Renormalization group approach to active biological systems

Mattia Scandolo
ID number 1715329

Thesis Director   PhD Board Advisor
Dr. Andrea Cavagna   Prof. Lara Benfatto

Academic Year 2022/2023

Thesis defended on February 21, 2024
in front of a Board of Examiners composed by:

Dr. Vito D. P. Servedio (chairman)
Prof. Francesco Zamponi
Prof. Chiu Fan Lee

External evaluators:

Prof. Chiu Fan Lee
Prof. Sriram Ramaswamy

Renormalization group approach to active biological systems
Ph.D. thesis. Sapienza University of Rome

This thesis has been typeset by LaTeX and the Sapthesis class.

Author's email: mattia.scandolo@gmail.com

Abstract

The renormalization group is a key set of ideas and quantitative tools of statistical physics that allow for the calculation of quantities that encompass the collective behaviour of different kinds of systems. According to the renormalization group theory, different collective behaviours can be organised into universality classes, based only on general properties of the underlying system, such as symmetries and conservation laws. Extension of the predictive power of the renormalization group, and its most fruitful consequence, namely universality, to collective biological systems would greatly strengthen the effort to put biophysics on a firm basis.

Living systems are very different from equilibrium systems statistical physics used to deal with. The ability to convert free energy from the environment into systematic movement, known as activity, drives living systems far from thermal equilibrium. Furthermore, the wide range of scales over which biological processes take place, from the chemical reactions of metabolism at the cell scale up to social interactions on inter-individual scales, makes the behaviour of living systems infinitely more complex. Given these premises, one may question whether the collective behaviour of a living system can solely be described by symmetries and conservation laws, challenging the idea of universality.

Here, by focusing on the case of natural swarms of insects, I provide one of the first successful tests of universality in active biological systems, by calculating the dynamic critical exponent of swarms using the renormalization group.

Swarms of midges in the field perform collective behaviour, as recent experiments highlighted. Despite the lack of global order, swarms exhibit strong scale-free connected correlations between midges' velocities. These findings, together with the observation of scaling laws, both static and dynamic, suggested that swarms behave as systems near a critical point, in which order is low but correlations are large and the capability to respond collectively to external perturbations is strong.

By focusing only on a few general properties of swarming midges, I developed a field theory aiming to describe their collective behaviour. Although based on experimental evidence, this approach entirely relies on the symmetries of the system, mainly the rotational symmetry, and the associated conservation laws entailed by the Noether theorem. The novelty of the field theory here developed is the combined presence of activity and inertia. Activity is represented by the ability of individuals to self-propel and thus accounts for the fact that the order parameter is the local direction of motion. Inertial behaviour, on the other hand, stems from the presence of a mode-coupling interaction with the conserved generator of the rotational symmetry of the direction of motion of midges and accounts for the observation of non-exponential relaxation of the temporal velocity-velocity correlation function.

I then perform a perturbative renormalization group analysis of this theory at first order in $\epsilon = 4 - d$, showing that a new fixed point where both activity and inertia are relevant emerges. At this fixed point, the dynamic critical exponent is found to be $z = 1.35$, in very good agreement with experiments on natural swarms ($z = 1.37 \pm 0.11$). On the path to this result, particular care has been taken to the effects of density fluctuations, which I show must be small in all active systems exhibiting collective behaviour in the absence of global order. This agreement

between theory and experiments suggests that statistical physics, particularly the renormalization group, can play a decisive role in describing collective behaviours in biological systems.

Finally, within the present work, I focus also on the development of a field-theoretical framework for models of flocking with discrete symmetry. Intending to understand the universal features of active systems near the flocking transition, I provide a comprehensive hydrodynamic approach to these systems, investigating their behaviour at the onset of flocking.

Contents

Introduction

Collective behaviour is a phenomenon that can be observed in a variety of different contexts, ranging from condensed matter systems like Ising [1, 2] or Heisenberg [3] ferromagnets near their critical temperature or superfluid helium [4], to biological systems such as birds flying in flocks [5, 6], sheep herds [7], and bacterial clusters [8].

Most of these biological systems exhibit collective order, suggesting a strong link between ordered dynamical structures and collective behaviour. This is the case of bird flocks and fish schools, which are strongly polarised systems where a spontaneously-selected direction of motion emerges. Is the presence of collective order in biological systems therefore necessary to achieve collective behaviour? The answer is no: what matters are correlations, and not order [9]. By thinking in terms of statistical physics systems, collective behaviour is related to the non-trivial presence of strong (connected) correlations among the fluctuations of the system, which measures to what extent a change in the state of one individual influences the change of the state of another individual [9]. Strong correlations thus allow the system to have an efficient, namely collective, response to external stimuli.

The misconception that collective behaviours and collective order are somewhat connected does not come out of nowhere. Strong and scale-free correlations are naturally achieved by systems in which collective order emerges via the spontaneous breaking of a continuous symmetry: when this happens, collective excitations can be represented as quasiparticles, known as Goldstone bosons, which have no energy gap and therefore can be exited by random fluctuations [10, 11]. Nevertheless, collective behaviour can be also performed by systems with no global order: this is the case of swarms of flies, mosquitoes or midges in the field [12]. Swarm formation plays a crucial role in the mating process of these insects, and thus understanding their properties is of great biophysical interest.

Insects gathering in swarms only apparently seem to behave as a cloud of non-interacting particles; in fact, their behaviour is strongly correlated, thus suggesting that interactions play a relevant role in the formation of swarms [12]. Furthermore, the observation of both static [12] and dynamic [13] scaling laws in natural swarms, together with the lack of global order, suggests that the proximity to a critical point can describe swarms and their collective behaviour. These observations paved the way for a theoretical investigation of swarms using the tools developed in the context of the physics of critical phenomena [1, 2, 14, 15, 16], above all the renormalization group [17].

The extension of the predictive power of the renormalization group (RG) and its fruitful consequence, namely universality, to collective biological systems would greatly strengthen the effort to put biophysics on a firm basis. Were universality

shown to play a decisive role in strongly correlated biological systems, it would allow one to describe collective behaviours in living systems based only on their general properties, such as dimensionality, symmetries and conservation laws. In the broader field of active matter [18], RG is already a key tool. The pioneering hydrodynamic theory of Toner and Tu [19, 20] has been studied through the RG both in the polarised [21, 22] and near ordering phase [23, 24], with applications in systems with nematic or polar order [25, 26, 27]. RG has also been employed to study motility-induced phase separation [28, 29], active membranes [30], bacterial chemotaxis [31], cellular growth [32]. Direct comparisons with experiments are few, though: the exponent of giant number fluctuations in $d = 2$ [22] was confirmed in experiments on vibrated polar disks [33], while in [34] the exponents of the Vicsek Model in the ordered phase were found to be incompatible with those conjectured by Toner and Tu [19]. Other RG exponents have been checked in numerical simulations [35, 36, 37, 38]. Comparisons with biological experiments are scarcer. Experiments studying giant number fluctuations in swimming filamentous bacteria displaying long-range nematic order [39] found an exponent in disagreement with RG predictions of active nematic [26] and polar [22] systems. To the best of my knowledge, prior to my recent work on swarms [MyPaper1], there has been no successful test of an RG prediction against experiments on active biological systems.

In the case of natural swarms, the presence of dynamic scaling [13] links the relaxation time τ to the correlation length ξ through a power law, $\tau \sim \xi^z$, where z is known as the dynamic critical exponent. The value of this dynamic exponent in swarms, of which the latest and most solid prediction is $z_{\text{exp}} = 1.37 \pm 0.11$ [MyPaper1], is far from that of any standard statistical model [13]. To give an example, in three dimensions, the dynamical critical exponent of a model for alignment interactions with no conservation laws is $z \approx 2$ (Model A [40]).

In my PhD thesis, I will use a field-theoretical approach to characterise the collective behaviour of insect swarms. To do this, I will focus on a theory that combines the presence of activity and behavioural inertia. The former, activity, is the ability of midges to perform self-propelled motion by consuming stored or ambient free energy. The latter, behavioural inertia, refers to the presence of inertia in the orientation dynamics of midges. Both these ingredients are motivated by strong experimental evidence [13]. Following recent literature [23, 41], I will attempt to build a field theory that properly accounts for collective swarming behaviour. Some challenges will arise during the discussion, mainly regarding the role of density fluctuations. Solving all these issues has been an integral part of my research work, and has led to the publication of the two papers [MyPaper2, MyPaper3]. Finally, the characterisation of the dynamic behaviour of swarms has been performed through a renormalization group approach, showing a remarkable agreement with both experimental and numerical results [MyPaper1].

Thesis structure

The thesis is organised as follows. In Chapter 1 I will introduce the reader to the main subject of my work, namely natural swarms of insects. An overview of their collective behaviours, together with a first characterisation of the interactions between midges

will be provided. The role of correlations will draw useful connections with statistical physics, as it allows one to describe swarms as systems in the proximity of a critical point. I will then move on by introducing, in Chapter 2, a set of minimal models developed to describe the collective behaviour of active matter, above all the Vicsek model [42]. In these models, individuals are self-propelled and move at a constant speed, and they interact with neighbours via an effective alignment of their direction of motion.

In Chapter 3 I introduce and discuss a general coarse-grained description of active matter systems, known as the Toner and Tu hydrodynamic theory [19]. This theory merges the relaxation dynamics of an equilibrium ferromagnetic system, known as Model A [40], with Navier-Stokes equations [43]. This theory provides a general description of the large-scale behaviour of Vicsek-like systems. After a detailed discussion of the Toner and Tu theory, I show through a linear stability analysis that the homogeneous steady-state is unstable in the proximity of the transition, a mechanism that turns the second-order transition of Model A into a first-order transition [44]. This mechanism is however suppressed when the compressibility vanishes, suggesting that swarms might behave as incompressible systems.

To perform a detailed analysis of the large-scale behaviour of the incompressible theory, and of other systems in the following, I review in Chapter 4 the main concepts and ideas behind the renormalization group, both in the case of static and dynamic systems.

The renormalization group calculation of the incompressible Toner and Tu theory near criticality of Chapter 5 is a review of a paper by Chen, Toner and Lee [23]. This calculation represents an important stepping stone towards the characterisation of swarming behaviour, as it addresses the effects of activity on the critical dynamics, and provides insightful technical details on how RG can be applied to active theories. For these reasons, I decided to dedicate a full chapter to this calculation although it is not original content. In their analysis, the authors of [23] find that incompressible active matter systems, with no conservation laws, have a dynamic exponent of $z = 1.73$ in the physical case of three dimensions. The shift from the value of $z \approx 2$ of equilibrium Model A dynamics to $z = 1.73$ for (incompressible) active systems is an encouraging result, as it shows that activity modifies the collective behaviour pushing z in the right direction. However, some missing ingredient is still needed to fill the gap between theory and experiments.

Before proceeding to the introduction of inertial behaviour, in Chapter 6 I ask myself whether the behaviour of swarms, which are not incompressible, can be truly characterised by enforcing incompressibility. Recent numerical evidence suggests that the dynamic critical behaviour of the compressible Vicsek model in the near-ordering phase is described by the incompressible universality class, as long as the density profile is homogeneous. To provide theoretical support to this hypothesis, I study a version of the Toner and Tu theory in which density fluctuations are partially suppressed by the presence of birth and death processes, known as Malthusian theory [45]. In this work, published in [MyPaper3], I find a crossover between a second-order phenomenology at finite scales and a first-order transition in the infinite size limit. Moreover, the scaling behaviour exhibited by finite-size systems is described by the exponents of the incompressible universality class [MyPaper3]. This result provides strong support for working under the assumption of incompressibility in the context

of homogeneous systems as swarms.

In Chapter 7, I tackle the problem of what other ingredient, in addition to alignment and activity, is needed to describe the collective behaviour of swarms. Following experimental evidence, I show that behavioural inertia in the orientation dynamics of the directions of motion might be the missing ingredient [13]. At the general level, inertial dynamics stems from the existence of a reversible coupling between the primary field (playing the role of the generalised coordinate) and the generator of the symmetry (playing the role of the generalised momentum); in the case at hand, the symmetry is the rotation of the direction of motion field, hence its generator has been called 'spin'. In the absence of explicit dissipation, a reversible mode-coupling dynamics leads to global spin conservation, which is known – at equilibrium – to significantly decrease the dynamical exponent, from $z \approx 2$ of Model A [40], to $z = 1.5$ of three-dimensional superfluid helium or quantum antiferromagnets (Models E/F and G [40]). At the end of Chapter 7, I introduce the reader to Self-Propelled Model G, the field theory in which inertia and self-propulsion merge.

The need to model natural swarms as incompressible systems, to account for the scaling laws observed in experiments, requires the direction of motion field to obey a solenoidal constraint [46]. In Chapter 8, I address the question of what are the consequences of this constraint on the dynamic behaviour of the spin field. Since this issue is unrelated to the presence of self-propulsion, I perform this analysis in the fixed-network approximation by studying a solenoidal-constrained version of Model G. I show that an additional interaction, relevant in the RG sense, is needed for the theory to pass some crucial consistency checks. Moreover, in the presence of this solenoidal constraint, I reveal that the dynamic universality class remains unchanged compared to Model G. This is remarkable, as the solenoidal constraint does instead modify the static universality class, usually believed to be more robust compared to the dynamic one. The results presented within this Chapter have been published in [MyPaper2].

Overall, the scenario presented so far suggests that the combined effect of activity *and* inertia may account for the experimental exponent of natural swarms. In Chapter 9 I, therefore, start to investigate this hypothesis, by performing a field-theoretical study of Self-Propelled Model G in the incompressible limit. In particular, I discuss in detail the equation of motion, provide arguments for the presence of some additional *anomalous* terms which were neglected in the introduction of Self-Propelled Model G in Chapter 7, and provide an equivalent field-theoretical description of the system using a Martin-Siggia-Rose formalism [47].

Chapter 10 is completely dedicated to the renormalization group calculation of Self-Propelled Model G. There, I discuss in detail the effects of the renormalization group transformation on the action of the theory and provide a primer of the calculation of the Feynman diagrams, which have not been reported explicitly. I also show that the anomalous terms, introduced in the previous Chapter, are generated by the renormalization group. This means that even if one started with equations of Chapter 7, the renormalization group would have singled out the presence of these interactions anyway. Most importantly, I reveal that the collective behaviour of Self-Propelled Model G is described by a novel fixed point, characterised by the presence of both activity and inertia.

In Chapter 11 I characterise the collective behaviours of the system in the proximity of this new RG fixed point, revealing its many interesting features. Above all, I compute the dynamic critical exponent z and find a new dynamic universality class, describing active inertial systems, characterised by $z = 1.34(8)$, in great agreement with both experimental ($z_{\text{exp}} = 1.37 \pm 0.11$) and numerical results ($z_{\text{num}} = 1.35 \pm 0.04$). The analysis performed in Chapters 9-11 is now published in [MyPaper1].

In the last Chapter, I present work done during a visiting period spent in Cambridge, in collaboration with Dr Pausch and Prof Cates. There, I investigate the behaviour of flocking models with discrete symmetry, known as Active Ising Models. I use a field-theoretical approach to study the emergent behaviours of these models, confirming some known results and presenting some new findings concerning the universality class of the system. Most of the results of Chapter 12 are now published in [MyPaper4], although some will be presented in a paper currently in preparation [MyPaper5].

Chapter 1

Collective behaviour in active biological systems

As physicists, we are usually interested in finding simple descriptions of the phenomena we observe in the world surrounding us. To do this, sophisticated tools and techniques have been developed throughout the centuries, both theoretical and experimental. In particular, statistical physics aims to provide a general framework to characterise emergent properties of a system using a *statistical* description of its constituents.

The great success of statistical physics in describing collective properties of matter, which culminated with the development of a theory of critical phenomena, found prolific applications in many areas of science and technology. Ferromagnetism is a typical example of an emerging property: thanks to the ability of neighbouring atoms in a material to locally align their spins, as a consequence of induced magnetic fields, the material can develop a global net magnetic field if the temperature is sufficiently low. Moreover, the response of the system to external perturbations - as an external magnetic field - is extremely efficient. Superconductors and superfluids also provide examples of collective behaviour. The vanishing electrical resistance in the former, and the vanishing viscosity in the latter both emerge from local interactions between the constituents of the system through the presence of collective excitations.

Similarly, emergent behaviour is also observed all the time in a wide variety of living systems: bird flocks move all in the same direction and respond efficiently to the attack of a falcon, resembling the aforementioned behaviour of ferromagnetic materials. Fish schooling, swarming midges and herds of mammals all provide other collective behaviour emerging from *local* interactions between the system's constituents. A unifying ingredient of collective behaviours in these living systems, which also provides an insightful connection with statistical physics, is the presence of strong correlations, which allow small fluctuations of an individual's behaviour to quickly propagate and influence the behaviour of others, hence allowing the system to respond collectively to external perturbations.

In contrast to ferromagnets, superfluids and superconductors, understanding the emergent behaviour of a living system within the boundaries of equilibrium physics would not be possible. Most biological systems are made of *active* self-driven

units, able to convert energy from the environment into mechanical motion at the individual's scale. This property, known as activity, drives the system far from thermal equilibrium, and often has far-reaching consequences on its large-scale behaviour [18, 26]. A typical example is flocking, namely, the collective coherent motion of a large group of self-propelled units, which can spontaneously emerge in a system moving on a surface [19]. In equilibrium systems, a phenomenon like flocking would violate the Mermin-Wagner-Hohenberg theorem, which states that no continuous symmetry can be spontaneously broken in two spatial dimensions [48, 49]. However, the presence of self-advection and the consequent rewiring of the interaction network gives rise to a feedback mechanism that stabilises the ordered flocking phase. It should therefore be no surprise that active matter physics represents one of the most prolific fields of the last decades since the introduction of a simple model to describe flocking by Vicsek et al. [42] paved the way for deep theoretical investigation of collective behaviours in living matter.

1.1   Is there universality in living systems?

One of the central questions I will address throughout this work is whether *universality* applies to strongly correlated biological systems, namely understanding if the collective behaviour observed in a biological system can be explained by looking at a few general properties, such as symmetries and conservation laws.

This concept of universality, according to which only a few *general* features contribute to the observed emergent properties in strongly correlated systems, has been proposed in the context of critical phenomena and phase transitions [14, 2, 15, 1]. As a system approaches a critical point, it exhibits fluctuations on increasingly wider length scales, which leads to the presence of a diverging correlation length. A set of phenomenological scaling laws have been proposed by Widom and Kadanoff [50, 51], which link the divergence of the free energy of the system, and its derivatives, to the proximity to the critical point through a set of *critical exponents*. Experiments soon reported that systems very different one from another, often shared the same critical exponents when approaching a phase transition [14], providing strong evidence for universality in physics.

Within the renormalization group (RG) developed by Wilson [17, 52], universality finds an elegant and rather simple explanation. In the RG context, each specific microscopic system can be identified by a different point in the parameter space. Universality consists of the fact that one single fixed point rules the long-wavelength behaviour of a large class of theories, all sharing only a few general properties, such as symmetries, conservation laws and dimensionality. Hence, at the critical point, all systems sharing these general properties will fall into the same *universality class* and have the same critical exponents. Moreover, the RG gives a constructive method to compute these exponents [53], making it one of the most powerful tools of the theory of critical phenomena, broadly employed to characterise the critical behaviour in equilibrium systems. The predictive power of the RG is not limited, however, to systems that are precisely tuned at the critical point: any system which has strong correlations, regardless of its proximity to a phase transition, can be treated through an RG approach.

Whether the RG and its most fruitful consequence, universality, can be applied to biological systems should not be taken for granted. Biological systems appear to be very far from the world of condensed matter physics, where the ideas of the renormalization group were first applied. In the first place, these systems are *active*, namely, they are able to convert stored or ambient free energy into movement, driving living systems far from thermal equilibrium. Secondly, and perhaps most importantly, living systems are way more complex than non-living ones. What one observes on the macroscopic scale is the result of a chain of different processes ranging on several scales: from chemical reactions in the Krebs cycle of cellular respiration up to the *social* interactions among different individuals, passing through the internal organisation into tissues and organs in the case of animals. Their large-scale properties might therefore depend on the concatenated effect of all these processes, challenging the foundations of universality.

Despite these striking differences, when it comes to collective behaviour all systems share the same features: they exhibit strong, scale-free, correlations between the system's components. In the realm of biological systems, this has been experimentally observed in a wide range of systems, from bird flocks [5] and sheep herds [7] to midge swarms [5] and bacterial clusters [8]. The presence of a strong scale-free correlation associated with collective behaviour, although not proving direct evidence of universality, can be hardly considered a coincidence. This calls for an attempt to employ the tools of critical phenomena to explain collective behaviours in biology.

1.2   The case of natural swarms of midges

Within the present thesis, I will put to test the renormalization group approach in the biophysical context by focusing on the case of natural swarms of insects. Before starting with any theoretical approach to swarms, it is useful to review some relevant experimental evidence.

The claim that flocks of birds or schools of fish behave collectively seems quite intuitive. In these systems individuals all move in the same direction and turn at the same time, hence giving rise to emergent phenomena which can usually be detected already "by eye". This common intuition would suggest that the presence of some ordered structure and collective behaviour are two faces of the same medal.

In this respect, natural swarms of insects represent a tricky case. Swarms consist of a relatively large group of insects, mainly males, that gather together to attract females [54, 55]. The group however does not seem to exhibit any emergent pattern nor does it move around as a whole. Rather, it remains stationary over a landmark, usually a water puddle or a street lamp [54]. The reproductive function of the swarm together with the absence of any evidence of *order* broadly intended, challenges the link between emergent order and collective behaviour.

1.2.1   Collective behaviour vs emergent phenomena

It is therefore important to settle this issue, by making clear what I intend as collective behaviour, and how it might differ from the presence of an emergent ordered pattern. An ordered pattern emerges when individuals *do all the same thing*, for example arranging their position in space in a given way, moving all in

the same direction, or synchronising some degree of freedom. Collective behaviours arise instead when behavioural changes throughout the group are synchronised. To put this in the words of a theoretical physicist, the presence of an ordered pattern is related to the properties of the *ground state* of the system, while a collective behaviour arises when the energy gap of *collective modes* vanishes.

In the language of statistical physics, this means that the (connected) correlation is the observable to watch for to understand collective behaviour [9]. An intuitive explanation of this fact can be given as follows: when correlations are large, small fluctuations of an individual's behaviour quickly propagate throughout the system, influencing the behaviour of others. This allows the system to *behave collectively*, and respond efficiently to external perturbations. At equilibrium, the connection between fluctuations and response is entailed by the Fluctuation-Dissipation Theorem. In non-equilibrium systems, as living matter, fluctuations and response are not directly linked to each other; nevertheless, the presence of strong correlations is usually linked to an efficient response to an external perturbation.

Please note that the association between collective behaviour and emerging order is not completely unjustified: whenever order emerges through the spontaneous breaking of continuous symmetry, as happens in flocks, Goldstone modes arise. These modes, often referred to as spin-waves in the context of ferromagnets, can be excited with a vanishing energetic cost and therefore are characterised by a diverging correlation length. Hence, in these cases collective behaviour *do arise* from the presence of emerging order. It is however important to be aware that this might not be the *only* mechanism through which collective behaviours arise. In general, emergent order might be present in the absence of collective behaviour and vice-versa.

1.2.2 Evidence of collective behaviour in swarms

In the previous section, I justified that collective behaviour can be detected by looking at the connected correlations in a system. In the case of natural swarms, this has been done by the Collective Behaviour in Biological Systems lab in [12], where swarms of midges have been recorded in urban parks in Rome, their trajectory reconstructed and the correlation between the velocity fluctuations of different midges computed.

Short-range metric aligning interactions

Midges in the field seem to interact mainly with sound-mediated interactions with an interaction range of only a few centimetres [57, 58], way smaller than the size of the swarms observed. The short-range nature of the interactions in swarms was also confirmed in [12], where the radius of the effective aligning interaction was estimated to be of $2-5$ cm, in agreement with acoustic interactions. Moreover, because correlations were found to be larger in denser swarms, midges are expected to interact through a metric perceptive apparatus: the strength of the perception decreases with the distance, so that when midges are further apart from each other the interaction is weaker. Note that this is different from what happens in flocks, where birds interact only with a fixed number of neighbours [59], hence giving rise
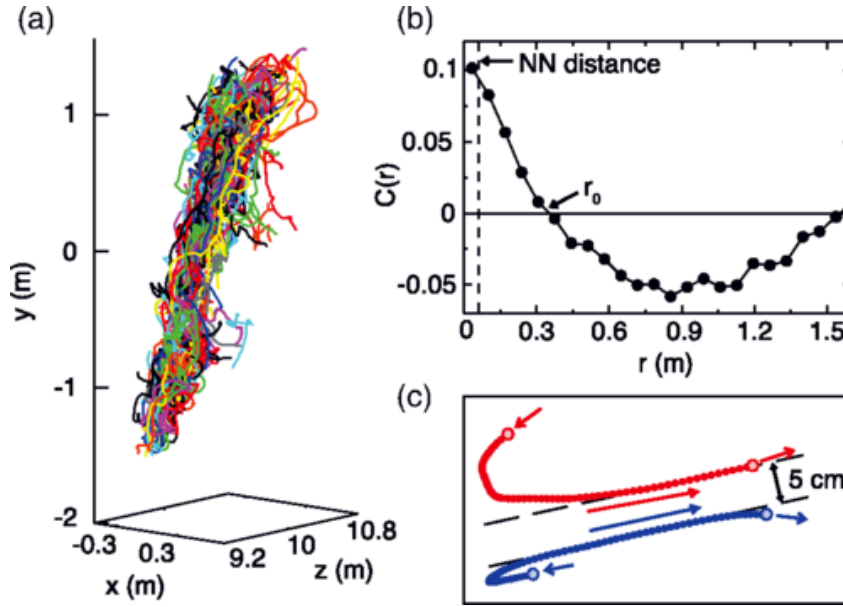
Figure 1.1. Natural swarms [56]. (a) 3D trajectories for swarm 20120907_A1 (see
[56]), $N = 169$. **(b)** Velocity correlation function. The correlation length, $\xi \sim r_0$, is
much larger than the nearest-neighbour distance. The correlation is averaged over the
whole time acquisition. **(c)** Alignment event between two midges (real trajectories).
*Permission to reuse granted by the American Physical Society under License Number
RNP/23/OCT/071428.*

to topological interactions. Finally, interactions between neighbouring swarms were
shown to promote alignment between their direction of motion [56]. This is not only
suggested by the presence of positive velocity-velocity corrections in neighbouring
midges, which *per se* suggests that a mechanism through which a change in direction
of one midge is followed by a similar change in a neighbouring one, but also observed
directly on real trajectories - see Fig 1.1, panel (c).

This overall picture suggests that midges effectively interact with their neighbours
through short-range metric alignment interactions. Although this behaviour emerges
from the complex interactions between many underlying biochemical processes,
it is under universality that one can hypothesise all these *details* do not matter,
allowing an effective description to be able to quantitatively account for the collective
properties. If this were true, from a theoretical point of view swarms could be cast in
the context of ferromagnetic-like models, where individuals tend to act to minimise
an effective energy [14]

$$H = J \sum_{ij} n_{ij} \boldsymbol{\psi}_i \boldsymbol{\psi}_j \,. \tag{1.1}$$

Here $\boldsymbol{\psi}_i = \boldsymbol{v}_i / |\boldsymbol{v}_i|$ is the direction of motion of the i-th individual, while n_{ij} is the
adjacency matrix, which tells whether two individuals i and j are interacting or not.

Lack of global order

To establish whether emergent order was present in the system, three order pa-
rameters were monitored: the alignment order parameter Φ, the rotational order
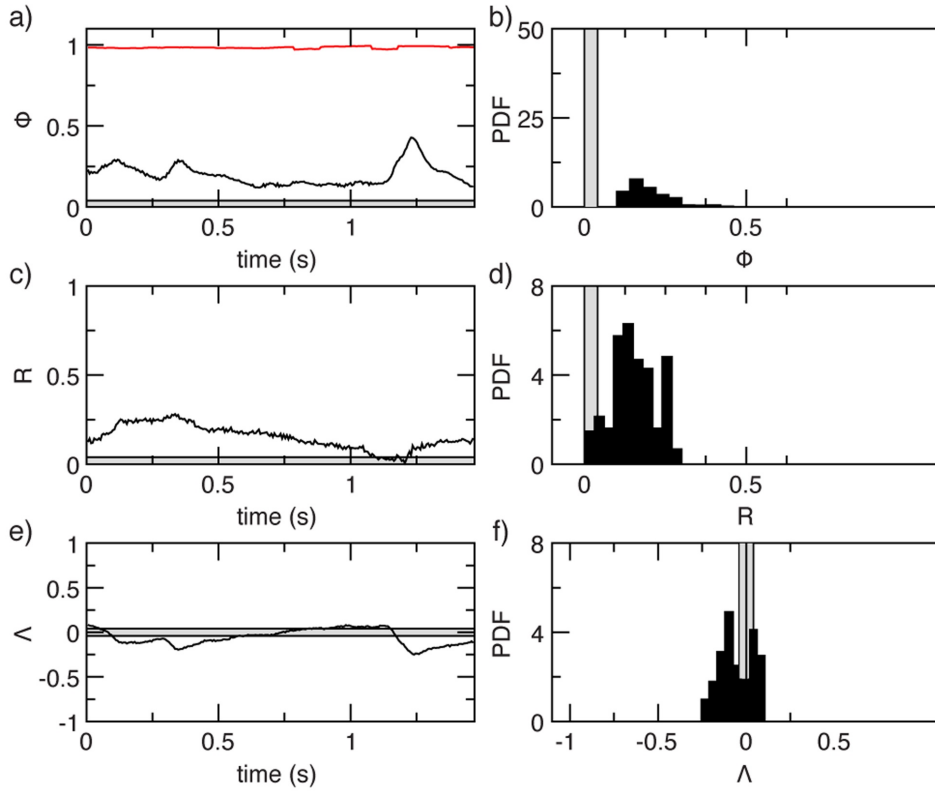
Figure 1.2. Natural swarms lack global order [56]. Order parameters in a typical natural swarm. In all panels, the grey band around zero is the expected amplitude of the fluctuations in a completely uncorrelated system. In the left panels, the time series of the order parameters are reported, in the right panels their probability distributions. **Top:** The alignment order parameter, known as polarisation, $\Phi \in [0:1]$ In red the reference value of the polarisation in a flock of starlings is reported. **Middle:** Rotational order parameter, $R \in [0:1]$ **Bottom:** Dilatational order parameter, $\Lambda \in [-1:1]$. *Permission to reuse granted under the terms of the Creative Commons Attribution License CC BY 4.0*

parameter R and the dilatational order parameter Λ (see Methods of [12] for definitions). The former provides a measure of *translational* modes, associated with collective motion, the second of *rotational* modes, as milling, and the latter of *pulsation* modes, observed when contractions and dilations follow one another cyclically. As can be seen from Fig. 1.2, all these order parameters are small [12], hence suggesting swarms belong to an overall *disordered* phase. Furthermore, let me note how none of these order parameters is conserved, as they all fluctuate in time.

Strong correlation and near-critical behaviour

On the other hand, however, connected velocity-velocity correlations were found to be large, and in particular to scale linearly with the size of the system [12, 56]. But even most remarkably, scaling laws were observed in natural swarms of insects [56]. Through a finite-size scaling analysis, data for natural swarms could be explained by the proximity to the critical point of an ordering transition, suggesting that

the collective behaviours of swarms are of the same nature as those observed in a ferromagnet near the Curie temperature.

Note that, however, being near to a critical point is not the only mechanism through which biological systems in general exhibit collective behaviour and scaling laws. Often, collective behaviour arise from other mechanisms, as the spontaneous breaking of continuous symmetries or the presence of conserved quantities. In the former case, Goldstone modes of large wave-length can be excited with arbitrary small energetic cost. Therefore, random fluctuations are able to give rise to strong collective behaviour. On the other hand, in systems with conservation laws scale invariant structures arise in the fluctuations of the conserved quantities. In these systems, universal collective behaviours are expected to emerge without the need of any fine-tuning of parameters, while in cases as swarms some fine-tuning near the critical point is required.

How swarms perform this fine tuning is a topic that will not be addressed here. Let me just mention that, although no definitive answer has been provided yet, two main scenarios are possible. One is that natural swarms do fine-tune their intrinsic parameters to achieve scale invariance. This would however require midges to be able to change their interactions with neighbours and tune them accordingly. A second possibility is that each swarm in the field has a given set of parameters, and tunes its size to maximise its susceptibility, namely the collective response. This mechanism, proposed in [56], lies on a simple assumption: midges gather in swarms only when it is convenient, namely when they maximise their ability to behave collectively and therefore to mate. This could happen due to interactions we are currently not aware of, that make the swarm unstable whenever its size is too large, naturally breaking it into smaller swarms until the collective response is maximal. This mechanisms would mean that swarms might be able to cut off their size close to that of their correlation length. Note that, whatever is the correct scenario, based on the results in [12, 56], swarms can be effectively described as a system near a critical point.

1.2.3 Dynamic scaling in swarms

While the finite-size scaling observed in [56] involved only static quantities, as the integrated same-time correlation function, the scaling analysis has been further expanded in [13] by probing the presence of *dynamic scaling* in natural swarms.

Dynamic scaling is a property exhibited by spatiotemporal correlations of critical systems, entangling the relaxation time-scales of large-scale modes with the correlation length [60, 61]. In particular, it states that the dynamic correlation function C, when expressed as a function of wave vector and frequency, takes the following simplified scaling form,

$$C\left(\boldsymbol{k}, \omega; \xi\right) = C_0\left(\boldsymbol{k}; \xi\right) F\left(\frac{\omega}{\omega_k}, k\xi\right) , \qquad (1.2)$$

where ξ is the correlation length and where the *static* correlation function C_0 has in turn the scaling form,

$$C_0(k, \xi) = k^{2-\eta} F_0\left(k\xi\right) \qquad (1.3)$$

and where the characteristic frequency at scale k is given by,

$$\omega_k = k^z \Omega\left(k\xi\right) \qquad (1.4)$$
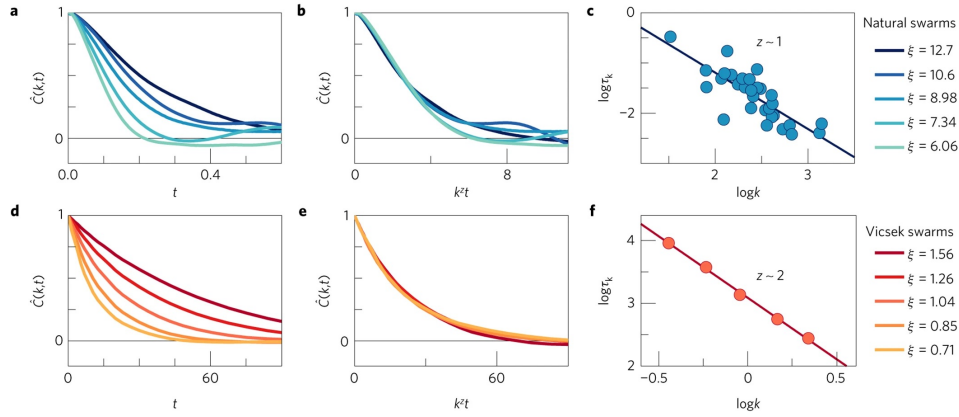
Figure 1.3. Dynamic scaling in swarms [13]. (a) Normalised time correlation function, $\hat{C}(k,t)$, evaluated at $k = 1/\xi$, in several natural swarms. Sizes range from $N = 100$ to $N = 300$, time is measured in seconds and correlation length ξ is centimetres. **(b)** $\hat{C}(k,t)$ as a function of the scaling variable $k^z t$ for the same events (here the value $z = 1.2$ was used). The quality of the collapse deteriorates for longer times because $\hat{C}(k,t)$ is the average over $t_{max} - t$ time pairs (t_{max} is the sequence duration); hence, large t data are noisier. **(c)** Characteristic timescale, τ_k, computed at $k = 1/\xi$, as a function of k (log-log scale). Each point corresponds to a different natural swarm; all experimental events of [13] are reported. $P - value = 10^{-6}$, $z = 1.12 \pm 0.16$, consistent with the estimate from the collapse in (b). **(d-f)** Dynamic scaling analysis of the 3D Vicsek model for $N = 128$, 256, 512, $1,024$, $2,048$ particles; τ_k scale with k with an exponent $z = 1.96 \pm 0.04$, which also produces an excellent collapse of the correlation functions. *Permission to reuse granted by Springer Nature under License Number 5655281510730.*

In the relations above, Ω, F_0 and F are well-behaved scaling functions, whose explicit form is inessential to capture the gists of dynamic scaling [60, 61]; η is the critical exponent for the static correlation function (normally called anomalous dimension [14]). The fundamental meaning of dynamic scaling is that in critical systems space and time do not scale independently from each other, but they are linked by the dynamic critical exponent z. The space-time correlation function has a very simple form, as its whole spatiotemporal dependence goes through the product $k\xi$. When $\boldsymbol{k} = 0$, the collective relaxation time τ of the system is linked to the correlation length ξ through the relation,

$$\tau \simeq \omega_{\boldsymbol{k}=0}^{-1} \sim \xi^z \tag{1.5}$$

This phenomenon is known as *critical slowing down* and it represents a consequence of the fact that the time τ needed to decorrelate a spatially correlated region grows with the region's size, namely with the correlation length ξ, making the latter the only relevant scale also at a dynamic level.

Notably, natural swarms of insects have been found to obey dynamic scaling [13], with a dynamical critical exponent z quite close to 1. In Fig. 1.3, one can appreciate the collapse of the correlation functions of swarms arising from the validity of Eq. (1.2). Note that the analysis of [13], where a Least Squares regression method [62] was used to infer z, predicted an exponent of $z = 1.12 \pm 0.16$. However, the addition of other data points to the analysis, and the realisation that the hypothesis underneath the Least Square method – negligible error bars on the abscissa – was

violated in the case of swarms, led to a revision of the analysis in [MyPaper1]. In this case, a Reduced Major Axis method [63, 64] has been used to take into account non-negligible error bars on both the ordinate and abscissa variables, which lead to the result [MyPaper1]

$$z_{\text{exp}} = 1.37 \pm 0.11 \,. \tag{1.6}$$

In conclusion, because the validity of scaling laws is one of the hallmarks of critical systems, the experimental evidence of static and dynamic scaling in natural swarms [12, 13] suggests that the swarming phase can be theoretically described as a near-ordering phase of ferromagnetic-like theories. The novelty of this dynamic critical exponent, not reported previously in any other theory to my knowledge, suggests swarms belong to a new universality class. In the present dissertation, I will attempt to first understand what features should characterise this new universality class, and then use a renormalization group approach to provide a theoretical estimate of this exponent.

Comparison with other systems

Let me try to put this exponent into context, and compare it to that of other systems sharing with swarms the same properties I discussed so far. As pointed out in Sec. 1.2.2, the presence of effective short-range alignment interactions between midges allows to model swarms as ferromagnetic-like systems, such as the Heisenberg model [3]. The proximity to a critical point further suggests collective swarming behaviour can be studied within the framework provided by the theory of dynamic critical phenomena [40].

The most simple dynamic behaviour, which takes into account the presence of effective alignment interactions between the order parameter field, but neglects any other feature, is known as Model A in Halperin and Hohenberg classification [40], and exhibits a dynamic critical exponent of $z \approx 2$ in $d = 3$, quite far from the value observed in natural swarms. When in addition the average magnetisation – which is the equivalent of the direction of motion in swarms – is conserved, as in Model B [40], the agreement becomes even worse, as $z \approx 4$.

Both Models A and B discussed here describe the dynamic behaviour of an equilibrium system in which no couplings with other conserved quantities are present. The following few Chapters will be therefore dedicated to understanding what ingredients, in addition to effective alignment, should be taken into account in a quantitative description of the collective behaviours of natural swarms of midges. As it will turn out, Model A fails to describe swarms both because it is an equilibrium model, while swarms are inherently active, and because a coupling with the conserved generator of the underlying rotational symmetry is neglected. Combining these two ingredients will therefore turn out to be crucial to understanding the collective behaviour of swarms.

Chapter 2

Activity through self-propulsion: minimal models

Although midges in a swarm interact via short-range effective alignment, their dynamic collective behaviour is hard to explain within the standard theories of ferromagnetic alignment. Midge-midge interactions might therefore not be the whole story: other ingredients must be taken if a quantitative description of swarming collective behaviour is aimed to be provided.

The first obvious candidate to lower the value of z from the value of 2 of Model A to the experimental value of swarms is activity, which represents the ability of a system to convert stored or ambient free energy into mechanical motion [18]. As such, active particles contain internal degrees of freedom able to dissipate this energy and, in the process, execute systematic movement [26]. Many biological systems indeed fit into this definition: from mammals to insects, from birds to bacteria, most living matter can sustain self-propelled movement. These motile organisms are usually able to intake nutrients from the environment, transform them into energy through metabolism, store this energy if necessary and then use it to perform work. This energy flow drives living systems far from thermodynamic equilibrium, allowing them to perform the biological functions that characterise the presence of life. The emergent behaviours of active systems are therefore expected to be way more complex compared to equilibrium systems.

In the context of equilibrium physics, when focusing on the large-scale properties of a system, universality [14] ensures that the precise details of the interactions are not usually necessary to describe its collective behaviour. Thus, a description in terms of some *general* effective features only – such as symmetries, conservation laws and dimensionality – is expected to be sufficient to characterise the observed emergent behaviours. Whether this holds also for biological systems is far from being completely understood. To probe the existence of universal behaviour in living systems, the route I will follow here is assuming universality holds, and check what conclusions can one draw based on this assumption. The main focus of the rest of the present thesis will be to attempt to provide *a posteriori* evidence in favour of the applicability of universality in biology by focusing on the case of natural swarms.

In the present chapter, I will start by discussing what activity is expected to be a relevant feature in the description of the large-scale behaviour of swarms. Then,

inspired by universality, I will introduce some particle-based models describing active systems with effective imitative alignment interactions among individuals, above all the Vicsek model [42]. Note that in what follows I will use the adjective "microscopic" to indicate these particle-based models. This choice is made to differentiate the behaviour of the system on the "microscopic" particle scale from the mesoscopic scales on which coarse-grained descriptions will become applicable and the macroscopic scales on which collective behaviour occurs.

2.1 Activity meets alignment: the Vicsek model

When self-propelled individuals group, *social* interactions among them usually take place, allowing living matter systems to give rise to fascinating collective behaviours. Among social interactions, imitation often plays a crucial role in allowing efficient responses to external stimuli. Imagine having a neighbour under attack by a predator: if they try to move away from the threat, by imitating them you avoid being attacked even if you are not able to directly detect the predator's presence. Countless biological systems, including swarms of midges [56], act guided by an imitative interaction, as individuals tend to align their motion to that of neighbours. Understanding the behaviour of active aligning systems is thus of fundamental interest in biophysics.

2.1.1 Relevance of activity in natural swarms

Before delving into the details of the Vicsek model, let me start the discussion by addressing the effective relevance of activity on the collective behaviour of natural swarms. While activity is indeed relevant on the scale of single midges, as it allows them to *move* in space, it is reasonable to question its relevance on the large-scale dynamics. There are several good reasons why this should be a good question to ask oneself. The first is that in other biological systems, such as flocks, local equilibrium behaviour has been reported [65]. In flocks, this happens because the time scale over which the network rearranges - a measure of the relevance of activity on large scales - is much larger than the time scale over which neighbouring birds align their directions of motion.

To understand whether this is what happens also in swarms, in [MyPaper1] the characteristic time scale of the network correlation function has been computed, and compared to the time scale of the velocity-velocity correlation. The results, reported in Fig. 2.1, leave little room for interpretation: these time scales are comparable, and hence activity has the same relevance as the alignment dynamics. As a consequence, guided by the spirit of universality, the large-scale behaviour of swarms is expected to be triggered by the combined presence of imitative interactions and activity. The former can be modelled as a *social* force whose effect is to align the direction of motion of neighbouring individuals. The latter property comes instead from the presence of an *internal* force that sustains movement. These are precisely the two features underlying the development of the model proposed by Vicsek et al. in [42].
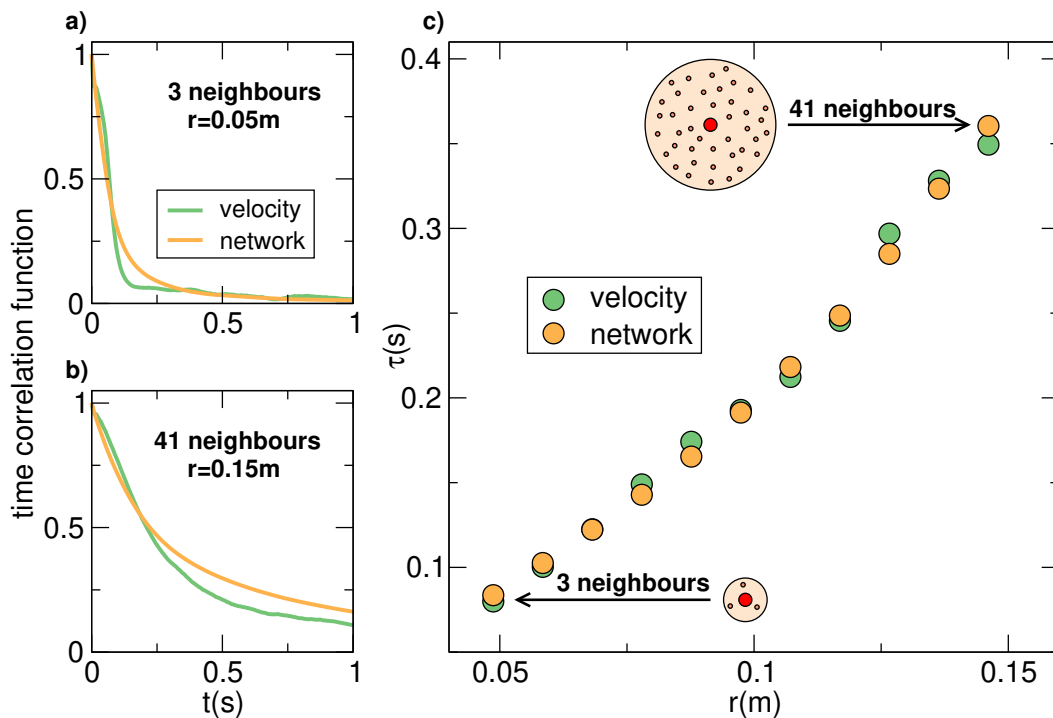
Figure 2.1. Swarms are strongly active. a, b: Network correlation (yellow) and velocity correlation (green) as a function of time, at two different spatial scales r. The network correlation measures the fraction of neighbours remaining within a region of size r around a given individual, after a time t; it therefore quantifies how quickly the interaction network rearranges on a given spatial scale. The two values of r considered correspond to neighbourhoods with - on average - 3 individuals and 41 individuals. **c:** Characteristic time of network and velocity correlation vs. r in the range $[0.05m, 0.15m]$, an interval within which the metric interaction range of real swarms certainly belongs to [12]. Results show that network rearrangement occurs on the same timescale as velocity relaxation both locally and for neighbourhoods containing many individuals. Data are from event 20150924_ACQ2, with $N = 781$ individuals (SI-Table 1 of [MyPaper1]).

2.1.2 Moving Ferromagnets

Fortunately, physics is not new to polar systems, whose aim is to align some vectorial degree of freedom. The classical theory of ferromagnetism is based exactly on the same principle: atoms in a certain material tend to align their spin. While spins align *simply* because of the presence of a magnetic field induced by neighbouring spins, social interactions inducing animals to align their direction of motion are way more complex, and require the coordination of biological functions of different organs and systems.

Claiming that animals are similar to ferromagnets is therefore an apparent blunder. However, the final effects of the very diverse processes in these two systems can be easily summarised with the same sentence: *individuals align to their neighbours.* The only macroscopic difference in this effective description is that atoms in ferromagnets are located on a fixed network, and spins therefore are simple *pointers* in space, while in active systems what is being aligned is the direction of

motion, which in turn affects how the network changes in time. This will be the only effective difference between these two systems I will take into account in this section. Yet, I will later show that this "tiny" difference has important consequences on the large-scale properties of the system.

The core idea behind most of the models aiming to describe collective behaviours in flocks and swarms is based on the empirical observation of combined self-propelled motion and imitative interactions between neighbours. Note that the biological mechanisms leading to alignment in these systems might be quite complex and perhaps not completely understood. It is not even clear whether in these systems individuals voluntarily tend to align one with the other, or whether alignment emerges as an effective consequence of other interactions. However, if the aim is to describe effectively the dynamics of these biological systems on large scales, it is reasonable to expect this deep understanding to not be needed.

In the most simple description, imitation can be encoded by the tendency of a given individual i to align its velocity to that of neighbours. Given that individuals are moving at a known velocity at time t, after a *small* time Δt the new velocity will get closer to the average velocity of neighbours $\langle \boldsymbol{v} \rangle_r$, following the update rule

$$\boldsymbol{v}_i \left(t + \Delta t\right) = v_0 \frac{\boldsymbol{v}_i \left(t\right) + \Delta t \left\langle \boldsymbol{v} \right\rangle_r \left(t\right)}{\left|\boldsymbol{v}_i \left(t\right) + \Delta t \left\langle \boldsymbol{v} \right\rangle_r \left(t\right)\right|} \tag{2.1}$$

To enforce the fact that particles are self-propelled, I am here considering individuals that move at a constant speed v_0, so that the velocity is not dissipated. More realistic assumptions might be made, such as a speed fluctuating with Gaussian statistics around an average speed v_0. Unless scale-free speed correlations are a feature one wants to reproduce, for which marginal models are required [66, 67], other choices that do not allow speed dissipation are expected to lead to analogue behaviours.

In the limit $\Delta t \to 0$, only the component of $\langle \boldsymbol{v} \rangle_r$ orthogonal to $\boldsymbol{v}_i$ contributes to the evolution of $\boldsymbol{v}_i$ itself, thus meaning that

$$\frac{\mathrm{d}\boldsymbol{v}_i}{\mathrm{d}t} \left(t\right) = \left\langle \boldsymbol{v} \right\rangle_r^\perp \left(t\right) \tag{2.2}$$

To take into account the self-propelled nature of the particles, this equation should be coupled to the temporal evolution of the positions

$$\frac{\mathrm{d}\boldsymbol{x}_i}{\mathrm{d}t} \left(t\right) = \boldsymbol{v}_i \left(t\right) \tag{2.3}$$

Systems with the same alignment interaction in which the ability to move is absent have been widely studied in the context of ferromagnetism. If (2.2) is not coupled to (2.3), namely if the limit $v_0 \to 0$ is taken, the positions $\boldsymbol{x}_i$ of each individual do not depend on time, and therefore the interaction network is fixed. In this limit, the magnitude of $\boldsymbol{v}_i$ vanishes, since it is equal to v_0. However, the direction of motion

$$\boldsymbol{\psi}_i = \frac{\boldsymbol{v}_i}{v_0} \tag{2.4}$$

remains well-defined at arbitrarily small v_0. When $v_0 = 0$ the vector $\boldsymbol{\psi}$ does not represent the direction of motion, since no motion is occurring, and equilibrium ferromagnetic models are recovered. However, the presence of movement through the

evolution of $\boldsymbol{x}_i$ radically changes the properties of the model. When $v_0 \neq 0$ then the positions are not fixed, and thus the adjacency matrix n_{ij}, that is a function of $\boldsymbol{x}_i$ and $\boldsymbol{x}_j$, will indirectly depend on time. This leads the system to be off-equilibrium.

2.1.3 The model

One of the first and most simple models proposed to describe the collective behaviour of active biological systems in the presence of an effective alignment interaction was proposed by Vicsek and collaborators in [42]. The Vicsek model (VM) describes the dynamics of a collection of self-propelled individuals with a ferromagnetic-like alignment interaction between their directions of motion. The model, originally introduced in the two-dimensional case in terms of the angular orientation of the velocity [42, 68], can be defined in a more general way by the following equations for the direction of motion $\boldsymbol{\psi}_i$ and the positions $\boldsymbol{x}_i$ of each individual i:

$$\frac{\mathrm{d}\boldsymbol{\psi}_i}{\mathrm{d}t} = \theta \left[\mathcal{J} \sum_j n_{ij} \boldsymbol{\psi}_j + \sqrt{2D_\psi} \boldsymbol{\zeta}_i \right] \tag{2.5}$$

$$\frac{\mathrm{d}\boldsymbol{x}_i}{\mathrm{d}t} = v_0 \boldsymbol{\psi}_i \tag{2.6}$$

Because the direction of motion $\boldsymbol{\psi}_i$ is, by definition, a unitary vector, the operator $\mathcal{R}$ is present to enforce the conservation of the moduli of $\boldsymbol{\psi}$. To fulfil this, θ must project its argument perpendicular to $\boldsymbol{\psi}_i$, so that no change in the magnitude of $\boldsymbol{\psi}$ occurs:

$$\theta \left[\boldsymbol{\varphi} \right] = \boldsymbol{\varphi} - \left(\boldsymbol{\psi}_i \cdot \boldsymbol{\varphi} \right) \boldsymbol{\psi}_i \tag{2.7}$$

The social force inducing imitative interactions, in virtue of the similarity with ferromagnetic-like alignment, can be written as arising from the following Hamiltonian

$$H = -\mathcal{J} \sum n_{ij} \boldsymbol{\psi}_i \cdot \boldsymbol{\psi}_j \tag{2.8}$$

and results in the term

$$F_i = -\frac{\partial H}{\partial \boldsymbol{\psi}_i} = \mathcal{J} \sum_j n_{ij} \boldsymbol{\psi}_j \tag{2.9}$$

in Eq. (2.5). In addition to alignment, $\boldsymbol{\zeta}_i$ is a noise term that encodes the presence of intrinsic errors in the ability of each individual to imitate the behaviour of neighbours. Note that this noise can be defined in many different ways, and depending on the precise form different phenomenologies may take place. In Eq (2.5) I wrote it as an additive noise, but other choices are possible. For what concerns here, let me assume this noise to be an additive random white noise with Gaussian statistics

$$\langle \zeta_i^\alpha(t) \zeta_j^\beta(t') \rangle_0 = \delta_{\alpha\beta} \delta_{ij} \delta \left(t - t' \right) . \tag{2.10}$$

The noise amplitude D_ψ in Eq. (2.5) plays the role of an effective temperature, a measure of *how much* individuals tend to make mistakes in their imitation.

Activity, which in this context is the ability to self-propel, is reflected by the presence of a fixed speed v_0 in (2.6). The velocity of each individual is therefore given by

$$\boldsymbol{v}_i = v_0 \boldsymbol{\psi}_i \tag{2.11}$$

The presence of activity causes the interaction matrix n_{ij} to not be fixed, but dependent on the specific configuration of the system at a given time. In the case of metric systems as swarms, where all individuals interact with a set of neighbours within a given distance r_0, this interaction matrix takes the form

$$n_{ij} = n\left(\boldsymbol{x}_i, \boldsymbol{x}_j\right) = \begin{cases} 1 & \text{if } |\boldsymbol{x}_i - \boldsymbol{x}_j| < r_0 \\ 0 & \text{else} \end{cases} \tag{2.12}$$

As a consequence, the effective energy H *is not* the Hamiltonian of the system, but should be viewed only as an objective function midges tend to minimise. Equations (2.5) and (2.6) therefore define what could be called a *moving ferromagnet*, in which $\boldsymbol{\psi}$ plays a double role: it is both the direction of motion of the single individual and the orientation to which neighbouring individuals tend to align.

2.1.4 The flocking phase

The Vicsek model displays two distinct phases as the temperature T and the density ρ changes [42]. The order parameter that rules this transition is the magnitude of the average direction of motion

$$\Psi = \frac{1}{N} \left| \sum_i \boldsymbol{\psi}_i \right| \tag{2.13}$$

At high temperatures or low densities, the system is in a disordered phase, where particles display a random motion. No emergent phenomena associated with the alignment interaction are detected: in this phase, the order parameter vanishes $\Psi \simeq 0$ meaning that the system displays no net group motion and the centre of mass remains stationary. This phase closely resembles the disordered high-temperature phase of ferromagnets.

On the other side, at low temperatures and high densities, a *flocking* phase emerges, characterised by the presence of net group motion on the macroscopic scale, associated with a non-vanishing order parameter $\Psi > 0$. Although the system has no *a priori* preferred direction of motion, in this phase all of the particles tend to move in the same direction. This mechanism whereby a given state of a system has fewer symmetries than the system itself, known as spontaneous symmetry breaking, is precisely what allows for ferromagnetism to arise. In analogy with the low-temperature phase of ferromagnetic systems, in this flocking phase, spin-wave-like excitations emerge, giving rise to interesting collective behaviours.

Long-range order in two dimensions

Despite the similarities with ferromagnets, the Vicsek model and ferromagnets exhibit many qualitative and quantitative differences. One of them is the presence of long-range order in two dimensions. As a consequence of the Mermin-Wagner-Hohenberg theorem [48, 49], a continuous symmetry can not be broken in equilibrium systems with short-range interactions at any finite temperature in dimensions $d \leq 2$. This prevents ferromagnetism in two dimensions and apparently suggests that no flocking phase should be possible in two dimensions either. However, numerical simulations have shown that this is incorrect, and Vicsek flocks can form even in $d = 2$ [42].

What makes this possible is the active nature of individuals in the Vicsek model, which poses the system out of equilibrium. This feature explicitly violates the hypothesis of the Mermin-Wagner-Hohenberg theorem, therefore solving the apparent contradiction. A naive argument to understand what is the physical mechanism that allows for long-range order in $d = 2$ is that the rewiring of the interaction network generates density fluctuations that couple to velocity fluctuations generating sound-wave propagation. This leads to a more efficient mechanism of information propagation, which is believed to stabilise the ordered phase of the Vicsek model in $d = 2$ [19, 20].

2.1.5 The swarming phase

Generally speaking, when two phases differ in their symmetries, a phase transition separating them is always expected, since it is not possible to *smoothly* go from one phase to the other. In the temperature-density plane, this phase transition occurs at a critical line $T_c(\rho)$, at which the symmetry spontaneously breaks.

In ferromagnetic systems, the behaviour near this transition is characterised by non-analyticity of the free energy, which in turn gives rise to the divergence of many thermodynamic quantities [50, 51]. Moreover, a set of scaling laws was shown to arise, linking all these divergences to the divergence of the correlation length. When this happens, non-trivial collective behaviours take place, as the system becomes strongly correlated and the response to external perturbations becomes extremely efficient. Note the difference between this near-ordering phase and the flocking phase: here the order parameter is still small since no symmetry is explicitly broken. Because of the analogy between this phase and natural swarms, characterised by small average polarisation and scaling laws, I will refer to this critical near-ordering phase as the swarming phase.

When scaling laws are observed and the order parameter continuously changes across the transition, a phase transition is called *second-order* or *continuous*. This is the case of transitions in ferromagnetic systems in the absence of an external magnetic field. On the other hand, if the order parameter experiences a *jump* as in the liquid-gas transition, this is referred to as *first-order* or *discontinuous* phase transition. Note that in the case of first-order phase transition, scaling laws are not expected to arise. On the other hand, when the transition is second-order the presence of scaling laws means that large-scale collective behaviours are taking place.

First-order ordering phase transition

The most relevant difference between the Vicsek model and the Heisenberg ferromagnet is the order of the phase transition. Heisenberg ferromagnets undergo a second-order continuous phase transition, while a system obeying equations (2.5)-(2.6) exhibits a first-order phase transition [44, 36]. The nature of the first-order transition is strongly related to the presence of density-velocity coupling. Near the phase transition, large density fluctuations arise. These density fluctuations couple to the velocity, generating a phase separation, typical of first-order transitions such as the liquid-gas transition. It has been observed that when the critical temperature is approached band structures arise, within which order is generated despite Ψ

remaining very close to 0. However, it has been shown that above the ordering transition, in the near-ordering swarming phase where density heterogeneities are less prone to develop, a constant density constraint gives results that apply also to the compressible case [69]. Because the incompressible model does not develop phase separation and thus undergoes a continuous phase transition, in the present work an incompressible constraint will be enforced to work in a near-critical phase. In Chapter 6 I will, however, address the question of what happens when weak density fluctuations are taken into account, and show that incompressible theories well-describe the behaviour of spatially homogeneous finite-size systems as swarms. It has to be stressed the fact that the main interest of the present work is on the near-ordering phase, and not on the phase transition itself. Therefore, a situation in which the correlation between velocity fluctuations is *large* but density fluctuations are very weak will be the ideal scenario in which to expect to find collective behaviour typical of swarms.

2.2   A general model for active particles

The Vicsek model introduced in the previous section represents the archetype of collective behaviour models in active living systems. However, its description completely neglects the potential collisions between the individuals and the particles that constitute the surrounding medium. A more complete and general description should therefore take into account both the ability to generate an *active* force ensuring self-propulsion and the presence of the effect of random collisions with the medium.

In this case, the two forces act on the system: one is the active force, which can be taken to a force with fixed magnitude f_0 in the direction of self-propulsion $\boldsymbol{\psi}$. The second is a damping force, which can be written as the sum of a drag term $-\gamma\boldsymbol{v}$ and a random Gaussian white noise with variance $\sqrt{2\tilde{D}}$. The dynamics of this system is thus given by

$$\dot{\boldsymbol{r}}_i = \boldsymbol{v}_i$$
$$m\dot{\boldsymbol{v}}_i = -\gamma\boldsymbol{v}_i + f_0\boldsymbol{\psi}_i + \sqrt{2\tilde{D}}\boldsymbol{\xi}_i$$
$$\dot{\boldsymbol{\psi}}_i = \mathcal{R}\left[\mathcal{J}\sum_j n_{ij}\boldsymbol{\psi}_j + \sqrt{2D_\psi}\boldsymbol{\zeta}_i\right]$$

(2.14)

Here $\boldsymbol{v}$ is the velocity of the individual and m its mass, while $\boldsymbol{\psi}$ is a unitary vector that points in the desired direction of motion of the particle i and undergoes the alignment dynamics as in the Vicsek model (2.5).

When the time-scale $m\gamma^{-1}$ on which the velocity relaxes is fast compared to that of ψ, one can approximate $\dot{\boldsymbol{v}}_i \approx 0$, and hence use

$$\boldsymbol{v}_i = v_0\boldsymbol{\psi}_i + \sqrt{2\gamma^{-2}\tilde{D}}\boldsymbol{\xi}_i\,,$$

(2.15)

where $v_0 = f_0/\gamma$ is the average self-propulsion speed. In this regime, the equations

of motion thus become

$$\dot{\boldsymbol{r}}_i = v_0 \boldsymbol{\psi}_i + \sqrt{2D_r}\, \boldsymbol{\xi}_I$$

$$\dot{\boldsymbol{\psi}}_i = \mathcal{R}\left[\mathcal{J}\sum_j n_{ij}\boldsymbol{\psi}_j + \sqrt{2D_\psi}\boldsymbol{\zeta}_i\right] \tag{2.16}$$

Where $D_r = \gamma^{-2}\tilde{D}$. When $D_r \to 0$, the Vicsek behaviour is recovered, with $\boldsymbol{\psi}$ coinciding with the direction of motion and the velocity being $\boldsymbol{v} = v_0\boldsymbol{\psi}$. If $D_r \neq 0$, the vector $\boldsymbol{\psi}$ is not the direction of motion anymore, since the velocity has also a stochastic component. However, because $\langle \boldsymbol{\xi} \rangle = 0$, it is still true that the average value of $\boldsymbol{\psi}$ is the average direction of motion. This holds whenever $v_0 \neq 0$. If instead $v_0 \to 0$, the spatial motion is decoupled from the behaviour of $\boldsymbol{\psi}$. One therefore recovers a model where diffusive agents align an *internal* degree of freedom $\boldsymbol{\psi}$, which is not linked to motion in any way. Nevertheless, note that in both cases, however, the adjacency matrix n_{ij} is not constant, potentially violating thermal equilibrium anyway.

2.2.1 Active Ising Models of flocking

Among the models that fall into this class, it is worth mentioning the case of Active Ising Models (AIMs) of flocking [70], [MyPaper4]. Contrary to the Vicsek model, where the system has a continuous rotational symmetry, AIMs are characterised by having a discrete symmetry, as individuals perform directed motion along a preferred direction in space. In AIMs, particles can be considered as *active spins*, which undergo diffusion in all directions but one, in which the value of the spin determines the preferred direction of motion. Spins of different particles undergo an alignment process with neighbouring particles, in a similar fashion with Ising-like dynamics - hence the name Active Ising Models.

Although AIMs have been originally introduced in an on-lattice formulation, numerical evidence is that their behaviour is equivalent to an off-lattice definition [71], where particles' position is updated according to:

$$\dot{\boldsymbol{r}}_i = v_0 s_i \hat{x} + \sqrt{2D_r}\, \boldsymbol{\zeta} \tag{2.17}$$

Here s_i is a spin-like variable, which can take ± 1 value, which undergoes an aligning process with neighbouring spins. This equation is quite similar to Eq. (2.16), with the main difference that $\boldsymbol{\psi} = s\hat{x}$ has a discrete symmetry rather than a continuous one.

Although in the active case, $v_0 \neq 0$, the presence of diffusion is not expected to affect the large-scale behaviour of the model, for weak activity $v_0 \to 0$ the presence of diffusion allows to keep the model out of equilibrium, as the adjacency matrix n_{ij} would still be time-dependent. From the theoretical point of view, this opens the question of whether the behaviour of systems with $v_0 = 0$ is affected by the presence of diffusion. To make progress in this direction, in Chapter 12 I will derive a field-theoretical approach to Active Ising Models.

Chapter 3

Hydrodynamic approach to self-propelled systems: the Toner and Tu theory

Numerical investigation of models like the Vicsek model, introduced in the previous Chapter, certainly represents one of the standard ways in which the collective behaviour of active systems can be investigated and characterised. However, dealing with finite-size effects and boundary conditions is often a nightmare in the context of numerical simulations. Establishing unambiguously what phenomena are associated with bulk behaviours and what with boundary effects becomes therefore a hard task. To circumvent these difficulties, coarse-grained approaches typically provide more solid and reliable tools to characterise bulk large-scale behaviours. I do not want to claim that coarse-grained approaches are better than simulations, but they provide a powerful complementary framework where some of the large-scale features can be better understood.

In the present Chapter, I will review the hydrodynamic theory of Toner and Tu. This *hydrodynamic theory of flocks* was introduced by J. Toner and Y. Tu in their seminal paper [19], to prove the stability of the flocking state observed numerically by Vicsek et. al. [42] in two spatial dimensions, in apparent violation of the Mermin-Wagner-Hohenberg theorem [48, 49]. The theory was developed to account for the large-scale behaviour of Vicsek-like models, combining the Navier-Stokes description of the velocity field in a fluid with a dynamical XY model, namely Model A in Halperin and Hohenberg classification [40], to account for velocity-velocity alignment interactions. The resulting theory, morally representing a coarse-grained description of the Vicsek model introduced in the previous Chapter, is expected to describe the collective behaviours of a wider class of systems, namely any collection of *self-propelled* agents with rotational and translational invariance.

Compared to Model A, in the Toner and Tu theory the consumption of energy at the microscopic scale, i.e. activity, allows each individual to self-propel. This *promotes* the order parameter from being a simple pointer in space - as in Model A dynamics - to be the direction of motion of individuals. As I will review in this Chapter, this has a huge impact on the large-scale behaviour of the system, leading to surprisingly new emergent behaviours. Particular attention will be dedicated

to what happens in the near-ordering phase, which is believed to describe natural swarms of insects.

3.1 The hydrodynamic approach: Navier-Stokes equations

To properly describe the collective modes of a system, a full description of the behaviour over all the physical scales is usually not necessary. This is because the collective modes represent the fluctuations around the steady-state occurring on *collective*, i.e. large, spatial and temporal scales. On such large scales, it is often more convenient to focus on a coarse-grained description of the system, in which the precise details of the microscopic interactions are averaged out. In these coarse-grained descriptions, only a few of the many degrees of freedom experience significant fluctuations and therefore contribute to the determination of the collective behaviours. Putting it in another way, the behaviour of the collective modes is expected to be universal, and not depend on the details of the system.

The relevant coarse-grained degrees of freedom are usually referred to as *hydro-dynamic modes*, or *slow modes*, as their characteristic frequency vanishes as the wave vector does. Interactions between slow and fast modes are encoded by two elements in the coarse-grained description. The first is the presence of effective phenomenological couplings, which cannot be computed within the coarse-grained approach, but in principle require the knowledge of the microscopic details, namely the dynamics of the fast modes, to be computed. Secondly, fluctuations of the fast modes might induce some slight change in the behaviour of slow modes. However, because these fluctuations relax on time scales much faster compared to the hydrodynamic modes, from the point of view of the latter the former behaves as a random white noise.

3.1.1 Coarse-grained degrees of freedom

In a coarse-grained description of the system, the large-scale degrees of freedom are usually represented by local averages of the microscopic ones. In particular, the systems of interest (as in the Vicsek model) are made of particles with a given position $\boldsymbol{x}_i$ and some additional degree of freedom, e.g. the velocity $\boldsymbol{v}_i$. By calling $\boldsymbol{\phi}_i$ the set of all degrees of freedom of the i-th particle, the coarse-grained variable associated with some local observable q_α can be written in the form

$$Q_\alpha(\boldsymbol{x}) = \frac{1}{V_{\partial x}} \sum_{j \in \partial \boldsymbol{x}} q_\alpha(\{\boldsymbol{\phi}_j\}).$$ (3.1)

where the sum runs over all the particles in a neighbourhood $\partial \boldsymbol{x}$ of $\boldsymbol{x}$. The volume of this neighbourhood, $V_{\partial \boldsymbol{x}}$, is taken to be proportional to h^d, with h being a coarse-graining scale and d being the spatial dimensionality. The precise form of this neighbourhood is not relevant, and it can be imagined to be a ball centred in $\boldsymbol{x}$. What is important is that h must be quite larger than the characteristic inter-particle distance a, say the interaction range. When this happens, $Q(\boldsymbol{x})$ is obtained by averaging over many particles and hence is expected to approach a smooth function of the spatial variable $\boldsymbol{x}$. Furthermore, h should also be much

smaller than the size of the system L, in such a way that $Q(\boldsymbol{x})$ describes fluctuations that are *local* in space. Substituting particle-based descriptions with continuous fields is a standard process in deriving hydrodynamic equations: the Navier-Stokes equations for example completely neglect the discrete microscopic nature of fluids and yet provide an excellent description of them [43].

Since these coarse-grained observables $Q(\boldsymbol{x})$ are obtained by averaging over volumes $V \sim h^d$, the coarse-grained theory has a spatial resolution of h. Variations of Q over length scales smaller than h have no physical meaning. The coarse-grained scale h can be usually assumed to be a multiple of the characteristic *microscopic* scale a, say the length of the individuals, hence $h \propto a$. As a consequence, in Fourier representation, the field Q does not take any contributions from wave-vectors

$$|\boldsymbol{k}| > \Lambda \sim \frac{1}{a}\,, \tag{3.2}$$

setting a natural cutoff in momentum space, where modes of higher wave vector do not enter the effective description, namely have already been coarse-grained. This requirement can be explicitly enforced on the real-space field Q by stating that

$$Q\left(\boldsymbol{x}\right) = \int\limits_{|\boldsymbol{k}|<\Lambda} \frac{\mathrm{d}^d k}{\left(2\pi\right)^d}\, Q\left(\boldsymbol{k}\right) \mathrm{e}^{\mathrm{i}\boldsymbol{x}\cdot\boldsymbol{k}} \tag{3.3}$$

Indeed, one might construct as many coarse-grained variables as one wants. However, only a few coarse-grained variables represent the hydrodynamic variables of the system. As previously discussed, these variables are characterised by the fact that they fluctuate on large spatiotemporal scales. This, in turn, means that hydrodynamic variables should vary slowly in both space and time and hence their spatial and temporal derivatives are small. This legitimates a gradient expansion in writing the coarse-grained equations for these variables.

Coarse-grained variables for Vicsek-like models

In the case of current interest, namely for Vicsek-like systems, the microscopic degrees of freedom for each particle are given by their position $\boldsymbol{x}_i$ and its velocity $\boldsymbol{v}_i$. The natural coarse-grained quantities associated with these two microscopic degrees of freedom are the density field and the velocity field, defined as

$$\rho(\boldsymbol{x}) = \frac{1}{V_{\partial x}} \sum_{j \in \partial x} 1\,, \tag{3.4}$$

$$\boldsymbol{v}(\boldsymbol{x}) = \frac{1}{\rho(\boldsymbol{x}) V_{\partial x}} \sum_{j \in \partial x} \boldsymbol{v}_j \tag{3.5}$$

In this definition, ρ is the average number of particles in a *small* volume around $\boldsymbol{x}$, while $\boldsymbol{v}$ is the average velocity of a particle in the same volume. These are the only two degrees of freedom I will assume to be relevant on the hydrodynamic scale. Conservation of the number of particles automatically makes the density ρ a hydrodynamic variable, as ρ must satisfy a continuity equation of the form

$$\partial_t \rho = -\nabla \cdot \boldsymbol{J}\,, \tag{3.6}$$

where the current $\boldsymbol{J}$ is given by $\boldsymbol{J} = \rho\boldsymbol{v}$. When decomposed in Fourier modes, the large wave-length fluctuations relax on long time scales, as a consequence of the presence of the ∇ on the r.h.s. of the continuity equation. In fact, in Fourier space the continuity equation reads $\partial_t \rho(\boldsymbol{k}, t) = -\mathrm{i}\boldsymbol{k} \cdot J(\boldsymbol{k})$, from which one can clearly see that $\partial_t \rho(\boldsymbol{k}) \to 0$ when $\boldsymbol{k} \to 0$, making ρ an hydrodynamic variable. The velocity field $\boldsymbol{v}$ is instead not always a hydrodynamic variable, as in some regimes it might relax on finite time-scales [72]. However, both in the ordered flocking phase and the near-ordering swarming phase, the velocity field *is* a hydrodynamic variable. In the former case, this is because the continuous rotational symmetry of $\boldsymbol{v}$ is spontaneously broken, and hence $\boldsymbol{v}$ develops $d-1$ Goldstone modes. In the swarming phase instead, the proximity to a second order phase transition with $|\langle\boldsymbol{v}\rangle|$ as an order parameter makes fluctuations of $\boldsymbol{v}$ to become slow modes too.

On the other hand, in some active matter systems, other quantities might be relevant at the hydrodynamic scale. A typical example is the nematic tensor for non-polar particles [73], e.g. rod-shaped bacteria. In this case, motion is performed along a preferred axis $\hat{\boldsymbol{n}}$ without a preferred direction along the axis. As a consequence, the local expected velocity vanishes, and the large-scale description of the system is made in terms of a coarse-grained nematic tensor

$$\boldsymbol{\mathcal{Q}}(\boldsymbol{x}) = \frac{1}{\rho(\boldsymbol{x})V_{\partial x}} \sum_{j\in\partial x} \left(\hat{\boldsymbol{n}}_j \otimes \hat{\boldsymbol{n}}_j - \frac{1}{d}\mathbb{I} \right) \tag{3.7}$$

Where $\mathbb{I}$ is the $d \times d$ identity matrix. This higher-order tensor is however expected to be a fast mode in the case of polar systems I will be interested in, and can be therefore dropped from the hydrodynamic description.

3.1.2 Coarse-grained active matter as a fluid

From the coarse-grained perspective introduced in the previous sections, hydrodynamic properties of polar active matter are well described by the behaviour of the density ρ and velocity $\boldsymbol{v}$ fields. The idea behind the Toner and Tu theory was to provide a hydrodynamic description of systems with rotational and translational invariance for which the hydrodynamic variables, whose relaxation time-scale vanishes at large wavelengths, are the velocity field $\boldsymbol{v}(\boldsymbol{x}, t)$ and the density field $\rho(\boldsymbol{x}, t)$.

In the context of fluid dynamics, the hydrodynamic behaviour of the velocity field $\boldsymbol{v}$ and the density field ρ is well-captured by the Navier-Stokes equations [43]. Active matter is indeed different from passive fluids. However, on scales much larger than their characteristic microscopic scales they both have similar coarse-grained descriptions: active matter on coarse-grained scales can be modelled as a fluid with the presence of an additional *active force*.

The dynamics of such a *polar active fluid* is thus expected to be ruled by some kind of generalisation of the Navier-Stokes equations [43]. In its most general form, the dynamics of the velocity in a fluid can be written as

$$\rho\partial_t v_\alpha + \rho\left(\boldsymbol{v} \cdot \nabla\right)v_\alpha = \partial_\gamma \sigma_{\alpha\gamma} + f_\alpha. \tag{3.8}$$

Here $\boldsymbol{\sigma}$ is the stress tensor while $\boldsymbol{f}$ are the volume forces. Because in the microscopic model, particles move in space, the local density ρ is not fixed. If the total number

of particles is conserved, ρ admits hydrodynamic fluctuations around its mean value ρ_0. The equation associated with this conservation law is the continuity equation for the density, which reads

$$\partial_t \rho + \nabla \cdot (\rho \, \boldsymbol{v}) = 0 \,. \tag{3.9}$$

Navier-Stokes equations for passive fluids are then derived by the additional requirements that *(i)* the momentum field $\boldsymbol{p} = \rho \boldsymbol{v}$ is globally conserved, namely $\partial_t P(t) = \partial_t \int \mathrm{d}^d x \boldsymbol{p}(\boldsymbol{x}, t) = 0$, and *(ii)* that the physical description is the same in all inertial reference frames, that is the equations are invariant under Galilean transformations. These requirements further limit the structure of the stress-tensor $\boldsymbol{\sigma}$ and the volume forces $\boldsymbol{f}$. It is however important to note that none of these two properties apply to polar active fluids, since they move in a frictional medium that acts as a momentum sink and serves as a preferred reference frame.

On Galilean invariance

So far, I have discussed the most general description possible of the behaviour of a fluid. In passive fluids, in addition to rotational and translational symmetries, and the conservation of the total density, a third symmetry is at play: Galilean invariance. A system obeys Galilean invariance if its physics is invariant when observed in two inertial reference frames, namely in two reference frames moving at fixed velocity one with respect to the other. The laws of physics, as the equations of motion, must therefore be invariant under the Galilean transformation

$$\boldsymbol{x}' = \boldsymbol{x} - \overline{\boldsymbol{v}} t \qquad\qquad t' = t \qquad\qquad \boldsymbol{v}'(\boldsymbol{x}', t') = \boldsymbol{v}(\boldsymbol{x}, t) - \overline{\boldsymbol{v}} \tag{3.10}$$

Where $\overline{\boldsymbol{v}}$ is the relative velocity of the two reference frames, $\boldsymbol{v}, \boldsymbol{x}, t$ are respectively velocity, position and time measured in the first reference frame. At the same time, prime quantities indicate they are measured in the second reference frame.

Interestingly, an operator which is invariant under a Galilean transformation is the material derivative

$$\mathcal{D}_t = \partial_t + \boldsymbol{v}(\boldsymbol{x}, t) \cdot \nabla \tag{3.11}$$

To show this operator is a Galilean invariant, let me apply it to a test function $f(\boldsymbol{x}, t)$ - not to be confused with the volume force:

$$\mathcal{D}_t f(\boldsymbol{x}, t) = [\partial_t + (\boldsymbol{v} \cdot \nabla)] \, f(\boldsymbol{x}, t) \tag{3.12}$$

Let me now perform the change of coordinates, by using $\boldsymbol{x}' = \boldsymbol{x} - \overline{\boldsymbol{v}} t$ and $\boldsymbol{v}' = \boldsymbol{v} - \overline{\boldsymbol{v}}$ - note that $t' = t$. To simplify the reading, I lighted the notation by implicitly assuming $\boldsymbol{v} = \boldsymbol{v}(\boldsymbol{x}, t)$ and $\boldsymbol{v}' = \boldsymbol{v}'(\boldsymbol{x}', t)$. Assuming that under a Galilean transformation the quantity f transforms as $f'(\boldsymbol{x}', t) = f(\boldsymbol{x}, t)$ - note that $t' = t$ - the temporal partial derivative can be written as follows:

$$\partial_t f(\boldsymbol{x}, t) = \frac{\mathrm{d}}{\mathrm{d}t} f'(\boldsymbol{x}'(\boldsymbol{x}, t), t) = \partial_t f'(\boldsymbol{x}', t) + (\partial_t \boldsymbol{x}'(\boldsymbol{x}, t)) \cdot \nabla' f'(\boldsymbol{x}', t) =$$
$$= \partial_t f'(\boldsymbol{x}', t) - \overline{\boldsymbol{v}} \cdot \nabla' f'(\boldsymbol{x}', t) \tag{3.13}$$

Where in the last equality I used the fact that $\partial_t \boldsymbol{x}'(\boldsymbol{x}, t) = -\overline{\boldsymbol{v}}$. The advective term $\boldsymbol{v} \cdot \nabla$ transforms instead in the following way

$$\boldsymbol{v} \cdot \nabla f(\boldsymbol{x}, t) = (\boldsymbol{v}' + \overline{\boldsymbol{v}}) \cdot \nabla' f'(\boldsymbol{x}', t) = \boldsymbol{v}' \cdot \nabla' f'(\boldsymbol{x}', t) + \overline{\boldsymbol{v}} \cdot \nabla' f'(\boldsymbol{x}', t) \qquad (3.14)$$

While the two operators, namely partial temporal derivative and advective term, are not independently invariant, their sum is, as

$$
\begin{aligned}
\mathcal{D}_t f(\boldsymbol{x}, t) =& \partial_t f(\boldsymbol{x}, t) + \boldsymbol{v} \cdot \nabla f(\boldsymbol{x}, t) = \\
=& \partial_t f'(\boldsymbol{x}', t) - \overline{\boldsymbol{v}} \cdot \nabla' f'(\boldsymbol{x}', t) + \boldsymbol{v}' \cdot \nabla' f'(\boldsymbol{x}', t) + \overline{\boldsymbol{v}} \cdot \nabla' f'(\boldsymbol{x}', t) = \quad (3.15) \\
=& \partial_t f'(\boldsymbol{x}', t) + \boldsymbol{v}' \cdot \nabla' f'(\boldsymbol{x}', t) = \mathcal{D}'_t f'(\boldsymbol{x}', t)
\end{aligned}
$$

Therefore, for a fluid to be Galilean-invariant the only requirement is that all terms contained in $\boldsymbol{f}$ and $\boldsymbol{\sigma}$ are themselves Galilean-invariant. At the lowest order in a gradient expansion, the Galilean-invariant terms contributing to $\boldsymbol{\sigma}$ are:

$$\boldsymbol{\sigma} = \Gamma_1 \partial_\alpha v_\beta + \Gamma_2 \partial_\beta v_\alpha + \Gamma_3 \delta_{\alpha\beta}(\partial_\gamma v_\gamma) + \delta_{\alpha\beta} \mathcal{P}(\rho) \qquad (3.16)$$

Here Γ_i are three coefficients, which contribute to bulk and shear viscosity, while $\mathcal{P}(\rho)$ is the pressure. On the other hand, the volume forces $\boldsymbol{f}$ might depend on the interactions with external objects, as the gravitational force, in which case $\boldsymbol{f} = -\rho \boldsymbol{g}$. What is important is that in the presence of Galilean invariance, $\boldsymbol{f}$ does not depend directly on the local velocity, as it would not be invariant under a change of reference frame.

3.2   Alignment interactions: Model A

Simple models of active fluids, such as the Vicsek and Toner and Tu models, and experimental systems confined to a substrate, are not Galilean invariant. In fact, in systems like the Vicsek model (introduced in the previous Chapter), the speed of each individual is fixed to be v_0 in a particular frame of reference, namely that of the substrate on which individuals are moving. The presence of a privileged reference frame violates Galilean invariance, thus allowing a more complex structure of the equations of motion compared to the standard Navier-Stokes equations.

To understand how the simplest introduction of activity violates Galilean invariance, let me focus on *how* to incorporate in the fluid-dynamics description the presence of a fixed speed v_0 at the microscopic level. As strange as it may sound, to understand how to incorporate this *active* force, I will get inspiration from the equilibrium counterpart of the Vicsek model, namely the relaxation dynamics of ferromagnetic Heisenberg model, obtained by sending $v_0 \to 0$. This is because, at the microscopic level, the effect of the active force is keeping the magnitude of $\boldsymbol{\psi}$ - and in turn the magnitude of the velocity, namely the speed - fixed. In a similar fashion, also in equilibrium ferromagnetic models the magnitude of the local "spin" $\boldsymbol{\psi}$ is fixed (its dynamic behaviour being described by Eq. (2.5)). Although in this case the force is not active, as the positions are fixed on a lattice, its effect is precisely what we need here: keeping the magnitude of the degree of freedom fixed.

3.2.1 The equilibrium limit

The Heisenberg model describes the behaviour of classical "spins", with fixed magnitude $|\boldsymbol{\psi}| = 1$, that align to the total magnetic field induced by neighbours. The dynamic behaviour of the Heisenberg model can be obtained by taking the $v_0 \to 0$ limit of the Vicsek model. This is not a surprise, as the Vicsek model was built to be an *off-equilibrium* version of the ferromagnetic models. In this limit $v_0 \to 0$, particles are fixed on a lattice and $\boldsymbol{\psi}$, which for $v_0 \neq 0$ used to represent the direction of motion, becomes a unity vector unrelated to the *external* position space. Its dynamic behaviour can be written by taking $v_0 \to 0$ in Eq (2.5), and reads

$$\frac{\mathrm{d}\boldsymbol{\psi}_i}{\mathrm{d}t} = \mathcal{R}\left[-\frac{\partial H}{\partial \boldsymbol{\psi}_i} + \boldsymbol{\zeta}_i\right], \qquad (3.17)$$

where the operator $\mathcal{R}$, defined in (2.7), projects its argument on the direction orthogonal to $\boldsymbol{\psi}_i$. The present dynamics approaches a steady-state in which the *static* features are well captured by the Gibbs-Boltzmann distribution $P \sim e^{-\beta H}$, with H being the Hamiltonian of the Heisenberg ferromagnet, namely

$$H = -\sum_{ij} n_{ij} \boldsymbol{\psi}_i \cdot \boldsymbol{\psi}_j. \qquad (3.18)$$

Here the adjacency matrix n_{ij} is fixed in time since for $v_0 \to 0$ positions are fixed on a network. This Hamiltonian was introduced to explain the ferromagnetic phase transition, characterised by a $O(n)$ rotational symmetry in the *internal* space of $\boldsymbol{\psi}$.

The large-scale description of this system can be given in terms of the coarse-grained field

$$\boldsymbol{\psi}(\boldsymbol{x}) = \frac{1}{N_{\partial x}} \sum_{j \in \partial x} \boldsymbol{\psi}_j, \qquad (3.19)$$

where $N_{\partial x}$ is the number of particles in the neighbourhood ∂x of $\boldsymbol{x}$. Note that, because positions are not updated for $v_0 \to 0$, the density field ρ is not even a fluctuating quantity, as it is fixed once and for all. In this coarse-grained description, the Hamiltonian H is replaced by an effective free energy $\mathcal{H}$, obtained by averaging over the degrees of freedom that have been integrated into the coarse-graining procedure. Performing this explicit calculation is usually quite long and tedious: for this reason, it is often easier to follow general principles, such as symmetries, to write down the effective free energy. The drawback of this procedure is not having an explicit connection between the parameters of the new effective free energy and the original microscopic model. However, this generality allows capturing the behaviour of several different models, irrespective of their precise microscopic formulation, as long as they share the same symmetries of the coarse-grained free energy. For systems with rotational symmetry, as the Heisenberg model, a quite general form for $\mathcal{H}$ is given by

$$\mathcal{H} = \int \mathrm{d}^d x \frac{1}{2} (\partial_\alpha \psi_\beta)(\partial_\alpha \psi_\beta) + V(\boldsymbol{\psi}). \qquad (3.20)$$

Here the $(\nabla \psi)^2$ term stems from local alignment since it suppresses fluctuations of $\boldsymbol{\psi}$ and favours uniform configurations. The potential $V(\boldsymbol{\psi})$, on the other hand, takes contributions both from the aligning interactions, which favours highly polarised

configurations with $|\boldsymbol{\psi}| \sim 1$, and from entropic effects, which favours configurations with higher number of associated micro-states, namely disordered configurations with $|\boldsymbol{\psi}| \sim 0$. Because of the rotational symmetry, V is expected to depend only on the absolute value of $\boldsymbol{\psi}$.

The simplest form of $V(\boldsymbol{\psi})$ arising from the above picture, which also turns out to capture the phase diagram of the Heisenberg model, is

$$V(\boldsymbol{\psi}) = \int \mathrm{d}^d x \frac{r}{2} \boldsymbol{\psi} \cdot \boldsymbol{\psi} + \frac{u}{4} (\boldsymbol{\psi} \cdot \boldsymbol{\psi})^2 \,, \tag{3.21}$$

where $u > 0$ ensures the magnitude of the average polarisation, $|\langle\boldsymbol{\psi}\rangle|$, to be bounded. The aforementioned *competition* between alignment and entropy is expected to allow r to take both positive and negative values. As r changes sign, a mean-field analysis predicts a transition between two phases (or ground states):

- a disordered phase for $r > 0$, where the average polarisation is $|\langle\boldsymbol{\psi}\rangle| = 0$;

- an ordered phase for $r < 0$, where the average polarisation is $|\langle\boldsymbol{\psi}\rangle| = \sqrt{-r/u}$.

This confirms the phenomenology observed in the Heisenberg model, where for high temperatures, namely high noise amplitudes, entropic effects dominate and $|\boldsymbol{\psi}| = 0$ configurations are favoured, while for low temperatures, namely low noise, alignment wins and $|\boldsymbol{\psi}| \sim 1$.

From a coarse-grained perspective, the dynamics of the Heisenberg ferromagnet is described by the relaxation dynamics

$$\partial_t \psi_\alpha = -\Gamma \frac{\delta \mathcal{H}}{\delta \psi_\alpha} + \sqrt{2\Gamma}\, \theta_\alpha \,, \tag{3.22}$$

where Γ is a kinetic coefficient, while $\boldsymbol{\theta}$ is a random Gaussian noise with unitary variance. Note that detailed balance conditions force the noise amplitude to be equal to the kinetic coefficient in this coarse-grained model. This dynamic behaviour is known as Model A in Halperin and Hohenberg classification [40]. As for its *microscopic* discrete counterpart, in Model A, the effective free energy $\mathcal{H}$ defines the steady-state probability distribution $P \sim e^{-\mathcal{H}}$. By explicitly using the form of $\mathcal{H}$ given in (3.20), the equation of motion of Model A can be written as

$$\partial_t \psi_\alpha = \Gamma \nabla^2 \psi_\alpha - \Gamma \frac{\delta V}{\delta \psi_\alpha} + \sqrt{2\Gamma}\, \theta_\alpha \,. \tag{3.23}$$

The zeros of $\delta V / \delta \boldsymbol{\psi}$ set the steady-state, while the $\nabla^2 \boldsymbol{\psi}$ term suppresses fluctuations around the steady-state, hence favouring local alignment. As in the Heisenberg Model, also in the Vicsek model the direction of motion $\boldsymbol{\psi}$ has a fixed magnitude at the microscopic level, which in turn allows to maintain a fixed microscopic speed v_0. The fixed magnitude of the *microscopic* velocity, which is what in the context of the Vicsek model represents activity, requires the presence of a bulk force in the equation for the coarse-grained velocity field analogue to the $-\Gamma \delta V / \delta \boldsymbol{\psi}$ term in Model A.

3.3 Self-Propelled Model A

The presence of alignment interaction on its own is not sufficient to explain the dynamic collective behaviours observed in natural swarms of insects. As I mentioned previously, the dynamic critical exponents for theories of relaxation dynamics with alignment interactions is $z \approx 2$, far from the experimental value of $z = 1.35$ [MyPaper1]. Besides alignment interactions, *activity* is a hallmark of biological systems as swarms.

To take activity into account in the coarse-grained description, I will follow the idea of Toner and Tu, who combined the Navier-Stokes equations with Model A dynamics to develop a hydrodynamic theory inspired by the Vicsek model [19]. I shall therefore refer to this theory, commonly known as the Toner and Tu theory, as Self-Propelled Model A. The reason for this is that, further on, I will build an active theory which has Model G, rather than Model A, as its equilibrium counterpart. Since I will call that theory Self-Propelled Model G, I use here Self-Propelled Model A to refer to the Toner and Tu theory.

This theory of Self-Propelled Model A (SPMA) describes *moving* ferromagnets, namely systems where individuals are self-propelled and align their direction of motion, as in the Vicsek model. To keep the connection with Model A, which must be recovered as the speed $v_0 \to 0$, I will describe the behaviour of the coarse-grained direction of motion $\boldsymbol{\psi}$ rather than the velocity $\boldsymbol{v}$. Since the Vicsek model, at the particle level, has $\boldsymbol{v}_i = v_0 \boldsymbol{\psi}_i$, the coarse-grained velocity field introduced in Eq. (3.5) can be expressed as

$$\boldsymbol{v}(\boldsymbol{x}) = \frac{1}{\rho(\boldsymbol{x}) V_{\partial x}} \sum_{j \in \partial x} v_0 \boldsymbol{\psi}_j = v_0 \boldsymbol{\psi}(\boldsymbol{x})$$

$$\boldsymbol{\psi}(\boldsymbol{x}) = \frac{1}{\rho(\boldsymbol{x}) V_{\partial x}} \sum_{j \in \partial x} \boldsymbol{\psi}_j \tag{3.24}$$

Let me note, once again, that while at the microscopic level $\boldsymbol{\psi}_j$ is a unitary vector, at the coarse-grained level this is not true anymore.

3.3.1 Minimal active theory

The conservation of $\left|\boldsymbol{\psi}_j\right| = 1$ in time, crucial to keeping the microscopic speed fixed to v_0, was explicitly enforced in the Vicsek dynamics of $\boldsymbol{\psi}_j$, Eq. (2.5). As I showed in the previous section, in the equilibrium limit $v_0 \to 0$ the requirement of $\left|\boldsymbol{\psi}_j\right| = 1$ at the microscopic level can be softened when coarse-graining, as long as a dynamic *force*

$$\partial_t \boldsymbol{\psi} \sim -\Gamma \frac{\delta V}{\delta \boldsymbol{\psi}} + \sqrt{2\tilde{\Gamma}}\, \theta_\alpha \tag{3.25}$$

is appropriately introduced in the coarse-grained dynamic equation of $\boldsymbol{\psi}$. Here V is a potential which can be taken of the form

$$V(\boldsymbol{\psi}) = \int \mathrm{d}^d x \frac{r}{2} \boldsymbol{\psi} \cdot \boldsymbol{\psi} + \frac{u}{4} (\boldsymbol{\psi} \cdot \boldsymbol{\psi})^2 \tag{3.26}$$

Now, since the system is active and thus far from thermal equilibrium, the coefficients Γ and $\tilde{\Gamma}$ need not be equal as in (3.22) as detailed balance is not expected to hold.

A minimal set of equations of motion can be thus derived by adding an *active force* like (3.25) to the Navier-Stokes equations. This leads to the theory proposed by Toner and Tu in their first paper of 1995 [19], namely

$$\partial_t \psi_\alpha + v_0 \left(\boldsymbol{\psi} \cdot \nabla \right) \psi_\alpha = \Gamma \nabla^2 \psi_\alpha + \Gamma_2 \partial_\alpha \left(\nabla \cdot \boldsymbol{\psi} \right) - \Gamma \frac{\delta V}{\delta \psi_\alpha} - \nabla \mathcal{P} + \sqrt{2\tilde{\Gamma}} \, \theta_\alpha \, ,$$

$$\partial_t \rho + v_0 \nabla \cdot \left(\rho \, \boldsymbol{\psi} \right) = 0 \, . \tag{3.27}$$

Here I took as stress-tensor of the same form of viscous Navier-Stokes equations [43], where $\mathcal{P}$ is a pressure force that depends on ρ, while the two Γ viscous terms can be interpreted, within the Toner and Tu theory, as aligning terms. The effect of viscosity is precisely that of suppressing strong fluctuations in the velocity field, in a similar fashion with alignment interactions.

Note that these equations can be also obtained by *promoting* the field $\boldsymbol{\psi}$ of Model A to be self-advected, namely by promoting the temporal derivative ∂_t to be a material derivative:

$$\partial_t \boldsymbol{\psi} \to \mathcal{D} \boldsymbol{\psi} = \partial_t \boldsymbol{\psi} + v_0 \left(\boldsymbol{\psi} \cdot \nabla \right) \boldsymbol{\psi} \tag{3.28}$$

where the self-advection term $\left(\boldsymbol{\psi} \cdot \nabla \right) \boldsymbol{\psi}$ is proportional to the microscopic speed v_0. From this point of view, the *active* term is given precisely by this self-advective term, which is what encodes activity. This double interpretation comes from the existence of two different ways of switching activity off in the microscopic dynamics: the first is to drop the constraint $\left| \boldsymbol{\psi}_j \right| = 1$, and thus the force $\delta V / \delta \boldsymbol{\psi}$ from the coarse-grained dynamics while keeping the presence of some local alignment interaction - namely the viscous gradient terms of Navier-Stokes equations. In this limit, one expects to recover precisely the Navier-Stokes behaviour, which is not at equilibrium but neither describes a self-propelled system.

On the other hand, a second more sound way to turn activity off is to send the self-propulsion speed to zero, $v_0 \to 0$. In this limit, the Vicsek model describes the equilibrium relaxation dynamics of a Heisenberg model with non-conserved magnetisation. This limit has also a clearer interpretation from a physical point of view: when $v_0 \to 0$, the system is *froze* on a lattice, and one can therefore probe the effects of the other interactions that characterise the dynamic behaviour. Since this procedure will turn quite useful in the following chapters, I stick to this second point of view and identify as *active terms* those coming from self-advection.

The presence of the *active* force has, however, a quite drastic effect on the symmetries of the system. When individuals move by self-propulsion, they do it by exerting a force opposite to motion on a given substrate/medium. The reference frame of this substrate/medium therefore represents a privileged frame of reference: in the context of the Vicsek model, for example, this is the frame in which the speed is v_0. The very existence of a privilege reference frame breaks Galilean invariance, and because the active force originates from self-propulsion, it does break Galilean invariance. This allows for the presence of other non-standard terms in the stress tensor $\boldsymbol{\sigma}$, and also in the force $\boldsymbol{f}$.

3.3.2 The Toner and Tu theory

The theory just proposed in the previous section does indeed account for the presence of both alignment interactions and self-propulsion. However, it is not the most general theory one can write down given the symmetries of the system. For example, I showed in the previous sections that the material derivative operator $\mathcal{D}_t = \partial_t + \boldsymbol{v} \cdot \nabla$ does obey Galilean invariance, and in doing so the coefficient in front of the $\boldsymbol{v} \cdot \nabla$ must be equal to unity. This property must be preserved under coarse-graining, and indeed in the contest of Navier-Stokes, it does [46]. However, when Galilean invariance is violated and detailed balance is violated, there is no reason to expect it to be equal to unity [74, 75]. Even if one did choose its bare value to be equal to unity, upon coarse-graining the RG flow of that coupling would likely drive it away from 1. The equation of motion of $\boldsymbol{\psi}$ can therefore be generalised by accounting for a non-Galilean invariant material derivative operator

$$\mathcal{D}_t = \partial_t + \gamma \boldsymbol{v} \cdot \nabla = \partial_t + v_0 \gamma \boldsymbol{\psi} \cdot \nabla \tag{3.29}$$

Similarly, other additional non-Galilean invariant terms can be identified, and perhaps the most general form possible of the theory of the Self-Propelled Mode A is given by

$$\partial_t \psi_\alpha + v_0 \gamma_1 \left(\psi_\gamma \partial_\gamma \right) \psi_\alpha + v_0 \gamma_2 \left(\partial_\gamma \psi_\gamma \right) \psi_\alpha + v_0 \gamma_3 \partial_\alpha \left(\psi_\gamma \psi_\gamma \right) = U \psi_\alpha +$$
$$+ \Gamma \nabla^2 \psi_\alpha + \Gamma_2 \partial_\alpha \left(\partial_\gamma \psi_\gamma \right) + \Gamma_3 \left(\psi_\gamma \partial_\gamma \right)^2 \psi_\alpha - \partial_\alpha \mathcal{P} - \psi_\alpha \left(\psi_\gamma \partial_\gamma \right) \mathcal{P}_2 + \sqrt{2 \tilde{\Gamma}} \theta_\alpha \tag{3.30}$$

$$\partial_t \rho + v_0 \partial_\gamma \left(\rho \psi_\gamma \right) = 0 \tag{3.31}$$

These are precisely the equations of the Toner and Tu theory, as proposed in their latest version in [76]. Here all coefficients are in principle functions of the density ρ and the magnitude of the alignment order parameter $|\boldsymbol{\psi}|$, but not of its direction, since a rotational symmetry is present in the system. In addition to the standard advective term, $\left(\psi_\gamma \partial_\gamma \right) \psi_\alpha$, other two terms with the same number of fields and derivatives are present, namely those proportional to γ_2 and γ_3. These will be referred to as *anomalous* advection terms, as they differ from the *standard* one of Navier-Stokes equations. The term $U \boldsymbol{\psi}$ is the one responsible of bounding $|\boldsymbol{\psi}|$, and will be here taken of the form

$$U(|\boldsymbol{\psi}|) = -m - J |\boldsymbol{\psi}|^2 \, , \tag{3.32}$$

with m and J potentially still functions of ρ. This is the minimal form that allows to recover the flocking transition as m goes from positive to negative. In addition to the two kinetic coefficients Γ and Γ_2, which in the Navier-Stokes context represent shear and bulk viscosity [43], a third anisotropic kinetic coefficient Γ_3 is also allowed by the symmetries. Similarly, also an anisotropic pressure $\mathcal{P}_2$ should be taken into account. The two pressures are usually expanded in the form

$$\mathcal{P} = \sum_{n=1}^{+\infty} \sigma_n(|\boldsymbol{\psi}|) \left(\rho - \rho_0 \right)^n \qquad \mathcal{P}_2 = \sum_{n=1}^{+\infty} \mu_n(|\boldsymbol{\psi}|) \left(\rho - \rho_0 \right)^n \tag{3.33}$$

Where ρ_0 is the (conserved) average density of the system.

3.3.3 Density-velocity feedback and first-order ordering transition

To understand how the Toner and Tu theory behaves in the proximity of the flocking transition, I will here perform a mean-field analysis, namely setting $\tilde{\Gamma} = 0$, of the phase diagram. I will then study the linear stability of homogeneous states of the system. To have a rough idea of how the phase diagram looks like, I will assume U to take the form of (3.32) with J roughly constant and always positive, and $m \propto (\rho_c - \rho_0)$, where ρ_c is some critical density at which a transition is expected to take place. In contrast with ferromagnets, I will show that the coupling of density and velocity fluctuations gives rise to an instability which is known to lead to a discontinuous, i.e. first-order, phase transition [44, 77].

Homogeneous solution

Spatially homogeneous but time-dependent solutions of the noiseless hydrodynamic equations are found by assuming $\boldsymbol{\psi}(\boldsymbol{x}, t) = \boldsymbol{\psi}(t)$ and $\rho(\boldsymbol{x}, t) = \rho(t)$ in the Toner and Tu equations, which then take the form

$$\partial_t \boldsymbol{\psi} = U\boldsymbol{\psi} \qquad\qquad \partial_t \rho = 0 \qquad\qquad (3.34)$$

The second of these expresses particle conservation: $\rho(t) \equiv \rho_0$, the initial density, for all times. In contrast, $\boldsymbol{\psi}$ relaxes, with an asymptotic solution $\lim_{t \to +\infty} |\boldsymbol{\psi}| = |\boldsymbol{\psi}|_0$. A *disordered* state with

$$|\boldsymbol{\psi}|_0 = 0\,, \qquad\qquad (3.35)$$

is always a steady-state solution, however, it is asymptotically stable only when $m > 0$, namely when $\rho_0 < \rho_c$. For $\rho_0 > \rho_c$, namely $m < 0$, another steady-state solution emerges, obtained by setting

$$U(|\boldsymbol{\psi}|_0\,, \rho_0) = 0 \Rightarrow |\psi|_0 = \sqrt{\frac{-m}{J}} \propto \sqrt{\rho_0 - \rho_c}\,. \qquad\qquad (3.36)$$

I will refer to this as the *flocking* state for obvious reasons. Note that for $m > 0$, this state does not even exist, while for $m < 0$ it turns out to be linearly stable for homogeneous perturbations. Based on this analysis, the system is therefore expected to undergo a phase transition at $m = 0$, where the continuous rotational symmetry is spontaneously broken for $m < 0$ and a phase with non-zero average polarisation $|\psi|_0$ emerges. Note that, precisely because of the rotational symmetry, the direction of $\boldsymbol{\psi}$ is spontaneously selected by the system and can not be determined *a priori*.

Linear stability analysis

The presence of a transition via spontaneous symmetry-breaking suggests some similarity with the phase transition in ferromagnetic systems, apparently suggesting the phase transition to be continuous. However, this would be true only if the homogeneous polarised state $|\boldsymbol{\psi}|_0 \neq 0$ was stable, for all $\rho_0 > \rho_c$, against spatially inhomogeneous perturbations. While this is the case for standard ferromagnetic theories, as Model A, I will now show that this is not the case for Self-Propelled Model A. In the latter case, there is a range of densities just above ρ_c where no homogeneous solution is stable, in which the system is driven towards a phase-separated state.

Let me assume the system for $\rho_0 > \rho_c$ is found in a state $\boldsymbol{\psi} = \psi_0 \hat{x}$, $\rho = \rho_0$, with $\hat{x}$ being the direction in which the $\boldsymbol{\psi}$ field spontaneously breaks the rotational symmetry. To check the linear stability of this homogeneous solution, I should examine the dynamic behaviour of small perturbations $\delta\boldsymbol{\psi} = \delta\psi_x \hat{x} + \delta\boldsymbol{\psi}^\perp$ and $\delta\rho$. For the sake of simplicity, let me here neglect the $\delta\boldsymbol{\psi}^\perp$ fluctuations in directions orthogonal to the flocking direction, and consider only fluctuations parallel to $\hat{x}$. At the linear level, these fluctuations obey the equations:

$$\partial_t \delta\psi_x + v_0 \psi_0 \gamma_x \partial_x \delta\psi_x = -2\,|m|\,\delta\psi_x - g\delta\rho + \Gamma\nabla^2\delta\psi_x + \Gamma_x\partial_x^2\delta\psi_x - \sigma\partial_x\delta\rho\,, \quad (3.37)$$

$$\partial_t \delta\rho + v_0\psi_0\partial_x\delta\rho + v_0\rho_0\partial_x\delta\psi_x = 0 \quad (3.38)$$

where I defined

$$\gamma_x = (\gamma_1 + \gamma_2 + 2\gamma_3) \qquad\qquad \Gamma_x = \Gamma_2 + \psi_0^2\Gamma_3 \quad (3.39)$$

$$g = \psi_0\left(\frac{\partial m}{\partial\rho} + \psi_0^2\frac{\partial J}{\partial\rho}\right) \qquad\qquad \sigma = \sigma_1 + \psi_0^2\mu_1 \quad (3.40)$$

In Fourier space, where the general field ϕ can be expressed as $\phi\left(\boldsymbol{k},t\right) = \int \mathrm{d}^d x\,\phi\left(\boldsymbol{x},t\right)e^{-\mathrm{i}\boldsymbol{x}\cdot\boldsymbol{k}}$, the linearised dynamics becomes

$$\partial_t\begin{pmatrix}\delta\rho \\ \delta\psi_x\end{pmatrix} = M\left(\boldsymbol{k}\right)\begin{pmatrix}\delta\rho \\ \delta\psi_x\end{pmatrix} \quad (3.41)$$

Here

$$M(\boldsymbol{k}) = \begin{pmatrix} -\mathrm{i}v_0 k_x & -\mathrm{i}\rho_0 k_x \\ -g - \sigma\mathrm{i}k_x & -2\,|m| - \mathrm{i}v_0\psi_0\gamma_x k_x - \Gamma k^2 - \Gamma_x k_x^2 \end{pmatrix} \quad (3.42)$$

and stability against perturbations at wave-vector $\boldsymbol{k}$ requires both eigenvalues of $M(\boldsymbol{k})$ to have a nonpositive real part. At small momenta, where the hydrodynamic approach is valid, the real part of the eigenvalues are given by

$$\Re[\lambda_1\left(\boldsymbol{k}\right)] = -2\,|m| + \mathcal{O}(k) \quad (3.43)$$

$$\Re[\lambda_2\left(\boldsymbol{k}\right)] = k_x^2\rho_0 v_0\frac{g^2 v_0\rho_0 + 2v_0\psi_0(\gamma_x - 1)g\,|m| - 4\,|m|^2\,\sigma}{8\,|m|^3} + \mathcal{O}(k^3) \quad (3.44)$$

While the first eigenvalue always has a negative real part for sufficiently small $\boldsymbol{k}$, the latter might not. In fact, close enough to ρ_c, namely for small enough $|m|$, the real part of λ_2 is $\Re[\lambda_2\left(\boldsymbol{k}\right)] \simeq k_x^2(\rho_0 v_0 g)^2/(8\,|m|^3)$, which is always positive, signalling the instability of the homogeneous flocking phase in the proximity of the phase transition.

The careful reader might have noticed that this instability is present only for wave-vectors pointing in the $\hat{x}$ direction: in fact, this instability leads to the formation of plane waves running orthogonal to the direction of motion, but moving along it. These are the band-like structures observed in numerical simulations of the Vicsek model [44, 36], which are responsible for turning the transition into first-order.

3.4   Conclusion

In the present Chapter, I introduced the Toner and Tu theory, a coarse-grained field theory able to capture the large-scale phenomenology of Vicsek-like models, where active, self-propelled particles align their direction of motion. I reviewed in detail what non-linear interactions are needed to go from an equilibrium theory for ferromagnetic alignment, as Model A, to the active Toner and Tu theory, also called Self-Propelled Model A. The minimal substitution to do so is to *promote* the temporal derivative to a material derivative, following $\partial_t \rightarrow \mathcal{D}_t = \partial_t + \gamma \boldsymbol{v} \cdot \nabla$, where $\gamma \neq 1$ as a consequence of the lack of Galilean invariance and activity. All this repertoire will turn out to be extremely useful later on, in Chapter 7, where to account for inertial behaviour in swarms I will build the Self-Propelled version of another equilibrium theory, namely Model G [40].

For the moment, let me focus on the effects of activity only on the dynamics in the near-ordering phase, which is believed to describe swarms. As I just mentioned in the last Section, the presence of self-propulsion allows the density to fluctuate. A feedback mechanism between velocity and density fluctuations makes the homogeneous state unstable in the proximity of the phase transition, turning the transition from second to first-order.

Systems in the proximity of a first-order transition do not exhibit scaling laws, while swarms do. Moreover, no trace of the heterogeneous spatial profiles that arise as a consequence of the instability has been observed in experiments on swarms. To explain both these phenomena at once, one can assume the system to be incompressible: as the inverse compressibility σ diverges, the real part of λ_2 becomes always negative, hence restoring the second-order nature of the phase transition. As I will show in Chapter 6, incompressibility is more than a simple simplifying assumption: in the presence of weak density fluctuations, finite-size systems with small enough compressibility do exhibit the same collective behaviours of incompressible theories.

To study the collective behaviour of the incompressible Toner and Tu theory, which will be performed in Chapter 5, it is however fundamental to first introduce the main tool that will be used for this purpose: the renormalization group. Hence, I will devote the following Chapter to discussing the main ideas and concepts of this powerful technique.

Chapter 4

The renormalization group

The introduction of coarse-grained descriptions of active matter systems has been motivated by the need to find a framework in which collective properties of biophysical systems, such as natural swarms, could be characterised and understood. The power of these coarse-grained, or hydrodynamic, descriptions is that they allow a simple description of large-scale properties in terms of interactions between few fields, e.g. chemical concentrations, particle density, and the local average velocity. Moreover, a hydrodynamic theory usually provides an accurate and comprehensive mesoscopic description of a wide range of microscopic models, all sharing the same emergent behaviour.

When interested in the description of large-scale collective modes, the renormalization group (RG) turns out to be a very useful tool. In a nutshell, the RG provides a way to study how the description of a system changes as one changes the wave-length resolution at which they observe the system, resulting in an extremely versatile tool. In the context of particle physics, for example, the RG is used to investigate the behaviour of small wavelength, i.e. high-energy, fluctuations of the quantum fields. On the other side, in the condensed matter physics attention is instead given to the large wavelength, i.e. low-energy, fluctuations of collective modes. In this latter case, when the system behaves collectively the large-scale physics is scale-invariant. In this scale-invariant regime, many observables exhibit a power-law behaviour, thus allowing one to encompass the description of the system in a set of few scaling exponents.

The momentum shell RG scheme developed by Wilson [17, 52] provides an explicit method to calculate scaling exponents. By integrating out the short-wavelength modes iteratively, the RG generates a flow in the parameter space of the effective action. This coarse-graining procedure tells how the effective action changes as one *zooms out* and looks at the system's behaviour on larger and larger scales. When this RG flow eventually converges towards an attractive fixed point, the study of the linearised flow equations near this fixed point allows computing explicitly the critical exponents of the theory. Universality, in this RG context, consists of the fact that one single fixed point rules the long-wavelength behaviour of a large class of theories, each one identified by a different initial point in the parameter space.

The best way to perform RG calculations is to have the system described by a field theory defined through a path-integral formulation, namely to have an *action*

$\mathcal{S}$ which defines the probability P of a given configuration ϕ through $P = e^{\mathcal{S}[\phi]}$. At equilibrium, it is the free energy functional that plays the role of the action. Therefore, one can directly attempt to build a suitable free energy in agreement with all the symmetries of the underlying system. This is exactly the process that led to the Landau-Ginzburg free energy for Ising-like systems. However, in non-equilibrium physics, the behaviour of a system usually cannot be described by a free energy. Instead, the dynamics of the system is often described by a set of stochastic Partial Differential Equations (PDEs), or by the Master-Equation ruling the evolution of the probability distribution. Many different tools have been developed to perform RG analysis of these systems. Here I will review the Martin-Siggia-Rose/Janssen-De Dominicis formalism [47, 78, 79], which allows to derive a field-theoretical action from stochastic PDEs, and the Doi-Peliti formalism [80, 81, 82], which allows to derive field-theory out of a Master-Equation.

4.1 Momentum-shell renormalization group

The starting point to understand the momentum-shell RG is to define an RG transformation of the effective action. This RG transformation consists of two steps:

i) the probability distribution of the fields is marginalised by integrating short-wavelength modes on the shell $b^{-1}\Lambda < k < \Lambda$, with $b > 1$, hence effectively decreasing the cutoff in momentum space;

ii) space and time are rescaled, to formally restore the same cutoff as the original theory.

The action obtained after one RG transformation has different parameters and it describes the system when it is observed on a larger scale. However, since the partition function remains the same up to a multiplicative constant, the physical observables are left unchanged. The iteration of such an RG transformation gives rise to a flow in the space of the actions. The flow equations are obtained in the form of recursive relations, describing how the parameters at the iteration $(l + 1)$ can be obtained starting from those at step l.

4.1.1 Shell integration

In the Gaussian theory, when all interaction terms vanish, the shell integration is harmless since modes at different wavelengths are independent [15], and thus the RG flow is trivial: essentially each parameter rescales according to naive dimensional analysis. However, when non-Gaussian interactions are present, the shell integration couples long and short wavelength modes, generating nontrivial corrections to the bare action. To perform the shell integration, it is convenient to split the fields in their Infra-Red (IR) and Ultra-Violet (UV) modes [15], and write the partition function as,

$$\mathcal{Z} = \int \mathcal{D}\phi \, e^{-S[\phi]} = \int \mathcal{D}\phi^< \mathcal{D}\phi^> \, e^{-S[\phi^< + \phi^>]} \tag{4.1}$$

where ϕ stands for all the fields of the theory, while superscripts $<$ and $>$ indicate whether the field has momenta lower (IR modes) or higher (UV modes) than $b^{-1}\Lambda$

respectively. The action S can then be written in the following form,

$$S[\phi^< + \phi^>] = S[\phi^<] + S_0[\phi^>] - \mathcal{V}[\phi^<, \phi^>] \tag{4.2}$$

where S_0 is the Gaussian part of the action while $\mathcal{V}$ represents all the UV-IR and UV-UV interactions. The goal now is to write down an *effective* action for the large-wavelength $\phi^<$ modes only, by integrating out the short-wavelength *details* $\phi^>$. To do this, it is best to write Eq. (4.1) in the following form,

$$\mathcal{Z} = \int \mathcal{D}\phi^< e^{S[\phi^<]} \int D\phi^> \, e^{S_0[\phi^>]} e^{-\mathcal{V}[\phi^<, \phi^>]} \tag{4.3}$$

From this equation, it is straightforward to achieve my aforementioned goal, since $\mathcal{Z}$ can be now written as

$$\mathcal{Z} = \mathcal{Z}_0^> \int \mathcal{D}\phi^< e^{-S^<[\phi^<]} , \qquad S^<[\phi^<] = S[\phi^<] + \Delta S[\phi^<] \tag{4.4}$$

The action $S^<$ represents what I wanted to achieve: an effective action for the IR modes only, independent of the UV ones. The UV modes do however leave their sign: the action for the $\phi^<$ acquired a correction $\Delta S[\phi^<]$, which is obtained by averaging $e^{\mathcal{V}[\phi^<, \phi^>]}$ over the Gaussian action of the UV fields with on-shell momentum, namely

$$e^{-\Delta S[\phi^<]} = \frac{1}{\mathcal{Z}_0^>} \int \mathcal{D}\phi^> e^{-S_0[\phi^>]} e^{\mathcal{V}[\phi^<, \phi^>]} \tag{4.5}$$

This process is known as *shell integration*, where all the UV modes with wave vectors belonging to the so-called momentum shell have been integrated out. The shell integration is typically performed under a thin-shell approximation, namely taking $b \to 1^+$: in this limit ΔS is proportional to the shell thickness $1 - b^{-1} \simeq \ln b$. The final result after the integration over the UV modes $\phi^>$ is an effective action with a new cutoff $b^{-1}\Lambda$ and modified parameters, namely,

$$\mathcal{P}_0 \to \mathcal{P}_0 + \mathcal{P}_0 \delta\mathcal{P} \ln b = \mathcal{P}_0 \left(1 + \delta\mathcal{P} \ln b\right) \simeq \mathcal{P}_0 b^{\delta\mathcal{P}} \tag{4.6}$$

where I used the relation $b^a \simeq 1 + a \ln b$ when b is close to 1, while $\delta\mathcal{P}$ is in general a function of the bare parameters $\mathcal{P}_0$. The typical aim of an RG calculation is to calculate the corrections to the parameters $\delta\mathcal{P}$.

4.1.2 Rescaling

At this point, I would like to *compare* the bare action with the new action obtained after shell integration. However, these two theories have at the moment different cutoffs, since the former has cutoff Λ while the latter $b^{-1}\Lambda$. To recover a *renormalized* theory with the same cutoff Λ of the bare theory, the space must be rescaled as $\boldsymbol{x}_b = b^{-1}\boldsymbol{x}$ or equivalently momenta must be rescaled as $\boldsymbol{k}_b = b\boldsymbol{k}$. While doing this rescaling, it is typically convenient to also rescale frequencies and fields in the following way

$$\boldsymbol{k} = b^{-1}\boldsymbol{k}_b \qquad \omega = b^{-z}\omega_b \qquad \phi(\boldsymbol{k}, \omega) = b^{-\chi_\phi}\phi_b(\boldsymbol{k}_b, \omega_b) \tag{4.7}$$

where z is the dynamical exponent and χ_ϕ the scaling dimension of the field. Note that although there might be some convenient choices to fix the exponents z and χ_ϕ, the physical predictions can not depend on this choice. Once this rescaling is done, the action has the same cutoff as the bare one, but its parameters and couplings change. Note that potentially new interaction terms might arise after shell integration: in this case, the couplings of these terms only *changed* from 0 to a finite value. These new values of the parameters, which will be denoted with a subscript b, are defined to absorb all the powers of b in front of them after shell integration and rescaling, and can be expressed as functions of the bare parameters,

$$\mathcal{P}_b = b^{\chi_\mathcal{P}(\mathcal{P}_0)}\mathcal{P}_0 \tag{4.8}$$

where $\chi_\mathcal{P}$ is the total scaling dimension of $\mathcal{P}$, and depends on the values of $\mathcal{P}_0$. This total scaling takes into account both naive scaling, coming from dimensional analysis, and the anomalous scaling due to the RG coupling of IR and UV modes. I may therefore write $\chi_\mathcal{P}$ as

$$\chi_\mathcal{P} = d_\mathcal{P} + \delta\mathcal{P} \tag{4.9}$$

where $d_\mathcal{P}$ is the naive physical dimension of $\mathcal{P}$ in units of momentum $\boldsymbol{k}$ while $\delta\mathcal{P}$ is RG correction, as defined in Eq (4.6). Thanks to this transformation, the partition function can be written as,

$$\mathcal{Z} \propto \int \mathcal{D}\boldsymbol{\phi}^< e^{-(S[\phi^<]+\Delta S[\phi^<])} \propto \int \mathcal{D}\boldsymbol{\phi} e^{-S_b[\phi]} \tag{4.10}$$

where $S_b[\phi]$ is the *renormalized action*, obtained after integration over a shell of thickness $\ln b$ and rescaling.

4.1.3   RG flow and fixed points

The iteration of this renormalization group transformation many times defines a flow in the parameter space, where the parameters after $l+1$ iterations are given by

$$\mathcal{P}_{l+1} = b^{\chi_\mathcal{P}(\mathcal{P}_l)}\mathcal{P}_l \tag{4.11}$$

where $\chi_\mathcal{P}(\mathcal{P}_l)$ means that the scaling dimension $\chi_\mathcal{P}$ is evaluated using the parameters at the step l. Furthermore, when a thin shell approximation $b \to 1^+$ is taken, one can define a continuous flow of the parameters of the theory, ruled by the equation

$$\dot{\mathcal{P}} = \beta_\mathcal{P}(\mathcal{P}) = \mathcal{P}\,\chi_\mathcal{P}(\mathcal{P}) \tag{4.12}$$

The beta-function $\beta_\mathcal{P}$ can be computed from Eq. (4.8), by taking the derivative of $\mathcal{P}$ with respect to $\ln b$, namely $\beta_\mathcal{P} = \partial\mathcal{P}/\partial\ln b = \mathcal{P}\,\chi_\mathcal{P}$. The values $\mathcal{P}^*$ to which the flow of $\mathcal{P}$ approaches when $l \to \infty$ are called fixed points, and play a crucial role in determining the critical behaviour of the theory [15]. Fixed points are given by the zeros of $\beta_\mathcal{P}$ since these are the points at which $\dot{\mathcal{P}} = \beta_\mathcal{P}|_{\mathcal{P}=\mathcal{P}^*} = 0$. Among these fixed points, some are (IR-)stable meaning that the flow is driven towards them, while others may have one or more directions of instability from which the RG flow escapes. Asymptotically IR-stable fixed points are those typically ruling the critical behaviour of systems in the thermodynamic limit. The power of the

RG lies in the fact that critical exponents can be inferred by the study of the RG flow in the neighbourhood of a fixed point. The fixed point at which the critical exponents should be evaluated usually is the stable one, since one expects the RG flow to eventually reach its stable fixed point.

4.1.4 Perturbation theory

Computing exactly the RG corrections is often an impossible task. To overcome this problem, the RG can be performed using a perturbative expansion. This is done by assuming the interaction couplings entering $\mathcal{V}$ to be *small* - an assumption that will be verified *a posteriori* at the stable fixed point. Within this perturbative approach, it is possible to expand $e^{\mathcal{V}}$ in powers of the couplings. The consequence of this is that also ΔS can be expressed in an expansion in these small couplings. In particular, it can be graphically represented as a series of Feynman diagrams, composed only by connected diagrams [15] in which the momenta k of the UV modes are integrated only over the shell $b^{-1}\Lambda < k < \Lambda$.

The *small* parameter in which the perturbative expansion is performed is $\epsilon = d_c - d$, where d_c is the upper critical dimension, namely the dimension above which mean-field theory is exact, while d is the spatial dimension. This well-established expansion method to compute the critical exponents, known as ϵ-expansion [53], often allows one to get good predictions of the scaling exponents of the theory already at first order.

4.2 renormalization group approach to dynamic phenomena

Most of the theories I will discuss in this dissertation are defined by a set of stochastic partial differential equations describing the temporal evolution of the hydrodynamic variables in the system. To employ the standard RG tools, introduced in the present Chapter, to the study of these theories I need a formalism that allows me to describe the system of interest through a field-theoretical action. Many possible strategies to do so have been formulated, but here I will follow the formalism proposed by Martin, Siggia, Rose [47], Janssen [78] and De Dominicis [79], which provides a mapping between the behaviour of fields evolving according to stochastic differential equations with a field-theory formulated using path integrals.

Let me assume the dynamic behaviour of the field ϕ is defined by the following Langevin equation with Ito time-discretisation:

$$\mathcal{F}[\phi] - \boldsymbol{\theta} = 0\,, \tag{4.13}$$

with the noise $\boldsymbol{\theta}$ characterised by the distribution P_θ, while $\mathcal{F}$ is the deterministic evolution operator. The expected value of a given observable O can be computed by averaging $O[\phi]$ over the possible noise realisations, requiring ϕ to obey (4.13), namely

$$\langle O \rangle = \frac{1}{Z} \int \mathcal{D}\phi\, O[\phi] \int \mathcal{D}\boldsymbol{\theta}\, P_\theta(\boldsymbol{\theta};\phi)\, \delta(\mathcal{F}[\phi] - \boldsymbol{\theta}) \tag{4.14}$$

where

$$Z = \int \mathcal{D}\phi \int \mathcal{D}\boldsymbol{\theta}\, P_\theta(\boldsymbol{\theta}; \boldsymbol{\phi})\, \delta(\boldsymbol{\mathcal{F}}[\boldsymbol{\phi}] - \boldsymbol{\theta})\,. \tag{4.15}$$

By means of an integral representation of the delta-function $\delta(x) = \int \mathrm{d}\hat{x}\, e^{\mathrm{i}\hat{x}\,x}$, one can write $\langle O \rangle$ as

$$\begin{aligned}
\langle O \rangle &= \frac{1}{Z} \int \mathcal{D}\phi \int \mathcal{D}\hat{\phi}\, O\,[\boldsymbol{\phi}]\, e^{-\mathrm{i}\hat{\boldsymbol{\phi}}\cdot\boldsymbol{\mathcal{F}}[\boldsymbol{\phi}]} \int \mathcal{D}\boldsymbol{\theta}\, P_\theta(\boldsymbol{\theta}; \boldsymbol{\phi})\, e^{\mathrm{i}\hat{\boldsymbol{\phi}}\cdot\boldsymbol{\theta}} = \\
&= \frac{1}{\mathrm{i}Z} \int \mathcal{D}\phi \int \mathcal{D}\hat{\phi}\, O\,[\boldsymbol{\phi}]\, e^{-\hat{\boldsymbol{\phi}}\cdot\boldsymbol{\mathcal{F}}[\boldsymbol{\phi}]+K_\theta[\hat{\phi},\phi]}
\end{aligned} \tag{4.16}$$

where I performed the substitution $\hat{\phi} \to \mathrm{i}\hat{\phi}$. Moreover

$$K_\theta[\boldsymbol{x}, \boldsymbol{\phi}] = \ln\left[\int \mathcal{D}\boldsymbol{\theta}\, P_\theta(\boldsymbol{\theta}; \boldsymbol{\phi})\, e^{\boldsymbol{x}\cdot\boldsymbol{\theta}} \right] \tag{4.17}$$

is the cumulant-generating function of the distribution P_θ. In the case of a Gaussian distribution with zero mean and covariance matrix $2L_{\alpha\beta}$, the cumulant-generating function is given by $K_\theta[\boldsymbol{x}] = x_\alpha L_{\alpha\beta} x_\beta$.

The bottom line of this algebraic manipulation is that the statistics generated by dynamic behaviour defined by Eq. (4.13) is reproduced by the field-theoretical action S given by,

$$S[\boldsymbol{\phi}, \hat{\boldsymbol{\phi}}] = \int \mathrm{d}\boldsymbol{x}\, \mathrm{d}t\, \hat{\boldsymbol{\phi}} \cdot \boldsymbol{\mathcal{F}}[\boldsymbol{\phi}] - K_\theta[\hat{\boldsymbol{\phi}}, \boldsymbol{\phi}] \tag{4.18}$$

The introduction of the hatted field $\hat{\boldsymbol{\phi}}$ in the action is the price that has to be paid to exploit the path integral formulation, using the standard rules of static renormalization and writing the perturbative series in terms of Feynman diagrams. The field theoretical description reproduces the stochastic dynamics in the sense that, for a given observable $O\,[\boldsymbol{\phi}]$,

$$\langle O \rangle = \langle O \rangle_S \tag{4.19}$$

where $\langle O \rangle$ is the average value of O over all possible realisations of the noise $\boldsymbol{\theta}$, while

$$\langle O \rangle_S = \frac{1}{\mathcal{Z}} \int \mathcal{D}\phi \int \mathcal{D}\hat{\phi}\, O\,[\boldsymbol{\phi}]\, e^{-S[\phi,\hat{\phi}]} \tag{4.20}$$

Thanks to this equivalence, the critical dynamics can be investigated by studying the action S through RG techniques. The Gaussian part of the action S derives from the linear dynamics, namely the linear part of the operator $\mathcal{F}$, while the interactions derive from non-linear terms. Within this formalism, an external source $\boldsymbol{h}$ introduced in the dynamical equation of $\boldsymbol{\phi}$ is coupled to $\hat{\boldsymbol{\phi}}$ in the effective action. Therefore, the response function, known also as the Green function or propagator, can be written as,

$$\frac{\delta\langle \phi_\alpha\,(\boldsymbol{x}, t)\rangle}{\delta h_\beta\,(\boldsymbol{x}', t')} = \langle \phi_\alpha(\boldsymbol{x}, t)\hat{\phi}_\beta(\boldsymbol{x}', t')\rangle \tag{4.21}$$

For this reason, $\hat{\boldsymbol{\phi}}$ takes the name 'response field'.

Note that the equivalence derived in this section works also the other way round: if one obtains a field theoretical action like (4.18) from other approaches, say a Doi-Peliti approach [16], the resulting behaviour of $\boldsymbol{\phi}$ is equivalent to that obtained if $\boldsymbol{\phi}$ obeyed Eq. (4.13).

Chapter 5

Incompressible Toner and Tu theory

The presence of instability of the homogeneous state in the proximity of the ordering phase transition in polar active matter systems, and its main consequence, namely the presence of a first-order transition, is in apparent contradiction with the simulations made by Vicsek et al. in their seminal paper [42] where a second order phenomenology was reported. After some debate among the community [44, 83, 84, 85], there is nowadays a quite large consensus on the first-order nature of the transition. The earlier belief of a second-order transition was likely a result of finite-size effects. While the coupling between velocity and density fluctuations drives the transition from second to first-order in infinitely large systems, finite-size systems are often not large enough to make this effect noticeable. This is the case of the simulations made in [42], where a second-order phenomenology appeared at finite scales, with no strong heterogeneous spatial structures, as bands, forming in the system in the ordered phase.

Quite interestingly, natural swarms of midges in the field were shown to be well described by the proximity to an ordering critical point [12, 56], because of their low polarisation but long-range velocity-velocity correlations. Midges however are self-propelled units that align to their neighbours [56], making swarms a polar active matter system that should undergo a first-order transition rather than a second-order one. Once again, the explanation for their critical behaviour might come from finite-size effects. Remarkably, midges and finite-size simulations of the Vicsek model not only have the observation of scaling laws in common but also the absence of heterogeneous spatial structures such as bands. This evidence suggests that the finite size of the system might suppress the density-velocity coupling responsible for turning the transition into a first-order one.

From the point of view of the large-scale dynamics of the direction of motion field, the suppression of density-velocity couplings means that density can be treated as a constant, hence calling for an investigation of a theory for incompressible polar active matter. Interestingly, as the compressibility of the longitudinal modes σ^{-1} becomes smaller, the range of values of ρ_0 for which the instability occurs gets smaller, eventually vanishing when $\sigma^{-1} \to 0$ (see (3.44) of Chapter 3). This suggests that the phase transition in the incompressible limit is continuous at all scales.

In their seminal paper [23], Chen, Toner and Lee performed a renormalization group calculation of the incompressible Toner and Tu theory near criticality, aiming to show that in this case, the transition is continuous. The finding on a new non-trivial fixed point ruling the large-scale behaviour of near-ordering incompressible active matter confirmed the expectations of the authors, proving the transition is second-order (i.e., continuous) in the incompressible limit. The authors of [23] probably did not have natural swarms in mind, and the dynamic critical exponent found in their active theory ($z = 1.73$ in $d = 3$) is not compatible with that observed in swarms. Nevertheless, their calculation is extremely valuable, both from a physical and from a technical point of view. Physically, it shows that being self-propelled can affect the large-scale dynamic behaviour. Even though self-propulsion on its own is not able to explain the dynamic exponent observed in swarms, compared to the non-active case z shifts in the right direction. From a technical point of view, instead, this calculation will represent a reference point for the RG analysis I will perform in Chapters 9-11. For these reasons, it is extremely useful to review in detail the calculation performed in [23], a topic to which I will dedicate the following sections.

5.1   The incompressible theory

Incompressibility is the requirement that the density field remains constant, namely that $\rho \equiv \rho_0$. This might happen for a variety of reasons, but when this happens the continuity equation of the density reduces to a solenoidal constraint on the direction of motion field:

$$\partial_t \rho + v_0 \partial_\alpha \left(\rho \psi_\alpha \right) = 0 \quad \Rightarrow \quad \partial_\alpha \psi_\alpha = 0 \tag{5.1}$$

With this constraint, the theory describing the large-scale behaviour of incompressible polar active fluids in the near-ordering phase [23] can be written in the form:

$$\partial_t \psi_\alpha + v_0 \gamma \left(\psi_\gamma \partial_\gamma \right) \psi_\alpha = \Gamma \nabla^2 \psi_\alpha - \Gamma \frac{\delta V}{\delta \psi_\alpha} - \partial_\alpha \mathcal{P} + \sqrt{2\tilde{\Gamma}}\, \theta_\alpha \,,$$
$$\partial_\alpha \psi_\alpha = 0 \,. \tag{5.2}$$

Here the pressure term $\mathcal{P}$, in which also the γ_3 term was absorbed, acts as a Lagrange multiplier enforcing the incompressibility condition $\partial_\alpha \psi_\alpha = 0$. On the l.h.s. of (5.2) one can recognise a modified material derivative $D_t \boldsymbol{\psi} = \partial_t \boldsymbol{\psi} + v_0 \gamma \left(\boldsymbol{\psi} \cdot \nabla \right) \boldsymbol{\psi}$, with $\gamma \neq 1$ in the general case since Galilean invariance is broken [20]. On the r.h.s. instead, there is the alignment force $\nabla^2 \boldsymbol{\psi}$, which from the fluid-dynamics perspective can also be interpreted as a shear viscosity, the active force coming from a Landau potential V, the pressure $\mathcal{P}$ and a Gaussian white noise of variance $2\tilde{\Gamma}$.

The parameter v_0, namely the microscopic speed, is what quantifies *activity*: when $v_0 = 0$, one recovers the behaviour of Model A [40] with a solenoidal constraint, which describes systems like dipolar ferromagnets [86]. The system thus effectively behaves as an equilibrium one. Any *active* field theory, aiming to describe collective behaviours of self-propelled units therefore requires the presence of advection, effectively captured by the presence of a material derivative, in addition to the presence of an active force.

On the other hand, it is relevant to observe that, when $m = J = 0$, one recovers the behaviour of an incompressible fluid stirred by a force which acts even at $k = 0$, namely Model B of [46].

5.1.1 The equations in Fourier space

In Fourier space, the incompressibility constraint has an expression which is local in the wave vector, namely

$$k_\alpha \psi_\alpha(\mathbf{k}) = 0\,, \tag{5.3}$$

Note that the real-space fields can be recovered via

$$\phi(\mathbf{x}) = \int_{\mathbf{k}} \mathrm{e}^{\mathrm{i}\mathbf{x}\cdot\mathbf{k}} \phi(\mathbf{k})\ . \tag{5.4}$$

Here and in the following, I will use the notation,

$$\int_{\mathbf{k}} = \int\limits_{|\mathbf{k}|<\Lambda} \frac{\mathrm{d}^d k}{(2\pi)^d} \tag{5.5}$$

The locality of the constraint in momentum space makes it a more convenient choice compared to real space, as the constraint can be easily imposed on the equation of motion. When written in Fourier spare, the dynamic equation (5.2) becomes

$$\partial_t \psi_\alpha(\mathbf{k}) + \mathrm{i} v_0 \gamma \int_{\mathbf{q}} \psi_\gamma(\mathbf{k}-\mathbf{q}) q_\gamma \psi_\alpha(\mathbf{q}) = -\Gamma k^2 \psi_\alpha(\mathbf{k}) - m\psi_\alpha(\mathbf{k}) -$$
$$- J \int_{\mathbf{q},\mathbf{h}} \psi_\gamma(\mathbf{q})\psi_\beta(\mathbf{h})\psi_\alpha(\mathbf{k}-\mathbf{q}-\mathbf{h}) - k_\alpha \mathcal{P}(\mathbf{k}) + \sqrt{2\tilde{\Gamma}}\,\theta_\alpha(\mathbf{k})\,, \tag{5.6}$$

which must be complemented by $k_\alpha \psi_\alpha(\mathbf{k}) = 0$. As done in [46], one can approach the implementation of this constraint as follows. The geometrical interpretation of incompressibility is that, in Fourier space, the direction of motion $\boldsymbol{\psi}(\mathbf{k})$ belongs to the plane orthogonal to $\mathbf{k}$, hence obeying the following relations

$$P^{\parallel}_{\alpha\beta}(\mathbf{k})\psi_\beta(\mathbf{k}) = 0 \qquad\qquad P^{\parallel}_{\alpha\beta}(\mathbf{k}) = \frac{k_\alpha k_\beta}{k^2}\,, \tag{5.7}$$

$$P^{\perp}_{\alpha\beta}(\mathbf{k})\psi_\beta(\mathbf{k}) = \psi_\alpha(\mathbf{k}) \qquad\qquad P^{\perp}_{\alpha\beta}(\mathbf{k}) = \delta_{\alpha\beta} - \frac{k_\alpha k_\beta}{k^2}\,. \tag{5.8}$$

Here $P^{\parallel}$ is an operator that projects on the direction of $\mathbf{k}$, while $P^{\perp} = 1 - P^{\parallel}$ projects on the plane orthogonal to $\mathbf{k}$ [46]. The reason why working in Fourier space is convenient is that one can enforce the constraint by simply applying $P^{\perp}$ to both sides of Eq. (5.6). By doing this, because $P^{\perp}_{\alpha\beta}k_\beta = 0$, no Lagrange multiplier needs to be explicitly used and hence the constraint is automatically satisfied. When performing this projection, the equation of motion becomes

$$\partial_t \psi_\alpha(\mathbf{k}) + \mathrm{i} v_0 \gamma P^{\perp}_{\alpha\beta}(\mathbf{k}) \int_{\mathbf{q}} \psi_\gamma(\mathbf{k}-\mathbf{q}) q_\gamma \psi_\beta(\mathbf{q}) = -\Gamma k^2 \psi_\alpha(\mathbf{k}) - m\psi_\alpha(\mathbf{k}) -$$
$$- J P^{\perp}_{\alpha\beta}(\mathbf{k}) \int_{\mathbf{q},\mathbf{h}} \psi_\gamma(\mathbf{q})\psi_\beta(\mathbf{h})\psi_\beta(\mathbf{k}-\mathbf{q}-\mathbf{h}) + \sqrt{2\tilde{\Gamma}}\,P^{\perp}_{\alpha\beta}(\mathbf{k})\theta_\beta(\mathbf{k})\,. \tag{5.9}$$

Using again the incompressible constraint $k_\alpha \psi_\alpha(\boldsymbol{k}) = 0$ allows one to write

$$\psi_\gamma(\boldsymbol{k} - \boldsymbol{q})q_\gamma = \psi_\gamma(\boldsymbol{k} - \boldsymbol{q})(k_\gamma - q_\gamma) + \psi_\gamma(\boldsymbol{k} - \boldsymbol{q})q_\gamma = \psi_\gamma(\boldsymbol{k} - \boldsymbol{q})k_\gamma \qquad (5.10)$$

This equality, when used in the γ term, leads to

$$\partial_t \psi_\alpha(\boldsymbol{k}) + \mathrm{i}v_0\gamma P^\perp_{\alpha\beta}(\boldsymbol{k})k_\gamma \int_{\boldsymbol{q}} \psi_\gamma(\boldsymbol{k} - \boldsymbol{q})\psi_\beta(\boldsymbol{q}) = -\Gamma k^2 \psi_\alpha(\boldsymbol{k}) - m\psi_\alpha(\boldsymbol{k}) -$$

$$- JP^\perp_{\alpha\beta}(\boldsymbol{k}) \int_{\boldsymbol{q},\boldsymbol{h}} \psi_\gamma(\boldsymbol{q})\psi_\beta(\boldsymbol{h})\psi_\beta(\boldsymbol{k} - \boldsymbol{q} - \boldsymbol{h}) + \sqrt{2\tilde{\Gamma}}\, P^\perp_{\alpha\beta}(\boldsymbol{k})\theta_\beta(\boldsymbol{k}). \quad (5.11)$$

For technical reasons, related to the calculation of Feynman diagrams, it is convenient to make the two interaction terms symmetric under the exchange of two $\boldsymbol{\psi}$ fields

$$\partial_t \psi_\alpha(\boldsymbol{k}) + \mathrm{i}\frac{v_0\gamma}{2}Y^\perp_{\alpha\beta\gamma}(\boldsymbol{k}) \int_{\boldsymbol{q}} \psi_\beta(\boldsymbol{q})\psi_\gamma(\boldsymbol{k} - \boldsymbol{q}) = -\Gamma k^2 \psi_\alpha(\boldsymbol{k}) - m\psi_\alpha(\boldsymbol{k}) -$$

$$- \frac{J}{3}Q^\perp_{\alpha\beta\gamma\nu}(\boldsymbol{k}) \int_{\boldsymbol{q},\boldsymbol{h}} \psi_\beta(\boldsymbol{q})\psi_\gamma(\boldsymbol{h})\psi_\nu(\boldsymbol{k} - \boldsymbol{q} - \boldsymbol{h}) + \sqrt{2\tilde{\Gamma}}\, P^\perp_{\alpha\beta}(\boldsymbol{k})\theta_\beta(\boldsymbol{k}). \quad (5.12)$$

Here two new tensors were defined, namely

$$Y^\perp_{\alpha\beta\gamma}(\boldsymbol{k}) = P^\perp_{\alpha\beta}(\boldsymbol{k})k_\gamma + P^\perp_{\alpha\gamma}(\boldsymbol{k})k_\beta \qquad (5.13)$$

$$Q^\perp_{\alpha\beta\gamma\nu}(\boldsymbol{k}) = P^\perp_{\alpha\beta}(\boldsymbol{k})\delta_{\gamma\nu} + P^\perp_{\alpha\gamma}(\boldsymbol{k})\delta_{\beta\nu} + P^\perp_{\alpha\nu}(\boldsymbol{k})\delta_{\beta\gamma} \qquad (5.14)$$

5.1.2 Linear theory

As in the Toner and Tu theory discussed in Chapter 3, also in this incompressible theory a mean-field analysis reveals the presence of an ordering transition when m turns from positive to negative [23]. Before approaching the field-theoretical analysis of the transition that allows one to go beyond mean-field, it is instructive to review the linear theory in the proximity of the transition. In the disordered near-critical phase, small fluctuations of $\boldsymbol{\psi}$ - which coincide with $\boldsymbol{\psi}$ itself, as $\langle \boldsymbol{\psi} \rangle = 0$ - are expected to behave as follows:

$$\partial_t \psi_\alpha = -(m + \Gamma k^2)\psi_\alpha + \sqrt{2\tilde{\Gamma}}\, P^\perp_{\alpha\beta}(\boldsymbol{k})\theta_\beta(\boldsymbol{k}). \qquad (5.15)$$

The presence of the $P^\perp$ operator in front of the noise term guaranteed that when $k_\alpha \psi_\alpha = 0$ at $t = 0$, the incompressibility constraint is conserved by the dynamics.

To obtain the response and correlation functions, it is easier to move to frequency space, namely performing a Fourier transform of the temporal variable, where the equations become

$$-\mathrm{i}\omega_k \psi_\alpha(\tilde{\boldsymbol{k}}) = -(m + \Gamma k^2)\psi_\alpha(\tilde{\boldsymbol{k}}) + \sqrt{2\tilde{\Gamma}}\, P^\perp_{\alpha\beta}(\boldsymbol{k})\theta_\beta(\tilde{\boldsymbol{k}}). \qquad (5.16)$$

Here the Fourier-transformed field $\psi(\tilde{\boldsymbol{k}})$ was introduced, with $\tilde{\boldsymbol{k}} = (\boldsymbol{k}, \omega_k)$, linked to the real space-time field using an inverse Fourier transformation, namely

$$\phi(\boldsymbol{x}, t) = \int_{\tilde{\boldsymbol{k}}} \mathrm{e}^{-\mathrm{i}\omega t + \mathrm{i}\boldsymbol{x}\cdot\boldsymbol{k}}\phi(\tilde{\boldsymbol{k}}), \qquad\qquad \int_{\tilde{\boldsymbol{k}}} = \int_{\boldsymbol{k}}\int_{-\infty}^{+\infty} \frac{\mathrm{d}\omega}{2\pi} \qquad (5.17)$$

Eq. (5.16) can be written in the form

$$\psi_\alpha(\tilde{\boldsymbol{k}}) = G_{\alpha\beta}(\tilde{\boldsymbol{k}})h_\beta(\tilde{\boldsymbol{k}}) \qquad G_{\alpha\beta}(\tilde{\boldsymbol{k}}) = \frac{1}{-\mathrm{i}\omega_k + m + \Gamma k^2}\delta_{\alpha\beta}\,, \qquad (5.18)$$

where G is the response function, which gives the response of ψ to external perturbations h, where in the present case h represents the noise: $h_\alpha = \sqrt{2\tilde{\Gamma}}\,P_{\alpha\beta}^\perp(\boldsymbol{k})\theta_\beta(\tilde{\boldsymbol{k}})$.

Knowing that the noise correlations are given by

$$\langle\theta_\alpha(\tilde{\boldsymbol{k}})\theta_\beta(\tilde{\boldsymbol{k}})\rangle = \delta_{\alpha\beta}\hat{\delta}(\tilde{\boldsymbol{k}} + \tilde{\boldsymbol{q}}) \qquad (5.19)$$

where

$$\hat{\delta}(\tilde{\boldsymbol{k}}) = (2\pi)^{d+1}\delta^{(d)}(\boldsymbol{k})\delta(\omega_k)\,, \qquad (5.20)$$

The correlation function for the direction of motion $\boldsymbol{\psi}$ can be computed in the following way:

$$\begin{aligned}
\langle\psi_\alpha(\tilde{\boldsymbol{k}})\psi_\beta(\tilde{\boldsymbol{q}})\rangle_0 &= 2\tilde{\Gamma}G_{\alpha\gamma}(\tilde{\boldsymbol{k}})G_{\beta\nu}(\tilde{\boldsymbol{q}})P_{\gamma\sigma}^\perp(\boldsymbol{k})P_{\nu\tau}^\perp(\boldsymbol{q})\langle\theta_\sigma(\tilde{\boldsymbol{k}})\theta_\tau(\tilde{\boldsymbol{k}})\rangle \\
&= 2\tilde{\Gamma}G_{\alpha\gamma}(\tilde{\boldsymbol{k}})G_{\beta\nu}(-\tilde{\boldsymbol{k}})P_{\gamma\nu}^\perp(\boldsymbol{k})\hat{\delta}(\tilde{\boldsymbol{k}} + \tilde{\boldsymbol{q}})
\end{aligned} \qquad (5.21)$$

Here the subscript 0 means that the average $\langle\cdot\rangle_0$ is performed within the linear theory. The expression in the last row is obtained by reminding that the delta function imposes $\tilde{\boldsymbol{q}} = -\tilde{\boldsymbol{k}}$, that $P_{\nu\tau}^\perp(-\boldsymbol{k}) = P_{\nu\tau}^\perp(\boldsymbol{k})$ and that $P_{\gamma\sigma}^\perp(\boldsymbol{k})P_{\nu\sigma}^\perp(\boldsymbol{q}) = P_{\gamma\nu}^\perp(\boldsymbol{k})$. Finally, by using the explicit form of $G_{\alpha\beta}(\tilde{\boldsymbol{k}})$ previously derived, one obtains

$$\langle\psi_\alpha(\tilde{\boldsymbol{k}})\psi_\beta(\tilde{\boldsymbol{q}})\rangle_0 = C_{\alpha\beta}(\tilde{\boldsymbol{k}})\hat{\delta}(\tilde{\boldsymbol{k}} + \tilde{\boldsymbol{q}}) \qquad C_{\alpha\beta}(\tilde{\boldsymbol{k}}) = \frac{2\tilde{\Gamma}}{\omega_k^2 + (m + \Gamma k^2)^2}P_{\alpha\beta}^\perp(\boldsymbol{k}) \qquad (5.22)$$

5.2 The field theoretical action

Contrary to what was done in [23], I will here use the Martin-Siggia-Rose/Janssen-De Dominicis (MSRJD) formalism discussed in Chapter 4 to study the near-critical behaviour of the theory and compute the corrections to mean-field. Note however that the two approaches are completely equivalent, and will lead to the same results. Following the MSRJD formalism, one can write a field-theoretical action which reproduces the same statistics of a stochastic Langevin equation - see Chapter 4 for details. The price to do this is the introduction of an auxiliary field $\hat{\boldsymbol{\psi}}$, known as the response field, which acts as a Lagrange multiplier enforcing the primary field $\boldsymbol{\psi}$ to obey the stochastic Langevin dynamics.

The action can be usually written in the form $\mathcal{S} = \mathcal{S}_0 + \mathcal{S}_I$, where $\mathcal{S}_0$ is the Gaussian action, coming from the linear dynamic terms, while $\mathcal{S}_I$ represents the interactions, arising from non-linear dynamics. In the case at hand, these two contributions read

$$\mathcal{S}_0 = \int_{\tilde{\boldsymbol{k}}}\left(-\mathrm{i}\omega_k + m + \Gamma k^2\right)\hat{\psi}_\alpha(-\tilde{\boldsymbol{k}})\psi_\alpha(\tilde{\boldsymbol{k}}) - \tilde{\Gamma}P_{\alpha\beta}^\perp(\boldsymbol{k})\hat{\psi}_\alpha(-\tilde{\boldsymbol{k}})\hat{\psi}_\beta(\tilde{\boldsymbol{k}}) \qquad (5.23)$$

$$\begin{aligned}
\mathcal{S}_I = &-\frac{J}{3}\int_{\tilde{\boldsymbol{k}},\tilde{\boldsymbol{q}},\tilde{\boldsymbol{h}}}Q_{\alpha\beta\gamma\gamma}^\perp(\boldsymbol{k})\hat{\psi}_\alpha(-\tilde{\boldsymbol{k}})\psi_\beta(\tilde{\boldsymbol{q}})\psi_\gamma(\tilde{\boldsymbol{h}})\psi_\nu(\tilde{\boldsymbol{k}} - \tilde{\boldsymbol{q}} - \tilde{\boldsymbol{h}})+ \\
&+\mathrm{i}\frac{v_0\gamma}{2}\int_{\tilde{\boldsymbol{k}},\tilde{\boldsymbol{q}}}Y_{\alpha\beta\gamma}^\perp(\boldsymbol{k})\hat{\psi}_\alpha(-\tilde{\boldsymbol{k}})\psi_\beta(\tilde{\boldsymbol{q}})\psi_\gamma(\tilde{\boldsymbol{k}} - \tilde{\boldsymbol{q}})
\end{aligned} \qquad (5.24)$$

5.2.1 Gaussian theory

Since the RG analysis will be performed using a perturbative expansion in the non-linear dynamic couplings γ and J, it is useful to first review the behaviour of the Gaussian theory. It should be perhaps not surprising that the Gaussian theory presented here reproduces the behaviour of the linear dynamics: in fact, the MSRJD action has been built to reproduce the behaviour of the stochastic Langevin dynamics.

The two correlation functions are given by

$$\langle \psi_\alpha(\tilde{\boldsymbol{k}})\hat{\psi}_\beta(\tilde{\boldsymbol{q}})\rangle_0 = G_{\alpha\beta}(\tilde{\boldsymbol{k}})\hat{\delta}(\tilde{\boldsymbol{k}}+\tilde{\boldsymbol{q}}) \quad G_{\alpha\beta}(\tilde{\boldsymbol{k}}) = \frac{1}{-\mathrm{i}\omega_k + m + \Gamma k^2}\delta_{\alpha\beta}, \qquad (5.25)$$

$$\langle \psi_\alpha(\tilde{\boldsymbol{k}})\psi_\beta(\tilde{\boldsymbol{q}})\rangle_0 = C_{\alpha\beta}(\tilde{\boldsymbol{k}})\hat{\delta}(\tilde{\boldsymbol{k}}+\tilde{\boldsymbol{q}}) \quad C_{\alpha\beta}(\tilde{\boldsymbol{k}}) = \frac{2\tilde{\Gamma}}{\omega_k^2 + (m + \Gamma k^2)^2}P_{\alpha\beta}^\perp(\boldsymbol{k}) \quad (5.26)$$

As one can see, the $\langle\psi\psi\rangle$ correlation function coincides with that of the linear dynamics, while the correlation $\langle\psi\hat{\psi}\rangle$ equals the linear response function of [23]. This is no coincidence as a source field h in the dynamics of ψ enters the action as $\int h\hat{\psi}$, and therefore the response function for small fields is given by $\partial\langle\psi\rangle/\partial h = \langle\psi\hat{\psi}\rangle$. This is the reason why $\hat{\psi}$ is known as the response field. Let me finally note that the $\langle\hat{\psi}\hat{\psi}\rangle$ always vanishes, as in all MSRJD theories, since a $\psi\psi$ term is missing in the action.

Graphically, the two non-vanishing correlation functions are represented by lines joining the two fields in the following way

$$\langle\psi_\alpha\hat{\psi}_\beta\rangle_0 \quad = \quad \longrightarrow\!\!\!\!\!\!\!- \qquad\qquad \langle\psi_\alpha\psi_\beta\rangle_0 \quad = \quad \underline{\qquad}, \qquad (5.27)$$

where the arrows in the propagators point in the direction of the response field $\hat{\psi}$.

5.2.2 Non-linear theory

Non-linear terms play a relevant role in the proximity of the phase transition, where $m \simeq 0$, as fluctuations become so large that linear theory is not enough to predict the large-scale properties. In this incompressible theory, there are two relevant non-linearities, respectively γ and J, which are responsible for mixing the short and long wavelength modes of the $\boldsymbol{\psi}$ field. In the diagrammatic framework, these interactions are graphically represented by Feynman vertices, in which different lines merge, each representing one of the fields involved in the interaction. In the representation I will use here, an *entering* arrow is used to identify the leg representing the response field. Moreover, vertices have opposite signs compared to the associated interaction; the convenience of this choice is that vertices play a crucial role in building Feynman diagrams, which come from the expansion of $\exp(-\mathcal{S}_\mathcal{I})$.

Therefore, incompressible SPMA has only two Feynman vertices, defined as

follows:

$$\hat{\psi}_\alpha(-\tilde{\boldsymbol{k}}) \quad\overset{\psi_\beta(\tilde{\boldsymbol{q}})}{\underset{\psi_\gamma(\tilde{\boldsymbol{p}})}{\bigg\langle}} \qquad : \quad \mathrm{i}\,\frac{v_0\gamma}{2}Y^\perp_{\alpha\beta\gamma}(\boldsymbol{k})\hat{\delta}(\tilde{\boldsymbol{k}}-\tilde{\boldsymbol{q}}-\tilde{\boldsymbol{p}})\ , \qquad (5.28)$$

$$\hat{\psi}_\alpha(-\tilde{\boldsymbol{k}}) \quad\overset{\psi_\beta(\tilde{\boldsymbol{q}})}{\underset{\psi_\gamma(\tilde{\boldsymbol{h}})}{\bigg\langle}}\ \psi_\gamma(\tilde{\boldsymbol{p}}) \quad : \quad -\frac{J}{3}Q^\perp_{\alpha\beta\gamma\nu}(\boldsymbol{k})\hat{\delta}(\tilde{\boldsymbol{k}}-\tilde{\boldsymbol{q}}-\tilde{\boldsymbol{p}}-\tilde{\boldsymbol{h}})\ , \qquad (5.29)$$

The first vertex (5.28) will be called the self-propulsion vertex, as it arises from the ability of the particle to be self-propelled at the microscopic level. This can be seen by the fact that this vertex is proportional to v_0, meaning that when the microscopic speed is sent to $v_0 \to 0$, this self-propulsion vertex vanishes too. This self-propulsion vertex is composed of the usual advective derivative term, proportional to γ, as the anomalous advective terms typical of the Toner and Tu theory, which are introduced because of the Galilean-invariance breaking, vanish as a consequence of incompressibility [23]. The second vertex (5.29) is the standard ferromagnetic relaxation vertex, characteristic of ferromagnetic theories belonging to the $\mathcal{O}(n)$ universality class [2, 3].

5.3 Critical behaviours at the ordering transition

Starting from the action introduced in the previous section, one can perform an RG analysis of the theory in the proximity of the ordering transition, namely near $m \sim 0$. In this regime, modes are massless, and therefore the coupling between short and large wavelength fluctuations induced by the non-linear terms gives rise to non-trivial corrections to the scaling predicted by the linear theory.

5.3.1 Shell integration

To work out these non-trivial corrections, the idea of the momentum shell RG is to integrate little by little the short-wavelength details. As detailed in Chapter 4, this is done by first integrating the short-wavelength modes over the momentum shell $\Lambda/b < |\boldsymbol{k}| < \Lambda$. When these modes are integrated, one is left with a new action $\mathcal{S}^< = \mathcal{S} + \Delta\mathcal{S}$ describing the behaviour of the modes with $|\boldsymbol{k}| < \Lambda/b$. As for the action $\mathcal{S}$, the corrections $\Delta\mathcal{S}$ can be written as the sum of a Gaussian part and an

interacting part, namely $\Delta\mathcal{S} = \Delta\mathcal{S}_0 + \Delta\mathcal{S}_I$, where each contribution takes the form

$$\Delta\mathcal{S}_0 = \int_{\tilde{\boldsymbol{k}}}^{<} \hat{\psi}_\alpha(-\tilde{\boldsymbol{k}})\Sigma_{\alpha\beta}(\tilde{\boldsymbol{k}})\psi_\beta(\tilde{\boldsymbol{k}}) - \hat{\psi}_\alpha(-\tilde{\boldsymbol{k}})\tilde{\Sigma}_{\alpha\beta}(\tilde{\boldsymbol{k}})\hat{\psi}_\beta(\tilde{\boldsymbol{k}})$$

$$\Delta\mathcal{S}_I = -\int_{\tilde{\boldsymbol{k}},\tilde{\boldsymbol{q}}}^{<} V_{\alpha\beta\gamma}^{\hat{\psi}\psi\psi}(\tilde{\boldsymbol{k}},\tilde{\boldsymbol{q}})\hat{\psi}_\alpha(-\tilde{\boldsymbol{k}}-\tilde{\boldsymbol{q}})\psi_\beta(\tilde{\boldsymbol{k}})\psi_\gamma(\tilde{\boldsymbol{q}}) - \tag{5.30}$$

$$-\int_{\tilde{\boldsymbol{k}},\tilde{\boldsymbol{q}},\tilde{\boldsymbol{p}}}^{<} V_{\alpha\beta\gamma\nu}^{\hat{\psi}\psi\psi\psi}(\tilde{\boldsymbol{k}},\tilde{\boldsymbol{q}},\tilde{\boldsymbol{p}})\hat{\psi}_\alpha(-\tilde{\boldsymbol{k}})\psi_\beta(\tilde{\boldsymbol{q}})\psi_\gamma(\tilde{\boldsymbol{p}})\psi_\nu(\tilde{\boldsymbol{k}}-\tilde{\boldsymbol{q}}-\tilde{\boldsymbol{p}})\,.$$

Here all momenta are integrated off-shell, $k < \Lambda/b$, while frequency integrals still run from $-\infty$ to ∞. This is the meaning of the superscript $<$ over the integral sign, which stems for

$$\int_{\tilde{\boldsymbol{k}}}^{<} = \int_{|\boldsymbol{k}|<\Lambda/b} \frac{\mathrm{d}^d k}{(2\pi)^d} \int_{-\infty}^{+\infty} \frac{\mathrm{d}\omega_k}{2\pi} \tag{5.31}$$

The quantities Σ and $\tilde{\Sigma}$ are known as the *self-energies* [40], which contribute to the perturbative corrections of the Gaussian part of the original action, while $V^{\hat{\psi}\psi\psi}$ and $V^{\hat{\psi}\psi\psi\psi}$ are known as *vertex-functions*, and correct the non-linear dynamic couplings. From a diagrammatic point of view, each self-energy and vertex-function is given by the sum of all amputated 1-particle irreducible diagrams with external fields $\hat{\psi}\psi$, $\hat{\psi}\hat{\psi}$, $\hat{\psi}\psi\psi$ and $\hat{\psi}\psi\psi\psi$ respectively. Graphically, they are represented by the blobs in the following diagrammatic scheme

$$\Sigma_{\alpha\beta}(\tilde{\boldsymbol{k}}) \quad : \quad \hat{\psi}_\alpha(-\tilde{\boldsymbol{k}}) \longrightarrow \bigcirc\!\!\!\!\!\diagdown\, \longrightarrow \psi_\beta(\tilde{\boldsymbol{k}}) \tag{5.32}$$

$$\tilde{\Sigma}_{\alpha\beta}(\tilde{\boldsymbol{k}}) \quad : \quad \hat{\psi}_\alpha(-\tilde{\boldsymbol{k}}) \longrightarrow \bigcirc\!\!\!\!\!\diagdown\, \longleftarrow \hat{\psi}_\beta(\tilde{\boldsymbol{k}}) \tag{5.33}$$

$$V_{\alpha\beta\gamma}^{\hat{\psi}\psi\psi}(\tilde{\boldsymbol{k}},\tilde{\boldsymbol{q}}) \quad : \quad \hat{\psi}_\alpha(-\tilde{\boldsymbol{k}}-\tilde{\boldsymbol{q}}) \tag{5.34}$$

$$V_{\alpha\beta\gamma\nu}^{\hat{\psi}\psi\psi\psi}(\tilde{\boldsymbol{k}},\tilde{\boldsymbol{q}},\tilde{\boldsymbol{h}}) \quad : \quad \hat{\psi}_\alpha(-\tilde{\boldsymbol{k}}) \tag{5.35}$$

To compute these self-energies and vertex functions, one can use a perturbative approach, by treating the coupling constants of the non-linear dynamic terms as *small*. This assumption will be justified *a posteriori*, by showing the validity of this

assumption in the proximity of the upper critical dimension $d_c = 4$. To compute the corrections to scaling at first order in $\epsilon = 4 - d$, a diagrammatic approach was used in [23].

At first order in ϵ, the self-energies and the vertex-functions take non-vanishing contributions from the diagrams listed in Appendix A. By expanding at relevant order in k and ω, the self-energies and the vertex-functions take the form

$$\Sigma_{\alpha\beta}(\tilde{\boldsymbol{k}}) = m_0 \, \delta m \, \delta_{\alpha\beta} \ln b + \Gamma_0 \, \delta\Gamma \, \delta_{\alpha\beta} \ln b \qquad\qquad \tilde{\Sigma}_{\alpha\beta}(\tilde{\boldsymbol{k}}) = 0 \,, \tag{5.36}$$

$$\begin{aligned} V^{\hat{\psi}\psi\psi}_{\alpha\beta\gamma}(\tilde{\boldsymbol{k}}, \tilde{\boldsymbol{q}}) &= \frac{v_0\gamma_0}{2} \delta\gamma \, Y^{\perp}_{\alpha\beta\gamma}(\boldsymbol{k}) \ln b \,, \\ V^{\hat{\psi}\psi\psi\psi}_{\alpha\beta\gamma\nu}(\tilde{\boldsymbol{k}}, \tilde{\boldsymbol{q}}, \tilde{\boldsymbol{h}}) &= \frac{J_0}{3} \delta J \, Q^{\perp}_{\alpha\beta\gamma\nu}(\boldsymbol{k}) \ln b \,, \end{aligned} \tag{5.37}$$

where

$$\delta m = \frac{d^2 + d - 2}{d} \frac{\tilde{\Gamma}_0 J_0}{\Gamma_0 m_0} K_d \Lambda^{d-2} \qquad \delta\gamma = -\frac{3d^2 - 8}{d(d+2)} \frac{\tilde{\Gamma}_0 J_0}{\Gamma^2} K_d \Lambda^{d-4} \,, \tag{5.38}$$

$$\delta\Gamma = \frac{d-2}{2d} \frac{\tilde{\Gamma}\gamma^2}{\Gamma^3} K_d \Lambda^{d-4} \qquad \delta J = -\frac{d^3 + 9d^2 + 2d - 12}{d(d+2)} \frac{\tilde{\Gamma}_0 J_0}{\Gamma^2} K_d \Lambda^{d-4} \,. \tag{5.39}$$

Here $K_d = S_d/(2\pi)^d$, with S_d being the surface of the d-dimensional sphere with unity radius. The mass term m has been set to 0 in all the corrections, apart from those to m itself. This is because keeping m in these terms leads to contributions of order at least ϵ^2, which are irrelevant for working out the critical exponents at order ϵ. Finally, for the same reason, one can set $d = 4$ in these corrections, obtaining

$$\delta m = \frac{9}{2} \frac{\tilde{\Gamma}_0 J_0}{\Gamma_0 m_0} K_d \Lambda^{d-2} \qquad\qquad \delta\gamma = -\frac{5}{3} \frac{\tilde{\Gamma}_0 J_0}{\Gamma^2} K_d \Lambda^{d-4} \,, \tag{5.40}$$

$$\delta\Gamma = \frac{1}{4} \frac{\tilde{\Gamma}\gamma^2}{\Gamma^3} K_d \Lambda^{d-4} \qquad\qquad \delta J = -\frac{17}{2} \frac{\tilde{\Gamma}_0 J_0}{\Gamma^2} K_d \Lambda^{d-4} \,. \tag{5.41}$$

The overall effect of the shell integration on the action can be summarised as follows:

$$\mathcal{S}^{<}_0 = \int_{\tilde{\boldsymbol{k}}}^{<} \left(-\mathrm{i}\omega_k + m_0(1 + \delta m \ln b) + \Gamma_0(1 + \delta\Gamma \ln b)k^2 \right) \hat{\psi}\psi - \tilde{\Gamma}_0 P^{\perp} \hat{\psi}^2 \tag{5.42}$$

$$\mathcal{S}^{<}_I = -\mathrm{i}\frac{v_0}{2} \gamma_0 (1 + \delta\gamma \ln b) \int_{\tilde{\boldsymbol{k}}, \tilde{\boldsymbol{q}}}^{<} Y^{\perp} \hat{\psi}\psi^2 + \frac{1}{3} J_0 (1 + \delta J \ln b) \int_{\tilde{\boldsymbol{k}}, \tilde{\boldsymbol{q}}, \tilde{\boldsymbol{h}}}^{<} Q^{\perp} \hat{\psi}\psi^3 \tag{5.43}$$

Here, for the benefit of the reader, I lightened the tensorial structure for easier reading. One can appreciate here how the shell integration affects the action by providing corrections to the bare parameters and couplings of the theory, denoted by a subscript 0. In principle, also corrections to the $-\mathrm{i}\omega_k\hat{\psi}\psi$ and $\tilde{\Gamma}_0\hat{\psi}^2$ might arise. However, in the present case the advection vertex is proportional to $\boldsymbol{k}$, and thus does not contribute to any correction to these terms. Furthermore, corrections from the ferromagnetic interaction are expected to be at least of order ϵ^2 as happens in Model A [40]. Note that the structure of $\mathcal{S}^{<}$ is the same as the original one. Higher order terms in the number of fields or terms with higher powers of k or ω may be generated by this shell integration; however, they turn out to be irrelevant at first-order in ϵ [52].

5.3.2 Rescaling

The second step of the RG consists of the following rescaling of momenta, frequencies and fields,

$$\boldsymbol{k}_b = \boldsymbol{k} b \qquad\qquad \omega_b = \omega b^z \qquad\qquad (5.44)$$

$$\hat{\boldsymbol{\psi}}(\boldsymbol{k}_b, \omega_b) = b^{\chi_{\hat{\psi}}} \hat{\boldsymbol{\psi}}(\boldsymbol{k}, \omega) \qquad\qquad \boldsymbol{\psi}(\boldsymbol{k}_b, \omega_b) = b^{\chi_{\psi}} \boldsymbol{\psi}(\boldsymbol{k}, \omega) \qquad\qquad (5.45)$$

Here the exponent z is called the *dynamical exponent* and it rules the interplay between spatial and temporal scales. Once this transformation is performed, the action recovers its original cutoff Λ.

Note that the scaling dimension of $\hat{\psi}$ can be fixed by requiring that the coefficient in front of the $-\mathrm{i}\omega\hat{\psi}\psi$ term remains equal to unity. Any non-unity coefficient in front of this term would reflect into a coefficient different from one in front of the partial temporal derivative of the ψ field in the Langevin equation (5.12). This coefficient can be easily removed by dividing by it both sides of the equation, which is equivalent to fixing the scaling dimension of $\hat{\psi}$ in the action.

Since the $-\mathrm{i}\omega$ term scales as

$$\int_{\tilde{k}} -\mathrm{i}\omega\hat{\psi}(-\tilde{\boldsymbol{k}})\psi(\tilde{\boldsymbol{k}}) = \int_{\tilde{k}_b} -\mathrm{i}b^{-\chi_{\psi}-\chi_{\hat{\psi}}-d-2z}\omega_b\hat{\psi}(-\tilde{\boldsymbol{k}}_b)\psi(\tilde{\boldsymbol{k}}_b)\,, \qquad\qquad (5.46)$$

The scaling dimension of $\hat{\psi}$ can be fixed to keep

$$-\chi_{\psi} - \chi_{\hat{\psi}} - d - 2z = 0 \Rightarrow \chi_{\hat{\psi}} = -\chi_{\psi} - d - 2z \qquad\qquad (5.47)$$

When all the other terms are concerned, the final action takes the same form as the bare action (5.23)-(5.24), but with renormalized coefficients:

$$m_b = m_0\, b^{\chi_m} \qquad\qquad \chi_m = z + \delta m \qquad\qquad (5.48)$$

$$\Gamma_b = \Gamma_0\, b^{\chi_\Gamma} \qquad\qquad \chi_\Gamma = z - 2 + \delta\Gamma \qquad\qquad (5.49)$$

$$\tilde{\Gamma}_b = \tilde{\Gamma}_0\, b^{\chi_{\tilde{\Gamma}}} \qquad\qquad \chi_{\tilde{\Gamma}} = 2\chi_\psi + d + 3z \qquad\qquad (5.50)$$

$$\gamma_b = \gamma_0\, b^{\chi_\gamma} \qquad\qquad \chi_\gamma = -\chi_\psi - d + \delta\gamma \qquad\qquad (5.51)$$

$$J_b = J_0\, b^{\chi_J} \qquad\qquad \chi_J = -2\chi_\psi + 2d + z + \delta J \qquad\qquad (5.52)$$

5.3.3 Effective couplings and RG flow equations

To carry out the RG flow equations properly, it is useful to focus on a set of effective couplings whose scaling dimension does not depend on the scaling exponents z and χ_ψ. The best choice for this set of couplings is

$$c_v = v_0^2 \frac{\tilde{\Gamma}\gamma^2}{\Gamma^3} K_d \Lambda^{d-4} \qquad\qquad \tilde{u} = \frac{\tilde{\Gamma}J}{\Gamma^2} K_d \Lambda^{d-4} \qquad\qquad \tilde{r} = \frac{m}{\Gamma}\Lambda^{-2} \qquad\qquad (5.53)$$

These three couplings are equivalent to the g_1, g_2 and a couplings of [23]. After an RG transformation, these couplings are modified as follows

$$c_{v,b} = c_{v,0} b^{\chi_{c_v}} \qquad\qquad \chi_{c_v} = 4 - d + 2\delta\gamma - 3\delta\Gamma \qquad\qquad (5.54)$$

$$\tilde{u}_b = \tilde{u}_0 b^{\chi_{\tilde{u}}} \qquad\qquad \chi_{\tilde{u}} = 4 - d + \delta J - 2\delta\Gamma \qquad\qquad (5.55)$$

$$\tilde{r}_b = \tilde{r}_0 b^{\chi_{\tilde{r}}} \qquad\qquad \chi_{\tilde{r}} = 2 + \delta m - \delta\Gamma \qquad\qquad (5.56)$$

It is crucial to notice that the perturbative corrections depend uniquely on these 3 effective couplings. Rewriting them in terms of these newly defined couplings leads to

$$\delta m = \frac{9}{2}\frac{\tilde{u}}{\tilde{r}} \qquad \delta\gamma = -\frac{5}{3}\tilde{u} \qquad \delta\Gamma = \frac{c_v}{4} \qquad \delta J = -\frac{17}{2}\tilde{u}. \qquad (5.57)$$

When many RG iterations are performed, in the thin shell limit $\ln b \to 1^+$, the effective parameters flow according to the following equations

$$\dot{\mathcal{P}} = \beta_{\mathcal{P}} \qquad\qquad\qquad \beta_{\mathcal{P}} = \mathcal{P}\chi_{\mathcal{P}} \qquad (5.58)$$

Where $\beta_{\mathcal{P}}$ is known as the beta-function of $\mathcal{P}$. In the present case, these beta-functions are given by

$$\beta_{c_v} = c_v\left(\epsilon - \frac{10}{3}\tilde{u} - \frac{3}{4}c_v\right) \qquad (5.59)$$

$$\beta_{\tilde{u}} = \tilde{u}\left(\epsilon - \frac{17}{2}\tilde{u} - \frac{1}{2}c_v\right) \qquad (5.60)$$

$$\beta_{\tilde{r}} = \tilde{r}\left(2 - \frac{c_v}{4}\right) + \frac{9}{2}\tilde{u} \qquad (5.61)$$

Critical exponents can be obtained by looking at the large-scale behaviour of these parameters, namely by searching fixed points of the RG flow and looking at the linearised flow in their surroundings. Fixed points can be found by searching for zeros of the beta-functions, namely by setting $\beta_{\mathcal{P}} = 0$. In the present case, four fixed points can be found by analytic inspection of the beta-functions. A plot of the RG flow trajectories, together with the four fixed points, can be found in Fig. 5.1.

Gaussian fixed point. The first is the trivial Gaussian fixed point, where $c_v^* = \tilde{u}^* = 0$. When starting the flow *on* the critical manifold, the mass $\tilde{r}$ flows to $\tilde{r}^* = 0$. At this fixed point, mean-field exponents are found. This fixed point is however unstable whenever $\epsilon > 0$, namely for all $d < 4$.

Dipolar ferromagnet fixed point. When $d < 4$, but activity is switched off by setting $v_0 = 0$, and thus $c_v = 0$, the coupling $\tilde{u}$ flows towards the fixed-point value of $\tilde{u}^* = 2\epsilon/17$, while $\tilde{r} = -9\epsilon/34$. This fixed point, which described the critical relaxation dynamics of a ferromagnet with dipolar interactions [87, 86], is unstable for any *active* perturbation below $d = 4$.

Incompressible stirred fluid fixed point. On the other hand, still for $d < 4$, when $\tilde{u} = 0$ but $c_v \neq 0$, the flow approaches the fixed point $c_v^* = 4\epsilon/3$, which describes the behaviour of turbulent incompressible fluids stirred by a random force at zero wave vector [46]. This fixed point is however unstable to any $\tilde{u}$ perturbation.

Incompressible polar active matter fixed point. Finally, when both activity and alignment interactions are relevant, the stable fixed point is given by that found in [23], where

$$c_v = \frac{124}{11}\epsilon \qquad\qquad \tilde{u}^* = \frac{6}{113}\epsilon \qquad\qquad \tilde{r}^* = -\frac{27}{226}\epsilon. \qquad (5.62)$$

This fixed point is expected to describe the critical behaviour of any incompressible polar active matter system with no conservation laws.
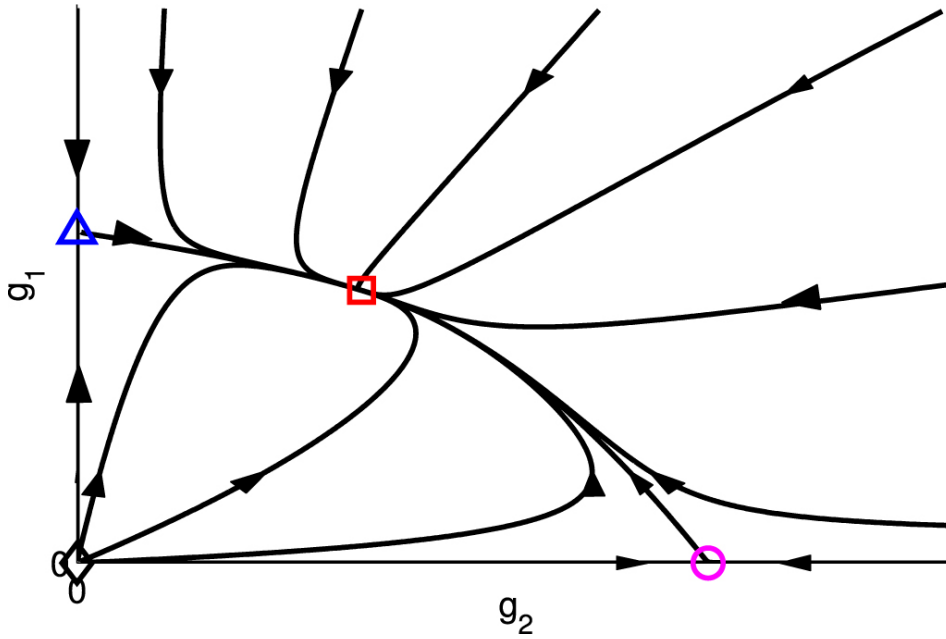
Figure 5.1. Renormalization group flow of the incompressible Toner-Tu theory
[**23**] RG flows on the critical surface. Besides the unstable Gaussian fixed point (black
diamond) and the stable fixed described in Equation (5.62) (red square), there are
two unstable fixed points: one at $c_v^* = 0$, $\tilde{u}^* = 2\epsilon/17$, which is the fixed point of an
isotropic ferromagnet with long-ranged dipolar interactions [86] (purple circle), and one
at $c_v^* = 4\epsilon/3$, $\tilde{u}^* = 0$, which is the fixed point of a fluid forced at zero wavevector (model
B of [46]) (blue triangle). *Permission to reuse granted under the terms of the Creative
Commons Attribution License CC BY 3.0*

5.3.4 Dynamic critical exponent and comparison with swarms

To check whether activity and alignment interactions are sufficient to account for
the collective behaviours observed in swarms, it is important to check whether there
is any agreement between the dynamic critical exponent of swarms with that of the
incompressible Toner and Tu theory.

The dynamic critical exponent of this incompressible theory can be computed by
requiring the relaxation coefficient Γ to remain finite at large scales. This ensures
that the relaxation timescale of the renormalized system remains finite at large
scales. Requiring Γ to remain finite is equivalent to asking for its scaling dimension
χ_Γ to approach zero, hence

$$\chi_\Gamma = 2 - z + \delta\Gamma = 0 \implies z = 2 - \delta\Gamma \tag{5.63}$$

Reminding the explicit form of $\delta\Gamma$, and the fixed point values of the effective couplings
at the incompressible polar active matter fixed point found in the previous section,
one finally obtained

$$z = 2 - \frac{31}{113}\epsilon \tag{5.64}$$

By sending $\epsilon \to 1$, an estimation of the dynamic critical exponent for three-

dimensional systems as swarms can be obtained. This leads to

$$z = 2 - \frac{31}{113} = \frac{195}{113} = 1.72(5) \tag{5.65}$$

Unfortunately, this result is quite far from the value of z in natural swarms, namely $z = 1.37 \pm 0.11$, suggesting some new physical ingredient is necessary to account for the collective behaviours observed in swarms.

One possible explanation of this discrepancy could be that this is an expansion in ϵ that was stopped at first order (one loop), hence maybe the second-order estimate of z could be closer to the experimental value; often second-order calculations are required to get exponents in satisfactory agreement with experiments and/or simulations. Unfortunately, this cannot be the case. Not only does the gap between 1.73 and 1.37 seem far too large to be bridged by a second loop correction, but most importantly this explanation clashes with the numerical evidence. A recent investigation of the near-critical Vicsek model in [69] has reported a dynamic exponent of $z \approx 1.7$, in good agreement with the result predicted by the first-order perturbative RG calculation [23]. This further strengthens the hypothesis that new physics, other than alignment and activity, is required to account for collective behaviours in biological systems as natural swarms.

5.4   Conclusions

The study of the incompressible Toner and Tu theory near criticality performed by Chen, Toner and Lee [23] represents an important stepping stone towards the characterisation of swarming behaviour. Although not in agreement with the experimental value of z observed in natural swarms, the one in [23] is the first successful attempt to characterise the universality class of an active matter system undergoing an ordering transition. To achieve quantitative agreement with experiments, however, some new ingredients must be taken into account. For example, as in the case of equilibrium dynamic critical phenomena [40], the presence of additional conservation laws are expected to give rise to other, new, universality classes of active matter. The development and study of a compelling theory for swarms will represent a crucial part of this thesis, to which I will dedicate Chapters from 7 to 11.

Before proceeding, there is still another issue that needs to be solved. As discussed at the beginning of the present Chapter, there are plenty of valid reasons for which one should expect density fluctuations in natural swarms to be *small*, above all the very observation of scaling laws and the homogeneous spatial profile. Nevertheless, whether the behaviour of homogeneous systems can be described by assuming incompressibility is not a given. Recent numerical simulations suggest homogeneous systems have the same dynamic critical exponent as incompressible ones [69]. On the other hand, in the context of equilibrium systems, the presence of a solenoidal constraint is known to change the universality class, as a consequence of the long-range interactions introduced by it. In the following Chapter, I will precisely try to address this question, by studying a version of the Toner and Tu theory in which density fluctuations are partially suppressed.

Chapter 6

Incompressibility as a tool to study collective homogeneous systems

The Heisenberg model is known to approach the ordered phase through a continuous, second-order, phase transition as the temperature of the system is lowered [3, 15]. However, I explained in Chapter 3 that the presence of self-propulsion makes the phase transition more similar to a first-order one rather than to a second-order one [44, 36, 88]. A naive explanation of why the transition in the Vicsek model is first order may be given by the following argument. In the presence of self-propulsion, particles' movement causes a rewiring of the interaction network, which generates positive feedback between density and velocity fluctuations. This mechanism favours the formation of spatially heterogeneous patterns, such as clusters, when velocity correlations become large, which in turn causes the equilibrium-like second-order behaviour to be replaced into an off-equilibrium first-order phase transition at the onset of collective motion [36, 88].

Despite being self-propelled, natural swarms of insects do not exhibit the expected phenomenology of systems near a first-order transition. Instead, they exhibit near-critical scaling laws, a hallmark of second-order transitions. Similarly, many numerical studies do report scaling behaviour in the near-ordering Vicsek model [42, 83, 69]. How can these observations be compatible with the first-order phenomenology expected from the linear instability of the ordered state I reported in Chapter 3? To answer this question, together with my former fellow PhD student Dr Luca Di Carlo, I studied the near-ordering behaviour of a version of the Toner and Tu theory in which density fluctuations are not conserved, known as Malthusian Toner and Tu theory. In [MyPaper2] we reported the presence of a crossover between two very distinct behaviours: a second-order phenomenology is observed at finite sizes, while in the large-size limit, the first-order behaviour is recovered. Remarkably, the finite-size behaviour of this Malthusian theory is ruled by the incompressible universality class discovered in [23]. These results not only confirm that finite-size systems might exhibit a second-order phenomenology [69] but also show that incompressibility becomes more than a simplifying hypothesis when characterising the behaviour of these systems.

6.1   Introducing fast density fluctuations

From a theoretical perspective, the large-scale properties of the Vicsek model are captured by its corresponding hydrodynamic theory: the celebrated Toner and Tu (TT) theory [20]. In the seminal paper [23] by Chen, Toner and Lee, the authors realised that the phase transition is however second-order if density fluctuations are *completely* suppressed, namely if the system is incompressible. As I showed in Chapter 5, an RG approach to the Toner and Tu theory in the incompressible limit allows one to find a novel non-equilibrium fixed-point that rules the critical dynamics of incompressible active matter [23]. This study revealed that although activity is an important feature and changes the critical dynamics, it is not responsible *per se* for turning the phase transition from second to first order. A feedback mechanism between density and velocity fluctuations seems to be a *fundamental ingredient* to explain the first-order phenomenology of the transition [89].

The results of [23] represent an important stepping stone in the understanding of why so many studies did report scaling laws in active matter systems. In fact, neither the numerical simulations performed by Vicsek et. al. in [42] nor experimental data of natural swarms of insects [12] seem to exhibit spatial clustering of any kind. This suggests that to understand why a second-order phenomenology is observed in finite-size active matter systems, the following question should be addressed: when do density fluctuations become strong enough to turn a second-order transition into an off-equilibrium first-order one?

To understand how the interplay between density and velocity fluctuations renders the phase transition first order, one would have to study the Toner and Tu theory in its near-ordering regime. However, precisely because of the presence of velocity-density couplings, this is not a piece of cake; and, from a mere technical point of view, many things could go wrong with trying to study the Toner and Tu theory in its critical phase. In the present Chapter, instead of the Toner and Tu theory I study a modification of it, namely the Malthusian Toner and Tu (MTT) theory [45], in its near-ordering phase [MyPaper2], which has never been done before.

The peculiarity of this MTT theory is that individuals reproduce and die. When this happens, the total density is not conserved and its local fluctuations quickly relax to a steady-state determined by the local velocity field. Apart from very fast transients, which may be neglected in the hydrodynamic limit, the density field is therefore *enslaved* to the velocity field. The density is therefore not an independent hydrodynamic variable, and thus the hydrodynamic behaviour of the velocity completely ignores density fluctuations. In this sense, the MTT theory can be viewed as analogue to an infinitely compressible limit of the TT theory.

Nevertheless, the MTT theory can be viewed as a case in which density fluctuations are partially suppressed: they are neither strictly constant, as in the ITT theory, nor they are an hydrodynamic variable, as in the TT theory. The density instead does fluctuate around a local steady-state value, but because of the lack of mass conservation, it relaxes *quickly*. In this sense, from the point of view of the strength of density fluctuations, the MTT theory poses in between the ITT theory and the TT theory. The MTT theory is easy enough to be tackled with perturbative renormalization group techniques; furthermore, recent numerical simulations [90] showed that the homogeneous flocking state is metastable, suggesting that the MTT

is rich enough to give rise to a phenomenology qualitatively different from the one of the incompressible Toner and Tu theory.

Note that by no means I am suggesting that in systems as natural swarms midges are born and die *while* flying: while this Malthusian theory might be relevant to describe other kinds of systems, it is not expected to be suitable to correctly describe swarms. However, this will serve as an important theoretical study case to understand the relevance of density fluctuations near the phase transition and shed light on how finite-size compressible systems exhibit scaling laws when approaching the phase transition.

6.1.1   The hydrodynamic equations

The Malthusian Toner and Tu theory, introduced by J. Toner in [45], is a model for self-propelled agents that reproduce and die. In its hydrodynamic description, the equations of motion (EOM) for the direction of motion field $\boldsymbol{\psi}$ and the density field ρ are [45]:

$$\partial_t \boldsymbol{\psi} + v_0 \gamma_v \left(\boldsymbol{\psi} \cdot \nabla \right) \boldsymbol{\psi} = \Gamma \nabla^2 \boldsymbol{\psi} - \Gamma \frac{\delta V}{\delta \boldsymbol{\psi}} - \nabla \mathcal{P} + \sqrt{2\tilde{\Gamma}} \, \boldsymbol{\theta} + \dots \tag{6.1}$$

$$\partial_t \rho + v_0 \nabla \left(\rho \, \boldsymbol{\psi} \right) = g(\rho) \tag{6.2}$$

The equation for $\boldsymbol{\psi}$ is the same as in the TT theory, where P is a pressure term, $\boldsymbol{\theta}$ is Gaussian white noise with variance $2\tilde{\Gamma}$, and $(\boldsymbol{\psi} \cdot \nabla)\boldsymbol{\psi}$ is the material derivative accounting for self-advection [43]. Dots stand for the possible presence of other, non-standard advective terms as those discussed in Chapter 3.

The force term $\boldsymbol{F}(\boldsymbol{\psi}) = -dV/d\boldsymbol{\psi}$ is responsible for the order/disorder phase transition, and it arises from the imitation/ferromagnetic interaction, encoded in the choice of V as a Landau potential, given by

$$V = \int \mathrm{d}^d x \, \frac{r}{2} \boldsymbol{\psi}^2 + \frac{u}{4} \boldsymbol{\psi}^4 \tag{6.3}$$

As in Model A and TT theory, the state of the system depends on the values of r and u [27]. While the coupling u must be positive - otherwise the potential V would be unbounded - the sign of r determines, at the mean-field level, whether or not the system is in a polarised phase $\langle \boldsymbol{\psi} \rangle \neq 0$. Precisely, if $r < 0$ the average polarisation of the system is non-zero,

$$r > 0 \implies \langle \boldsymbol{\psi} \rangle = 0$$

$$r < 0 \implies \langle \boldsymbol{\psi} \rangle = \sqrt{\frac{|r|}{u}} \tag{6.4}$$

6.1.2   Birth and death processes

The main difference with the *immortal* Toner and Tu theory lie in the presence of the $g(\rho)$ term in the equation for the density, which accounts for the birth/death process [45, 91]. This $g(\rho)$ term represents the net, local growth rate of the density field in the absence of motion. Before trying to understand how this affects collective

motion, let me first focus on what happens in the absence of self-propulsion, namely when $v_0 = 0$. In this case, the density's dynamics simply becomes

$$\partial_t \rho = g(\rho) \,, \tag{6.5}$$

Which also represents a sort of mean-field equation for the local density.

But what is a possible form of g? A very basic case is that in which individuals die at a given fixed rate α and are spawned in random positions at some rate λ. The process give $g(\rho) = -\alpha\rho + \lambda$, describing the following mean-field density dynamics

$$\partial_t \rho = -\alpha\rho + \lambda \tag{6.6}$$

The only steady-state solution in this case is given by $\rho_0 = \lambda/\alpha$, and since $g'(\rho) \equiv -\alpha$, this state turns out to be stable at mean-field level. If the local density is $\rho < \rho_0$ or $\rho > \rho_0$, it will relax back to the steady-state with a non-hydrodynamic time scale of $\tau_\rho = \alpha^{-1}$.

Other more complicated death and birth processes are of course possible. Whenever these processes rely on the realistic hypothesis that population growth is limited by the finiteness of resources, then $\lim_{\rho \to \infty} g(\rho) < 0$. This is because positive g at large ρ would lead to uncontrolled population growth. If the population does not go extinct, this is because there is some steady-state value $\rho_0 \neq 0$ at which $g(\rho) = 0$. Although this is often called *active* state, this name would be misleading in the present contest, in which activity is referred to self-propulsion. Absorbing phase transitions usually occur when $\rho_0 \to 0$, however, I am here interested only in cases where ρ_0 is far from 0.

For ρ_0 to be a stable steady-state, the following conditions are required

$$g(\rho_0) = 0 \qquad\qquad g'(\rho_0) < 0 \,. \tag{6.7}$$

Therefore, near to ρ_0 the function $g(\rho)$ acts as a harmonic restoring force, $\partial_t \rho = g'(\rho_0)\delta\rho$, with $\delta\rho = \rho - \rho_0$. At first glance, the birth/death mechanism seems to further complicate the problem, but it is a significant simplification. Because of the term $g(\rho)$, density is not a conserved field [45]. For *conserved* quantities, fluctuations of large wave-vectors $\boldsymbol{k}$ relax on timescales proportional to powers of $|\boldsymbol{k}|$, meaning that sufficiently smooth fluctuations might take ages to relax to their steady-state. On the other hand, *non-conserved* density fluctuations relax on finite time scales, regardless of their wave-vector. In this Malthusian case, the field ρ stops from being an independent hydrodynamic variable [26], and can be likely dropped from the large-scale description.

Note that when $v_0 \neq 0$, the presence of the density-velocity coupling in (6.2) slightly changes this picture. While the steady state of ρ is still expected to be ρ_0, fluctuations $\delta\rho$ will not relax quickly to 0. To see this, let me expand (6.2) at linear order in the fluctuations:

$$\partial_t \delta\rho + v_0 \rho_0 \nabla \cdot \boldsymbol{\psi} = g'(\rho_0)\delta\rho \tag{6.8}$$

Near-ordering, $\boldsymbol{\psi}$ is known to relax on hydrodynamic time scales, which are much slower than the relaxation time scale of $\delta\rho$. Assuming this scale separation, one can

consider $\boldsymbol{\psi}$ spatial fluctuations to be *frozen* on the short time scales of $\delta\rho$ dynamics. Therefore, $\delta\rho$ will not relax to 0, but to [45, 92]

$$\delta\rho(\boldsymbol{x}, t) = -\frac{\rho_0 v_0}{|g'(\rho_0)|} \nabla \cdot \boldsymbol{\psi}(\boldsymbol{x}, t) \tag{6.9}$$

This equation *enslaves* density fluctuations $\delta\rho$ to fluctuations of the order parameter $\boldsymbol{\psi}$, making it possible to get rid of the former when attempting to describe large-scale fluctuations of the latter.

6.1.3 Non-galilean invariant interactions

Before explicitly deriving the EOM, a remark is in order. In general, the TT theory breaks Galilean invariance [43, 27, 76], and the Malthusian TT theory is no exception. Galilean invariance is the symmetry under a change of reference frame, and it is defined by the following transformation [43]:

$$\boldsymbol{x}' = \boldsymbol{x} + v_0 \bar{\psi} t \qquad t' = t \qquad \boldsymbol{\psi}' = \boldsymbol{\psi} + \bar{\psi} \tag{6.10}$$

implying that the derivatives in the new reference frame $(\nabla', \partial_{t'})$ are different from the derivates in the old reference frame (∇, ∂_t) :

$$\nabla' = \nabla \qquad \partial_{t'} = \partial_t - v_0 \bar{\psi} \cdot \nabla \tag{6.11}$$

The force term $\boldsymbol{F}(\boldsymbol{\psi})$ breaks explicitly Galilean invariance, and the TT theory is not invariant under the transformation (6.117). In the hydrodynamic approach, symmetries determine which terms are allowed in the equation [1, 3], and particularly in Galilean-invariant theories the only allowed term, with one derivative and two fields, is $\boldsymbol{\psi} \cdot \nabla\boldsymbol{\psi}$ [43]. Conversely, in a theory with broken Galilean invariance, as the TT theory, one must include all the possible terms with one derivative and two fields, namely $\boldsymbol{\psi}\nabla \cdot \boldsymbol{\psi}$ and $\nabla\psi^2$ [76]. I anticipate that, as will be later shown, even if I did not consider these terms the RG would generate them spontaneously, suggesting that indeed they must be included in the theory.

The first of these two terms can be interpreted as a density-dependent alignment force [93]. To understand this, let me write explicitly Eq. (6.1):

$$\partial_t \boldsymbol{\psi} + v_0 \gamma_v (\boldsymbol{\psi} \cdot \nabla) \boldsymbol{\psi} = \Gamma \nabla^2 \boldsymbol{\psi} - m\boldsymbol{\psi} - J |\boldsymbol{\psi}|^2 \boldsymbol{\psi} - \nabla\mathcal{P} + \sqrt{2\tilde{\Gamma}} \,\boldsymbol{\theta} \tag{6.12}$$

Where I defined $m = \Gamma r$ and $J = \Gamma u$. By assuming that the aligning force depends also on the local density, the *mass m* might take the form

$$m(\rho) = m_0 + m'(\rho_0)\delta\rho \ \ . \tag{6.13}$$

Using the relation (6.9), I can write the term $m\boldsymbol{\psi}$ in the equation of ψ as

$$m(\rho)\boldsymbol{\psi} = m(\rho_0)\boldsymbol{\psi} - m'(\rho_0)\frac{\rho_0 v_0}{|g'(\rho_0)|} (\nabla \cdot \boldsymbol{\psi}) \boldsymbol{\psi} \tag{6.14}$$

where the second term reproduces the expected structure $\boldsymbol{\psi}\nabla \cdot \boldsymbol{\psi}$.

The second non-Galilean-invariant term can be interpreted as a non-linear pressure term, of the kind $\mathcal{P} \sim -v_0 \gamma_3 \boldsymbol{\psi}^2$, which would lead to the following pressure force:

$$-\nabla\mathcal{P}(\rho, \boldsymbol{\psi}) = -\nabla\mathcal{P}(\rho) + v_0 \gamma_3 \nabla\boldsymbol{\psi}^2 \tag{6.15}$$

which reproduces the structure of the second non-Galilean-invariant term, $\nabla\boldsymbol{\psi}^2$.

6.1.4   Pressure forces

The last step needed to derive an EOM for the velocity alone is an explicit expression for the pressure force $\nabla \mathcal{P}$. Following standard literature on active matter [27], the pressure term $\mathcal{P}$ can be expressed as a series in powers of density fluctuations:

$$\mathcal{P}(\rho) = \sum_{n=1} \sigma_n \delta \rho^n \ . \tag{6.16}$$

Using equation (6.9), at the leading order in the fluctuations the pressure force reduces to

$$\mathcal{P} \simeq \sigma_1 \delta \rho = -\sigma_1 \frac{\rho_0 v_0}{|g'(\rho_0)|} \nabla \cdot \boldsymbol{\psi} \ . \tag{6.17}$$

6.2   The Malthusian Toner and Tu theory

Finally, I am ready to write down the final EOM for the Malthusian Toner and Tu theory. This is an equation for the direction of motion only, since the relation (6.9) *enslaves* density fluctuations to velocity fluctuations. Taking into account all the dynamic terms discussed in the previous paragraphs, the dynamics of the direction of motion field in the MTT theory is described by the following EOM:

$$\begin{aligned}
\partial_t \boldsymbol{\psi} + v_0 \gamma_1 \left(\boldsymbol{\psi} \cdot \nabla\right) \boldsymbol{\psi} + v_0 \gamma_2 \boldsymbol{\psi} \left(\nabla \cdot \boldsymbol{\psi}\right) + v_0 \gamma_3 \nabla \left(\psi^2\right) = \\
= \Gamma \nabla^2 \boldsymbol{\psi} + \Gamma_2 \nabla(\nabla \cdot \boldsymbol{\psi}) - \left(m + J\,\psi^2\right) \boldsymbol{\psi} + \sqrt{2\widetilde{\Gamma}}\,\boldsymbol{\theta}
\end{aligned} \tag{6.18}$$

Where $\boldsymbol{\theta}$ is a Gaussian white noise with unitary variance, namely

$$\langle \theta_\alpha(\boldsymbol{x}, t) \theta_\beta(\boldsymbol{y}, s) \rangle = \delta_{\alpha\beta} \delta^d(\boldsymbol{x} - \boldsymbol{y}) \delta(t - s) \tag{6.19}$$

Note that I obtained an EOM for the sole velocity field; however, a relic of the coupling with density is hidden in the parameters γ_2 and Γ_2, given by

$$\gamma_2 = m'(\rho_0) \frac{\rho_0}{|g'(\rho_0)|} \qquad\qquad \Gamma_2 = \sigma_1 \frac{\rho_0}{|g'(\rho_0)|} \tag{6.20}$$

A final remark is in order: both Eq. (6.18) and the equation of motion of the incompressible theory [23] can be obtained by taking the Toner and Tu theory of Chapter 3 and *dropping* the equation for the density. The real technical difference between the two cases resides in the fact that in the incompressible case, the velocity field is also constrained to be divergence-free. In this sense, both the incompressible theory and the MTT theory lack an associated hydrodynamic equation for the density. Nevertheless, in the MTT the density is not constant, as density fluctuations can always be computed through equation (6.9).

6.2.1   Linear theory

I will now analyse the linearised equations of motion. This will turn out to be necessary for two reasons. The first is that it serves as a starting point for the renormalization group study I will perform later on. The core idea of the perturbative RG is to perform an expansion in small non-linear couplings. Therefore, the linear

(free) theory will represent the expansion point of my RG analysis. The second is that, within this linear theory, one can better understand *how* to properly recover the incompressible limit.

The linear theory is obtained by setting to zero all the non-linear terms, $\gamma_i = 0$, $J = 0$, in the equation of motion (6.18). In Fourier space, hence using the variables $\boldsymbol{k}$ and t, the linearised equation of motion is:

$$\partial_t \boldsymbol{\psi} = -m\boldsymbol{\psi} - \Gamma k^2 \boldsymbol{\psi} - \sigma_1 \frac{v_0 \rho_0}{|g'(\rho_0)|} \boldsymbol{k}\,(\boldsymbol{k} \cdot \boldsymbol{\psi}) + \sqrt{2\tilde{\Gamma}}\,\boldsymbol{\theta} \tag{6.21}$$

where the real-space fields can be recovered via

$$\phi(\boldsymbol{x}) = \int_{\boldsymbol{k}} e^{i\boldsymbol{x}\cdot\boldsymbol{k}} \phi(\boldsymbol{k})\ . \tag{6.22}$$

Here and in the following, I will – as usual – use the notation,

$$\int_{\boldsymbol{k}} = \int\limits_{|\boldsymbol{k}|<\Lambda} \frac{\mathrm{d}^d k}{(2\pi)^d} \tag{6.23}$$

In equation (6.21), one can distinguish two different types of terms: relaxation terms that are in the same direction of the field $\boldsymbol{\psi}(\boldsymbol{k})$, and pressure-like terms that are always in the direction of the wave vector $\boldsymbol{k}$. Because of this, the dynamics of the Fourier transformed fields $\boldsymbol{\psi}^{\parallel}(\boldsymbol{k},t)$ and $\boldsymbol{\psi}^{\perp}(\boldsymbol{k},t)$ are different, where $\boldsymbol{\psi}^{\parallel}$ and $\boldsymbol{\psi}^{\perp}$ are respectively the component of $\boldsymbol{\psi}(\boldsymbol{k},t)$ parallel and orthogonal to the wave vector $\boldsymbol{k}$. Note that, since the $\boldsymbol{k}$-space analogue of equation (6.9) links density fluctuations to $\boldsymbol{k} \cdot \boldsymbol{\psi} = k\psi^{\parallel}$, this means that density fluctuations are present only if $\psi^{\parallel}$ fluctuations are not suppressed.

For this reason it is practical to introduce the transverse $P_{\alpha\beta}^{\perp}(k)$ and longitudinal $P_{\alpha\beta}^{\parallel}(k)$ projection operators,

$$P_{\alpha\beta}^{\perp}(\boldsymbol{k}) = \delta_{\alpha\beta} - \frac{k_\alpha k_\beta}{k^2} \qquad\qquad P_{\alpha\beta}^{\parallel}(\boldsymbol{k}) = \frac{k_\alpha k_\beta}{k^2}\ . \tag{6.24}$$

In this way, the $\boldsymbol{\psi}^{\parallel}$ and $\boldsymbol{\psi}^{\perp}$ modes are simply given by

$$\psi_\alpha^{\perp} = P_{\alpha\beta}^{\perp}(\boldsymbol{k})\psi_\alpha \qquad\qquad \psi_\alpha^{\parallel} = P_{\alpha\beta}^{\parallel}(\boldsymbol{k})\psi_\alpha\ . \tag{6.25}$$

Using (6.24), the equation of motion (6.21) can be written as,

$$\partial_t \psi_\alpha = -(m + \Gamma^{\perp} k^2) P_{\alpha\beta}^{\perp} \psi_\beta - (m + \Gamma^{\parallel} k^2) P_{\alpha\beta}^{\parallel} \psi_\beta + \sqrt{2\tilde{\Gamma}}\theta_\alpha\,, \tag{6.26}$$

where $\Gamma^{\perp} = \Gamma$ and $\Gamma^{\parallel} = \Gamma + \Gamma_2$ are the transverse and longitudinal kinetic coefficients respectively. This makes it more evident that longitudinal and transverse fluctuations behave differently. Intuitively, since longitudinal fluctuations are coupled to density fluctuations, as shown in equation (6.9), they relax faster than transverse fluctuations and $\Gamma^{\parallel} > \Gamma^{\perp}$.

Solving Eq. (6.26) is easier when it is written in frequency space. This is because in frequency space the temporal derivative is transformed according to $\partial_t \to -i\omega$. The solution for $\boldsymbol{\psi}$ can be therefore easily computed and leads to

$$\psi_\alpha(\boldsymbol{k},\omega) = \sqrt{2\tilde{\Gamma}} G_{\alpha\beta}(\boldsymbol{k},\omega)\theta_\alpha(\boldsymbol{k},\omega)\,, \tag{6.27}$$

Note that the field in real space-time can be computed through an inverse Fourier transformation, given by

$$\phi\left(\boldsymbol{x}, t\right) = \int_{\boldsymbol{k}} \int_{-\infty}^{+\infty} \frac{\mathrm{d}\omega}{2\pi} \mathrm{e}^{-\mathrm{i}\omega t + \mathrm{i}\boldsymbol{x}\cdot\boldsymbol{k}} \phi\left(\boldsymbol{k}, \omega_k\right) \ . \tag{6.28}$$

In Eq. (6.27), the tensor $G_{\alpha\beta}(\boldsymbol{k}, \omega)$ is the bare linear response function of $\boldsymbol{\psi}$, which quantifies variations of $\boldsymbol{\psi}$ in the presence of *small* external fields. This linear response function is given by

$$G_{\alpha\beta}(\boldsymbol{k}, \omega) = G_0^{\perp}(\boldsymbol{k}, \omega) P_{\alpha\beta}^{\perp}(\boldsymbol{k}) + G_0^{\parallel}(\boldsymbol{k}, \omega) P_{\alpha\beta}^{\parallel}(\boldsymbol{k}) \tag{6.29}$$

$$G_0^{\perp,\parallel}(\boldsymbol{k}, \omega) = \frac{1}{-i\omega + \Gamma^{\perp,\parallel} k^2 + m} \tag{6.30}$$

Notice that the response function naturally decomposes in a longitudinal $G_0^{\parallel}$ and orthogonal $G_0^{\perp}$ component to $\boldsymbol{k}$. These two response functions precisely represent the response function of the $\psi^{\parallel}$ and $\psi^{\perp}$ modes respectively.

In the case of Eq. (6.27), the behaviour of $\boldsymbol{\psi}$ is completely determined once the noise is specified. Here, the noise is assumed to be a white Gaussian noise with zero mean and variance

$$\langle\theta_{\alpha}(\boldsymbol{k}, \omega_k)\theta_{\beta}(\boldsymbol{q}, \omega_q)\rangle = (2\pi)^d \delta_{\alpha\beta}\delta^d(\boldsymbol{k} + \boldsymbol{q})\delta(\omega_k + \omega_q)\,, \tag{6.31}$$

Note that this variance is precisely the Fourier-space analogue of Eq. (6.19). The knowledge of the noise variance allows one to easily compute the velocity-velocity correlations. To do this, let me recall that the correlations are given by

$$\langle\psi_{\alpha}(\boldsymbol{k}, \omega_k)\psi_{\beta}(\boldsymbol{q}, \omega_q)\rangle = 2\tilde{\Gamma} G_{\alpha\gamma}(\boldsymbol{k}, \omega_k)G_{\beta\nu}(\boldsymbol{q}, \omega_q)\langle\theta_{\alpha}(\boldsymbol{k}, \omega_k)\theta_{\beta}(\boldsymbol{q}, \omega_q)\rangle\,. \tag{6.32}$$

By reminding the form of the noise-variance (6.19), it is straightforward to compute the correlations, finding that

$$\langle\psi_{\alpha}(\boldsymbol{k}, \omega_k)\psi_{\beta}(\boldsymbol{q}, \omega_q)\rangle = C_{\alpha\beta}(\boldsymbol{k}, \omega)(2\pi)^d \delta_{\alpha\beta}\delta^d(\boldsymbol{k} + \boldsymbol{q})\delta(\omega_k + \omega_q) \tag{6.33}$$

$$C_{\alpha\beta}(\boldsymbol{k}, \omega) = 2\tilde{\Gamma} G_{\alpha\gamma}^0(\boldsymbol{k}, \omega)G_{\beta\nu}^0(-\boldsymbol{k}, -\omega) \tag{6.34}$$

Similarly to the response function G, also $C_{\alpha\beta}^0(\boldsymbol{k}, \omega)$ can be decomposed in a longitudinal and orthogonal component to $\boldsymbol{k}$, namely

$$C_{\alpha\beta}(\boldsymbol{k}, \omega) = C_0^{\perp}(\boldsymbol{k}, \omega) P_{\alpha\beta}^{\perp}(\boldsymbol{k}) + C_0^{\parallel}(\boldsymbol{k}, \omega) P_{\alpha\beta}^{\parallel}(\boldsymbol{k}) \tag{6.35}$$

$$C_0^{\perp,\parallel}(\boldsymbol{k}, \omega) = \frac{2D_0}{\omega^2 + (\Gamma_0^{\perp,\parallel} \boldsymbol{k}^2 + m_0)^2} \ . \tag{6.36}$$

Note that expressions (6.30) and (6.36) can also be obtained through the Martin-Siggia-Rose formalism detailed in Chapter 4.

6.2.2 Recovering the incompressible limit

To address the relevance of density fluctuations $\delta\rho$, one must understand the strength of their correlations. As I pointed out, even if one removed density from the equation of motion of velocity, density is still a fluctuating field. Larger correlations might lead to heterogeneous spatial structures, while incompressible behaviour is expected to be recovered when these correlations become small. To compute this correlation function, I can once again make use of Eq. (6.9), linking fluctuations of ρ to those of $\boldsymbol{\psi}$. The density-density correlation function can be therefore written as

$$\langle \rho(\boldsymbol{k},\omega_k)\rho(\boldsymbol{q},\omega_q)\rangle = -\left(\frac{\rho_0 v_0}{|g'(\rho_0)|}\right)^2 q_\alpha k_\beta \langle \psi_\alpha(\boldsymbol{k},\omega_k)\psi_\beta(\boldsymbol{q},\omega_q)\rangle \tag{6.37}$$

Using the explicit form of velocity-velocity correlations, given by Eq. (6.33), one can finally obtain the form of the density correlations, given by

$$\langle \rho(\boldsymbol{k},\omega_k)\rho(\boldsymbol{q},\omega_q)\rangle = C_{\rho\rho,0}(\boldsymbol{k},\omega)(2\pi)^d \delta_{\alpha\beta}\delta^d(\boldsymbol{k}+\boldsymbol{q})\delta(\omega_k+\omega_q)\,, \tag{6.38}$$

$$C_{\rho\rho,0}(\boldsymbol{k},\omega) = \left(\frac{\rho_0 v_0}{|g'(\rho_0)|}\right)^2 \frac{2\tilde{\Gamma}\,k^2}{\omega^2 + (\Gamma^\parallel k^2 + m)^2}\,. \tag{6.39}$$

By looking at the poles of the correlation function of the (linear) theory, it is possible to understand on what time scales the system is relaxing. These poles are

$$\omega_\perp(k) = \pm\mathrm{i}(m + \Gamma^\perp k^2) \tag{6.40}$$

$$\omega_{\parallel/\rho}(k) = \pm\mathrm{i}(m + \Gamma^\parallel k^2) \tag{6.41}$$

Here $\omega_\perp$ are the poles of the transverse correlation function $C_0^\perp$, while $\omega_\parallel$ are the poles of the longitudinal correlation function $C_0^\parallel$. Poles ω_ρ of the density correlation function $C_{\rho\rho,0}$ are equal to $\omega_\parallel$, since the two fluctuations are linked by Eq. (6.9). The time scale over which these correlations relax is given by the inverse of the imaginary part of the pole. Near criticality, where $m \approx 0$, density fluctuations relax slower when $\Gamma^\parallel > \Gamma^\perp$. When $\Gamma^\parallel \ll \Gamma^\perp$, on the other hand, density fluctuations (as well as longitudinal $\psi^\parallel$ fluctuations) relax much faster than the transverse $\psi^\perp$ fluctuations, hence becoming irrelevant.

The important parameter, ruling the relevance of density fluctuations, is therefore given by the ratio between the transverse and longitudinal kinetic coefficients,

$$\mu = \frac{\Gamma^\parallel}{\Gamma^\perp} = 1 + \sigma_1 \frac{\rho_0}{|g'(\rho_0)|\Gamma} \quad . \tag{6.42}$$

At the linear level, the MTT theory becomes equivalent to the ITT when $\mu \to \infty$, namely when $\Gamma^\parallel \gg \Gamma^\perp$. In this regime, both bare correlation and response functions of the longitudinal mode vanish, which means that as in incompressible theories, the field fluctuates only in the transverse direction [23, 46]. To further convince ourselves that $\mu = \infty$ corresponds to the incompressible regime, I recall that the difference between longitudinal and transverse kinetic coefficients arises from the pressure force $\mathcal{P} \simeq \sigma_1 \delta\rho$, where σ_1 is proportional to the inverse compressibility χ:

$$\chi = \frac{1}{\rho}\frac{\partial\rho}{\partial\mathcal{P}}\bigg|_{\rho_0} = \frac{1}{\rho_0}\frac{\partial\delta\rho}{\partial\mathcal{P}}\bigg|_{\delta\rho=0} = \frac{1}{\rho_0\sigma_1} \tag{6.43}$$

Since ρ_0 is finite, a system is incompressible ($\chi = 0$) if $\sigma_1 \to \infty$, which corresponds to $\mu \to \infty$. The parameter μ plays an important role in ruling the relevance of density fluctuations not only in the linear theory but also at the non-linear level. The renormalization group analysis of Sec. 6.3 will reveal that the phase transition is second-order in the $\mu \to \infty$ limit, with a large-scale behaviour ruled by the incompressible universality class found in [23], namely with $z = 1.73$ in $d = 3$.

The question of whether this $\mu \to \infty$ fixed point is stable or not naturally arises. In other words, one may wonder whether a system with very small, but non-zero compressibility χ will still be ruled by the $\mu \to \infty$ fixed point in the large-size limit. To answer this question, naive scaling analysis is not enough. In fact, by simple power-counting, one can convince themselves that $\Gamma^{\perp/\parallel}$ must have the same scaling dimensions, and hence μ has a scaling dimension of 0. Non-linear effects are therefore crucial to address this question. This will be done in Sec. 6.4, where I will show that this incompressible fixed point is indeed unstable against density fluctuations.

6.2.3 The field-theoretical action of MTT

To prepare the RG analysis that will be performed in the next Section, I will hereby use a Martin-Siggia-Rose/Janssen-De Dominicis (MSRJD) formalism [1], a standard technique that allows writing a stochastic differential equation as a field theory, formulated using path integrals. This path integral representation will be the starting point of the renormalization group computation.

The details of the MSRJD formalism can be found in Chapter 4.2, but let me review it very quickly here. Let ϕ be a field whose dynamics is ruled by a stochastic differential equation, determined by a deterministic evolution operator $\mathcal{F}$ and a Gaussian noise θ with zero mean and $2D_{\alpha\beta}$ variance,

$$\mathcal{F}[\phi] - \theta = 0 \quad , \tag{6.44}$$

Then, the same statistics of this stochastic PDE – i.e. its correlation and response functions – is reproduced by the field-theoretical action

$$\mathcal{S}[\hat{\phi}, \phi] = \int \mathrm{d}^d x \mathrm{d}t \left[\hat{\phi}_\alpha \mathcal{F}_\alpha[\phi] - \hat{\phi}_\alpha D_{\alpha\beta} \hat{\phi}_\beta \right] \quad , \tag{6.45}$$

where averages $\langle \cdot \rangle$ are performed over the pseudo-probability distribution $\mathcal{P}[\hat{\phi}, \phi] = e^{-\mathcal{S}}$. The auxiliary field $\hat{\phi}$ is known as *response field*, since the response function $G(\tilde{k})$, computed in the previous section, can be written as [94]:

$$\langle \hat{\phi}_\alpha(\tilde{k}) \phi_\beta(\tilde{q}) \rangle = G_{\alpha\beta}(\tilde{k}) \hat{\delta}(\tilde{k} + \tilde{q}) \quad , \tag{6.46}$$

To compact the notation, I defined $\tilde{k}$ and $\tilde{\delta}(\tilde{k})$ as follows:

$$\tilde{k} = (k, \omega_k) \qquad\qquad \hat{\delta}(\tilde{k}) = (2\pi)^{d+1} \delta^d(k) \delta(\omega_k) \tag{6.47}$$

Applying this procedure to the equation of motion of the Malthusian Toner and Tu theory, given by Eq. (6.18), leads to the MSRJD action $\mathcal{S} = \mathcal{S}_0 + \mathcal{S}_I$. I distinguish between the Gaussian and non-Gaussian parts of the action: $\mathcal{S}_0$ is the Gaussian action, corresponding to the linear terms in the equation of motion (6.1),

and $\mathcal{S}_I$ is the non-Gaussian action, corresponding to the non-linear terms in the equation of motion (6.1). These two contributions are given by

$$\mathcal{S}_0 = \int_{\tilde{k}} \left[(-i\omega + m + \Gamma^{\parallel} k^2) P_{\alpha\beta}^{\parallel} + (-i\omega + m + k^2 \Gamma^{\perp}) P_{\alpha\beta}^{\perp} \right] \hat{\psi}_\alpha(-\tilde{k})\psi_\beta(\tilde{k}) - \tilde{\Gamma}\hat{\psi}_\alpha(-\tilde{k})\hat{\psi}_\alpha(\tilde{k})$$

$$\mathcal{S}_I = i\, v_0 \int_{\tilde{k},\tilde{q}} \left[\gamma_1 \delta_{\alpha\beta} q_\gamma + \gamma_2 \delta_{\alpha\gamma} q_\beta + \gamma_3 \delta_{\beta\gamma} k_\alpha \right] \hat{\psi}_\alpha(-\tilde{k})\psi_\beta(\tilde{q})\psi_\gamma(\tilde{k}-\tilde{q}) -$$

$$- J \int_{\tilde{k},\tilde{q},\tilde{p}} Q_{\alpha\beta\gamma\nu} \hat{\psi}_\alpha(-\tilde{k})\psi_\beta(\tilde{q})\psi_\gamma(\tilde{p})\psi_\nu(\tilde{k}-\tilde{q}-\tilde{p})$$

$$(6.48)$$

Where I used the notation

$$\int_{\tilde{k}} = \int\limits_{|\boldsymbol{k}|<\Lambda} \frac{\mathrm{d}^d k}{(2\pi)^d} \int\limits_{-\infty}^{+\infty} \frac{\mathrm{d}\omega}{2\pi} \tag{6.49}$$

And defined the tensor

$$Q_{\alpha\beta\gamma\nu} = \delta_{\alpha\beta}\delta_{\gamma\nu} + \delta_{\alpha\gamma}\delta_{\beta\nu} + \delta_{\alpha\nu}\delta_{\beta\gamma} \tag{6.50}$$

I remark that the action has the standard structure shown in equation (6.44): the linear part in the auxiliary field $\hat{\psi}$ multiplies the deterministic part of the equation of motion, while the quadratic term in the auxiliary field $\hat{\psi}$ multiplies the noise amplitude.

Linear correlation functions

In this section, I will provide an alternative derivation of the linear response and bare correlation function, starting from the MSRJD action. In the Malthusian Toner and Tu theory, because of the anisotropy given by the pressure force, the two-point functions are not diagonal in the spatial indices, which means that $\langle \psi_\alpha \psi_\beta \rangle$ is not proportional to $\delta_{\alpha\beta}$. To derive the two-point function, I write the Gaussian action $\mathcal{S}_0$ in the form:

$$\mathcal{S}_0 = \frac{1}{2} \int_{\tilde{k}} \phi_\alpha(\tilde{k}) \mathbb{M}_{\alpha\beta}(\tilde{k}) \phi_\beta(-\tilde{k}) \,,$$

$$\mathbb{M}_{\alpha\beta}(\tilde{k}) = \begin{pmatrix} 0 & A^{\perp} P_{\alpha\beta}^{\perp} + A^{\parallel} P_{\alpha\beta}^{\parallel} \\ \bar{A}^{\perp} P_{\alpha\beta}^{\perp} + \bar{A}^{\parallel} P_{\alpha\beta}^{\parallel} & -2D_0 \delta_{\alpha\beta} \end{pmatrix} \,, \tag{6.51}$$

where the vector $\boldsymbol{\phi}$ is defined as $\boldsymbol{\phi}(\tilde{k}) = (\boldsymbol{\psi}(\tilde{k}), \hat{\boldsymbol{\psi}}(\tilde{k}))$, while $A^{\perp}$ and $A^{\parallel}$ are defined as follows

$$A^{\perp,\parallel} = -i\omega + m_0 + \Gamma_0^{\perp,\parallel} k^2, \tag{6.52}$$

and $\bar{A}^{\parallel,\perp}$ are the respective complex conjugate. I remark that the matrix $\mathbb{M}$ is a $2d \times 2d$ matrix, and each block of the matrix, as defined in equation (6.51), is a $d \times d$ block.

Correlation and response functions are obtained by inverting the matrix $\mathbb{M}_{\alpha\beta}(\tilde{k})$. The matrix $\mathbb{M}_{\alpha\beta}$ is a block matrix, and also will be its inverse $\mathbb{G}$:

$$\mathbb{G}_{\alpha\gamma}(\tilde{k})\mathbb{M}_{\gamma\beta}(\tilde{k}) = \begin{pmatrix} \delta_{\alpha\beta} & 0 \\ 0 & \delta_{\alpha\beta} \end{pmatrix} \qquad \mathbb{G}_{\alpha\beta} = \begin{pmatrix} C_{\alpha\beta} & \bar{G}_{\alpha\beta} \\ G_{\alpha\beta} & 0 \end{pmatrix} \qquad , \tag{6.53}$$

The matrix elements of $\mathbb{G}_{\alpha\beta}(\tilde{\boldsymbol{k}})$ are the Gaussian correlation and response function [2, 1]; $C_{\alpha\beta}$ is the Gaussian correlation function, and $G_{\alpha\beta}$ is the Gaussian response function,

$$\langle \hat{\psi}_\alpha(\tilde{\boldsymbol{k}})\psi_\beta(\tilde{\boldsymbol{q}})\rangle = G_{\alpha\beta}(\tilde{\boldsymbol{k}})\hat{\delta}(\tilde{\boldsymbol{k}}+\tilde{\boldsymbol{q}}) \qquad \langle \psi_\alpha(\tilde{\boldsymbol{k}})\psi_\beta(\tilde{\boldsymbol{q}})\rangle = C_{\alpha\beta}(\tilde{\boldsymbol{k}})\hat{\delta}(\tilde{\boldsymbol{k}}+\tilde{\boldsymbol{q}})\,. \qquad (6.54)$$

By explicitly computing the inverse matrix $\mathbb{G}$, one finds that the response function $G_{\alpha\beta}$ and the correlation function $C_{\alpha\beta}$ are precisely given by those found in Sec. 6.2.1, namely Eq. (6.29), (6.35). As made explicit by Eq. (6.29)-(6.35) the transverse and longitudinal modes are non-interacting in the linear theory. This means that the longitudinal and transverse fluctuations of the velocity field are independent at the Gaussian level.

Non-linear terms

Of course, even if the longitudinal and transverse fluctuations are not coupled at the Gaussian level, they interact at the non-linear level. There are four non-linearities, respectively γ_1, γ_2, γ_3, and J, which mix the longitudinal and transverse components of the velocity field. In the diagrammatic framework, these interactions are graphically represented by Feynman vertices, in which different lines merge, each representing one of the fields involved in the interaction. In the representation I will use here, an *entering* arrow is used to identify the leg representing the response field. Moreover, I shall choose vertices to have opposed signs with respect to the interactions; the convenience of this choice is that vertices play a crucial role in building Feynman diagrams, which come from the expansion of $\exp(-\mathcal{S})$.

In principle, each Feynman vertex represents a non-linearity, however since the first three non-linearities involve two fields $\boldsymbol{\psi}$ and one field $\hat{\boldsymbol{\psi}}$, one can represent them with only one Feynman vertex. Therefore, the theory has only two Feynman vertices, defined as follows:

$$\hat{\psi}_\alpha(-\tilde{\boldsymbol{k}}) \quad\begin{matrix}\psi_\beta(\tilde{\boldsymbol{q}})\\ \\ \psi_\gamma(\tilde{\boldsymbol{p}})\end{matrix} \qquad : \qquad -\frac{iv_0}{2}Y_{\alpha\beta\gamma}(\boldsymbol{q},\boldsymbol{p})\hat{\delta}(\tilde{\boldsymbol{k}}-\tilde{\boldsymbol{q}}-\tilde{\boldsymbol{p}})\,, \qquad (6.55)$$

$$\hat{\psi}_\alpha(-\tilde{\boldsymbol{k}}) \quad\begin{matrix}\psi_\beta(\tilde{\boldsymbol{q}})\\ \psi_\gamma(\tilde{\boldsymbol{p}})\\ \psi_\gamma(\tilde{\boldsymbol{h}})\end{matrix} \qquad : \qquad -\frac{J}{3}Q_{\alpha\beta\gamma\nu}\hat{\delta}(\tilde{\boldsymbol{k}}-\tilde{\boldsymbol{q}}-\tilde{\boldsymbol{p}}-\tilde{\boldsymbol{h}})\,, \qquad (6.56)$$

where the tensor $Q_{\alpha\beta\gamma\nu}$ is given by (6.50), while $Y_{\alpha\beta\gamma}(\boldsymbol{q},\boldsymbol{p})$ is defined as follows:

$$Y_{\alpha\beta\gamma}(\boldsymbol{q},\boldsymbol{p}) = \gamma_1(\delta_{\alpha\gamma}p_\beta + \delta_{\alpha\beta}q_\gamma) + \gamma_2(\delta_{\alpha\gamma}q_\beta + \delta_{\alpha\beta}p_\gamma) + 2\gamma_3\delta_{\beta\gamma}(q_\alpha + p_\alpha) \qquad (6.57)$$

I remark that each non-linearity has been symmetrised here, for each interaction term to be symmetric under the exchange of the direction of motion field. The first vertex (6.55) is called the self-propulsion vertex since it arises from the particle being self-propelled at the microscopic level. This can be seen by the fact that this vertex is proportional to v_0, meaning that when the microscopic speed is sent to $v_0 \to 0$, this self-propulsion vertex vanishes too. This self-propulsion vertex is composed by the convective derivative term, proportional to γ_1, and by the two terms, γ_2 and γ_3, which are introduced because of the Galilean-invariance breaking. The second vertex (6.56) is the standard ferromagnetic relaxation vertex, characteristic of ferromagnetic theories belonging to the $\mathcal{O}(n)$ universality class [2, 3].

6.3 Renormalization group calculation

In the present section, I will perform the one-loop RG calculation for the near-critical behaviour of the Malthusian Toner and Tu theory. This work, now published in [MyPaper2], provides one of the first RG evidence that the phase transition in active matter is first-order for large enough systems. But more importantly for my purposes, it also proves that fine-size effects might lead to the observation of a second-order phenomenology even in compressible systems. Remarkably, the associated scaling exponents are shown to belong to the incompressible universality class. These results, in agreement with numerical studies [42, 69], provide a compelling and solid explanation of why swarms behave like incompressible systems. This will allow me to study their critical properties by analysing an incompressible theory.

To understand the large-scale behaviour of the MTT theory, I will undertake a momentum-shell renormalization group approach. As detailed in Chapter 4, the momentum-shell RG unfolds through two stages. The first stage consists of integrating out large momenta fluctuations, precisely fluctuations inside the momentum shell $\Lambda/b < k < \Lambda$. The key point is that b, which determines how many modes one is integrating out, is close to one, $b \simeq 1$; this means that a *thin* shell of modes is integrated out, defining in this way a continuous transformation. After the integration, one is left with a theory whose cut-off is not Λ anymore, but it is Λ/b. To recover the original cutoff Λ, and compare apples with apples, a second step consisting of rescaling momenta, frequencies and fields is performed. This will allow me to obtain the recursion relations for the parameters of the theory, enabling me to investigate the large-scale properties.

6.3.1 Shell integration and perturbative corrections

When the short-wavelength modes, with wave-vector belonging to the momentum-shell with $\Lambda/b < k < \Lambda$ are integrated out in the Malthusian Toner and Tu theory (6.48), one ends up with an action $\mathcal{S}^< = \mathcal{S} + \Delta\mathcal{S}$ for the modes with $k < \Lambda/b$. For convenience, I will split the corrections $\Delta\mathcal{S} = \Delta\mathcal{S}_0 + \Delta\mathcal{S}_I$, with $\Delta\mathcal{S}_0$ being the corrections to the Gaussian part and $\Delta\mathcal{S}_I$ those to the interacting part of the action.

These two contributions take the form

$$\Delta\mathcal{S}_0 = \int_{\tilde{\boldsymbol{k}}}^{<} \hat{\psi}_\alpha(-\tilde{\boldsymbol{k}})\Sigma_{\alpha\beta}(\tilde{\boldsymbol{k}})\psi_\beta(\tilde{\boldsymbol{k}}) - \hat{\psi}_\alpha(-\tilde{\boldsymbol{k}})\tilde{\Sigma}_{\alpha\beta}(\tilde{\boldsymbol{k}})\hat{\psi}_\beta(\tilde{\boldsymbol{k}})$$

$$\Delta\mathcal{S}_I = -\int_{\tilde{\boldsymbol{k}},\tilde{\boldsymbol{q}}}^{<} V_{\alpha\beta\gamma}^{\hat{\psi}\psi\psi}(\tilde{\boldsymbol{k}},\tilde{\boldsymbol{q}})\hat{\psi}_\alpha(-\tilde{\boldsymbol{k}}-\tilde{\boldsymbol{q}})\psi_\beta(\tilde{\boldsymbol{k}})\psi_\gamma(\tilde{\boldsymbol{q}})- \qquad (6.58)$$

$$-\int_{\tilde{\boldsymbol{k}},\tilde{\boldsymbol{q}},\tilde{\boldsymbol{p}}}^{<} V_{\alpha\beta\gamma\nu}^{\hat{\psi}\psi\psi\psi}(\tilde{\boldsymbol{k}},\tilde{\boldsymbol{q}},\tilde{\boldsymbol{p}})\hat{\psi}_\alpha(-\tilde{\boldsymbol{k}})\psi_\beta(\tilde{\boldsymbol{q}})\psi_\gamma(\tilde{\boldsymbol{p}})\psi_\nu(\tilde{\boldsymbol{k}}-\tilde{\boldsymbol{q}}-\tilde{\boldsymbol{p}})\,.$$

Here all momenta are integrated off-shell, $k < \Lambda/b$, while frequency integrals still run from $-\infty$ to ∞. This is the meaning of the superscript $<$ over the integral sign, which stems for

$$\int_{\tilde{\boldsymbol{k}}}^{<} = \int_{|\boldsymbol{k}|<\Lambda/b} \frac{\mathrm{d}^d k}{(2\pi)^d} \int_{-\infty}^{+\infty} \frac{\mathrm{d}\omega_k}{2\pi} \qquad (6.59)$$

The quantities Σ and $\tilde{\Sigma}$ are known as the *self-energies* [40], which contribute to the perturbative corrections of the Gaussian part of the original action, while $V^{\hat{\psi}\psi\psi}$ and $V^{\hat{\psi}\psi\psi\psi}$ are known as *vertex-functions*, and correct the non-linear dynamic couplings. From a diagrammatic point of view, each self-energy and vertex-function is given by the sum of all amputated 1-particle irreducible diagrams with external fields $\hat{\psi}\psi$, $\hat{\psi}\hat{\psi}$, $\hat{\psi}\psi\psi$ and $\hat{\psi}\psi\psi\psi$ respectively. Graphically, they are represented by the blobs in the following diagrammatic scheme

$$\Sigma_{\alpha\beta}(\tilde{\boldsymbol{k}}) \quad : \quad \hat{\psi}_\alpha(-\tilde{\boldsymbol{k}}) \longrightarrow \!\!\!\text{⬤}\!\!\!\longrightarrow \psi_\beta(\tilde{\boldsymbol{k}}) \qquad (6.60)$$

$$\tilde{\Sigma}_{\alpha\beta}(\tilde{\boldsymbol{k}}) \quad : \quad \hat{\psi}_\alpha(-\tilde{\boldsymbol{k}}) \longrightarrow \!\!\!\text{⬤}\!\!\!\longleftarrow \hat{\psi}_\beta(\tilde{\boldsymbol{k}}) \qquad (6.61)$$

$$V_{\alpha\beta\gamma}^{\hat{\psi}\psi\psi}(\tilde{\boldsymbol{k}},\tilde{\boldsymbol{q}}) \quad : \quad \hat{\psi}_\alpha(-\tilde{\boldsymbol{k}}-\tilde{\boldsymbol{q}}) \qquad (6.62)$$

$$V_{\alpha\beta\gamma\nu}^{\hat{\psi}\psi\psi\psi}(\tilde{\boldsymbol{k}},\tilde{\boldsymbol{q}},\tilde{\boldsymbol{h}}) \quad : \quad \hat{\psi}_\alpha(-\tilde{\boldsymbol{k}}) \qquad (6.63)$$

Let me remark that the structure of this novel action is the same as the original one. Higher order terms in the number of fields or terms with higher powers of k or ω may be generated, but they turn out to be irrelevant at first-order in ϵ [52]. The

complete list of diagrams contributing to these self-energies and vertex-functions relevant at first order in ϵ is given in Appendix B.

Each of these self-energies and vertex-functions contributes to giving corrections to different parameters of the bare action (6.48). In particular

- the self-energy $\Sigma_{\alpha\beta}$ corrects the mass term m, the kinetic coefficients $\Gamma^{\perp/\parallel}$, and it will eventually provide a correction to the term proportional to $-\mathrm{i}\omega$;

- the self energy $\tilde{\Sigma}_{\alpha\beta}$ corrects the noise amplitude $\tilde{\Gamma}$;

- the three-point function $V^{\hat{\psi}\psi\psi}$ corrects the couplings γ_1, γ_2 and γ_3;

- the four point function $V^{\hat{\psi}\psi\psi\psi}$ corrects the ferromagnetic coupling J.

It is, therefore, useful to expand these terms in $\boldsymbol{k}$ and ω, to better identify the terms they are correcting. At leading order in this expansion, the self-energies read

$$\begin{aligned}
\Sigma_{\alpha\beta}(\tilde{\boldsymbol{k}}) &= (-\mathrm{i}\omega\,\delta\Omega + m_0\,\delta m)\,\delta_{\alpha\beta}\,\ln b + \\
&\quad + \Gamma_0^{\parallel}k^2\,\delta\Gamma^{\parallel}\,P_{\alpha\beta}^{\parallel}(\boldsymbol{k})\,\ln b + \Gamma_0^{\perp}k^2\,\delta\Gamma^{\perp}\,P_{\alpha\beta}^{\perp}(\boldsymbol{k})\,\ln b + \dots, \quad (6.64) \\
\tilde{\Sigma}_{\alpha\beta}(\tilde{\boldsymbol{k}}) &= \tilde{\Gamma}_0\,\delta\tilde{\Gamma}\,\delta_{\alpha\beta}\,\ln b + \dots.
\end{aligned}$$

Here I denoted the bare parameters with the subscript 0, and the ellipses stand for higher order terms in ω and $\boldsymbol{k}$, which are irrelevant in determining the critical behaviour at first order in ϵ. Notice that all the corrections are proportional to the volume of the momentum shell, which is proportional to $1 - b^{-1} \simeq \ln b$. It is possible to appreciate that the structure of the self-energy $\Sigma_{\alpha\beta}(\boldsymbol{k}, \omega)$ has a quite complicated $\boldsymbol{k}$ dependence since it contains isotropic, longitudinal and transverse corrections respectively proportional to $\delta_{\alpha\beta}$, $P_{\alpha\beta}^{\parallel}(\boldsymbol{k})$ and to $P_{\alpha\beta}^{\perp}(\boldsymbol{k})$. The new action $\mathcal{S}^<$ can be therefore written in the same form as the bare action (6.48), but with modified coefficients. Note moreover that the presence of the $\delta\Omega$ corrections leads to a modification of the unity coefficient in front of the $-\mathrm{i}\omega\hat{\psi}\psi$ term. To take care of this and keep this coefficient equal to one during the RG flow, rescaling will play a crucial role. For the moment however, the Gaussian part of $\mathcal{S}^<$ is modified as follows

$$\begin{aligned}
\mathcal{S}_0^< &= \int_{\tilde{\boldsymbol{k}}}^< -\mathrm{i}\omega\,(1 + \delta\Omega\ln b)\,\hat{\psi}\psi + \Gamma_0(1 + \delta\Gamma\ln b)k^2\hat{\psi}\psi + m_0(1 + \delta m\ln b)\hat{\psi}\psi + \\
&\quad + \int_{\tilde{\boldsymbol{k}}}^< \Gamma_0^{\perp}(1 + \delta\Gamma^{\perp}\ln b)k^2 P^{\perp}\hat{\psi}\psi + \Gamma_0^{\parallel}(1 + \delta\Gamma^{\parallel}\ln b)k^2 P^{\parallel}\hat{\psi}\psi - \\
&\quad - \int_{\tilde{\boldsymbol{k}}}^< \tilde{\Gamma}_0\left(1 + \delta\tilde{\Gamma}\ln b\right)\hat{\psi}\hat{\psi}
\end{aligned}$$

$$(6.65)$$

where the tensorial structure of the action was omitted to facilitate the reading.

The vertex-functions, which I remind give corrections to the non-Gaussian part

of the action, can be expanded as

$$
V^{\hat{\psi}\psi\psi}_{\alpha\beta\gamma}(\tilde{\boldsymbol{k}}, \tilde{\boldsymbol{q}}) = -\frac{iv_0}{2}\gamma_{1,0}\,\delta\gamma_1\,(\delta_{\alpha\gamma}q_\beta + \delta_{\alpha\beta}k_\gamma)\ln b-
$$
$$
-\frac{iv_0}{2}\gamma_{2,0}\,\delta\gamma_2\,(\delta_{\alpha\gamma}k_\beta + \delta_{\alpha\beta}q_\gamma)\ln b- \tag{6.66}
$$
$$
- iv_0\gamma_{3,0}\,\delta\gamma_3\,\delta_{\beta\gamma}\,(q_\alpha + k_\alpha)\ln b + \dots,
$$
$$
V^{\hat{\psi}\psi\psi\psi}_{\alpha\beta\gamma\nu}(\tilde{\boldsymbol{k}}, \tilde{\boldsymbol{q}}, \tilde{\boldsymbol{p}}) = -\frac{J_0}{3}Q_{\alpha\beta\gamma\nu}\delta J\ln b + \dots,
$$

Again, I recall that I denoted the bare parameters with the subscript 0, while the ellipses stand for higher orders terms in ω and $\boldsymbol{k}$, which are irrelevant in determining the critical behaviour at first order in ϵ. Let me note that the vertex correction $V^{\hat{\psi}\psi\psi}$ has quite an intricate tensorial structure, which however reproduces that of the tensor $Y_{\alpha\beta\gamma}$. Once these vertex functions are computed, the new non-Gaussian action $\mathcal{S}^<_I$ takes the following form

$$
\mathcal{S}^<_0 = -\frac{iv_0}{2}\int^<_{\tilde{\boldsymbol{k}},\tilde{\boldsymbol{q}}}\gamma_{1,0}(1 + \delta\gamma_1\ln b)\,(\delta_{\alpha\gamma}q_\beta + \delta_{\alpha\beta}k_\gamma)\hat{\psi}_\alpha(-\tilde{\boldsymbol{k}} - \tilde{\boldsymbol{q}})\psi_\beta(\tilde{\boldsymbol{k}})\psi_\gamma(\tilde{\boldsymbol{q}})-
$$
$$
-\frac{iv_0}{2}\int^<_{\tilde{\boldsymbol{k}},\tilde{\boldsymbol{q}}}\gamma_{2,0}(1 + \delta\gamma_2\ln b)(\delta_{\alpha\gamma}k_\beta + \delta_{\alpha\beta}q_\gamma)\hat{\psi}_\alpha(-\tilde{\boldsymbol{k}} - \tilde{\boldsymbol{q}})\psi_\beta(\tilde{\boldsymbol{k}})\psi_\gamma(\tilde{\boldsymbol{q}})-
$$
$$
- iv_0\int^<_{\tilde{\boldsymbol{k}},\tilde{\boldsymbol{q}}}\gamma_{3,0}(1 + \delta\gamma_3\ln b)\delta_{\beta\gamma}\,(q_\alpha + k_\alpha)\hat{\psi}_\alpha(-\tilde{\boldsymbol{k}} - \tilde{\boldsymbol{q}})\psi_\beta(\tilde{\boldsymbol{k}})\psi_\gamma(\tilde{\boldsymbol{q}})+ \tag{6.67}
$$
$$
-\frac{J_0}{3}\int^<_{\tilde{\boldsymbol{k}},\tilde{\boldsymbol{q}},\tilde{\boldsymbol{p}}}Q_{\alpha\beta\gamma\nu}J_0(1 + \delta J\ln b)\,,
$$

Note once again that $\mathcal{S}^<$ has the same form of the bare action (6.48), but with modified couplings.

6.3.2 Rescaling

The second step of the RG consists of the following rescaling of momenta, frequencies and fields,

$$
\boldsymbol{k}_b = \boldsymbol{k}b \qquad\qquad\qquad \omega_b = \omega b^z \tag{6.68}
$$
$$
\hat{\boldsymbol{\psi}}(\boldsymbol{k}_b, \omega_b) = b^{\chi_{\hat{\psi}}}\hat{\boldsymbol{\psi}}(\boldsymbol{k}, \omega) \qquad\qquad \boldsymbol{\psi}(\boldsymbol{k}_b, \omega_b) = b^{\chi_\psi}\boldsymbol{\psi}(\boldsymbol{k}, \omega) \tag{6.69}
$$

Once this transformation is performed, the action recovers its original cutoff Λ.

Before looking at the full action, let me focus on what happens to the $-i\omega\hat{\psi}\psi$ term after this RG step. Once both shell-integration and rescaling are performed, this terms is modified as follows

$$
\int_{\tilde{\boldsymbol{k}}} -i\omega\hat{\psi}(-\tilde{\boldsymbol{k}})\psi(\tilde{\boldsymbol{k}}) = \int_{\tilde{\boldsymbol{k}}_b} -ib^{-\chi_\psi - \chi_{\hat{\psi}} - d - 2z}(1 + \delta\Omega\ln b)\omega_b\hat{\psi}(-\tilde{\boldsymbol{k}}_b)\psi(\tilde{\boldsymbol{k}}_b)\,. \tag{6.70}
$$

In other words, the *renormalized* field theory acquires a non-unity coefficient in front of the $-i\omega_b\hat{\psi}\psi$ term. In terms of Langevin equations, this would mean having a coefficient different from 1 in front of the temporal derivative $\partial_t\psi$ term. It is easy to understand that one can easily get rid of this coefficient, by simply dividing both

sides of the equation by it. In the context of MSRJD field theories, this same result is achieved by *fixing* the scaling dimension of the auxiliary $\hat{\psi}$ field, requiring its scaling to keep this coefficient equal to unity. Therefore, I will require $\chi_{\hat{\psi}}$ to satisfy

$$b^{-\chi_\psi - \chi_{\hat{\psi}} - d - 2z}(1 + \delta\Omega \ln b) = 1 \;\Rightarrow\; \chi_{\hat{\psi}} = -\chi_\psi - d - 2z - \delta\Omega \qquad (6.71)$$

Here I used the fact that for $b \sim 1$ one can express $1 + \delta\Omega \ln b \simeq b^{\delta\Omega}$.

With this caveat in mind, let me now turn my attention to the new action, which takes the form

$$\begin{aligned}
\mathcal{S}_{0,b} &= \int_{\tilde{\boldsymbol{k}}_b} \left(-\mathrm{i}\omega_b + m_b + k_b^2\,\Gamma_b^\perp \right) P_{\alpha\beta}^\perp \hat{\psi}_\alpha(-\tilde{\boldsymbol{k}}_b)\psi_\beta(\tilde{\boldsymbol{k}}_b) + \\
&\quad + \int_{\tilde{\boldsymbol{k}}_b} \left(-\mathrm{i}\omega_b + m_b + k_b^2\,\Gamma_b^\| \right) P_{\alpha\beta}^\| \hat{\psi}_\alpha(-\tilde{\boldsymbol{k}}_b)\psi_\beta(\tilde{\boldsymbol{k}}_b) - \\
&\quad - \int_{\tilde{\boldsymbol{k}}_b} \tilde{\Gamma}_b \hat{\psi}_\alpha(-\tilde{\boldsymbol{k}}_b)\hat{\psi}_\beta(\tilde{\boldsymbol{k}}_b)\,, \\
\mathcal{S}_{I,b} &= -\frac{\mathrm{i}v_0}{2}\int_{\tilde{\boldsymbol{k}}_b,\tilde{\boldsymbol{q}}_b} Y_{\alpha\beta\gamma}^{(b)}(\tilde{\boldsymbol{k}}_b,\tilde{\boldsymbol{q}}_b)\hat{\psi}_\alpha(-\tilde{\boldsymbol{k}}_b)\psi_\beta(\tilde{\boldsymbol{q}}_b)\psi_\gamma(\tilde{\boldsymbol{k}}_b - \tilde{\boldsymbol{q}}_b) - \\
&\quad - \frac{J_b}{3}\int_{\tilde{\boldsymbol{k}}_b,\tilde{\boldsymbol{q}}_b,\tilde{\boldsymbol{p}}_b} Q_{\alpha\beta\gamma\nu}\hat{\psi}_\alpha(-\tilde{\boldsymbol{k}}_b)\psi_\beta(\tilde{\boldsymbol{q}}_b)\psi_\gamma(\tilde{\boldsymbol{p}}_b)\psi_\nu(\tilde{\boldsymbol{k}}_b - \tilde{\boldsymbol{q}}_b - \tilde{\boldsymbol{p}}_b)
\end{aligned} \qquad (6.72)$$

Where the tensor $Y_{\alpha\beta\gamma}^{(b)}$ is the same of $Y_{\alpha\beta\gamma}$, but with $\gamma_{i,b}$ instead of γ_i, namely

$$Y_{\alpha\beta\gamma}^b(\boldsymbol{k},\boldsymbol{q}) = \gamma_{1,b}(\delta_{\alpha\gamma}q_\beta + \delta_{\alpha\beta}k_\gamma) + \gamma_{2,b}(\delta_{\alpha\gamma}k_\beta + \delta_{\alpha\beta}q_\gamma) + 2\gamma_{3,b}\delta_{\beta\gamma}(q_\alpha + k_\alpha) \quad (6.73)$$

The subscript b indicates that this is the action after an RG transformation with shell-thickness $\ln b$. These new parameters are defined to reabsorb all the powers of b comparing in front of them. Once the perturbative corrections are computed, these new parameters are linked to the bare ones through the following relations

$$m_b = m_0\; b^{-\chi_\psi - \chi_{\hat{\psi}} - d - z}(1 + \delta m \ln b) \qquad (6.74)$$

$$\Gamma_b^\perp = \Gamma_0^\perp\; b^{-\chi_\psi - \chi_{\hat{\psi}} - d - z - 2}(1 + \delta\Gamma^\perp \ln b) \qquad (6.75)$$

$$\Gamma^\| = \Gamma_0^\|\; b^{-\chi_\psi - \chi_{\hat{\psi}} - d - z - 2}(1 + \delta\Gamma^\| \ln b) \qquad (6.76)$$

$$\gamma_{i,b} = \gamma_{i,0}\; b^{-2\chi_\psi - \chi_{\hat{\psi}} - 2d - 2z - 1}(1 + \delta\gamma_i \ln b) \qquad (6.77)$$

$$J_b = J_0\; b^{-3\chi_\psi - \chi_{\hat{\psi}} - 3d - 3z}(1 + \delta J \ln b) \qquad (6.78)$$

$$\tilde{\Gamma}_b = \tilde{\Gamma}_0\; b^{-2\chi_{\hat{\psi}} - d - z}(1 + \delta\tilde{\Gamma} \ln b) \qquad (6.79)$$

where I remind all the perturbative corrections $\delta\mathcal{P}$ are functions of the bare parameters, while $\chi_{\hat{\psi}}$ takes the form derived in Eq. (6.71). The scaling exponents z and χ_ψ are instead yet to be determined.

6.3.3 RG flow equations

The action after the RG transformation differs from the original one because of two different kinds of contributions: naive rescaling and perturbative contributions. The perturbative contributions are given by the momentum shell integral, and they are

determined by the terms $\Sigma_{\alpha\beta}$, $\tilde{\Sigma}_{\alpha\beta}$, $V_{\alpha\beta\gamma}^{\hat{\psi}\psi\psi}$ and $V_{\alpha\beta\gamma\nu}^{\hat{\psi}\psi\psi\psi}$. The actions (6.48) and (6.72) have the same structure, but their parameters are different. The parameters after and before the RG transformation are linked by the following recursion relations,

$$m_b = m_0 \; b^{\chi_m} \qquad\qquad \chi_m = z + \delta m - \delta\Omega \qquad\qquad (6.80)$$

$$\Gamma_b^{\|,\perp} = \Gamma_0^{\|,\perp} \; b^{\chi_{\|,\perp}} \qquad\qquad \chi_{\|,\perp} = z - 2 + \delta\Gamma^{\|,\perp} - \delta\Omega \qquad (6.81)$$

$$\tilde{\Gamma}_b = \tilde{\Gamma}_0 \; b^{\chi_{\tilde{\Gamma}}} \qquad\qquad \chi_{\tilde{\Gamma}} = 2\chi_\psi + d + 3z + \delta\tilde{\Gamma} - 2\delta\Omega \qquad (6.82)$$

$$\gamma_{i,b} = \gamma_{i,0} \; b^{\chi_{\gamma_i}} \qquad\qquad \chi_{\gamma_i} = -\chi_\psi - d + \delta\gamma_i - \delta\Omega \qquad (6.83)$$

$$J_b = J_0 \; b^{\chi_J} \qquad\qquad \chi_J = -2\chi_\psi + 2d + z + \delta J - \delta\Omega \qquad (6.84)$$

where I denote with $\mathcal{P}_b$ the parameter $\mathcal{P}$ after the RG transformation, and with $\delta\mathcal{P}$ the perturbative contribution to the parameter $\mathcal{P}$. The fact that perturbative corrections are proportional to $\ln b$ is here taken into account by noticing that $1 + \delta\mathcal{P} \simeq b^{\delta\mathcal{P}}$ when $b \sim 1$, as in the present case. Finally, the quantities $\chi_\mathcal{P}$ are the scaling dimensions of the parameters and tell how the parameters scale when an RG transformation is made. Note that $\chi_\mathcal{P}$ is given by the *naive* dimension of $\mathcal{P}$ plus perturbative corrections coming from Feynman diagrams. It is precisely these latter contributions, which come from the coupling of IR and UV fluctuations, that give rise to non-trivial scaling behaviours.

Before proceeding, it is useful to define a set of effective parameters and effective couplings, whose scaling dimension is independent of the exponents χ_ψ and z. This will allow their RG flow equations to depend only on the effective parameters themselves, making their RG flow closed. For the theory in study, the effective parameters are given by:

$$\mu_0 = \frac{\Gamma_0^\|}{\Gamma_0^\perp} \qquad\qquad g_{i,0} = \frac{\gamma_{i,0}}{\Gamma_0^\perp}\sqrt{\frac{\tilde{\Gamma}_0}{\Gamma_0^\perp}}\sqrt{\Lambda^{4-d}K_d} \qquad (6.85)$$

$$r_0 = \frac{m_0}{\Gamma_0^\perp} \qquad\qquad \tilde{u}_0 = \frac{J_0}{\Gamma_0^\perp}\frac{\tilde{\Gamma}_0}{\Gamma_0^\perp}\Lambda^{4-d}K_d \qquad (6.86)$$

where Λ is the cutoff of the theory and $K_d = S_d/(2\pi)^d$, being S_d the surface of the d-dimensional hyper-sphere. Note that r coincides with the mass r of the Landau potential (6.3), while the relation between u of (6.3) and the effective coupling $\tilde{u}$ is given by $\tilde{u} \propto \tilde{\Gamma}u/\Gamma$.

One can obtain the recursion relations of the effective parameters from the recursion relations (6.80)-(6.84):

$$r_b = r_0 b^{\chi_r} \qquad\qquad \chi_r = 2 + \delta m - \delta\Gamma^\perp \qquad (6.87)$$

$$\mu_b = \mu_0 b^{\chi_\mu} \qquad\qquad \chi_\mu = \delta\Gamma^\| - \delta\Gamma^\perp \qquad (6.88)$$

$$u_b = u_0 b^{\chi_u} \qquad\qquad \chi_u = \epsilon + \delta J + \delta D - 2\delta\Gamma^\perp - \delta\Omega \qquad (6.89)$$

$$g_{1,b} = g_{1,0}b^{\chi_{g_1}} \qquad \chi_{g_1} = \epsilon/2 + \delta\gamma_1 + \frac{1}{2}\delta\tilde{\Gamma} - \frac{3}{2}\delta\Gamma^\perp - \delta\Omega \qquad (6.90)$$

$$g_{2,b} = g_{2,0}b^{\chi_{g_2}} \qquad \chi_{g_2} = \epsilon/2 + \delta\gamma_2 + \frac{1}{2}\delta\tilde{\Gamma} - \frac{3}{2}\delta\Gamma^\perp - \delta\Omega \qquad (6.91)$$

$$g_{3,b} = g_{3,0}b^{\chi_{g_3}} \qquad \chi_{g_3} = \epsilon/2 + \delta\gamma_3 + \frac{1}{2}\delta\tilde{\Gamma} - \frac{3}{2}\delta\Gamma^\perp - \delta\Omega \qquad (6.92)$$

The scaling dimension of an effective parameter $\mathcal{P}$ can be written as the sum of its naive dimension $d_{\mathcal{P}}$ and perturbative contributions, namely

$$\chi_{\mathcal{P}} = d_{\mathcal{P}} + \text{perturbative corrections} \tag{6.93}$$

To assess the relevance of each parameter, it is useful to look at their *naive* dimension: this will tell when a given coupling becomes relevant near the Gaussian fixed point. The naive scaling dimensions of the effective parameters are:

$$d_{\mu} = 0 \qquad\qquad d_{g_i} = \epsilon/2 \qquad\qquad d_u = \epsilon \qquad\qquad d_r = 2 \tag{6.94}$$

The effective coupling constant u has naive scaling dimension ϵ, suggesting that its fixed point value must also be of order ϵ. Similarly, since the coupling constants g_i have naive scaling dimension $\epsilon/2$, their fixed point will be of order $\epsilon^{1/2}$. The parameter r represents the distance from the transition point, and it is analogous to the distance from the critical temperature $T - T_c$ in equilibrium systems. At the mean-field level, the transition point corresponds to $r = 0$; however, because of the non-linear terms, the transition point is shifted of $\mathcal{O}(g_i^2, u)$ from its naive value. One also concludes that the critical value of r must be of the same order $r_c = \mathcal{O}(\epsilon)$. Since an expansion in powers of ϵ is performed, I can neglect, at the leading order in ϵ, the r dependence in most of the Feynman diagrams, since this would lead to corrections of order ϵ^2.

In the present calculation, perturbative corrections are computed in the thin-shell limit $b \to 1^+$. Each RG step therefore provides an infinitesimal correction to the parameters of the theory, proportional to $\ln b$. As shown in Chapter 4, in this limit the iteration of many RG steps defines a continuous flow of the parameters of the theory, ruled by the equation

$$\dot{\mathcal{P}} = \beta_{\mathcal{P}}(\mathcal{P}) = \mathcal{P}\,\chi_{\mathcal{P}}(\mathcal{P}) \tag{6.95}$$

Where $\beta_{\mathcal{P}}$ are known as the beta-functions. The values $\mathcal{P}^*$ of the parameters to which the flow eventually approaches are called fixed points, and play a crucial role in determining the critical behaviour of the theory. These fixed points are given by the zeros of $\beta_{\mathcal{P}}$. The beta-functions for the effective parameters and coupling are therefore given by

$$\beta_r = r\left(2 + \delta m - \delta\Gamma^{\perp}\right) \tag{6.96}$$

$$\beta_{\mu} = \mu\left(\delta\Gamma^{\parallel} - \delta\Gamma^{\perp}\right) \tag{6.97}$$

$$\beta_{\tilde{u}} = \tilde{u}\left(\epsilon + \delta J + \delta D - 2\delta\Gamma^{\perp} - \delta\Omega\right) \tag{6.98}$$

$$\beta_{g_1} = g_1\left(\frac{\epsilon}{2} + \delta\gamma_1 + \frac{\delta\tilde{\Gamma}}{2} - \frac{3}{2}\delta\Gamma^{\perp} - \delta\Omega\right) \tag{6.99}$$

$$\beta_{g_2} = g_2\left(\frac{\epsilon}{2} + \delta\gamma_2 + \frac{\delta\tilde{\Gamma}}{2} - \frac{3}{2}\delta\Gamma^{\perp} - \delta\Omega\right) \tag{6.100}$$

$$\beta_{g_3} = g_3\left(\frac{\epsilon}{2} + \delta\gamma_3 + \frac{\delta\tilde{\Gamma}}{2} - \frac{3}{2}\delta\Gamma^{\perp} - \delta\Omega\right) \tag{6.101}$$

6.3.4 Fixed points

This section discusses some consistency checks that the recursion relations must pass. The Malthusian Toner-Tu theory, just as the Toner-Tu theory, combines the Landau-Ginzburg $\lambda\phi^4$ theory and the Navier-Stokes theory equations of fluid dynamics. The first one accounts for the ferromagnetic-like interaction, while the latter brings the theory off-equilibrium and accounts for the particle's movement at the microscopic level. Therefore, when all active elements are removed, the theory must reproduce the behaviour of equilibrium isotropic and dipolar ferromagnets. Similarly, when all the $\mathcal{O}(n)$ $\lambda\phi^4$-like terms are set to zero, the theory must reproduce the behaviour of a stirred fluid, discussed in [46]. To summarise, it is possible to divide the terms of the equation of motion into three groups:

$$
\begin{array}{lll}
1 \text{ - Landau Ginzburg} & m\boldsymbol{\psi}, \ J\psi^2\boldsymbol{\psi} & \\
2 \text{ - Navier Stokes} & v_0\gamma_1(\boldsymbol{\psi}\cdot\nabla)\boldsymbol{\psi} & (6.102) \\
3 \text{ - Galilean invariance breaking} & v_0\gamma_2(\nabla\cdot\boldsymbol{\psi})\boldsymbol{\psi}, v_0\gamma_3\nabla\psi^2 &
\end{array}
$$

The first class represents the equilibrium terms of the theory, while the second and third classes contain mostly off-equilibrium, active, terms. I shall show how setting to zero some of these terms in the Malthusian Toner-Tu theory allows to recover many of the know fixed points. Furthermore, I will provide two additional consistency checks of the theory.

Equilibrium ferromagnet

The first, obvious, fixed point of the Malthusian Toner and Tu theory can be obtained by setting to zero all the Navier-Stokes and Galilean invariance breaking non-linear terms, namely $\gamma_i = 0$. This leads to the behaviour of an equilibrium ferromagnet, in which transverse and longitudinal fluctuations relax differently, governed by the following equation of motion

$$
\partial_t\boldsymbol{\psi} = -\Gamma\frac{\delta\mathcal{H}}{\delta\boldsymbol{\psi}} + \sqrt{2\tilde{\Gamma}}\,\boldsymbol{\theta} \quad \mathcal{H} = \int d^d x \frac{1}{2}(\nabla\psi)^2 + \frac{\mu-1}{2}(\nabla\cdot\boldsymbol{\psi})^2 + \frac{r}{2}\psi^2 + \frac{u}{4}\psi^4\,,
$$

(6.103)

in which the force term can be expressed as the derivative of an effective free-energy $\mathcal{H}$. This theory interpolates between an ordinary isotropic ferromagnet, at $\mu = 1$, and a ferromagnet with dipolar interactions, $\mu = \infty$, where the configurations with $\nabla\cdot\boldsymbol{v} \neq 0$ are completely suppressed (their Boltzmann weight $e^{-\mathcal{H}}$ vanishes). This analogy is explained by the fact that dipolar interactions suppress all the longitudinal fluctuations of $\boldsymbol{\psi}$.

In this limit the beta functions (6.96)-(6.101) reduce to

$$
\beta_r = r\left(2 + 3\tilde{u}\frac{(3\mu+1)\Lambda^2 + 4r}{2r(r+\Lambda^2)(r+\mu\Lambda^2)}\right) \qquad \beta_\mu = 0 \qquad (6.104)
$$

$$
\beta_{\tilde{u}} = \tilde{u}\left(\epsilon - \tilde{u}\frac{17\mu^2 + 2\mu + 5}{2\mu^2}\right) \qquad \beta_{g_i} = 0 \qquad (6.105)
$$

The fact that $\beta_{g_i} = 0$ confirms that, if one switches of all the g_I couplings, they are not generated in any way by the RG. What is instead a peculiarity of the one-loop approximation, is the fact that $\beta_\mu = 0$. Were this result exact, one would find a manifold of fixed points, namely infinitely many fixed points, one for each value of μ. Higher order RG calculations have however shown that only $\mu = 1$ and $\mu = +\infty$ are fixed points when higher order corrections are taken into account [95], with the latter being unstable under RG. These two fixed point coincide with the Wilson-Fisher fixed point [53] for isotropic ferromagnets and that of ferromagnets with dipolar interactions [87].

The first fixed point, for $\mu = 1$, is given by

$$r^* = -\frac{1}{4}\epsilon\Lambda^2 \qquad\qquad \mu^* = 1 \qquad\qquad (6.106)$$

$$u^* = \frac{1}{12}\epsilon \qquad\qquad g_i^* = 0 \quad . \qquad\qquad (6.107)$$

At the leading order in $\epsilon = 4 - d$, this fixed point gives the following critical exponents,

$$\nu = \frac{1}{2} + \frac{\epsilon}{8} \qquad\qquad \eta = 0 \qquad\qquad z = 2 \,. \qquad (6.108)$$

reproducing correctly the critical behaviour of an isotropic ferromagnet, or in the classification of Halperin and Hoenberg the critical behaviour of model A of critical dynamics [40].

The second fixed point, for $\mu = +\infty$, is instead given by

$$r^* = -\frac{9}{34}\epsilon\Lambda^2 \qquad\qquad \mu^* = +\infty \qquad\qquad (6.109)$$

$$u^* = \frac{2}{17}\epsilon \qquad\qquad g_i^* = 0 \quad . \qquad\qquad (6.110)$$

and the associated critical exponents, in agreement with the literature [87], are

$$\nu = \frac{1}{2} + \frac{9}{68}\epsilon \qquad\qquad \eta = 0 \qquad\qquad z = 2 \qquad . \qquad (6.111)$$

An equilibrium consistency check

Besides the equilibrium case investigated in the previous paragraphs, there is an even more general equilibrium model which can be recovered from the Malthusian Toner and Tu theory. This is given by an equilibrium model with dynamics arising from the following free-energy:

$$\mathcal{F} = \int d^d\boldsymbol{x} \frac{1}{2}(\nabla\psi)^2 + \frac{\mu - 1}{2}\left(\nabla \cdot \boldsymbol{\psi}\right)^2 + \frac{r}{2}\psi^2 + \frac{u}{4}\psi^4 + \lambda\psi^2\left(\nabla \cdot \boldsymbol{\psi}\right) , \qquad (6.112)$$

which is a $\lambda\phi^4$-like theory, as the one define in (6.103), at which the term $\psi^2(\nabla \cdot \boldsymbol{\psi})$ was added in the free energy. It is possible to obtain this theory from the equation of motion of the Malthusian Toner and Tu theory by setting $\gamma_1 = 0$, and $\gamma_2 = -2\gamma_3 = -2\lambda/\Gamma$.

Clearly, the fact that this model is at equilibrium depends crucially on the condition $\gamma_2 = -2\gamma_3$. This constraint must be preserved by the renormalization

group - it would be strange that the large-scale properties of an equilibrium theory revealed to be off-equilibrium. Requiring that the RG transformation preserves this constraint, $\gamma_2 = -2\gamma_3$, implies that the perturbative contributions $\delta\gamma_2$ and $\delta\gamma_3$ must coincide when one sets $\gamma_1 = 0$ and $\gamma_2 = -2\gamma_3$. One can easily check that this is the case, as

$$\delta\gamma_2 = \delta\gamma_3 = g_3^2 \frac{3\mu + 4}{\mu^2} - u\frac{9\mu^2 - 2\mu + 5}{2\mu^2} \tag{6.113}$$

Incompressible stirred fluid

When, opposite to the equilibrium case, one sets the Landau-Ginzburg terms together with the Galilean invariance breaking terms to zero, in the incompressible limit one expects to recover the behaviour of an incompressible Navier-Stokes equation with a stochastic force stirring the fluid even at zero wave-vector. This model, called Model B in the classification of [46], is governed by the following equations of motion

$$\partial_t \boldsymbol{\psi} + v_0\gamma_1 \left(\boldsymbol{\psi} \cdot \nabla \right) \boldsymbol{\psi} = \Gamma\nabla^2\boldsymbol{\psi} + \sqrt{2\tilde{\Gamma}}\boldsymbol{\theta} \tag{6.114}$$

Complemented by the incompressible condition $\nabla \cdot \boldsymbol{\psi} = 0$, which in the present case is expected to be recovered for $\mu = +\infty$.

To check this, I set $g_{2,3} = \tilde{u} = r = 0$ in the flow equations, and then take the $\mu \to \infty$ limit. In this limit, all the flow equations besides that of g_1 vanish, while g_1 flows according to

$$\beta_{g_1} = g_1 \left(\frac{\epsilon}{2} - \frac{3}{8}g_1^2 \right) \tag{6.115}$$

Besides the gaussian fixed point, this flow equations admits one non-trivial fixed point, namely $g_1 = 2\sqrt{\epsilon/3}$, which coincides with that found for Model B in [46].

Consistency of Galilean invariance

More generally, whenever the theory is found to be Galilean invariant, this property is expected to be preserved by the RG flow. Within the Malthusian Toner and Tu theory, the most general form of a theory obeying Galilean invariance is given by

$$\partial_t \boldsymbol{\psi} + v_0\gamma_1 \left(\boldsymbol{\psi} \cdot \nabla \right) \boldsymbol{\psi} = \Gamma\nabla^2\boldsymbol{\psi} + \Gamma_2\nabla \left(\nabla \cdot \boldsymbol{\psi} \right) + \sqrt{2\tilde{\Gamma}}\boldsymbol{\theta} \tag{6.116}$$

This theory is obtained by setting $m = J = \gamma_{2,3} = 0$, which are all the terms that violate Galilean invariance, namely that do not leave the equations of motion invariant under the a change of reference frame [43]:

$$\boldsymbol{x}' = \boldsymbol{x} - v_0\gamma_1\bar{\boldsymbol{\psi}}t \qquad t' = t \qquad \boldsymbol{\psi}' = \boldsymbol{\psi} + \bar{\boldsymbol{\psi}} \tag{6.117}$$

This transformation also implies that the derivatives in the new reference frame are different,

$$\nabla' = \nabla \qquad \partial_{t'} = \partial_t - \bar{\boldsymbol{v}} \cdot \nabla \quad , \tag{6.118}$$

where the prime indicates the derivatives in the new reference frame. It can be easily seen that the force terms proportional to m, J, γ_2, and γ_3 explicitly break this

symmetry; this means that if one applied the transformation (6.117) to the equation of motion, they would get a theory different from the original one.

The presence of Galilean invariance, which must be preserved under the RG flow, guarantees that the material derivative $\mathcal{D}_t = \partial_t + (\boldsymbol{v} \cdot \boldsymbol{\nabla})$, which is a Galilean-invariant operator, does not take perturbative RG contributions. As expected, when $m = J = \gamma_2 = \gamma_3 = 0$, or equivalently when $r = u = g_2 = g_3 = 0$, we have that

$$\delta\Omega = \delta\gamma_1 = 0 \tag{6.119}$$

Incompressible active matter

Here, I will show that in the $\mu \to \infty$ limit, the Malthusian Toner and Tu theory precisely reproduces the critical behaviour of incompressible active matter studied by Chen *et al.* in [23]. To check this, let me show how do the flow equations look on the $\mu = \infty$ manifold. In this limit, the β-functions read

$$\beta_{\tilde{u}} = \tilde{u}\left(\epsilon - \frac{1}{2}g_1^2 - \frac{17}{2}\tilde{u}\right) \tag{6.120}$$

$$\beta_r = r\left(2 - \frac{9}{2}\frac{r - \Lambda^2}{r}\tilde{u} - \frac{1}{4}g_1^2\right) \tag{6.121}$$

$$\beta_{g_1} = g_1\left(\frac{\epsilon}{2} - \frac{3}{8}g_1^2 - \frac{5}{3}\tilde{u}\right) \tag{6.122}$$

$$\beta_{g_2} = g_2\left(\frac{\epsilon}{2} - \frac{3}{8}g_1^2 + \frac{9}{2}\tilde{u} - \frac{11}{12}\frac{g_1\tilde{u}}{g_2}\right) \tag{6.123}$$

$$\beta_{g_3} = g_3\left(\frac{\epsilon}{2} - \frac{3}{8}g_1^2 + \frac{9}{2}\tilde{u} - \frac{13}{17}\frac{g_1\tilde{u}}{g_3}\right) , \tag{6.124}$$

Quite remarkably, the behaviour of r, $\tilde{u}$ and g_1 decouples from the coupling constants g_2 and g_3. But what turns out to be even more surprising is that the recursion relations for r, $\tilde{u}$ and g_1 (6.120)-(6.122) take the same form as in [23], thus leading to the same fixed-point structure.

These flow equations give rise to three unstable fixed points, namely the trivial Gaussian fixed point, with $g_i^* = u^* = r^* = 0$, the incompressible Navier-Stokes fixed point [46] where $u^* = r^* = 0$ but $g_1^* \neq 0$ and the equilibrium dipolar Model A fixed point where $g_i^* = 0$ [23]. The stable fixed point, describing incompressible active matter systems, is given by

$$g_1^* = 2\sqrt{\frac{31}{113}\epsilon} \qquad g_2^* = \frac{11}{17}\sqrt{\frac{31}{113}\epsilon} \qquad g_3^* = \frac{13}{17}\sqrt{\frac{31}{113}\epsilon} \tag{6.125}$$

$$\mu^* = \infty \qquad \tilde{u}^* = \frac{6}{113}\epsilon \qquad r^* = -\frac{27}{226}\epsilon\Lambda^2 , \tag{6.126}$$

at which both advection g_i and ferromagnetic u effective couplings have a finite fixed-point value. The critical exponents of this fixed point coincide with the ones found in [23]. I give here the expression of the critical exponents ν, η and z

$$\nu = \frac{1}{2} + \frac{29}{226}\epsilon \qquad \eta = \frac{31}{113} \qquad z = 2 - \frac{31}{113}\epsilon \tag{6.127}$$

Interestingly, the critical behaviour of incompressible active matter was derived without imposing any constraint on the order parameter. In [23] the authors impose a constraint on the order parameter at the beginning of the computation; that is the reason why the equilibrium limit of their model is a dipolar ferromagnet and not a simple isotropic ferromagnet. To some extent, the incompressible limit of the Malthusian Toner-Tu theory looks quite different from the strictly incompressible Toner-Tu Theory, since here no constraint was imposed. It is therefore remarkable that these two theories reproduce the same critical behaviour.

6.3.5 Examples of RG flow

The careful reader might have noticed that no active fixed point with $\mu < \infty$ has been discussed so far. The full RG flow equation are too intricate to be solved analytically, but in the present section I will try to show some behaviours of the RG flow, integrated numerically by starting in different regions of the parameter space.

The first initial condition I shall look at is what happens when all parameters are chosen to be close to the equilibrium manifold, which is for γ_i small. The RG flow of a selection of parameters is showed in Fig. 6.1, from which one can clearly see that the RG first approaches the equilibrium fixed point, but then leaves the equilibrium manifold entering a region of runaway RG trajectories. Interestingly, no fixed point is approached in the IR limit, an interesting feature of this Malthusian system that will better discussed in the following section.

To further strength the idea that no active compressible RG fixed point is present, I also simulated the RG flow equations by starting with parameters all of order 1. In this case, no transient arises, and the flow enters a runaway trajectory phase immediately. The RG flow for these initial conditions is shown in Fig. 6.2. Interestingly, in both cases the runaway trajectory regime is anticipated by a change
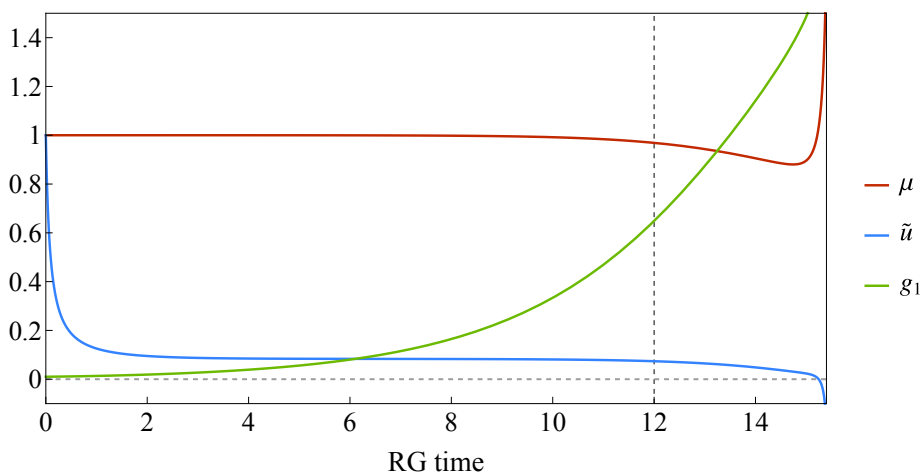
Figure 6.1. Renormalization group flow near equilibrium. In this example, the flow starts in the nearly equilibrium manifold, with $\tilde{u} = \mu = 1$ and $g_i = 10^{-2}$. As the flow escapes from the equilibrium manifold, namely as g_1 grows, the ferromagnetic coupling u_b (blue curve) eventually becomes negative, and then the flow is characterised by run-away trajectories.
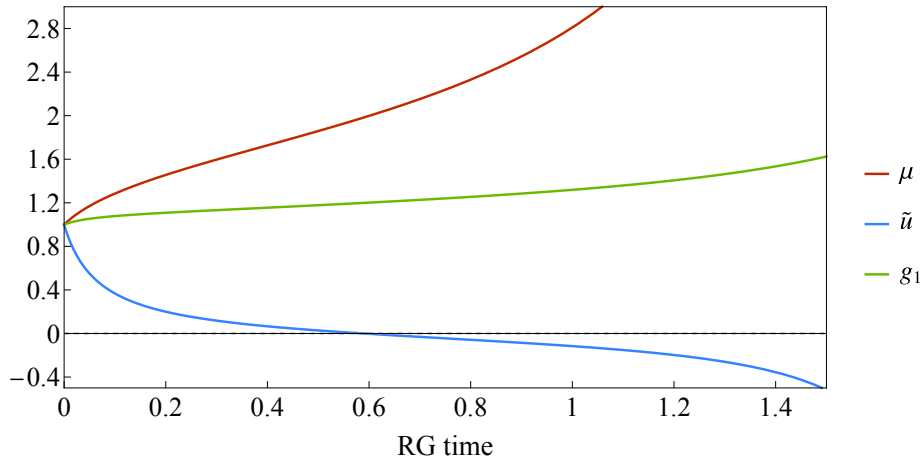
Figure 6.2. Renormalization group flow far from equilibrium. In this example, the flow starts in the far from equilibrium regime, with all coupling constants of order 1, namely $\tilde{u} = \mu = g_i = 1$. The coupling u_b (blue curve) quickly becomes negative, and then the flow is then characterised by run-away trajectories.

of sign of the coupling constant $\tilde{u}$, which flows from positive values to negative values.

6.4 Evidence of fluctuation induced first-order transition in active matter

Among many other fixed points, all reported in [MyPaper2], and reviewed in the previous the one on which I will focus my attention at the moment is the one describing incompressible active matter. As anticipated in Sec. 6.2.3, from the linearised theory one understands that the system becomes incompressible when $\mu \to \infty$, namely when $\Gamma^{\parallel} \gg \Gamma^{\perp}$. In this limit, fluctuations of $\boldsymbol{\psi}$ parallel to $\boldsymbol{k}$ are suppressed, and in turn, so are the fluctuations of the density field ρ. The RG calculation performed in the previous Section allowed me to confirm that this holds also at the non-linear level, recovering the incompressible theory for $\mu \to \infty$.

6.4.1 Stability of the incompressible fixed point

Let me now address the question of whether the incompressible active matter fixed point is stable or not. While a full linear stability analysis can be performed, I prefer here to take a simpler and more insightful approach, which will lead to the same results.

   Since I know the incompressible fixed point to be stable in the incompressible manifold $\mu \to \infty$, the only instability could come from the presence of small density fluctuations. In such a system, the value of μ would be large but finite, therefore still belonging to the neighbourhood of the incompressible fixed point. Near this

fixed point, the recursion relation of μ takes the form,

$$\mu_b = \mu_0 \left[1 - \frac{g_1^2}{4} \ln b \right] = \mu_0 b^{-g_1^2/4} \qquad \text{as} \quad \mu \gg 1 \ , \tag{6.128}$$

This reveals that the incompressible fixed point is unstable under a small deviation from incompressibility, since its scaling dimension $-g_1^2/4$ is negative. For large but finite μ, the RG flow therefore *escapes* this fixed point. Not everything is lost however: as I will show in the next section, the larger μ - i.e. the less the system is compressible - the longer the RG flow lingers near the incompressible active matter fixed point. This will give rise to a crossover [1], where depending on its size a finite system might still exhibit large-scale behaviours ruled by this incompressible active matter fixed point.

6.4.2   Crossover between second- and first-order transition

The properties of the Malthusian Toner and Tu theory in the vicinity of the transition are determined by the RG flow equations (6.96)-(6.101). These recursion relations are complicated, and it is unfortunately not easy to study them analytically. Therefore, to try to understand what happens near the transition, a set of initial values of the parameters were chosen and the flow equations were simulated numerically. Usually, this procedure leads the system's parameters to an IR-stable fixed point; however, things are more complicated in the MTT theory. As I will show here, the RG flow enters an unstable region, suggesting the presence of a fluctuation-induced first-order phase transition.

The first-order transition

In Fig. 6.3 I show the RG flow obtained by numerical integration, where initial conditions were chosen with a large initial value of μ, meaning that the RG flow starts in a neighbourhood of the incompressible active matter fixed point. As soon as the flow escapes this fixed point - which means that the longitudinal fluctuations, along with density fluctuations, become relevant - the RG flow enters an unstable region, where the ferromagnetic coupling $\tilde{u}$ becomes negative. After that, the RG flow is characterised by run-away trajectories, and the couplings blow up to larger and larger values. The condition $\tilde{u} > 0$ ensures that the pseudo-potential V of Eq. (6.3) is bounded, and as shown in Fig. 6.3 after the potential enters the $\tilde{u} < 0$ region, the potential becomes unbounded.

To have an idea of what is happening, let me consider how the pseudo-potential V changes along the RG flow. At the beginning of the RG flow, this potential takes a double-well shape, characteristic of $\lambda\varphi^4$ theories [1], guaranteeing that the order parameter is small. However, if the flow enters the $\tilde{u} < 0$ region, the pseudo-potential becomes unbounded. The interpretation of this is that the order parameter is not fluctuating around zero anymore, suggesting a breakdown of the perturbative expansion. The situation may seem puzzling: all the theories along an RG trajectory describe the same system, which means that if the system is stable at the beginning of the flow, it should remain stable along the whole RG trajectory, but figure 6.3 clearly shows the contrary.
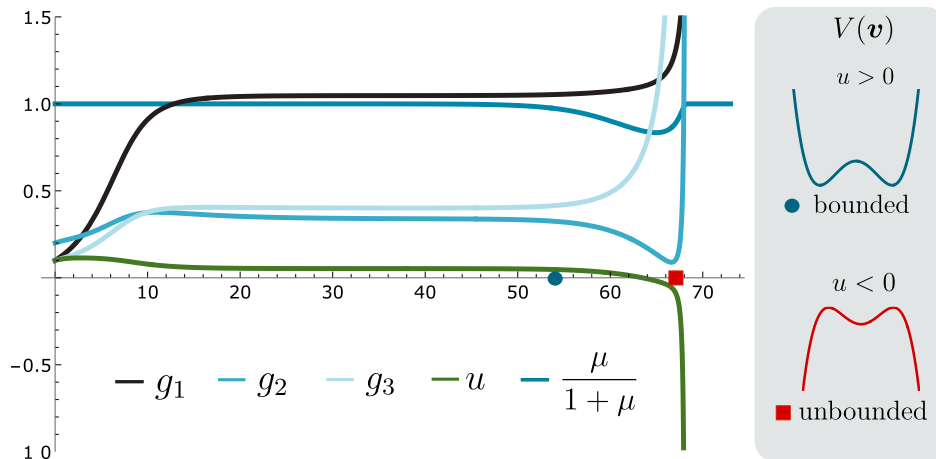
Figure 6.3. Renormalization group flow of the Malthusian Toner-Tu theory [MyPaper2] In this example, the flow starts in the nearly incompressible regime, $\mu \gg 1$ and $\mu/(1+\mu) \simeq 1$; as soon as the flow escapes from the incompressible regime, the ferromagnetic coupling u_b (green curve) becomes negative, and then the flow is characterised by run-away trajectories. In the $u_b < 0$ regime the system is unstable. In the inserts, it is qualitatively shown how the pseudo-potential $V(\psi)$ changes before (blue dot) and after (red square) the flow enters the unstable region; when u_b becomes negative the pseudo-potential is unbounded.

This apparent contradiction can be solved considering that the RG transformation may generate additional couplings that grant the stability of the theory also in the $\tilde{u} < 0$ region. In Fig. 6.4 (right) I show two Feynman diagrams that generate a ψ^6 term in the potential V of Eq. (6.3), which may stabilise the system whenever $u < 0$ (I remind that $\tilde{u}$ is proportional to the coupling u in V). Even if the coefficient u becomes negative, a force term $-\Gamma\mathcal{K}\psi^4\boldsymbol{\psi}$ could still guarantee the stability of the equation of motion, provided that $\mathcal{K} > 0$. Adding this novel force term in the equation of motion is equivalent to modifying the pseudo-potential V_{new} as follows:

$$V_{\text{new}} = \frac{r}{2}\psi^2 + \frac{u}{4}\psi^4 + \frac{\mathcal{K}}{6}\psi^6 \qquad (6.129)$$

If $\mathcal{K}$ is zero, the potential V develops a non-zero minimum only for $r < 0$; moreover, these minima are arbitrarily close to zero provided that r is small enough. This scenario gives rise to the phenomenology of a second-order phase transition. Conversely, if $\mathcal{K} > 0$, the potential V may develop a minimum which is not close to zero when u becomes negative. As shown in figure 6.4, when the constant u becomes negative the potential may develop a global minimum far from $\boldsymbol{\psi} = 0$, provided that both r and $\mathcal{K}$ remain positive; *this would result in a discontinuous, first-order, phase transition.*

In the literature, this scenario, where one or more couplings become negative and then run away, is often, but not always [96, 97], related to a fluctuation-induced first-order transition. The Heisenberg model with cubic anisotropy and the scalar electrodynamics [98] are two paradigmatic examples in which run-away trajectories result in a first-order phase transition. Non-perturbative techniques are often needed to prove that a run-away RG trajectory results in a first-order phase transition
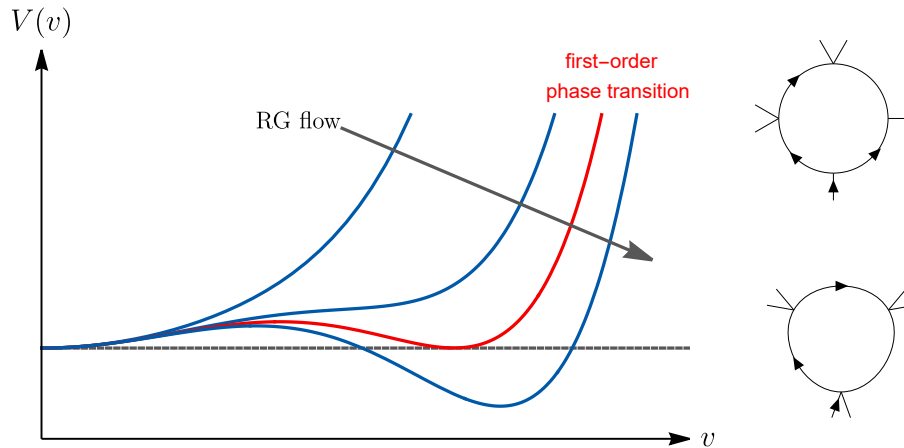
Figure 6.4. The RG generates new interactions [MyPaper2]. Left - An idea of how the inclusion of the ψ^6 term in the potential, $V_b = \frac{r_b}{2}\psi^2 + \frac{u_b}{2}\psi^4 + \frac{\mathcal{K}_b}{6}\psi^6$, may affect the renormalization group flow of the Malthusian Toner-Tu theory. u_b becoming negative, while both r_b and $\mathcal{K}_b$ staying positive, could lead to a first-order phase transition phenomenology. When the RG flow enters the $u_b < 0$ region (red curve), the perturbative expansion breaks down. **Right** - Two of the 39 possible Feynman diagrams contributing to the generation of the coupling $\mathcal{K}$.

[99, 98], but this is beyond the purposes of this perturbative RG calculation.

The RG allows to investigate properties of a system on larger and larger scales. What I just have shown is that, at sufficiently large scales, the RG flow enters an unstable $u < 0$ region; when it happens because of the strong fluctuations, the phase transition becomes first-order [98]. In this sense, I refer to this phase transition as a fluctuation-induced first-order phase transition [98].

The crossover

To understand how finite-size compressible systems, as natural swarms of insects, may still be ruled by the incompressible fixed point, I will here analyse the crossover between this fixed point and the first-order transition. Let me consider a system with relatively small compressibility, namely large μ_0. This system therefore lives *close* to the incompressible manifold $\mu = \infty$. For large enough μ, the RG flow is therefore expected to rapidly approach the incompressible fixed point, linger around it for quite a while and eventually enter the unstable region of the RG flow.

While this is the general picture for an infinite-size system exactly *at* criticality ($\xi = \infty$), the system might behave differently if $\xi < \infty$. To determine whether or not the critical dynamics is ruled by the incompressible fixed point one must consider the stopping condition of the RG flow. The RG flow stops when the correlation length becomes of the order of the inverse cutoff, namely when $\xi_{\text{stop}} = \Lambda^{-1}$. Reminding that the correlation length ξ after l RG steps trivially scales as

$$\xi_l = \frac{\xi_{l-1}}{b} = \frac{\xi_0}{b^l} \, , \tag{6.130}$$

one can derive the number of RG iterations before stopping l_{stop} by requiring that $\xi_{l_{\text{stop}}} = \Lambda^{-1}$, which leads to $l_{\text{stop}} = \log_b(\Lambda\xi)$. If at the end of the RG flow μ_{stop} is still large, the incompressible active matter fixed point rules the critical dynamics.

Let me now show what this can tell us about the size of the system. As shown in Eq. (6.128), the scaling of μ, at large μ, is given by

$$\mu_l = \mu_{l-1} b^{-g_1^2/4} = \mu_0 b^{-\int_0^l \mathrm{d}l'\, g_1(l')^2/4}\,. \tag{6.131}$$

After the last equality, at the exponential, I have the integral over the RG flow trajectory of the scaling exponent $\chi_\mu = -g_1^2/4$. When the RG starts close enough to the incompressible manifold, the parameters rapidly converge towards the incompressible fixed point and linger there for many RG iterations. If by the time the number of iterations reaches l_{stop}, the parameters are still in the proximity of the incompressible point, the large-scale behaviour is ruled by this fixed point. When this happens, for most of the RG time $g_1(l) = g_1^*$, with g_1^* being the fixed point value of g_1, given by Eq. (6.125). Therefore, the integral on the r.h.s. of (6.131) can be approximated by $\int \mathrm{d}l\, g_1(l)^2/4 \approx l_{\text{stop}}(g_1^*)^2/4$. With this in mind, let me turn my attention back to the value of μ at this stopping condition, given by

$$\mu_{\text{stop}} = \mu_0 b^{-l_{\text{stop}}\phi} = \mu_0(\xi\Lambda)^{-\phi} \qquad\qquad \phi = \frac{(g_1^*)^2}{4} = \frac{31}{113}\epsilon \tag{6.132}$$

Since I assumed the parameters are still in the proximity of the incompressible manifold, $\mu_{\text{stop}} \gg 1$. As a consequence, the correlation length of a system whose behaviour is ruled by the incompressible active matter fixed point (6.127) is bounded by

$$\xi \ll \Lambda^{-1}\mu_0^\phi \qquad, \qquad \phi = \frac{31}{113}\epsilon\,, \tag{6.133}$$

Here ϕ is the so-called crossover exponent [1].

In finite systems, the correlation length is always bounded by the system size L, and a relation akin to (6.133) can be derived. If

$$L \ll \Lambda^{-1}\mu^\phi \tag{6.134}$$

the critical dynamics is ruled by the incompressible fixed point, meaning that the results of Chen et al. [23] also hold in sufficiently small systems with mild density fluctuations $\mu \gg 1$, as it has been observed numerically in [69]. Conversely, if the system size is large enough, $L \gg \mu^\phi$, its properties at the transition point are not described by the incompressible active matter fixed point and the system crosses over to a first-order behaviour. Let me remark that μ can be measured by looking at the system's transverse and longitudinal correlation functions, and, at least in principle, it could be measured both in numerical simulations and in real experiments.

6.4.3   Take-home message for swarms

The analysis of this Malthusian Toner and Tu theory revealed the presence of a crossover between an unstable incompressible critical point and a first-order phenomenology. To understand how this applies to swarms, let me recall that midges are indeed active and they have been shown to align with their neighbours.

Based on these simple observations, one should in principle conclude that swarms' dynamics is described by some Vicsek-like model, and therefore undergo a first-order transition. However, the very observation of scaling laws - a hallmark of second-order phenomenology - in swarms, together with the absence of phase separation - usually encountered near the phase transition-, suggests that compressibility should be low. In [69] this idea was tested in numerical simulations, showing that Vicsek swarms with homogeneous density profiles are well-described by the incompressible active matter fixed point found in [23]. Here, I gave additional support to this interpretation through a renormalization group analysis. I furthermore demonstrated that the scaling laws for these finite-size systems are ruled by incompressible exponents even if the system is not strictly incompressible, as long as their size is smaller than a critical scale μ^{ϕ}. These results will allow me to theoretically study swarms through an *incompressible* theory, simplifying the task by getting rid of density fluctuations.

Chapter 7

The role of behavioural inertia in biological systems

In the analysis performed in Chapter 3, I showed that the combined effect of activity and alignment, both properties detected in natural swarms of insects, give rise to a rich phenomenology. Because of the presence of an instability of the ordered state near the phase transition, it has been argued that this is turned into a first-order phase transition where no scaling laws should be expected. Since, in natural swarms, no strong spatial heterogeneity has been detected, it might be tempting to enforce incompressibility and hope that the behaviour of swarms is equivalent to that of systems where density fluctuations are completely suppressed. When incompressibility is enforced, the transition is shown to be second-order [23].

Further analysis on the role of density fluctuations has been performed in Chapter 6, where a renormalization group approach strongly supports the idea that incompressibility is not only a mere simplification when attempting to describe natural swarms but a valid hypothesis. I showed that, whenever scale-free velocity-velocity correlations are observed in a near-critical active matter system, the associated critical exponents belong to the incompressible universality class even if the system of interest is not incompressible. Therefore, although the system might allow mild density fluctuations, on large scales it behaves as if it was incompressible. This extends the results of [23], reviewed in Chapter 3, to finite-size compressible polar active systems.

In principle, one would expect natural swarms of insects to fall into this class. They exhibit scaling laws [13] and are indeed active [MyPaper1]. However, swarms' dynamic critical exponent of $z_{\text{exp}} = 1.37 \pm 0.11$ [MyPaper1] is far from the RG prediction of $z = 1.73$ of the incompressible Toner and Tu theory [23]. In the present chapter, in an attempt to fill this gap, I will introduce the concept of inertial behaviour and show that it is required to correctly describe swarms' dynamic behaviour. Following symmetries and conservation laws, I will then show in the equilibrium case what are the effects of introducing inertia on the structure of the field theory. Finally, I will review how these changes in the field theory's structure give rise to a change in universality class, from that of Model A to that of Model G [40].

7.1 Experimental evidence suggests the presence of inertial behaviour

The first hints about the necessity of restoring inertial dynamics in the description of collective behaviour in biological systems came from experiments on bird flocks. When a flock undergoes a collective turn, local variations in the direction of motion propagate linearly in time with surprising efficiency [100]. Although "sound" modes arise in the Toner and Tu hydrodynamic theory as a consequence of density-velocity coupling, they are known to lead to giant density fluctuations [27] that have not been observed in turning flocks. To explain these observations, a different physical mechanism responsible for the propagating sound waves during turns has been proposed in [100], namely the presence of *inertia* in the orientational dynamics of the particles.

In the case of natural swarms of insects, hints of something missing in the description provided by the Toner and Tu theory come from direct inspection of the temporal correlation functions. These correlation functions exhibit a non-exponential decay on short timescales [13], which cannot be explained within the context of systems falling in the hydrodynamic description provided by the Toner and Tu theory. Note that density-velocity couplings, present in Toner and Tu theory, do generate sound modes, and thus might in principle give rise to a non-exponential decay for short times. However, as discussed in Chapter 6, these couplings are negligible in swarms's description. When density fluctuations are suppressed, the dynamic equation of the Toner and Tu theory is first-order in time and thus cannot give rise to sound modes. This implies that temporal relaxation is exponential in time, as observed in numerical simulations of the Vicsek model [13]. Therefore, to recover the proper *inertial* shape of the correlation function, some other coupling that recovers second-order dynamics is required.

To see this, in [13] the following function was introduced, whose limit in for $x \to 0$ gives useful information on the presence of inertia:

$$h(x) = -\frac{1}{x} \log \hat{C}(\tau x) \qquad , \quad x \equiv \frac{t}{\tau}. \tag{7.1}$$

Here $\hat{C}(t) = C(t)/C(0)$ is the normalised temporal correlation function, while τ is the characteristic decorrelation time-scale. For a vanishing derivative in $t = 0$, $\hat{C}'(0) = 0$, the quantity $h(x)$ vanishes near $x = 0$. To see this, one can use the Bernoulli-De l'Hospital rule:

$$\lim_{x \to 0^+} h(x) = -\lim_{x \to 0^+} \frac{\log \hat{C}(\tau x)}{x} \overset{H}{=} -\lim_{x \to 0^+} \frac{\tau \hat{C}'(\tau x)}{\hat{C}(\tau x)} \tag{7.2}$$

Reminding that $\hat{C}(0) = 1$ for normalisation, one finally obtains that

$$\lim_{x \to 0^+} h(x) = -\tau \hat{C}'(0) \tag{7.3}$$

Therefore, if $\hat{C}'(0) = 0$, then $h(0) = 0$.

On the other hand, if one considers the case of purely exponential correlations $\hat{C}(t) = e^{-t/\tau}$, the derivative of $\hat{C}$ for small times is finite, $\hat{C}'(0) = -\tau^{-1}$, and

therefore the function $h(x)$ approaches 1 for $x \to 0$. In fact, for purely exponential correlations $h(x) \equiv 1$ for all x. Summarising, one can say to observe

$$\cdot \text{Inertial Behaviour, if:} \qquad \lim_{x \to 0^+} h(x) = 0 \qquad (7.4)$$

$$\cdot \text{Non-inertial Behaviour if:} \qquad \lim_{x \to 0^+} h(x) = 1 \qquad (7.5)$$

In [13], the behaviour of the function h in natural swarms was compared to that obtained in numerical simulations of the Vicsek model. As shown in Fig. 7.1, the difference in the behaviour of h is remarkable: Vicsek dynamics exhibits a clear non-inertial behaviour, while in natural swarms $h \to 0$ as $x \to 0$, a hallmark of inertial behaviour.

7.1.1   Inertial vs non-inertial behaviour: a toy model

To better understand how inertia can be recovered, let me here focus on the simplest case possible where inertial vs non-inertial behaviour can be appreciated: the stochastic harmonic oscillator [101]. This will serve as a toy model to better understand the concept of behavioural inertia, and how it connects to the shape of the temporal correlation function.

The stochastic harmonic oscillator is defined by the equation

$$m\ddot{u} = -\gamma\dot{u} - \frac{\partial U}{\partial u} + \sqrt{2\gamma T}\,\theta\,, \qquad (7.6)$$

which directly follows from Newton's second law. Here u is some generalised coordinate, say the position, γ the viscosity, T the temperature and $U = \frac{1}{2}\kappa u^2$ the harmonic potential. The quantity m, which is the mass if u is a position, is often referred to as *inertia* and represents a sort of *resistance* in the change of behaviour. This resistance inhibits sudden changes in the system's configuration, thus delaying decorrelation and giving the correlation function the characteristic inertial shape. The white noise θ is Gaussian, delta-correlated in time and with unitary variance. This second-order differential equation can be written as a system of two coupled first-order differential equations

$$\begin{cases} \dot{u} = \frac{p}{m} \\ \dot{p} = -\frac{\gamma}{m}p - \frac{\partial U}{\partial u} + \sqrt{2\gamma T}\,\theta \end{cases}, \qquad (7.7)$$

where $p = m\dot{u}$ is the conjugate momentum of u, namely linear momentum in the present case.

The overdamped limit

Let me start my analysis by looking at what happens in the *overdamped* limit, namely on timescales much larger than m/γ. On these timescales, the conjugate momenta relaxes to a steady-state value, and hence $\dot{p} \approx 0$. Therefore from the second equation, one can work out the steady-state value of p, namely

$$\frac{p}{m} = -\frac{1}{\gamma}\frac{\partial U}{\partial u} + \sqrt{2\frac{T}{\gamma}}\theta \qquad (7.8)$$
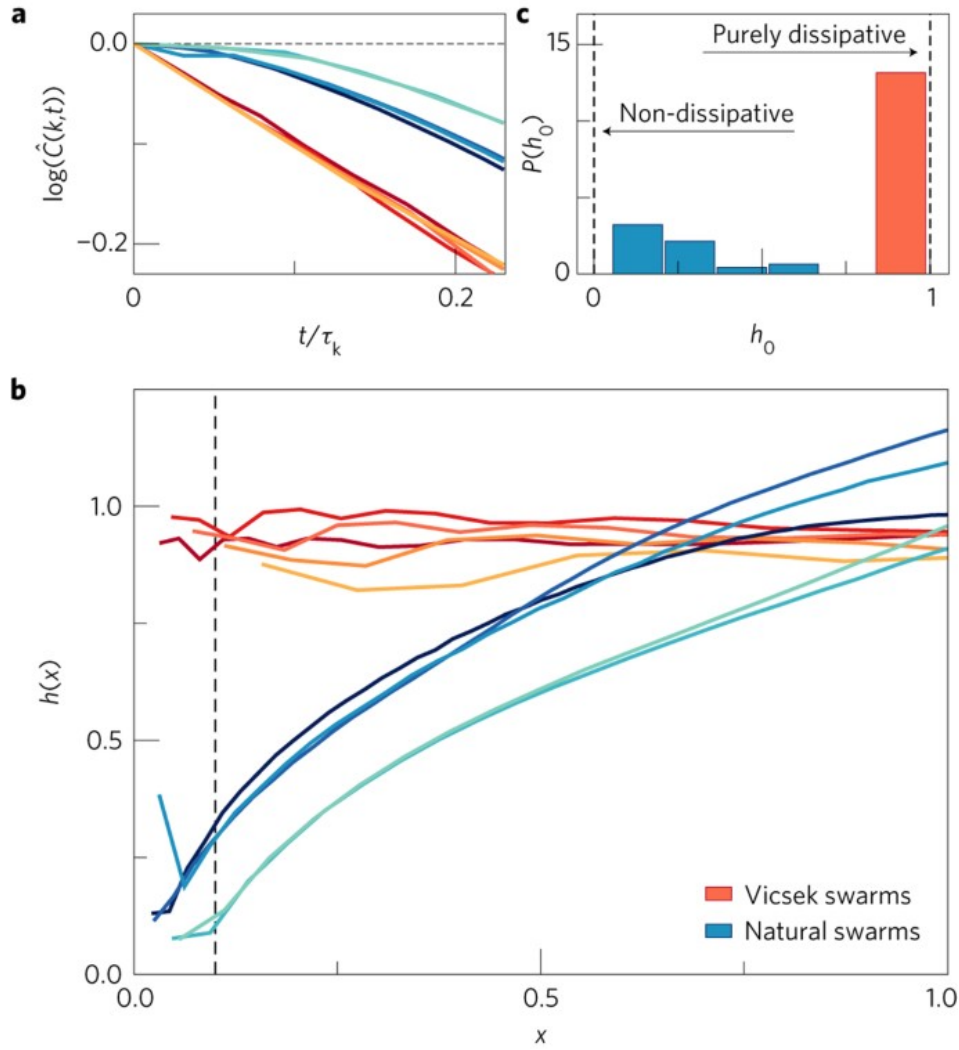
Figure 7.1. Inertial behaviour in swarms [13]: **a)** The correlation in Vicsek swarms displays exponential relaxation (linear decay in semi-log scale), while natural swarms have a strongly non-exponential correlation function (flat derivative for small t). **b)** To quantify the different forms of the correlation the function $h(x)$ defined in (7.1) was calculated, where $x = t/\tau$; in contrast with Vicsek, natural swarms are characterised by a small value of $h(x)$ in the interval $0 < t < \tau$. **c)** The estimated intercept $h_0 = h(x = 0.1)$ was computed for all data [13] and its distribution reported here: all natural swarms have a low first derivative, indicating the existence of non-dissipative modes, while Vicsek swarms have a purely dissipative peak at $h_0 \sim 1$. *Permission to reuse granted by Springer Nature under License Number 5655281510730.*

which, if inserted in the first equation, leads to

$$\gamma\dot{u} = -\frac{\partial U}{\partial u} + \sqrt{2\gamma T}\theta \tag{7.9}$$

Note that this equation is equivalent to taking $m = 0$ in the equation (7.6): in fact, the overdamped limit can be defined as the limit for $m\kappa/\gamma^2 \to 0$. In this limit, the timescale needed for inertial effects to remain relevant $\tau_m = m/\gamma$ is infinitely smaller

than the timescale over which the harmonic force exerts its influence $\tau_\kappa = \gamma/\kappa$.

The correlation function of this kind of dynamics can be obtained by standard techniques, leading to the usual *overdamped* form

$$\hat{C}(t) = \mathrm{e}^{-t/\tau} \qquad\qquad \tau = \frac{\kappa}{\gamma} \qquad\qquad (7.10)$$

which, according to the aforementioned classification of inertial vs non-inertial dynamics, clearly falls in the latter case as $h(t \to 0) \to 1$. The overdamped description is however valid *only* as $t \gg m/\gamma$, or equivalently when the limit $m\kappa/\gamma^2 \to 0$ is taken. Only in this limit, the dynamics becomes exactly first-order, and the overdamped description here presented is correct.

Finally, let me highlight the striking similarity between both Model A dynamics (3.22) and the (incompressible) Toner and Tu theory (5.2), and the overdamped dynamics of the stochastic harmonic oscillator (7.9): in both cases the dynamics is first-order in time. This explains the lack of inertial behaviour observed in the Vicsek model (see Fig. 7.1), supporting the idea that alignment and activity on their own are not expected to be enough to describe collective behaviours in swarms.

The underdamped regime

The statistics of the stochastic harmonic oscillator can be worked out also in the general case, as its dynamics is linear. In particular, after a little effort, one can show that the normalised temporal correlation function of the system takes the form [13, 101]

$$\hat{C}(t) = \frac{C(t)}{C(0)} = \mathrm{e}^{-t/\tau} \left(\cos(\omega t) + \frac{1}{\tau\omega} \sin(\omega t) \right) , \qquad\qquad (7.11)$$

where

$$\tau = \frac{2m}{\gamma} \qquad\qquad \omega = \sqrt{\frac{\kappa}{m} - \frac{\gamma^2}{4m^2}} \qquad\qquad (7.12)$$

The temporal derivative of this correlation function is given by

$$\hat{C}'(t) = -\frac{\mathrm{e}^{-t/\tau}\left(\tau^2\omega^2 + 1\right)\sin(\omega t)}{\tau^2\omega} \overset{t \to 0}{\nrightarrow} 0 \qquad\qquad (7.13)$$

Therefore, for any $m \neq 0$, even if very *small*, the limit $h(x \to 0^+) = 0$, hence meaning that inertial behaviour is present when the dynamics is second-order in time.

This apparently seems to contradict the result found in the previous section, in which I showed that for $m/\gamma \ll \gamma/\kappa$ non-inertial behaviour was found, namely that $\hat{C}' \neq 0$ as $t \to 0$. To solve this puzzle, one has to keep in mind that the overdamped limit $(m\kappa/\gamma^2 \to 0)$ and the $t \to 0$ limit taken in (7.13) do not commute. Therefore, for *any* finite m the correlation functions will *always* display inertial behaviour, while only if $m\kappa/\gamma^2 = 0$ then the dynamics is non-inertial and thus $\hat{C}'(0) \neq 0$. However, the timescale separating these two different behaviours of h is precisely $\tau_m = m/\gamma$: therefore, in the $m \to 0$ inertial behaviour is detectable only if the data are sufficiently time-resolved.

7.1.2 Relevance of inertial behaviour for collective behaviours swarms

From the discussion of the previous section, I hope I convinced the reader that experimental evidence clearly shows swarms are systems where inertial behaviour is present at the time resolution of current experiments. At this point, a key question to answer is whether this inertial behaviour is relevant in describing the collective behaviours of swarms. The property of being inertial seems deeply related to the small time behaviour, while collective behaviours characterise the *large* time behaviour of a system.

To answer this question one has to look at the behaviour of $h(x)$ over larger values of x. In particular, one expects that in the presence of some viscosity coefficient γ, for large enough x, namely for large enough times, the overdamped description gets better and better. The function $h(x)$ is therefore expected to eventually saturate at the overdamped value $\lim_{x \to +\infty} h(x) = 1$. To address the relevance of inertia, one has to look at the scale $x^* = t^*/\tau$ where the crossover between overdamped and underdamped behaviour occurs. If $x^* \ll 1$, namely if the time-scale on which h saturates is $t^* \ll \tau$, the large-scale properties are expected to be well-described by the overdamped theory since inertial effects influence the dynamics only on very short scales $t < t^* \ll \tau$.

On the other hand, in systems like natural swarms where the decorrelation time increases with the size of the system $\tau \sim L^z$, inertial effects are relevant in the large-scale description of the system whenever $x^* \sim 1$, namely when t^* and τ are of the same order. In this way, a large portion of the modes of the theory are affected by the presence of inertial behaviour. Inertia should thus be taken into account in an effective description of the large-scale modes. By a direct inspection of the behaviour of $h(x)$ in swarms (see Fig. 7.1.c), it is clear that t^* and τ are of the same order, and hence inertial behaviour is expected to be relevant in the description of collective behaviours in swarms.

7.2 Behavioural inertia from a symmetry perspective

Given that inertial behaviour is a relevant feature of the description of natural swarms of insects, as shown in the previous section, the natural following question is *how* to account for this inertial behaviour. Therefore, I will review what in the context of swarms (and flocks) is the most proper way to achieve inertial dynamics.

7.2.1 Recovering a Hamiltonian structure

As one can see from the case of the stochastic harmonic oscillator, the critical difference between an overdamped, non-inertial dynamics (7.9) and an inertial one (7.7) is the structure of the equations of motion. In the former case, the *force* coming from the harmonic potential acts directly on the dynamics of the order parameter u, while in the latter it is *mediated* by the linear momentum p.

To recover inertial behaviour, I need to introduce a similar symplectic structure for Self-Propelled Model A. One of the best ways of doing so, proposed in [100] for the case of flocks, is by recognising that although Self-Propelled Model A is invariant under rotations, there is no trace of an associated conservation law.

However, according to Noether's theorem, when a system is invariant under a given symmetry group, the generator of this symmetry should be conserved. The presence of conservation laws heavily affects the critical properties of a system, potentially changing its dynamic behaviour. Since Self-Propelled Model A was explicitly built to be invariant under a rotational symmetry, the idea is to recover inertial behaviour by coupling (5.2) with the conservation law associated with rotational invariance.

The Inertial Spin Model

A possible way to restore inertial behaviour has been proposed in [102], where a model named Inertial Spin Model (ISM) has been introduced to provide a theoretical explanation for information propagation in flocks [100]. The ISM shares many common features with the Vicsek model, but has one main (and crucial) difference: the aligning force does not act directly on the equation of the direction of motion $\boldsymbol{\psi}_i$ but is mediated by the local generator of rotational symmetry $\boldsymbol{s}_i$, in the following way:

$$
\begin{aligned}
\frac{\mathrm{d}\boldsymbol{\psi}_i}{\mathrm{d}t} &= \frac{\boldsymbol{\psi}_i \times \boldsymbol{s}_i}{\chi} \\
\frac{\mathrm{d}\boldsymbol{s}_i}{\mathrm{d}t} &= -\frac{\eta}{\chi}\boldsymbol{s}_i + \left[\mathcal{J}n_{ij}\boldsymbol{\psi}_j + \boldsymbol{\zeta}_i\right] \times \boldsymbol{\psi}_i
\end{aligned}
\tag{7.14}
$$

Here χ is usually referred to as *inertia*, since it plays a role similar to that of the mass for the stochastic harmonic oscillator, while η is the dissipation, playing a role analogue to viscosity. As in the case of the stochastic harmonic oscillator, the overdamped limit is reached for times $t \ll \chi/\eta$. In this limit, the behaviour of the Vicsek model is properly recovered, as when $t \ll \chi/\eta$ the spin *quickly* approaches a steady-state, where $\boldsymbol{s}_i/\chi = \boldsymbol{\psi}_i \times \left[\mathcal{J}n_{ij}\boldsymbol{\psi}_j + \boldsymbol{\zeta}_j\right]$, and hence

$$
\frac{\mathrm{d}\boldsymbol{\psi}_i}{\mathrm{d}t} = \boldsymbol{\psi}_i \times \left[\left(\mathcal{J}n_{ij}\boldsymbol{\psi}_j + \boldsymbol{\zeta}_j\right) \times \boldsymbol{\psi}_i\right] = \mathcal{R}\left[\mathcal{J}n_{ij}\boldsymbol{\psi}_j + \boldsymbol{\zeta}_i\right]
\tag{7.15}
$$

The local generator of rotational symmetry $\boldsymbol{s}$, in analogy with quantum mechanics, has been called *spin*, since it represents the generator of rotations in the *internal* space of the velocities. It must not be confused with angular momentum, which is the generator of rotations in positions' space. To put this new quantity into context, it can be viewed as a measure of how much an individual is rotating around its own axis; more precisely, it is proportional to the curvature of the trajectory, namely to the inverse of its radius of curvature: all individuals sharing the same spin undergo equal radius turns rather than parallel-path turns [100].

Conservation (or slow dissipation) of the total spin has a huge impact on the dynamics of the system. The presence of a spin-velocity coupling makes the spin responsible for carrying information, giving rise to second-sound propagation in flocks. The presence of second-sound modes even close to the ordering transition (called 'paramagnons' in condensed matter) was also found experimentally in natural swarms [13], supporting the idea that spin-velocity mode-coupling is also an essential mechanism of these systems.

Inertia at the hydrodynamic level

When shifting my attention to hydrodynamics, inertia can be restored by dynamically coupling the direction of motion field with to spin field [41]. The global conservation of the spin induced by the Noether theorem allows it to fluctuate on space-time scales comparable with those of critical fluctuations, thus making spin-velocity couplings relevant in the RG sense. To simplify the discussion, I will first discuss the effects of restoring inertia in the absence of activity, namely using a fixed network approximation. This approximation is indeed not suitable for swarms since network rearrangements induced by activity are indeed relevant in the description of swarms, as I showed in Chapter 3. Nevertheless, understanding how inertia can be restored in the equilibrium context of Model A will help me develop the correct self-propelled theory, in a similar fashion to how Toner and Tu developed the self-propelled version of Model A.

At equilibrium, namely when $v_0 \to 0$, a mode-coupling interaction between the order parameter $\boldsymbol{\psi}$ and its spin $\boldsymbol{s}$ arises from their Poisson-bracket relation [40]

$$\left\{ s_{\alpha\beta}\left(\boldsymbol{x}\right), \psi_\gamma\left(\boldsymbol{x}'\right) \right\} = 2\, g\, \mathbb{I}_{\alpha\beta\gamma\nu} \psi_\nu\left(\boldsymbol{x}\right) \delta\left(\boldsymbol{x} - \boldsymbol{x}'\right) , \tag{7.16}$$

which encodes the fact that $\boldsymbol{s}$ is the generator of rotations of $\boldsymbol{\psi}$. The parameter g is the reversible coupling regulating the symplectic structure, i.e. the inertial coupling between polarisation and spin. In general, when the order parameter is a n-dimensional vector, the generator of its rotations $\boldsymbol{s}$ is a $n \times n$ anti-symmetric tensor [103]. The tensor $\mathbb{I}$ represents the identity in the space of $s_{\alpha\beta}$, and it is given by,

$$\mathbb{I}_{\alpha\beta\gamma\nu} = \frac{\delta_{\alpha\gamma}\delta_{\beta\nu} - \delta_{\alpha\nu}\delta_{\beta\gamma}}{2} , \tag{7.17}$$

with the factor $\frac{1}{2}$ ensuring that $\mathbb{I}_{\alpha\beta\gamma\nu} s_{\gamma\nu} = s_{\alpha\beta}$ and $\mathbb{I}_{\alpha\beta\sigma\tau}\mathbb{I}_{\sigma\tau\gamma\nu} = \mathbb{I}_{\alpha\beta\gamma\nu}$.

Working with an order parameter of generic dimension n, rather than set directly $n = 3$ as in the physical case, might seem inconvenient at first glance. When $n = 3$ the spin $\boldsymbol{s}$ can be written as a 3-dimensional vector, lightening the tensorial structure and reducing the number of indices. This comes from the fact that when $n = 3$, the plane on which the rotation occurs can be uniquely identified by the vector orthogonal to it, while this does not happen when $n > 3$. However, there is an important reason to work with a tensorial spin, rather than a vectorial one. In the active case, which will be studied later, the velocity $\boldsymbol{v}$ has the same dimension d as space, and therefore so will the order parameter $\boldsymbol{\psi}$, the direction of motion. Although the physical case is given by $n = d = 3$, the RG perturbative expansion is performed by expanding d near the upper critical dimension $d_c = 4$, hence one is forced to work with an order parameter of dimension $n = d \sim d_c$ to correctly perform the RG perturbative expansion.

7.3 Restoring behavioural inertia at equilibrium: Model G

The equilibrium dynamics of a near-critical system in which $\boldsymbol{s}$ is conserved, known respectively as Model E and G for a two- and three-dimensional order parameter

[40] and generalised by the Sasvari-Schwabl-Szepfalusy (SSS) model in n dimensions [103, 104], can be constructed following the Mori-Zwanzig formalism [105, 106] and it is given by [103, 107],

$$\partial_t \psi_\alpha = -\Gamma \frac{\delta \mathcal{H}}{\delta \psi_\alpha} + g\,\psi_\beta \frac{\delta \mathcal{H}}{\delta s_{\alpha\beta}} + \theta_\alpha\,, \tag{7.18}$$

$$\partial_t s_{\alpha\beta} = -\Lambda_{\alpha\beta\gamma\nu} \frac{\delta \mathcal{H}}{\delta s_{\gamma\nu}} + 2g\,\mathbb{I}_{\alpha\beta\gamma\nu}\psi_\gamma \frac{\delta \mathcal{H}}{\delta \psi_\nu} + \zeta_{\alpha\beta}\,. \tag{7.19}$$

Here, and in the following, summation over repeated index is understood.

To encode the presence of alignment, free energy functional $\mathcal{H}$ is chosen to take the usual Landau-Ginzburg form for the critical field $\boldsymbol{\psi}$ while it is purely Gaussian for the spin field, namely

$$\mathcal{H} = \int \mathrm{d}^d x \frac{1}{2}(\partial_\alpha \psi_\beta)(\partial_\alpha \psi_\beta) + V(\boldsymbol{\psi}) + \int \mathrm{d}^d x \frac{1}{4} s_{\alpha\beta} s_{\alpha\beta}\,. \tag{7.20}$$

Here the $(\nabla\psi)^2$ term tends to suppress the presence of strong fluctuations, namely favouring local alignment between neighbouring regions, while the potential is

$$V(\boldsymbol{\psi}) = \int \mathrm{d}^d x \frac{r}{2} \boldsymbol{\psi} \cdot \boldsymbol{\psi} + \frac{u}{4} (\boldsymbol{\psi} \cdot \boldsymbol{\psi})^2\,, \tag{7.21}$$

Inertia is restored thanks to the presence of mode-coupling interactions that encode the conservative nature of the dynamics, arising as a consequence of the Poisson-bracket relation (7.16). The term $\partial_t s \sim g\psi \times \delta_\psi \mathcal{H}$ represents the action of the *force* on the dynamics of the spin, rather than directly on the order parameter. The indirect action of this force on the dynamics of $\boldsymbol{\psi}$ is guaranteed by the term $\partial_t \psi \sim g\psi \times \delta_s \mathcal{H}$, which expresses the rotation of $\boldsymbol{\psi}$ induced by the conservation of $\boldsymbol{s}$. This mode-coupling mechanism restores the inertial structure of the equations of motion, thus allowing one to describe the behaviour observed experimentally in swarms in the field [13].

On the other hand, the terms $\partial_t \psi = -\Gamma \delta_\psi \mathcal{H}$ and $\partial_t s \sim -\Lambda \delta_s \mathcal{H}$ represent dynamic relaxations, giving rise to the diffusion and transport phenomenology typical of stochastic statistical systems. These relaxation terms are thus complemented by the white Gaussian noises $\boldsymbol{\theta}$ and $\boldsymbol{\zeta}$, whose variances are given by Einstein relations when the system is at equilibrium. The dissipative constant (or kinetic coefficient) Γ rules the relaxation of the order parameter and it is a crucial player in determining the dynamic exponent z since it fixes the time scale on which relaxation occurs. Similarly, the kinetic tensor $\Lambda_{\alpha\beta\gamma\nu}$ rules the relaxation of the spin. When the total spin is conserved, the tensor Λ is proportional to ∇^2 [40], and in the isotropic theory it takes the form,

$$\Lambda_{\alpha\beta\gamma\nu} = -\lambda\,\nabla^2\,\mathbb{I}_{\alpha\beta\gamma\nu}\,. \tag{7.22}$$

With the choice of $\mathcal{H}$ in (7.20), the equations of Model G can be written as follows:

$$\partial_t \psi_\alpha = \Gamma\nabla^2 \psi_\alpha - m\psi_\alpha - J\psi_\beta\psi_\beta\psi_\alpha + g\,s_{\alpha\beta}\psi_\beta + \theta_\alpha\,, \tag{7.23}$$

$$\partial_t s_{\alpha\beta} = \lambda\nabla^2 s_{\alpha\beta} - 2g\,\mathbb{I}_{\alpha\beta\gamma\nu}\psi_\gamma\nabla^2\psi_\nu + \zeta_{\alpha\beta}\,. \tag{7.24}$$

where I introduced $m = \Gamma r$ and $J = \Gamma u$.

In this theory, the total spin is conserved. To see this, one can exploit the fact that $\mathbb{I}_{\alpha\beta\gamma\nu} = -\mathbb{I}_{\alpha\beta\nu\gamma}$ to rewrite the mode-coupling term in the equation for $\boldsymbol{s}$:

$$\mathbb{I}_{\alpha\beta\gamma\nu}\psi_\gamma\nabla^2\psi_\nu = \mathbb{I}_{\alpha\beta\gamma\nu}\partial_\sigma\left(\psi_\gamma\partial_\sigma\psi_\nu\right). \tag{7.25}$$

Therefore, the equation for $\boldsymbol{s}$ can be written in the form of a continuity equation. If also the noise is conservative, namely if its variance is proportional to a Laplacian ∇^2, the total integral of the spin is conserved

$$\dot{S}_{\alpha\beta}(t) = \frac{\mathrm{d}}{\mathrm{d}t}\int \mathrm{d}^d x\; s_{\alpha\beta}(x,t) = 0. \tag{7.26}$$

7.3.1 Dynamic critical behaviour of Model G

To understand if the introduction of behavioural inertia helps to fill the gap between experimental evidence in natural swarms and theoretical results, it is useful to briefly review the dynamic RG analysis of Model G. I will not perform any diagrammatic calculation here, but only go through the argument for which the dynamic critical exponent can be computed non-perturbatively, yielding $z = d/2$ for all $d < 4$, namely $z = 1.5$ in the physical case of interest for swarms $d = 3$.

Let me review the naive scaling generated by a scaling transformation

$$\boldsymbol{x} = b\,\boldsymbol{x}_b\,, \qquad\qquad\qquad t = b^z t_b\,, \tag{7.27}$$
$$\boldsymbol{\psi}(\boldsymbol{x},t) = b^{-\chi_\psi}\boldsymbol{\psi}_b(\boldsymbol{x}_b,t_b)\,, \qquad\qquad \boldsymbol{s}(\boldsymbol{x},t) = b^{-\chi_s}\boldsymbol{s}_b(\boldsymbol{x}_b,t_b)\,. \tag{7.28}$$

Please note that, contrary to all the other scaling transformations carried out in the other sections, this is performed directly in real space rather than in Fourier space. The naive scaling dimensions of the fields will therefore not match. A relation between the fields' scaling dimensions in real and Fourier space is provided by the relation

$$\chi_{\phi(\boldsymbol{x},t)} = \chi_{\phi(\boldsymbol{k},\omega)} + d + z\,, \tag{7.29}$$

where the relation between $\phi(\boldsymbol{x},t)$ and $\phi(\boldsymbol{k},\omega)$ is given by the usual Fourier transform

$$\phi(\boldsymbol{x},t) = \int_{|\boldsymbol{k}|<\Lambda}\frac{\mathrm{d}^d k}{(2\pi)^d}\int_{-\infty}^{+\infty}\frac{\mathrm{d}\omega}{2\pi}\;\mathrm{e}^{-\mathrm{i}t\omega + \mathrm{i}\boldsymbol{k}\cdot\boldsymbol{x}}\phi(\boldsymbol{k},\omega)\,. \tag{7.30}$$

With this set of scaling relations in mind, the rescaled equations of motion read

$$\partial_{t_b}\psi_\alpha = \Gamma\,b^{z-2}\nabla_b^2\psi_\alpha - m\,b^z\psi_\alpha - J\,b^{z-2\chi_\psi}\psi_\beta\psi_\beta\psi_\alpha + gb^{z-\chi_s}s_{\alpha\beta}\psi_\beta + \theta_\alpha\,, \tag{7.31}$$

$$\partial_t s_{\alpha\beta} = \lambda\,b^{z-2}\nabla_b^2 s_{\alpha\beta} - 2g\,b^{z-2+\chi_s-2\chi_\psi}\mathbb{I}_{\alpha\beta\gamma\nu}\psi_\gamma\nabla_b^2\psi_\nu + \zeta_{\alpha\beta}\,. \tag{7.32}$$

When the total spin is conserved, and the equation for the spin can be written in the form of a continuity equation, no diagrammatic correction can arise to the $\partial_t s_{\alpha\beta}$ term. This implies that the scaling dimension of s gets no anomalous contribution [107], and remains equal to its naive value $\chi_s = d/2$, which can be derived by requiring $\mathcal{H}$ to be dimensionless.

Furthermore, a Ward identity for the response function [107] prevents the coupling g from getting any correction from the RG. Therefore, the scaling of the mode-coupling term in the equation of ψ is *exact*. To make inertia relevant in the large-scale description of the system, one must have

$$z = \chi_s = \frac{d}{2} \,. \tag{7.33}$$

I would like to drive the attention of the reader on how, in three dimensions, this mode-coupling mechanism gives $z = 1.5$, a value significantly closer to the experimental window $z = 1.37 \pm 0.11$ than the value $z = 1.73$ found in active dissipative models. This result indicates that an inertial dynamical coupling is necessary to develop a theory of natural swarms fully consistent with experiments.

7.3.2   On possible violations of spin conservation

The mode-coupling dynamics introduced in the previous section was mainly motivated by symmetry arguments and associated conservation laws. However, in real biological systems, information is not expected to be propagated forever with zero dissipation, as damping effects may become relevant over longer and longer distances. Thus, a (small) spin dissipation cannot be excluded in real biological systems. Note that the introduction of this dissipation does not violate the rotational symmetry of the problem, since all hydrodynamic equations are still invariant upon rotations.

Spin dissipation without symmetry violation

To understand why the violation of spin conservation does not come from a weak violation of symmetry, let me discuss an example in a case with which the reader might be more familiar. In a translational invariant system - say a collection of marbles -, the Noether theorem states that the *total* linear momentum is conserved. If one had complete control of all degrees of freedom, namely position q and momentum p of each marble, the system could be described through Hamilton equations $\dot{p}_i = -\frac{\partial H}{\partial q_I}$, $\dot{q}_i = \frac{\partial H}{\partial p_i}$. In this case, Noether theorem can be explicitly tested: since all the interactions in H must obey translational invariance $q_i \to q_i + \delta q$, the time derivative of the total momentum $P = \sum_i p_i$ vanishes. In which cases can momentum conservation be violated? The first case is when the system is closed in a box. In this case, collisions with the walls of the box violate momentum conservation. This lack of conservation *is* due to the violation of symmetry: the presence of a wall in a precise point of space manifestly violates translational invariance.

If instead these marbles were surrounded by some medium, say a fluid, an exchange of momentum between the system and the medium is allowed. Hence, when observing the momentum of the collections of marbles only, it might be that violations of momentum conservation are detected. Does this mean that the symmetry is violated? Of course not: Noether theorem ensures conservation of the total momentum of all degrees of freedom, including those describing the medium. What happens to the total momentum of the marbles only depends on the interactions between fluid and marbles. When one aims to describe only the degrees of freedom of the system of marbles, non-Hamiltonian effective interactions

must be taken into account to describe the effect of those degrees of freedom that were coarse-grained (the medium). These interactions between the system and the medium can be effectively described as a dissipation of the momentum, apparently violating the conservation law associated with the symmetry. Instead, this effective dissipation arises as a consequence of not taking into account all the possible degrees of freedom; the symmetry and its associated conservation law are still in place.

Similarly, if the swarm were an isolated system, its total spin would be exactly conserved. Nevertheless, midges in a swarm interact not only with each other but also with the surroundings. Due to the global rotational symmetry, in virtue of Noether's theorem, the total spin of all degrees of freedom is expected to be conserved. However, Self-Propelled Model G is an effective description of swarms, in which the interactions with the environment have been coarse-grained. Hence, some spin dissipation may arise as the effect of external forces on the swarms. Whether these interactions between midges and the environment allow some spin exchange is out of current knowledge, and hence they cannot be excluded. Indeed, *if* spin exchange was possible, it has to be weak since the presence of inertial effects in the correlation functions [13] indicates that the spin dissipation is small. Nevertheless, for the sake of completeness, in the renormalization group analysis performed in Chapter 10, I will also address the question of what happens in the presence of spin dissipation.

Spin dissipation in Model G

To introduce spin-dissipation, a *k*-independent term must be added to the kinetic coefficient of the spin, $\Lambda_{\alpha\beta\gamma\nu} \to \Lambda_{\alpha\beta\gamma\nu} + \eta\mathbb{I}_{\alpha\beta\gamma\nu}$ where η represents spin-dissipation. The new form of $\Lambda_{\alpha\beta\gamma\nu}$, in isotropic theories, is therefore given by

$$\Lambda_{\alpha\beta\gamma\nu} = \eta\mathbb{I}_{\alpha\beta\gamma\nu} - \lambda\nabla^2\mathbb{I}_{\alpha\beta\gamma\nu} \ . \tag{7.34}$$

From a purely hydrodynamic perspective - i.e. at long wavelengths and long times - the existence of spin dissipation η would make the field **s** a fast mode that can be dropped from the hydrodynamic description [40]. Hence, any spin dissipation would eventually make inertia to become irrelevant.

This *naive* argument was indeed shown to be true in [41, 108], where the authors studied the critical behaviour of Model G in the presence of dissipation, showing that the stable fixed point is given by Model A behaviour, reached for $\eta \to +\infty$. However, inertial effects might be still relevant in the description of finite-size systems if the spin dissipation η is small enough. This phenomenology can be explained in terms of a crossover between an underdamped and an overdamped regime. Consider a system with linear size L: when dissipation is weak, namely $\eta \ll \lambda L^{-2}$ ($k \sim L^{-1}$ being the largest wavelength mode), the system is in its underdamped regime and conservative Model G dynamics ($\eta = 0$) effectively describes the behaviour of the system over all the physically accessible scales. On the other hand, when the size of the system becomes large enough, an overdamped regime is accessed, where dissipative effects prevail and the non-conservative behaviour of Model A is recovered. These two regimes are separated by a crossover length-scale $\mathcal{R} = \sqrt{\lambda/\eta}$, determined by the extent of dissipation: for modes with wave-vector $k \gg \mathcal{R}^{-1}$, the critical dynamics has a conservative nature (as if $\eta = 0$), with $z = 1.5$ [41]. On the other hand, on
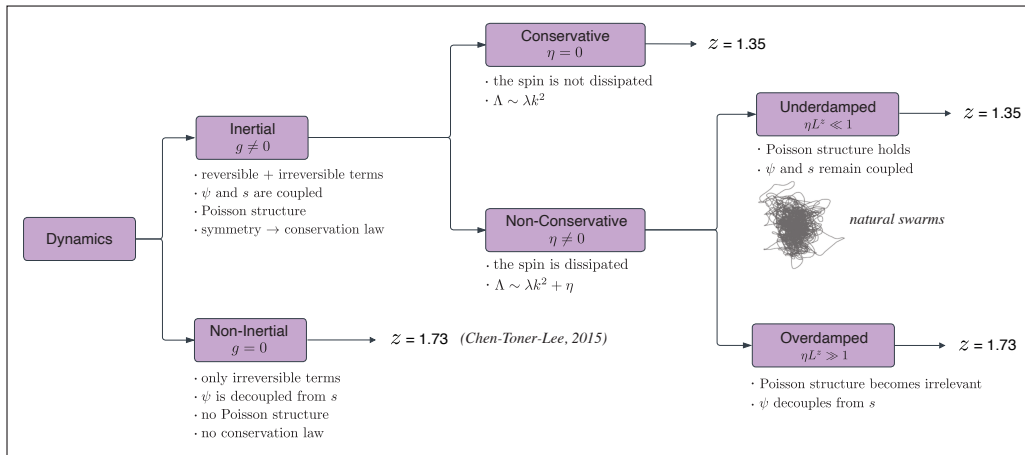
Figure 7.2. Map of the active theory. The difference between inertial and non-inertial dynamics, conservative and non-conservative behaviour, and underdamped and overdamped regimes is presented synthetically.

length scales larger than $\mathcal{R}$, $k \ll \mathcal{R}^{-1}$, the dissipation overcomes and the dissipative result of Model A is recovered.

Natural swarms definitively have a finite size. Moreover, in natural swarms, the spin dissipation must be small enough to keep the system in its underdamped phase, as otherwise, the temporal correlation functions of the theory would not reproduce the experimental ones [13] (see Sec 7.1.2). This implies that the crossover length-scale $\mathcal{R}$ must be larger than the system's size, so that experimentally one observes the conservative inertial dynamics at all the accessible scales [41]. For this reason, I will be particularly interested in the neighbourhood of the conservative $\eta = 0$ plane, even though η turns out to be a relevant perturbation in the RG sense.

At this point, a lot of different concepts have been introduced: *inertial*, *conservative*, *underdamped*. Although the reader might feel they are all synonyms, they are not. Let me try to clarify here, once and for all, the difference between these terms. The coarse-grained dynamical equations may either have or not have the reversible couplings, arising from the Poisson-bracket relation (7.16) between the polarisation ψ (i.e. the generalised coordinate) and the spin s (i.e. the generalised momentum). In the first case ($g \neq 0$) one has an *inertial* theory, with a Poisson structure expressing the fact that s is the generator of the rotational symmetry. In this case, correlation functions exhibit the inertial shape discussed in Sec. 7.1. If the reversible coupling is structurally absent ($g \equiv 0$) one recovers the *non-inertial* theory of [23], where polarisation is decoupled from the spin and the symmetry does not entail any Poisson structure. In this case, one recovers the result of $z = 1.73$.

On the other hand, in the inertial theory, the irreversible kinetic coefficient of the spin $\Lambda_{\alpha\beta\gamma\nu}$ may be either conservative or non-conservative. In the *conservative* case there is no spin-dissipation ($\eta = 0$), and a fixed point yet to be determined (see Chapter 10) will rule the large-scale behaviour of this inertial-conservative. In the *non-conservative* case, the kinetic coefficient contains a dissipative term ($\eta \neq 0$). The impact of a non-conserved spin on the collective properties, however, depends

on the interplay between the strength of spin dissipation and the size of the system. In the *underdamped* regime, where either the spin dissipation or the system's size are *small*, collective fluctuations are still ruled by the inertial-conservative fixed point; this is the regime in which I expect to find natural swarms [41]. Conversely, in the infinite-size limit, the *overdamped* regime is entered. Here the Poisson structure, which is still present in the underlying dynamics, is washed out by the finite time-scale over which the spin relaxes, namely η^{-1}. The spin therefore drops out of the calculation and collective fluctuations are ruled by the fully non-conservative fixed point, hence giving $z = 1.73$.

A useful "map" of these concepts is provided in Fig. 7.2. To summarise:

- *inertial* behaviour is related to the short-time shape of the correlation function, discussed in Sec 7.1. From a field-theoretical point of view, it manifests through the presence of a coupling between the order parameter and the spin ($g \neq 0$);

- *conservative* behaviour is related to the conservation of the spin ($g \neq 0$ and $\eta = 0$), which therefore renders the behaviour inertial over all scales;

- *underdamped* behaviour is instead the behaviour observed in a finite-size inertial non-conservative system for small enough spin dissipation ($g \neq 0$ and $\eta \ll 1$).

7.4 Towards a new field theory for swarms

I now have all the *ingredients* a field theory for natural swarms should have, namely local alignment interactions, self-propulsion and inertial behaviour. If universality holds in living systems, the combination of these three features is expected to describe collective behaviour observed in swarms, as their effects on the dynamic behaviour can be all described by the presence of symmetries and conservation laws.

To build out an active inertial field theory, I will take a similar path to that taken by Toner and Tu when first deriving their theory of flocking [19], reviewed in Chapter 3: merging an equilibrium model for alignment with Navier-Stokes. The only, crucial, difference is that to reproduce inertial behaviour, Model G rather than Model A will be used as a starting point. Hence, in the following the field theory for swarms will be built by merging Model G, namely the inertial counterpart of Model A, and Navier-Stokes dynamics. The resulting equations will be therefore referred to as Self-Propelled Model G, in opposition to Self-Propelled Model A, which represents the Toner and Tu theory.

Similarly to the path followed in Sec. 3.3.1, this can be done in Model G by *promoting* the order parameter $\boldsymbol{\psi}$ to be proportional to the velocity field, through the relation

$$\boldsymbol{v}\left(\boldsymbol{x}, t\right) = v_0 \boldsymbol{\psi}\left(\boldsymbol{x}, t\right) \ . \tag{7.35}$$

Here v_0 is the speed of the individuals at the *microscopic* level, which is typically assumed to be fixed. From the field-theoretical point of view, this "promotion" of $\boldsymbol{\psi}$ can be encoded by substituting the temporal derivative ∂_t with a material derivative:

$$\partial_t \to \mathcal{D}_t = \partial_t \boldsymbol{\psi} + v_0 \left(\boldsymbol{\psi} \cdot \nabla\right) \ , \tag{7.36}$$

Note that in Model G $\boldsymbol{\psi}$ is not only responsible for self-advection, but advects also the spin field $\boldsymbol{s}$. Moreover, in this active case the behaviour of a third field must be taken into account, namely the density field ρ, which is not fixed anymore as a consequence of particles moving. This leads to the presence of a pressure force in the equation for the speed.

A minimal theory for active inertial systems can be therefore written starting from Model G structure and taking into account the advection generated by $\boldsymbol{\psi}$. This results into [109]:

$$\mathcal{D}_t \psi_\alpha = -\Gamma \frac{\delta \mathcal{H}}{\delta \psi_\alpha} + g \psi_\beta \frac{\delta \mathcal{H}}{\delta s_{\alpha\beta}} - \partial_\alpha \mathcal{P} + \theta_\alpha \ , \tag{7.37}$$

$$\mathcal{D}_t s_{\alpha\beta} = -\Lambda_{\alpha\beta\gamma\nu} \frac{\delta \mathcal{H}}{\delta s_{\gamma\nu}} + 2g \mathbb{I}_{\alpha\beta\gamma\nu} \psi_\gamma \frac{\delta \mathcal{H}}{\delta \psi_\nu} + \zeta_{\alpha\beta} \tag{7.38}$$

$$\partial_t \rho + v_0 \partial_\gamma \left(\rho \psi_\gamma \right) = 0 \tag{7.39}$$

Note that here all the couplings might depend on the local density. Unlike other approaches, this theory should be considered only as a *minimal* theory, in the sense that other terms compatible with the symmetries of the problem could be introduced, some of which will be discussed in Chapter 9. Nevertheless, Eqquations (7.37)-(7.39) will represent the starting point for the field-theoretical approach presented here, and already include all the necessary ingredients needed to capture the collective behaviour of swarms of insects.

As discussed in detail in Chapters 3 and 6, density fluctuations are not expected to play a relevant role in near-ordering systems exhibiting scaling behaviour as natural swarms. When this happens, density fluctuations can be completely suppressed by enforcing incompressibility [MyPaper2], see Chapter 6. Suppressing density fluctuations is desirable also from a technical point of view, as it allows handling a field theory with two fields, $\boldsymbol{\psi}$ and $\boldsymbol{s}$, rather than one with three. This reduces enormously the number of interactions, and hence the complexity of the RG calculation, which as I will show in Chapters 9-11 is already quite hard in the presence of two fields.

Enforcing incompressibility, namely requiring the density to be fixed $\rho \equiv \rho_0$, can be done by imposing a *solenoidal* constraint on $\boldsymbol{\psi}$,

$$\nabla \cdot \boldsymbol{\psi} = 0 \,. \tag{7.40}$$

In a non-inertial theory, enforcing this constraint has been proven to be relatively straightforward [23], see Chapter 5, as a *projection* of the equation for $\boldsymbol{\psi}$ allows to get rid of fluctuations of $\boldsymbol{\psi}$ which would lead to a violation of incompressibility. How this requirement affects the behaviour of the spin is however something that never had been investigated previously. Before tackling the study of the critical behaviour of Self-Propelled Model G in the incompressible limit, understanding the effects of such a limit on the behaviour of $\boldsymbol{s}$ turns out to be a necessary task, which has surprising consequences even at equilibrium.

Chapter 8

Enforcing incompressibility in the equilibrium limit

Recent experimental evidence has shown that natural swarms of insects display collective phenomena even in the absence of collective order [12]. Remarkably, correlation functions in swarms exhibit both static and dynamic scaling laws [12, 13], a hallmark of near-critical systems. This evidence made a renormalization group approach to swarming behaviour seem particularly appealing. The previous chapters have focused on the different *ingredients* required to account for the dynamic behaviour of natural swarms. Local alignment between the direction of motion of each midge can qualitatively explain collective behaviours in swarms, posing swarms near a critical ordering transition [56], but fails to explain the low dynamic critical exponent z. Model A, the dissipative dynamics of aligning systems, predicts $z \approx 2$ [40] as opposed to $z = 1.37 \pm 0.11$ observed in natural swarms [MyPaper1]. Two possible mechanisms can explain a drop in the value of the dynamic critical exponent in natural swarms compared to that of standard ferromagnetic systems in the Model A class.

As discussed in the previous Chapter, one factor that may lower the value of z, and that is relevant in the description of both insect swarms and bird flocks, is the presence of inertial dynamics, namely a coupling between the direction of motion field $\psi(\boldsymbol{x}, t)$ and the generator of its rotations, known as the spin $\boldsymbol{s}(\boldsymbol{x}, t)$ [100, 13]. This mechanism lowers the dynamic critical exponent to the value of $z = 1.5$ in $d = 3$ [40, 41]. The second relevant feature of swarms, explored in Chapter 3, is midges' activity. The ability of individuals to self-propel leads to a time-dependent network of interactions between the particles' velocities, thus driving the system out of equilibrium. The rewiring of the interaction network due to activity leads to a more efficient propagation of the information, which is responsible for lowering z from 2 to the value of 1.73 three-dimensional incompressible systems [23].

A theory that keeps into account both the off-equilibrium active nature of swarms *and* the mode-coupling nature of their interaction, may provide a value of the dynamical critical exponent close to the experimental one. The bad news is that in a full-fledged out-of-equilibrium field theory, the presence of activity gives rise to density fluctuations, thus meaning that in addition to the direction of motion field $\psi(\boldsymbol{x}, t)$ and spin field $\boldsymbol{s}(\boldsymbol{x}, t)$, also the density field $\rho(\boldsymbol{x}, t)$ must be included in the

hydrodynamic description of the system [19, 20]. The presence of 3 fields, of which only one is scalar, leads to a large number of couplings between them and a near-prohibitive level of intricacy. However, I gave evidence in Chapter 6 that to observe scaling laws, the compressibility of the system must be *small* so that collective modes effectively behave as if the system was incompressible. Therefore, to make theoretical progress, one needs to make the simplifying assumption of incompressibility, obtained by enforcing a solenoidal constraint on the order parameter field $\nabla \cdot \boldsymbol{\psi} = 0$.

In the present Chapter, I will address the problem of understanding the effects of incompressibility on the mode-coupling dynamics. To do this, I will work in the fixed-network approximation, namely taking the equilibrium limit by sending the microscopic speed $v_0 \rightarrow 0$ while keeping the solenoidal constraint active. The resulting field theory, which I shall refer to as Solenoidal Model G, therefore describes the dynamics of an inertial system where the order parameter $\boldsymbol{\psi}$ obeys $\nabla \cdot \boldsymbol{\psi} = 0$.

8.1 The solenoidal constraint

To join activity and inertia into one single dynamical field theory, one needs to write equations for three coupled fields - density, direction of motion and spin - with several non-linear couplings among them, giving rise to a diagrammatic RG proliferation that is impossible to keep under control without any simplifying assumption. One such simplification is that of incompressibility. The first, huge, advantage of working under the hypothesis of incompressibility is that the density field drops out the theoretical description [46, 23], thus reducing the number of fields that have to be studied from three to two, hence dramatically simplifying the theoretical investigation. One may worry that incompressibility introduces some non-local interactions in the system, potentially changing the critical exponents compared to the compressible case. However, numerical simulations of the standard *compressible* Vicsek model have found the dynamic scaling exponent to be in perfect agreement with theoretical RG predictions of the *incompressible* theory [69], thus indicating that the effects of activity on the dynamical critical exponent are independent of whether incompressibility is enforced or not. This is very useful indeed, as it means that incompressibility can be used as a simplifying tool, without changing critical dynamics.

Not only do numerical simulations support this idea, but also the RG analysis performed in Chapter 6 points in the same direction. The presence of density fluctuations in the system turns the ordering phase transition of Vicsek-like models into a first-order (i.e. discontinuous) transition [44]. In incompressible systems, however, the absence of density fluctuations suppresses the dynamic instability leading to a first-order transition, hence always recovering a second-order (continuous) behaviour [23]. Scaling behaviour is thus observed at all sizes and all the complications about phase separation are avoided. A crossover between these two regimes, discussed in Chapter 6, has been shown to arise for finite-size systems with mild density fluctuations [MyPaper2]: sufficiently small systems in the near-ordering phase exhibit scaling laws with exponents falling in the incompressible universality class, while in the infinite size limit, a first-order transition is recovered. The very observation of scaling behaviour, combined with the absence of heterogeneous spatial structures

in natural swarms [12, 56], strongly suggests their collective properties behave as if the system was incompressible. In this sense, incompressibility is not merely a simplifying hypothesis, but also a sound theoretical description of actual empirical data.

Incompressibility in the RG study of the Navier-Stokes equations was first used in the seminal paper by Forster, Nelson and Stephen [46], while it was used first in the context of dynamical field theories for active matter in [23]. This hypothesis seems quite reasonable both in natural insect swarms and bird flocks, because experiments show that density fluctuations are indeed very limited in these systems, and they do not seem to be a crucial ingredient in their collective behaviour [12, 65].

Following the results discussed in Chapter 6, I expect that also in the presence of mode-coupling dynamics, the presence of scaling laws in active systems can be explained by a finite size crossover in the compressibility. The observed large-scale behaviour of natural swarms is therefore ruled by the incompressible fixed point, yet to be determined, describing the active inertial universality class.

The dynamic behaviour of density fluctuations in systems with a conserved number of individuals is ruled by the continuity equation

$$\partial_t \rho + \nabla \cdot (\rho \boldsymbol{v}) = \partial_t \rho + \boldsymbol{v} \cdot \nabla + \rho \nabla \cdot \boldsymbol{v} = 0 \tag{8.1}$$

Incompressible can be achieved by requiring the density to be fixed to its average value $\rho \equiv \rho_0$, thus meaning that both its temporal and spatial derivatives vanish. Thanks to the continuity equation (8.1), the condition of incompressibility reduces to imposing a solenoidal constraint on the velocity field,

$$\nabla \cdot \boldsymbol{v} = 0 \,. \tag{8.2}$$

Incompressible swarms in the fully dissipative case (i.e. without inertial mode-coupling) have been studied in [23]. When moving to the inertial case, where the coupling with the conserved spin is at work, the introduction of a solenoidal constraint on the primary field within mode-coupling dynamics is far from trivial. In the case of a theory with one single field (the velocity), the solenoidal constraint is simply enforced by projecting the force acting on the velocity onto the direction orthogonal to the wave vector $\boldsymbol{k}$ in Fourier space [46, 23]; in this way, the constraint is naturally conserved during the temporal evolution of the system. But in systems with mode-coupling dynamics, incompressibility cannot be achieved in this simple way, as the aligning forces now act also on the spin, rather than solely on the velocity. Since the spin is not subject to the solenoidal constraint, an apparently paradoxical situation emerges: the assumption that was supposed to radically simplify the calculation, reducing from three to two the number of fields, creates a new challenge.

Instead of giving up the crucial simplification of incompressibility, I choose to try and solve the problem of how to impose a solenoidal constraint in a mode-coupling theory. The only encouraging thing is that the complications arising are completely unrelated to activity, so it seems sound to first find a conceptually consistent way to impose the solenoidal constraint on a theory at equilibrium and then use this result to make progress off-equilibrium. Indeed, surprising as this may seem, the problem of how to impose the solenoidal constraint on a mode-coupling theory has never been investigated in the literature before. My work on solenoidal constrained

mode-coupling theories, now published in [MyPaper2], therefore represents the first attempt to tackle this issue. By solving this problem, pushing the calculation out-of-equilibrium, still retaining the incompressibility condition, will become an easier task. Therefore, in this Chapter activity will be neglected by assuming the adjacency network to be fixed in time. The virtue of this approach is that any future calculation performed in the active case must have the present calculation as a limit in the zero-speed case.

Notice that in the absence of activity, it does not make much sense to refer to any kind of velocity field $\boldsymbol{v}$, as it would identically vanish. This happens because in the microscopic description of Vicsek-like systems, each individual has a fixed speed v_0, and the fixed-network approximation can be formally seen as a limit where v_0 vanishes, which is equivalent to *freeze* the position of each particle. While in this limit the velocity field acquires a singular behaviour, since no particle is moving, the coarse-grained direction of motion $\boldsymbol{\psi}$, defined by the relation

$$\boldsymbol{v}\left(\boldsymbol{x},t\right) = v_0\,\boldsymbol{\psi}\left(\boldsymbol{x},t\right) \tag{8.3}$$

still has a smooth behaviour when $v_0 \to 0$, and therefore represents the ideal candidate to be the order parameter in the fixed network approximation. Because of this connection, the solenoidal constraint given by Eq. (8.2) must hold also for $\boldsymbol{\psi}$ at any finite value of v_0. Therefore, in the equilibrium limit of an incompressible theory, the order parameter $\boldsymbol{\psi}$ must still obey

$$\nabla \cdot \boldsymbol{\psi}(\boldsymbol{x},t) = 0\,. \tag{8.4}$$

8.1.1 Static critical behaviour of the solenoidal theory

Before moving on with the study of the dynamic properties of inertial theories with a solenoidal constraint, let me first focus on reviewing, for the benefit of the reader, what happens to the static behaviour in the presence of such a constraint. The static behaviour of inertial systems as Model G is completely determined once the free energy functional $\mathcal{H}$ is given, which in the case of models with aligning interactions, that are invariant under a $O(n)$ symmetry group, takes the usual Landau-Ginzburg form

$$\mathcal{H} = \int \mathrm{d}^d x \frac{1}{2}\left(\partial_\alpha \psi_\beta\right)\left(\partial_\alpha \psi_\beta\right) + \frac{r}{2}\psi_\alpha\psi_\alpha + \frac{u}{4}\left(\psi_\alpha\psi_\alpha\right)^2 \tag{8.5}$$

Note that summation is implicit in the presence of repeated indices. When r changes sign while $u > 0$, these systems undergo a phase transition from a disordered state with $|\langle\boldsymbol{\psi}\rangle| = 0$ to an ordered state with $|\langle\boldsymbol{\psi}\rangle| = \sqrt{-r/u}$. At the transition, the collective properties are ruled by the universality class of $O(n)$ systems [110]. But what happens if I now require the order field $\boldsymbol{\psi}$ to obey a solenoidal constraint?

In the non-solenoidal theory, the behaviour of the system is described by the partition function

$$Z[\boldsymbol{J}] = \int \mathcal{D}\boldsymbol{\psi} e^{-\mathcal{H} - \int \mathrm{d}^d x J_\alpha \psi_\alpha} \tag{8.6}$$

Within this framework, the addition of a solenoidal constraint can be done by simply adding a Dirac delta function enforcing this constraint in the integral defining

Z, which suppresses any configuration of $\boldsymbol{\psi}$ which does not obey the constraint. Therefore the solenoidal contained theory is characterised by the partition function

$$Z[\boldsymbol{J}] = \int \mathcal{D}\boldsymbol{\psi}\,\delta(\nabla \cdot \boldsymbol{\psi})e^{-\mathcal{H} - \int \mathrm{d}^d x J_\alpha \psi_\alpha} \tag{8.7}$$

By representing the delta function as the limit of a Gaussian distribution $\delta(x) = \lim_{a \to \infty}(a/\pi)^{1/2}e^{-a\,x^2}$, one can see how the behaviour of the solenoidal theory is described by the free energy

$$\mathcal{H} = \int \mathrm{d}^d x \frac{1}{2}\left(\partial_\alpha \psi_\beta\right)\left(\partial_\alpha \psi_\beta\right) + \frac{a}{2}\left(\partial_\alpha \psi_\alpha\right)^2 + \frac{r}{2}\psi_\alpha \psi_\alpha + \frac{u}{4}\left(\psi_\alpha \psi_\alpha\right)^2 \tag{8.8}$$

in the limit $a \to \infty$. Note that this Hamiltonian is equivalent to that of antiferromagnets with dipolar interactions in the absence of lattice anisotropies, derived in [95], which in the $a \to \infty$ limit is known to reproduce the critical behaviour of ferromagnets with dipolar interactions [87, 86, 111].

This parallelism between solenoidal constraint and dipolar ferromagnets can be perhaps better understood by shifting the attention to Fourier space, where the solenoidal constraint reads

$$k_\alpha \psi_\alpha\left(\boldsymbol{k}\right) = 0 \tag{8.9}$$

Note that the Fourier-transformed fields are defined by the relation

$$\psi_\alpha\left(\boldsymbol{x}\right) = \int_{\boldsymbol{k}} \mathrm{e}^{\mathrm{i}\boldsymbol{k}\cdot\boldsymbol{x}}\psi_\alpha\left(\boldsymbol{k}\right) \tag{8.10}$$

where $\int_{\boldsymbol{k}} = \int_{|\boldsymbol{k}|<\Lambda} \frac{\mathrm{d}^d k}{(2\pi)^d}$. In Eq. (8.10) the cutoff Λ is the value of the wave-vector above which fluctuations have no physical meaning. Since a field theory, in the context of biophysics, is obtained by coarse-graining a discrete model, fluctuations cannot occur on distances shorter than a given coarse-graining length scale a, therefore meaning that the cutoff can be taken to be $\Lambda \sim a^{-1}$.

The relation (8.9) tells me that fluctuations of $\boldsymbol{\psi}$ longitudinal to the wave vector $\boldsymbol{k}$ are completely suppressed. An equivalent way of stating this is by saying that the field $\boldsymbol{\psi}$ belongs to the plane orthogonal to $\boldsymbol{k}$, which means that

$$P_{\alpha\beta}^\perp\left(\boldsymbol{k}\right)\psi_\beta\left(\boldsymbol{k}\right) = \psi_\alpha\left(\boldsymbol{k}\right) \tag{8.11}$$

Here $P^\perp$ is the transverse projection operator, which projects vectors in the transverse direction to $\boldsymbol{k}$, and thus takes the form

$$P_{\alpha\beta}^\perp\left(\boldsymbol{k}\right) = \delta_{\alpha\beta} - \frac{k_\alpha k_\beta}{k^2} \tag{8.12}$$

In general, dipolar ferromagnets may exhibit both longitudinal and transverse fluctuations. However, the non-critical nature of the longitudinal mode leads to their full suppression in the long-wavelength limit, meaning that an RG analysis finds a stable fixed point that describes a solenoidal-constrained theory. The renormalization group analysis of isotropic dipolar ferromagnets, performed to order $\epsilon = 4 - d$ in [87], shows a recursive relation for the ferromagnetic coupling constant given by

$$\frac{\mathrm{d}u}{\mathrm{d}l} = u\left(\epsilon - \frac{17}{2}u\Lambda^{-\epsilon}K_d\right). \tag{8.13}$$

In dimension $d < 4$, namely $\epsilon > 0$, the stable fixed point u^* ruling the critical behaviour of dipolar ferromagnets is thus given by [87]

$$u^* = \frac{2}{17} K_d \epsilon \tag{8.14}$$

Even though the change in the static universality class is very interesting at the theoretical level, it must be said that the new critical exponents are so close to those of the standard $O(n)$ universality class that the difference is often experimentally difficult to observe [111]. A two-loop estimation of the critical exponents ν, ruling the behaviour of the mass r while the transition is approached, and η, modifying the spatial dependence of the correlation function, are reported in Table 8.1. Here it is clear the little difference between the scaling behaviour of dipolar ferromagnets class and Landau-Ginzburg class.

8.2 The solenoidal mode-coupling theory

I will now turn my attention to the derivation and the study of a solenoidal inertial theory. The corresponding coarse-grained dynamic equations will hence describe the critical behaviour of a field ψ which is coupled to the generator of its rotations, s, in the presence of the solenoidal constrain, $\nabla \cdot \psi = 0$. I shall refer to this theory as Solenoidal Model G (SMG) because, in the absence of the solenoidal constraint, this field theory is known in the literature as Model G [40]. This classic model for equilibrium quantum antiferromagnets, which has been discussed in detail in Chapter 7, will therefore represent the starting point of the derivation of SMG equations.

8.2.1 The Sasvari-Schwabl-Szepfalusy model: a necessary generalization

The first problem one faces is that the presence of the solenoidal constraint,

$$\nabla \cdot \psi = 0 \tag{8.15}$$

forces the order parameter to have the same dimensionality as the space in which the theory is defined. Thus, since in the following sections I will need to perform an RG expansion near $d = 4$, I must work with the generalisation of Model G to arbitrary dimensions, known as the Sasvari-Schwabl-Szepfalusy (SSS) model [103, 104]. Given that I will be calculating the properties of the Solenoidal Sasvari-Schwabl-Szepfalusy model, strictly speaking, I should use the nomenclature "SSSS model"; however,

Table 8.1. Values of ν and η up to order ϵ^2 [111]

	Mean-field	Landau-Ginzburg ϵ-expansion	$\epsilon = 1$	Dipolar Ferromagnets ϵ-expansion	$\epsilon = 1$
ν	$\frac{1}{2}$	$\frac{1}{2} + \frac{1}{8}\epsilon + \frac{1}{16}\epsilon^2$	0.6875	$\frac{1}{2} + \frac{9}{68}\epsilon + \frac{7013}{117912}\epsilon^2$	0.692
η	0	$\frac{1}{48}\epsilon^2$	0.0208	$\frac{20}{867}\epsilon^2$	0.0231

chiefly for aesthetic reasons, I prefer not to do that and rather stick to Solenoidal Model G even in generic dimension d.

In the SSS model, the spin $\boldsymbol{s}$ is an anti-symmetric $d \times d$ matrix, with one independent component for each possible plane around which a rotation can be performed. The Poisson-bracket relation between $\boldsymbol{s}$ and ψ, a hallmark of the presence of inertial behaviour, is still given by

$$\left\{ s_{\alpha\beta}\left(\boldsymbol{x}\right), \psi_{\gamma}\left(\boldsymbol{x}'\right) \right\} = 2g\,\mathbb{I}_{\alpha\beta\gamma\rho}\psi_{\rho}\left(\boldsymbol{x}\right)\delta^{(d)}\left(\boldsymbol{x} - \boldsymbol{x}'\right) \tag{8.16}$$

where repeated greek-letter indices are intended to be summed, if not otherwise indicated, and the tensor $\mathbb{I}$ is the identity tensor in the space of $d \times d$ anti-symmetric matrices given by

$$\mathbb{I}_{\alpha\beta\gamma\rho} = \frac{1}{2}\left(\delta_{\alpha\gamma}\delta_{\beta\rho} - \delta_{\alpha\rho}\delta_{\beta\gamma}\right) \tag{8.17}$$

The factor $\frac{1}{2}$ in the definition of $\mathbb{I}$ arises as a consequence of the fact that, when $\boldsymbol{s}$ is represented as an anti-symmetric matrix, each independent component appears twice.

The static properties of the SSS model are fully determined by its effective Hamiltonian, which reflects the fact that $\boldsymbol{\psi}$ is a critical field with $O\left(d\right)$ symmetry group and local interactions, having the static critical properties of the Landau-Ginzburg universality class, while $\boldsymbol{s}$ is a non-critical massive field. The effective Hamiltonian of the system takes the following natural generalisation,

$$\mathcal{H} = \int \mathrm{d}^{d}x \left[\frac{1}{2}\left(\partial_{\alpha}\psi_{\beta}\right)\left(\partial_{\alpha}\psi_{\beta}\right) + \frac{r}{2}\psi_{\alpha}\psi_{\alpha} + \frac{u}{4}\left(\psi_{\alpha}\psi_{\alpha}\right)^{2} + \frac{s_{\alpha\beta}s_{\alpha\beta}}{4}\right] \tag{8.18}$$

The equations of motion of the critical SSS model have been derived in Chapter 7 starting from the Poisson-bracket relation (8.16) and the effective free energy (8.18) by following a procedure coming from the works of Mori *et al.* [105] and Zwanzig [106] (see [112] and [113]) These equations are given by

$$\frac{\partial \psi_{\alpha}}{\partial t} = -\Gamma \frac{\delta \mathcal{H}}{\delta \psi_{\alpha}} + g \frac{\delta \mathcal{H}}{\delta s_{\alpha\beta}}\psi_{\beta} + \theta_{\alpha} \tag{8.19}$$

$$\frac{\partial s_{\alpha\beta}}{\partial t} = \lambda \nabla^{2} \frac{\delta \mathcal{H}}{\delta s_{\alpha\beta}} + 2g\mathbb{I}_{\alpha\beta\gamma\nu}\,\psi_{\gamma}\frac{\delta \mathcal{H}}{\delta \psi_{\nu}} + \zeta_{\alpha\beta} \tag{8.20}$$

where θ and ζ are two Gaussian white noises, with variance

$$\left\langle \theta_{\alpha}\left(\boldsymbol{x}, t\right)\theta_{\beta}\left(\boldsymbol{x}', t'\right)\right\rangle = 2\Gamma\delta_{\alpha\beta}\delta^{(d)}\left(\boldsymbol{x} - \boldsymbol{x}'\right)\delta\left(t - t'\right) \tag{8.21}$$

$$\left\langle \zeta_{\alpha\beta}\left(\boldsymbol{x}, t\right)\zeta_{\gamma\nu}\left(\boldsymbol{x}', t'\right)\right\rangle = -4\lambda\mathbb{I}_{\alpha\beta\gamma\nu}\nabla^{2}\delta^{(d)}\left(\boldsymbol{x} - \boldsymbol{x}'\right)\delta\left(t - t'\right) \tag{8.22}$$

The $\lambda\nabla^{2}$ terms in the stochastic parts of the dynamics of $\boldsymbol{s}$ ensure that the spin is conserved.

8.2.2 Dynamic behaviour of the solenoidal inertial theory

In this crucial section, the dynamical equations of the mode-coupling theory subject to a solenoidal constraint will be derived through the classic Mori-Zwanzig formalism

[106, 105] by using the Poisson relation (8.16), the effective free energy of the SSS model and the suppression of fluctuations longitudinal to $\boldsymbol{k}$.

Because the field $\boldsymbol{\psi}$ is subject to the constraint,

$$k_\alpha \psi_\alpha\left(\boldsymbol{k}\right) = 0 \tag{8.23}$$

the most natural representation in which one would like to derive the equations of motion is,

$$\boldsymbol{\psi}\left(\boldsymbol{k}\right) = \psi_\parallel\left(\boldsymbol{k}\right) \hat{\boldsymbol{e}}^\parallel\left(\boldsymbol{k}\right) + \sum_{i=1}^{d-1} \psi_{\perp,i}\left(\boldsymbol{k}\right) \hat{\boldsymbol{e}}^{\perp,i}\left(\boldsymbol{k}\right) \tag{8.24}$$

where $\hat{\boldsymbol{e}}^\parallel = \boldsymbol{k}/\left|\boldsymbol{k}\right|$ is the unitary vector identifying the direction of $\boldsymbol{k}$, while the $\hat{\boldsymbol{e}}^{\perp,i}$ are orthogonal unitary vectors spanning the space perpendicular to $\boldsymbol{k}$, in such a way that $\hat{\boldsymbol{e}}^\parallel \cdot \hat{\boldsymbol{e}}^{\perp,i} = 0$ and $\hat{\boldsymbol{e}}^{\perp,i} \cdot \hat{\boldsymbol{e}}^{\perp,j} = \delta_{ij}$; indeed, within this set of coordinates, the constraint simply reads,

$$\psi_\parallel\left(\boldsymbol{k}\right) = 0 \tag{8.25}$$

leaving only the $(d-1)$ independent modes $\psi_{\perp,i}\left(\boldsymbol{k}\right)$ to take care of. The advantage of this notation is that the constrained field theory can be formulated in terms of the $(d-1)$ independent transverse modes and not in terms of a constrained set of d cartesian coordinates, ψ_α, to which it is not clear how to apply the Mori-Zwanzig procedure. However, the explicit form of both the effective free energy $\mathcal{H}$ and of the Poisson bracket relation is given in terms of the cartesian coordinates, ψ_α, while their form in terms of the $\psi_{\perp,i}$ would be extremely cumbersome. What I shall do, then, will be to first obtain the equation of motions for the $\psi_{\perp,i}$ and then to go back to the standard ψ_α fields by using the chain rule. In doing that, something new will pop out in the spin equation.

The dynamic behaviour of the constrained variables ψ_α is given, in terms of the independent variables $\psi_\perp$, by

$$\frac{\partial \psi_\alpha}{\partial t}\left(\boldsymbol{k}, t\right) = \sum_{i=1}^{d-1} \hat{e}_\alpha^{\perp,i}\left(\boldsymbol{k}\right) \frac{\partial \psi_{\perp,i}}{\partial t}\left(\boldsymbol{k}, t\right) \tag{8.26}$$

Following the Mori-Zwanzig procedure, the equations of motion for the $(d-1)$ independent fields $\psi_{\perp,i}$ and $\boldsymbol{s}$ take the following form

$$\partial_t \psi_{\perp,i}\left(\boldsymbol{k}, t\right) = -\Gamma \frac{\delta \mathcal{H}}{\delta \psi_{\perp,i}\left(-\boldsymbol{k}\right)} + $$
$$+ \frac{1}{2} \int_{\boldsymbol{q}} \left\{s_{\gamma\nu}\left(-\boldsymbol{q}\right), \psi_{\perp,i}\left(\boldsymbol{k}\right)\right\} \frac{\delta \mathcal{H}}{\delta s_{\gamma\nu}\left(-\boldsymbol{q}\right)} + \hat{e}_\beta^{\perp,i}\left(\boldsymbol{k}\right) \tilde{\theta}_\beta \tag{8.27}$$

$$\partial_t s_{\alpha\beta}\left(\boldsymbol{k}, t\right) = -\Lambda_{\alpha\beta\gamma\nu}\left(\boldsymbol{k}\right) \frac{\delta \mathcal{H}}{\delta s_{\gamma\nu}\left(-\boldsymbol{k}\right)} - $$
$$- \sum_{i=1}^{d-1} \int_{\boldsymbol{q}} \left\{s_{\alpha\beta}\left(\boldsymbol{k}\right), \psi_{\perp,i}\left(-\boldsymbol{q}\right)\right\} \frac{\delta \mathcal{H}}{\delta \psi_{\perp,i}\left(-\boldsymbol{q}\right)} + \zeta_{\alpha\beta} \tag{8.28}$$

where the t dependence is always understood even when not made explicit for reasons of space. In Eqs. (8.27) and (8.28) $\mathcal{H}$ is the free energy given by Eq. (8.18) in which

$\psi_{\parallel}$ is set to 0; $\tilde{\boldsymbol{\theta}}$, $\boldsymbol{\zeta}$ are white gaussian noises with variance respectively given by $2\Gamma\delta_{\alpha\beta}$ and $4\Lambda_{\alpha\beta\gamma\nu}(\boldsymbol{k})$. The tensor $\Lambda_{\alpha\beta\gamma\nu}(\boldsymbol{k})$ is a function of the wave-vector $\boldsymbol{k}$. In the field theory without constraint, it takes the simple form $\Lambda_{\alpha\beta\gamma\nu} = k^2\lambda\mathbb{I}_{\alpha\beta\gamma\nu}$; however, since the solenoidal constraint generates an anisotropy in Fourier space for the order parameter, I expect that anisotropic effects can affect also the spin dynamics. Therefore, to generalise I will allow λ to take different values for the longitudinal and transverse components of $\boldsymbol{s}$, namely by taking,

$$\Lambda_{\alpha\beta\gamma\nu}(\boldsymbol{k}) = k^2\lambda^{\perp}\mathbb{P}^{\perp}_{\alpha\beta\gamma\nu}(\boldsymbol{k}) + k^2\lambda^{\parallel}\mathbb{P}^{\parallel}_{\alpha\beta\gamma\nu}(\boldsymbol{k}) \tag{8.29}$$

where $\mathbb{P}^{\perp}$ is the generalisation of the projection operator $P^{\perp}$ defined in Eq. (8.12) acting on the space of 2-indices antisymmetric tensors, and takes the following form

$$\mathbb{P}^{\perp}_{\alpha\beta\gamma\nu}(\boldsymbol{k}) = \mathbb{I}_{\alpha\beta\gamma\nu} - \mathbb{I}_{\alpha\beta\sigma\tau}P^{\perp}_{\sigma\gamma}(\boldsymbol{k})P^{\perp}_{\tau\nu}(\boldsymbol{k}) \tag{8.30}$$

On the other hand, the projection operator $\mathbb{P}^{\parallel}$ represent the generalisation of $P^{\parallel}$, and takes the form

$$\mathbb{P}^{\parallel}_{\alpha\beta\gamma\nu}(\boldsymbol{k}) = \mathbb{I}_{\alpha\beta\gamma\nu} - \mathbb{P}^{\perp}_{\alpha\beta\gamma\nu}(\boldsymbol{k}) \tag{8.31}$$

Note that when $\lambda^{\perp} = \lambda^{\parallel} = \lambda$, the tensor Λ reduces to the standard isotropic form of Model G, namely $\Lambda = k^2\lambda\mathbb{I}$.

To find the equations of motion of ψ_{α} and $\boldsymbol{s}_{\alpha\beta}$, I will proceed by making explicit the terms in Eqs. (8.27) and (8.28) exploiting the chain rule between the fields $\psi_{\perp}$ and ψ_{α}. The chain rule applied to the variations of the free energy with respect to $\psi_{\perp,i}$ reads,

$$\frac{\delta\mathcal{H}}{\delta\psi_{\perp,i}(-\boldsymbol{k})} = \int \mathrm{d}^d p \, \frac{\delta\psi_{\beta}(-\boldsymbol{p})}{\delta\psi_{\perp,i}(-\boldsymbol{k})}\frac{\delta\mathcal{H}}{\delta\psi_{\beta}(-\boldsymbol{p})} = \hat{e}^{\perp,i}_{\beta}(\boldsymbol{k})\frac{\delta\mathcal{H}}{\delta\psi_{\beta}(-\boldsymbol{k})} \tag{8.32}$$

while the Poisson-bracket relation between $\boldsymbol{s}$ and $\psi_{\perp,i}$ can be written as

$$\{s_{\gamma\nu}(-\boldsymbol{q}), \psi_{\perp,i}(\boldsymbol{k})\} = \int \mathrm{d}^d p \, \{s_{\gamma\nu}(-\boldsymbol{q}), \psi_{\beta}(\boldsymbol{p})\}\frac{\delta\psi_{\perp,i}(\boldsymbol{k})}{\delta\psi_{\beta}(\boldsymbol{p})} =$$
$$= \hat{e}^{\perp,i}_{\beta}(\boldsymbol{k})\{s_{\gamma\nu}(-\boldsymbol{q}), \psi_{\beta}(\boldsymbol{k})\} \tag{8.33}$$

In the last equality of both Eq. (8.32) and (8.33), I made use of the relation between the two representations of $\boldsymbol{\psi}$, given by the relations

$$\frac{\delta\psi_{\perp,i}(\boldsymbol{k})}{\delta\psi_{\beta}(\boldsymbol{p})} = \hat{e}^{\perp,i}_{\beta}(\boldsymbol{k})\delta^{(d)}(\boldsymbol{k} - \boldsymbol{p}), \tag{8.34}$$

$$\frac{\delta\psi_{\beta}(\boldsymbol{p})}{\delta\psi_{\perp,i}(\boldsymbol{k})} = \hat{e}^{\perp,i}_{\beta}(\boldsymbol{k})\delta^{(d)}(\boldsymbol{k} - \boldsymbol{p}). \tag{8.35}$$

Thanks to Eq. (8.32) and (8.33) it is possible to write the mode-coupling term of the dynamics of the spin in the following way:

$$\sum_{i=1}^{d-1}\int_{\boldsymbol{q}} \{s_{\alpha\beta}(\boldsymbol{k}), \psi_{\perp,i}(-\boldsymbol{q})\}\frac{\delta\mathcal{H}}{\delta\psi_{\perp,i}(-\boldsymbol{q})} =$$
$$= \int_{\boldsymbol{q}} \{s_{\alpha\beta}(\boldsymbol{k}), \psi_{\nu}(-\boldsymbol{q})\}\left[\sum_{i=1}^{d-1}\hat{e}^{\perp,i}_{\nu}(\boldsymbol{q})\hat{e}^{\perp,i}_{\rho}(\boldsymbol{q})\right]\frac{\delta\mathcal{H}}{\delta\psi_{\rho}(-\boldsymbol{q})} =$$
$$= \int_{\boldsymbol{q}} \{s_{\alpha\beta}(\boldsymbol{k}), \psi_{\nu}(-\boldsymbol{q})\}P_{\nu\rho}(\boldsymbol{q})\frac{\delta\mathcal{H}}{\delta\psi_{\rho}(-\boldsymbol{q})}, \tag{8.36}$$

where I used the following alternative definition of $P^\perp$, equivalent to (8.12), which follows directly from the definition of the unitary vectors $\hat{e}^{\perp,i}$

$$P_{\alpha\beta}(\boldsymbol{k}) = \sum_{i=1}^{d-1} \hat{e}_\alpha^{\perp,i}(\boldsymbol{k})\, \hat{e}_\beta^{\perp,i}(\boldsymbol{k}) \;. \tag{8.37}$$

Thanks to the equalities (8.32), (8.33) and (8.36), it is now possible to write the equations of motion Eq. (8.27) and (8.28) in the following form

$$\partial_t \psi_{\perp,i}(\boldsymbol{k},t) = \hat{e}_\beta^{\perp,i}(\boldsymbol{k}) \left[-\Gamma \frac{\delta\mathcal{H}}{\delta\psi_\beta(-\boldsymbol{k})} + \frac{1}{2}\int_{\boldsymbol{q}} \{s_{\gamma\nu}(-\boldsymbol{q}), \psi_\beta(\boldsymbol{k})\} \frac{\delta\mathcal{H}}{\delta s_{\gamma\nu}(-\boldsymbol{q})} + \tilde{\theta}_\beta \right] \tag{8.38}$$

$$\partial_t s_{\alpha\beta}(\boldsymbol{k},t) = -\Lambda_{\alpha\beta\gamma\nu} \frac{\delta\mathcal{H}}{\delta s_{\gamma\nu}(-\boldsymbol{k})} - \int_{\boldsymbol{q}} \{s_{\alpha\beta}(\boldsymbol{k}), \psi_\nu(-\boldsymbol{q})\} P_{\nu\rho}(\boldsymbol{q}) \frac{\delta\mathcal{H}}{\delta\psi_\rho(-\boldsymbol{q})} + \zeta_{\alpha\beta} \tag{8.39}$$

The equation for $\boldsymbol{\psi}$ in Cartesian coordinates can be derived by making use of Eq. (8.26). By plugging the equation for $\psi_{\perp,i}$ (8.38) into Eq. (8.26), reminding that $P^\perp$ is given by (8.37) and using the explicit Poisson-bracket relation given in Eq. (8.16), the equations of motion for the Cartesian components ψ_α and for $s_{\alpha\beta}$ can finally be written as

$$\partial_t \psi_\alpha(\boldsymbol{k},t) = -\Gamma P_{\alpha\beta}(\boldsymbol{k}) \frac{\delta\mathcal{H}}{\delta\psi_\beta(-\boldsymbol{k})} + g P_{\alpha\rho}(\boldsymbol{k}) \mathbb{I}_{\rho\beta\gamma\nu} \int_{\boldsymbol{q}} \psi_\beta(\boldsymbol{k}-\boldsymbol{q}) \frac{\delta\mathcal{H}}{\delta s_{\gamma\nu}(-\boldsymbol{q})} + \theta_\alpha \tag{8.40}$$

$$\partial_t s_{\alpha\beta}(\boldsymbol{k},t) = -\Lambda_{\alpha\beta\gamma\nu}(\boldsymbol{k}) \frac{\delta\mathcal{H}}{\delta s_{\gamma\nu}(-\boldsymbol{k})} + 2\,g\mathbb{I}_{\alpha\beta\gamma\nu} \int_{\boldsymbol{q}} \psi_\gamma(\boldsymbol{k}-\boldsymbol{q}) P_{\nu\rho}(\boldsymbol{q}) \frac{\delta\mathcal{H}}{\delta\psi_\rho(-\boldsymbol{q})} + \zeta_{\alpha\beta} \tag{8.41}$$

Here the free energy $\mathcal{H}$ can be taken to be the same as the SSS model, since all the terms involving derivatives of $\mathcal{H}$ with respect to $\boldsymbol{\psi}$ are already projected. Moreover, the two Gaussian random white noises $\boldsymbol{\zeta}$ and $\boldsymbol{\theta}$ have variance

$$\langle \theta_\alpha(\boldsymbol{k},t)\, \theta_\beta(\boldsymbol{k}',t') \rangle = 2\Gamma\, P_{\alpha\beta}(\boldsymbol{k})\, \hat{\delta}^{(d)}(\boldsymbol{k}+\boldsymbol{k}')\, \delta(t-t') \tag{8.42}$$

$$\langle \zeta_{\alpha\beta}(\boldsymbol{k},t)\, \zeta_{\gamma\nu}(\boldsymbol{k}',t') \rangle = 4\Lambda_{\alpha\beta\gamma\nu}(\boldsymbol{k})\, \hat{\delta}^{(d)}(\boldsymbol{k}+\boldsymbol{k}')\, \delta(t-t') \tag{8.43}$$

where I remind that $\hat{\delta}(x) = (2\pi)\delta(x)$.

8.2.3   Effects of the constraint

The solenoidal constraint has a triple effect on the equations of motion of Model G. The first, and maybe the most trivial, is that the equation of motion for $\boldsymbol{\psi}$ is projected orthogonally to $\boldsymbol{k}$, as it happens in incompressible field theories with no mode-coupling interaction [46, 23]. The second effect is that it allows a more complex form of the spin relaxation tensor Λ: while up to this point there no reason to claim that this tensor *must* take such a complex form, I will show in the following sections how the RG naturally generates two different relaxation coefficients $\lambda^\perp$ and $\lambda^\parallel$ even if one starts with $\lambda^\perp = \lambda^\parallel$.

The last effect is the less obvious one, and it is represented by the presence of a projection operator $P_{\nu\rho}(\boldsymbol{q})$ in the mode coupling interaction of the spin dynamics. The existence of this projector is a consequence of the fact that, in the presence of a solenoidal constraint, the conservative *Hamiltonian* force is not simply,

$$\mathbb{F}_\nu(\boldsymbol{q}) = -\frac{\delta\mathcal{H}}{\delta\psi_\nu(-\boldsymbol{q})} \tag{8.44}$$

but rather,

$$\mathbb{F}_\nu(\boldsymbol{q}) = -P_{\nu\rho}(\boldsymbol{q})\frac{\delta\mathcal{H}}{\delta\psi_\rho(-\boldsymbol{q})} \tag{8.45}$$

The linear part of the force is not affected by this new projector, but the non-linear terms are. This can be seen by writing explicitly the new force,

$$\mathbb{F}_\nu(\boldsymbol{q}) = -\left(r+q^2\right)\psi_\nu(\boldsymbol{q}) + uP_{\nu\rho}(\boldsymbol{q})\int_{\boldsymbol{p},\boldsymbol{h}}\psi_\rho(\boldsymbol{p})\,\psi_\sigma(\boldsymbol{h})\,\psi_\sigma(\boldsymbol{q}-\boldsymbol{p}-\boldsymbol{h}) \tag{8.46}$$

where in the first linear term I used the fact that $P_{\nu\rho}(\boldsymbol{q})\psi_\rho(\boldsymbol{q}) = \psi_\nu(\boldsymbol{q})$. The linear part of the force contributes to the dynamics of $\boldsymbol{s}$ with the same term as Model G [40]

$$\partial_t s_{\alpha\beta}(\boldsymbol{k}) \sim g\mathbb{I}_{\alpha\beta\gamma\nu}\int_{\boldsymbol{q}}\left[q^2 - (k-q)^2\right]\psi_\gamma(\boldsymbol{k}-\boldsymbol{q})\,\psi_\nu(\boldsymbol{q}) \tag{8.47}$$

Here the factor $q^2 - (k-q)^2$ arises as a consequence of mode-coupling and it vanishes as $\boldsymbol{k} \to 0$, thus conserving the total spin $\boldsymbol{S}(t) = \int d^d x\, \boldsymbol{s}(\boldsymbol{x},t) = \boldsymbol{s}(\boldsymbol{k}=0,t)$. But now, thanks to the presence of the projector, the non-linear term also contributes to the dynamics of the spin. More precisely, it does so through a novel dynamical interaction term given by,

$$\partial_t s_{\alpha\beta}(\boldsymbol{k}) \sim 2gu\mathbb{I}_{\alpha\beta\gamma\nu}\int_{\boldsymbol{q},\boldsymbol{h},\boldsymbol{p}}\psi_\gamma(\boldsymbol{k}-\boldsymbol{q})\,P_{\nu\rho}(\boldsymbol{q})\,\psi_\rho(\boldsymbol{p})\,\psi_\sigma(\boldsymbol{h})\,\psi_\sigma(\boldsymbol{q}-\boldsymbol{p}-\boldsymbol{h}) \tag{8.48}$$

This is a completely new term, which mixes the static ferromagnetic interaction (the coupling constant u) with the dynamic mode-coupling interaction (the coupling constant g); such vertex is absent in the non-constrained theory, since when $P_{\nu\rho}$ is substituted by $\delta_{\nu\rho}$, as in the non-solenoidal case, the r.h.s. of Eq. (8.48) vanishes. I will call this new interaction the *DYS vertex*, which stands for DYnamic - Static vertex since it mixes the dynamic mode-coupling structure to the static ψ^4 term. As I will show later on, the DYS vertex is crucial to keep closed and self-consistent the RG calculation and to recover the correct static critical exponents.

Remarkably, the DYS interaction does not vanish when $\boldsymbol{k} \to 0$, meaning that the equation of motion of $\boldsymbol{s}$ cannot be written as a continuity equation any more and thus that the total spin $\boldsymbol{S}(t)$ is no longer conserved. However, in the following section, I will show that no spin dissipation is generated by the DYS vertex, suggesting that the violation of the spin conservation is equivalent to a generalized precession of the total spin vector.

8.3 Field theoretical description of Solenoidal Model G

To set up the renormalization of the theory I will follow the procedure proposed by Martin, Siggia, Rose [47], Janssen [78] and De Dominicis [79] to write stochastic

differential equations as a field theory formulated using path integrals, reviewed in Chapter 4. Thanks to this procedure, the behaviour of a field ϕ governed by a stochastic differential equation with a deterministic evolution operator $\mathcal{F}$ and a Gaussian noise θ

$$\mathcal{F}[\phi] - \theta = 0 \tag{8.49}$$

can be described through a field-theoretical action that correctly reproduces its statistics, i.e. the correlation and response functions,

$$\mathcal{S}[\hat{\phi}, \phi] = \int \mathrm{d}^d x \mathrm{d}t \left[\hat{\phi}_\alpha \mathcal{F}_\alpha[\phi] - \hat{\phi}_\alpha L_{\alpha\beta} \hat{\phi}_\beta \right] \tag{8.50}$$

where $2L_{\alpha\beta}$ is the variance of the Gaussian noise θ, while $\hat{\phi}$ is an auxiliary field. The presence of this additional field is the cost which has to be paid to exploit standard path integral formulation, which allows one to use the standard rules of static renormalization and write the perturbative series in terms of Feynman diagrams.

The Martin-Siggia-Rose (MSR) action for the stochastic differential equations (8.40) and (8.41) takes the following form

$$\mathcal{S}[\hat{\psi}, \psi, \hat{s}, s] = \mathcal{S}_{0,\psi}[\hat{\psi}, \psi] + \mathcal{S}_{0,s}[\hat{s}, s] + \mathcal{S}_I[\hat{\psi}, \psi, \hat{s}, s] \tag{8.51}$$

where $\mathcal{S}_{0,\psi}$ and $\mathcal{S}_{0,m}$ are the two Gaussian actions of the two fields, which reproduce the linear dynamic theory, while $\mathcal{S}_I$, which takes contributes from the non-linear dynamic terms, represents the *interacting* part of the action. These contributions are respectively given by

$$\mathcal{S}_{0,\psi} = \int_{\tilde{\boldsymbol{k}}} \hat{\psi}_\alpha(-\tilde{\boldsymbol{k}}) \left(-\mathrm{i}\omega + \Gamma k^2 + m \right) \psi_\alpha(\tilde{\boldsymbol{k}}) - \hat{\psi}_\alpha(-\tilde{\boldsymbol{k}}) \Gamma P_{\alpha\beta}(\boldsymbol{k}) \hat{\psi}_\beta(\tilde{\boldsymbol{k}}) \tag{8.52}$$

$$\mathcal{S}_{0,s} = \frac{1}{2} \int_{\tilde{\boldsymbol{k}}} \hat{s}_{\alpha\beta}(-\tilde{\boldsymbol{k}}) \left[-\mathrm{i}\omega \mathbb{I}_{\alpha\beta\gamma\nu} + \Lambda_{\alpha\beta\gamma\nu}(\boldsymbol{k}) \right] s_{\gamma\nu}(\tilde{\boldsymbol{k}}) - \hat{s}_{\alpha\beta}(-\tilde{\boldsymbol{k}}) \Lambda_{\alpha\beta\gamma\nu}(\boldsymbol{k}) \hat{s}_{\gamma\nu}(\tilde{\boldsymbol{k}}) \tag{8.53}$$

while $\mathcal{S}_I$, which takes contributes from the non-linear dynamic terms and represents the *interaction* part of the action, is given by

$$
\begin{aligned}
\mathcal{S}_I = &-g\,\mathbb{I}_{\rho\beta\gamma\nu} \int_{\tilde{\boldsymbol{k}},\tilde{\boldsymbol{q}}} P_{\alpha\rho}(\boldsymbol{k}) \hat{\psi}_\alpha(-\tilde{\boldsymbol{k}}) \psi_\beta(\tilde{\boldsymbol{q}}) s_{\gamma\nu}(\tilde{\boldsymbol{k}} - \tilde{\boldsymbol{q}}) - \\
&+\frac{J}{3} \int_{\tilde{\boldsymbol{k}},\tilde{\boldsymbol{q}},\tilde{\boldsymbol{p}}} Q_{\alpha\beta\gamma\nu}(\boldsymbol{k}) \hat{\psi}_\alpha(-\tilde{\boldsymbol{k}}) \psi_\beta(\tilde{\boldsymbol{q}}) \psi_\gamma(\tilde{\boldsymbol{p}}) \psi_\nu(\tilde{\boldsymbol{k}} - \tilde{\boldsymbol{q}} - \tilde{\boldsymbol{p}}) - \\
&-g\,\mathbb{I}_{\alpha\beta\gamma\nu} \int_{\tilde{\boldsymbol{k}},\tilde{\boldsymbol{q}}} \boldsymbol{k} \cdot \boldsymbol{q}\, \hat{s}_{\alpha\beta}(-\tilde{\boldsymbol{k}}) \psi_\gamma(-\tilde{\boldsymbol{q}} + \tilde{\boldsymbol{k}}/2) \psi_\nu(\tilde{\boldsymbol{q}} + \tilde{\boldsymbol{k}}/2) + \\
&-\frac{\kappa}{12} \int_{\tilde{\boldsymbol{k}},\tilde{\boldsymbol{q}},\tilde{\boldsymbol{p}},\tilde{\boldsymbol{h}}} K_{\alpha\beta\gamma\nu\sigma\tau}(\boldsymbol{k},\boldsymbol{q},\boldsymbol{p},\boldsymbol{h},\boldsymbol{k} - \boldsymbol{q} - \boldsymbol{p} - \boldsymbol{h}) \times \\
&\qquad\qquad \times \hat{s}_{\alpha\beta}(-\tilde{\boldsymbol{k}}) \psi_\gamma(\tilde{\boldsymbol{q}}) \psi_\nu(\tilde{\boldsymbol{p}}) \psi_\sigma(\tilde{\boldsymbol{h}}) \psi_\tau(\tilde{\boldsymbol{k}} - \tilde{\boldsymbol{q}} - \tilde{\boldsymbol{h}} - \tilde{\boldsymbol{p}})
\end{aligned}
\tag{8.54}
$$

where I have introduced the new parameters,

$$m = \Gamma r \qquad\qquad J = \Gamma u \qquad\qquad \kappa = ug \tag{8.55}$$

Here m and J represent a sort of dynamical generalization of the mass and the ferromagnetic coupling constant, respectively, while κ is the coupling constant associated with the DYS vertex. It will be crucial to check, in what follows, that the renormalization of all the couplings maintains the validity of these relations along the RG flow since otherwise the system would not be at equilibrium. Moreover, in Eq. (8.54) the following new tensors have been introduced

$$Q_{\alpha\beta\gamma\nu}\left(\boldsymbol{k}\right) = P_{\alpha\beta}\left(\boldsymbol{k}\right)\delta_{\gamma\nu} + P_{\alpha\gamma}\left(\boldsymbol{k}\right)\delta_{\beta\nu} + P_{\alpha\nu}\left(\boldsymbol{k}\right)\delta_{\beta\gamma} \tag{8.56}$$

$$K_{\alpha\beta\gamma\nu\sigma\tau}\left(\boldsymbol{k},\boldsymbol{p}_1,\boldsymbol{p}_2,\boldsymbol{p}_3,\boldsymbol{p}_4\right) = \mathbb{I}_{\alpha\beta\gamma\rho}Q_{\rho\nu\sigma\tau}\left(\boldsymbol{k}-\boldsymbol{p}_1\right) + \mathbb{I}_{\alpha\beta\nu\rho}Q_{\rho\gamma\sigma\tau}\left(\boldsymbol{k}-\boldsymbol{p}_2\right) + \\ + \mathbb{I}_{\alpha\beta\sigma\rho}Q_{\rho\gamma\nu\tau}\left(\boldsymbol{k}-\boldsymbol{p}_3\right) + \mathbb{I}_{\alpha\beta\tau\rho}Q_{\rho\gamma\nu\sigma}\left(\boldsymbol{k}-\boldsymbol{p}_4\right) \tag{8.57}$$

Note that the fields in Fourier space for both the spatial and temporal domains, introduced in the previous equations, are related to real-space fields as follows

$$\phi\left(\boldsymbol{x},t\right) = \int_{\tilde{\boldsymbol{k}}} \mathrm{e}^{\mathrm{i}(\boldsymbol{k}\cdot\boldsymbol{x}-\omega t)}\phi(\tilde{\boldsymbol{k}}) \tag{8.58}$$

where $\tilde{\boldsymbol{k}} = (\boldsymbol{k},\omega)$ and $\int_{\tilde{\boldsymbol{k}}} = \int_{\boldsymbol{k}}\int_{-\infty}^{\infty}\frac{\mathrm{d}\omega}{2\pi}$.

Free theory

The starting point to build the perturbative expansion of the equations of motion is the free, or Gaussian, dynamic theory, obtained by setting to 0 all the dynamic non-linear couplings, namely g and u. From the Gaussian part of the action, given by Eqs. (8.52) and (8.53), the expressions for the bare propagators and correlation functions for the effective field theory can be easily derived, and are given by:

$$\langle\psi_\alpha(\tilde{\boldsymbol{k}})\hat{\psi}_\beta(\tilde{\boldsymbol{q}})\rangle_0 = \mathbb{G}^{0,\psi}_{\alpha\beta}(\tilde{\boldsymbol{k}})\hat{\delta}(\tilde{\boldsymbol{k}}+\tilde{\boldsymbol{q}}) \tag{8.59}$$

$$\langle s_{\alpha\beta}(\tilde{\boldsymbol{k}})\hat{s}_{\gamma\nu}(\tilde{\boldsymbol{q}})\rangle_0 = \mathbb{G}^{0,s}_{\alpha\beta\gamma\nu}(\tilde{\boldsymbol{k}})\hat{\delta}(\tilde{\boldsymbol{k}}+\tilde{\boldsymbol{q}}) \tag{8.60}$$

$$\langle\psi_\alpha(\tilde{\boldsymbol{k}})\psi_\beta(\tilde{\boldsymbol{q}})\rangle_0 = \mathbb{C}^{0,\psi}_{\alpha\beta}(\tilde{\boldsymbol{k}})\hat{\delta}(\tilde{\boldsymbol{k}}+\tilde{\boldsymbol{q}}) \tag{8.61}$$

$$\langle s_{\alpha\beta}(\tilde{\boldsymbol{k}})s_{\gamma\nu}(\tilde{\boldsymbol{q}})\rangle_0 = \mathbb{C}^{0,s}_{\alpha\beta\gamma\nu}(\tilde{\boldsymbol{k}})\hat{\delta}(\tilde{\boldsymbol{k}}+\tilde{\boldsymbol{q}}) \tag{8.62}$$

where $\hat{\delta}(\tilde{\boldsymbol{h}}) = (2\pi)^{d+1}\delta^{(d)}(\boldsymbol{h})\delta(\omega_h)$. The subscripted 0 on thermal averages indicate that they are computed within the non-interacting theory, namely by setting $u = g = 0$ (and thus also $J = \kappa = 0$). The tensors $\mathbb{G}$ and $\mathbb{C}$ are given by

$$\mathbb{G}^{0,\psi}_{\alpha\beta}(\tilde{\boldsymbol{k}}) = G_{0,\psi}(\tilde{\boldsymbol{k}})\delta_{\alpha\beta} \tag{8.63}$$

$$\mathbb{C}^{0,\psi}_{\alpha\beta}(\tilde{\boldsymbol{k}}) = C_{0,\psi}(\tilde{\boldsymbol{k}})P^{\perp}_{\alpha\beta}(\boldsymbol{k}) \tag{8.64}$$

$$\mathbb{G}^{0,s}_{\alpha\beta\gamma\nu}(\tilde{\boldsymbol{k}}) = G^{\perp}_{0,s}(\tilde{\boldsymbol{k}})\mathbb{P}^{\perp}_{\alpha\beta\gamma\nu}(\boldsymbol{k}) + G^{\parallel}_{0,s}(\tilde{\boldsymbol{k}})\mathbb{P}^{\parallel}_{\alpha\beta\gamma\nu}(\boldsymbol{k}) \tag{8.65}$$

$$\mathbb{C}^{0,s}_{\alpha\beta\gamma\nu}(\tilde{\boldsymbol{k}}) = C^{\perp}_{0,s}(\tilde{\boldsymbol{k}})\mathbb{P}_{\alpha\beta\gamma\nu}(\boldsymbol{k})^{\perp} + C^{\parallel}_{0,s}(\tilde{\boldsymbol{k}})\mathbb{P}^{\parallel}_{\alpha\beta\gamma\nu}(\boldsymbol{k}) \tag{8.66}$$

In Eq. (8.63), (8.65), (8.64) and (8.66) I have,

$$G_{0,\psi}\left(\boldsymbol{k},\omega\right) = \frac{1}{-\mathrm{i}\omega + \Gamma k^2 + m} \qquad C_{0,\psi}\left(\boldsymbol{k},\omega\right) = \frac{2\Gamma}{\omega^2 + (m + \Gamma k^2)^2} \tag{8.67}$$

$$G^{\perp}_{0,s}\left(\boldsymbol{k},\omega\right) = \frac{2}{-\mathrm{i}\omega + \lambda^{\perp}k^2} \qquad C^{\perp}_{0,s}\left(\boldsymbol{k},\omega\right) = \frac{4\lambda^{\perp}k^2}{\omega^2 + (\lambda^{\perp}k^2)^2} \tag{8.68}$$

$$G^{\parallel}_{0,s}\left(\boldsymbol{k},\omega\right) = \frac{2}{-\mathrm{i}\omega + \lambda^{\parallel}k^2} \qquad C^{\parallel}_{0,s}\left(\boldsymbol{k},\omega\right) = \frac{4\lambda^{\parallel}k^2}{\omega^2 + (\lambda^{\parallel}k^2)^2} \tag{8.69}$$

In the diagrammatic framework, bare propagators and correlation functions are represented in the following way

$$\langle \psi_\alpha \hat{\psi}_\beta \rangle_0 \quad = \quad \xrightarrow{\hspace{2cm}} \qquad \langle s_{\alpha\beta} \hat{s}_{\gamma\nu} \rangle_0 \quad = \quad \text{\raisebox{-2pt}{\rule{1cm}{0pt}}} \qquad (8.70)$$

$$\langle \psi_\alpha \psi_\beta \rangle_0 \quad = \quad \text{\rule{1.5cm}{0.4pt}} \qquad \langle s_{\alpha\beta} s_{\gamma\nu} \rangle_0 \quad = \quad \text{\raisebox{-2pt}{\rule{1cm}{0pt}}} \qquad (8.71)$$

where the arrows in the propagators always point in the direction of the response field.

Non-linear terms: the vertices

The four terms that compose $\mathcal{S}_I$ represent the non-linear interactions in the equations of motion. Two of them involve one field $\hat{\psi}$, since they derive from the equation of motion of ψ, while the other two involve one field $\hat{s}$ since they derive from the equation of motion of s. In the diagrammatic framework, these interactions are represented by vertices, in which different lines merge, each representing one of the fields involved in the interaction. Here I will be representing with a solid line the fields ψ and $\hat{\psi}$, with wavy lines the fields s and $\hat{s}$. Moreover, an arrow is used to recognise which legs represent a response field.

The first vertex - namely interaction - involving $\hat{\psi}$, represents the mode coupling non-linearity,

$$\hat{\psi}_\alpha(-\tilde{\boldsymbol{k}}) \qquad \psi_\beta(\tilde{\boldsymbol{q}}) \qquad s_{\gamma\nu}(\tilde{\boldsymbol{p}}) \qquad = g P_{\alpha\rho}(\boldsymbol{k}) \, \mathbb{I}_{\rho\beta\gamma\nu} \hat{\delta}(\tilde{\boldsymbol{k}} - \tilde{\boldsymbol{q}} - \tilde{\boldsymbol{p}}) \qquad (8.72)$$

This interaction represents a purely dynamic interaction since it is proportional only to the dynamic coupling g.

The second vertex involving $\hat{\psi}$ comes from the ferromagnetic quartic interaction of the static free energy, ensuring that the field ψ relaxes towards the static equilibrium distribution, and therefore is proportional to static coupling u. It is represented by the term

$$\hat{\psi}_\alpha(-\tilde{\boldsymbol{k}}) \qquad \psi_\beta(\tilde{\boldsymbol{q}}) \qquad \psi_\gamma(\tilde{\boldsymbol{p}}) \qquad \psi_\gamma(\tilde{\boldsymbol{h}}) \qquad = -\frac{J}{3} Q_{\alpha\beta\gamma\nu}(\boldsymbol{k}) \, \hat{\delta}(\tilde{\boldsymbol{k}} - \tilde{\boldsymbol{q}} - \tilde{\boldsymbol{p}} - \tilde{\boldsymbol{h}}) \qquad (8.73)$$

The other two vertices involve one field $\hat{s}$, and both derive from the mode-coupling interaction in the equation for s. The first comes from the linear part of the "force" defined in Eq. (8.45), representing a purely dynamic interaction proportional to g,

and it takes the same form as in the non-constrained theory

$$
\hat{s}_{\alpha\beta}(-\tilde{\boldsymbol{k}}) \quad\text{[diagram]}\quad \begin{matrix} \psi_\gamma(\tilde{\boldsymbol{q}}) \\ \\ \psi_\nu(\tilde{\boldsymbol{p}}) \end{matrix} \quad = \frac{g}{2}\left(p^2 - q^2\right)\mathbb{I}_{\alpha\beta\gamma\nu}\hat{\delta}(\tilde{\boldsymbol{k}} - \tilde{\boldsymbol{q}} - \tilde{\boldsymbol{p}}) \tag{8.74}
$$

Here the factor $(p^2 - q^2)$, coming from the cross-product structure of the mode-coupling interaction, guarantees that this interaction vanishes when $\boldsymbol{k} = 0$. This is a consequence of the symmetry of the non-constrained theory, which conserves the total instantaneous spin $\boldsymbol{S}(t) = \boldsymbol{s}(\boldsymbol{k} = 0, t)$.

The last interaction term is the DYS vertex, given by the novel non-linear contribution peculiar to the solenoidal theory, discussed at the end of Sec. 8.2.2. This interaction mixes static and dynamic terms since it represents the effects of the static quartic interaction on the dynamics of $\boldsymbol{s}$, mediated by the mode-coupling dynamic interaction. Therefore, the DYS vertex is proportional to the product of the static coupling u_0 and the dynamic coupling g_0 and it takes the following form,

$$
\hat{s}_{\alpha\beta}(-\tilde{\boldsymbol{k}}) \quad\text{[diagram]}\quad \begin{matrix} \psi_\gamma(\tilde{\boldsymbol{q}}_1) \\ \psi_\nu(\tilde{\boldsymbol{p}}_2) \\ \psi_\sigma(\tilde{\boldsymbol{p}}_3) \\ \psi_\tau(\tilde{\boldsymbol{p}}_4) \end{matrix} \quad = \frac{\kappa}{12}K_{\alpha\beta\gamma\nu\sigma\tau}\left(\boldsymbol{k}, \boldsymbol{p}_1, \boldsymbol{p}_2, \boldsymbol{p}_3, \boldsymbol{p}_4\right)\hat{\delta}(\tilde{\boldsymbol{k}} - \tilde{\boldsymbol{p}}_1 - \tilde{\boldsymbol{p}}_2 - \tilde{\boldsymbol{p}}_3 - \tilde{\boldsymbol{p}}_4) \tag{8.75}
$$

The DYS vertex arises as a consequence of the solenoidal constraint since the tensor $K_{\alpha\beta\gamma\nu\sigma\tau}$ vanishes in the non-constrained theory. At variance with the vertex (9.56), DYS causes a violation of the spin conservation because the order parameter has lost the $O(d)$ symmetry as a consequence of the solenoidal constraint, meaning that it does not vanish when $\boldsymbol{k} = 0$. However, the fact that the total spin is not conserved does not mean that it is dissipated. I will show in the following sections that at first order in perturbation theory, no spin dissipation is generated by the RG after the shell integration as a consequence of the presence of the DYS vertex, reinforcing the hypothesis according to which $\boldsymbol{s}$ is a hydrodynamic slow-variable of the system. Note that, were this not the case, the RG flow would lead to the stable fixed point of solenoidal Model A [41].

8.4 Renormalization group calculation

The key idea behind the renormalization group is that, under the assumption of a large correlation length, scaling laws and critical exponents can be obtained by looking at how the parameters of a theory change by changing the length scale at which the system is observed [17]. The RG itself consists of a transformation through which a set of equations describing the dependence of the couplings from the length scale, namely the β-functions, can be derived.

I will use Wilson's momentum shell approach [17], detailed in Chapter 4, which in a nutshell is performed by following a two-step procedure: *i)* integrating out the short wavelength details, hence decreasing the cutoff in momentum space; *ii)* rescaling space and time, to formally reinstate the same original cutoff.

8.4.1 Self-energies

In the first step, one integrates out the small length scale (large momenta) fluctuations, namely fluctuations with momenta $\Lambda/b < k < \Lambda$. The effect of this integration is twofold: *i)* it changes the cut-off of the theory since now only fluctuation $k < \Lambda/b$ are allowed; *ii)* it changes the value of the parameters of the model, which acquires corrections due to the coupling between low and high momenta fluctuations. When focusing the attention on the Gaussian action, shell integration corrects the parameters in the following way

$$
\begin{aligned}
\mathcal{S}_0^< = \int_{\tilde{\boldsymbol{k}}}^< \hat{\psi} \left[-\mathrm{i}\omega + \Gamma(1 + \delta\Gamma \ln b)k^2 + m(1 + \delta m \ln b) \right] \psi + \\
+ \frac{1}{2} \int_{\tilde{\boldsymbol{k}}}^< \hat{s} \left[-\mathrm{i}\omega + \lambda^\perp(1 + \delta\lambda^\perp \ln b)k^2 + \lambda^\parallel(1 + \delta\lambda^\parallel \ln b)k^2 \right] s + \dots,
\end{aligned}
\tag{8.76}
$$

where the ellipses stand for higher order terms in $\boldsymbol{k}$ and ω, which turn out to be irrelevant at first-order in ϵ. Here I omitted the tensorial structure of the action for easier reading. Note that because the shell integration has been already performed, the integral over $\boldsymbol{k}$ runs from 0 to Λ/b, as denoted by the $<$ superscript to the integral sign, namely

$$
\int_{\tilde{\boldsymbol{k}}}^< = \int_{|\boldsymbol{k}|<\Lambda/b} \frac{\mathrm{d}^d k}{(2\pi)^d} \int_{-\infty}^\infty \frac{\mathrm{d}\omega}{2\pi}
\tag{8.77}
$$

Moreover, because diagrams will be computed in the thin shell limit $b \to 1^+$, all the corrections are proportional to the volume of the momentum shell, which is proportional to $1 - b^{-1} \simeq \ln b$.

In general, also corrections to the $-\mathrm{i}\omega\hat{\psi}\psi$ and $-\mathrm{i}\omega\hat{s}s$ terms in (8.76) might arise. However, this is not the case for the present calculation. The absence of corrections to $-\mathrm{i}\omega\hat{s}s$ is a relic of the rotational symmetry of the unconstrained theory: even though the constrained theory is not $O(n)$-invariant and the dynamics of the spin can not be written as a continuity equation because of the DYS vertex, no corrections to $-\mathrm{i}\omega\hat{s}s$ arise. I will provide a more complete argument for why this happens later. The absence of corrections to $-\mathrm{i}\omega\hat{\psi}\psi$ is instead only a consequence of the order in the perturbation theory I am working at. Corrections to this term would contribute to the anomalous dimension η, which is known to be $O(\epsilon^2)$ in the static universality class of dipolar ferromagnets [111] SMG is expected to belong to (see Sec. 8.1.1).

Diagrammatic expansion

The standard way to compute the corrections to the bare parameters of the model is using perturbation theory; to be more precise I will compute the corrections $\delta\mathcal{P}$ using a Feynman diagram expansion. The diagrams that contribute to these

perturbative corrections to the Gaussian parameters of the action, namely m, Γ, $\lambda^\perp, \lambda^\parallel$, are known as Self-Energies, and take the following form:

$$\Sigma_{\alpha\beta}(\tilde{\boldsymbol{k}}) \quad : \quad \hat{\psi}_\alpha(-\tilde{\boldsymbol{k}}) \longrightarrow \!\!\!\!\!\!\bigcirc\!\!\!\!\!\!\longrightarrow \psi_\beta(\tilde{\boldsymbol{k}}) \tag{8.78}$$

$$\Pi_{\alpha\beta\gamma\nu}(\tilde{\boldsymbol{k}}) \quad : \quad \hat{s}_{\alpha\beta}(-\tilde{\boldsymbol{k}}) \sim\!\!\!\!\bigcirc\!\!\!\!\sim s_{\gamma\nu}(\tilde{\boldsymbol{k}}) \tag{8.79}$$

which corrects the action as follows:

$$\Delta\mathcal{S}_0 = \int_{\tilde{\boldsymbol{k}}}^< \hat{\psi}_\alpha(-\tilde{\boldsymbol{k}})\Sigma_{\alpha\beta}(\tilde{\boldsymbol{k}})\psi_\beta(\tilde{\boldsymbol{k}}) + \hat{s}_{\alpha\beta}(-\tilde{\boldsymbol{k}})\Pi_{\alpha\beta\gamma\nu}(\tilde{\boldsymbol{k}})s_{\gamma\nu}(\tilde{\boldsymbol{k}}) \tag{8.80}$$

Therefore $\Sigma_{\alpha\beta}$ corrects Γ and m, while $\Pi_{\alpha\beta\gamma\nu}$ corrects $\lambda^\perp$ and $\lambda^\parallel$. Here all momenta are integrated off-shell, $k < \Lambda/b$, while frequency integrals still run from $-\infty$ to ∞. The quantities Σ and Π are the *self-energies*, which contribute to the perturbative corrections of the Gaussian parameters of the original action. At first order in ϵ, the self-energies are given by the following Feynman diagrams:

$$\Sigma_{\alpha\beta} = \longrightarrow\!\!\!\bigcirc\!\!\!\longrightarrow \; + \; \longrightarrow\!\!\!\bigcirc\!\!\!\longrightarrow \; + \; \longrightarrow\!\!\!\bigcirc\!\!\!\longrightarrow \tag{8.81}$$

$$\Pi_{\alpha\beta\gamma\nu} = \sim\!\!\!\bigcirc\!\!\!\sim \tag{8.82}$$

These diagrams can be written as integrals, using the standard Feynman diagrammatic rules, and read

$$\Sigma_{\alpha\beta}(\tilde{\boldsymbol{k}}) = - JQ_{\alpha\beta\sigma\tau}(\boldsymbol{k})\int_{\tilde{\boldsymbol{p}}}^> \mathbb{C}^{0,\psi}_{\sigma\tau}(\tilde{\boldsymbol{p}})+$$

$$+ g^2 P^\perp_{\alpha\rho}(\boldsymbol{k})\int_{\tilde{\boldsymbol{p}}}^> P^\perp_{\tau\mu}(\boldsymbol{p}_+)\mathbb{G}^{0,\psi}_{\sigma\tau}(-\tilde{\boldsymbol{p}}_+)\mathbb{C}^{0,s}_{\rho\sigma\mu\beta}(\tilde{\boldsymbol{p}}_-) \tag{8.83}$$

$$+ g^2 P^\perp_{\alpha\rho}(\boldsymbol{k})\int_{\tilde{\boldsymbol{p}}}^> (k^2 - p^2_-)\mathbb{G}^{0,s}_{\rho\sigma\tau\beta}(-\tilde{\boldsymbol{p}}_+)\mathbb{C}^{0,\psi}_{\sigma\tau}(\tilde{\boldsymbol{p}}_-)$$

$$\Pi_{\alpha\beta\gamma\nu}(\tilde{\boldsymbol{k}}) = g^2\mathbb{I}_{\alpha\beta\sigma\mu}\mathbb{I}_{\rho\tau\gamma\nu}\int_{\tilde{\boldsymbol{p}}}^> (p^2_+ - p^2_-)P^\perp_{\iota\rho}(\boldsymbol{p}_+)\mathbb{G}^{0,\psi}_{\mu\iota}(-\tilde{\boldsymbol{p}}_+)\mathbb{C}^{0,\psi}_{\sigma\tau}(\tilde{\boldsymbol{p}}_-) \tag{8.84}$$

where $\tilde{\boldsymbol{p}}_+ = \tilde{\boldsymbol{p}}+\frac{\tilde{\boldsymbol{k}}}{2}$, while $\tilde{\boldsymbol{p}}_- = \tilde{\boldsymbol{p}}-\frac{\tilde{\boldsymbol{k}}}{2}$. The integration over the frequency is performed explicitly, as ω has no cutoff, while the integration in the wave vector is performed on the momentum shell $\Lambda/b < k < \Lambda$, as the $>$ superscript to the integral sign suggests:

$$\int_{\tilde{\boldsymbol{p}}}^> = \int_{\frac{\Lambda}{b}}^\Lambda \frac{\mathrm{d}^d p}{(2\pi)^d} \int_{-\infty}^\infty \frac{\mathrm{d}\omega}{2\pi} \tag{8.85}$$

When working in the thin-shell limit, which is achieved by sending $b \to 1^+$; the diagrams of $\Sigma_{\alpha\beta}$ and $\Pi_{\alpha\beta\gamma\nu}$ can be computed exactly up to the relevant order in $\boldsymbol{k}$, namely up to order k^2. This calculation gives:

$$\Sigma_{\alpha\beta}(\tilde{\boldsymbol{k}}) = -(m + \Gamma k^2)\delta_{\alpha\beta}\frac{3(1 + 3w + 2x)f}{4(1 + w)(x + w)}\ln b + \delta_{\alpha\beta}\frac{9}{2}\tilde{u}(m - \Gamma\Lambda^2)\ln b$$

$$\Pi_{\alpha\beta\gamma\nu}(\tilde{\boldsymbol{k}}) = -\frac{1}{2}\lambda^\perp\mathbb{P}^\perp_{\alpha\beta\gamma\nu}k^2\frac{f}{6x}\ln b - \frac{1}{2}\lambda^\parallel k^2\mathbb{P}^\parallel_{\alpha\beta\gamma\nu}\frac{f}{3}\ln b \tag{8.86}$$

These results are given in terms of the following *effective parameters*, whose meaning will be discussed in the following section,

$$f = \frac{g^2}{\Gamma \lambda^{\|}} K_d \Lambda^{d-4} \qquad \tilde{u} = \frac{J}{\Gamma} K_d \Lambda^{d-4} \qquad r = \frac{m}{\Gamma} \qquad w = \frac{\Gamma}{\lambda^{\|}} \qquad x = \frac{\lambda^{\perp}}{\lambda^{\|}}. \qquad (8.87)$$

Here $K_d = S_d/(2\pi)^d$, with S_d being the surface of the d-dimensional sphere, while Λ is the cutoff of the theory (not to be confused with the relaxation tensor of the spin $\Lambda_{\alpha\beta\gamma\nu}$). Moreover, because I am working on the critical manifold $T = T_c$ when results at first order in ϵ are concerned one can set $r = m = 0$ in all corrections but those of m itself.

From (8.86) it is possible to read the perturbative correction to the parameters $\Gamma, m, \lambda^{\perp}, \lambda^{\|}$:
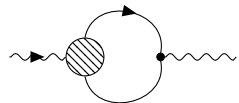
$$\delta\Gamma = \frac{3(1 + 3w + 2x)}{4(1 + w)(x + w)} f \qquad (8.88)$$

$$\delta m = -\frac{9}{2}\tilde{u}(1 - r^{-1}\Lambda^2) + \frac{3(1 + 3w + 2x)}{4(1 + w)(x + w)} f \qquad (8.89)$$

$$\delta\lambda^{\perp} = \frac{f}{6x} \qquad\qquad\qquad \delta\lambda^{\|} = \frac{f}{3} \qquad (8.90)$$

Absence of spin dissipation

It is important at this point to emphasise a key result: the self-energy $\Pi_{\alpha\beta\gamma\nu}(k, \omega)$ vanishes when $k \to 0$. This fact has two very important implications: the first is that the RG is not generating a dissipative term for the spin $-\eta\hat{s}s$, namely a linear term in the spin equation of motion which is finite at $k = 0$. The second is that no correction to the $-i\omega\hat{s}s$ term arises. This result is strictly related to the particular structure of the mode coupling vertex of the spin's equation of motion (9.56), and in particular to the fact that this vertex vanishes at zero external momentum k. I believe that this result, which was proven here only at one loop level, could be valid at all orders in perturbation theory. Indeed, the most general diagram that can generate a dissipation is given by,

$$\Pi_{\alpha\beta\gamma\nu} = \quad \text{} \qquad (8.91)$$

where the blob represents the sum of all 1-particle irreducible diagrams compatible with the given external legs, namely the renormalized mode coupling spin vertex, in which all the possible diagrammatic corrections (at all orders) are taken into account. If the renormalized spin mode coupling vertex vanishes at zero external momentum k, then Π is zero too at $k = 0$, implying that no dissipation is generated. Therefore, as far as the structure of the spin mode coupling vertex is preserved under RG, no spin dissipation can be generated. Even though in this work I explicitly showed that the structure of this vertex is preserved under RG only at one loop level, there are

some hints suggesting that this result could remain valid at all order in perturbation theory.

It can be shown, by computing the Fokker-Planck equation of SMG from the Langevin equations (8.40) and (8.41), that the probability density of the system approaches the equilibrium Gibbs-Boltzmann stationary state, $P \sim \exp\left(-\mathcal{H}\right)$. This non-perturbative result relies on the specific structure of the mode coupling vertices, which means that if the structure of the mode coupling interactions (8.74) and (8.72) were different, the system would not have a stationary equilibrium distribution. This is similar to what was observed in the case of (non-solenoidal) Models E/F in [114]. As this result is not perturbative, it is reasonable to think that the RG does not violate it; indeed, it would be very strange if under coarse-graining an equilibrium model flowed to an out-of-equilibrium one. Therefore, the structure of the mode coupling vertices should be preserved by the RG at all orders in perturbation theory. Since an essential requirement to generate a spin dissipation is that the RG changes the structure of the mode coupling spin vertex (9.56), one concludes that no dissipation is generated at any orders in perturbation theory. Note also that this result ensures that in the presence of a small bare dissipation, the same crossover observed in [41, 108] between a conservative and a dissipative dynamics is expected to arise.

Finally, I remark once again that the absence of spin dissipation does *not* imply that the total spin is instantaneously conserved: due to the presence of the novel DYS vertex (8.48), which is not zero at $k = 0$, conservation is broken, even though it is still true that the *mean* value of the total spin vector is conserved, suggesting that a generalised spin precession occurs: similarly to a standard angular momentum without dissipation but in presence of an external force, which performs a periodic precession with constant time average, so the total spin in presence of the solenoidal constraint has a non-dissipative time dynamics that conserves its mean value. To see why this happens, let me notice that the DYS vertex is the only contribution to the dynamics of the total spin $S(t) = \int \mathrm{d}^d x s(\boldsymbol{x}, t) = s(\boldsymbol{k} = 0, t)$, which takes the form

$$\dot{S}(t) = 2\kappa \mathbb{I}_{\alpha\beta\gamma\nu} \int_{\boldsymbol{q},\boldsymbol{h},\boldsymbol{p}} \psi_\gamma\left(-\boldsymbol{q}\right) P_{\nu\rho}\left(\boldsymbol{q}\right) \psi_\rho\left(\boldsymbol{p}\right) \psi_\sigma\left(\boldsymbol{h}\right) \psi_\sigma\left(\boldsymbol{q} - \boldsymbol{p} - \boldsymbol{h}\right) \qquad (8.92)$$

The average value $\langle \dot{S}(t) \rangle$ can be computed through a diagrammatic approach as the amputated diagram

$$\langle \dot{S}(t) \rangle = \quad \text{} \qquad (8.93)$$

Where the blob stands for the sum of all diagrams with one $\hat{s}(\tilde{\boldsymbol{k}})$ external leg evaluated ad $\tilde{\boldsymbol{k}} = 0$. Since the mode-coupling vertex is proportional to $\boldsymbol{k}$, this will not contribute to $\langle \dot{S}(t) \rangle$. At first order in perturbation theory, the DYS vertex contributes to $\langle \dot{S}(t) \rangle$ through the diagram,

$$(8.94)$$

This diagram can be shown to vanish identically, supporting the idea that although $\dot{S}(t)$ might fluctuate, it is not *dissipated* by the presence of the DYS vertex.

Perturbative corrections from the noise terms

It is quite crucial to notice how in the action (8.52)-(8.53) the coefficients Γ, $\lambda^\perp$ and $\lambda^\parallel$ do not appear only in the $\hat{\psi}\psi$ and $\hat{s}s$ terms, but also in the $\hat{\psi}\hat{\psi}$ and $\hat{s}\hat{s}$ terms. While the former terms arise from the deterministic relaxation dynamics, the latter arise from the Gaussian noises. In the presence of detailed balance, relaxation coefficients and noise amplitudes are linked by Einstein's relations. In this equilibrium theory, the relaxation coefficients must be equal to the amplitude of noise correlations. This equality follows from the presence of detailed balance with respect to the equilibrium Gibbs-Boltzmann distribution $e^{-\mathcal{H}}$.

It is crucial for this relation to also hold at a coarse-grained level, namely after applying an RG transformation. Therefore, the corrections $\delta\Gamma$ and $\delta\lambda^{\perp\parallel}$ appearing in (8.76) should equal the corrections to the $\hat{\psi}\hat{\psi}$ and $\hat{s}\hat{s}$ terms respectively. These noise terms get corrected from the shell integration in the following way:

$$
\begin{aligned}
\mathcal{S}_0^< = &-\int_{\tilde{\boldsymbol{k}}}^< \hat{\psi}\,\Gamma(1+\delta\Gamma\ln b)\,\hat{\psi}- \\
&-\frac{1}{2}\int_{\tilde{\boldsymbol{k}}}^< \hat{s}\left[\lambda^\perp(1+\delta\lambda^\perp\ln b)k^2 + \lambda^\parallel(1+\delta\lambda^\parallel\ln b)k^2\right]\hat{s} + \dots ,
\end{aligned}
\tag{8.95}
$$

To verify this, I compute here the following Self-energies

$$
\tilde{\Sigma}_{\alpha\beta}(\tilde{\boldsymbol{k}}) \quad : \quad \hat{\psi}_\alpha(-\tilde{\boldsymbol{k}}) \longrightarrow \bigcirc \longleftarrow \hat{\psi}_\beta(\tilde{\boldsymbol{k}})
\tag{8.96}
$$

$$
\tilde{\Pi}_{\alpha\beta\gamma\nu}(\tilde{\boldsymbol{k}}) \quad : \quad \hat{s}_{\alpha\beta}(-\tilde{\boldsymbol{k}}) \rightsquigarrow \bigcirc \rightsquigarrow \hat{s}_{\gamma\nu}(\tilde{\boldsymbol{k}})
\tag{8.97}
$$

which correct the $\hat{\psi}\hat{\psi}$ and $\hat{s}\hat{s}$ terms in the action as follows:

$$
\Delta\mathcal{S}_0 = \int_{\tilde{\boldsymbol{k}}}^< \hat{\psi}_\alpha(-\tilde{\boldsymbol{k}})\tilde{\Sigma}_{\alpha\beta}(\tilde{\boldsymbol{k}})\hat{\psi}_\beta(\tilde{\boldsymbol{k}}) + \hat{s}_{\alpha\beta}(-\tilde{\boldsymbol{k}})\tilde{\Pi}_{\alpha\beta\gamma\nu}(\tilde{\boldsymbol{k}})\hat{s}_{\gamma\nu}(\tilde{\boldsymbol{k}})
\tag{8.98}
$$

Therefore $\tilde{\Sigma}_{\alpha\beta}$ corrects Γ, while $\tilde{\Pi}_{\alpha\beta\gamma\nu}$ corrects $\lambda^\perp$ and $\lambda^\parallel$. At first order in ϵ, the noise self-energies are given by the following Feynman diagrams:

$$
\tilde{\Sigma}_{\alpha\beta} = \qquad\qquad\qquad \tilde{\Pi}_{\alpha\beta\gamma\nu} = \qquad\qquad
\tag{8.99}
$$

These diagrams can be written as integrals, using the standard Feynman diagrammatic rules, and read

$$
\tilde{\Sigma}_{\alpha\beta}(\tilde{\boldsymbol{k}}) = g^2 P_{\alpha\rho}^\perp(\boldsymbol{k})P_{\beta\mu}^\perp(\boldsymbol{k})\int_{\tilde{\boldsymbol{p}}}^> \mathbb{G}_{\sigma\tau}^{0,\psi}(-\tilde{\boldsymbol{p}}_+)\mathbb{C}_{\rho\sigma\mu\tau}^{0,s}(\tilde{\boldsymbol{p}}_-)
\tag{8.100}
$$

$$
\Pi_{\alpha\beta\gamma\nu}(\tilde{\boldsymbol{k}}) = g^2\mathbb{I}_{\alpha\beta\sigma\mu}\mathbb{I}_{\rho\tau\gamma\nu}\int_{\tilde{\boldsymbol{p}}}^> (p_+^2 - p_-^2)P_{\iota\rho}^\perp(\boldsymbol{p}_+)\mathbb{G}_{\mu\iota}^{0,\psi}(-\tilde{\boldsymbol{p}}_+)\mathbb{C}_{\sigma\tau}^{0,\psi}(\tilde{\boldsymbol{p}}_-)
\tag{8.101}
$$

where $\tilde{\boldsymbol{p}}_+ = \tilde{\boldsymbol{p}} + \frac{\tilde{\boldsymbol{k}}}{2}$, while $\tilde{\boldsymbol{p}}_- = \tilde{\boldsymbol{p}} - \frac{\tilde{\boldsymbol{k}}}{2}$.

When working in the thin-shell limit, which is achieved by sending $b \to 1^+$; the diagrams of $\tilde{\Sigma}_{\alpha\beta}$ and $\tilde{\Pi}_{\alpha\beta\gamma\nu}$ can be computed exactly up to the relevant order in $\boldsymbol{k}$, which is k^0 for $\tilde{\Sigma}$ and k^2 for $\tilde{\Pi}$. This calculation gives:

$$\tilde{\Sigma}_{\alpha\beta}(\tilde{\boldsymbol{k}}) = \Gamma P_{\alpha\beta}^{\perp}(\boldsymbol{k}) \frac{3(1 + 3w + 2x)f}{4(1+w)(x+w)} \ln b$$

$$\tilde{\Pi}_{\alpha\beta\gamma\nu}(\tilde{\boldsymbol{k}}) = \frac{1}{2}\lambda^{\perp}\mathbb{P}_{\alpha\beta\gamma\nu}^{\perp} k^2 \frac{f}{6x} \ln b + \frac{1}{2}\lambda^{\parallel}k^2 \mathbb{P}_{\alpha\beta\gamma\nu}^{\parallel} \frac{f}{3} \ln b \tag{8.102}$$
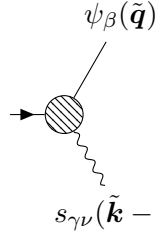
From (8.102) it is possible to read the perturbative correction to the parameters $\Gamma, \lambda^{\perp}, \lambda^{\parallel}$:
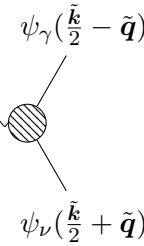
$$\delta\Gamma = \frac{3(1 + 3w + 2x)}{4(1+w)(x+w)}f \qquad \delta\lambda^{\perp} = \frac{f}{6x} \qquad \delta\lambda^{\parallel} = \frac{f}{3} \tag{8.103}$$

Remarkably, these results coincide with those of (8.88) and (8.90), derived from the corrections to the relaxation terms.

8.4.2 Mode coupling vertex corrections

The corrections to the mode coupling constant g are given by the following vertex functions,

$$V_{\alpha\beta\gamma\nu}^{\hat{\psi}\psi s}(\tilde{\boldsymbol{k}}, \tilde{\boldsymbol{q}}) = \hat{\psi}_\alpha(-\tilde{\boldsymbol{k}}) \quad \tag{8.104}$$

$\psi_\beta(\tilde{\boldsymbol{q}})$

$s_{\gamma\nu}(\tilde{\boldsymbol{k}} - \tilde{\boldsymbol{q}})$

$$V_{\alpha\beta\gamma\nu}^{\hat{s}\psi\psi}(\tilde{\boldsymbol{k}}, \tilde{\boldsymbol{q}}) = \hat{s}_{\alpha\beta}(-\tilde{\boldsymbol{k}}) \quad \tag{8.105}$$

$\psi_\gamma(\frac{\tilde{\boldsymbol{k}}}{2} - \tilde{\boldsymbol{q}})$

$\psi_\nu(\frac{\tilde{\boldsymbol{k}}}{2} + \tilde{\boldsymbol{q}})$

These two vertex functions correct the action as follows:

$$\Delta\mathcal{S} = \int_{\tilde{\boldsymbol{k}},\tilde{\boldsymbol{q}}}^{<} \hat{\psi}_\alpha(-\tilde{\boldsymbol{k}})\psi_\beta(\tilde{\boldsymbol{q}})s_{\gamma\nu}(\tilde{\boldsymbol{k}} - \tilde{\boldsymbol{q}})V_{\alpha\beta\gamma\nu}^{\hat{\psi}\psi s}(\tilde{\boldsymbol{k}}, \tilde{\boldsymbol{q}})$$

$$+ \int_{\tilde{\boldsymbol{k}},\tilde{\boldsymbol{q}}}^{<} \hat{s}_{\alpha\beta}(-\tilde{\boldsymbol{k}})\psi_\gamma(\tilde{\boldsymbol{k}}/2 - \tilde{\boldsymbol{q}})\psi_\nu(\tilde{\boldsymbol{k}}/2 + \tilde{\boldsymbol{q}})V_{\alpha\beta\gamma\nu}^{\hat{s}\psi\psi}(\tilde{\boldsymbol{k}}, \tilde{\boldsymbol{q}}) \tag{8.106}$$

Note that it is a crucial requirement for these equilibrium theories that g renormalizes in the same way in both terms. I am interested in how these vertex functions change the value of the mode coupling constant, hence one can compute $V^{\hat{\psi}\psi s}$ at the zeroth order in the momenta, and $V^{\hat{s}\psi\psi}$ up the second order in the momentum because the $g\hat{s}\psi\psi$ term in the action is of second order in the wave vector.

A first key consistency check: perturbative renormalization vs symmetry generator

The coupling g is the parameter conjugated to the generator of the rotational symmetry (the spin), hence it plays a central role in the definition of the Poisson structure and for this reason, it cannot take perturbative contributions from the RG calculation. Therefore, I expect both $V^{\hat{\psi}\psi s}$ and $V^{\hat{s}\psi\psi}$ to be zero, and fortunately this is indeed the case in the present calculation. From the technical point of view, however, the fact that these vertex functions are zero is extremely nontrivial and it is worth showing, as it is a vital consistency check of the calculation and in particular of the necessity of the new DYS vertex. The vertex function $V^{\hat{\psi}\psi s}$ is given by the following Feynman diagrams:

$$V^{\hat{\psi}\psi s}_{\alpha\beta\gamma\nu} = \quad\text{(8.107)}$$

To compute the corrections to g one must compute $V^{\hat{\psi}\psi s}$ at the zeroth order it the momentum. As it happens in the non-constrained case [40], these four diagrams, at zero external momenta $\tilde{\boldsymbol{k}}$, $\tilde{\boldsymbol{q}}$, sum up to zero.

$$V^{\hat{\psi}\psi s}_{\alpha\beta\gamma\nu}(0,0) = 0 \tag{8.108}$$

The vertex function $V^{\hat{s}\psi\psi}_{\alpha\beta\gamma\nu}(\tilde{\boldsymbol{k}}, \tilde{\boldsymbol{q}})$, on the other hand, is given by the following nonzero Feynman diagrams:

$$V^{\hat{s}\psi\psi}_{\alpha\beta\gamma\nu} = \quad\text{(8.109)}$$

The first two diagrams (the triangles) cancel each other, exactly as in the non-solenoidal case. The other two diagrams are, on the other hand, specific to the solenoidal case. The first diagram, which vanishes in the non-constrained theory [108], is nonzero when the solenoidal constraint is present, due to the suppression of the longitudinal $\psi^{\parallel}$ mode,

$$= -\frac{gu}{8}\mathbb{I}_{\alpha\beta\sigma\tau}\left(k_\sigma k_\gamma \delta_{\tau\nu} + k_\sigma k_\nu \delta_{\tau\gamma}\right)\Lambda^{d-4}K_d \ln b + \dots \tag{8.110}$$

where the ellipses stand for higher order in the momentum expansion, representing corrections to RG-irrelevant interactions. These vertex corrections not only would give to g a perturbative correction due to the shell integration, but it would *generate* a novel interaction term too since it does not have the same tensorial structure as the original interaction (9.56). If no other diagram cancelling it were present, the RG

would not have a closed structure, meaning that the equations of motion would not be eigenstates of the RG transformation, since the shell integration generates new interaction terms that were not present in the bare theory. In the general case, as in the off-equilibrium theory that I will study in the following chapters, this and other novel interaction terms will be generated anyway by activity. When this happens, it is sufficient to take into add these novel terms to the bare equations and start the RG procedure once again. However, as far as this equilibrium case is concerned, one would not expect any term other than those derived from the Mori-Zwanzig formalism to be generated by the RG. This unpleasant scenario, in which a new relevant interaction arises during the RG flow, is avoided by the key presence of a new Feynman diagram formed by a bubble connection of two lines of the DYS vertex, namely,

$$
\text{} = \frac{\kappa}{8} \mathbb{I}_{\alpha\beta\sigma\tau} \left(k_\sigma k_\gamma \delta_{\tau\nu} + k_\sigma k_\nu \delta_{\tau\gamma} \right) \Lambda^{d-4} K_d \ln b + \dots \tag{8.111}
$$

where, as before, the ellipses stand for higher order in the momentum expansion. The presence of this diagram is fundamental, since for $\kappa = ug$ as in the present case, it *exactly cancels* the contributions of diagram (8.110), therefore curing the anomalies that the latter carries and making the solenoidal RG calculation self-consistent. I therefore consider the following diagrammatic equation a key result of the present calculation:

$$
\text{} = 0 \tag{8.112}
$$

This calculation not only showed that g does not take any perturbative correction, but it also indirectly showed that no terms of $O(k = 0)$ are generated by the DYS vertex. Although the DYS vertex contributes to the dynamic behaviour of s also at $k = 0$, namely violating the conservation of the total spin, the last diagram vanishes at $k = 0$. The fact that the simplest one-loop diagram that can be constructed starting from the DYS vertex does not give any perturbative contribution at vanishing momenta suggests that no spin dissipation should arise, not even at higher orders in the ϵ-expansion. This is related to the fact that the DYS vertex violates the conservation of the spin in a *weak* way, leading to a sort of generalised precession that keeps its average value fixed.

8.4.3 Ferromagnetic vertex corrections

In contrast to the mode coupling vertex, the ferromagnetic coupling does have perturbative corrections due to the shell integration. The coupling J is corrected by

the four-field vertex function $V^{\hat\psi\psi\psi\psi}$,

$$V^{(\hat\psi\psi\psi\psi)}_{\alpha\beta\gamma\nu}(\tilde{\boldsymbol{k}},\tilde{\boldsymbol{q}},\tilde{\boldsymbol{p}}) = \quad \hat\psi_\alpha(-\tilde{\boldsymbol{k}}) \; \longrightarrow \;$$

$$\tag{8.113}$$

that corrects the action as follows:

$$\Delta\mathcal{S} = \int^{<}_{\tilde{\boldsymbol{k}},\tilde{\boldsymbol{q}},\tilde{\boldsymbol{p}}} \hat\psi_\alpha(-\tilde{\boldsymbol{k}})\psi_\beta(\tilde{\boldsymbol{p}})\psi_\gamma(\tilde{\boldsymbol{q}})\psi_\nu(\tilde{\boldsymbol{k}}-\tilde{\boldsymbol{q}}-\tilde{\boldsymbol{p}}) \; V^{\hat\psi\psi\psi\psi}_{\alpha\beta\gamma\nu}(\tilde{\boldsymbol{k}},\tilde{\boldsymbol{q}},\tilde{\boldsymbol{p}}) \tag{8.114}$$

At one loop, only the following Feynman diagrams contribute to the vertex function $V^{\hat\psi\psi\psi\psi}$ in a non-trivial way:

$$\tag{8.115}$$

The first term is the classic fish diagram of the standard ferromagnetic theory; the second diagram is generated by joining a mode-coupling vertex with the DYS vertex; the last three diagrams are of purely mode-coupling origin. Computing $V^{\hat\psi\psi\psi\psi}$ at the zeroth order in the external momenta, gives,

$$V^{\hat\psi\psi\psi\psi}_{\alpha\beta\gamma\nu}(\tilde{\boldsymbol{k}},\tilde{\boldsymbol{q}},\tilde{\boldsymbol{p}}) = -\frac{J}{3}Q_{\alpha\beta\gamma\nu}(\boldsymbol{k})\left[-\frac{17}{2}\tilde{u} + \frac{3(1+3w+2x)}{4(1+w)(x+w)}f\right]\ln b \tag{8.116}$$

so that the perturbative correction to the coupling J_0 is

$$\delta J = -\frac{17}{2}\tilde{u} + \frac{3(1+3w+2x)}{4(1+w)(x+w)}f \tag{8.117}$$

A second key consistency check: statics vs dynamics

The dynamical RG calculation (at equilibrium) must, of course, contain in itself the static RG calculation; more specifically, if a coupling constant is present also in the static case, its dynamical renormalization must be the same as its static renormalization. This is the case for the ferromagnetic coupling, which is perfectly well-defined also within a purely static framework. Therefore, in this section, I show that this consistency between statics and dynamics is achieved by this calculation.
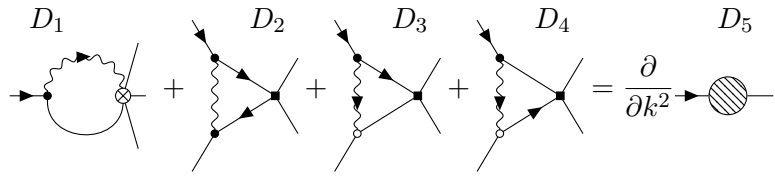
First of all, I recall that the *actual* ferromagnetic coupling, namely the coupling constant that appears in the static Hamiltonian, is $u = J/\Gamma$ (see (8.55)). Hence, the static ferromagnetic coupling u gets perturbative corrections both from J and Γ,

$$\delta u = \delta J - \delta\Gamma \tag{8.118}$$

and from equations (8.117) and (8.88) one has,

$$\delta u = -\frac{17}{2}\tilde{u} = -\frac{17}{2}\Lambda^{d-4}K_d u \tag{8.119}$$

Hence, the static coupling u does *not* receive any perturbative corrections from the dynamic coupling g, which is healthy. But the crucial check is whether the recursive relation I get for u from the dynamic RG is the same as the static one, equation (8.13). Fortunately, it is. Let me stress that this key consistency is recovered in an extremely nontrivial way; in particular, the DYS vertex plays a crucial role. The cancellation of the dynamical coupling g in the perturbative correction of the static coupling is achieved through the following diagrammatic identity:

$$\tag{8.120}$$

$$D_1 = -\frac{f}{4(w+x)}$$

$$D_2 + D_3 + D_4 = \frac{(2+5w+3x)}{2(1+w)(x+w)}f$$

$$D_5 = \frac{3(1+3w+2x)}{4(1+w)(x+w)}f$$

where the l.h.s of the equation is computed at zero external momenta. The diagram D_1 is the product of the interplay between the mode-coupling vertex and the DYS vertex, which is therefore crucial - once again - in recovering the correct static behaviour.

8.4.4 DYS vertex corrections

There is a third, and subtler, consistency check that is related to the renormalization of the ferromagnetic coupling constant. The coupling u not only appears in front of the ferromagnetic vertex but - due to the static-dynamic coupling induced by the solenoidal constraint - it also appears in front of the DYS vertex, which is indeed proportional to $\kappa = gu$ (see equation (8.75)). I showed that g does not acquire perturbative corrections, hence any diagrammatic correction to the DYS vertex must be billed to u; but u has been already corrected by its natural ferromagnetic corrections $V^{\hat{\psi}\psi\psi\psi}$, in the static-compliant way that I have just seen, equation (8.119). Hence, it seems two potentially *independent* corrections to u might arise, one coming from the *bona fide* ferromagnetic vertex, and a second one from the DYS vertex. If these diagrammatic corrections were different from each other, I would have a serious problem, as there would be a bifurcation of the ferromagnetic interaction, with highly dubious physical interpretation, not to mention the impossible recovery of the equilibrium static results. Once again, fortunately, the calculation does not

disappoint me, even though in a very nontrivial way. The DYS vertex function $V^{\hat{s}\psi\psi\psi}$ has (at one loop) the following non-vanishing diagrammatic contribution,

$$V^{\hat{s}\psi\psi\psi\psi}_{\alpha\beta\gamma\nu\sigma\tau} = \quad\quad\quad\quad\quad\quad\quad\quad\quad\quad\quad\quad (8.121)$$

Computing this Feynman diagram I get,

$$V^{\hat{s}\psi\psi\psi\psi}_{\alpha\beta\gamma\nu\sigma\tau}(\tilde{\boldsymbol{k}}, \tilde{\boldsymbol{q}}, \tilde{\boldsymbol{h}}, \tilde{\boldsymbol{p}}) = \frac{\kappa}{12}\frac{17}{2}\tilde{u}\, K_{\alpha\beta\gamma\nu\sigma\tau}\left(\boldsymbol{k}, \boldsymbol{q}, \boldsymbol{h}, \boldsymbol{p}, \boldsymbol{k} - \boldsymbol{q} - \boldsymbol{h} - \boldsymbol{p}\right) \quad (8.122)$$

and therefore the correction to κ that one obtains from the DYS vertex is

$$\delta\kappa = -\frac{17}{2}\tilde{u} \quad\quad\quad\quad\quad\quad (8.123)$$

Because $\kappa = gu$, the following relation between the perturbative correction of κ, g and u is expected to hold:

$$\delta u = \delta\kappa - \delta g \quad\quad\quad\quad\quad\quad (8.124)$$

Since $\delta g = 0$, as shown previously, I obtain the same correction to u as the one obtained from the ferromagnetic vertex, namely $\delta u = -17/2\tilde{u}$, which saves the day.

8.4.5 Rescaling

Now that the shell integration has been performed, it is time to move to the second step of the RG transformation. This second step consists of re-scaling momenta, frequencies and fields according to

$$\boldsymbol{k} = b^{-1}\,\boldsymbol{k}_b\,, \quad\quad\quad\quad\quad \omega = b^{-z}\omega_b\,, \quad\quad\quad\quad (8.125)$$

$$\boldsymbol{\psi}(\boldsymbol{k}, \omega) = b^{-\chi_\psi}\boldsymbol{\psi}(\boldsymbol{k}_b, \omega_b)\,, \quad\quad\quad \hat{\boldsymbol{\psi}}(\boldsymbol{k}, \omega) = b^{-\chi_{\hat{\psi}}}\hat{\boldsymbol{\psi}}(\boldsymbol{k}_b, \omega_b)\,, \quad\quad (8.126)$$

$$\boldsymbol{s}(\boldsymbol{k}, \omega) = b^{-\chi_s}\boldsymbol{s}(\boldsymbol{k}_b, \omega_b)\,, \quad\quad\quad \hat{\boldsymbol{s}}(\boldsymbol{k}, \omega) = b^{-\chi_{\hat{s}}}\hat{\boldsymbol{s}}(\boldsymbol{k}_b, \omega_b)\,. \quad\quad (8.127)$$

After this rescaling, one recovers an action with the same cutoff Λ but with new renormalized parameters and couplings, which will be denoted with a subscript b in what follows.

Note that by χ_ϕ I indicated here the scaling dimension of the field ϕ written in momentum-frequency space. Since the physical real-space fields $\psi(\boldsymbol{x}, t)$ and $s(\boldsymbol{x}, t)$ are linked to χ_ψ and χ_s by a Fourier transform, their scaling dimensions are given by

$$\chi_{\psi(x,t)} = \chi_\psi + d + z \quad\quad\quad\quad \chi_{s(x,t)} = \chi_s + d + z \quad\quad (8.128)$$

These scaling dimensions of real-space fields are fixed by the requirement that the coefficients in front of the terms $(\partial\psi)^2$ and s^2 in the Hamiltonian (8.18) remain equal to the unity under static RG flow and therefore are

$$\chi_{\psi(x,t)} = \frac{d - 2 + \eta}{2} \qu\quad\quad\quad\quad \chi_{s(x,t)} = \frac{d}{2} \qu\quad\quad (8.129)$$

where η is critical exponent characterising the anomalous dimension of the $\langle\psi\psi\rangle$ correlation function. Because I am working at first order in ϵ, and $\eta = O(\epsilon^2)$ in the

static universality class of reference, i.e. dipolar ferromagnets [87], I will here work at $\eta = 0$.

The scaling dimensions of the response fields $\hat{\psi}$ and $\hat{s}$ can be determined by requiring the coefficient in front of $\partial_t \psi$ and $\partial_t s$ in the equations of motion to remain equal to one along the RG flow. In Fourier space, this is equivalent to requiring that the coefficient in front of the $-\mathrm{i}\omega$ terms in the action (8.52)-(8.53) remains equal to unity. With these requirements, at first order in ϵ, one gets that

$$\chi_\psi = -\frac{6+d}{2} \qquad\qquad \chi_s = -\frac{4+d}{2} \qquad\qquad (8.130)$$

$$\chi_{\hat{\psi}} = -\frac{2+d}{2} \qquad\qquad \chi_{\hat{s}} = -\frac{4+d}{2} \qquad\qquad (8.131)$$

The effect of this rescaling step is to restore the original cut-off of the theory. Moreover, after this step, all the parameters of the model acquire a naive scaling factor, corresponding to their naive/engineering scaling dimension:

$$\Gamma \to b^{z-2}\Gamma \qquad\qquad \lambda^\perp \to b^{z-2}\lambda^\perp \qquad\qquad \lambda^\| \to b^{z-2}\lambda^\| \qquad\qquad (8.132)$$

$$g \to b^{z-\frac{d}{2}}g \qquad\quad J \to b^{2z-d}J \qquad\quad \kappa \to b^{3z-3d/2}\kappa \qquad\quad m \to b^z m \qquad (8.133)$$

where z is the dynamic critical exponents, which determines how the order parameter relaxes close to the critical point.

8.5 The critical dynamics of solenoidal Model G

After an RG step, namely after both shell integration and rescaling are performed, one ends up with a theory defined by a *new set of parameters*:

$$\Gamma_b = b^{z-2+\delta\Gamma}\,\Gamma \qquad\qquad m_b = b^{z+\delta m}\,m \qquad\qquad (8.134)$$

$$\lambda_b^\| = b^{z-2+\delta\lambda^\|}\,\lambda^\| \qquad\qquad \lambda_b^\perp = b^{z-2+\delta\lambda^\perp}\,\lambda^\perp \qquad\qquad (8.135)$$

$$g_b = b^{z-\frac{d}{2}+\delta g}\,g \qquad\qquad J_b = b^{2z-d+\delta J}\,J \qquad\qquad (8.136)$$

$$\kappa_b = b^{3z-\frac{3}{2}d+\delta\kappa} \qquad\qquad (8.137)$$

Here I used the fact that in the thin shell limit $b \to 1^+$, the perturbative corrections $1 + \delta\mathcal{P} \simeq b^{\delta\mathcal{P}}$. How the parameters change iterating this procedure defines the renormalization group flow, and the fixed point of this flow rules the critical dynamics of the system.

8.5.1 Effective parameters and RG flow equations

Even though I have seven equations for seven parameters, it is possible to reduce the complexity of the problem by using the set of five effective parameters introduced in Eq. (8.87). Let me recall here, for the benefit of the reader, what these effective parameters look like:

$$f = \frac{g^2}{\Gamma\lambda^\|}K_d\Lambda^{d-4} \qquad \tilde{u} = \frac{J}{\Gamma}K_d\Lambda^{d-4} \qquad r = \frac{m}{\Gamma} \qquad w = \frac{\Gamma}{\lambda^\|} \qquad x = \frac{\lambda^\perp}{\lambda^\|}, \qquad (8.138)$$

Please note also that all perturbative corrections computed in the previous section depend unambiguously on these effective parameters. The parameter r is precisely the coefficient in front of the quadratic ψ term in the free energy (8.18). Also, the coupling $\tilde{u}$ has connections with the *static* free energy, since it can be written as $\tilde{u} = u\Lambda^{d-4}K_d$: hence it is not a new effective coupling constant. I just went back to the original static ferromagnetic coupling constant u of (8.18) multiplied by $\Lambda^{d-4}K_d$ for computational convenience. Finally, note that in principle I should add a fifth coupling $\tilde{u}_\kappa = \kappa/g\Lambda^{d-4}K_d$. However, because at equilibrium $\kappa = ug$, then $\tilde{u}_\kappa = \tilde{u}$.

The effective coupling constants, through equations (8.134)-(8.137), are regulated in a closed manner by the following four equations:

$$f_b = b^{\epsilon + 2\delta g - \delta\Gamma - \delta\lambda^{\parallel}} f$$
$$\tilde{u}_b = b^{\epsilon + \delta J - \delta\Gamma} \tilde{u}$$
$$w_b = b^{\delta\Gamma - \delta\lambda^{\parallel}} w \tag{8.139}$$
$$x_b = b^{\delta\lambda^{\perp} - \delta\lambda_{\parallel}} x$$
$$r_b = b^{2 + \delta m - \delta\Gamma} r$$

The flow equation for $\tilde{u}_\kappa$ would take instead the form $\tilde{u}_{\kappa,b} = b^{\epsilon + \delta\kappa - \delta g} \tilde{u}_\kappa$. However, as I checked explicitly in Sec. 8.4.4, $\delta J - \delta\Gamma = \delta\kappa - \delta g$, hence maintaining the crucial relation $\tilde{u}_\kappa = \tilde{u}$ also along the RG. Let me point out that if I were to set $\lambda^{\parallel} = \lambda^{\perp} \equiv \lambda$ the effective parameters (8.138) would coincide with the one of the standard, unconstrained Model G [40].

By iterating this RG transformation, one obtains a set of recursive relations defining the RG flow, which link the parameters at the step $l+1$ to those at the step l:

$$f_{l+1} = b^{\epsilon + 2\delta g - \delta\Gamma - \delta\lambda^{\parallel}} f_l$$
$$\tilde{u}_{l+1} = b^{\epsilon + \delta J - \delta\Gamma} \tilde{u}_l$$
$$w_{l+1} = b^{\delta\Gamma - \delta\lambda^{\parallel}} w_l \tag{8.140}$$
$$x_{l+1} = b^{\delta\lambda^{\perp} - \delta\lambda_{\parallel}} x_l$$
$$r_{l+1} = b^{2 + \delta m - \delta\Gamma} r_l$$

In the thin shell limit the $b \to 1^+$, these recursive relations can be written in terms of a continuous number of step variable l as

$$\frac{\mathrm{d}f}{\mathrm{d}l} = \beta_f = (\epsilon + 2\delta g - \delta\Gamma - \delta\lambda^{\parallel})f \tag{8.141}$$

$$\frac{\mathrm{d}\tilde{u}}{\mathrm{d}l} = \beta_{\tilde{u}} = (\epsilon + \delta J - \delta\Gamma)\tilde{u} \tag{8.142}$$

$$\frac{\mathrm{d}w}{\mathrm{d}l} = \beta_w = (\delta\Gamma - \delta\lambda^{\parallel})w \tag{8.143}$$

$$\frac{\mathrm{d}x}{\mathrm{d}l} = \beta_x = (\delta\lambda^{\perp} - \delta\lambda_{\parallel})x \tag{8.144}$$

$$\frac{\mathrm{d}r}{\mathrm{d}l} = \beta_r = (2 + \delta m - \delta\Gamma)r \tag{8.145}$$

Note that explicit expression of the various perturbative corrections $\delta\Gamma, \delta\lambda^{\perp/\parallel}, \delta m, \delta J$ have been calculated in the previous sections, and can be found in Eq. (8.88)-(8.90) and Eq. (8.117), while $\delta g = 0$ as shown in Sec. 8.4.2.

The fixed point value of these parameters will determine the value of the critical exponents of the model. Let me notice that the naive scaling dimension of the effective couplings f and $\tilde{u}$ is $\epsilon = 4 - d$, which suggests that their fixed point will be of order ϵ. Moreover, the naive scaling dimension of r is 2, which means that r will be a relevant perturbation in the RG sense: the critical manifold is unstable to perturbations of r. This is related to the fact that $r \propto T - T_0$, with T_0 being the mean-field transition temperature, and hence for values of r different from a given *critical* value $r \neq r_c$, the RG flow is driven towards the non-critical infinite-temperature or zero-temperature fixed points.

8.5.2 Fixed point

I am ready to finally calculate the dynamical critical exponent z at one loop in a mode-coupling theory subject to a solenoidal constraint, that is in solenoidal Model G. To do this, I need to find the fixed points of the RG flow equations. Since the calculation here is performed at one loop, the static coupling u does not contribute to the renormalization of the dynamic parameters, therefore completely decoupling the dynamic behaviour from the static one. Because I have already abundantly checked that the renormalization of u is compatible with the static behaviour of dipolar ferromagnets, I will simply drop this equation from now on.

Fixed points can be searched by looking at the zeros of the β-functions of the effective parameters f, w and x, obtained in Eqs. (8.141), (8.143) and (8.144), are given by:

$$\beta_f = f\left(\epsilon - \frac{f}{3} - \frac{3\left(1 + 3w + 2x\right)}{4\left(1 + w\right)\left(x + w\right)}f\right) \tag{8.146}$$

$$\beta_w = wf\left(\frac{3\left(1 + 3w + 2x\right)}{4\left(1 + w\right)\left(x + w\right)} - \frac{1}{3}\right) \tag{8.147}$$

$$\beta_x = \frac{f}{3}\left(\frac{1}{2} - x\right) \tag{8.148}$$

Since I am interested in a genuine mode-coupling dynamical regime, I will not consider the trivial fixed points with $f^* = 0$, since they lead to the overdamped dynamics with $z = 2$ (at one loop) typical of Model A [40]. I find a set of non-trivial fixed points, among which only one is IR-stable while all the others are unstable. This stable fixed point is given by,

$$f^* = \frac{3\epsilon}{2} \quad , \quad w^* = \frac{21 + \sqrt{697}}{8} \quad , \quad x^* = \frac{1}{2} \tag{8.149}$$

As expected the effective coupling constant is of order $\epsilon = 4 - d$ at this fixed point.

The stability of the new fixed point $\vec{p}^* = (f^*, w^*, x^*)$ can be verified by studying the RG flow of small perturbations $\delta\vec{p} = \vec{p} - \vec{p}^*$. The linearized flow equation in the surroundings of $\vec{p}^*$ is given by

$$\frac{d\vec{p}}{dl} \simeq W \cdot \delta\vec{p} \tag{8.150}$$
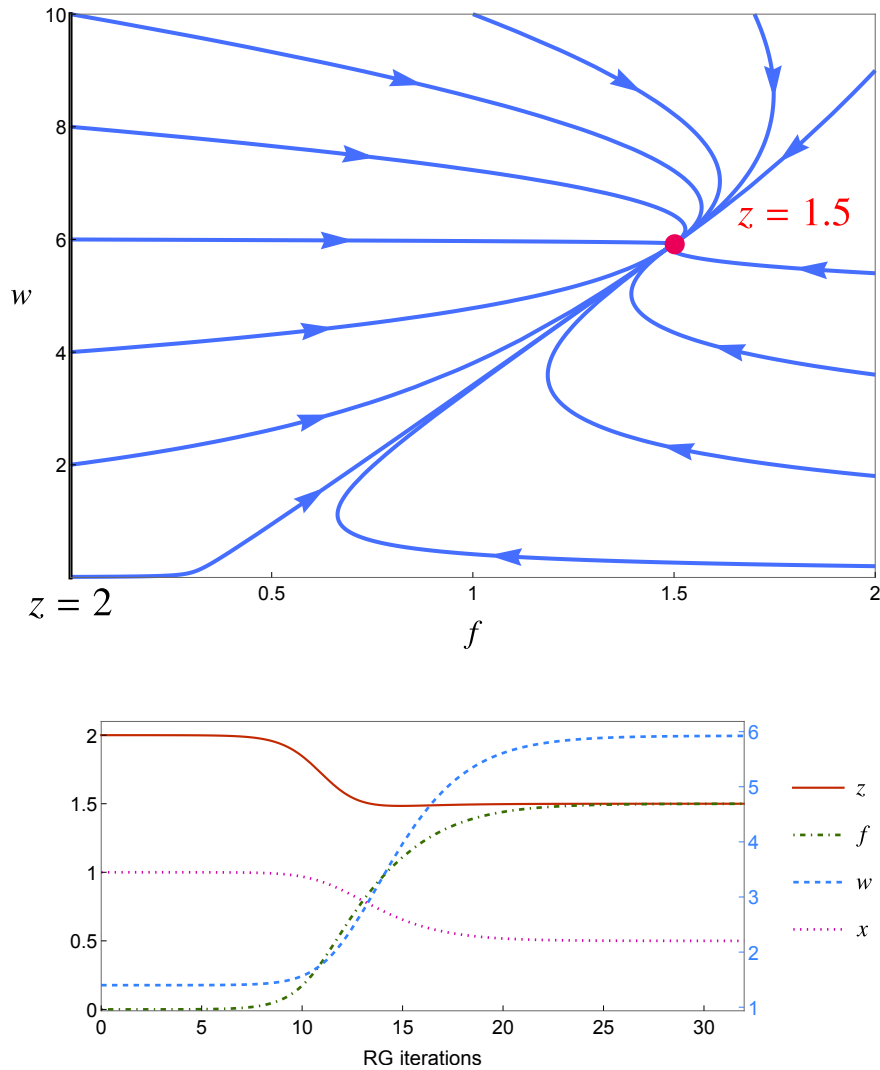
Figure 8.1. Renormalization group flow [MyPaper2]. Top: RG flow in the (f, w) plane in $d = 3$ at $x = \frac{1}{2}$. The $f = 0$ black line represents the set of unstable Gaussian fixed points. The RG flow converges towards the stable fixed point (red dot). Bottom: running parameters and critical exponent z as a function of the iteration step. *Permission to reuse granted under the terms of the Creative Commons Attribution License CC BY 4.0*

where the matrix W is the Jacobian of the β-functions $\vec{\beta} = (\beta_f, \beta_w, \beta_x)$, namely

$$W = \begin{pmatrix} \frac{\partial \beta_f}{\partial f} & \frac{\partial \beta_f}{\partial w} & \frac{\partial \beta_f}{\partial x} \\ \frac{\partial \beta_w}{\partial f} & \frac{\partial \beta_w}{\partial w} & \frac{\partial \beta_w}{\partial x} \\ \frac{\partial \beta_x}{\partial f} & \frac{\partial \beta_x}{\partial w} & \frac{\partial \beta_x}{\partial x} \end{pmatrix} \tag{8.151}$$

When the eigenvalues of the Jacobian matrix are negative, Eq. (8.150) guarantees

that small deviations $\delta\vec{p}$ form the fixed point flow back towards $\vec{p}^*$. At the fixed point (8.149) the matrix W has eigenvalues

$$e_1 = -\frac{\epsilon}{2}; \qquad e_2 = -\epsilon; \qquad e_3 = -\left(\frac{3\sqrt{697}}{4} - \frac{697}{36}\right)\epsilon \approx -0.44\epsilon \qquad (8.152)$$

which are all strictly negative for $\epsilon > 0$, thus making the novel fixed point stable in $d < d_c = 4$. In Fig. 8.1 (upper panel) I plot the RG flow in the (f, w) plane at $x = 1/2$ in $d = 3$ (upper panel), which converges to the stable fixed point (8.149) as expected. In the lower panel, I show the flow of the running couplings as a function of the RG step, from which one can see that the parameters flow from the Gaussian fixed point with $f = 0$ and $z = 2$ towards the new fixed point with $z = \frac{d}{2}$.

8.5.3 Anisotropy in the spin dynamics

In Model G the absence of anisotropic effects leads to the implicit assumption that all the different directions of the fields, both in real and Fourier space, meaning that transverse and parallel modes must be equal and therefore $\lambda = \lambda^\perp = \lambda^\parallel$, namely $x = 1$. However, at the new stable fixed point of the solenoidal Model G described by Eq. (8.149) $x^* = 1/2$, meaning that the anisotropy due to the suppression of the longitudinal ψ-mode leads to different dynamic behaviour of the two s-modes $\boldsymbol{s}^\perp$ and $\boldsymbol{s}^\parallel$, in such a way that $\lambda^{\parallel*} = 2\lambda^{\perp*}$. This result directly follows from the fact that the perturbative corrections $\delta\lambda^\perp$ and $\delta\lambda^\parallel$, given in Eq. (8.90), obey the relation

$$\delta\lambda^\parallel = 2x\,\delta\lambda^\perp \qquad (8.153)$$

It is not yet clear to me whether this factor 2 between $\lambda^\perp$ and $\lambda^\parallel$ can be guessed through a direct analysis of the equations of motion, or if it is valid only in the long-wavelength and long-time dynamic behaviour.

In any case, since the diagram contributing to $\delta\lambda^\perp$ and $\delta\lambda^\parallel$ involves neither propagators nor correlators of the field s, this result is a pure consequence of the suppression of the $\psi^\parallel$ modes. Even if I had naively left $\lambda_0 = \lambda_0^\perp = \lambda_0^\parallel$ at a bare level, the RG transformation would have led to two different perturbative corrections $\delta\lambda^\perp$ and $\delta\lambda^\parallel$, meaning that the infrared behaviour of this theory has two different diffusive coefficients for the $\boldsymbol{s}^\perp$ and $\boldsymbol{s}^\parallel$ modes.

8.5.4 The dynamical critical exponent z

To find the dynamic critical exponent, following [40] and [1], I require that the kinetic coefficient of the primary field, Γ, is non-singular at the RG fixed point, thus ensuring that the effective RG theory has a non-singular characteristic time scale. This amounts to imposing the condition,

$$\Gamma^* = \lim_{l\to\infty} \Gamma_l = O(1) \qquad (8.154)$$

and thus I need to write explicitly the recursive RG equation for the kinetic coefficient; that equation can be found in equations (8.134), complemented by its perturbative corrections, equation (8.88), thus giving,

$$\Gamma_{l+1} = b^{\chi_\Gamma}\,\Gamma \qquad\qquad \chi_\Gamma = z - 2 + \frac{3(1 + 3w_l + 2x_l)f_l}{4(1 + w_l)(x_l + w_l)} \qquad (8.155)$$

By requiring $\Gamma^* = O(1)$, which means asking that at the fixed point $\chi_\Gamma = 0$, I finally get

$$z = 2 - \frac{3\left(1 + 3w^* + 2x^*\right)f^*}{4\left(1 + w^*\right)\left(x^* + w^*\right)} \tag{8.156}$$

and once I use the one-loop values of the parameters at the stable fixed point (8.149), I obtain

$$z = \frac{d}{2} \tag{8.157}$$

Despite the difference of all effective parameters and coupling constants at the stable fixed point, this is exactly the same dynamic critical exponent as the standard unconstrained Model G [40]. This result is somewhat surprising. The solenoidal constraint *does* change the static universality class: the static critical exponents are different from the Landau-Ginzburg class, and define the novel dipolar ferromagnet class (see Table I and [87]). According to the common wisdom in the theory of critical phenomena, one would expect a change also in the dynamic universality class, as universality is normally broader at the static level than at the dynamic level. For example, Ising-like ferromagnets, have the same static critical exponents, while the dynamical critical exponents varies depending on whether the order parameter is conserved (Model B) or not (Model A). Here, I see something different: the dynamic universality class *does not* change due to the solenoidal constraint. Even though I have derived this conclusion perturbatively, this is probably a non-perturbative result due to the great power of the symmetry; the lack of diagrammatic renormalization of the coupling constant conjugated to the generator of the rotations, g, leads to the recursive relation,

$$g_{l+1} = b^{z - \frac{d}{2}} g_l \tag{8.158}$$

If one now asks that g does not change *at all*, they get $z = d/2$ at the non-perturbative level.

The fact that the solenoidal constraint does not alter the dynamical critical exponent is an encouraging result since it suggests that using the incompressibility condition to simplify the dynamical equations of active matter with mode coupling interactions is reasonable, as in the case of equilibrium systems it does to change the dynamical behaviour of the system.

8.6 Conclusions

I have studied the effects of a solenoidal constraint on the critical dynamics of a field $\boldsymbol{\psi}$ with $O(d)$-symmetry in the presence of mode-coupling interaction with the generator of the rotational symmetry $\boldsymbol{s}$, called spin; more succinctly, I have studied Solenoidal Model G. The presence of the constraint leads to the suppression of the ψ-mode parallel to the wave-vector $\boldsymbol{k}$, namely $\psi^{\parallel}(\boldsymbol{k}) = \boldsymbol{k} \cdot \boldsymbol{\psi}(\boldsymbol{k}) / |k|$, violating the $O(d)$-symmetry and modifying the static behaviour. The equations of motion of the constrained theory have been derived starting from the symmetries and Poisson-bracket relations between the hydrodynamic variables, namely the order parameter $\boldsymbol{\psi}$ and the spin $\boldsymbol{s}$. I performed a one-loop renormalization group calculation to investigate the long wave-length and long time behaviour in the critical region. The closed structure of the RG transformation and the consistency of the RG flow with

the static behaviour of dipolar ferromagnets provide a self-consistent proof that no RG-relevant interaction has been omitted and that the equations of motion I derived are correct.

Two main dynamic effects arise as a consequence of the solenoidal constraint. The first, and most predictable one, is the projection on the plane orthogonal to $\boldsymbol{k}$ of the equation of motion for the order parameter $\boldsymbol{\psi}$. On the contrary, no similar projection of the equation for $\boldsymbol{s}$ can be performed to obtain the spin dynamics; instead, the suppression of $\psi^{\parallel}(\boldsymbol{k})$ leads to a novel non-linear interaction - the DYS vertex - combining the effect of the static ferromagnetic coupling of the field $\boldsymbol{\psi}$ and the mode-coupling dynamic interaction. The presence of this new mixed interaction is the second, less intuitive, effect of the constraint, which adapts the spin dynamics to the presence of the constraint by making the static quartic coupling contributing to the torque-like interaction $\partial_t \boldsymbol{s} \sim g_0 \boldsymbol{\psi} \times \delta_\psi \mathcal{H}$. Moreover, the DYS vertex contributes to the time-derivative of the spin also at zero wave vector, therefore violating the conservation of the total spin.

The lack of conservation of the spin is not something strange: the order parameter is not rotational-invariant, due to the solenoidal constraint, and therefore the generator of its rotations is not a conserved quantity. It is however crucial to understand whether the spin is dissipated or not, since the presence of a dissipation generated by the RG would make the spin stop being an hydrodynamic variable, therefore suppressing any inertial behaviour in the critical region. The torque-like nature of the DYS vertex, which is the only dynamic term violating the spin conservation, indicates that this violation gives rise to a generalized precession of the total spin, rather than a dissipation. At one loop, the perturbative expansion confirms this interpretation, since the self-energy of the spin Π does not contain any perturbative corrections at $\boldsymbol{k} = 0$. Moreover, I have shown that the presence of any dissipative term in the linear dynamics of the spin can arise only if the dynamic mode-coupling vertex in the equation of $\boldsymbol{s}$ did not vanish when $\boldsymbol{k} = 0$, which seems not to be the case for this theory.

Our RG calculation passed several nontrivial consistency checks. First of all, the fact that the equations of motion appear to be eigenstates of the RG, in the sense that the shell integration step does not generate new interaction terms, ensures that I did not miss any relevant coupling in the problem description. Secondly, the RG recursive relations for the dynamic theory reproduce the behaviour of dipolar ferromagnets, ensuring that the static behaviour is correctly reproduced by the dynamics. Let me remark that both these results directly follow from the presence of the new DYS vertex, in the absence of which the theory would not describe correctly the dynamics of the system; therefore meaning that this new non-trivial interaction plays a crucial role in making the dynamic behaviour of the spin compatible with the constraint.

From the study of the RG recursive relations, the dynamic behaviour has been shown to be characterised by a critical exponent $z = \frac{d}{2}$, which is the same as the non-constrained theory. This result was somewhat unexpected. In general, static properties are more robust compared to dynamical properties; models with different dynamical critical behaviours are often characterised by the same static behaviour, such as Model A and Model G of [40]. On the contrary, in my model the solenoidal constraint changes the static universality class, leaving unchanged the

critical dynamics of the system. This suggests that the dynamic critical behaviour of homogeneous systems does not change when a solenoidal constraint, i.e. incompressibility, is enforced; this indicates that one can try and understand their dynamic critical behaviour by studying their incompressible version. Homogeneous systems are governed by equations of motion in which incompressibility is, in general, not required, but where density fluctuations, and therefore density-velocity couplings, are negligible. Incompressibility, though, completely suppresses density fluctuations and therefore represents a stronger requirement than homogeneity. Moreover, requiring incompressibility, hence imposing a solenoidal constraint on the velocity field, generates long-range interactions that could change the properties of a system; while this is indeed the case for the static behaviour of the present theory, the long-range interactions are not sufficient to modify its dynamic universality class. Numerical pieces of evidence of this fact have already been discussed in [69], where it was shown that homogeneous active systems exhibit similar dynamic collective behaviours to their incompressible counterpart. Furthermore, the analysis performed in Chapter 6 provides a theoretical explanation of why this happens. With the addition of the results obtained within the present Chapter, evidence that imposing incompressibility is justified in the description of natural swarms is extremely solid, as the solenoidal constraint resulting from it does not affect the critical dynamic behaviour in the presence of either activity or mode-coupling terms. This result is therefore very encouraging, as it allows one to study the homogeneous phase of the off-equilibrium Inertial Spin Model under an incompressible hypothesis, where the absence of the density field leads to a great simplification of the calculation.

This result is an important stepping stone towards developing an RG theory for natural swarms. The DYS interaction vertex in the spin dynamics that I derived in this chapter, which emerges as an effect of the solenoidal constraint, must certainly characterise also the equations of motion of an incompressible out-of-equilibrium field theory, in which terms coupling the order parameter to its generator of rotations are present. It would have been extremely difficult to derive the DYS vertex had one tackled the problem directly in the presence of activity. Despite this step forward, though, the complexity of the present calculation suggests that significantly more theoretical efforts will be needed to carry out the full-fledged out-of-equilibrium mode-coupling RG study of natural swarms.

Chapter 9

Field theory for natural swarms

So far, a comprehensive description of what features a field theory for collective swarming behaviour should account for has been provided. The lack of global order and the presence of long-range, scale-free velocity-velocity correlations suggest swarms belong to a near-ordering phase. Their collective behaviour therefore arises from the critical nature of the velocity fluctuations in a system near a second-order transition.

The need to account for alignment interactions and self-propulsion suggested that swarms can be modelled within the framework of the Toner and Tu theory [19] (see Chapter 3), describing the behaviour of an active rotational invariant system. However, the lack of consistency between theoretical predictions and experimental data [13] suggested some additional relevant feature was missing in this description. Experimental evidence highlighted this missing ingredient was *inertial behaviour*, as discussed in Chapter 7. To account for this inertia, a coupling with the *conserved* generator of the rotational symmetry, known as *spin*, has been proposed [100, 102]. This coupling leads, at equilibrium, to the universality class of Model G in Halperin and Hohenberg classification [40, 41].

Starting from these ingredients, I presented in Chapter 7 a minimal field theory for swarms, describing the fluctuations of the direction of motion field ψ, the spin field s and the density field ρ. However, to account for the observations of scaling laws in natural swarms, in Chapter 6 I gave evidence that density fluctuations are expected to be negligible [MyPaper2]. Incompressibility, namely a solenoidal constraint on ψ, should be therefore imposed, a task which turned out to be not so straightforward in the presence of a mode-coupling interaction between ψ and s. By working in a fixed-network approximation, I showed in Chapter 8 that in the presence of incompressibility, a new interaction arises in the dynamics of s.

This long route will allow me to finally provide in the present and following Chapters a field-theoretic description able to explain the dynamic collective behaviour observed in natural swarms of insects. By starting from the minimal active inertial field theory presented in Chapter 7, I will here present the complete version of an active inertial theory, which I shall call Self-Propelled Model G. This will allow me, in the following chapters, to perform a renormalization group analysis of this field theory aiming to characterise dynamic collective properties and compare them to experiments and numerical results.

9.1 Self-Propelled Model G

In the present section, I will present the equations of motion of Self-Propelled Model G (SPMG) in the incompressible limit. The behaviour of SPMG describes active systems in which inertia in the orientational dynamics of the velocity is relevant.

9.1.1 Effective interactions in natural swarms

Before proceeding, let me briefly review, for the benefit of the reader, what effective interactions are required to capture swarms' behaviour from a field-theoretical perspective. As these aspects have been widely discussed in the previous Chapters, the reader familiar with them can skip the present section and proceed directly to Sec. 9.1.2, where the field theory for swarms is introduced.

Effective alignment in the near-ordering phase

Evidence in swarms is that midges interact in such a way that they align their direction of motion to that of neighbours when they become sufficiently close [56]. These interactions are metric, probably mediated by sound, and short-range [12, 56]. From a field-theoretical point of view, the best framework to model this kind of behaviour is that of Landau-Ginzburg theory, originally employed to describe alignment interactions in ferromagnets. According to this theory, the effective free energy of a system as swarms in which individuals tend to align their direction of motion $\boldsymbol{\psi}$ is given by

$$\mathcal{H}_{LG} = \int \mathrm{d}^d x \frac{1}{2} (\partial_\alpha \psi_\beta)(\partial_\alpha \psi_\beta) + V(|\boldsymbol{\psi}|) \tag{9.1}$$

The summation over repeated index is understood. Here the $(\partial \psi)^2$ term tends to suppress the presence of strong fluctuations, namely favouring local alignment between neighbouring regions. The potential can usually be taken in the form

$$V(\psi) = \frac{r}{2}\psi^2 + \frac{u}{4}\psi^4 \, . \tag{9.2}$$

When r is positive the ground state is given by $\boldsymbol{\psi} = 0$, thus well describing a disordered phase with zero global magnetisation. For $r < 0$ instead, a flocking phase with $|\boldsymbol{\psi}|^2 = \frac{|r|}{u}$ arises at mean-field level. Swarms are instead expected to be described by the critical near-ordering phase, namely where $r \simeq 0$.

Behavioural inertia and mode-coupling interactions

The main difference between inertial and non-inertial behaviour can be detected by looking at the correlation function at small times. Correlations of non-inertial systems decay exponentially also in this limit, with a finite negative slope, whereas inertial systems have a vanishing derivative near $t = 0$. Evidence of inertial behaviour in swarms is strong [13], and in Chapter 7 I showed that inertia is present at all scales.

As discussed in Chapter 7, at equilibrium inertial behaviour in the orientational dynamics is described by Model G [40], in which the order parameters $\boldsymbol{\psi}$ is coupled

to its local generator of rotations $\boldsymbol{s}$. This new variable, in analogy with quantum mechanics, has been called *spin* since it represents the generator of rotations in the *internal* space of the velocities. It must not be confused with angular momentum, which is the generator of rotations in positions' space. The dynamic mode-coupling between between the direction of motion $\boldsymbol{\psi}$ and the spin $\boldsymbol{s}$ arises from the presence of a Poisson-bracket relation [40, 41],

$$\left\{ s_{\alpha\beta}\left(\boldsymbol{x}\right), \psi_{\gamma}\left(\boldsymbol{x}'\right) \right\} = 2\,g\,\mathbb{I}_{\alpha\beta\gamma\nu}\psi_{\nu}\left(\boldsymbol{x}\right)\delta\left(\boldsymbol{x} - \boldsymbol{x}'\right) \ , \tag{9.3}$$

which encodes the fact that $\boldsymbol{s}$ is the generator of rotations of $\boldsymbol{\psi}$.

Midges move in space: the role of active self-propulsion

The final feature of midges is their ability to self-propel, which drives the system far from thermal equilibrium. This property of being active is well encoded by the relation between the order parameter $\boldsymbol{\psi}$, which is not simply a pointer in space but rather represents the local coarse-grained average of the direction of motion of the individuals, and the velocity field:

$$\boldsymbol{v}\left(\boldsymbol{x}, t\right) = v_0 \boldsymbol{\psi}\left(\boldsymbol{x}, t\right) \ . \tag{9.4}$$

The parameter v_0, namely the microscopic speed, is what quantifies *activity*: when $v_0 = 0$ the system effectively behaves as an equilibrium one. When describing the dynamics of the system, the relation (9.4) states that the order parameter $\boldsymbol{\psi}$ is responsible for the presence of advection. At a coarse-grained level, the system can be hence described as an *active* fluid. This can be done by adding the presence of a pressure force in the equation for $\boldsymbol{\psi}$ and substituting the temporal derivative with the material derivative

$$\partial_t \to \mathcal{D}_t = \partial_t + v_0\left(\psi_{\gamma}\partial_{\gamma}\right) \ . \tag{9.5}$$

Any *active* field theory, aiming to describe collective behaviours of self-propelled units therefore requires the presence of advection, effectively captured by the presence of a material derivative, in addition to the presence of an active force.

9.1.2 The equations of motion

The combined effect of alignment, inertia and self-propulsion, led me to introduce the field theory of Self-Propelled Model G at the end of Chapter 7. The equations of motion for this theory have been derived from those of Model G, already accounting for both alignment and inertia, by adding activity through the minimal substitution (9.5), which encodes the fact that $\boldsymbol{\psi}$ *advects* both itself and the spin. This leads to the following set of equations:

$$\mathcal{D}_t \psi_{\alpha} = -\Gamma \frac{\delta\mathcal{H}}{\delta\psi_{\alpha}} + g\psi_{\beta}\frac{\delta\mathcal{H}}{\delta s_{\alpha\beta}} - \partial_{\alpha}\mathcal{P} + \theta_{\alpha} \ , \tag{9.6}$$

$$\mathcal{D}_t s_{\alpha\beta} = -\Lambda_{\alpha\beta\gamma\nu}\frac{\delta\mathcal{H}}{\delta s_{\gamma\nu}} + 2g\mathbb{I}_{\alpha\beta\gamma\nu}\psi_{\gamma}\frac{\delta\mathcal{H}}{\delta\psi_{\nu}} + \zeta_{\alpha\beta} \tag{9.7}$$

where the material derivatives are given by

$$\mathcal{D}_t \psi_\alpha = \partial_t \psi_\alpha + v_0 \gamma_v \left(\psi_\nu \partial_\nu\right) \psi_\alpha \tag{9.8}$$

$$\mathcal{D}_t s_{\alpha\beta} = \partial_t s_{\alpha\beta} + v_0 \gamma_s \left(\psi_\nu \partial_\nu\right) s_{\alpha\beta} \tag{9.9}$$

These equations are almost equivalent to those introduced at the end of Chapter 7, (7.37) and (7.38), with the exception that here I introduced two couplings in the material derivative, namely $\gamma_{\psi/s}$. In contrast with the case of Navier-Stokes equations, $\gamma_{\psi/s}$ need not be equal to 1 nor to each other, since activity breaks Galilean invariance.

Although in equilibrium systems Γ needed to be a coefficient, rather than a matrix, because of the rotational symmetry, out of equilibrium the possibility of having non-symmetric interactions allows in principle for more complex tensorial structures, making $\Gamma_{\alpha\beta}$ a matrix rather than a real coefficient. However, non-symmetric linear couplings between the different components of ψ_α are typically known to lead to totally different phase transition phenomenology, very different from that in which I am interested [115]. Hence, for the sake of simplicity, I shall assume that $\Gamma_{\alpha\beta}$ has no anti-symmetric component. Because of the rotational symmetry, the only symmetric form $\Gamma_{\alpha\beta}$ can take is that proportional to the identity: $\Gamma_{\alpha\beta} = \Gamma \delta_{\alpha\beta}$.

The theory presented in Eq. (9.6)-(9.7) will be studied in the incompressible case, for the reasons discussed in Chapter 6, therefore I omit all terms incompatible with this constraint, such as - for example - the two non-standard advective terms $\boldsymbol{\psi} \left(\nabla \cdot \boldsymbol{\psi}\right)$ and $\nabla \psi^2$ arising in the compressible Toner and Tu theory as a consequence of the absence of Galilean invariance [20]. Incompressibility, however, does not forbid the presence of non-standard advection terms in the equation of motion for the spin. As I will demonstrate in Section 10.1.4 through a Renormalisation Group analysis, two of these advection-like (adv) terms will be needed to correctly describe the large-scale behaviour. These terms are given by

$$\begin{aligned} V^{\mathrm{adv},1}_{\alpha\beta} &= v_0 \, \mu_1 \, \gamma_s \, \partial_\nu \left(s_{\alpha\nu}\psi_\beta - s_{\beta\nu}\psi_\alpha\right) \ , \\ V^{\mathrm{adv},2}_{\alpha\beta} &= v_0 \, \mu_2 \, \gamma_s \left[\partial_\alpha \left(\psi_\nu s_{\nu\beta}\right) - \partial_\beta \left(\psi_\nu s_{\nu\alpha}\right)\right] \ . \end{aligned} \tag{9.10}$$

Moreover, the RG also *generates* two of other anomalous terms in the equation of the spin (see Section 10.1.4). Because of the similar structure they share with the interaction arising from mode-coupling, I shall refer to them as anomalous mode-coupling (mc) terms. These terms read

$$\begin{aligned} V^{\mathrm{mc},1}_{\alpha\beta} &= \phi_1 \, g \, \left[\partial_\alpha \left(\psi_\nu \partial_\nu \psi_\beta\right) - \partial_\beta \left(\psi_\nu \partial_\nu \psi_\alpha\right)\right] \ , \\ V^{\mathrm{mc},2}_{\alpha\beta} &= \phi_2 \, g \, \partial_\nu \left[\psi_\nu \left(\partial_\alpha \psi_\beta - \partial_\beta \psi_\alpha\right)\right] \ . \end{aligned} \tag{9.11}$$

Crucially, each one of these anomalous terms is the divergence of a current, implying that the RG does not generate non-conserved (k-independent) spin dissipation: the conservation of the total spin, $\dot{S}_{\alpha\beta}(t) = 0$, a hallmark of the mode-coupling theories [40], is preserved even out of equilibrium. The novel vertices are accompanied by four new dimensionless couplings $\mu_1, \mu_2, \phi_1, \phi_2$.

Some other terms could be included in the calculation. It is the case of linear couplings between spin and velocity described in [116], which near criticality take

the form $\partial_t \psi_\alpha \sim \partial_\beta s_{\alpha\beta}$ and $\partial_t s_{\alpha\beta} \sim \nabla^2 (\partial_\alpha \psi_\beta - \partial_\beta \psi_\alpha)$. These terms modify the structure of linearised hydrodynamic equations, allowing the presence of propagators and correlation functions that mix the fields $\boldsymbol{s}$ and $\boldsymbol{\psi}$. However, if such terms were included, the number of diagrams (which are not few even in the present calculation) would inevitably become enormous and impossible to manage. Moreover, the presence of these new linear terms does not modify the dynamic critical exponent z of the linear theory, while the presence of advection or inertial mode-coupling alone has a great impact on it. Therefore, the presence of these additional linear terms is expected only to perturb the effect of non-linear interactions on the critical exponents. Hence, I decided to focus on the study of spin-velocity couplings due to non-linear interactions only by working on the sub-manifold of the parameter space where such linear terms are not present. Because the RG calculation is in perfect agreement with numerical simulations even in the case in which these linear terms are ignored, I believe that including them from the beginning should not really affect the results I find here.

The resulting equations of motion therefore become,

$$\partial_t \psi_\alpha + v_0 \gamma_v \left(\psi_\nu \partial_\nu \right) \psi_\alpha = -\Gamma \frac{\delta \mathcal{H}}{\delta \psi_\alpha} + g \psi_\beta \frac{\delta \mathcal{H}}{\delta s_{\alpha\beta}} - \partial_\alpha \mathcal{P} + \theta_\alpha \ , \qquad (9.12)$$

$$\partial_t s_{\alpha\beta} + v_0 \gamma_s \left(\psi_\nu \partial_\nu \right) s_{\alpha\beta} + v_0 \, \mu_1 \, \gamma_s \, \partial_\nu \left(s_{\alpha\nu} \psi_\beta - s_{\beta\nu} \psi_\alpha \right) +$$
$$+ \, v_0 \, \mu_2 \, \gamma_s \left[\partial_\alpha \left(\psi_\nu s_{\nu\beta} \right) - \partial_\beta \left(\psi_\nu s_{\nu\alpha} \right) \right] = -\Lambda_{\alpha\beta\gamma\nu} \frac{\delta \mathcal{H}}{\delta s_{\gamma\nu}} + 2 g \mathbb{I}_{\alpha\beta\gamma\nu} \psi_\gamma \frac{\delta \mathcal{H}}{\delta \psi_\sigma} +$$
$$+ \, \phi_1 \, g \, \left[\partial_\alpha \left(\psi_\nu \partial_\nu \psi_\beta \right) - \partial_\beta \left(\psi_\nu \partial_\nu \psi_\alpha \right) \right] + \phi_2 \, g \, \partial_\nu \left[\psi_\nu \left(\partial_\alpha \psi_\beta - \partial_\beta \psi_\alpha \right) \right] + \zeta_{\alpha\beta} \quad (9.13)$$

In principle, these equations should be coupled to an additional equation for the density field ρ. However, as discussed in Chapter 6, when interested in characterising scaling laws in active systems, it is possible to get rid of the density field by studying incompressible systems.

Although the system I am dealing with is out of equilibrium, it is possible to identify the truly non-equilibrium dynamic terms from those arising from a free energy functional $\mathcal{H}$ that would survive also in the equilibrium limit $v_0 \to 0$. In this limit, the theory resembles the dynamical structure of Model G [40]. Therefore equations (9.12), (9.13) can be viewed as given by the merging of this equilibrium model with Navier-Stokes equation [46]. The latter takes into account the active motion of particles, as it happens for the Toner and Tu theory.

Because the system is out of equilibrium, Einstein's relations between the kinetic coefficients and the corresponding noise variances are not expected to hold. Therefore, $\boldsymbol{\theta}$ and $\boldsymbol{\zeta}$ of Eq. (9.12), (9.13) are white Gaussian noises with zero mean $\langle \boldsymbol{\theta} \rangle = \langle \boldsymbol{\zeta} \rangle = 0$ and variance given by

$$\langle \theta_\alpha \left(\boldsymbol{x}, t \right) \theta_\beta \left(\boldsymbol{x}', t' \right) \rangle = 2 \tilde{\Gamma} \delta_{\alpha\beta} \delta \left(\boldsymbol{x} - \boldsymbol{x}' \right) \delta \left(t - t' \right) \ , \qquad (9.14)$$

$$\langle \zeta_{\alpha\beta} \left(\boldsymbol{x}, t \right) \zeta_{\gamma\nu} \left(\boldsymbol{x}', t' \right) \rangle = 4 \tilde{\Lambda}_{\alpha\beta\gamma\nu} \delta \left(\boldsymbol{x} - \boldsymbol{x}' \right) \delta \left(t - t' \right) \ , \qquad (9.15)$$

where $\tilde{\Gamma} \neq \Gamma$ and the amplitude $\tilde{\Lambda}$ to take the same form of Λ but with different coefficients ($\tilde{\lambda} \neq \lambda$ and $\tilde{\eta} \neq \eta$).

All the other terms, which cannot be written as derivatives of a free energy functional, represent genuinely off-equilibrium interactions; these are advection and anomalous terms, which all occur as a consequence of the fact that individuals are not fixed on a network. As I already mentioned, the couplings of the advective terms γ_v and γ_s need not be equal to 1 nor to each other, due to the absence of Galilean invariance [20]. Together with these active terms, a pressure force $-\partial_\alpha \mathcal{P}$ was added to (9.12), as it happens in Navier-Stokes, as well as in Toner-Tu equations.

The equations of motion I just derived in the present section describe inertial active matter. By tuning the different parameters, these equations are expected to be able to describe many different phases of active matter. As discussed in Chapter 1, since swarms have large, scale-free correlations but no net global polarisation [12, 56], they are expected to be described by the near-critical regime of the present field-theory. The absence of any intrinsic length scale in the correlations of swarms suggests that the renormalized mass of the field theory has to vanish. This means that the bare mass r is expected to be *small*.

9.2 Enforcing incompressibility

As discussed previously, equations (9.12) and (9.13) must be complemented by incompressibility, which is merely a solenoidal constraint on the field $\boldsymbol{v}$ and, consequently, on the polarisation $\boldsymbol{\psi}$:

$$\nabla \cdot \boldsymbol{\psi} = 0 \tag{9.16}$$

In Fourier space, this constraint translates into the following two equivalent statements,

$$k_\alpha \psi_\alpha (\boldsymbol{k}) = 0 \quad , \quad P^\perp_{\alpha\beta} (\boldsymbol{k}) \, \psi_\beta (\boldsymbol{k}) = \psi_\alpha (\boldsymbol{k}) \ , \tag{9.17}$$

where I have (re-)defined (see Eq. (6.24)) an object which is rather central to this calculation, namely the projector onto the subspace orthogonal to $\boldsymbol{k}$,

$$P^\perp_{\alpha\beta} (\boldsymbol{k}) = \delta_{\alpha\beta} - \frac{k_\alpha k_\beta}{k^2} \tag{9.18}$$

and where,

$$\phi (\boldsymbol{x}) = \int_{\boldsymbol{k}} \mathrm{e}^{\mathrm{i}\boldsymbol{x} \cdot \boldsymbol{k}} \phi (\boldsymbol{k}) \ . \tag{9.19}$$

Here and in the following, I will use the notation,

$$\int_{\boldsymbol{k}} = \int\limits_{|\boldsymbol{k}| < \Lambda} \frac{\mathrm{d}^d k}{(2\pi)^d} \, , \tag{9.20}$$

where Λ is the ultraviolet cutoff of the theory, of the order of the inverse of the microscopic inter-particle distance, which must not be confused with the relaxation tensor of the spin $\Lambda_{\alpha\beta\gamma\nu}$. Summation over repeated indices is always understood.

In Chapter 8, I showed that enforcing this solenoidal constraint at equilibrium has a triple effect on the equations of motion. The first, and maybe the most trivial, is that the equation of motion for $\boldsymbol{\psi}$ is projected orthogonally to $\boldsymbol{k}$, as it happens in incompressible field theories with no mode-coupling interaction [46, 23] - see

Chapter 5. The second is that the relaxation tensor $\Lambda_{\alpha\beta\gamma\nu}$ of $\boldsymbol{s}$, since the theory is not isotropic in $\boldsymbol{k}$-space, will take the general anisotropic form

$$\Lambda_{\alpha\beta\gamma\nu}\left(\boldsymbol{k}\right) = \eta\,\mathbb{I}_{\alpha\beta\gamma\nu} + \lambda^{\perp}\mathbb{P}^{\perp}_{\alpha\beta\gamma\nu}\left(\boldsymbol{k}\right) + \lambda^{\parallel}\mathbb{P}^{\parallel}_{\alpha\beta\gamma\nu}\left(\boldsymbol{k}\right) \qquad (9.21)$$

where $\mathbb{P}^{\perp}$ and $\mathbb{P}^{\parallel}$ are the generalisation of the projection operator $P^{\perp}$ and $P^{\parallel}$ defined in Eq. (6.24) acting on the space of 2-indices antisymmetric tensors, namely

$$\mathbb{P}^{\perp}_{\alpha\beta\gamma\nu}\left(\boldsymbol{k}\right) = \mathbb{I}_{\alpha\beta\gamma\nu} - \mathbb{I}_{\alpha\beta\sigma\tau}P^{\perp}_{\sigma\gamma}\left(\boldsymbol{k}\right)P^{\perp}_{\tau\nu}\left(\boldsymbol{k}\right) \ , \qquad (9.22)$$

while $\mathbb{P}^{\parallel} = \mathbb{I} - \mathbb{P}^{\perp}$. Let me recall that $\mathbb{I}$ is the identity tensor in the space of $\boldsymbol{s}$, which reads

$$\mathbb{I}_{\alpha\beta\gamma\nu} = \frac{\delta_{\alpha\gamma}\delta_{\beta\nu} - \delta_{\alpha\nu}\delta_{\beta\gamma}}{2} \ . \qquad (9.23)$$

The third effect is less obvious, and it is represented by the presence of a projection operator $P_{\nu\rho}\left(\boldsymbol{q}\right)$ in the mode-coupling interaction of the spin dynamics. The existence of this projector comes from the fact that in the presence of a solenoidal constrain the conservative Hamiltonian force must be projected also in the mode-coupling term of Eq. (9.13), namely

$$\frac{\delta\mathcal{H}}{\delta\psi_{\nu}\left(-\boldsymbol{q}\right)} \quad \Rightarrow \quad P_{\nu\rho}\left(\boldsymbol{q}\right)\frac{\delta\mathcal{H}}{\delta\psi_{\rho}\left(-\boldsymbol{q}\right)} \ . \qquad (9.24)$$

The linear part of the force is not affected by this new projector, but the non-linear terms are. The presence of the projector in (9.24) gives rise to an additional non-linear term that contributes to the dynamics of the spin. More precisely, it does so through a novel dynamical interaction term, known as DYS vertex, given by [MyPaper2],

$$\partial_t s_{\alpha\beta}\left(\boldsymbol{k}\right) \sim 2\kappa\mathbb{I}_{\alpha\beta\gamma\nu}\int_{\boldsymbol{q},\boldsymbol{h},\boldsymbol{p}}\psi_{\gamma}\left(\boldsymbol{k}-\boldsymbol{q}\right)P_{\nu\rho}\left(\boldsymbol{q}\right)\psi_{\rho}\left(\boldsymbol{p}\right)\psi_{\sigma}\left(\boldsymbol{h}\right)\psi_{\sigma}\left(\boldsymbol{q}-\boldsymbol{p}-\boldsymbol{h}\right) \ . \qquad (9.25)$$

Such vertex is absent in the non-constrained theory, since when $P_{\nu\rho}$ is substituted by $\delta_{\nu\rho}$ in Eq. (9.24), as in the non-solenoidal case, the r.h.s. of Eq. (9.25) vanishes.

Finally, note that while at equilibrium $\kappa = g\,u$, off-equilibrium effects may lead to a violation of the relation between κ, g and u meaning that, in general, one can have,

$$\kappa \neq g\,u \ . \qquad (9.26)$$

In the active case, it is not even clear whether this new interaction is needed to account for the description of natural swarms. For example, repulsive interactions among individuals, encoded in the pressure term $\mathcal{P}$, might be responsible on their own to keep the density constant. Remarkably, I shall demonstrate in the next Chapter that at the new off-equilibrium inertial fixed point, u and g remain finite, while κ vanishes. One might be therefore tempted to neglect the κ vertex in the discussion. However, although it vanishes, there are two good reasons to keep a trace of this coupling. First, it allows maintaining a connection with the equilibrium theory of [MyPaper2], in particular, recovering the same result as in equilibrium when $v_0 \to 0$ is an important consistency check in such a complicated calculation. Secondly, the presence of this vertex is crucial for an additional reason: the high

dimensionality of the parameter space (16 dimensions) and the intricate form of the beta-functions will not allow me to find analytically the RG fixed points. To perform a successful numerical integration of the RG flow equations, it is convenient to choose the initial condition in a region of the parameters space close to the equilibrium theory with solenoidal constraint. For the RG flow to go smoothly from the equilibrium to the off-equilibrium novel fixed point, it is technically crucial to keep this interaction in the calculation, even though it eventually flows to zero at the new RG fixed point. In other words, although the DYS vertex is not relevant at the novel fixed point so that it does not contribute to the new value of the dynamical critical exponent, the DYS vertex is technically relevant to *find* the new fixed point in the large parameter space.

9.2.1 The final equations for incompressible active inertial swarms

I am now ready to write down the equations of SPMG, (9.12) and (9.13), in the incompressible limit. After projecting Eq. (9.12), adding the DYS vertex to Eq. (9.13), and symmetrising terms containing powers of the same field, the incompressible equations of motion in k-space, finally become

$$\partial_t \psi_\alpha (\boldsymbol{k}, t) + \left(k^2 \Gamma + m \right) \psi_\alpha (\boldsymbol{k}, t) = \theta_\alpha - v_0 \frac{\mathrm{i}\gamma_v}{2} P_{\alpha\beta\gamma} (\boldsymbol{k}) \int_{\boldsymbol{q}} \psi_\beta (\boldsymbol{q}, t) \psi_\gamma (\boldsymbol{k} - \boldsymbol{q}, t)$$

$$- \frac{J}{3} Q_{\alpha\beta\gamma\nu} (\boldsymbol{k}) \int_{\boldsymbol{q},\boldsymbol{h}} \psi_\beta (\boldsymbol{q}, t) \psi_\gamma (\boldsymbol{h}, t) \psi_\nu (\boldsymbol{k} - \boldsymbol{q} - \boldsymbol{h}, t)$$

$$+ g P_{\alpha\rho}^\perp (\boldsymbol{k}) \mathbb{I}_{\rho\beta\gamma\nu} \int_{\boldsymbol{q}} \psi_\beta (\boldsymbol{k} - \boldsymbol{q}, t) s_{\gamma\nu} (\boldsymbol{q}, t) \ ,$$

$$(9.27)$$

$$\partial_t s_{\alpha\beta} (\boldsymbol{k}, t) + \Lambda_{\alpha\beta\gamma\nu} s_{\gamma\nu} (\boldsymbol{k}, t) = \zeta_{\alpha\beta} - v_0 \, \mathrm{i} \, \gamma_s \, \mathbb{I}_{\alpha\beta\gamma\nu} k_\rho \int_{\boldsymbol{q}} s_{\gamma\nu} (\boldsymbol{q}, t) \psi_\rho (\boldsymbol{k} - \boldsymbol{q}, t)$$

$$- 2 \, v_0 \, \mathrm{i} \, \mu_1 \, \gamma_s \, \mathbb{I}_{\alpha\beta\rho\eta} \mathbb{I}_{\rho\tau\gamma\nu} k_\tau \int_{\boldsymbol{q}} s_{\gamma\nu} (\boldsymbol{q}, t) \psi_\eta (\boldsymbol{k} - \boldsymbol{q}, t)$$

$$- 2 \, v_0 \, \mathrm{i} \, \mu_2 \, \gamma_s \, \mathbb{I}_{\alpha\beta\rho\sigma} \mathbb{I}_{\rho\eta\gamma\nu} k_\sigma \int_{\boldsymbol{q}} s_{\gamma\nu} (\boldsymbol{q}, t) \psi_\eta (\boldsymbol{k} - \boldsymbol{q}, t)$$

$$+ 2 \, g \, \mathbb{I}_{\alpha\beta\gamma\nu} \int_{\boldsymbol{q}} \boldsymbol{k} \cdot \boldsymbol{q} \, \psi_\gamma (-\boldsymbol{q} + \boldsymbol{k}/2, t) \, \psi_\nu (\boldsymbol{q} + \boldsymbol{k}/2, t)$$

$$+ 2 \, \Phi_1 \, g \, \mathbb{I}_{\alpha\beta\rho\sigma} \mathbb{I}_{\rho\tau\gamma\nu} \int_{\boldsymbol{q}} k_\sigma q_\tau \psi_\gamma (-\boldsymbol{q} + \boldsymbol{k}/2, t) \, \psi_\nu (\boldsymbol{q} + \boldsymbol{k}/2, t)$$

$$+ 2 \, \Phi_2 \, g \, \mathbb{I}_{\alpha\beta\rho\sigma} \mathbb{I}_{\rho\tau\gamma\nu} \int_{\boldsymbol{q}} k_\tau q_\sigma \psi_\gamma (-\boldsymbol{q} + \boldsymbol{k}/2, t) \, \psi_\nu (\boldsymbol{q} + \boldsymbol{k}/2, t)$$

$$+ \frac{\kappa}{6} \int_{\boldsymbol{q},\boldsymbol{h},\boldsymbol{p}} K_{\alpha\beta\gamma\nu\sigma\tau} (\boldsymbol{k}, \boldsymbol{q}, \boldsymbol{h}, \boldsymbol{p}, \boldsymbol{k} - \boldsymbol{q} - \boldsymbol{h} - \boldsymbol{p}) \times$$

$$\times \, \psi_\gamma (\boldsymbol{q}, t) \, \psi_\nu (\boldsymbol{h}, t) \, \psi_\sigma (\boldsymbol{p}, t) \, \psi_\tau (\boldsymbol{k} - \boldsymbol{q} - \boldsymbol{h} - \boldsymbol{p}, t) \ ,$$

$$(9.28)$$

where the following tensors were introduced,

$$P_{\alpha\beta\gamma}^\perp (\boldsymbol{k}) = k_\beta P_{\alpha\gamma}^\perp (\boldsymbol{k}) + k_\gamma P_{\alpha\beta}^\perp (\boldsymbol{k}) \ , \qquad (9.29)$$

$$Q^\perp_{\alpha\beta\gamma\nu}\left(\boldsymbol{k}\right) = P^\perp_{\alpha\beta}\left(\boldsymbol{k}\right)\delta_{\gamma\nu} + P^\perp_{\alpha\gamma}\left(\boldsymbol{k}\right)\delta_{\beta\nu} + P^\perp_{\alpha\nu}\left(\boldsymbol{k}\right)\delta_{\beta\gamma} \ , \tag{9.30}$$

$$\begin{aligned} K_{\alpha\beta\gamma\nu\sigma\tau}\left(\boldsymbol{k},\boldsymbol{p}_1,\boldsymbol{p}_2,\boldsymbol{p}_3,\boldsymbol{p}_4\right) =& \mathbb{I}_{\alpha\beta\gamma\rho}Q^\perp_{\rho\nu\sigma\tau}\left(\boldsymbol{k}-\boldsymbol{p}_1\right) + \mathbb{I}_{\alpha\beta\nu\rho}Q^\perp_{\rho\gamma\sigma\tau}\left(\boldsymbol{k}-\boldsymbol{p}_2\right) + \\ &+ \mathbb{I}_{\alpha\beta\sigma\rho}Q^\perp_{\rho\gamma\nu\tau}\left(\boldsymbol{k}-\boldsymbol{p}_3\right) + \mathbb{I}_{\alpha\beta\tau\rho}Q^\perp_{\rho\gamma\nu\sigma}\left(\boldsymbol{k}-\boldsymbol{p}_4\right) \ , \end{aligned} \tag{9.31}$$

and the noises have correlations,

$$\left\langle\theta_\alpha\left(\boldsymbol{k},t\right)\theta_\beta\left(\boldsymbol{k}',t'\right)\right\rangle = 2\left(2\pi\right)^d\tilde{\Gamma}P^\perp_{\alpha\beta}\left(\boldsymbol{k}\right)\delta^{(d)}\left(\boldsymbol{k}+\boldsymbol{k}'\right)\delta\left(t-t'\right) \ , \tag{9.32}$$

$$\left\langle\zeta_{\alpha\beta}\left(\boldsymbol{k},t\right)\zeta_{\gamma\nu}\left(\boldsymbol{k}',t'\right)\right\rangle = 4\left(2\pi\right)^d\tilde{\Lambda}_{\alpha\beta\gamma\nu}\left(\boldsymbol{k}\right)\delta^{(d)}\left(\boldsymbol{k}+\boldsymbol{k}'\right)\delta\left(t-t'\right) \ , \tag{9.33}$$

To simplify the notation, in (9.27), (9.28) the following reduced parameters have been defined,

$$\begin{aligned} J &= \Gamma u & \Phi_1 &= -2\left(\phi_1+\phi_2\right) \ , \tag{9.34} \\ m &= \Gamma r & \Phi_2 &= -2\phi_2 \ . \tag{9.35} \end{aligned}$$

9.3 The field-theoretical action of SPMG

I now proceed with the field-theoretical approach by deriving the field-theoretical action for Self-Propelled Model G. This is done by following the standard Martin-Siggia-Rose technique, detailed in Sec. 4.2, which allows to derive a path-integral field theory from a set of Langevin equations.

9.3.1 The action

The MSRDJ action $\mathcal{S}$ for the stochastic equations (9.27) and (9.28) depends upon four fields: $\boldsymbol{\psi}$, $\hat{\boldsymbol{\psi}}$, $\boldsymbol{s}$ and $\hat{\boldsymbol{s}}$. The action can be split into the following terms,

$$\mathcal{S}[\boldsymbol{\psi},\hat{\boldsymbol{\psi}},\boldsymbol{s},\hat{\boldsymbol{s}}] = \mathcal{S}_{0,\psi}[\boldsymbol{\psi},\hat{\boldsymbol{\psi}}] + \mathcal{S}_{0,s}[\boldsymbol{s},\hat{\boldsymbol{s}}] + \mathcal{S}_I[\boldsymbol{\psi},\hat{\boldsymbol{\psi}},\boldsymbol{s},\hat{\boldsymbol{s}}] \tag{9.36}$$

where $\mathcal{S}_{0,\psi}$ and $\mathcal{S}_{0,s}$ are the Gaussian parts of the action, respectively coming from the linear dynamic terms of the equations of motion of $\boldsymbol{\psi}$ and $\boldsymbol{s}$, while $\mathcal{S}_I$ is the interacting part. From Eq. (4.18),

$$\mathcal{S}_{0,\psi}[\boldsymbol{\psi},\hat{\boldsymbol{\psi}}] = \int_{\tilde{\boldsymbol{k}}}\left[-\mathrm{i}\omega + \Gamma k^2 + m\right]\hat{\psi}_\alpha(-\tilde{\boldsymbol{k}})\,\psi_\alpha(\tilde{\boldsymbol{k}}) - \tilde{\Gamma}P^\perp_{\alpha\beta}\left(\boldsymbol{k}\right)\hat{\psi}_\alpha(-\tilde{\boldsymbol{k}})\,\hat{\psi}_\beta(\tilde{\boldsymbol{k}}) \tag{9.37}$$

$$\mathcal{S}_{0,s}[\boldsymbol{s},\hat{\boldsymbol{s}}] = \frac{1}{2}\int_{\tilde{\boldsymbol{k}}}\left[-\mathrm{i}\omega\mathbb{I}_{\alpha\beta\gamma\nu} + \Lambda_{\alpha\beta\gamma\nu}\right]\hat{s}_{\alpha\beta}(-\tilde{\boldsymbol{k}})\,s_{\gamma\nu}(\tilde{\boldsymbol{k}}) - \tilde{\Lambda}_{\alpha\beta\gamma\nu}\hat{s}_{\alpha\beta}(-\tilde{\boldsymbol{k}})\,\hat{s}_{\gamma\nu}(\tilde{\boldsymbol{k}}) \tag{9.38}$$

$$
\begin{aligned}
\mathcal{S}_I[\boldsymbol{\psi}, \hat{\boldsymbol{\psi}}, \boldsymbol{s}, \hat{\boldsymbol{s}}] = {} & -g \int_{\tilde{\boldsymbol{k}}, \tilde{\boldsymbol{q}}} P_{\alpha\rho}^{\perp}(\boldsymbol{k}) \, \mathbb{I}_{\rho\beta\gamma\nu} \hat{\psi}_{\alpha}(-\tilde{\boldsymbol{k}}) \psi_{\beta}(\tilde{\boldsymbol{k}} - \tilde{\boldsymbol{q}}) s_{\gamma\nu}(\tilde{\boldsymbol{q}}) + \\
& -g \, \mathbb{I}_{\alpha\beta\rho\sigma} \mathbb{I}_{\rho\tau\gamma\nu} \int_{\tilde{\boldsymbol{k}}, \tilde{\boldsymbol{q}}} [\boldsymbol{k}\cdot\boldsymbol{q}\,\delta_{\sigma\tau} + \Phi_1 k_\sigma q_\tau + \Phi_2 q_\sigma k_\tau] \times \\
& \hspace{3cm} \times \hat{s}_{\alpha\beta}(-\tilde{\boldsymbol{k}}) \psi_\gamma(-\tilde{\boldsymbol{q}} + \tilde{\boldsymbol{k}}/2)\,\psi_\nu(\tilde{\boldsymbol{q}} + \tilde{\boldsymbol{k}}/2) - \\
& +v_0 \frac{\mathrm{i}\gamma_v}{2} \int_{\tilde{\boldsymbol{k}}, \tilde{\boldsymbol{q}}} P_{\alpha\beta\gamma}^{\perp}(\boldsymbol{k}) \, \hat{\psi}_\alpha(-\tilde{\boldsymbol{k}}) \psi_\beta(\tilde{\boldsymbol{q}}) \psi_\gamma(\tilde{\boldsymbol{k}} - \tilde{\boldsymbol{q}}) - \\
& +v_0 \frac{\mathrm{i}\gamma_s}{2} \mathbb{I}_{\alpha\beta\rho\sigma} \mathbb{I}_{\rho\tau\gamma\nu} \int_{\tilde{\boldsymbol{k}}, \tilde{\boldsymbol{q}}} [k_\eta \delta_{\sigma\tau} + 2\mu_1 k_\tau \delta_{\sigma\eta} + 2\mu_2 k_\sigma \delta_{\tau\eta}] \times \\
& \hspace{3cm} \times \hat{s}_{\alpha\beta}(-\tilde{\boldsymbol{k}}) s_{\gamma\nu}(\tilde{\boldsymbol{q}})\,\psi_\eta(\tilde{\boldsymbol{k}} - \tilde{\boldsymbol{q}}) - \\
& +\frac{J}{3} \int_{\tilde{\boldsymbol{k}}, \tilde{\boldsymbol{q}}, \tilde{\boldsymbol{h}}} \hat{\psi}_\alpha(-\tilde{\boldsymbol{k}}) Q_{\alpha\beta\gamma\nu}^{\perp}(\boldsymbol{k})\,\psi_\beta(\tilde{\boldsymbol{q}}) \psi_\gamma(\tilde{\boldsymbol{h}}) \psi_\nu(\tilde{\boldsymbol{k}} - \tilde{\boldsymbol{q}} - \tilde{\boldsymbol{h}}) + \\
& -\frac{\kappa}{12} \int_{\tilde{\boldsymbol{k}}, \tilde{\boldsymbol{q}}, \tilde{\boldsymbol{h}}, \tilde{\boldsymbol{p}}} \hat{s}_{\alpha\beta}(-\tilde{\boldsymbol{k}}) K_{\alpha\beta\gamma\nu\sigma\tau}(\boldsymbol{k}, \boldsymbol{q}, \boldsymbol{h}, \boldsymbol{p}, \boldsymbol{k} - \boldsymbol{q} - \boldsymbol{h} - \boldsymbol{p}) \times \\
& \hspace{3cm} \times \psi_\gamma(\tilde{\boldsymbol{q}}) \psi_\nu(\tilde{\boldsymbol{h}}) \psi_\sigma(\tilde{\boldsymbol{p}}) \psi_\tau(\tilde{\boldsymbol{k}} - \tilde{\boldsymbol{q}} - \tilde{\boldsymbol{h}} - \tilde{\boldsymbol{p}})
\end{aligned}
\tag{9.39}
$$

Here I wrote the effective action in k and ω space, where the generic field ϕ is given by

$$
\phi(\boldsymbol{x}, t) = \int_{\tilde{\boldsymbol{k}}} \mathrm{e}^{\mathrm{i}(\boldsymbol{x}\cdot\boldsymbol{k} - t\omega)} \phi(\tilde{\boldsymbol{k}})\,,
\tag{9.40}
$$

with $\tilde{\boldsymbol{k}} = (\boldsymbol{k}, \omega)$ and

$$
\int_{\tilde{\boldsymbol{k}}} = \int\limits_{|\boldsymbol{k}|<\Lambda} \frac{\mathrm{d}^d k}{(2\pi)^d} \int\limits_{-\infty}^{\infty} \frac{\mathrm{d}\omega}{2\pi}\,.
\tag{9.41}
$$

Notice that there is no cutoff in the frequency ω.

9.3.2 Free theory: propagators and correlation functions

The starting point to build the perturbative expansion of the equations of motion is the free theory, obtained by setting to zero all the dynamic non-linear couplings, namely g, γ_v, γ_s, J and κ. From the Gaussian part of the action, given by Eqs. (9.37) and (9.38), it is possible to derive the expressions for the bare propagators and correlation functions for the effective field theory, which are very similar to those of Model G with solenoidal constraint [MyPaper2], and are given by,

$$
\langle \psi_\alpha(\tilde{\boldsymbol{k}}) \hat{\psi}_\beta(\tilde{\boldsymbol{q}}) \rangle_0 = \mathbb{G}_{\alpha\beta}^{0,\psi}(\tilde{\boldsymbol{k}}) \hat{\delta}(\tilde{\boldsymbol{k}} + \tilde{\boldsymbol{q}})\,, \quad \langle s_{\alpha\beta}(\tilde{\boldsymbol{k}}) \hat{s}_{\gamma\nu}(\tilde{\boldsymbol{q}}) \rangle_0 = \mathbb{G}_{\alpha\beta\gamma\nu}^{0,s}(\tilde{\boldsymbol{k}}) \hat{\delta}(\tilde{\boldsymbol{k}} + \tilde{\boldsymbol{q}})\,,
\tag{9.42}
$$

$$
\langle \psi_\alpha(\tilde{\boldsymbol{k}}) \psi_\beta(\tilde{\boldsymbol{q}}) \rangle_0 = \mathbb{C}_{\alpha\beta}^{0,\psi}(\tilde{\boldsymbol{k}}) \hat{\delta}(\tilde{\boldsymbol{k}} + \tilde{\boldsymbol{q}})\,, \quad \langle s_{\alpha\beta}(\tilde{\boldsymbol{k}}) s_{\gamma\nu}(\tilde{\boldsymbol{q}}) \rangle_0 = \mathbb{C}_{\alpha\beta\gamma\nu}^{0,s}(\tilde{\boldsymbol{k}}) \hat{\delta}(\tilde{\boldsymbol{k}} + \tilde{\boldsymbol{q}})\,,
\tag{9.43}
$$

where $\hat{\delta}(\tilde{\boldsymbol{h}}) = (2\pi)^{d+1} \delta^{(d)}(\boldsymbol{h}) \delta(\omega_h)$. The subscripted zeros on thermal averages indicate that they are computed within the non-interacting theory. The tensors $\mathbb{G}$ and $\mathbb{C}$ are given by,

$$
\mathbb{G}_{\alpha\beta}^{0,\psi}(\tilde{\boldsymbol{k}}) = G_{0,\psi}(\tilde{\boldsymbol{k}}) \delta_{\alpha\beta}
\tag{9.44}
$$

$$
\mathbb{C}_{\alpha\beta}^{0,\psi}(\tilde{\boldsymbol{k}}) = C_{0,\psi}(\tilde{\boldsymbol{k}}) P_{\alpha\beta}^{\perp}(\boldsymbol{k})
\tag{9.45}
$$

$$
\mathbb{G}_{\alpha\beta\gamma\nu}^{0,s}(\tilde{\boldsymbol{k}}) = G_{0,s}^{\perp}(\tilde{\boldsymbol{k}}) \mathbb{P}_{\alpha\beta\gamma\nu}^{\perp}(\boldsymbol{k}) + G_{0,s}^{\parallel}(\tilde{\boldsymbol{k}}) \mathbb{P}_{\alpha\beta\gamma\nu}^{\parallel}(\boldsymbol{k})
\tag{9.46}
$$

$$
\mathbb{C}_{\alpha\beta\gamma\nu}^{0,s}(\tilde{\boldsymbol{k}}) = C_{0,s}^{\perp}(\tilde{\boldsymbol{k}}) \mathbb{P}_{\alpha\beta\gamma\nu}^{\perp}(\boldsymbol{k}) + C_{0,s}^{\parallel}(\tilde{\boldsymbol{k}}) \mathbb{P}_{\alpha\beta\gamma\nu}^{\parallel}(\boldsymbol{k})
\tag{9.47}
$$

where,

$$G_{0,\psi}\left(\boldsymbol{k},\omega\right) = \frac{1}{-\mathrm{i}\omega + \Gamma k^2 + m} \qquad C_{0,\psi}\left(\boldsymbol{k},\omega\right) = \frac{2\tilde{\Gamma}}{\omega^2 + (m + \Gamma k^2)^2} \qquad (9.48)$$

$$G_{0,s}^{\perp}\left(\boldsymbol{k},\omega\right) = \frac{2}{-\mathrm{i}\omega + \eta + \lambda^{\perp}k^2} \qquad C_{0,s}^{\perp}\left(\boldsymbol{k},\omega\right) = \frac{4\tilde{\lambda}^{\perp}k^2}{\omega^2 + (\eta + \lambda^{\perp}k^2)^2} \qquad (9.49)$$

$$G_{0,s}^{\parallel}\left(\boldsymbol{k},\omega\right) = \frac{2}{-\mathrm{i}\omega + \eta + \lambda^{\parallel}k^2} \qquad C_{0,s}^{\parallel}\left(\boldsymbol{k},\omega\right) = \frac{4\tilde{\lambda}^{\parallel}k^2}{\omega^2 + (\eta + \lambda^{\parallel}k^2)^2} \qquad (9.50)$$

In the diagrammatic framework, the fields $\boldsymbol{\psi}$ and $\hat{\boldsymbol{\psi}}$ are represented with a solid line, while the fields $\boldsymbol{s}$ and $\hat{\boldsymbol{s}}$ are represented with wavy lines. Bare propagators and correlation functions thus take the following graphical representation

$$\langle\psi_\alpha\hat{\psi}_\beta\rangle_0 \quad = \quad \longrightarrow \qquad\qquad \langle s_{\alpha\beta}\hat{s}_{\gamma\nu}\rangle_0 \quad = \quad \sim\!\!\sim\!\!\blacktriangleright\!\!\sim\!\!\sim \qquad (9.51)$$

$$\langle\psi_\alpha\psi_\beta\rangle_0 \quad = \quad \underline{\qquad} \qquad\qquad \langle s_{\alpha\beta}s_{\gamma\nu}\rangle_0 \quad = \quad \sim\!\!\sim\!\!\sim\!\!\sim \qquad (9.52)$$

where the arrows in the propagators always point in the direction of the response field.

9.3.3 Non-linear terms: the vertices

The six terms that compose $\mathcal{S}_I$ represent the non-linear interactions in the equations of motion. Each interaction involves one response field, identifying the equation of motion in which the corresponding non-linearity appears: $\hat{\boldsymbol{\psi}}$ if the vertex comes from a non-linearity in the equation of $\boldsymbol{\psi}$; $\hat{\boldsymbol{s}}$ if it comes from a non-linearity in the equation of $\boldsymbol{s}$. In the diagrammatic framework, these interactions are graphically represented by vertices, in which different lines merge, each representing one of the fields involved in the interaction. Full lines will represent $\hat{\boldsymbol{\psi}}$ and $\boldsymbol{\psi}$ fields, while $\hat{\boldsymbol{s}}$ and $\boldsymbol{s}$ fields will be represented by wavy lines. Moreover, an *entering* arrow is used to identify the leg representing the response field. I shall choose vertices to have opposed signs with respect to the interactions; the convenience of this choice is that vertices play a crucial role in building Feynman diagrams, which come from the expansion of $\exp(-\mathcal{S})$.

The first vertex involving $\hat{\boldsymbol{\psi}}$ represents the mode coupling non-linearity proportional to the reversible dynamic coupling g,

$$: \quad gP_{\alpha\rho}^{\perp}\left(\boldsymbol{k}\right)\mathbb{I}_{\rho\beta\gamma\nu}\hat{\delta}(\tilde{\boldsymbol{k}} - \tilde{\boldsymbol{q}} - \tilde{\boldsymbol{p}}) , \qquad (9.53)$$

The second interaction involving $\hat{\boldsymbol{\psi}}$ is the self-propulsion (or advection) interaction coming from the convective derivative in the equation of motion. This vertex is

proportional to $v_0\gamma_v$, and it vanishes when the microscopic speed does. Graphically, this interaction is represented by

$$\hat{\psi}_\alpha(-\tilde{\boldsymbol{k}}) \qquad \psi_\beta(\tilde{\boldsymbol{q}}) \qquad \psi_\gamma(\tilde{\boldsymbol{p}}) \qquad : \qquad -v_0\frac{\mathrm{i}\gamma_v}{2}P_{\alpha\beta\nu}(\boldsymbol{k})\,\hat{\delta}(\tilde{\boldsymbol{k}}-\tilde{\boldsymbol{q}}-\tilde{\boldsymbol{p}})\ , \qquad (9.54)$$

The third vertex involving $\hat{\boldsymbol{\psi}}$ derives from the ferromagnetic ψ^3 Landau-Ginzburg interaction, proportional to J. It is represented by the term,

$$\hat{\psi}_\alpha(-\tilde{\boldsymbol{k}}) \qquad \psi_\beta(\tilde{\boldsymbol{q}}) \quad \psi_\gamma(\tilde{\boldsymbol{p}}) \qquad \psi_\gamma(\tilde{\boldsymbol{h}}) \qquad : \qquad -\frac{J}{3}Q_{\alpha\beta\gamma\nu}(\boldsymbol{k})\,\hat{\delta}(\tilde{\boldsymbol{k}}-\tilde{\boldsymbol{q}}-\tilde{\boldsymbol{p}}-\tilde{\boldsymbol{h}})\ , \qquad (9.55)$$

The other three vertices involve one field $\hat{\boldsymbol{s}}$ and derive from the equation for the spin. The first one represents the dynamic mode-coupling interaction proportional to g with the addition of the two mode-coupling anomalous terms, with different tensorial structures,

$$\hat{s}_{\alpha\beta}(-\tilde{\boldsymbol{k}}) \qquad \psi_\gamma(\tilde{\boldsymbol{h}}) \qquad \psi_\nu(\tilde{\boldsymbol{p}}) \qquad : \qquad \frac{g}{2}\mathbb{I}_{\alpha\beta\rho\sigma}\mathbb{I}_{\rho\tau\gamma\nu}\hat{\delta}(\tilde{\boldsymbol{k}}-\tilde{\boldsymbol{h}}-\tilde{\boldsymbol{p}})\times$$
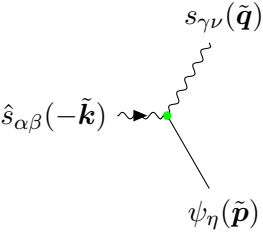
$$\times\left[\left(p^2-h^2\right)\delta_{\sigma\tau}+\Phi_1 p_\sigma^{(+)}p_\tau^{(-)}+\Phi_2 p_\sigma^{(-)}p_\tau^{(+)}\right]\ , \qquad (9.56)$$

where $\boldsymbol{p}^{(+)}=\boldsymbol{p}+\boldsymbol{h}$ while $\boldsymbol{p}^{(-)}=\boldsymbol{p}-\boldsymbol{h}$. This vertex vanishes when $\boldsymbol{h}=\boldsymbol{p}$, guaranteeing that this interaction does not contribute to the dynamics of the total spin $S(t)=s(\boldsymbol{k}=0,t)$. The anomalous mode coupling terms are those proportional to $\Phi_{1,2}$. From a technical point of view, it is essential to note that this vertex can be rewritten in an alternative form; by using the delta function, together with a symmetric distribution of the external momenta, one has,

$$\hat{s}_{\alpha\beta}(-\tilde{\boldsymbol{k}}) \qquad \psi_\gamma(\tilde{\boldsymbol{k}}/2-\tilde{\boldsymbol{q}}) \qquad \psi_\nu(\tilde{\boldsymbol{k}}/2+\tilde{\boldsymbol{q}}) \qquad : \qquad g\,\mathbb{I}_{\alpha\beta\rho\sigma}\mathbb{I}_{\rho\tau\gamma\nu}\left[\boldsymbol{k}\cdot\boldsymbol{q}\,\delta_{\sigma\tau}+\Phi_1\,k_\sigma q_\tau+\Phi_2\,q_\sigma k_\tau\right]\ .$$

$$(9.57)$$

This second form is convenient for two reasons: first, it has a simpler structure, which makes it easier to recognise corrections to the coupling constant g; secondly, in this form, it is more transparent to demonstrate the diagrammatic origin of the anomalous terms, a derivation that will be given later on in Section 10.1.4. On the other hand, the first form of this same vertex, equation (9.56), is handier when calculating diagrams in which $\hat{s}_{\alpha\beta}$ appears as an internal leg.

The second vertex involving $\hat{s}$ is the self-propulsion interaction, coming from the fact that s is advected by the velocity $v_0\psi$, and it is proportional to $v_0\gamma_s$. Graphically, this interaction is represented by,

$$
s_{\gamma\nu}(\tilde{\boldsymbol{q}})
$$

$$
\hat{s}_{\alpha\beta}(-\tilde{\boldsymbol{k}}) \qquad\qquad \psi_{\eta}(\tilde{\boldsymbol{p}}) \qquad : \qquad -v_0\frac{\mathrm{i}\gamma_s}{2}\mathbb{I}_{\alpha\beta\rho\sigma}\mathbb{I}_{\rho\tau\gamma\nu}\left[k_{\eta}\delta_{\sigma\tau}+2\mu_1 k_{\tau}\delta_{\sigma\eta}+2\mu_2 k_{\sigma}\delta_{\tau\eta}\right]\hat{\delta}(\tilde{\boldsymbol{k}}-\tilde{\boldsymbol{q}}-\tilde{\boldsymbol{p}})\,,
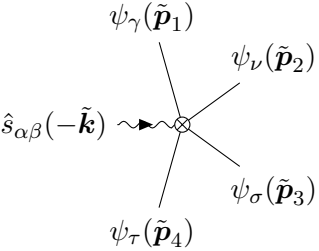$$

$$(9.58)$$

This interaction also vanishes when $\boldsymbol{q}=\boldsymbol{p}$, and therefore does not contribute to the dynamics of the total spin either. This vertex takes into account also the anomalous advection of s through the terms proportional to $\mu_{1,2}$.

The last interaction term is the DYnamic-Static (DYS) vertex [MyPaper2] introduced in Chapter 8. This interaction mixes the ferromagnetic-like interaction and the mode-coupling dynamic term, as a consequence of the presence of incompressibility. It represents the effects of the Landau confining potential on the dynamics of s, mediated by the mode-coupling dynamic interaction. It takes the following form,

$$
\psi_{\gamma}(\tilde{\boldsymbol{p}}_1)
$$
$$
\psi_{\nu}(\tilde{\boldsymbol{p}}_2)
$$

$$
\hat{s}_{\alpha\beta}(-\tilde{\boldsymbol{k}}) \qquad\qquad \psi_{\sigma}(\tilde{\boldsymbol{p}}_3) \qquad : \qquad \frac{\kappa}{12}K_{\alpha\beta\gamma\nu\sigma\tau}\left(\boldsymbol{k},\boldsymbol{p}_1,\boldsymbol{p}_2,\boldsymbol{p}_3,\boldsymbol{p}_4\right)\hat{\delta}(\tilde{\boldsymbol{k}}-\tilde{\boldsymbol{p}}_1-\tilde{\boldsymbol{p}}_2-\tilde{\boldsymbol{p}}_3-\tilde{\boldsymbol{p}}_4)\,.
$$
$$
\psi_{\tau}(\tilde{\boldsymbol{p}}_4)
$$

$$(9.59)$$

This interaction does not vanish when $\boldsymbol{k}=0$, and thus it contributes to the dynamics of the total spin. However, it is important not to confuse the absence of conservation with the presence of dissipation. If the spin was largely dissipated, it would become a non-hydrodynamic variable whose behaviour does not affect that of the order parameter. As shown in Chapter 8, where the fixed network approximation of the incompressible theory developed here is analysed, even though the spin may not be globally conserved due to the DYS interaction, it represents still a hydrodynamic slow mode. This is because the DYS vertex does not involve the spin, and thus represents the effects of the slow-mode ψ. Even if this effect remains finite as $\boldsymbol{k}\to 0$, it may only be responsible for slow variations of the total spin s. Hence, although the total spin is not conserved, it is not even dissipated and thus it undergoes a generalised precession caused by the DYS vertex [MyPaper2].

Chapter 10

Renormalization group calculation for swarms

The derivation of a field theory for natural swarms, a topic to which I have devoted the previous Chapter, is only the starting point of a deeper analysis of swarms. Characterising the collective behaviour exhibited by Self-Propelled Model G is the next step required to provide a quantitative assessment of inertia as a key ingredient in describing natural swarms.

In the present Chapter, the tools of the theory of critical phenomena [15, 2, 14] will be used to investigate the collective behaviours in Self-Propelled Model G. The core of this Chapter is represented by the perturbative renormalization group (RG) calculation, which I will perform in the momentum-shell scheme. In a nutshell, the momentum-shell RG unfolds through two stages: i) Integrating out small length-scale details, on the so-called momentum shell $\Lambda/b < k < \Lambda$, where $b < 1$, but close to 1; ii) Rescaling of momenta, together with frequencies and fields, to restore the cutoff Λ. The reader can refer to Chapter 4 for a more complete discussion of the RG procedure. Let me highlight only that the effect of step (ii) is to rescale each parameter by its corresponding naive dimension, while shell-integration (i) provides each parameter with an *anomalous* dimension. This last step is usually done by using the Feynman diagram technique [53]. It is therefore the very presence of Feynman diagrams that allows non-trivial collective behaviours to take place.

Following this structure, Sec. 10.1 will be dedicated to the computation of Feynman diagrams of Self-Propelled Model G, while in Sec. 10.2 the rescaling process will be discussed in detail. Through the computation of diagrams, I will prove the need to take into account some dynamic interactions, compatible with the symmetries of the system, not included in the heuristic derivation of Self-Propelled Model G given in Sec. 9.1.1.

Combining the perturbative and the naive scaling dimensions leads to a set of recursion relations, which determine how the parameters of the model have changed. Iterating the RG transformation results in a flow in the space of theories, all describing the same system at different length scales [1], known as the *renormalization group flow*. Analysis of the large-scale behaviour of the RG flow allows one to obtain the collective properties of the system. Section 10.4 will be devoted precisely to the study of the RG flow. First, the flow of Self-Propelled Model G in the absence of

spin dissipation will be analysed, revealing the presence of a novel active-inertial fixed point. Finally, the RG flow in the presence of dissipation will be studied.

10.1 The shell-integration

To obtain an effective description of the large-scale behaviour of a system, the first crucial step is to integrate the short-wavelength details, represented by those modes with wave-vector $\boldsymbol{k}$ on the momentum-shell $\Lambda/b < k < \Lambda$. Due to the presence of non-linear dynamic interactions, the shell integration couples short- and long-wavelength modes, giving rise to non-trivial corrections to the parameters of the bare action of the theory (9.36). Understanding how these corrections affect the action is the main purpose of the present section.

In what follows, I will split the discussion in two: first I will discuss the corrections to the Gaussian part of the action $\mathcal{S}_0$ (see (9.37) and (9.38)), known as Self-energies, and later those to the interacting part of the action $\mathcal{S}_I$ (see (9.39)), known as Vertex-functions. Since I am interested in the dynamic behaviour near criticality, the bare mass m_0 of the field theory is set to 0 in all diagrams [15], except for those giving corrections to the mass itself.

10.1.1 Self-Energies

Self-energies are the corrections to the Gaussian action arising from the shell integration, and are customary to write in the following way [40],

$$
\begin{aligned}
\Delta \mathcal{S}_0 = &\int \hat{\psi}_\alpha(-\tilde{\boldsymbol{k}})\Sigma_{\alpha\beta}(\tilde{\boldsymbol{k}})\psi_\beta(\tilde{\boldsymbol{k}}) - \hat{\psi}_\alpha(-\tilde{\boldsymbol{k}})\tilde{\Sigma}_{\alpha\beta}(\tilde{\boldsymbol{k}})\hat{\psi}_\beta(\tilde{\boldsymbol{k}}) + \\
&+ \int \hat{s}_{\alpha\beta}(-\tilde{\boldsymbol{k}})\Pi_{\alpha\beta\gamma\nu}(\tilde{\boldsymbol{k}})s_{\gamma\nu}(\tilde{\boldsymbol{k}}) - \hat{s}_{\alpha\beta}(-\tilde{\boldsymbol{k}})\tilde{\Pi}_{\alpha\beta\gamma\nu}(\tilde{\boldsymbol{k}})\hat{s}_{\gamma\nu}(\tilde{\boldsymbol{k}}) \; ,
\end{aligned}
\tag{10.1}
$$

Here all momenta are integrated off-shell, $k < \Lambda/b$, while frequency integrals still run from $-\infty$ to ∞. The quantities Σ, $\tilde{\Sigma}$, Π and $\tilde{\Pi}$ are the *self-energies*, which contribute to the perturbative corrections of the Gaussian parameters of the original action. Notice that all the corrections are proportional to the volume of the momentum shell, which is given by $1 - b^{-1} \simeq \ln b$.

It is possible to distinguish four different self-energies, one for each combination of fields appearing in $\mathcal{S}_0$, namely $\hat{\psi}\psi$, $\hat{\psi}\hat{\psi}$, $\hat{s}s$ and $\hat{s}\hat{s}$. From a diagrammatic point of view, each self-energy is given by the sum of all amputated 1-particle irreducible diagrams with external fields $\hat{\psi}\psi$, $\hat{\psi}\hat{\psi}$, $\hat{s}s$ and $\hat{s}\hat{s}$ respectively. Graphically, they are represented by the blobs in the following diagrammatic scheme

$$
\Sigma_{\alpha\beta}(\tilde{\boldsymbol{k}}) \quad : \quad \hat{\psi}_\alpha(-\tilde{\boldsymbol{k}}) \longrightarrow \!\!\!\!\otimes\!\!\!\!\longrightarrow \psi_\beta(\tilde{\boldsymbol{k}})
\tag{10.2}
$$

$$
\tilde{\Sigma}_{\alpha\beta}(\tilde{\boldsymbol{k}}) \quad : \quad \hat{\psi}_\alpha(-\tilde{\boldsymbol{k}}) \longrightarrow \!\!\!\!\otimes\!\!\!\!\longleftarrow \hat{\psi}_\beta(\tilde{\boldsymbol{k}})
\tag{10.3}
$$

$$
\Pi_{\alpha\beta\gamma\nu}(\tilde{\boldsymbol{k}}) \quad : \quad \hat{s}_{\alpha\beta}(-\tilde{\boldsymbol{k}}) \rightsquigarrow\!\!\!\!\otimes\!\!\!\!\rightsquigarrow s_{\gamma\nu}(\tilde{\boldsymbol{k}})
\tag{10.4}
$$

$$
\tilde{\Pi}_{\alpha\beta\gamma\nu}(\tilde{\boldsymbol{k}}) \quad : \quad \hat{s}_{\alpha\beta}(-\tilde{\boldsymbol{k}}) \rightsquigarrow\!\!\!\!\otimes\!\!\!\!\leftsquigarrow \hat{s}_{\gamma\nu}(\tilde{\boldsymbol{k}})
\tag{10.5}
$$

To identify perturbative corrections of the Gaussian parameters, one needs to expand the self energies in ω and $\boldsymbol{k}$ and keep only the leading terms. By comparing the corrections $\Delta \mathcal{S}_0$ in Eq. (10.1). with the form of the bare action $\mathcal{S}_0$ in Eq. (9.37)-(9.38), I can define the perturbative corrections to the Gaussian parameters through the relations,

$$\Sigma_{\alpha\beta}(\tilde{\boldsymbol{k}}) = \left[-\mathrm{i}\omega\, \delta\Omega + m_0\, \delta m + k^2 \Gamma_0\, \delta\Gamma \right] \ln b\; P^{\perp}_{\alpha\beta}(\boldsymbol{k}) + \dots \tag{10.6}$$

$$\tilde{\Sigma}_{\alpha\beta}(\tilde{\boldsymbol{k}}) = \tilde{\Gamma}_0\, \delta\tilde{\Gamma} \ln b\; P^{\perp}_{\alpha\beta}(\boldsymbol{k}) + \dots \tag{10.7}$$

$$\Pi_{\alpha\beta\gamma\nu}(\tilde{\boldsymbol{k}}) = \frac{1}{2}k^2 \lambda^{\perp}_0\, \delta\lambda^{\perp} \ln b\; \mathbb{P}^{\perp}_{\alpha\beta\gamma\nu}(\boldsymbol{k}) + \frac{1}{2}k^2 \lambda^{\|}_0\, \delta\lambda^{\|} \ln b\; (\mathbb{I} - \mathbb{P}^{\perp})_{\alpha\beta\gamma\nu}(\boldsymbol{k}) + \dots \tag{10.8}$$

$$\tilde{\Pi}_{\alpha\beta\gamma\nu}(\tilde{\boldsymbol{k}}) = \frac{1}{2}k^2 \tilde{\lambda}^{\perp}_0\, \delta\tilde{\lambda}^{\perp} \ln b\; \mathbb{P}^{\perp}_{\alpha\beta\gamma\nu}(\boldsymbol{k}) + \frac{1}{2}k^2 \tilde{\lambda}^{\|}_0\, \delta\tilde{\lambda}^{\|} \ln b\; (\mathbb{I} - \mathbb{P}^{\perp})_{\alpha\beta\gamma\nu}(\boldsymbol{k}) + \dots \tag{10.9}$$

where I denoted the bare parameters with the subscript 0 and where the ellipses stand for higher order terms in ω and $\boldsymbol{k}$, which are irrelevant in determining the critical behaviour at first order in ϵ. The $\ln b$ factors present in all terms reflect the fact that perturbative corrections are proportional to the volume of the momentum shell. After the shell integration, the Gaussian action takes the following form,

$$\mathcal{S}_0^< = \int_{\tilde{\boldsymbol{k}}}^< \left[-\mathrm{i}\omega\, (1 + \delta\Omega \ln b)\, \hat{\psi}\psi + \Gamma_0(1 + \delta\Gamma \ln b)k^2\hat{\psi}\psi + m_0(1 + \delta m \ln b)\hat{\psi}\psi \right] -$$

$$- \int_{\tilde{\boldsymbol{k}}}^< \tilde{\Gamma}_0 \left(1 + \delta\tilde{\Gamma} \ln b \right) \hat{\psi}\hat{\psi} +$$

$$+ \frac{1}{2} \int_{\tilde{\boldsymbol{k}}}^< \left[-\mathrm{i}\omega\hat{s}s + \eta_0\hat{s}s + \lambda^{\perp}_0(1 + \delta\lambda^{\perp} \ln b)k^2\hat{s}s + \lambda^{\|}_0(1 + \delta\lambda^{\|} \ln b)k^2\hat{s}s \right] -$$

$$- \frac{1}{2} \int_{\tilde{\boldsymbol{k}}}^< \left[\tilde{\eta}_0\hat{s}\hat{s} + \tilde{\lambda}^{\perp}_0(1 + \delta\tilde{\lambda}^{\perp} \ln b)k^2\hat{s}\hat{s} + \tilde{\lambda}^{\|}_0(1 + \delta\tilde{\lambda}^{\|} \ln b)k^2\hat{s}\hat{s} \right] \tag{10.10}$$

where the tensorial structure of the action was omitted to facilitate the reading, and the integral $\int_{\tilde{\boldsymbol{k}}}^<$ is given by

$$\int_{\tilde{\boldsymbol{k}}}^< = \int\limits_{|\boldsymbol{k}| < \Lambda/b} \frac{\mathrm{d}^d k}{(2\pi)^d} \int\limits_{-\infty}^{\infty} \frac{\mathrm{d}\omega}{2\pi} \tag{10.11}$$

The self-energies thus give perturbative corrections to the Gaussian parameters Γ, m, $\tilde{\Gamma}$, $\lambda^{\perp/\|}$ and $\tilde{\lambda}^{\perp/\|}$. Moreover, the self-energy Σ has also a non-vanishing term linear in ω, namely $\delta\Omega$, which gives a perturbative correction to $-\mathrm{i}\omega\hat{\psi}\psi$; because this term is not multiplied by any parameter in the original bare action, the only way to reabsorb this correction will be through a modification of the scaling dimension of the fields $\hat{\psi}$ and ψ. On the other hand, analogous perturbative terms do not arise in the self-energy Π, because all one-loop diagrams are at least of order $\boldsymbol{k}$ as a consequence of the particular properties of the vertices (9.56) and (9.58), which vanish at $\boldsymbol{k} = 0$, so that the term $-\mathrm{i}\omega\hat{s}s$ acquires only $\boldsymbol{k}$-dependent perturbative corrections that vanish when $\boldsymbol{k} = 0$. Another – rather crucial – consequence of

the fact that all corrections to Π and $\tilde{\Pi}$ are proportional to $\boldsymbol{k}$, is that there are no perturbative corrections to neither $\eta_0 \hat{s} s$ nor $\tilde{\eta}_0 \hat{s} \hat{s}$, and hence no $\delta\eta$ and $\delta\tilde{\eta}$ corrections are present in Eq. (10.8) and (10.9). This is no coincidence, but it is a result deeply related to the presence of the underlying (rotational) symmetry of the problem. Although terms explicitly violating the conservation of the spin s are present, namely the dissipative terms η and $\tilde{\eta}$, the symmetry is still at work and the non-linear interactions are not able to generate any perturbative corrections to the dissipative coefficients η and $\tilde{\eta}$.

The standard way to explicitly perform this shell integration, and to compute the corrections to the bare parameters of the model, is using perturbation theory. The corrections $\delta\mathcal{P}$ are thus computed using a Feynman diagram expansion. At order ϵ, the non-vanishing diagrams contributing to the self-energies are provided in Appendix C.1.

10.1.2 Vertex-functions

As happens to the Gaussian part of the action, the non-Gaussian interactions in $\mathcal{S}_I$ also acquire corrections due to shell integration. To distinguish them from the Self-energies, I shall refer to them as Vertex-functions.

The corrections to the interacting part of the action (9.39) can be written in the form,

$$
\begin{aligned}
\Delta\mathcal{S}_I = \int \hat{\psi}_\alpha(-\tilde{\boldsymbol{k}}) V^{\hat{\psi}\psi s}_{\alpha\beta\gamma\nu}(\tilde{\boldsymbol{k}}, \tilde{\boldsymbol{q}}) \psi_\beta(\tilde{\boldsymbol{k}} - \tilde{\boldsymbol{q}}) s_{\gamma\nu}(\tilde{\boldsymbol{q}}) + \\
+ \int \hat{s}_{\alpha\beta}(-\tilde{\boldsymbol{k}}) V^{\hat{s}\psi\psi}_{\alpha\beta\gamma\nu}(\tilde{\boldsymbol{k}}, \tilde{\boldsymbol{q}}) \psi_\gamma(-\tilde{\boldsymbol{q}} + \tilde{\boldsymbol{k}}/2) \psi_\nu(\tilde{\boldsymbol{q}} + \tilde{\boldsymbol{k}}/2) + \\
+ \int \hat{\psi}_\alpha(-\tilde{\boldsymbol{k}}) V^{\hat{\psi}\psi\psi}_{\alpha\beta\gamma}(\tilde{\boldsymbol{k}}, \tilde{\boldsymbol{q}}) \psi_\beta(\tilde{\boldsymbol{q}}) \psi_\gamma(\tilde{\boldsymbol{k}} - \tilde{\boldsymbol{q}}) + \\
+ \int \hat{s}_{\alpha\beta}(-\tilde{\boldsymbol{k}}) V^{\hat{s}s\psi}_{\alpha\beta\gamma\nu\eta}(\tilde{\boldsymbol{k}}, \tilde{\boldsymbol{q}}) s_{\gamma\nu}(\tilde{\boldsymbol{q}}) \psi_\eta(\tilde{\boldsymbol{k}} - \tilde{\boldsymbol{q}}) + \\
+ \int \hat{\psi}_\alpha(-\tilde{\boldsymbol{k}}) V^{\hat{\psi}\psi\psi\psi}_{\alpha\beta\gamma\nu}(\tilde{\boldsymbol{k}}, \tilde{\boldsymbol{q}}, \tilde{\boldsymbol{h}}) \psi_\beta(\tilde{\boldsymbol{q}}) \psi_\gamma(\tilde{\boldsymbol{h}}) \psi_\nu(\tilde{\boldsymbol{k}} - \tilde{\boldsymbol{q}} - \tilde{\boldsymbol{h}}) + \\
+ \int \hat{s}_{\alpha\beta}(-\tilde{\boldsymbol{k}}) V^{\hat{s}\psi\psi\psi\psi}_{\alpha\beta\gamma\nu\sigma\tau}(\tilde{\boldsymbol{k}}, \tilde{\boldsymbol{q}}, \tilde{\boldsymbol{h}}, \tilde{\boldsymbol{p}}) \psi_\gamma(\tilde{\boldsymbol{q}}) \psi_\nu(\tilde{\boldsymbol{h}}) \psi_\sigma(\tilde{\boldsymbol{p}}) \psi_\tau(\tilde{\boldsymbol{k}} - \tilde{\boldsymbol{q}} - \tilde{\boldsymbol{h}} - \tilde{\boldsymbol{p}}) \, ,
\end{aligned}
\tag{10.12}
$$

where the various *Vertex-functions* Vs give perturbative corrections to the coupling constants of the non-linear interactions. Notice that, as for Self-energies, all vertex-functions are proportional to the volume of the momentum shell, which is given by $1 - b^{-1} \simeq \ln b$. These vertex functions can be diagrammatically expressed through the sum of all the amputated connected diagrams having as external fields the same fields of the vertex they are correcting. The six vertex functions of the present theory, one for each bare vertex, can be graphically represented through the blobs in the following expressions. The two Mode-Coupling vertex-functions, correcting

the mode-coupling terms, are

$$V_{\alpha\beta\gamma\nu}^{\hat{\psi}\psi s}(\tilde{\boldsymbol{k}}, \tilde{\boldsymbol{q}}): \quad \hat{\psi}_\alpha(-\tilde{\boldsymbol{k}}) \;\; , \quad V_{\alpha\beta\gamma\nu}^{\hat{s}\psi\psi}(\tilde{\boldsymbol{k}}, \tilde{\boldsymbol{q}}): \quad \hat{s}_{\alpha\beta}(-\tilde{\boldsymbol{k}}) \tag{10.13}$$

with external legs $\psi_\beta(\tilde{\boldsymbol{k}} - \tilde{\boldsymbol{q}})$, $s_{\gamma\nu}(\tilde{\boldsymbol{q}})$ and $\psi_\gamma(\tilde{\boldsymbol{k}}/2 - \tilde{\boldsymbol{q}})$, $\psi_\nu(\tilde{\boldsymbol{k}}/2 + \tilde{\boldsymbol{q}})$.

The advection vertex-functions, correcting the advective terms of the theory, are given by

$$V_{\alpha\beta\gamma}^{\hat{\psi}\psi\psi}(\tilde{\boldsymbol{k}}, \tilde{\boldsymbol{q}}): \quad \hat{\psi}_\alpha(-\tilde{\boldsymbol{k}}) \qquad V_{\alpha\beta\gamma\nu\eta}^{\hat{s}s\psi}(\tilde{\boldsymbol{k}}, \tilde{\boldsymbol{q}}): \quad \hat{s}_{\alpha\beta}(-\tilde{\boldsymbol{k}}) \tag{10.14}$$

Then there is the ferromagnetic Vertex-Function, correcting the standard $\hat{\psi}\psi^3$ dynamic coupling coming from the Landau potential

$$V_{\alpha\beta\gamma\nu}^{\hat{\psi}\psi\psi\psi}(\tilde{\boldsymbol{k}}, \tilde{\boldsymbol{q}}, \tilde{\boldsymbol{h}}): \quad \hat{\psi}_\alpha(-\tilde{\boldsymbol{k}}) \longrightarrow \psi_\gamma(\tilde{\boldsymbol{h}}) \tag{10.15}$$

Finally, the last Vertex-Function is that giving corrections to the DYS vertex, given by

$$V_{\alpha\beta\gamma\nu\sigma\tau}^{\hat{s}\psi\psi\psi\psi}(\tilde{\boldsymbol{k}}, \tilde{\boldsymbol{q}}, \tilde{\boldsymbol{h}}, \tilde{\boldsymbol{p}}): \quad \hat{s}_{\alpha\beta}(-\tilde{\boldsymbol{k}}) \tag{10.16}$$

The full list of non-vanishing one-loop diagrams associated with each Vertex-Function is provided in Appendix C.2. For the moment, it is useful to remind that each vertex function contributes to the corrections of couplings and parameters of Eqs.

(9.53)-(9.59) in the following way,

$$V_{\alpha\beta\gamma\nu}^{\hat{\psi}\psi s}(\tilde{\boldsymbol{k}}, \tilde{\boldsymbol{q}}) = g\, \delta g_\psi\, P_{\alpha\rho}^\perp(\boldsymbol{k})\, \mathbb{I}_{\rho\beta\gamma\nu} \tag{10.17}$$

$$V_{\alpha\beta\gamma}^{\hat{\psi}\psi\psi}(\tilde{\boldsymbol{k}}, \tilde{\boldsymbol{q}}) = -v_0 \frac{\mathrm{i}\gamma_v}{2} \delta\gamma_v P_{\alpha\beta\nu}(\boldsymbol{k}) \tag{10.18}$$

$$V_{\alpha\beta\gamma\nu}^{\hat{\psi}\psi\psi\psi}(\tilde{\boldsymbol{k}}, \tilde{\boldsymbol{q}}, \tilde{\boldsymbol{h}}) = -\frac{J}{3} \delta J\, Q_{\alpha\beta\gamma\nu}(\boldsymbol{k}) \tag{10.19}$$

$$V_{\alpha\beta\gamma\nu}^{\hat{s}\psi\psi}(\tilde{\boldsymbol{k}}, \tilde{\boldsymbol{q}}) = g\, \mathbb{I}_{\alpha\beta\rho\sigma}\mathbb{I}_{\rho\tau\gamma\nu}\left[\delta g_s\, \boldsymbol{k}\cdot\boldsymbol{q}\, \delta_{\sigma\tau} + \Phi_1\, \delta g_{s1}\, k_\sigma q_\tau + \Phi_2\, \delta g_{s2}\, q_\sigma k_\tau\right] \tag{10.20}$$

$$V_{\alpha\beta\gamma\nu\eta}^{\hat{s}s\psi}(\tilde{\boldsymbol{k}}, \tilde{\boldsymbol{q}}) = -v_0 \frac{\mathrm{i}\gamma_s}{2}\mathbb{I}_{\alpha\beta\rho\sigma}\mathbb{I}_{\rho\tau\gamma\nu}\left[\delta\gamma_s\, k_\eta\delta_{\sigma\tau} + 2\mu_1\, \delta\gamma_{s1}\, k_\tau\delta_{\sigma\eta} + 2\mu_2\, \delta\gamma_{s2}\, k_\sigma\delta_{\tau\eta}\right]$$
$$\tag{10.21}$$

$$V_{\alpha\beta\gamma\nu\sigma\tau}^{\hat{s}\psi\psi\psi\psi}(\tilde{\boldsymbol{k}}, \tilde{\boldsymbol{q}}, \tilde{\boldsymbol{h}}, \tilde{\boldsymbol{p}}) = \frac{\kappa}{12}\delta\kappa\, K_{\alpha\beta\gamma\nu\sigma\tau}(\boldsymbol{k}, \boldsymbol{q}, \boldsymbol{h}, \boldsymbol{p}, \boldsymbol{k}-\boldsymbol{q}-\boldsymbol{h}-\boldsymbol{p}) \tag{10.22}$$

Higher orders in ω and $\boldsymbol{k}$ turn out to be irrelevant in determining the critical behaviour at the first order in ϵ. The perturbative corrections to the anomalous terms have been defined as,

$$\delta g_{s1} \equiv \delta\left(g\,\Phi_1\right) \quad, \quad \delta g_{s2} \equiv \delta\left(g\,\Phi_2\right) \tag{10.23}$$

$$\delta\gamma_{s1} \equiv \delta\left(\gamma_s\,\mu_1\right) \quad, \quad \delta\gamma_{s2} \equiv \delta\left(\gamma_s\,\mu_2\right) \tag{10.24}$$

(because they represent corrections to the *products* $g\,\Phi_{1,2}$ and $\gamma_s\,\mu_{1,2}$, they were not simply called $\delta\Phi_{1,2}$ and $\delta\mu_{1,2}$). At one loop, the non-vanishing diagrams contributing to the vertex functions are given in Appendix C.2.

10.1.3 A primer of the diagrammatic expansion

The one-loop Feynman diagrams generated by the action's expansion, and necessary to calculate all the corrections $\delta\mathcal{P}$ to the parameters and coupling constants, are given in Appendix C; not only they are many, but they are also quite complicated due to the tensorial structure of the theory. The integrals represented by each of these diagrams have been computed analytically with the help of *Mathematica*, and for space reasons will not be explicitly reported here.

However, I will perform in this Section the explicit calculation of one diagram, hoping that this may help the interested reader in picking up the general technique. The diagram I calculate is a contribution to the self-energy Σ defined in (10.2),

$$D_{\alpha\beta}(\boldsymbol{k}, \omega_k) \quad : \qquad \tag{10.25}$$

To facilitate the reader to follow the calculation and understand it better, I shall set $\eta = \tilde{\eta} = 0$ in the following paragraphs. The generalisation of the following calculation in the case with η and $\tilde{\eta}$ is straightforward. The integral expression corresponding

to this diagram can written following the definitions of lines and vertices given in Sections 9.3.2 and 9.3.3,

$$
D_{\alpha\beta}(\boldsymbol{k},\omega_k) = \int \frac{\mathrm{d}^d p}{(2\pi)^d} \frac{\mathrm{d}\omega_p}{2\pi} \; [g\, P_{\alpha\theta}(\boldsymbol{k})\mathbb{I}_{\theta\gamma\rho\sigma}] \left[g\, P_{\nu\eta} \left(\frac{\boldsymbol{k}}{2} - \boldsymbol{p} \right) \mathbb{I}_{\eta\beta\mu\lambda} \right] \times
$$
$$
\times\, \mathbb{G}^{0,\psi}_{\gamma\nu} \left(\frac{\boldsymbol{k}}{2} - \boldsymbol{p}, \frac{\omega_k}{2} - \omega_p \right) \mathbb{C}^{0,s}_{\rho\sigma\mu\lambda} \left(\frac{\boldsymbol{k}}{2} + \boldsymbol{p}, \frac{\omega_k}{2} + \omega_p \right) \tag{10.26}
$$

where I remind the reader that summation over repeated indexes is understood. While the momentum integral is restricted to the momentum shell, $\Lambda/b < p < \Lambda$, the frequency integral is extended over the whole spectrum $(-\infty, +\infty)$. Furthermore, I notice that the integrand (10.26) depends on the frequency ω_p only through the correlation functions $\mathbb{G}^{0,\psi}$ and $\mathbb{C}^{0,s}$ defined in Section 9.3.2; this is in general true for any Feynman diagram present in this work. All the correlation functions (9.44)-(9.47) have at most two poles in the complex plane, and it is always possible to compute the frequency integral using the residue theorem. In the case of this diagram the integration over ω_p yields,

$$
D_{\alpha\beta}(\boldsymbol{k},\omega_k) = g^2 \int \frac{\mathrm{d}^d p}{(2\pi)^d} P_{\alpha\theta}(\boldsymbol{k})\mathbb{I}_{\theta\gamma\rho\sigma} P_{\nu\eta}(\boldsymbol{k}/2 - \boldsymbol{p})\mathbb{I}_{\eta\beta\mu\lambda} \times
$$
$$
\times \left[\frac{2\tilde{\lambda}^{\perp}\, \delta_{\gamma\nu}\mathbb{P}^{\perp}_{\rho\sigma\mu\lambda}(\boldsymbol{k}/2 - \boldsymbol{p})}{\lambda^{\perp}[\Gamma(\boldsymbol{k}/2 - \boldsymbol{p})^2 + \lambda^{\perp}(\boldsymbol{k}/2 + \boldsymbol{p})^2 - \mathrm{i}\omega_k + m]} + \right. \tag{10.27}
$$
$$
\left. + \frac{2\tilde{\lambda}^{\parallel}\, \delta_{\gamma\nu}(\mathbb{P}^{\perp}_{\rho\sigma\mu\lambda}(\boldsymbol{k}/2 - \boldsymbol{p}) - \mathbb{I}_{\rho\sigma\mu\lambda})}{\lambda^{\parallel}[\Gamma(\boldsymbol{k}/2 - \boldsymbol{p})^2 + \lambda^{\parallel}(\boldsymbol{k}/2 + \boldsymbol{p})^2 - \mathrm{i}\omega_k + m]} \right]
$$

When not explicitly interested in the corrections to the mass m, since I am going to work at first order in $\epsilon = 4 - d$ (one loop), it is possible to drop the m dependence in the Feynman diagrams, because this would lead to higher order corrections. Although this diagram does give contributions to the correction of the mass, I will set $m = 0$ in the following. This is done to avoid giving very long, complicated and perhaps not very insightful expressions, which would not allow the reader to get any additional information and in fact would take me away from the goal of this section.

The integral over the modulus of the momentum becomes trivial if one assumes that the RG transformation is infinitesimal, namely if $b \simeq 1$; this means that the thickness of the momentum shell is infinitesimal and it is possible to approximate the integral of a generic function $f(\boldsymbol{p})$ as follows,

$$
\int_{\Lambda/b}^{\Lambda} \mathrm{d}^d p\; f(\boldsymbol{p}) = \int f(p)d\Omega_d p^{d-1}dp = \ln b\; \Lambda^d \int f(p)\Big|_{|p|=\Lambda} d\Omega_d \tag{10.28}
$$

which corresponds to approximating the integral as the value of the function at $|p| = \Lambda$ times the volume of the momentum shell $\Lambda^d(1 - 1/b) \simeq \ln b$. After this step, the integrand may still depend on the direction of the momentum $\hat{\boldsymbol{p}} = \boldsymbol{p}/|p|$, which

is a unit vector. Applying this procedure to equation (10.27) leads to,

$$D_{\alpha\beta}(\boldsymbol{k},\omega_k) = g^2 \int \frac{d\Omega_d}{(2\pi)^d} \Lambda^d \ln b \ P_{\alpha\theta}(\boldsymbol{k}) \mathbb{I}_{\theta\gamma\rho\sigma} P_{\nu\eta}(\boldsymbol{k}/2 - \Lambda\hat{\boldsymbol{p}}) \mathbb{I}_{\eta\beta\mu\lambda} \times$$

$$\times \left[\frac{2\tilde{\lambda}^{\perp} \ \delta_{\gamma\nu} \mathbb{P}^{\perp}_{\rho\sigma\mu\lambda}(\boldsymbol{k}/2 - \Lambda\hat{\boldsymbol{p}})}{\lambda^{\perp}[\Gamma(\boldsymbol{k}/2 - \Lambda\hat{\boldsymbol{p}})^2 + \lambda^{\perp}(\boldsymbol{k}/2 + \Lambda\hat{\boldsymbol{p}})^2 - \mathrm{i}\omega_k]} + \right. \quad (10.29)$$

$$\left. + \frac{2\tilde{\lambda}^{\|} \ \delta_{\gamma\nu}(\mathbb{P}^{\perp}_{\rho\sigma\mu\lambda}(\boldsymbol{k}/2 - \Lambda\hat{\boldsymbol{p}}) - \mathbb{I}_{\rho\sigma\mu\lambda})}{\lambda^{\|}[\Gamma(\boldsymbol{k}/2 - \Lambda\hat{\boldsymbol{p}})^2 + \lambda^{\|}(\boldsymbol{k}/2 + \Lambda\hat{\boldsymbol{p}})^2 - \mathrm{i}\omega_k]} \right]$$

where the unit vector $\hat{\boldsymbol{p}}$ is integrated over the d-dimensional sphere Ω_d. The main advantage of having an expression of this kind is that all the dependence on the cut-off Λ is made explicit.

To recognise within this diagram the corrections to the various parameters of the original action, one has to expand in small external momenta and frequency, as I did in (10.6). The order in which it is convenient to perform this expansion depends on the particular Feynman diagram I am considering and the specific parameters or coupling constants that it corrects. For example, the diagram I am studying here gives rise to perturbative corrections to the $\hat{\psi}\psi$ term in the Gaussian action (9.37); hence this diagram must be expanded up to the second order in the external momentum $\boldsymbol{k}$ and up to the first order in the external frequency ω_k. In this example, I will calculate explicitly only the contribution of order ω_k of this diagram, even though the diagram gives also contributions of $\mathcal{O}(1)$ and of $\mathcal{O}(k^2)$. The diagram at order ω_k is,

$$D_{\alpha\beta}(\boldsymbol{k},\omega_k) = \mathrm{i}\omega_k g^2 \Lambda^{d-4} \ln b \ \int \frac{d\Omega_d}{(2\pi)^d} P_{\alpha\theta}(\boldsymbol{k}) \mathbb{I}_{\theta\gamma\rho\sigma} P_{\nu\eta}(\hat{\boldsymbol{p}}) \mathbb{I}_{\eta\beta\mu\lambda} \delta_{\gamma\nu} \times$$

$$\times \left[2\tilde{\lambda}^{\perp} \frac{\mathbb{P}^{\perp}_{\rho\sigma\mu\lambda}(\hat{\boldsymbol{p}})}{\lambda^{\perp}(\Gamma + \lambda^{\perp})^2} + 2\tilde{\lambda}^{\|} \frac{\mathbb{P}^{\perp}_{\rho\sigma\mu\lambda}(\hat{\boldsymbol{p}}) - \mathbb{I}_{\rho\sigma\mu\lambda}}{\lambda^{\|}(\Gamma + \lambda^{\|})^2} \right] \quad (10.30)$$

Expanding all the tensors in equation (10.30), using the definitions (9.18), (9.22) and (9.23), I obtain,

$$D_{\alpha\beta}(\boldsymbol{k},\omega_k) = \mathrm{i}\omega_k g^2 \Lambda^{d-4} \ln b \ P_{\alpha\theta}(\boldsymbol{k}) \int \frac{d\Omega_d}{(2\pi)^d} \left[\frac{\tilde{\lambda}^{\perp}}{\lambda^{\perp}(\Gamma + \lambda^{\perp})^2}(1-d)\hat{p}_{\beta}\hat{p}_{\theta} + \right.$$

$$\left. + \frac{\tilde{\lambda}^{\|}}{\lambda^{\|}(\Gamma + \lambda^{\|})^2}(d-2)(\hat{p}_{\beta}\hat{p}_{\theta} - \delta_{\alpha\beta}) \right] \quad (10.31)$$

To perform the integral over the d-dimensional sphere $\mathrm{d}\omega_d$, it is useful to remember the following two relations,

$$\langle \hat{p}_{\alpha}\hat{p}_{\beta} \rangle_{\hat{p}} = \frac{1}{d}\delta_{\alpha\beta} \ , \qquad \langle \hat{p}_{\alpha}\hat{p}_{\beta}\hat{p}_{\gamma}\hat{p}_{\nu} \rangle_{\hat{p}} = \frac{1}{d(d+2)}\left(\delta_{\alpha\beta}\delta_{\gamma\nu} + \delta_{\alpha\gamma}\delta_{\beta\nu} + \delta_{\alpha\nu}\delta_{\beta\gamma} \right) \ ,$$

$$(10.32)$$

where the brackets indicate the average over the d-dimensional sphere,

$$\langle \cdot \rangle = \frac{1}{\Omega_d} \int \ \cdot \ \mathrm{d}\omega_d \quad (10.33)$$

While the average of an even number of uni vectors $\hat{\boldsymbol{p}}$ is nonzero, the angular average of an odd number of momenta vanishes by symmetry. This leads to the following expression for the diagram (10.25),

$$D_{\alpha\beta}(\boldsymbol{k}, \omega_k) = -\mathrm{i}\omega_k g^2 \; \Lambda^{d-4} \frac{d-1}{d} \left[\frac{\tilde{\lambda}^\perp}{\lambda^\perp (\Gamma + \lambda^\perp)^2} + \frac{\tilde{\lambda}^\|}{\lambda^\| (\Gamma + \lambda^\|)^2}(d-2) \right] \; \ln b \; P_{\alpha\beta}^\perp(\boldsymbol{k}) \tag{10.34}$$

Since an ϵ-expansion around the upper critical dimension $d_c = 4$ is performed here, I can set $d = 4$ in all the Feynman diagrams when results at first order in ϵ are concerned. In the end, by comparing this expression to the expansion of the self-energy in (10.6), the correction $\delta\Omega$ coming from this one diagram can be derived and is given by

$$\delta\Omega = g^2 \left[\frac{3}{4} \frac{\tilde{\lambda}^\perp}{\lambda^\perp (\Gamma + \lambda^\perp)^2} + \frac{3}{2} \frac{\tilde{\lambda}^\|}{\lambda^\| (\Gamma + \lambda^\|)^2} \right] + \dots \tag{10.35}$$

where the dots indicates the corrections from *all* other diagrams contributing to the self-energy Σ, which are listed in Appendix C.1.1.

10.1.4   Generation of the anomalous terms

The equations of motion proposed initially at the beginning of Sec. 9.1.2, namely (9.6) and (9.7), in which the anomalous terms proportional to μ_1, μ_2, Φ_1 or Φ_2 do not appear, have a (relatively) clear physical interpretation. However, as previously pointed out, in the absence of some additional terms, the equations of motion are not RG-invariant; basically, what happens is that the RG generates some terms that were not present in the original action. To see how this happens, I perform here a shell integration starting from a theory with bare coefficients $\Phi_{10} = \Phi_{20} = \mu_{10} = \mu_{20} = 0$ and show that these anomalous terms are spontaneously generated by the renormalization group transformation. I also hope that this further direct analysis of some highly non-trivial diagrams may provide the reader with a more robust technique to perform the entire calculation. Since the generation of these non-linear terms does not rely on the presence of η and $\tilde{\eta}$, as in the previous section they will be set both to 0. Once again, the hope is that this makes the calculation easier to follow.

Anomalous Mode-Coupling terms

Without anomalies, the non-Gaussian action (9.39) has only one term proportional to $\hat{s}\psi\psi$, corresponding to the following vertex,

$$\psi_\gamma(\tilde{\boldsymbol{k}}/2 - \tilde{\boldsymbol{q}})$$

$$\hat{s}_{\alpha\beta}(-\tilde{\boldsymbol{k}}) \qquad\qquad\qquad : \quad g\mathbb{I}_{\alpha\beta\gamma\nu}\boldsymbol{k}\cdot\boldsymbol{q} \tag{10.36}$$

$$\psi_\nu(\tilde{\boldsymbol{k}}/2 + \tilde{\boldsymbol{q}})$$

which is the same mode coupling vertex as (9.57), but without the anomalous terms. To compute the perturbative corrections to this vertex, all the diagrams with an incoming $\hat{s}$ line and two outcoming ψ lines must be considered; these are 12 diagrams, listed in Appendix C.2.2, most of which produce anomalous corrections. Here, as an example, I limit myself to consider only the first *two* of all these diagrams namely,

$$\tag{10.37}$$

where I explicitly wrote also the momentum of internal field lines. These diagrams can be converted into integral expressions following the usual Feynman rules. It is important to note, though, that this is exactly one of the cases in which it is more convenient to write the spin mode-coupling vertex as in (9.56) (but of course with $\Phi_1 = \Phi_2 = 0$), rather than as in (9.57). This results in the following expressions for the two diagrams,

$$
\begin{aligned}
D^{\mathrm{mc},1}_{\alpha\beta\gamma\nu} = g^3 \int\limits_{\Lambda/b<|\boldsymbol{p}|<\Lambda} \frac{\mathrm{d}^d p}{(2\pi)^d} \int\limits_{-\infty}^{\infty} \frac{\mathrm{d}\omega_p}{2\pi}\, P^{\perp}_{\mu\eta}\left(\boldsymbol{p}+\frac{\boldsymbol{k}}{2}+\frac{\boldsymbol{q}}{2}\right) \mathbb{I}_{\eta\gamma\xi\zeta}\times \\
\times\, \mathbb{I}_{\alpha\beta\sigma\rho}\left[\left(\boldsymbol{p}+\frac{\boldsymbol{k}}{2}+\frac{\boldsymbol{q}}{2}\right)^2 - \left(\boldsymbol{p}-\frac{\boldsymbol{k}}{2}+\frac{\boldsymbol{q}}{2}\right)^2\right]\times \\
\times\, \mathbb{I}_{\phi\chi\tau\nu}\left[\left(\boldsymbol{q}+\frac{\boldsymbol{k}}{2}\right)^2 - \left(\boldsymbol{p}-\frac{\boldsymbol{k}}{2}+\frac{\boldsymbol{q}}{2}\right)^2\right]\times \\
\times\, \mathbb{G}^{0,\psi}_{\rho\mu}\left(\tilde{\boldsymbol{p}}+\frac{\tilde{\boldsymbol{k}}}{2}+\frac{\tilde{\boldsymbol{q}}}{2}\right) \mathbb{G}^{0,s}_{\xi\zeta\phi\chi}\left(\tilde{\boldsymbol{p}}-\frac{\tilde{\boldsymbol{q}}}{2}\right) \mathbb{C}^{0,\psi}_{\sigma\tau}\left(\tilde{\boldsymbol{p}}-\frac{\tilde{\boldsymbol{k}}}{2}+\frac{\tilde{\boldsymbol{q}}}{2}\right),
\end{aligned}
$$

$$\tag{10.38}$$

$$D^{\text{mc},2}_{\alpha\beta\gamma\nu} = g^3 \int\limits_{\Lambda/b<|\boldsymbol{p}|<\Lambda} \frac{\mathrm{d}^d p}{(2\pi)^d} \int\limits_{-\infty}^{\infty} \frac{\mathrm{d}\omega_p}{2\pi} \left[\left(\boldsymbol{p} + \frac{\boldsymbol{k}}{2} + \frac{\boldsymbol{q}}{2} \right)^2 - \left(\boldsymbol{p} - \frac{\boldsymbol{k}}{2} + \frac{\boldsymbol{q}}{2} \right)^2 \right] \times$$

$$\times \mathbb{I}_{\alpha\beta\sigma\rho} P^{\perp}_{\mu,\eta} \left(\boldsymbol{p} + \frac{\boldsymbol{k}}{2} + \frac{\boldsymbol{q}}{2} \right) \mathbb{I}_{\eta\gamma\xi\zeta} P^{\perp}_{\sigma,\delta} \left(\boldsymbol{p} - \frac{\boldsymbol{k}}{2} + \frac{\boldsymbol{q}}{2} \right) \mathbb{I}_{\phi\chi\tau\nu} \times \tag{10.39}$$

$$\times \mathbb{G}^{0,\psi}_{\rho\mu} \left(\tilde{\boldsymbol{p}} + \frac{\tilde{\boldsymbol{k}}}{2} + \frac{\tilde{\boldsymbol{q}}}{2} \right) \mathbb{C}^{0,s}_{\xi\zeta\phi\chi} \left(\tilde{\boldsymbol{p}} - \frac{\tilde{\boldsymbol{q}}}{2} \right) \mathbb{G}^{0,\psi}_{\delta\tau} \left(-\tilde{\boldsymbol{p}} + \frac{\tilde{\boldsymbol{k}}}{2} - \frac{\tilde{\boldsymbol{q}}}{2} \right) .$$

At leading order in the momentum-frequency expansion, after integrals and index contraction are performed, the sum of these two diagrams can be written as

$$D^{\text{mc},1}_{\alpha\beta\gamma\nu} + D^{\text{mc},2}_{\alpha\beta\gamma\nu} = g\mathbb{I}_{\alpha\beta\rho\sigma}\mathbb{I}_{\rho\tau\gamma\nu}[\delta g_s \; \boldsymbol{k}\cdot\boldsymbol{q}\delta_{\sigma\tau} + A \; k_\sigma q_\tau + B \; q_\sigma k_\tau]\ln b \quad, \tag{10.40}$$

where the constants δg_s, A and B are,

$$\delta g_s = g^2 w \frac{\tilde{\lambda}^{\perp}w(w+1)^2 + \tilde{\Gamma}x(w(x-5)-3x-1) - \tilde{\lambda}^{\|}(w-3)wx(w+x)}{12\Gamma^3(w+1)^2x(w+x)}$$

$$A = -g^2 w \frac{-3\tilde{\lambda}^{\perp}w(w+1)^2 + \tilde{\Gamma}x(w(6w+3x+11)+5x+3) - \tilde{\lambda}^{\|}w(3w+5)x(w+x)}{12\Gamma^3(w+1)^2x(w+x)}$$

$$B = g^2 w \frac{-5\tilde{\lambda}^{\perp}w(w+1)^2 + \tilde{\Gamma}x(w(7-5x)-3x+5) + \tilde{\lambda}^{\|}w(5w+3)x(w+x)}{12\Gamma^3(w+1)^2x(w+x)}$$

$$\tag{10.41}$$

with $w = \Gamma/\lambda^{\|}$ and $x = \lambda^{\perp}/\lambda^{\|}$. These two Feynman diagrams correct the interacting part of the action relative to the mode-coupling of the spin as follows,

$$\Delta\mathcal{S}_{\text{mc}} = \mathbb{I}_{\alpha\beta\rho\sigma}\mathbb{I}_{\rho\tau\gamma\nu}\ln b \int_0^{\Lambda/b} d\tilde{\boldsymbol{k}} \; d\tilde{\boldsymbol{q}}\hat{s}_{\alpha\beta}(-\tilde{\boldsymbol{k}})\psi_\gamma(\tilde{\boldsymbol{k}}/2-\tilde{\boldsymbol{q}})\psi_\nu(\tilde{\boldsymbol{k}}/2+\tilde{\boldsymbol{q}})\times$$

$$\times g \; [\; \underbrace{\delta g_s \; \boldsymbol{k}\cdot\boldsymbol{q} \; \delta_{\sigma\tau}}_{\text{bare structure}} + \underbrace{A \; k_\sigma q_\tau + B \; q_\sigma k_\tau}_{\text{absent in the bare theory}} \;], \tag{10.42}$$

Note that, in terms of the corrections defined in Eq. (10.20), the terms A and B contribute to $\Phi_1\delta g_{s1} = A + \dots$ and $\Phi_2\delta g_{s2} = B + \dots$, where the ellipses stand for contributions coming from diagrams other than $D^{\text{mc},1}$ and $D^{\text{mc},2}$.

The core idea of the renormalization group is that the perturbative contributions generated by Feynman diagrams can be reabsorbed into a redefinition of the model's parameters. Comparing equations (10.36) and (10.42) it is evident that the first term, proportional to $\mathbb{I}_{\alpha\beta\gamma\nu} \; \boldsymbol{k}\cdot\boldsymbol{q}$, has the same form as the bare vertex (10.36), hence it can be reabsorbed in the coupling, $g \to g(1 + \delta g_s \ln b)$. However, it is not possible to reabsorb the second and third terms of equation (10.42) as correction of any pre-existing parameters, because of the different tensorial structure. For this reason two novel terms, proportional to $\mathbb{I}_{\alpha\beta\rho\sigma}\mathbb{I}_{\rho\tau\gamma\nu} \; k_\sigma q_\tau$ and $\mathbb{I}_{\alpha\beta\rho\sigma}\mathbb{I}_{\rho\tau\gamma\nu} \; q_\sigma k_\tau$ respectively, must be included in the action. These two terms coincide with the two *anomalous* terms Φ_1 and Φ_2 in equations (9.39). Let me note that most of the diagrams listed in Appendix C.2.2 *generate* the same anomalous terms with different coefficients A and B. It is crucial to note that, if the model is at equilibrium, $v_0 = 0$, $\tilde{\Gamma} = \Gamma$ and $\tilde{\lambda}^{\perp,\|} = \lambda^{\perp,\|}$, all these perturbative contributions vanish: $A = B = \delta g_s = 0$, so that no anomalous terms are generated in the non-active case.

Anomalous Advection terms

The same procedure can be used to prove that the two anomalous advection terms, proportional to μ_1 and μ_2, are fundamental to guarantee the closure of the theory under the RG transformation. I use the same strategy: even assuming that the anomalous terms are zero in the bare theory, $\mu_1 = \mu_2 = 0$, they are spontaneously generated by the renormalization group transformation. If one assumes that $\mu_1 = \mu_2 = 0$, there is only one term proportional to $\hat{s}s\psi$ in the non-Gaussian action (9.39), corresponding to the advective derivative. In the diagrammatic expansion, this corresponds to modifying the vertex,

$$
\begin{array}{c}
s_{\gamma\nu}(\tilde{\boldsymbol{k}}/2 - \tilde{\boldsymbol{q}}) \\[1em]
\hat{s}_{\alpha\beta}(-\tilde{\boldsymbol{k}}) \\[1em]
\psi_\eta(\tilde{\boldsymbol{k}}/2 + \tilde{\boldsymbol{q}})
\end{array}
\qquad : \qquad -v_0 \frac{\mathrm{i}\gamma_s}{2}\mathbb{I}_{\alpha\beta\gamma\nu}k_\eta
\tag{10.43}
$$

The term proportional to $\hat{s}s\psi$ in the action is corrected by the Feynman diagrams with an incoming $\hat{s}$, one outcoming s and ψ line. These are only 3 diagrams, listed in Appendix C.2.4, so I calculate here all three of them, namely,

$$
D^{\mathrm{adv},1} \quad : \quad
\begin{array}{c}
\tilde{\boldsymbol{k}}/2 - \tilde{\boldsymbol{q}}, \gamma\nu \\
\frac{\tilde{\boldsymbol{k}}}{2} + \frac{\tilde{\boldsymbol{q}}}{2} + \tilde{\boldsymbol{p}} \\
-\tilde{\boldsymbol{k}}, \alpha\beta \qquad \tilde{\boldsymbol{p}} - \frac{\tilde{\boldsymbol{q}}}{2} \\
\frac{\tilde{\boldsymbol{k}}}{2} - \frac{\tilde{\boldsymbol{q}}}{2} - \tilde{\boldsymbol{p}} \\
\tilde{\boldsymbol{k}}/2 + \tilde{\boldsymbol{q}}, \eta
\end{array}
\quad ,
$$

$$
D^{\mathrm{adv},2} \quad : \quad
\begin{array}{c}
\tilde{\boldsymbol{k}}/2 - \tilde{\boldsymbol{q}}, \gamma\nu \\
\frac{\tilde{\boldsymbol{k}}}{2} + \frac{\tilde{\boldsymbol{q}}}{2} + \tilde{\boldsymbol{p}} \\
-\tilde{\boldsymbol{k}}, \alpha\beta \qquad \tilde{\boldsymbol{p}} - \frac{\tilde{\boldsymbol{q}}}{2} \\
\frac{\tilde{\boldsymbol{k}}}{2} - \frac{\tilde{\boldsymbol{q}}}{2} - \tilde{\boldsymbol{p}} \\
\tilde{\boldsymbol{k}}/2 + \tilde{\boldsymbol{q}}, \eta
\end{array}
\quad ,
\tag{10.44}
$$

$$
D^{\mathrm{adv},3} \quad : \quad
\begin{array}{c}
\tilde{\boldsymbol{k}}/2 - \tilde{\boldsymbol{q}}, \gamma\nu \\
\frac{\tilde{\boldsymbol{k}}}{2} + \frac{\tilde{\boldsymbol{q}}}{2} + \tilde{\boldsymbol{p}} \\
-\tilde{\boldsymbol{k}}, \alpha\beta \qquad \tilde{\boldsymbol{p}} - \frac{\tilde{\boldsymbol{q}}}{2} \\
\frac{\tilde{\boldsymbol{k}}}{2} - \frac{\tilde{\boldsymbol{q}}}{2} - \tilde{\boldsymbol{p}} \\
\tilde{\boldsymbol{k}}/2 + \tilde{\boldsymbol{q}}, \eta
\end{array}
\quad .
$$

The integral expressions of these Feynman diagrams are:

$$
D^{\text{adv},1} = -\mathrm{i}v_0 \frac{\gamma_s g^2}{2} \int\limits_{\Lambda/b<|\boldsymbol{p}|<\Lambda} \frac{\mathrm{d}^d p}{(2\pi)^d} \int\limits_{-\infty}^{\infty} \frac{\mathrm{d}\omega_p}{2\pi} \mathbb{I}_{\alpha\beta\xi\zeta} k_\rho \times
$$

$$
\times P_{\mu\iota}^{\perp} \left(\boldsymbol{p} + \frac{\boldsymbol{k}}{2} + \frac{\boldsymbol{q}}{2}\right) \mathbb{I}_{\iota\sigma\gamma\nu} P_{\tau\delta}^{\perp} \left(\boldsymbol{p} - \frac{\boldsymbol{q}}{2}\right) \mathbb{I}_{\delta\eta\phi\chi} \times \tag{10.45}
$$

$$
\times \mathbb{G}_{\rho\mu}^{0,\psi} \left(\tilde{\boldsymbol{p}} + \frac{\tilde{\boldsymbol{k}}}{2} + \frac{\tilde{\boldsymbol{q}}}{2}\right) \mathbb{G}_{\sigma\tau}^{0,\psi} \left(\tilde{\boldsymbol{p}} - \frac{\tilde{\boldsymbol{q}}}{2}\right) \mathbb{C}_{\xi\zeta\phi\chi}^{0,s} \left(\tilde{\boldsymbol{p}} - \frac{\tilde{\boldsymbol{k}}}{2} + \frac{\tilde{\boldsymbol{q}}}{2}\right) ,
$$

$$
D^{\text{adv},2} = -\mathrm{i}v_0 \frac{\gamma_s g^2}{2} \int\limits_{\Lambda/b<|\boldsymbol{p}|<\Lambda} \frac{\mathrm{d}^d p}{(2\pi)^d} \int\limits_{-\infty}^{\infty} \frac{\mathrm{d}\omega_p}{2\pi} \mathbb{I}_{\alpha\beta\xi\zeta} k_\rho \times
$$

$$
\times P_{\mu\iota}^{\perp} \left(\boldsymbol{p} + \frac{\boldsymbol{k}}{2} + \frac{\boldsymbol{q}}{2}\right) \mathbb{I}_{\iota\sigma\gamma\nu} \left[\left(\boldsymbol{q} + \frac{\boldsymbol{k}}{2}\right)^2 - \left(\boldsymbol{p} - \frac{\boldsymbol{q}}{2}\right)^2\right] \mathbb{I}_{\phi\chi\tau\eta} \times \tag{10.46}
$$

$$
\times \mathbb{G}_{\rho\mu}^{0,\psi} \left(\tilde{\boldsymbol{p}} + \frac{\tilde{\boldsymbol{k}}}{2} + \frac{\tilde{\boldsymbol{q}}}{2}\right) \mathbb{C}_{\sigma\tau}^{0,\psi} \left(\tilde{\boldsymbol{p}} - \frac{\tilde{\boldsymbol{q}}}{2}\right) \mathbb{G}_{\xi\zeta\phi\chi}^{0,s} \left(-\tilde{\boldsymbol{p}} + \frac{\tilde{\boldsymbol{k}}}{2} - \frac{\tilde{\boldsymbol{q}}}{2}\right) ,
$$

$$
D^{\text{adv},3} = -\mathrm{i}v_0 \frac{\gamma_s g^2}{2} \int\limits_{\Lambda/b<|\boldsymbol{p}|<\Lambda} \frac{\mathrm{d}^d p}{(2\pi)^d} \int\limits_{-\infty}^{\infty} \frac{\mathrm{d}\omega_p}{2\pi} \mathbb{I}_{\alpha\beta\xi\zeta} k_\rho \times
$$

$$
\times P_{\sigma\iota}^{\perp} \left(-\boldsymbol{p} + \frac{\boldsymbol{q}}{2}\right) \mathbb{I}_{\iota\mu\gamma\nu} \left[\left(\boldsymbol{q} + \frac{\boldsymbol{k}}{2}\right)^2 - \left(\boldsymbol{p} - \frac{\boldsymbol{q}}{2}\right)^2\right] \mathbb{I}_{\phi\chi\tau\eta} \times
$$

$$
\times \mathbb{C}_{\rho\mu}^{0,\psi} \left(\tilde{\boldsymbol{p}} + \frac{\tilde{\boldsymbol{k}}}{2} + \frac{\tilde{\boldsymbol{q}}}{2}\right) \mathbb{G}_{\sigma\tau}^{0,\psi} \left(-\tilde{\boldsymbol{p}} + \frac{\tilde{\boldsymbol{q}}}{2}\right) \mathbb{G}_{\xi\zeta\phi\chi}^{0,s} \left(-\tilde{\boldsymbol{p}} + \frac{\tilde{\boldsymbol{k}}}{2} - \frac{\tilde{\boldsymbol{q}}}{2}\right) ,
$$

$$
\tag{10.47}
$$

At leading order in the momentum-frequency expansion, after integrals and index contraction are performed, the sum of these three diagrams can be written as

$$
D^{\text{adv},1} + D^{\text{adv},2} + D^{\text{adv},3} = -v_0 \frac{\mathrm{i}\gamma_s}{2} \mathbb{I}_{\alpha\beta\rho\sigma} \mathbb{I}_{\rho\tau\gamma\nu} \left[\delta\gamma_s\, k_\eta \delta_{\sigma\tau} + C\, k_\tau \delta_{\sigma\eta} + D\, k_\sigma \delta_{\tau\eta}\right] \ln b \tag{10.48}
$$

with the constants $\delta\gamma_s$, C and D, given by,

$$
\delta\gamma_s = -g^2 \frac{-x(x-1)(1+2w+x)\tilde{\Gamma} + wx(w+x)^2\tilde{\lambda}^{\|} - w(1+w)^2\tilde{\lambda}^{\perp}}{12\Gamma^3(1+w)^2 x(w+x)^2}
$$

$$
C = -g^2 \frac{-x(5+10w+12w^2+14wx+7x^2)\tilde{\Gamma} + 7wx(w+x)^2\tilde{\lambda}^{\|} + 5w(1+w)^2\tilde{\lambda}^{\perp}}{12\Gamma^3(1+w)^2 x(w+x)^2}
$$

$$
D = -g^2 \frac{-x(x-1)(1+2w+x)\tilde{\Gamma} + wx(w+x)^2\tilde{\lambda}^{\|} - w(1+w)^2\tilde{\lambda}^{\perp}}{12\Gamma^3(1+w)^2 x(w+x)^2} ,
$$

$$
\tag{10.49}
$$

These three Feynman diagrams correct the interacting part of the action relative to the advection of the spin as follows,

$$\Delta\mathcal{S}_{\text{adv}} = v_0 \frac{-\mathrm{i}\gamma_s}{2} \, \mathbb{I}_{\alpha\beta\rho\sigma}\mathbb{I}_{\rho\tau\gamma\nu} \int_0^{\Lambda/b} d\tilde{\boldsymbol{k}} \, d\tilde{\boldsymbol{q}}\hat{s}_{\alpha\beta}(-\tilde{\boldsymbol{k}})s_{\gamma\nu}(\tilde{\boldsymbol{k}}/2 - \tilde{\boldsymbol{q}})\psi_\eta(\tilde{\boldsymbol{k}}/2 + \tilde{\boldsymbol{q}})\times$$
$$\times [\, \underbrace{\delta\gamma_s k_\eta \delta_{\sigma\tau}}_{\text{bare structure}} + \underbrace{C \, k_\tau \, \delta_{\sigma\eta} + D \, k_\sigma \delta_{\tau\eta}}_{\text{absent in the bare theory}}]\,, \tag{10.50}$$

Comparing equations (10.50) and (10.43) it is evident that the term proportional to $\mathbb{I}_{\alpha\beta\rho\sigma}\mathbb{I}_{\rho\tau\gamma\nu}k_\eta\delta_{\sigma\tau} = \mathbb{I}_{\alpha\beta\gamma\nu}k_\eta$ is the same as in the bare case and it can be reabsorbed as a correction of the advection coupling, γ_s. On the other hand, the two terms proportional to $\mathbb{I}_{\alpha\beta\rho\sigma}\mathbb{I}_{\rho\tau\gamma\nu} \, k_\tau \, \delta_{\sigma\eta}$ and $\mathbb{I}_{\alpha\beta\rho\sigma}\mathbb{I}_{\rho\tau\gamma\nu} \, k_\sigma\delta_{\tau\eta}$ have a tensorial structure different from the bare action so that they require the addition of two new anomalous advection terms, which are exactly the ones proportional to μ_1 and μ_2 in equation (9.39). In terms of the corrections of Eq. (10.21), the terms C and D thus contribute to $2\mu_1\delta\gamma_{s1} = C$ and $2\mu_2\delta\gamma_{s2} = D$.

Summary of the anomalous terms

I have shown explicitly that some vertex-correction diagrams generate the following mode-coupling and advective *anomalous* terms in the equation of motion for the spin,

$$\left\{ \begin{array}{l} \psi_\gamma(\tilde{\boldsymbol{k}}/2 - \tilde{\boldsymbol{q}})\psi_\nu(\tilde{\boldsymbol{k}}/2 + \tilde{\boldsymbol{q}})\mathbb{I}_{\alpha\beta\rho\sigma}k_\sigma q_\tau\mathbb{I}_{\rho\tau\gamma\nu} \\ \psi_\gamma(\tilde{\boldsymbol{k}}/2 - \tilde{\boldsymbol{q}})\psi_\nu(\tilde{\boldsymbol{k}}/2 + \tilde{\boldsymbol{q}})\mathbb{I}_{\alpha\beta\rho\sigma}q_\sigma k_\tau\mathbb{I}_{\rho\tau\gamma\nu} \end{array} \right. \longrightarrow \left\{ \begin{array}{l} [\partial_\alpha\,(\psi_\nu\partial_\nu\psi_\beta) - \partial_\beta\,(\psi_\nu\partial_\nu\psi_\alpha)] \\ \partial_\nu\,[\psi_\nu\,(\partial_\alpha\psi_\beta - \partial_\beta\psi_\alpha)] \end{array} \right. ,$$
$$\tag{10.51}$$

$$\left\{ \begin{array}{l} s_{\gamma\nu}(\tilde{\boldsymbol{k}}/2 - \tilde{\boldsymbol{q}})\psi_\eta(\tilde{\boldsymbol{k}}/2 + \tilde{\boldsymbol{q}})\mathbb{I}_{\alpha\beta\rho\sigma}\mathbb{I}_{\rho\tau\gamma\nu} \, k_\tau\delta_{\sigma\eta} \longrightarrow \partial_\nu\,(s_{\alpha\nu}\psi_\beta - s_{\beta\nu}\psi_\alpha) \\ s_{\gamma\nu}(\tilde{\boldsymbol{k}}/2 - \tilde{\boldsymbol{q}})\psi_\eta(\tilde{\boldsymbol{k}}/2 + \tilde{\boldsymbol{q}})\mathbb{I}_{\alpha\beta\rho\sigma}\mathbb{I}_{\rho\tau\gamma\nu} \, k_\sigma\delta_{\tau\eta} \longrightarrow [\partial_\alpha\,(\psi_\nu s_{\nu\beta}) - \partial_\beta\,(\psi_\nu s_{\nu\alpha})] \end{array} \right. .$$
$$\tag{10.52}$$

which have been summarised here together with the real-space form that I anticipated in (9.10) and (9.11). Notice a complication: while each one of the two advection terms in k space gives rise to one term in x space, both mode-coupling anomalous terms in k space contribute to both terms in x space. For this same reason the couplings of the mode-coupling anomalous terms in momentum space, Φ_1, Φ_2 are a linear combination of those in real space, ϕ_1, ϕ_2 (see equations (9.34) and (9.35)).

The crucial result of the diagrammatic calculation is that *all* mode-coupling and advection diagrams generating anomalous terms (including all diagrams that I have not explicitly analyzed in this Section), generate *only* terms with one of these four tensorial structures. In this sense, the RG calculation is closed once I include these four vertices in the action. Notice also that the total perturbative amplitudes of these terms are not simply given by the coefficients A, B, C, D calculated here, indeed because these anomalous terms will give rise to additional self-correcting contributions.

10.2 Rescaling

Once the shell integration is performed, one is left with an effective action with a smaller cutoff Λ/b, a coefficient different from 1 in front of the $-\mathrm{i}\omega\hat{\psi}\psi$ term and modified parameters, namely

$$\mathcal{P}_0 \to \mathcal{P}_0(1 + \delta\mathcal{P}\ln b) \simeq \mathcal{P}_0 b^{\delta\mathcal{P}} \tag{10.53}$$

Following Section 4, to be able to compare apples with apples, one must perform a scaling transformation which restores the previous cutoff Λ. This in principle requires rescaling only $\boldsymbol{k}$; However, it is convenient to rescale also the frequency and the fields, according to

$$\boldsymbol{k} = b^{-1}\boldsymbol{k}_b\,, \qquad\qquad \omega = b^{-z}\omega_b\,, \tag{10.54}$$

$$\boldsymbol{\psi}(\boldsymbol{k},\omega) = b^{-\chi_\psi}\boldsymbol{\psi}(\boldsymbol{k}_b,\omega_b)\,, \qquad\qquad \hat{\boldsymbol{\psi}}(\boldsymbol{k},\omega) = b^{-\chi_{\hat\psi}}\hat{\boldsymbol{\psi}}(\boldsymbol{k}_b,\omega_b)\,, \tag{10.55}$$

$$\boldsymbol{s}(\boldsymbol{k},\omega) = b^{-\chi_s}\boldsymbol{s}(\boldsymbol{k}_b,\omega_b)\,, \qquad\qquad \hat{\boldsymbol{s}}(\boldsymbol{k},\omega) = b^{-\chi_{\hat s}}\hat{\boldsymbol{s}}(\boldsymbol{k}_b,\omega_b)\,. \tag{10.56}$$

After this rescaling, one recovers an action with the same cutoff Λ but with new renormalized parameters and couplings, which will be denoted with a subscript b in what follows.

To understand how this works in practice, let me first focus on what happens to the $-\mathrm{i}\omega$ terms under rescaling. Once the shell integration is performed, the rescaling procedure defined by Eq. (10.54)-(10.56) transforms these terms as follows

$$\int\limits_{|\boldsymbol{k}|<\Lambda/b} \mathrm{d}^d k \int\limits_{-\infty}^{+\infty} d\omega \left[-\mathrm{i}\omega\left(1 + \delta\Omega\ln b\right)\hat{\psi}(-\boldsymbol{k},-\omega)\psi(\boldsymbol{k},\omega)\right] =$$

$$= b^{-\chi_{\hat\psi}-\chi_\psi-d-2z+\delta\Omega} \int\limits_{|\boldsymbol{k}_b|<\Lambda} \mathrm{d}^d k_b \int\limits_{-\infty}^{+\infty} d\omega_b \left[-\mathrm{i}\omega_b\hat{\psi}(-\boldsymbol{k}_b,-\omega_b)\psi(\boldsymbol{k}_b,\omega_b)\right]\,, \tag{10.57}$$

$$\int\limits_{|\boldsymbol{k}|<\Lambda/b} \mathrm{d}^d k \int\limits_{-\infty}^{+\infty} d\omega \left[-\mathrm{i}\omega\hat{s}(-\boldsymbol{k},-\omega)s(\boldsymbol{k},\omega)\right] =$$

$$= b^{-\chi_{\hat s}-\chi_s-d-2z} \int\limits_{|\boldsymbol{k}_b|<\Lambda} \mathrm{d}^d k_b \int\limits_{-\infty}^{+\infty} d\omega_b \left[-\mathrm{i}\omega_b\hat{s}(-\boldsymbol{k}_b,-\omega_b)s(\boldsymbol{k}_b,\omega_b)\right]\,, \tag{10.58}$$

where I remind that the $-\mathrm{i}\omega\hat{s}s$ term has no perturbative corrections because of the rotational symmetry – see Sec. 9.3.3 for a discussion on this. As previously mentioned, these terms lack a coupling constant to redefine. Hence, the scaling dimensions of the fields must be properly chosen to restore the same structure of the bare action, namely

$$\chi_{\hat\psi} + \chi_\psi = -d - 2z + \delta\Omega \qquad\qquad \chi_{\hat s} + \chi_s = -d - 2z \tag{10.59}$$

With this choice, the renormalized theory will still have a coefficient equal to one in front of the time derivative of the equation of motion. This requirement allows me to fix the scaling dimension of the response fields $\chi_{\hat{\psi}}$ and $\chi_{\hat{s}}$,

$$\chi_{\hat{\psi}} = -\chi_{\psi} - d - 2z + \delta\Omega \qquad\qquad \chi_{\hat{s}} = -\chi_s - d - 2z \ . \qquad (10.60)$$

Rescaling can be performed on all the other terms of the action in the same way as it was done in Eq. (10.57)-(10.58). In these cases, however, the powers of b appearing after rescaling can be reabsorbed by defining new *renormalized* parameters of the theory. These new values of the parameters can be expressed as functions of the bare parameters, through the perturbative corrections, the dynamic exponent z and the scaling dimensions χ of the fields. Scaling dimensions for time and fields are not known *a priori* but can be determined by imposing additional conditions. For what concerns the Gaussian action, the renormalized parameters are given by

$$\Gamma_b = \Gamma_0 b^{\chi_\Gamma} \qquad\qquad \chi_\Gamma = -\chi_{\hat{\psi}} - \chi_\psi - d - 2 - z + \delta\Gamma \qquad (10.61)$$

$$\tilde{\Gamma}_b = \tilde{\Gamma}_0 b^{\chi_{\tilde{\Gamma}}} \qquad\qquad \chi_{\tilde{\Gamma}} = -2\chi_{\hat{\psi}} - d - z + \delta\tilde{\Gamma} \qquad (10.62)$$

$$\lambda_b^{\perp/\|} = \lambda_0^{\perp/\|} b^{\chi_{\lambda^{\perp/\|}}} \qquad\qquad \chi_{\lambda^{\perp/\|}} = -\chi_{\hat{s}} - \chi_s - d - 2 - z + \delta\lambda^{\perp/\|} \qquad (10.63)$$

$$\tilde{\lambda}_b^{\perp/\|} = \tilde{\lambda}_0^{\perp/\|} b^{\chi_{\tilde{\lambda}^{\perp/\|}}} \qquad\qquad \chi_{\tilde{\lambda}^{\perp/\|}} = -2\chi_{\hat{s}} - d - 2 - z + \delta\tilde{\lambda}^{\perp/\|} \qquad (10.64)$$

$$\eta_b = \eta_0 b^{\chi_\eta} \qquad\qquad \chi_\eta = -\chi_{\hat{s}} - \chi_s - d - z \qquad (10.65)$$

$$\tilde{\eta}_b = \tilde{\eta}_0 b^{\chi_{\tilde{\eta}}} \qquad\qquad \chi_{\tilde{\eta}} = -2\chi_{\hat{s}} - d - z \qquad (10.66)$$

$$m_b = m_0 b^{\chi_m} \qquad\qquad \chi_m = -\chi_{\hat{\psi}} - \chi_\psi - d - z + \delta m \qquad (10.67)$$

By taking advantage of Eq. (10.60) it is furthermore possible to write all the scaling dimensions of the parameters in terms of the scaling dimensions of the frequency and physical fields only, namely of z, χ_ψ and χ_s:

$$\chi_\Gamma = z - 2 + \delta\Gamma - \delta\Omega \qquad\qquad \chi_{\tilde{\Gamma}} = 2\chi_\psi + d + 3z + \delta\tilde{\Gamma} - 2\delta\Omega \qquad (10.68)$$

$$\chi_{\lambda^{\perp/\|}} = z - 2 + \delta\lambda^{\perp/\|} \qquad\qquad \chi_{\tilde{\lambda}^{\perp/\|}} = 2\chi_s + d + 3z - 2 + \delta\tilde{\lambda}^{\perp/\|} \qquad (10.69)$$

$$\chi_\eta = z \qquad\qquad \chi_{\tilde{\eta}} = 2\chi_s + d + 3z \qquad (10.70)$$

$$\chi_m = z + \delta m - \delta\Omega \qquad (10.71)$$

Let me note here a crucial fact: since the dynamic critical exponent z is always positive, so is the scaling dimension χ_η of the dissipation η. Due to this, η grows exponentially when the RG transformation is iterated over and over, eventually diverging. This makes η a relevant parameter, with a role similar to that of the mass m: while m is the relevant parameter that drives the system away from the critical manifold, similarly η drives the system away from the conservative plane (while remaining on the critical manifold). Hence, independent of all the other parameters, I expect η to diverge under the RG flow whenever its bare value is non-zero. This will have important consequences that I will discuss later on.

When turning the attention to the non-Gaussian part of the action, the renor-

malized couplings and parameters are given by

$$\gamma_{\psi b} = \gamma_{\psi 0} b^{\chi_{\gamma_\psi}} \qquad \chi_{\gamma_\psi} = -\chi_{\hat{\psi}} - 2\chi_\psi - 2d - 1 - 2z + \delta\gamma_\psi \qquad (10.72)$$

$$\gamma_{s b} = \gamma_{s 0} b^{\chi_{\gamma_s}} \qquad \chi_{\gamma_s} = -\chi_{\hat{s}} - \chi_s - \chi_\psi - 2d - 1 - 2z + \delta\gamma_s \qquad (10.73)$$

$$\mu_{1 b} = \mu_{10} b^{\chi_{\mu_1}} \qquad \chi_{\mu_1} = \delta\gamma_{s1} - \delta\gamma_s \qquad (10.74)$$

$$\mu_{2 b} = \mu_{20} b^{\chi_{\mu_2}} \qquad \chi_{\mu_2} = \delta\gamma_{s2} - \delta\gamma_s \qquad (10.75)$$

$$g_b^{(\psi)} = g_0 b^{\chi_{g^{(\psi)}}} \qquad \chi_{g^{(\psi)}} = -\chi_{\hat{\psi}} - \chi_\psi - \chi_s - 2d - 2z + \delta g_\psi \qquad (10.76)$$

$$g_b^{(s)} = g_0 b^{\chi_{g^{(s)}}} \qquad \chi_{g^{(s)}} = -\chi_{\hat{s}} - 2\chi_\psi - 2d - 2 - 2z + \delta g_s \qquad (10.77)$$

$$\Phi_{1 b} = \Phi_{10} b^{\chi_{\Phi_1}} \qquad \chi_{\Phi_1} = \delta g_{s1} - \delta g_s \qquad (10.78)$$

$$\Phi_{2 b} = \Phi_{20} b^{\chi_{\Phi_2}} \qquad \chi_{\Phi_2} = \delta g_{s2} - \delta g_s \qquad (10.79)$$

$$J_b = J_0 b^{\chi_J} \qquad \chi_J = -\chi_{\hat{\psi}} - 3\chi_\psi - 3d - 3z + \delta J \qquad (10.80)$$

$$\kappa_b = \kappa_0 b^{\chi_\kappa} \qquad \chi_\kappa = -\chi_{\hat{s}} - 4\chi_\psi - 4d - 4z + \delta\kappa \qquad (10.81)$$

By using Eq. (10.60) I can write all the scaling dimensions of the interaction couplings in terms of the scaling dimensions of the frequency and physical fields, namely of z, χ_ψ and χ_s:

$$\chi_{\gamma_\psi} = -\chi_\psi - d - 1 + \delta\gamma_\psi - \delta\Omega \qquad \chi_{\gamma_s} = -\chi_\psi - d - 1 + \delta\gamma_s \qquad (10.82)$$

$$\chi_{\mu_1} = \delta\gamma_{s1} - \delta\gamma_s \qquad \chi_{\mu_2} = \delta\gamma_{s2} - \delta\gamma_s \qquad (10.83)$$

$$\chi_{g^{(\psi)}} = -\chi_s - d + \delta g_\psi - \delta\Omega \qquad \chi_{g^{(s)}} = \chi_s - 2\chi_\psi - d - 2 + \delta g_s \qquad (10.84)$$

$$\chi_{\Phi_1} = \delta g_{s1} - \delta g_s \qquad \chi_{\Phi_2} = \delta g_{s2} - \delta g_s \qquad (10.85)$$

$$\chi_J = -2\chi_\psi - 2d - z + \delta J - \delta\Omega \qquad \chi_\kappa = \chi_s - 4\chi_\psi - 3d - 2z + \delta\kappa \qquad (10.86)$$

By looking at Eqs. (10.76) and (10.77) it may seem that one has *two* different mode-coupling constants; however, this is not the case. I defined two different renormalized coupling constants $g^{(\psi)}$ and $g^{(s)}$ only because the perturbative corrections δg_ψ and δg_s arising in Eqs. (10.17) and (10.20) are completely independent of each other, but this does not mean that there are two different *physical* constants. In fact, there must be only one mode-coupling constant, because g arises in the derivation of the equations of motion as the consequence of a symmetry, encoded by the Poisson-bracket relation $\{s, \psi\} \propto g\psi$, stating that $\boldsymbol{s}$ is the generator of the rotations of $\boldsymbol{\psi}$. The mode-coupling terms in both the equations of motion derive from this one Poisson-bracket relation; therefore, the existence of two different couplings would mean losing the connection with the underlying symmetry and Poisson structure. As I mentioned before, the scaling behaviour of the physical fields $\boldsymbol{\psi}$ and $\boldsymbol{s}$ is arbitrary, which allows a certain freedom in determining the scaling dimensions χ_ψ and χ_s, which enter Eqs. (10.76) and (10.77). Hence, it is possible to use this freedom to restore the identity of the two mode-coupling constants,

$$g_b^{(\psi)} = g_b^{(s)} = g_b \qquad (10.87)$$

by simply asking that χ_s is chosen in such a way that,

$$\chi_{g^{(\psi)}} = \chi_{g^{(s)}} \qquad (10.88)$$

Essentially, I am requiring the field $\boldsymbol{s}$ to scale in such a way that the coupling regulating the symmetry has one unique scaling behaviour.

10.3   Effective coupling constants

As it is always the case in RG calculations, it is now possible to define a set of effective parameters whose scaling behaviour does not depend on z, χ_ψ and χ_s, so that all physical quantities turn out to depend on the parameters of the theory only via these effective couplings. The effective couplings can be found by looking at the scaling dimensions of the parameters of the theory, given in Eqs. (10.68)-(10.70), (10.82)-(10.86). By recalling that the scaling dimension of the product of two couplings is given by the sum of the respective scaling dimensions, namely,

$$\mathcal{C}_b = \mathcal{A}_b \mathcal{B}_b = b^{\chi_\mathcal{A} + \chi_\mathcal{B}} \mathcal{A}_0 \mathcal{B}_0 = b^{\chi_\mathcal{C}} \mathcal{C}_0 \qquad \rightarrow \qquad \chi_\mathcal{C} = \chi_\mathcal{A} + \chi_\mathcal{B} \tag{10.89}$$

it is always possible to find a set of combinations of coupling constants and parameters of the theory that have a scaling behaviour which is independent of z, χ_ψ and χ_s [107]. For example, let me consider the coupling constant J: its scaling, given by Eq. (10.86), depends on χ_ψ and z. To compensate for the dependence on χ_ψ one can multiply it by the noise strength $\tilde{\Gamma}$, which also has a χ_ψ scaling dependence; thus, the product $\tilde{\Gamma} J$ does not depend anymore on χ_ψ. Similarly, the dependence on z can be compensated by dividing by Γ^2, making the scaling behaviour of the combination $\tilde{\Gamma} J / \Gamma^2$ depending only on d and perturbative corrections, which are computed through Feynman diagrams. A similar procedure can be applied at any other constant; multiplying it by appropriate powers of $\tilde{\lambda}^{\perp/\parallel}$ or $\tilde{\Gamma}$ to compensate the dependence on χ_s or χ_ψ respectively, and by appropriate powers of Γ, $\lambda^{\perp/\parallel}$ to compensate the dependence on z. There is some arbitrariness on the choice of whether to use $\tilde{\lambda}^\perp$ or $\tilde{\lambda}^\parallel$ to compensate χ_s and whether to use Γ, $\lambda^\perp$ or $\lambda^\parallel$ to compensate z. However, as long as these parameters are not singular (and they will not be at the fixed point), this choice is irrelevant.

The effective parameters for (9.12)-(9.13) are,

$$w = \frac{\Gamma}{\lambda^\parallel} , \quad x = \frac{\lambda^\perp}{\lambda^\parallel} , \quad \theta^\perp = \frac{\tilde{\Gamma} \lambda^\perp}{\Gamma \tilde{\lambda}^\perp} \frac{g^{(s)}}{g^{(\psi)}} , \quad \theta^\parallel = \frac{\tilde{\Gamma} \lambda^\parallel}{\Gamma \tilde{\lambda}^\parallel} \frac{g^{(s)}}{g^{(\psi)}} , \tag{10.90}$$

where $\theta^{\perp,\parallel} \neq 1$ if the system is out-of-equilibrium. Although the technical definition of $\theta^{\perp/\parallel}$ contains the ratio $g^{(s)}/g^{(\psi)}$, the physical case is given by $g^{(s)} = g^{(\psi)}$, as argued in Sec. 10.2 . Hence, the physical meaning of $\theta^{\perp/\parallel}$ is that of the ratio between the effective temperatures of the two fields, $T_\psi = \tilde{\Gamma}/\Gamma$ and $T_s^{\perp/\parallel} = \tilde{\lambda}^{\perp/\parallel}/\lambda^{\perp/\parallel}$, namely

$$\theta^\perp = \frac{T_\psi}{T_s^\perp} = \frac{\tilde{\Gamma} \lambda^\perp}{\Gamma \tilde{\lambda}^\perp} , \quad \theta^\parallel = \frac{T_\psi}{T_s^\parallel} = \frac{\tilde{\Gamma} \lambda^\parallel}{\Gamma \tilde{\lambda}^\parallel} . \tag{10.91}$$

From the dissipative coefficients η and $\tilde{\eta}$, two effective parameters can be obtained

$$\hat{\eta} = \frac{\eta}{\lambda^\parallel \Lambda^2 + \eta} , \quad \breve{\eta} = \frac{\tilde{\eta}}{\tilde{\lambda}^\parallel \Lambda^2 + \tilde{\eta}} \tag{10.92}$$

Here the presence of Λ is needed for dimensional reasons. In terms of these *reduced* dissipations, the conservative dynamics is recovered when $\hat{\eta} = \breve{\eta} = 0$, while the fully dissipative dynamics is recovered when $\hat{\eta} = \breve{\eta} = 1$, namely when $\eta \gg \lambda^{\parallel/\perp} \Lambda^2$, $\tilde{\eta} \gg \tilde{\lambda}^{\parallel/\perp} \Lambda^2$.

The effective coupling constants regulating activity are,

$$c_v = v_0 \frac{\gamma_v}{\Gamma} \sqrt{\frac{\tilde{\Gamma}}{\Gamma}} \sqrt{K_d \Lambda^{d-4}} \quad , \quad c_s = v_0 \frac{\gamma_s}{\lambda^{\parallel}} \sqrt{\frac{\tilde{\Gamma}}{\Gamma}} \sqrt{K_d \Lambda^{d-4}} \; , \tag{10.93}$$

the ferromagnetic coupling J and the mass m have effective couplings given by

$$\tilde{u} = \frac{\tilde{\Gamma}}{\Gamma} \frac{J}{\Gamma} K_d \Lambda^{d-4} = \frac{\tilde{\Gamma}}{\Gamma} u \, K_d \Lambda^{d-4} \quad , \quad \tilde{r} = \frac{m}{\Gamma} K_d \Lambda^{d-2} = \frac{\tilde{\Gamma}}{\Gamma} r K_d \Lambda^{d-2} \; ; \tag{10.94}$$

while the mode-coupling and the DYS effective coupling constants respectively are,

$$f = \frac{\tilde{\lambda}^{\parallel}}{\lambda^{\parallel}} \frac{g^2}{\lambda^{\parallel}\Gamma} K_d \Lambda^{d-4} \quad , \quad \tilde{u}_\kappa = \frac{\tilde{\Gamma}}{\Gamma} \frac{\kappa}{g} K_d \Lambda^{d-4} \; ; \tag{10.95}$$

where Λ is the cutoff of the theory and K_d is the surface of the unitary sphere in d dimensions. The presence of Λ to the power $4-d$ in all effective couplings except for r suggests that the upper critical dimension of the theory is $d_c = 4$, which means that all couplings are relevant in $d < 4$, while mean-field behaviour is recovered for $d \geq 4$. The dependence of r on Λ^{d-2} indicates instead that the mass is always a relevant perturbation above $d = 2$, driving the system away from the critical manifold. Therefore, this requires the mass to be fine-tuned to be near the critical point. At equilibrium, where $v_0 = 0$ and $\tilde{\Gamma} = \Gamma, \tilde{\lambda} = \lambda, \kappa = ug$, all the effective couplings become identical to their standard equilibrium counterpart [40], with the equilibrium result $\tilde{u} = \tilde{u}_\kappa$ [MyPaper2] being recovered.

Finally, the four adimensional parameters regulating the anomalous mode-coupling and self-propulsion non-linearities, namely

$$\Phi_1 \quad , \quad \Phi_2 \quad , \quad \mu_1 \quad , \quad \mu_2 \, . \tag{10.96}$$

should be added to the list of effective parameters.

10.4   RG flow equations and β-functions

The flow of the effective couplings can be obtained by iterating the RG transformation, thus defining a set of recursive relations. After l iterations, the new parameters will take the form,

$$\mathcal{P}_{l+1} = b^{\chi_\mathcal{P}} \mathcal{P}_l \tag{10.97}$$

where $\chi_\mathcal{P}$ is evaluated using the values of the parameters at step l. The values $\mathcal{P}^*$ to which the flow of $\mathcal{P}$ approaches when $l \to \infty$ are called fixed points, and play a crucial role in determining the critical behaviour of the theory [15]. To study the RG flow of the present theory, it is convenient to rewrite Eq. (10.97) in the thin shell limit $\ln b \to 0$. In this limit, the flow equations become

$$\dot{\mathcal{P}} = \frac{\partial \mathcal{P}}{\partial \ln b} \equiv \beta_\mathcal{P} \tag{10.98}$$

where $\beta_\mathcal{P}$, known as β-function, is defined as the derivative of $\mathcal{P}$ with respect to $\ln b$. The fixed points $\mathcal{P}^*$ of the RG-flow are given by the zeros of $\beta_\mathcal{P}$, since these are the points at which

$$\dot{\mathcal{P}} = \beta_\mathcal{P}|_{\mathcal{P}=\mathcal{P}^*} = 0 \, . \tag{10.99}$$

Among these fixed points, some are (IR-)stable meaning that the flow is driven towards them, while others may have one or more directions of instability from which the RG flow escapes. Asymptotically IR-stable fixed points are those typically ruling the critical behaviour of systems in the thermodynamic limit. Note that, as previously discussed, the mass coupling r always represents a source of instability since it drives the system away from criticality. Hence, stability is intended as stability in all directions except r.

The β-function of the generic parameter $\mathcal{P}$ is given by $\beta_{\mathcal{P}} = \mathcal{P}\chi_{\mathcal{P}}$. Hence, for the parameters defined in Eqs. (10.90)-(10.95) the beta-functions take the following form,

$$\beta_w = w\left(\delta\Gamma - \delta\lambda^{\|}\right) \tag{10.100}$$

$$\beta_x = x\left(\delta\lambda^{\perp} - \delta\lambda^{\|}\right) \tag{10.101}$$

$$\beta_{\theta\perp} = \theta^{\perp}\left(\delta\tilde{\Gamma} - \delta\Gamma + \delta\lambda^{\perp} - \delta\tilde{\lambda}^{\perp} + \delta g_s - \delta g_{\psi}\right) \tag{10.102}$$

$$\beta_{\theta\|} = \theta^{\perp}\left(\delta\tilde{\Gamma} - \delta\Gamma + \delta\lambda^{\|} - \delta\tilde{\lambda}^{\|} + \delta g_s - \delta g_{\psi}\right) \tag{10.103}$$

$$\beta_{\hat{\eta}} = \hat{\eta}\left(1 - \hat{\eta}\right)\left(2 - \delta\lambda^{\|}\right) \tag{10.104}$$

$$\beta_{\breve{\eta}} = \breve{\eta}\left(1 - \breve{\eta}\right)\left(2 - \delta\tilde{\lambda}^{\|}\right) \tag{10.105}$$

$$\beta_{\tilde{r}} = \tilde{r}\left(2 + \delta m - \delta\Gamma\right) \tag{10.106}$$

$$\beta_{c_v} = \frac{1}{2}c_v\left(\epsilon + \delta\tilde{\Gamma} + 2\delta\gamma_{\psi} - 3\delta\Gamma - \delta\Omega\right) \tag{10.107}$$

$$\beta_{c_s} = \frac{1}{2}c_s\left(\epsilon + \delta\tilde{\Gamma} + 2\delta\gamma_s - \delta\Gamma - 2\delta\lambda^{\|} - \delta\Omega\right) \tag{10.108}$$

$$\beta_f = f\left(\epsilon + \delta\tilde{\lambda}^{\|} + 2\delta g_{\psi} - 2\delta\tilde{\lambda}^{\|} - \delta\Gamma - \delta\Omega\right) \tag{10.109}$$

$$\beta_{\tilde{u}} = \tilde{u}\left(\epsilon + \delta\tilde{\Gamma} + \delta J - 2\delta\Gamma - \delta\omega_{\psi}\right) \tag{10.110}$$

$$\beta_{\tilde{u}_{\kappa}} = \tilde{u}_{\kappa}\left(\epsilon + \delta\tilde{\Gamma} + \delta\kappa - \delta\Gamma - \delta g_s - \delta\Omega\right) \tag{10.111}$$

$$\beta_{\mu_1} = \mu_1\left(\delta\gamma_{s1} - \delta\gamma_s\right) \tag{10.112}$$

$$\beta_{\mu_2} = \mu_2\left(\delta\gamma_{s2} - \delta\gamma_s\right) \tag{10.113}$$

$$\beta_{\Phi_1} = \Phi_1\left(\delta g_{s1} - \delta g_s\right) \tag{10.114}$$

$$\beta_{\Phi_2} = \Phi_2\left(\delta g_{s2} - \delta g_s\right) \tag{10.115}$$

where all the perturbative corrections $\delta\mathcal{P}$ are obtained from the Feynman diagram expansion. The explicit expressions of these beta-functions are given in the Mathematica notebook from [MyPaper1].

Before I proceed, let me draw the reader's attention to the beta functions of the reduced dissipative coefficients, $\hat{\eta}$ and $\breve{\eta}$, Eq. (10.104) and (10.105). Within the perturbative approach, near 4 dimensions the parameters $\hat{\eta}$ and $\breve{\eta}$ may take only two possible fixed point values: 0 or 1. This is because the perturbative corrections

$\delta\lambda^{\parallel}$ and $\delta\tilde{\lambda}^{\parallel}$ are both of $\mathcal{O}(\epsilon)$; hence the quantities $2 - \delta\lambda^{\parallel}$ and $2 - \delta\tilde{\lambda}^{\parallel}$ will always be strictly positive and close to 2; hence, the only way in which $\beta_{\hat{\eta}} = 0$ is by setting $\hat{\eta} = 0$ or $\hat{\eta} = 1$. Similarly, $\beta_{\breve{\eta}} = 0$ is achieved only when $\breve{\eta} = 0$ or $\breve{\eta} = 1$. Near the conservative manifold $\hat{\eta} = \breve{\eta} = 0$, the scaling dimensions of both $\hat{\eta}$ and $\breve{\eta}$ are positive, meaning that the flow drives the system away from it. On the other hand, the fully dissipative manifold $\hat{\eta} = \breve{\eta} = 1$ is attractive. Hence, both $\hat{\eta}$ and $\breve{\eta}$ flow from the conservative value of 0 towards the dissipative value of 1, regardless of what all the other parameters do. In terms of the dissipations coefficients η and $\tilde{\eta}$, the stability of the $\hat{\eta} = \breve{\eta} = 1$ manifold reflects the fact that both parameters grow under the RG flow, eventually diverging: $\eta \to \infty$, $\tilde{\eta} \to \infty$. This means that the asymptotically stable behaviour of the theory is given by the overdamped limit.

10.5 Properties of the RG solution in the absence of dissipation

The power of the RG lies in the fact that critical exponents can be inferred by the study of the RG flow in the neighbourhood of a fixed point. The fixed point at which the critical exponents should be evaluated usually is the stable one, since one expects the RG flow to eventually reach its stable fixed point. However, unstable fixed points often play a crucial role in determining the behaviour of *finite-size* systems, since crossover phenomena may take place.

In the following section, I will show that this is indeed the case for the field theory I have introduced. Although the IR-stable fixed point in the presence of spin dissipation is that of the incompressible Toner and Tu theory [23], an RG crossover takes place for small dissipation $\hat{\eta} \ll 1$, as in [41, 108]. The (IR-unstable) fixed point ruling the behaviour of systems with small dissipation can be found by focusing on the RG flow of the conservative theory. It is worth noting that the conservative subspace is RG-invariant, since $\beta_{\hat{\eta}} = \beta_{\breve{\eta}} = 0$ when $\hat{\eta} = \breve{\eta} = 0$. Hence, I shall first restrict myself to the sub-space $\hat{\eta} = \breve{\eta} = 0$, and come back to the dissipative theory later on in Section 10.6.

10.5.1 Flow and fixed points

In simple cases, fixed points can be found by solving analytically the set of equations $\beta_{\mathcal{P}} = 0$ in the parameters $\mathcal{P}$. Here this was not possible. Instead, I tackled this problem by integrating numerically the set of partial differential equations defining the RG flow, namely (10.98), and looking at what values of the parameters the flow converges. If the flow does converge, the point to which it will converge is a fixed point of the theory. This procedure does not allow me to find any fixed point, but only the ones that are stable in the manifold I decide to restrict myself to, which is the $\hat{\eta} = \breve{\eta} = 0$ manifold in the present case.

To perform this numerical integration, great care must be taken in the choice of initial conditions of the parameters and couplings, as a large portion of this 14-dimensional coupling space is expected to be just unphysical. Therefore, before proceeding with the search for a new active inertial fixed point, it is useful to identify the most relevant fixed points I already know about. As I will here show, a rich

fixed-point structure emerges.

Model A fixed point. The first, most trivial fixed point that the present theory exhibits is given by Model A [40] with solenoidal constraint. To find this fixed point, I first have to set $f = 0$, effectively decoupling the dynamics of the order parameter from that of the spin, hence turning off inertial effects. At this point, one can therefore forget about the equation for the spin and focus only on the dynamic of the order parameter. Model A dynamics is completely recovered when $v_0 = 0$ ($c_v = 0$), switching activity off. On this equilibrium non-inertial manifold, the only remaining coupling is the ferromagnetic coupling $\tilde{u}$, which flows to the fixed point of classical ferromagnets with dipolar interactions [87, 86, 111]. This *equilibrium non-inertial* fixed point thus describes non-active systems, as classical ferromagnets, where the polarisation is not coupled to the spin. This fixed point is however unstable both against activity *and* inertial perturbations.

Model G fixed point. By keeping the system at equilibrium, but turning on inertia the equilibrium inertial manifold can be now accessed. This manifold is represented by set of parameters $v_0 = 0$ (and thus $c_v = c_s = 0$), $\theta^{\perp/\parallel} = 1$, $\Phi_1 = \Phi_2 = 0$ and $\tilde{u} = \tilde{u}_\kappa \neq 0$, representing the equilibrium limit of the present theory – Eq. (9.12) (9.13). On this manifold, the couplings w, f and $\tilde{u}$ eventually approach the Solenoidal Model G fixed point [MyPaper2]. In the absence of solenoidal constraints, this fixed point is known to describe equilibrium superfluids and antiferromagnets (Models E/F and G of [40]). While this fixed point is stable on the equilibrium manifold, it is unstable against activity perturbations.

Self-Propelled Model A fixed point. On the other hand, it is possible to turn on activity while keeping inertial effects irrelevant. This is done by setting $f = 0$, but allowing $v_0 \neq 0$ (and hence $c_v \neq 0$). On this manifold, the inertial reversible terms are absent from the dynamics, hence the polarisation is decoupled from the spin. This leads to Self-Propelled Model A fixed point, which was first discovered in [23]. This *active non-inertial* fixed point is stable against fluctuations of c_v, but as soon as one perturbs it with an inertial coupling, $f \neq 0$, the RG flow diverges. There is a sound reason for this: the correct way to attain non-inertial dynamics is not to kill the reversible coupling between coordinate and momentum, but to introduce dissipation and let it take over in the overdamped limit. This analysis will be performed later on, in Sec. 10.6.

Let me now come back to my original goal, namely finding a new *active inertial* fixed point. As previously mentioned, this turns out to be not feasible by analytically solving $\beta_\mathcal{P} = 0$. Therefore, the RG flow must be solved numerically from a sound initial condition in order to find this new fixed point. Since any inertial system with *small*, but non-vanishing activity v_0 belongs to the neighbourhood of the equilibrium limit, the surroundings of Model G fixed point seem as a good starting point. If activity is relevant, and indeed I will show it is, the corresponding coupling constants c_v and c_s should grow along the RG flow and drive the system towards an out-of-equilibrium active fixed point if it exists. Let me remark that I do not start close to equilibrium because I expect activity to be weak in swarms; in fact, quite the opposite: activity in natural swarms is strong [MyPaper1]. I start close to the equilibrium fixed point for a mere technical point: I need a safe path through a very dangerous parameter space in which it is far too easy for the RG flow to go bonkers if one deviates too much from a physical initial condition.
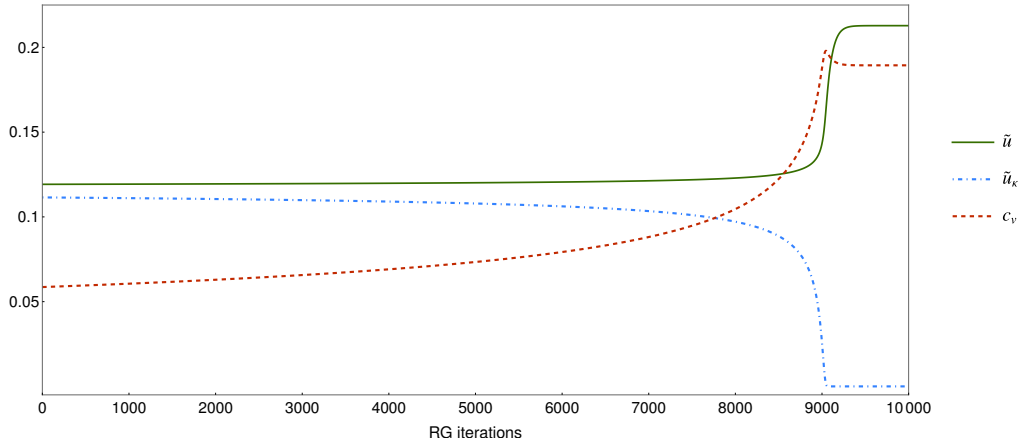
Figure 10.1. RG flow of $\tilde{u}$, $\tilde{u}_\kappa$ and c_v [MyPaper1]. As an example, I show a portion of the RG flow of the couplings $\tilde{u}$, $\tilde{u}_\kappa$ and c_v from the unstable equilibrium fixed point towards the stable off-equilibrium fixed point. From the plot, one can see that as activity increases, $\tilde{u}$ and $\tilde{u}_\kappa$ become different from the other. As the fixed point is approached, the value of $\tilde{u}_\kappa$ drops to 0. *Permission to reuse granted under the terms of the Creative Commons Attribution License CC BY 4.0*

The constants μ_1 and μ_2 have undefined values in the equilibrium limit since they are both multiplied by $v_0\gamma_s$ in the equations of motion and thus there are no *a priori* arguments to fix their value near equilibrium. However, I find that the β-functions of these two parameters, namely β_{μ_1} and β_{μ_2}, vanish when μ_1 and μ_2 take the following values

$$\mu_1 = \frac{1}{2} \quad , \quad \mu_2 = -\frac{1}{2} \tag{10.116}$$

$$\mu_1 = -1 \quad , \quad \mu_2 = 0 \tag{10.117}$$

independently of the values of all other parameters. This means that both these combinations of $\mu_{1,2}$ remain constant along with the RG flow, whatever the other couplings and parameters are doing. The first solution of $\mu_{1,2}$ turns out to be unstable for small perturbations of their values, at least near the equilibrium fixed point, while the second solution is stable. Hence, I fix from the beginning $\mu_1 = -1$ and $\mu_2 = 0$ and check the consistency of this choice by checking *a posteriori* the stability of the RG flow with respect to perturbations in μ_1 and μ_2, thus reducing the problem to 11 coupled equations instead of 13.

Self-Propelled Model G fixed point. I then simulate the RG flow starting from various initial conditions close to equilibrium by using the built-in *NDSolve* function of the software *Mathematica*, and always find the same attractive fixed point,

$$\tilde{u}^* = 0.213\epsilon \qquad \tilde{u}_\kappa^* = 0 \qquad c_v^* = 0.189\sqrt{\epsilon} \tag{10.118}$$

$$f^* = 1.68\epsilon \qquad \Phi_1 = -0.762 \qquad \Phi_2^* = -0.137 \tag{10.119}$$

$$c_s^* = 0.882\sqrt{\epsilon} \qquad \mu_1 = -1 \qquad \mu_2 = 0 \tag{10.120}$$

$$x^* = 0.369 \qquad \theta_\perp^* = 1.34 \qquad \hat{\eta}^* = 0 \tag{10.121}$$

$$w^* = 3.95 \qquad \theta_\parallel^* = 0.920 \qquad \breve{\eta}^* = 0 \tag{10.122}$$
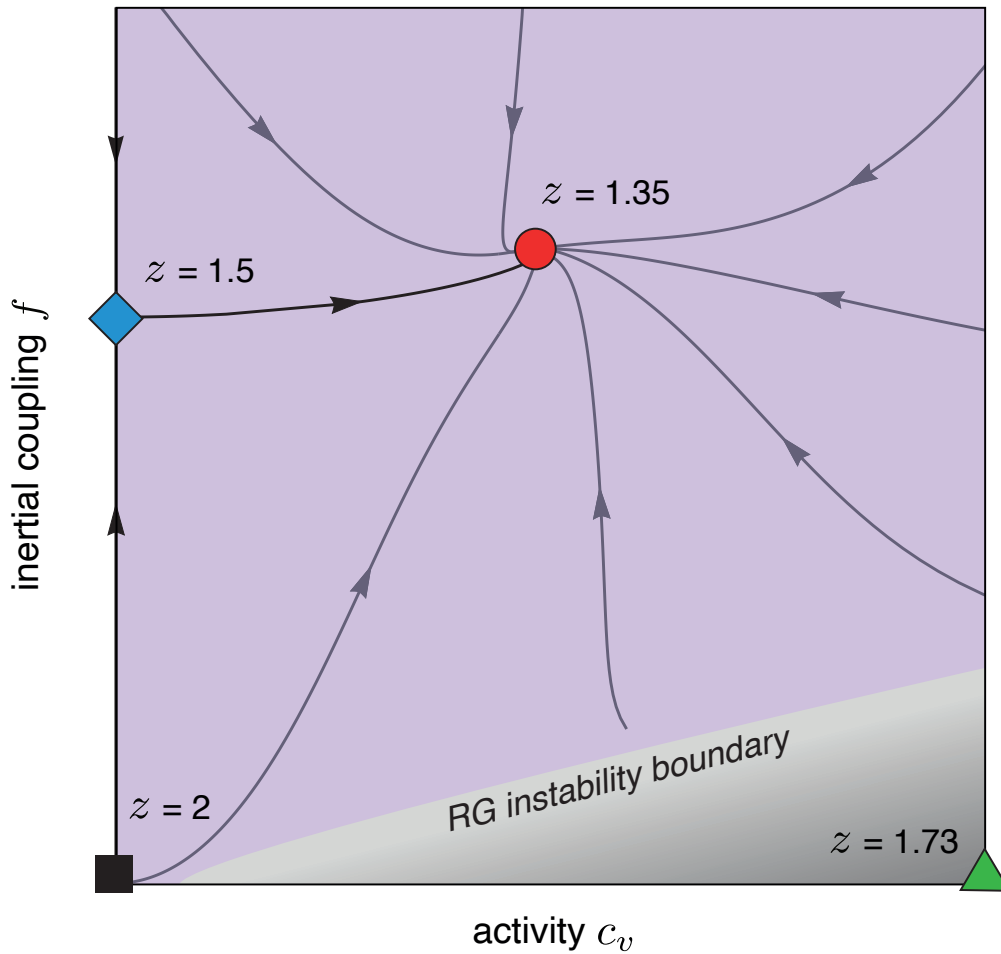
Figure 10.2. RG flow in the conservative case [MyPaper1]: The novel fixed point (red circle), with non-zero off-equilibrium activity and non-zero inertial coupling, is the only stable one, with a dynamical critical exponent $z = 1.35$ in $d = 3$. The equilibrium non-inertial fixed point (black square), $z = 2.0$, corresponds to standard ferromagnets (Model A of [40]); the equilibrium inertial fixed point (blue diamond), $z = 1.5$, corresponds to superfluids and quantum antiferromagnets (Models E and G of [40]); finally, the active non-inertial fixed point (green triangle), $z = 1.73$, corresponds to active matter without reversible coupling between velocity and spin [23]; this last fixed point is not connected to the active inertial one onto this plane. *Permission to reuse granted under the terms of the Creative Commons Attribution License CC BY 4.0*

The typical RG flow of a selected number of couplings is represented in Fig. 10.1, while the full picture of the RG flow in the conservative plane is represented in Fig. 10.2. Since c_v, c_s and f have a finite fixed point value, both activity and mode-coupling are relevant at this fixed point, making it the ideal candidate to describe incompressible inertial active matter. The stability of the novel fixed point is analysed by looking at the Jacobian matrix of the beta functions

$$\mathbb{J}_\beta = \frac{\partial \vec{\beta}}{\partial \vec{\mathcal{P}}} \tag{10.123}$$

The eigenvalues of $\mathbb{J}_\beta$ at the new fixed point are given by

$$-2.26\epsilon\,, \qquad\qquad -1.66\epsilon\,, \qquad\qquad -1.00\epsilon\,, \qquad\qquad (10.124)$$
$$-0.562\epsilon\,, \qquad\qquad -0.498\epsilon\,, \qquad\qquad -0.315\epsilon\,, \qquad\qquad (10.125)$$
$$-0.0584\epsilon\,, \qquad\qquad -0.0532\epsilon\,, \qquad\qquad -0.0167\epsilon\,, \qquad\qquad (10.126)$$

$$(-0.724 + 0.107\,\mathrm{i})\epsilon\,, \qquad\qquad (-0.724 - 0.107\,\mathrm{i})\epsilon\,, \qquad\qquad (10.127)$$
$$(-0.247 + 0.00185\,\mathrm{i})\epsilon\,, \qquad\qquad (-0.247 - 0.00185\,\mathrm{i})\epsilon\,, \qquad\qquad (10.128)$$
$$2 - 0.816\epsilon\,, \qquad\qquad 2 - 0.651\epsilon \qquad\qquad (10.129)$$

A negative (positive) real part of an eigenvalue indicates that the flow near the fixed point converges (diverges) exponentially along the direction of the associated eigenvector. On the other hand, the presence of an imaginary part of the eigenvalues stems from a spiralling convergence or divergence of the flow in the direction of the eigenvalue.

The last two eigenvalues of $\mathbb{J}_\beta$, namely $2 - 0.816\epsilon$ and $2 - 0.651\epsilon$, are positive for all values of ϵ that may be of physical interest ($0 \leq \epsilon \leq 2$). They indicate the presence of two directions of instability of the fixed point. From an analysis of the eigenvectors, it is possible to see that these instabilities point in the direction of $\hat{\eta}$ and $\breve{\eta}$ respectively, indicating that this fixed point is *not* stable with respect to spin-dissipation. However, since the real part of all other eigenvalues is negative when $\epsilon > 0$, I can conclude that this new fixed point is stable in the subspace $\hat{\eta} = \breve{\eta} = 0$ for $d < 4$ and thus it is expected to rule the long-wavelength behaviour of active inertial systems for $d = 3$.

10.6 Properties of the RG solution in the presence of dissipation

Up to now, I analysed the RG flow only in its fully conservative manifold, namely at $\hat{\eta} = \breve{\eta} = 0$, since expectations are that finite size systems with small dissipation are well described by fixed points in this manifold. In the present section, I will test the validity of these expectations. First, I will look at the behaviour of the RG flow in the strong-dissipation limit, showing that the behaviour of Self-Propelled Model A is recovered. Secondly, I will focus on the crossover between underdamped (small dissipation) and overdamped (strong dissipation) dynamics by analysing the RG flow in the proximity of the new active, inertial conservative fixed point found in Section 10.5.1.

10.6.1 Dissipative fixed point

As discussed at the end of Sec. 10.4, whenever $\hat{\eta} = \breve{\eta} \neq 0$ the RG flow makes them grow, approaching the fully dissipative manifold $\hat{\eta} = \breve{\eta} = 1$. When $\hat{\eta} = \breve{\eta} = 1$, the β-functions of the parameters and coupling constants of the theory take a simplified form. In particular, the β-functions of c_v and $\tilde{u}$ become independent from all the other parameters, while all the critical exponents can be expressed in terms of c_v and $\tilde{u}$ alone. This is a consequence of the fact that, in the presence of spin-dissipation,
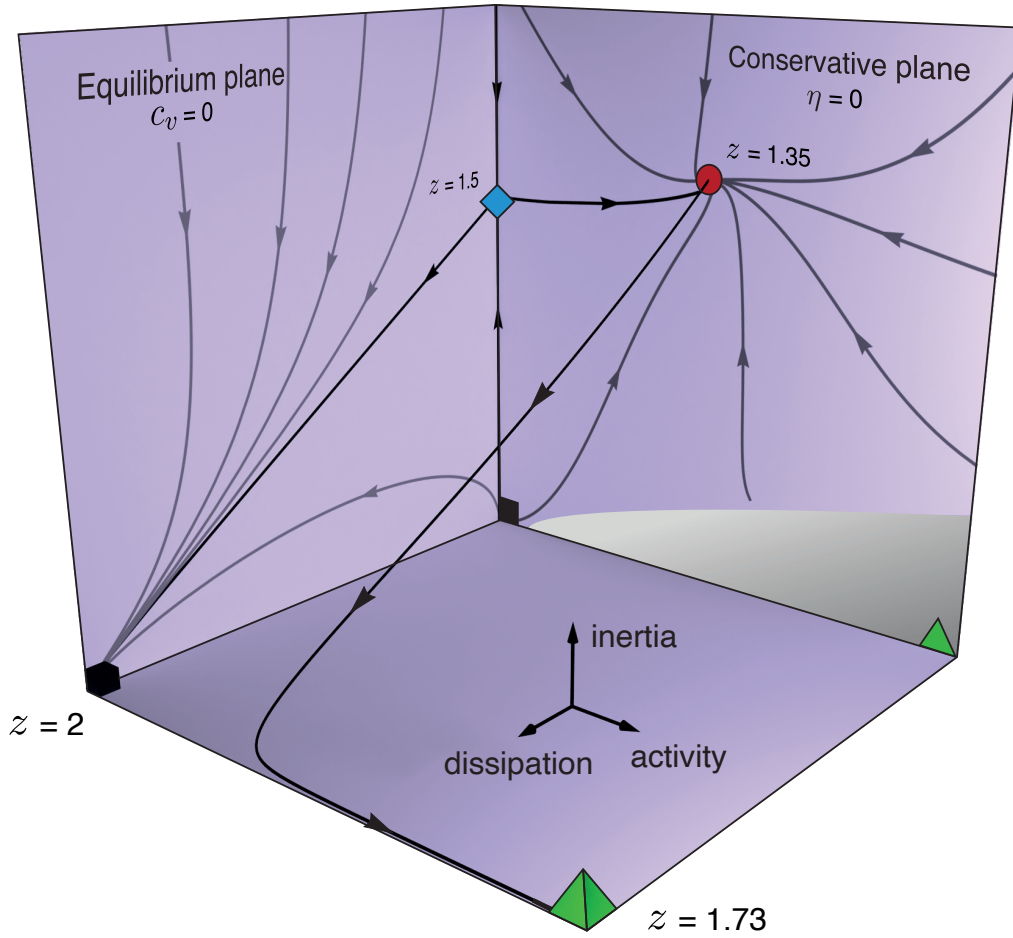
Figure 10.3. RG flow with spin dissipation [MyPaper1]: Spin dissipation, η, is a relevant parameter that brings the flow out of the conservative plane (bottom right plane of the cube). Perturbing the active inertial fixed point, $z = 1.35$, with some dissipation, the RG flow leaves the $\hat{\eta} = 0$ plane, until it eventually reaches the active overdamped fixed point for $\hat{\eta} = 1$ (green pyramid), where $z = 1.73$. This fixed point is best seen as belonging to the overdamped $\hat{\eta} = 1$ line, rather than to the conservative but non-inertial line, $\eta = 0$, $f = 0$: even though the value of $\hat{f}$ is the same on the two lines, only the first one corresponds to the correct overdamped limit. All flow lines are actual numerical solutions of the RG equations. *Permission to reuse granted under the terms of the Creative Commons Attribution License CC BY 4.0*

the actual mode-coupling effective constant in the perturbative expansion is no longer f, but rather

$$q = \frac{\tilde{\lambda}^{\|}}{\lambda^{\|}} \frac{g^2}{\eta\Gamma} K_d \Lambda^{d-2} \tag{10.130}$$

whose scaling dimension in proportional to $2 - d$, suggesting that mode-coupling is relevant only below 2 dimensions, and not 4, when dissipation is present. The upper critical dimension of the field theory however remains $d_c = 4$, since both c_v and $\tilde{u}$ still become relevant below 4 dimensions. The physical reason behind this change of dimension at which mode-coupling is relevant is the fact that the spin
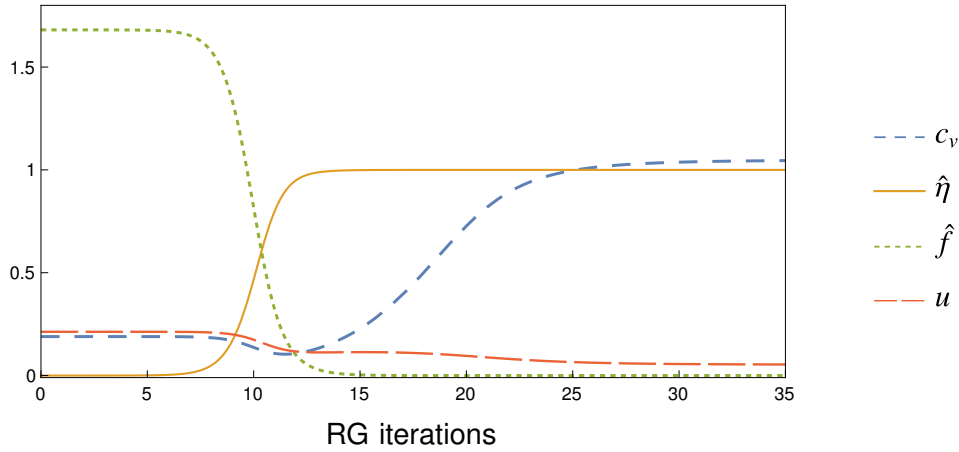
Figure 10.4. RG flow in the presence of dissipation [MyPaper1]: I show the RG flow of the couplings c_v, $\hat{\eta}$, $\hat{f} = (1 - \hat{\eta}) f$ and $\tilde{u}$ from the conservative active fixed point towards the dissipative active fixed point. Note that the coupling $\hat{f}$ interpolates between f and q, as the parameter η runs from 0 to ∞. From the plot, one can see that as dissipation increases, c_v and $\tilde{u}$ flow to the fixed point values of [23]. *Permission to reuse granted under the terms of the Creative Commons Attribution License CC BY 4.0*

becomes a *fast mode*. When $\eta \neq 0$, the finite relaxation time for the spin η^{-1} will become, close to criticality, much smaller than the velocity relaxation time $\tau = \xi^z$. Hence, the effect of the spin on the order parameter becomes irrelevant, since its effect can be represented as noise. The presence of dissipation strongly modifies the asymptotic critical behaviour, since near criticality only the modes fluctuating on the same scales of the order parameter may affect universal quantities [40]. Therefore, when dissipation is present, the *asymptotic* critical dynamics in the large-size limit is unaffected by the presence of the spin-velocity coupling.

In this limit, where $\hat{\eta} = \breve{\eta} = 1$, the present theory should become equivalent to the overdamped incompressible theory of [23]. In all perturbative corrections to the equation of motion of $\boldsymbol{\psi}$, the diagrams proportional to f are always also proportional to $(1 - \hat{\eta})$. This suggests the best choice of inertial coupling constant should be

$$\hat{f} = (1 - \hat{\eta})\, f\,. \tag{10.131}$$

This constant correctly interpolates between f when $\hat{\eta} = 0$ and q when $\hat{\eta} = 1$. When $\hat{f} = 0$, all these diagrams vanish, giving no contributions to the critical exponents. The velocity field $\boldsymbol{\psi}$ thus fully decouples from the spin $\boldsymbol{s}$ in the overdamped limit, making the behaviour of the fast mode $\boldsymbol{s}$ irrelevant in determining the universal quantities, so that for $\hat{\eta}, \breve{\eta} \to 1$, or equivalently for $\hat{f} \to 0$, I obtain,

$$\beta_{c_v} = \frac{1}{2}\, c_v \left(\epsilon - \frac{3}{4} c_v^2 - \frac{10}{3} \tilde{u} \right) \tag{10.132}$$

$$\beta_{\tilde{u}} = \tilde{u} \left(\epsilon - \frac{1}{2} c_v^2 - \frac{17}{2} \tilde{u} \right) \tag{10.133}$$

$$\beta_{\tilde{r}} = \tilde{r} \left(2 - \frac{c_v^2}{4} \right) + \frac{9}{2} \tilde{u} \tag{10.134}$$

$$\beta_{\hat{f}} = -2 \hat{f} \tag{10.135}$$

which are the same RG flow equations obtained by Chen, Toner and Lee in [23], analysed in Chapter 5. The stable fixed point of these flow equations is thus represented by [23]:

$$\tilde{u}^* = \frac{6}{113}\epsilon \qquad c_v^* = \sqrt{\frac{124}{133}}\epsilon \qquad \tilde{r}^* = -\frac{27}{226}\epsilon \qquad \hat{f}^* = 0 \,. \qquad (10.136)$$

Note that the coupling constant of activity used here, c_v, is the square root of that used in Chapter 5 and [23].

This prediction is confirmed also by the numerical integration of the full RG flow. As shown in Fig.10.4, $\hat{f}$ flows to 0 as expected, while the couplings c_v and $\tilde{u}$ approach the active overdamped fixed-point values of Self-Propelled Model A. As required by physical consistency, the overdamped limit of the theory is given by the non-inertial theory of [23]. Full RG flow, in terms of c_v, $\hat{f}$ and $\hat{\eta}$ is depicted in Fig. 10.3.

Finally, it is interesting to observe how, at this fixed point, $\hat{f}^* = 0$ while $f^* \neq 0$. This means that the coupling between the direction of motion and the spin remains finite along the RG flow, providing an interesting confirmation of the common belief that couplings with fast modes do not affect large-scale properties. Nevertheless, as I will argue in the next Chapter, this only holds when one is interested in the asymptotic large-size regime. At finite sizes, instead, the presence of a mode-coupling between order parameter and spin will be shown to play a crucial role in the collective behaviour of systems in which spin-dissipation is small, as in the case of swarms.

10.7   Conclusion

In the present Chapter, I presented the full RG calculation of the field theory of Self-Propelled Model G, developed to describe the collective behaviour of natural swarms of insects. In particular, I showed that a rich fixed-point structure emerges. In the absence of dissipation, $\hat{\eta} = 0$, in addition to the previously reported universality classes of equilibrium non-inertial Model A ($c_v = 0$, $\hat{f} = 0$), equilibrium inertial Model G ($c_v = 0$, $\hat{f} \neq 0$) and active non-inertial Self-Propelled Model A ($c_v \neq 0$, $\hat{f} = 0$), a new universality class emerges, described by a fixed point at which both activity and inertia are important features. Its stability, within the conservative plane, indicates that this is the fixed point ruling the large-scale behaviour of Self-Propelled Model G.

In the presence of spin dissipation $\hat{\eta} \neq 0$, the conservation of the total spin is violated and the system therefore does not belong anymore to the conservative plane. The RG relevance of the parameter $\hat{\eta}$ makes the conservative plane unstable to the presence of an arbitrary weak spin dissipation, and the RG flow therefore drives the system back to the Self-Propelled Model A universality class. This same mechanism has already been reported at equilibrium, where spin dissipation in Model G has been shown to lead to Model A university class [41]. This can be viewed as the consequence of the fact that, when spin dissipation is present, the spin ceases to be a hydrodynamic variable and can be therefore dropped from the large-scale description of the systems.

In the following chapter, I will address how this RG calculation can be applied to the case of natural swarms of insects. In particular, I will argue that the

Self-Propelled Model G dynamic universality class properly describes the dynamic collective behaviour observed in swarms, therefore suggesting universality might play an important role in the description of living systems.

Chapter 11

Collective behaviours near the swarms' fixed point

The renormalization group calculation performed in Chapter 10 allowed to organise the large-scale behaviour of Self-Propelled Model G in different *universality classes*, one for each fixed point that was found. In addition to several well-known universality classes, my results show the existence of a novel fixed point at which both activity and inertial behaviour are important. In the absence of explicit spin-dissipation, this new fixed point is found to be stable within the critical manifold. This finding suggests this is the fixed point ruling the collective properties of any near-critical active *and* inertial system. However, the presence of spin dissipation challenges the relevance of inertial effects, weakening the effects of the spin-velocity coupling at large scales.

The plans for the present Chapter are to characterise the *universal* collective properties exhibited by critical systems ruled by the active-inertial fixed point. To provide a quantitative assessment of experimental results, I will focus on the computation of the dynamic critical exponents z, which links the relaxation time-scale τ and the correlation length ξ through $\tau \sim \xi^z$, known as critical slowing down. Because this is the most robust prediction of an exponent in natural swarms, I will take it as the principal quantity to be compared in order to judge the suitableness of Self-Propelled Model G in describing swarms' behaviour. Estimations of other critical exponents are however also provided.

A second feature of the new active inertial fixed point which deserves attention is the exact conservation of the spin. Although in inertial systems such as Model G the spin is expected to be conserved [40], as I showed in Chapter 8 introducing incompressibility, namely a solenoidal constraint on the order parameter, may violate this exact conservation [MyPaper2]. This spin-conservation violation, which I remember does not give rise to any spin dissipation, arises at equilibrium as a consequence of the *artificial* introduction of the solenoidal constraint. Quite remarkably, the interaction which is responsible for this spin-conservation violation is found to be irrelevant near the active inertial fixed point, hence restoring effective spin-conservation at large scales.

Finally, to keep the present analysis as general as possible, I study what happens to systems with *small* spin dissipation. What I find is a crossover between inertial

behaviour at small scales and non-inertial behaviour at large scales, similar to that reported in [41]. As swarms have a finite size, this analysis suggests they would still exhibit active inertial collective behaviour even if some small spin-dissipation was present.

11.1   Scaling laws and their exponents

The proximity to a critical point is always characterised by the presence of scaling laws [50, 51], expressing the divergence of some thermodynamic or quantities or correlation functions as the critical point is approached. One of the best examples is the divergence of the correlation length of the system: when a given control parameter T, which depending on the system might be e.g. the temperature, the noise amplitude or the density, approaches its *critical* value T_c, the correlation length is known to diverge according to $\xi \sim |T - T_c|^{-\nu}$, with ν being a critical exponent. In the framework of the RG, each fixed point can be associated with a given set of exponents, which uniquely determine the behaviour in the proximity of the critical point. This feature is known as *universality*.

Among the exponents ruling the divergence of different quantities, one usually distinguishes between the so-called *static* exponents, which rule the divergence of equal-time observables, and the *dynamic* exponent. The latter provides an estimation of how *quickly* the systems decorrelates and is strictly entangled to the specific dynamic structure. It is common knowledge that many equilibrium systems sharing the same static universality class might have different dynamic exponents. This is because, at equilibrium, the static exponents are completely determined by the free energy, while the dynamical one further depends on the specific dynamic rules and conservation laws. Take Model A and Model B [40] for example: they both describe the behaviour of Ising spins, but the former has a relaxation dynamics with non-conserved magnetisation, while in the latter the total magnetisation is conserved. They both share the universality class of the Ising Model, described by the Landau-Ginzburg free energy. Their dynamic exponent is however different: Model A relaxes with $z \approx 2$, while Model B has $z \approx 4$ [40]. This leads to the common misconception that dynamic universality classes provide uniquely an *internal* subdivision of the larger static class.

I call this misconception because, despite it is often true, there are some cases where it is not. Remarkably, inertial behaviour *is* one of those cases. In the presence of inertia, the equilibrium reference model is indeed given by Models E/F/G, which have been extensively studied throughout this thesis. In the presence of inertial behaviour at equilibrium, the symmetries are so powerful that the dynamic critical exponent is $z = d/2$ *regardless* of the dimension of the order parameter, and event on what is the functional form of the free energy. In fact, despite their static universality being different, Model G and Solenoidal Model G both share this same exponent. It therefore appears to be clear that the dynamic exponent in an inertial system is less sensible to these differences than the static exponents.

11.1.1 The dynamical critical exponent

The spatiotemporal behaviour of a collective system is described by the two-point connected correlation function of the order parameter, $C(\boldsymbol{x}, t)$. In general, the correlation function encodes a very complicated relation between space and time and it depends on the set of parameters $\mathcal{P}$ defining the state of the system. In the case of critical systems, the parameters enter the correlation function only through the correlation length $\xi(\mathcal{P})$. This property is known as *dynamic scaling* [60, 61], and it states that the correlation function C, when expressed as a function of wave-vector and frequency, obeys the following scaling form,

$$C(\boldsymbol{k}, \omega; \mathcal{P}) = C_0(\boldsymbol{k}; \xi) \; F\left(\frac{\omega}{\omega_k(\mathcal{P})}, k\xi\right) \tag{11.1}$$

where $\xi = \xi(\mathcal{P})$ is the correlation length and where the static correlation function C_0 has in turn the scaling form,

$$C_0(k, \xi) = k^{2-\eta} F_0(k\xi) \tag{11.2}$$

while the characteristic frequency at scale k is given by,

$$\omega_k(\mathcal{P}) = k^z \Omega(k\xi(\mathcal{P})) \tag{11.3}$$

In the relations above, Ω, F_0 and F are well-behaved scaling functions, whose explicit form is not relevant for my purposes; η is the critical exponent for the static correlation function (normally called anomalous dimension of the order parameter [14]), which must *not* be confused with the dissipation. What dynamic scaling asserts is that the divergence of space correlations and time correlations are not independent near the critical point, but they are connected by the dynamic critical exponent z. To find the critical exponent z, following a standard procedure [1, 40] I require that the kinetic coefficient of the velocity field is not singular at the RG stable fixed point, namely,

$$\Gamma^* = O(1) \quad \rightarrow \quad \chi_\Gamma = 0 \tag{11.4}$$

By plugging $\chi_\Gamma = 0$ into Eq. (10.68), I find,

$$z = 2 - \delta\Gamma + \delta\Omega \tag{11.5}$$

Once the diagrammatic results for $\delta\Gamma$ and $\delta\Omega$ at $\hat{\eta} = \breve{\eta} = 0$ are plugged in the equation for z, one can obtain the following expression for the dynamic critical exponent,

$$z = 2 - \frac{3f(3w + 2x + 1)}{4(w + 1)(w + x)} - \frac{c_v^2}{4} + \frac{f(\theta^\perp - 1)(13w^2 + 12wx + 5x^2)}{12\theta^\perp(w + x)^3} - $$

$$- \frac{f(\theta^\| - 1)(13w^3 + w^2(4x + 75) + w(48x + 51) + 24x + 9)}{12(w + 1)^3(w + x)} - $$

$$- \frac{f(\theta^\| - 1)(\theta^\perp - 1)(13w^2 + 12wx + 5x^2)}{12\theta^\perp(w + x)^3} - \frac{f\theta^\| \Phi_1 x(3w + 2x)}{4(w + x)^3} - $$

$$- \frac{f\theta^\| \Phi_2 \left(9w^3 x + 2w^2 \left(4x^2 + 9x - 1\right) + wx \left(2x^2 + 16x + 3\right) + 2x^2(2x + 1)\right)}{12(w + 1)^2(w + x)^3}$$

$$\tag{11.6}$$

The value of z at any fixed point is then simply obtained by plugging into (11.6) the fixed point values of the parameters. At the active inertial fixed point discovered in Sec 10.5.1, this gives,

$$z = 2 - 0.65(2)\epsilon \tag{11.7}$$

For $d = 3$ ($\epsilon = 1$), I finally obtain the RG prediction for the dynamic critical exponents of the active inertial theory,

$$z = 1.34(8) \, . \tag{11.8}$$

The correction 0.65ϵ with respect to the free value $z = 2$ might seem large for a first-order term in a perturbative expansion, in particular when I set $\epsilon = 1$ in $d = 3$. However, comparing this result with the equilibrium non-inertial theory of Model A might be misleading. The new Self-Propelled Model G fixed point has been found by adding non-linear activity to Model G [40], which has a *non-perturbative* dynamic critical exponent $z = \frac{d}{2} = 2 - \frac{\epsilon}{2}$ [107]. Thus, the present result should be considered as a 0.15ϵ departure from Model G's non-perturbative exponent, rather than a 0.65ϵ correction to Model A. To compare this result with previous ones in a similar context, Self-Propelled Model A (Toner and Tu theory) has a dynamic critical exponent of $z = 2 - 0.27\epsilon$ [23], with a perturbative departure of 0.27ϵ from equilibrium Model A's exponent, which is its natural expansion point. This makes the active inertial dynamic exponent closer to its reference value compared to the active non-inertial exponent.

Note that both exponents are obtained by working in a first-order approximation in ϵ. In principle, although first-order results almost always give qualitative insights on the exponents of a system, they often still fail to provide quantitative agreement with the measured exponents in $d = 3$, namely when $\epsilon = 1$. Nevertheless, in the active fixed points I study here, both inertial and non-inertial, the agreement with numerical simulations is surprising. Concerning non-inertial dynamics, when setting $\epsilon = 1$ the one-loop analysis of Self-Propelled Model A predicts an exponent $z = 1.73$. Numerical simulations of Vicsek model in $d = 3$ found a dynamic exponent of $z \simeq 1.7$ [69], showing that the dynamic exponent found in [23] holds with remarkable accuracy also in $d = 3$, namely when $\epsilon = 1$. Similarly, simulations of the Inertial Spin Model [102], near criticality and at low values of spin dissipation [MyPaper1], have found a numerical dynamic exponent of

$$z_{\text{num}} = 1.35 \pm 0.04 \, , \tag{11.9}$$

in remarkable agreement with the RG theoretical prediction. Note that neither the simulations in [69] nor those of [MyPaper1] imposed incompressibility. This gives additional support to the idea expressed in Chapter 6 that the incompressible theory can indeed be used to describe finite-size compressible systems, as long as density fluctuations are not strong.

Finally, I am ready to check whether Self-Propelled Model G accurately describes the dynamic behaviours of natural swarms of midges in the field. To this day, the most reliable estimation of the dynamic exponent of swarms is [MyPaper1]

$$z_{\text{exp}} = 1.37 \pm 0.11 \, , \tag{11.10}$$

Contrary to the first estimations provided by [13], this new estimation relies not only on a larger swarm data set, counting swarms with up to 800 midges, but also on a more suitable method to perform the linear regression of $\ln \tau$ vs $\ln \xi$. In [13] z was fitted through a standard Least Squares regression, which gave $z_{\mathrm{exp}} = 1.12 \pm 0.16$ on the dataset of [13], and $z_{\mathrm{exp}} = 1.16 \pm 0.12$ on the larger dataset of [MyPaper1]; the problem with Least Squares, though, is that it assumes that experimental uncertainty is only present in the dependent variable y, which is not true for experimental data on swarms, as both τ and ξ are subject to experimental uncertainty; when using it on a dataset where the error affects also x, Least Squares systematically underestimate the slope [117]. Therefore, Least Squares is not a good method in this case. Reduced Major Axis regression, on the other hand, is a method that works under the hypothesis that both x and y are affected by uncertainties [63, 64]. Hence, a value of z fitted through a Reduced Major Axis regression appears to be more reliable than one obtained through a Least Squares regression.

In conclusion, because the value of z obtained from my RG calculation is in remarkable agreement with experiments on natural swarms *and* numerical simulations of an active inertial system, I can confidently claim Self-Propelled Model G correctly describes the dynamic universality class of natural swarms of insects.

11.1.2 Static critical exponents

In the present section, I will derive some of the static critical exponents relative to the active inertial fixed point found in the previous Chapter. Before proceeding, however, an important caveat is in order. The present RG calculation was performed by imposing a solenoidal constraint on the primary field, $\nabla \cdot \boldsymbol{\psi} = 0$, to enforce incompressibility. In non-active equilibrium systems, the presence of the solenoidal constraint is known to change the *static* universality class [87, 86], while leaving unchanged the *dynamic* universality class [MyPaper2]; this means that an equilibrium RG calculation with solenoidal constraint would find the same dynamic critical exponent z as a simulation without solenoidal constraint, but would fail to reproduce the static critical exponents of that same simulation. It is not known how this scenario generalises to the active off-equilibrium case, but some caution is certainly required: although in active systems with mild density fluctuations incompressibility is a reasonable hypothesis to calculate the dynamic critical exponents, one must be careful about the static exponents, as there is no certainty that they must be the same as in system where the solenoidal constraint is not imposed, as in natural swarms or numerical simulations.

Critical exponent ν

The first exponent I shall compute is ν, which characterises the divergence of the correlation length as the transition is approached via

$$\xi \sim |T - T_c|^{-\nu} \ . \tag{11.11}$$

Here T is the control parameter (the temperature in the case of ferromagnetic equilibrium systems, or the nearest neighbour distance in the case of swarms [56])

and T_c its value at the critical point. This exponent can be computed from the runaway behaviour of the mass, namely from the mass β-function. Let me define,

$$y_m = \left.\frac{\partial \beta_m}{\partial m}\right|_{\mathcal{P}=\mathcal{P}^*} . \tag{11.12}$$

where $\mathcal{P}^*$ are the values of the parameters at the fixed point. Therefore, the RG flow of the mass near the critical fixed point will be given by

$$\dot{m} = y_m(m - m^*) . \tag{11.13}$$

This gives the following runaway from the critical point m^*

$$\delta m(l) \sim e^{y_m l} , \tag{11.14}$$

where l is the number of RG iterations.

To compute ν, one can remember that the correlation length scales as $\xi(l) \sim e^{-l}$. This allows one to derive the following relation between ν and y_m, which reads

$$\nu = \frac{1}{y_m} \simeq \frac{1}{2} + 0.248(0)\epsilon , \tag{11.15}$$

which in $d = 3$ yields,

$$\nu \simeq 0.748(0) . \tag{11.16}$$

Critical exponent η

The second exponent I shall compute here is anomalous dimension η (not to be confused with the spin dissipation), which defines how the (connected) correlation function of the order parameter ψ decays with space. In particular, near criticality the equal-time correlation function is expected to have a scaling form that behaves as

$$C(b\boldsymbol{x}) = b^{-2\chi_{\psi(r,t)}} C(\boldsymbol{x}) . \tag{11.17}$$

Here $\chi_{\psi(r,t)}$ is the scaling dimension of ψ in position and time space, which is often referred to as roughness exponent. In the standard literature of critical phenomena, the roughness exponent is usually expressed as

$$-2\chi_{\psi(r,t)} = 2 - d - \eta , \tag{11.18}$$

where η gives the deviation from the mean-field scaling exponent of $2 - d$. Positive (negative) values of η indicate that correlation decay faster (slower) compared to mean-field.

In principle, to compute the exponent η one should compute correlation functions at small distances, or equivalently at large $\boldsymbol{k}$ if working in Fourier space, and use equalities derived from the RG flow to determine the exponents. In some cases, as for the evaluation of z in the previous section, this can be avoided and alternative methods can be used. In the case of z, requiring that $\Gamma^* = \mathcal{O}(1)$ is a well-established and well-understood prescription, both in and out of equilibrium [112, 114, 40, 69], and it has been validated by countless simulations and experiments. To my knowledge, on the other hand, there is no standard validated prescription to fix χ_ψ.

Nevertheless, as all the effective coupling constants flow to a finite fixed-point value, it seems reasonable imagine that the amplitude of the fluctuations of the field is determined by the amplitudes of the noise terms. If this was true, as it happens in [23], one can compute η by requiring that, in addition to $\Gamma^* = O(1)$, also the noise strength is not singular at the stable fixed point, namely

$$\tilde{\Gamma}^* = O(1) \quad \rightarrow \quad \chi_{\tilde{\Gamma}} = 0 \tag{11.19}$$

By plugging $\chi_{\tilde{\Gamma}} = 0$ into Eq. (10.68) and using (11.5), I find

$$\eta = \delta\Gamma + \delta\Omega - \delta\tilde{\Gamma}\,. \tag{11.20}$$

By evaluating the perturbative corrections at the stable fixed point, I find that

$$\eta = -0.217(5)\epsilon\,, \tag{11.21}$$

which leads to the prediction of $\eta = -0.217(5)$ in $d = 3$.

To put this exponent into perspective, let me focus on how can we compare this exponent with the experimental results obtained in [56]. There, the authors looked at the scaling behaviour of the *integrated equal-time correlation function*, which they refer to as 'generalised susceptibility', naming it χ. It is important to stress that, despite the name, this is not a susceptibility, namely it doesn't describe the response of the system to external perturbations. It is rather a measure of the degree of correlation of the system.

In [56], it has been observe that χ scales with the size of the system L through a power law, $\chi \sim L^{\gamma/\nu}$, with $\gamma/\nu \simeq 2.57$. The choice of the name of the exponent is unfortunately ambiguous, as γ is usually the exponent associated with response functions, while χ is *not* a response function, but the integrated correlation function. Translating the definition of χ given in [56] in the field-theoretical formalisms used here, its expression in terms of $C(\boldsymbol{x})$ can be written as

$$\chi = \int_{\Lambda^{-1}}^{\xi} d^d x\, C(\boldsymbol{x})\,. \tag{11.22}$$

Thus, this variable χ is expected to scale as

$$\chi \sim \xi^{2-\eta}\,. \tag{11.23}$$

It might have become now clear why the choice of calling this exponent γ/ν in [56] is misleading. While in equilibrium systems it is true that $\gamma/\nu = (2 - \eta)$, because of a well known hyper-scaling relation arising from the fluctuation dissipation theorem, the same relation might not hold out of equilibrium. In fact, in the present case I will show later on that when γ is taken to be the exponent of the response function, then

$$\frac{\gamma}{\nu} \neq (2 - \eta)\,. \tag{11.24}$$

The exponent γ/ν computed in [56] should be compared with $2 - \eta$, which in $d = 3$ reads

$$2 - \eta = 2.217(5) \tag{11.25}$$

Although the matching is not exact, we can appreciate the shift of $2 - \eta$ towards the experimental value 2.57 compared to the mean-field value of 2.

Critical exponent γ

The third exponent I will compute, γ, characterises the response of the system to a small external field $\boldsymbol{H}$ coupled to the order parameter. Assuming linear response of $\boldsymbol{\psi}$ on $\boldsymbol{H}$, $\langle\boldsymbol{\psi}\rangle = \chi_H \boldsymbol{H}$, the exponent γ characterises the divergence of the susceptibility χ_H in the proximity to the phase transition,

$$\chi_H \sim |T - T_c|^{-\gamma} \tag{11.26}$$

where T is the control parameter. Since $\chi_H = \frac{\partial\langle\boldsymbol{\psi}\rangle}{\partial H}$, the exponent γ will be given by,

$$\gamma = \nu\left(-\chi_{\psi(r,t)} + y_H\right), \tag{11.27}$$

where $\chi_{\psi(r,t)}$ is the scaling dimension of $\boldsymbol{\psi}$ in position and time space, and y_H is the scaling dimension of the field $\boldsymbol{H}$. It is crucial here, to compute these exponents up to one loop, to notice that no one loop graphical corrections to such a field term appear in the calculation. The absence of graphical correction to $\boldsymbol{H}$ at one loop, namely the absence of diagrams with only one external field $\hat{\psi}$, implies that y_H can be determined only by power counting, as happens in [23]. To determinate y_H, let me recall how $\boldsymbol{H}$ would enter the equation of motion for $\boldsymbol{\psi}$: $\partial_t\psi \sim \boldsymbol{H}$, hence leading to $y_H = z + \chi_{\psi(r,t)} + \mathcal{O}\left(\epsilon^2\right)$. At first order in ϵ, the exponent γ is thus given by,

$$\gamma = \nu z \simeq 1 + 0.171\epsilon, \tag{11.28}$$

which in $d = 3$ becomes

$$\gamma \simeq 1.171. \tag{11.29}$$

Let me remark, once again, that this exponent *does not* quantify the divergence of the space integral of the connected correlation function, as it would be the case for equilibrium systems because the fluctuation-dissipation relation linking the susceptibility χ_H to the correlation function loses its validity when the system is out-of-equilibrium. This is precisely the case here, where one can directly check that

$$\gamma \neq \nu(2 - \eta) \tag{11.30}$$

11.2 Off-equilibrium activity restores the conservation of the spin

One of the most intriguing features of the novel active inertial fixed point is the vanishing of the DYS vertex effective coupling constant, namely $\tilde{u}_\kappa^* = 0$. At equilibrium, the presence of the DYS vertex, with $\tilde{u}_\kappa = \tilde{u}$, had such a crucial role in keeping the dynamics of $\boldsymbol{s}$ consistent with the solenoidal constraint on $\boldsymbol{\psi}$ [MyPaper2] that it seems surprising to find that this vertex disappears when the system is the off-equilibrium active phase. Moreover, the couplings $\tilde{u}$ and $\tilde{u}_\kappa$ both derive from derivatives of the $u\psi^4$ term in the free energy functional $\mathcal{H}$, and thus one would expect a deep connection between the two. However, the fact that the DYS vertex vanishes at this novel fixed point avoids the odd scenario of having two different ferromagnetic couplings; both at equilibrium and off-equilibrium, the RG suggests

that only *one* ferromagnetic coupling should exist, by requiring in the former case that $\tilde{u} = \tilde{u}_\kappa$ and in the latter $\tilde{u}_\kappa = 0$.

But by far the most surprising consequence of the off-equilibrium vanishing of the DYS vertex is that when $\tilde{u}_\kappa = 0$ (and when the dissipation $\eta = 0$) the global spin turns out to be conserved. As mentioned in Section(9.3.3) and discussed in [MyPaper2], the DYS vertex is the only interaction that contributes to the dynamics of the spin at $k = 0$, thus violating the spin conservation (although it does not violate it strongly, e.g. through dissipation). Since $\tilde{u}_\kappa$ is the effective coupling associated with the DYS interaction, the fact that it vanishes means that this vertex is irrelevant at the novel fixed point and thus the spin becomes globally conserved. The restored spin conservation in the active off-equilibrium case is surprising, and it can hardly be a mere accident of the RG calculation. To understand its meaning one has to go back to the underlying symmetry and conservation law in the theory.

At equilibrium, and in the absence of any constraint on the field, the presence of an exact rotational symmetry guarantees that the spin is globally conserved since it is the generator of the symmetry. This is exactly what happens in Model G, described in Chapter 7. When added, a solenoidal constraint breaks the rotational invariance: as it is clear from Fig.11.1-left, if one starts from a solenoidal configuration of the field and rotate each vector by the same constant amount, they obtain a new field configuration which violates the solenoidal constraint. At the field-theoretical level, this manifests itself by the RG generation of the DYS vertex discussed in Chapter 8, which indeed breaks the symmetry and conservation of the spin [MyPaper2]. This is what happens at equilibrium, namely in the non-active case.

According to the RG, when turning from the inactive solenoidal case to the active incompressible one, the presence of activity restores the full power of the rotation symmetry - at least on long wavelengths - by making the spin conserved once again. This suggests that - at variance with the inactive case - activity preserves incompressibility under local rotations. A qualitative cartoon of this mechanism can be seen in Fig.11.1-right: in the active case a local rotation generated by the spin has a twofold effect: *i)* it rotates the field (as in the inactive case); *ii)* it also rotates the positions, through the self-propelled part of the equations, $\dot{\vec{x}} = \vec{v}$ (at variance with the inactive case). These two rotations balance each other, giving rise to a new field configuration that is still solenoidal, i.e. incompressible (Fig.11.1-right). I stress that this is far from being a general mathematical proof, as it is restricted to the very simple case of a purely rotational field, while one would need to generalise this argument to a generic solution of the dynamical equations. It may be that the full proof of spin conservation in the case of active incompressible dynamics is the very RG calculation that I carried out here; even though one would hope for a simpler and more direct way to prove this result, I could not find it.

In fact, when one reflects on the whole RG flow, rather than restricting themselves to the fixed point, the situation becomes even more intriguing. As I wrote above, I found the new active incompressible inertial fixed point by starting close to the inactive (equilibrium) incompressible inertial fixed point. At the starting point, $\tilde{u}_\kappa^* \neq 0$, because - as I said - at equilibrium, the DYS vertex is required to enforce incompressibility; along with the flow which goes from equilibrium to off-equilibrium, the coupling $\tilde{u}_\kappa^*$ decreases weakly (see Fig.10.1) until it abruptly goes to zero right before arriving at the new fixed point. If one tried to start the flow with all
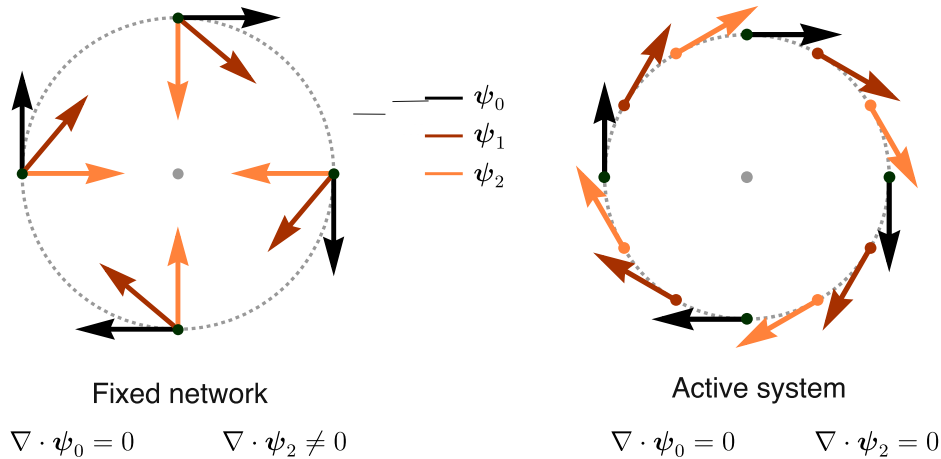
Figure 11.1. Incompressibility in the inactive vs. active case [MyPaper1]. Left: in the inactive case, if one starts from a solenoidal configuration of the field (ψ_0, black) and let a constant uniform spin rotate the field, they obtain a non-solenoidal configuration (ψ_2, orange). This is equivalent to saying that the solenoidal constraint breaks rotational invariance at equilibrium. Right: in the active case the particles are dragged by the field, hence the rotation generated by the spin rotates both the field *and* the position of the field, giving rise to a new configuration that is equally solenoidal (that is incompressible).

parameters close to their equilibrium values, but with $\tilde{u}_\kappa^* = 0$ from the outset, they would *not* reach the new off-equilibrium fixed point, and the RG flow would simply go bonkers. Hence, not only the symmetry-breaking coupling $\tilde{u}_\kappa^*$ is necessary *at* equilibrium, but it is also necessary to accompany the RG flow to the off-equilibrium fixed point; only there $\tilde{u}_\kappa^*$ is finally allowed to vanish. Clearly, this phenomenon deserves a deeper study.

11.3 The crossover from underdamped to overdamped dynamics

While the active inertial fixed point found in Chapter 10 is stable in the conservative manifold, a linear stability analysis clearly revealed its instability with respect to spin dissipation. In this latter case, the asymptotic stable fixed point was found to be given by the active non-inertial fixed point already discovered in [23]. This is no surprise since the presence of spin-dissipation makes the spin $\boldsymbol{s}$ a non-hydrodynamic mode, which is turn not expected to influence the critical behaviour.

Unstable fixed points can still play a crucial role in determining critical exponents for *finite-size* systems [41]. It often happens that for small enough sizes, the critical properties of a system are determined by the closest fixed point, rather than the fully stable one. As the size of the system is increased, a crossover between different regimes emerges, changing the critical properties of the system. What I am interested in here is understanding how *small* the system must be in order to observe the behaviour associated with the active inertial fixed point.

In general, I expect a finite-size system with small enough dissipation to initially behave as if it were inertial, and turn to the overdamped, non-inertial behaviour only when the large-size limit is approached. At the theoretical level, this crossover between a finite-size physics influenced by inertia, and an asymptotic non-inertial physics manifests itself as a crossover between different RG fixed points. Hence, following [41, 108], I will investigate the crossover between the underdamped dynamic behaviour, ruled by the novel active inertial fixed point with $z = 1.35$, and the dissipative incompressible theory with $z = 1.73$.

The starting point of this analysis is the observation that the ratio between dissipation η and conservative kinetic coefficient $\lambda^{\parallel}$ naturally defines, by simple power counting, a length-scale $\mathcal{R}$ given by [41, 108],

$$\mathcal{R} = \sqrt{\frac{\lambda^{\parallel}}{\eta}} \tag{11.31}$$

An alternative length-scale could be also $\sqrt{\lambda^{\perp}/\eta}$. However, it turns out this second length-scale has the same scaling behaviour as $\mathcal{R}$, hence it makes no difference what definition one uses.

The parameter $\mathcal{R}$ plays the role of a conservation length-scale, in the sense that fluctuations occurring on length-scales smaller than $\mathcal{R}$ obey a conservative dynamics, while beyond $\mathcal{R}$ fluctuations are insensitive to inertia and conservation laws. The scaling dimension of $\mathcal{R}$ is that of a length, but only at the naive (non-interacting) level; in fact, the RG coupling between the UV and IR degrees of freedom generates non-trivial modifications of naive scaling dimensions of $\lambda^{\parallel}$ and in principle also of η. The RG flow of $\mathcal{R}$ can be written – defining its scaling dimension $\chi_{\mathcal{R}}$ – as (see Eq. (10.97)),

$$\mathcal{R}_{l+1} = b^{\chi_{\mathcal{R}}} \, \mathcal{R}_l \, , \tag{11.32}$$

and from equations (11.31),(10.69) and (10.70) I obtain,

$$\chi_{\mathcal{R}} = \frac{1}{2}(\chi_{\lambda^{\parallel}} - \chi_{\eta}) = -1 + \frac{1}{2}\delta\lambda^{\parallel} \tag{11.33}$$

where -1 is the naive dimension of $\mathcal{R}$, which allowed one to naively identify it as a length-scale, while $\delta\lambda^{\parallel}$ the correction to the kinetic coefficient $\lambda^{\parallel}$.

I recall that η has no perturbative correction, $\delta\eta = 0$, due to the symmetry of the problem. The physical origin of this fact is that all diagrams contributing to the self-energy Π (which contains corrections to both η and $\lambda^{\parallel}$) vanish at $k = 0$ as a consequence of the form of the mode-coupling and the self-propulsion vertices for $\boldsymbol{s}$. This has been verified in the present calculation at first order in perturbation theory, where higher order effects of diagrams containing the DYS vertex on Π are not taken into account; however, if the result $\kappa^* = 0$ is exact to all orders, the DYS vertex is always irrelevant and thus no diagrams could ever generate dissipation. This is what I expect, as $\kappa^* = 0$ implies a global conservation of the spin (at $\eta = 0$), which does not seem like a perturbative accident (see Section 11.2). But even in the unlikely case in which the result $\kappa^* = 0$ were an accident of first-order perturbation theory, I prove here that the dissipation of the spin still can *never* receive any perturbative corrections. In general, the self-energy Π takes contributions only from the following

two distinct classes of diagrams,

$$\Pi = \quad \text{[diagram]} \quad + \quad \text{[diagram]} \tag{11.34}$$

where the blobs represent the renormalized mode-coupling and self-propulsion vertices respectively, in which all the possible diagrammatic corrections (at all orders in $\boldsymbol{k}$ and $\boldsymbol{q}$) are taken into account. Because the renormalized spin mode-coupling and self-propulsion vertices vanish at zero external momentum $\boldsymbol{k}$, these diagrams are zero at $k = 0$, implying that no dissipation is generated. Therefore, as long as the structure of the equations of motion (9.12) and (9.13) is preserved under the RG, no spin dissipation can be generated.

To work out the correction $\delta\lambda^{\parallel}$ I need a different argument. As I previously showed, the ratio $w = \Gamma/\lambda^{\parallel}$ is finite at the novel fixed point, $w^* = 3.95$ (equation (10.122)); moreover, the kinetic coefficient of the primary field is also finite at the fixed point, $\Gamma^* = O(1)$ (this is how one works out the dynamic exponent z), implying that also the kinetic coefficient of the spin is finite, $\lambda^{\parallel^*} = O(1)$, and thus that $\chi_{\lambda^{\parallel}} = 0$. From (10.68) I conclude,

$$\delta\lambda^{\parallel} = 2 - z \ . \tag{11.35}$$

From equations (11.33) and (11.35), one finally obtains the scaling dimension of $\mathcal{R}$ near the active conservative fixed point,

$$\chi_{\mathcal{R}} = -\frac{z}{2} \ . \tag{11.36}$$

where z is the dynamic exponent of the conservative inertial fixed point one is interested in. The fact that the scaling dimension of $\mathcal{R}$ is negative implies (through (11.32)) that it *decreases* along the RG flow, making the length-scale within which critical dynamics is underdamped shorter and shorter; this is another way to see that dissipation eventually takes over in the hydrodynamic limit. However, thanks to (11.36), I can now quantitatively describe the RG crossover from the conservative active fixed point to the dissipative one, or – more precisely – describe the departure of the RG flow from the conservative active fixed point when one starts close to it. Close to criticality, the correlation length scales as,

$$\xi_l = b^{-1}\xi_{l-1} = b^{-l}\xi_0 \ , \tag{11.37}$$

where ξ_0 is its physical value in the original system under study. The RG flow stops when the system is far from the critical manifold, namely when the correlation length becomes of the same size of the microscopic scale Λ^{-1}, giving $b^{l_{\text{stop}}} = \xi_0\Lambda$ [40, 1]. Let me consider a system with small bare dissipation, η_0, and therefore with a large conservation length-scale $\mathcal{R}_0$ (the subscript zero indicates the bare values of the parameter, namely the starting values of the RG flow or the parameters that are those of the equations of motion). The RG flow will rapidly approach the conservative fixed point, remaining in its neighbourhood for a large number of RG iterations and eventually flowing towards the dissipative fixed point [108]. Whether
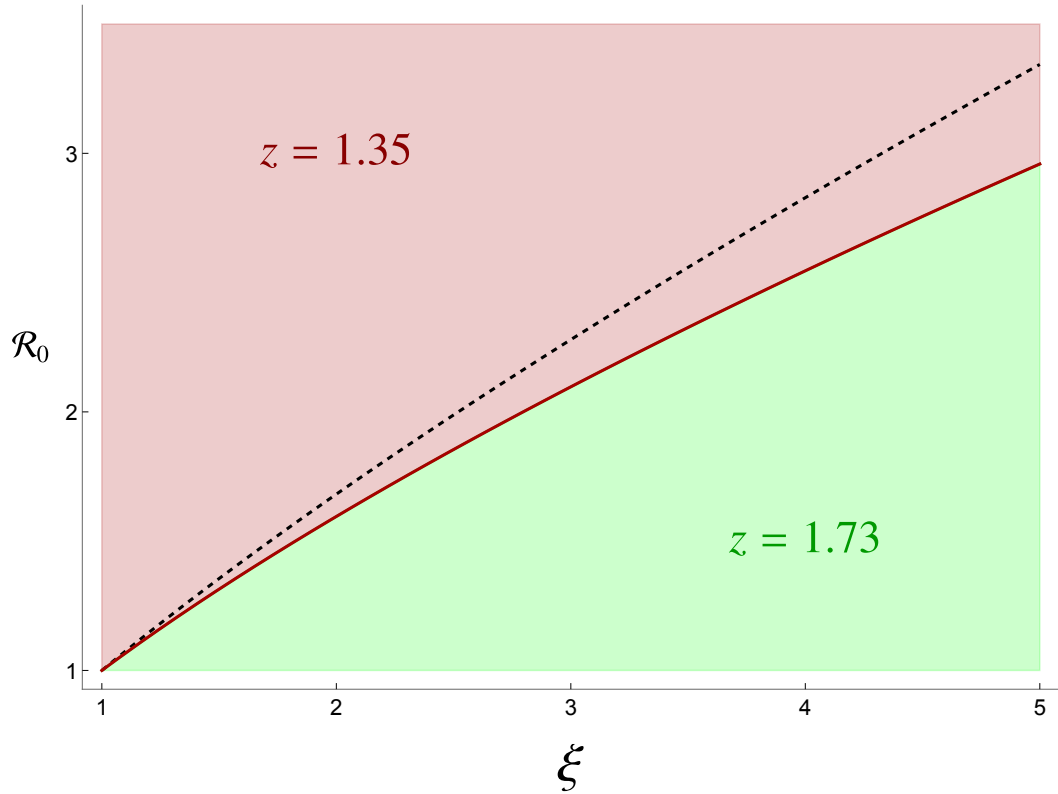
Figure 11.2. Crossover between different critical regions [MyPaper1]. Different values of $\mathcal{R}_0$ lead to different critical behaviour, depending on the correlation length ξ. I restrict myself to the physical range $\xi_0 > \Lambda^{-1}$, and measure lengths in units of Λ^{-1}. The figure refers to the $d = 3$ case. The dark red region is where dissipation is weak enough that conservative dynamics still hold, thus leading to $z = 1.35$: this is the underdamped regime. In the light green region, dissipation overcomes and an overdamped regime is achieved, where the dynamic behaviour is controlled by $z = 1.73$. The red line represents L_c, the threshold between the two behaviours in the active case. The black dashed line represents instead the threshold between underdamped and overdamped dynamics at equilibrium: since the underdamped region is lower here, I conclude that activity protects underdamped behaviour up to high scales.

the system is ruled by the conservative or dissipative fixed point depends on how large $\mathcal{R}_{l_{\text{stop}}}$ is when the RG flow leaves the critical region: if when the flow stops $\mathcal{R}_{l_{\text{stop}}} \gg \Lambda^{-1}$, the critical behaviour is ruled by the conservative fixed point; this is equivalent to the condition,

$$\mathcal{R}_0(b^{\chi_\mathcal{R}})^{l_{\text{stop}}} = \mathcal{R}_0(\xi_0\Lambda)^{\chi_\mathcal{R}} \gg \Lambda^{-1} \tag{11.38}$$

that is,

$$\xi_0 \ll (\mathcal{R}_0\Lambda)^{-\frac{1}{\chi_\mathcal{R}}}\Lambda^{-1} \ . \tag{11.39}$$

By using equation (11.36) and by measuring all lengths in units of the microscopic scale Λ^{-1} (which is equivalent to simply set $\Lambda = 1$ in all equations), one obtains the following condition for active underdamped dynamics,

$$\xi_0 \ll \mathcal{R}_0^{2/z} \ , \tag{11.40}$$

where $\kappa = 2/z$ is the so-called *crossover exponent*, which determines how slowly the dissipative dynamics becomes relevant. Beyond this regime, the overdamped fixed point with dynamic exponent 1.73 takes over. In Fig. 11.2 I show the regions corresponding to the two dynamical behaviours. In the case of finite-size systems as natural swarms, the size of the system L is a physical upper bound to the correlation length ξ_0. Therefore, if the dissipation η_0 is small enough to have $L \ll \mathcal{R}_0^{2/z}$, the ruling fixed point is the active inertial one. By recalling the definition of $\mathcal{R}$, equation (11.31), I get,

$$L \ll \left(\frac{\lambda_0^{\parallel}}{\eta_0} \right)^{1/z} \longrightarrow \quad z = 1.35 \ . \tag{11.41}$$

Because $\lambda_0^{\parallel}$ is always finite, the condition above can be finally rewritten as,

$$\eta_0 L^z \ll 1 \longrightarrow \quad z = 1.35 \ , \tag{11.42}$$

which clearly shows that the regime of the system (underdamped vs. overdamped) depends essentially on the balance between system size and spin dissipation.

A final remark is in order. From (11.41) one clearly sees that the smaller is z, the larger the system can be before crossing over to the dissipative fixed point. Since the new active inertial critical exponent, $z = 1.35$ is smaller than its equilibrium inertial counterpart, $z = 1.5$, this means that in the active off-equilibrium case, conservative dynamics rules the collective behaviour of the system up to larger scales compared to the equilibrium case (see Fig. (11.2)); this means that activity *protects* the conservative structure against dissipation, rather than thwarting it, which is quite remarkable.

11.4   Conclusions

In the present and previous two Chapters, I studied the near-ordering collective behaviour of Self-Propelled Model G, a field theory which combines activity and inertia. Through a one-loop renormalization group calculation, I was able to find a new RG fixed point ruling the large-scale behaviour of the theory. At this new fixed point, both the couplings controlling inertia and activity have a non-zero value, and the dynamic critical exponent is $z = 1.35$ in the physical case of three dimensions. Remarkably, this result is in very good agreement with the value measured in experiments on natural swarms of insects, $z_{\mathrm{exp}} = 1.37 \pm 0.11$ [MyPaper1], for which both activity and inertia were found to be important features (see Chapters 2 and 7). Symmetries and conservation laws, which are the only features on which the RG result relies, are therefore sufficient to provide a theoretical prediction of z which explains the experimental data. This calculation represents the first confirmation that universality, namely the independence of the collective behaviour from the microscopic details, applies also to active biological systems.

The active inertial fixed point of Self-Propelled Model G describes, in principle, systems that exhibit an exact conservation of the generator of the rotational symmetry of the order parameter (the spin). Because a weak dissipation of the spin cannot be ruled out *a priori* in swarms, I addressed its effects on collective behaviour. For infinite-size systems, I find that any spin dissipation makes inertia irrelevant on large

scales, therefore recovering the fixed point found by Chen, Toner and Lee [23], where $z = 1.73$ in three dimensions. However, for finite sizes, this is not necessarily the case: a crossover, similar to that reported in [41], occurs between an underdamped and an overdamped regime. Finite-size systems are described by the active inertial fixed point with $z = 1.35$, provided that spin-dissipation is small enough, while the non-inertial exponent of $z = 1.73$ is recovered at large size. As shown in Chapter 7, experiments show that swarms exhibit strong inertial behaviour over all scales, indicating that spin-dissipation, if present, must be weak, so that inertial behaviour is present over all scales. Therefore, swarms would in any case live in the underdamped regime, where $z = 1.35$. The result strengthens the applicability of the theoretical prediction attained here, extending its validity to finite-size systems with weak violations of the conversation of the spin.

The confirmation of the presence of universality in biological systems, provided in the present thesis, opens new research prospects and offers deeper connections between biology and physics. Natural swarms of midges might be just the first of many living systems whose collective behaviour can be characterised within a renormalization group approach. The case of flocks of birds, for example, is a paradigmatic example of collective behaviour in biology. In contrast to swarms, whose collective behaviours are described by the proximity to a critical point, flocks behave collectively because they spontaneously break a continuous symmetry [20]. Nevertheless, inertial behaviour has shown to be particularly relevant in describing their collective turns [100]. Therefore, possibilities are that Self-Propelled Model G might, in its spontaneously broken phase, describe also the collective behaviour of flocks in addition to those of swarms.

While in swarms activity is indeed strong, as the interaction network rearrangement occurs on the same time scales of alignment, in flocks these two time scales are well separated. Alignment of neighbouring birds thus occurs in a context of local equilibrium [65]. It would be therefore of great interest to compare the extent of activity in these two systems. To do this, entropy production is the quantity to watch out for. While entropy is always produced at the individual's scale, as a consequence of self-propelled motion, it might be not on the large scale. Using the tools of non-equilibrium statistical mechanics, it is possible to estimate the entropy production in an active field theory [118, 119] as Self-Propelled Model G, both in the swarming and in the flocking phase. A comparison between the two cases would help in understanding to what extent activity affects collective behaviour in flocks.

Chapter 12

Active Ising Models of flocking

Flocking, namely the coherent collective motion of a group of self-propelled particles, is an emergent phenomenon displayed by a wide variety of biological and soft-matter systems [27]. To achieve this behaviour, the presence of effective alignment interactions is required, hence creating many similarities between flocking and ferromagnetism. This precise analogy led Vicsek *et al.* to introduce in [42] a flocking model, which I discussed in Chapter 2, where the velocity of neighbouring individuals align as spins in ferromagnets.

Despite the similarity with ferromagnets, flocks are inherently active, and driven far from thermal equilibrium. Because of the presence of activity, under the form of self-propulsion, flocking models exhibit a richer phenomenology compared to ferromagnets. Although much recent research has addressed collective behaviour and phase transitions in flocking models, there are still many unanswered questions [18]. This is often related to the fact that these flocking models are quite hard to analyse from a theoretical point of view.

To help understand some of the aspects of the flocking transition, Solon and Tailleur introduced a simplified toy model, where flocking can emerge only along one privileged axis (the x-axis, say). This class of modes took the name of Active Ising Models [70, 71], as the discrete nature of the system, with motion occurring mainly along a privileged axis, resembles that of an equilibrium Ising model. Although *the* Active Ising Model was introduced with a specific choice of spin-alignment dynamics, in the present Chapter I will refer to any model in which velocities locally tend to align along a fixed axis as *an* Active Ising Model (or AIM).

Although direct numerical simulations of active matter models are often able to reveal many of their interesting features, it is only through field-theoretical approaches that their large-scale bulk behaviour can be investigated. To prove the ordering transition observed in the two-dimensional Vicsek model [42] was not some kind of finite-size effect, Toner and Tu studied a hydrodynamic theory describing a coarse-grained version of the Vicsek model. Only within this framework, they were able to show that activity breaks the precepts of the Mermin-Wagner-Hohenberg theorem, stabilising the ordered phase even in two dimensions [19, 20, 76]. Moreover, to give evidence that the phase transition from disorder to the ordered (flocked) phase is first-order also required hydrodynamic (or field-theoretical) descriptions [44, 36], [MyPaper3].

In the present Chapter, I study the behaviour of various AIMs through a field-theoretical approach. As in equilibrium, the main advantage of using field theory is that the collective behaviour of the system does not depend on the specific microscopic details, allowing a description of the large-scale properties in terms of interactions between coarse-grained fields. When this happens, once the hydrodynamic variables are identified, an expansion in small, slowly variating fluctuations is typically possible – either directly, or by re-expressing as an expansion in dimensionality via the renormalisation group (RG).

Below, starting from the Master Equation for AIM systems, I will derive a field theory through a coherent-state path-integral representation. This approach leads to what is known as the Doi-Peliti field theory of the system, which offers an exact mapping between the coefficients of the microscopic model and the bare couplings of a field-theoretic action. It not only enables standard field-theoretical approximations including RG, but also gives the exact deterministic hydrodynamic equations, together with their lowest order fluctuation corrections [16]. Using a field theoretical approach, I will present several new results, some in line with prior expectations based on less formal analyses, but some others contradicting such expectations. The research I will present in this Chapter was performed in collaboration with Dr Pausch and Prof Cates during a visiting period spent at the University of Cambridge between March and July 2022, and is now published in [MyPaper4].

12.1 Active Ising Models

An Active Ising Model (AIM) is a minimal description of a system in which individuals align their directions of motion. Contrary to the Vicsek model [42], where collective motion may occur in any possible direction in space, in an AIM, individuals prefer to move parallel to a given axis, which I identify without loss of generality as the x axis. The *state* of each particle is thus defined by its lattice position and a spin variable ± 1 that tells which direction $\pm \hat{x}$ it prefers to move in. The particles sit on a d-dimensional square lattice *without any occupation number constraint* and move through space by hopping onto neighbouring sites. In the x direction (only) the hopping rates are actively biased: particles with positive (negative) spin will hop preferentially towards more positive (negative) x values. In all directions other than x, particles undergo unbiased, diffusive hopping. Finally, imitative behaviour among individuals, effectively encoded in a ferromagnetic spin alignment interaction among particles on the same site, creates a tendency towards mutual alignment and hence collective motion [70, 71].

Thus an AIM represents a minimal, Ising-like model of flocking, with a discrete symmetry replacing the full rotational symmetry of the Vicsek model. Two crucial differences between an AIM and the equilibrium Ising Model must be kept in mind: *(i)* an AIM has no occupancy constraint on each lattice site, and *(ii)* the alignment interaction occurs only between same-site particles instead of between particles on nearest neighbour sites. The former means that particles are never blocked from hopping by excluded volume, allowing a simpler treatment of the bias. The latter choice is likewise made for simplicity in the hope that same-site interactions are

sufficient to describe emergent properties; in most cases one expects diffusion to mix particles enough that on-site and nearest-neighbour alignment interactions are equivalent.

The state of the k-th particle is defined by its position on the lattice $\boldsymbol{i}^{(k)} = \left(i_1^{(k)}, \ldots, i_d^{(k)}\right)$ and its spin $s_k = \pm 1$. The state of the whole system can then be identified via the number of $+1$ and -1 spin particles on each site $\boldsymbol{i}$, respectively $n_{\boldsymbol{i}}^+$ and $n_{\boldsymbol{i}}^-$, or equivalently via the local density $\rho_{\boldsymbol{i}} = n_{\boldsymbol{i}}^+ + n_{\boldsymbol{i}}^-$, and magnetisation $m_{\boldsymbol{i}} = n_{\boldsymbol{i}}^+ - n_{\boldsymbol{i}}^-$. With no occupational constraint, $\rho_{\boldsymbol{i}}$ has no upper bound, but the magnetisation $m_{\boldsymbol{i}}$ is bounded by $\rho_{\boldsymbol{i}}$, since $-\rho_{\boldsymbol{i}} \leq m_{\boldsymbol{i}} \leq \rho_{\boldsymbol{i}}$.

12.1.1 Description using reactions

Due to its on-lattice definition, the dynamics of an AIM can be described as a set of reactions between two particle species $A_{\boldsymbol{i}}$ and $B_{\boldsymbol{i}}$, representing respectively particles at site $\boldsymbol{i}$ having $+1$ and -1 spin. The model is completely defined once the following two processes are specified:

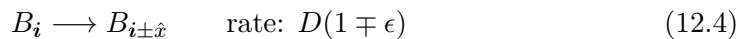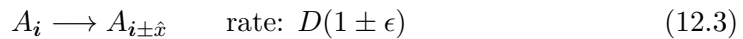*i)* how particles move in space, namely with what rates they undergo hopping reactions

$$A_{\boldsymbol{i}} \longrightarrow A_{\boldsymbol{j}} \qquad B_{\boldsymbol{i}} \longrightarrow B_{\boldsymbol{j}} \tag{12.1}$$
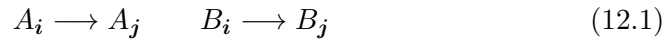
ii) how particles change direction, namely with what rate they undergo the spin-flip reactions

$$A_{\boldsymbol{i}} \longrightarrow B_{\boldsymbol{i}} \qquad B_{\boldsymbol{i}} \longrightarrow A_{\boldsymbol{i}} \tag{12.2}$$
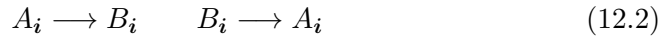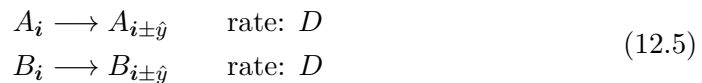
I will next address these processes separately.

Hopping

In an AIM, particles are assumed to hop with a fixed rate D in all spatial directions, except for the $\hat{x}$ direction where there is a preferred motion set by the spin variable. The biased hopping reactions in the $\hat{x}$ direction are therefore given by

$$A_{\boldsymbol{i}} \longrightarrow A_{\boldsymbol{i}\pm\hat{x}} \qquad \text{rate: } D(1 \pm \epsilon) \tag{12.3}$$
$$B_{\boldsymbol{i}} \longrightarrow B_{\boldsymbol{i}\pm\hat{x}} \qquad \text{rate: } D(1 \mp \epsilon) \tag{12.4}$$

In all other directions $\hat{y} \neq \hat{x}$ instead, the hopping is unbiased and hence

$$\begin{aligned} A_{\boldsymbol{i}} \longrightarrow A_{\boldsymbol{i}\pm\hat{y}} \qquad \text{rate: } D \\ B_{\boldsymbol{i}} \longrightarrow B_{\boldsymbol{i}\pm\hat{y}} \qquad \text{rate: } D \end{aligned} \tag{12.5}$$

Here the bias parameter $0 \leq \epsilon \leq 1$ quantifies self-propulsive activity. The hopping reactions are not influenced by the presence of other particles and hence are independent of particle concentration.
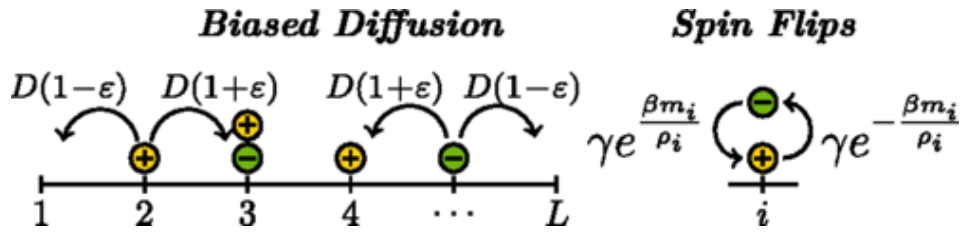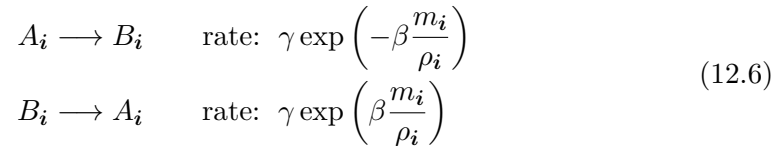
Figure 12.1. AIM0 hopping and spin-flipping processes [71]. Sketch of the two possible actions and their rates of occurrence. The ferromagnetic interaction between particles is purely on-site and particles diffuse freely. Beyond the biased diffusion shown here, particles also hop symmetrically in all other directions with equal rates D. *Permission to reuse granted by the American Physical Society under License Number RNP/23/OCT/071565.*

Spin-flipping

In this Chapter, I will address three different types of AIM (AIM0, AIM1 and AIM2, the latter with several sub-variants), which are distinguished by different choices of spin-flip reaction rates [MyPaper4].

AIM0: Original Ising flip rates

In the original formulation of the AIM, as introduced in [70], the rates for a spin-flipping event took inspiration from equilibrium dynamics of a fully-connected Ising model in the canonical ensemble. This means that, in the absence of any hopping, each *site* behaves as a fully-connected Ising model. In terms of reactions between A and B particles, this choice of rates leads to
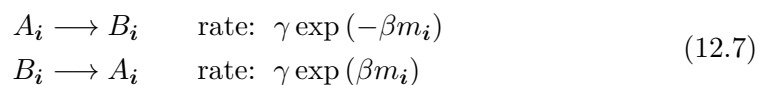
$$
\begin{aligned}
A_i &\longrightarrow B_i \qquad \text{rate: } \gamma \exp\left(-\beta \frac{m_i}{\rho_i}\right) \\
B_i &\longrightarrow A_i \qquad \text{rate: } \gamma \exp\left(\beta \frac{m_i}{\rho_i}\right)
\end{aligned}
\tag{12.6}
$$

which I shall refer to as AIM0. Here γ is the rate of particle flipping in the $m = 0$ case, while β plays the role of an inverse temperature. A schematic representation of the reactions of AIM0 is presented in Fig. 12.1.

This choice of flip rates is however unfeasible to implement in a Doi-Peliti framework: although it is possible to formally derive a field-theoretical action for this choice, I could not express it in terms of simple functions but only as an infinite series, as I will detail in the following. Given that the choice of rates in [70] is somewhat arbitrary, I am at liberty to make others for which the field theory is simpler.

AIM1: Alternative Ising-like flip rates

From a technical point of view, what makes it difficult to study the rates of (12.6) is the presence of the ρ_i in the denominator of the exponential argument. Hence, a choice of reactions which still mimics the equilibrium dynamics of Ising spins is given by [120]

$$
\begin{aligned}
A_i &\longrightarrow B_i \qquad \text{rate: } \gamma \exp\left(-\beta m_i\right) \\
B_i &\longrightarrow A_i \qquad \text{rate: } \gamma \exp\left(\beta m_i\right)
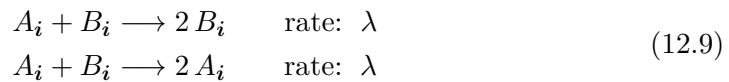\end{aligned}
\tag{12.7}
$$

I shall refer to this model as AIM1. The two sets of reactions (12.6) and (12.7) are expected to give qualitatively similar phase diagrams, but quantitative agreement is not expected. In particular, strong differences are expected to arise in the zero and infinite density limits, where the absence of normalisation of m_i by ρ_i might lead to drastic consequences. However, I will later show that, at finite densities, the behaviour near the ordering transition is extremely similar.

AIM2: Collisional flip rates In the context of off-equilibrium systems such as active matter, one has no particular reason to argue that the flip dynamics should mimic that of any equilibrium spin system. The rates that will be introduced here are inspired by the process of multiple-particle collisions, involving a finite and fixed number of particles (chosen at random from the same site), in contrast with the equilibrium-inspired rates, where all particles on the same site interact to set the rates. I consider the following three reaction processes:
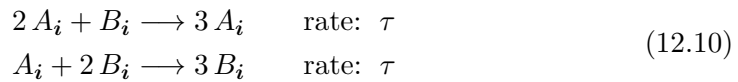
AIM2.1: One-body collisional flip rate

$$
\begin{aligned}
A_i &\longrightarrow B_i \qquad \text{rate: } \gamma \\
B_i &\longrightarrow A_i \qquad \text{rate: } \gamma
\end{aligned}
\tag{12.8}
$$

AIM2.2: Two-body collisional flip rate

$$
\begin{aligned}
A_i + B_i &\longrightarrow 2\,B_i \qquad \text{rate: } \lambda \\
A_i + B_i &\longrightarrow 2\,A_i \qquad \text{rate: } \lambda
\end{aligned}
\tag{12.9}
$$

AIM2.3: Three-body collisional flip rate

$$
\begin{aligned}
2\,A_i + B_i &\longrightarrow 3\,A_i \qquad \text{rate: } \tau \\
A_i + 2\,B_i &\longrightarrow 3\,B_i \qquad \text{rate: } \tau
\end{aligned}
\tag{12.10}
$$

The one-body collision (or random) spin-flipping AIM2.1 introduces a random error in the alignment process, not dissimilar to thermal noise. Not surprisingly, the rates in (12.8) are exactly equivalent to the infinite-temperature limit $\beta \to 0$ of both AIM0 (12.6) and AIM1 (12.7). It amounts to a random interconversion of A and B particles, and there is no phase transition.

On the other hand, the two-body (12.9) and three-body (12.10) collisional terms favour alignment. For both cases, in the absence of any additional random spin-flipping, the two fully ordered states (all A or all B particles) are absorbing states: once the system reaches them, it will remain there forever. One might therefore expect AIM2.2 and AIM2.3 to give rise to a phenomenology similar to the original AIM0, at least qualitatively, with spontaneous symmetry breaking leading to a strongly flocked state of positive or negative spins. However, in Sec. 12.4, I will show how this expectation fails for AIM2.2: the two-body flip reaction cannot create order in the presence of any random (one-body) spin-flipping rate, no matter how small. Therefore a three-body interaction (AIM2.3) will be needed below to get an ordering transition. With this term present, one can add back two- and one-body collisional flips without qualitatively altering the outcome; I use the inclusive nomenclature 'AIM2' for this most general case.
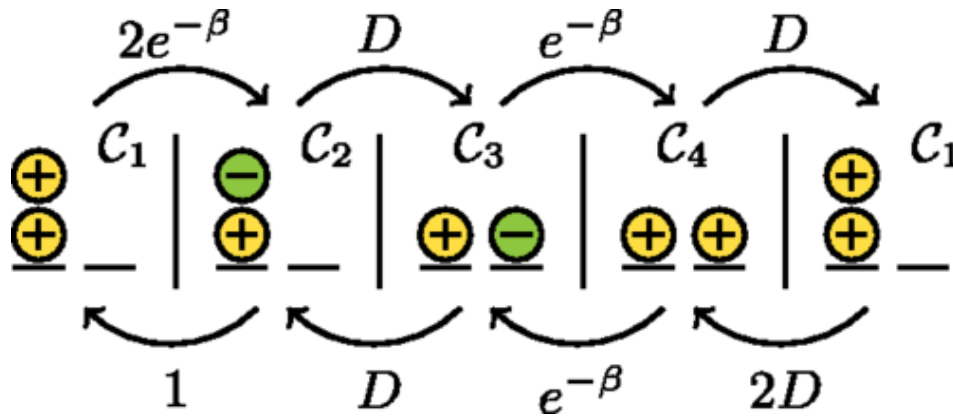
Figure 12.2. AIM0 violates detailed balance in absence of biased-diffusion [71]. A loop of four configurations involving two particles on two sites that breaks Kolmogorov's criterion [121], thus showing that the system does not satisfy detailed balance even when $\epsilon = 0$. The numbers associated with the arrows are the transition rates for $\epsilon = 0$. The product of the transition rates along $\mathcal{C}_1 \to \mathcal{C}_2 \to \mathcal{C}_3 \to \mathcal{C}_4 \to \mathcal{C}_1$ (left to right) is $2\,D^2\mathrm{e}^{-2\beta}$, whereas the reverse order (right to left) yields $2\,D^2\mathrm{e}^{-\beta}$. *Permission to reuse granted by the American Physical Society under License Number RNP/23/OCT/071565.*

12.1.2 Phase diagram of the AIM0

To understand what features an AIM is expected to exhibit, I will start here by reviewing the main features of the phase diagram of the AIM0, with the spin-flipping rates originally introduced and studied in [70, 71]. The phase diagram of the AIM0 has been characterised as the bias diffusion parameters ϵ, the inverse effective temperature β and the average density ρ_0 were changed. At low temperatures $T = \beta^{-1}$ and high densities ρ_0 a homogeneous ordered liquid phase has been observed, while at high temperatures and low densities, the system is found in a homogeneous disordered gas phase. Whenever $\epsilon \neq 0$, the two phases are separated by a region of phase-coexistence, in which dense ordered bands move on a low-density disordered background. Hence, the transition between the two homogeneous phases has been claimed to look like a liquid-gas transition [71]. The phase diagram of the AIM0 is shown in Fig. 12.3.

Interestingly, the width of the region of phase-coexistence vanishes as $\epsilon \to 0$, with the transition between the liquid and gas phases becoming continuous. This might seem not too surprising: when $\epsilon = 0$ the dynamics in space is purely diffusive, and no *active* processes seem to be in place. Moreover, at $\epsilon = 0$ spin alignment does not generate any collective motion, as the spin state does not influence how the particle moves in space and particles stop being self-propelled. However, the hopping and spin-flip rules do not obey detailed balance even in this propulsion-free limit [71]. In Fig. 12.2 an example of a loop violating Kolmogorov's criterion [121] for the AIM0 is provided. It is possible to construct different AIM variants in which detailed balance is recovered in the limit $\epsilon \to 0$[71, 122], but I will not address these variants here. Numerical simulations on the AIM performed in [71] showed that while the system is out-of-equilibrium, in $2d$ the phase transition falls in the Ising universality class, suggesting that the violation of detailed balance is not sufficient
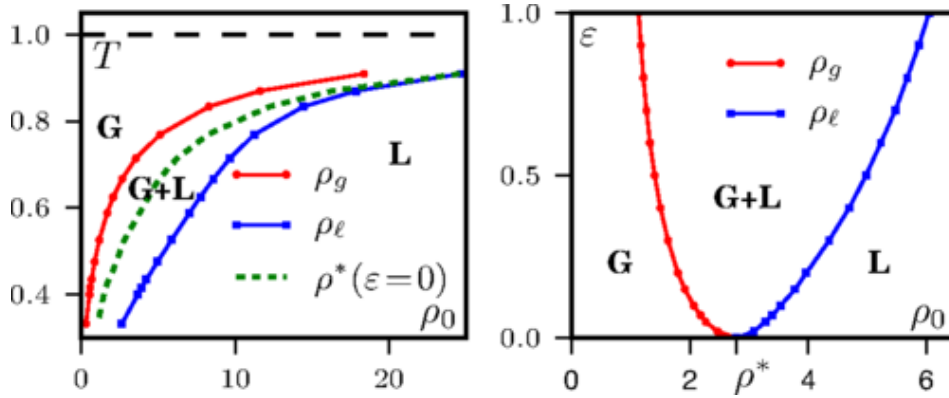
Figure 12.3. Phase diagram of the AIM [71]. The red and blue lines delimit the region of existence of phase-separated profiles (G+L) between the disordered gas phase (G) and the ordered liquid phase (L). On the left, it is shown the phase diagram at fixed $\epsilon = 0.9$, $D = 1$, $\gamma = 1$, as a function of ρ_0 and $T = \beta^{-1}$. The green dashed line corresponds to the case $\epsilon = 0$, in which the red and blue lines collapse onto one single line. On the right, the phase diagram at fixed $\beta = 1.9$, $D = 1$, $\gamma = 1$. *Permission to reuse granted by the American Physical Society under License Number RNP/23 OCT 071565.*

to perturb the long-scale behaviour of the system. Moreover, it was conjectured that the universality class of unbiased AIMs might have been that of Model C in Halperin and Hohenberg classification [40]. The reason this was conjectured is that Model C describes systems in which the order parameter (the local magnetisation) is coupled to a conserved diffusive quantity (the density). I will address the issue of the universality class of AIMs later on, showing that non-equilibrium effects prevent the critical behaviour from being described by the Model C universality class.

12.1.3 Master Equation for AIMs

Having specified the hopping and flip rates, the behaviour of the model can be studied via a Master Equation

$$\partial_t P = \mathcal{L}\,[P] \tag{12.11}$$

for the probability distribution $P(\boldsymbol{n}^+, \boldsymbol{n}^-; t)$ in configuration space. Crucially, the operator $\mathcal{L}$ is linear in the probability distribution P, and therefore each different process gives an independent contribution to $\mathcal{L}$:

$$\mathcal{L}\,[P] = \mathcal{L}_{\text{hop}}\,[P] + \mathcal{L}_{\text{flip}}\,[P]\,, \tag{12.12}$$

where $\mathcal{L}_{\text{hop}}$ is the contribution coming from the hopping processes, while $\mathcal{L}_{\text{flip}}$ that of the alignment processes. It is convenient to further split $\mathcal{L}_{\text{hop}}$ in two:

$$\mathcal{L}_{\text{hop}} = \mathcal{L}_D\,[P] + \mathcal{L}_\epsilon\,[P]\,. \tag{12.13}$$

Here $\mathcal{L}_D$ arises from the unbiased hopping dynamics while $\mathcal{L}_\epsilon$ takes into account the hopping bias and is linear in the bias parameter ϵ. The contribution $\mathcal{L}_D$ is therefore what remains after the limit $\epsilon \to 0$ is taken, and is expected to give rise to standard diffusive dynamic, while directed motion is contained in $\mathcal{L}_\epsilon$.

In the cases of AIM2, the alignment contribution can be also further written as $\mathcal{L}_{\text{flip}} = \mathcal{L}_\gamma + \mathcal{L}_\lambda + \mathcal{L}_\tau$, with terms stemming from reaction (12.8), (12.9) and (12.10) respectively.

12.2 The Doi-Peliti field theory

When dealing with reaction-diffusion processes, the Master Equation can be *exactly* represented by a field-theoretic action, constructed through a coherent-state path integral representation of the evolution operator $\mathcal{L}$, following the second-quantisation formalism introduced by Doi [80, 81] and Peliti [82]. Although originally introduced to describe reaction-diffusion systems, it has recently started being used to study active matter systems as well [123, 124]. For a pedagogical review of Doi-Peliti formalism, which is beyond the scope of the present work, I shall refer the reader to [16, 125]. I will however quickly review, for the benefit of the reader, the main features of this approach.

12.2.1 Building the action

Consider the Master Equation of a given microscopic model, written in the form

$$\partial_t P(\boldsymbol{n}, t) = \mathcal{L}\left[P(\boldsymbol{n}, t)\right] . \tag{12.14}$$

Here $\mathcal{L}$ is a linear operator acting on $P(\boldsymbol{n}, t)$ in which $\boldsymbol{n}$ specifies a micro-state at time t. (That is, $\boldsymbol{n}$ lists the occupancies of each type of particle at every site in the system.)

Second-quantisation formalism

The first step is to define a second-quantised Fock space representation: for a single site and particle type I will call $|n\rangle$ the state in which n particles are present. More generally, one has a Fock state $|n_1, n_2, n_3, \ldots\rangle = |\boldsymbol{n}\rangle$. The state of the system at time t, represented by the probability generating function, can be written as a superposition in Fock space as

$$|\psi(t)\rangle = \sum_{\boldsymbol{n}} P(\boldsymbol{n}, t)|\boldsymbol{n}\rangle . \tag{12.15}$$

On this Fock space, one can furthermore define a bosonic ladder operator algebra, with a creation operator $a^\dagger$ and annihilation operator a that act on the system in the following way

$$a_i^\dagger|n_i\rangle = |n_i + 1\rangle \qquad a_i|n_i\rangle = n_i|n_i - 1\rangle . \tag{12.16}$$

Note that this normalisation convention differs from that usually introduced in many-body quantum systems. However, the usual commutation relations still hold

$$\left[a_i, a_j\right] = \left[a_i^\dagger, a_j^\dagger\right] = 0 \qquad \left[a_i, a_j^\dagger\right] = \delta_{ij} . \tag{12.17}$$

In this new notation, one can express $|\psi(t)\rangle$ as

$$|\psi(t)\rangle = \sum_{\boldsymbol{n}} P(\boldsymbol{n}, t) \prod_i \left(a_i^\dagger\right)^{n_i} |0\rangle , \tag{12.18}$$

where $|0\rangle$ is the vacuum state, where no particles are present.

Master equations as an imaginary-time Schrödinger equation

The Master Equation is then written in a second-quantisation formalism, such that the *state* of the system $|\psi(t)\rangle$ – namely the probability generating function – evolves via an imaginary-time Schrödinger equation with an evolution operator $\hat{H}$ derived from $\mathcal{L}$. The evolution of $|\psi(t)\rangle$ is thus described by

$$\partial_t |\psi(t)\rangle = -\hat{H} |\psi(t)\rangle. \tag{12.19}$$

Given $\mathcal{L}$ in (12.14), an explicit expression of the operator $\hat{H}$ in (12.19) can be explicitly constructed from it by using the relation between $|\psi\rangle$ and P provided in Eq. (12.18).

The coherent-state path integral representation

From this imaginary-time Schrödinger equation, a field theory can be derived through a coherent-state path integral representation. The coherent states, defined as the eigenstates of the creation and annihilation operators, are given by

$$|\boldsymbol{\phi}\rangle = \left(\prod_i e^{\phi_i a_i^\dagger} \right) |0\rangle \qquad\qquad \langle \boldsymbol{\phi}^* | = \langle 0 | \left(\prod_i e^{\phi_i^* a_i} \right) \tag{12.20}$$

Note that, in this representation, for each particle species, two fields are introduced, ϕ and ϕ^*, representing the eigenvalues of the annihilation and creation operators respectively. Therefore, ϕ and ϕ^* will be referred to as annihilation and creation fields.

The field-theoretical action S for these fields is obtained by computing the matrix elements of $\hat{H}$ in the basis of the coherent states, of which the fields are the associated eigenvalues. The action of the Doi-Peliti field theory is therefore given by

$$\mathcal{S} = \sum_i \int \mathrm{d}t\, \phi_i^*(t) \partial_t \phi_i(t) + \int \mathrm{d}t\, \frac{\langle \boldsymbol{\phi}^*(t)| \hat{H} |\boldsymbol{\phi}(t)\rangle}{\langle \boldsymbol{\phi}^*(t)|\boldsymbol{\phi}(t)\rangle} \tag{12.21}$$

The last step to get an explicit form for the Doi-Peliti action is to compute the second term of (12.21), and in particular the numerator $\langle \boldsymbol{\phi}^*(t)| \hat{H} |\boldsymbol{\phi}(t)\rangle$. This is straightforward if $\hat{H}$ is normal-ordered, but might become a more complicated task when it is not. Operationally, one therefore first writes $\hat{H}$ in normal ordered form and then replaces annihilation and creation operators with their corresponding fields. If difficulties arise, one can revert to finding the normal ordered form directly by computing $\langle \boldsymbol{\phi}^*(t)| \hat{H} |\boldsymbol{\phi}(t)\rangle$, bearing in mind that

$$e^{\phi_i a_i^\dagger} = \sum_l \frac{(\phi_i)^l}{l!} \left(a_i^\dagger \right)^n \qquad\qquad e^{\phi_i^* a_i} = \sum_l \frac{(\phi_i^*)^l}{l!} \left(a_i \right)^n \tag{12.22}$$

Doi shift

The evolution operator $\mathcal{L}$ in Eq. (12.14) must satisfy a basic condition: it must keep the probability distribution P normalised to unity. The fulfilment of this requirement implies that the second-quantised evolution operator $\hat{H}$ vanishes when all creation

operators are set equal to unity, $a_i^\dagger \to 1$ [125]. This property is reflected in the fact that the action $\mathcal{S}$ vanishes when all creation fields are set to unity, $\phi^* \to 1$. It is therefore often convenient to perform what is known as a Doi shift, namely shifting the creation field according to:

$$\tilde{\phi} = \phi^* - 1 \,. \tag{12.23}$$

12.2.2 Building the operators

The main drawback of the Doi-Peliti formalism is that the fields it describes are of difficult physical interpretation. In fact, not only does the evolution operator have to be written in a second-quantised formalism, but so do the observables of the theory. For simplicity, let me consider a model with a single species of particles on a lattice. The number of particles on a given site i can then be expressed as $n_i = a_i^\dagger a_i$, where $a^\dagger$ and a are creation and annihilation operators. Say we wanted to compute the expectation value of some observable containing products of n_i at different sites and times. The rule to construct the corresponding field-theoretical operator is very similar to that needed to build the action. First, particle numbers are written in terms of creation and annihilation operators, then such operators have to be normal-ordered, and then operators are substituted by fields. A simplifying feature of the Doi-Peliti theory is that any creation operators appearing at the last of the chosen times can then be dropped. The underlying reason is causality: the event of a particle *created* after all the measurements should not affect the averages one is computing.

Accordingly, the field-theoretical operator whose average is equal to the expected value of n_i at time t is constructed as follows:

$$n_i(t) \to a_i^\dagger(t) a_i(t) \to \phi_i(t) \,, \tag{12.24}$$

with ϕ the annihilation field. (The creation operator at time t can be dropped as stated above.) Therefore, the following relation for the expected value of n holds

$$\mathbb{E}\left[n_i(t)\right] = \langle \phi_i(t) \rangle \tag{12.25}$$

where we denote with $\mathbb{E}\left[\cdot\right]$ expected values for the microscopic stochastic process, while $\langle \cdot \rangle$ indicates the average over the field-theoretic measure, namely

$$\langle O \rangle = \frac{1}{\mathcal{Z}} \int \mathcal{D}\phi \int \mathcal{D}\phi^* \, O \, e^{-S[\phi, \phi^*]} \tag{12.26}$$

Here S is the field-theoretic action, while the factor $\mathcal{Z}$ ensures the correct normalisation $\langle 1 \rangle = 1$. This case is simple, but more complicated operators are not always so intuitive. For example, to compute the correlation between n_i at time t and n_j at time $t' < t$, one has to compute the field-theoretical average of

$$n_i(t) n_j(t') \to a_i^\dagger(t) a_j^\dagger(t') a_i(t) a_j(t') \to \phi_i(t) \phi_j^*(t') \phi_j(t') \,, \tag{12.27}$$

where ϕ^* is the creation field. This is because the $a_i^\dagger$ operator, acting at time $t > t'$, can be dropped, while the $a_j^\dagger$ at time t' cannot, leading to

$$\mathbb{E}\left[n_i(t)\, n_j(t')\right] = \langle \phi_i(t) \phi_j^*(t') \phi_j(t') \rangle = \langle \phi_i(t) \tilde{\phi}_j(t') \phi_j(t') \rangle + \langle \phi_i(t) \phi_j(t') \rangle \tag{12.28}$$

Meanwhile, the equal time and equal position correlation obeys

$$\mathbb{E}\left[n_{\boldsymbol{i}}(t)^2\right] = \langle \phi_{\boldsymbol{i}}(t)^2 \rangle + \langle \phi_{\boldsymbol{i}}(t) \rangle \tag{12.29}$$

This follows from normal-ordering, whereby

$$n_{\boldsymbol{i}}^2 \rightarrow \left(a_{\boldsymbol{i}}^\dagger a_{\boldsymbol{i}}\right)^2 = a_{\boldsymbol{i}}^\dagger a_{\boldsymbol{i}}^\dagger a_{\boldsymbol{i}} a_{\boldsymbol{i}} + a_{\boldsymbol{i}}^\dagger a_{\boldsymbol{i}} \rightarrow \phi_{\boldsymbol{i}}^2 + \phi_{\boldsymbol{i}}\,. \tag{12.30}$$

12.2.3 Doi-Peliti field theory for Active Ising Models

Active Ising Models have two distinct particle types A, B, corresponding to spins ± 1 respectively, so alongside annihilation and creation fields ϕ, ϕ^* for species A, I need counterparts ψ and ψ^* for B.

Just as for the Master Equation, the spacetime action $\mathcal{S}$ of the field theory is additive over the various hopping and jump processes, and also over spatial (site) and temporal variables. The action can be therefore written in the form [MyPaper4]:

$$\mathcal{S} = \sum_i \int \mathrm{d}t\, \mathcal{A} \tag{12.31}$$
$$\mathcal{A} = \phi_{\boldsymbol{i}}^*(t)\partial_t \phi_{\boldsymbol{i}}(t) + \psi_{\boldsymbol{i}}^*(t)\partial_t \psi_{\boldsymbol{i}}(t) + \mathcal{A}_D + \mathcal{A}_\epsilon + \mathcal{A}_{\text{flip}}$$

Here $\mathcal{A}$ is the action density. Since the spin-flip dynamics involves only same-site particles, $\mathcal{A}_{\text{flip}}$ is fully local in both space and time, while the diffusive $\mathcal{A}_D$ and propulsive $\mathcal{A}_\epsilon$ hopping contributions connect neighbouring sites. The explicit form of these various contributions for the different AIMs, derived in Appendix D.2, is given as follows. For later convenience, I will give the form of the action without performing the Doi shift of the creation fields.

Hopping

The action for the hopping processes is given by [MyPaper4]

$$\mathcal{A}_D = \frac{D}{2} \sum_{\boldsymbol{j}:|\boldsymbol{i}-\boldsymbol{j}|=h} \left[\left(\phi_{\boldsymbol{i}}^*(t) - \phi_{\boldsymbol{j}}^*(t)\right)\left(\phi_{\boldsymbol{i}}(t) - \phi_{\boldsymbol{j}}(t)\right) + \left(\psi_{\boldsymbol{i}}^*(t) - \psi_{\boldsymbol{j}}^*(t)\right)\left(\psi_{\boldsymbol{i}}(t) - \psi_{\boldsymbol{j}}(t)\right) \right]$$
$$\tag{12.32}$$
$$\mathcal{A}_\epsilon = -\epsilon\, D \left[\left(\phi_{\boldsymbol{i}+h\hat{x}}^*(t) - \phi_{\boldsymbol{i}-h\hat{x}}^*(t)\right)\phi_{\boldsymbol{i}}(t) - \left(\psi_{\boldsymbol{i}+h\hat{x}}^*(t) - \psi_{\boldsymbol{i}-h\hat{x}}^*(t)\right)\psi_{\boldsymbol{i}}(t) \right] \tag{12.33}$$

Here h is the lattice spacing, separating two neighbouring sites. Moreover, here and in what follows I am omitting the temporal dependence on t.

Spin-flipping

I will here present the results for the action of the three choices of flipping rates introduced in Sec. 12.1.1. Since flipping processes all occur on the same site, the subscript $\boldsymbol{i}$ will be omitted.

AIM0 action. As anticipated, the process of deriving the action for the AIM0 leads to an infinite series of terms, which I was not able to sum up. This series is

given by:

$$\mathcal{A}_{\text{flip}} = -\gamma \, e^{-\beta - \psi\psi^* - \phi\phi^*} (\phi^* - \psi^*) \sum_k \frac{\phi \left(\psi\psi^* e^{\frac{2\beta}{k+1}} + \phi\phi^* \right)^k - \psi \left(\phi\phi^* e^{\frac{2\beta}{k+1}} + \psi\psi^* \right)^k}{k!}$$

(12.34)

Details of the derivation are provided in Appendix D.2.2. Because of this, from now on I will restrict my attention mainly to the AIM1 and AIM2, whose actions I compute below.

AIM1 action. For the flipping rates of AIM1, the action takes the same form as that of AIM0, except for the fact that all the $k+1$ factors in the denominator of the exponentials are absent. In this case, the sum over k can be performed exactly, and leads to [MyPaper4]:

$$\mathcal{A}_{\text{flip}} = \gamma \, (\phi^* - \psi^*) e^{-\beta - \psi^*\psi - \phi^*\phi} \left(\phi \, \exp\left[e^\beta \psi^*\psi + e^{-\beta} \phi^*\phi \right] - \psi \, \exp\left[e^{-\beta} \psi^*\psi + e^\beta \phi^*\phi \right] \right)$$

(12.35)

AIM2 action. In the case of the AIM2, the action $\mathcal{A}_{\text{flip}}$ can be split into three different contributions [MyPaper4]

$$\mathcal{A}_{\text{flip}} = \mathcal{A}_\gamma + \mathcal{A}_\lambda + \mathcal{A}_\tau \,, \tag{12.36}$$

where:

$$\mathcal{A}_\gamma = \gamma \, (\phi^* - \psi^*) \, (\phi - \psi) \,, \tag{12.37}$$

$$\mathcal{A}_\lambda = -\lambda \, (\phi^* - \psi^*)^2 \, \phi \, \psi \,, \tag{12.38}$$

$$\mathcal{A}_\tau = -\frac{\tau}{2} \, (\phi^* - \psi^*) \left[(\phi^*)^2 \, \phi - (\psi^*)^2 \, \psi \right] \, \phi \, \psi \,. \tag{12.39}$$

12.3   The hydrodynamic limit

Here I will derive hydrodynamic-level equations for the various Active Ising Models proposed in Sec. 12.1. The case of the AIM0 will be excluded because, as mentioned previously, its Doi-Peliti action is intractable.

The derivation is lengthy but it offers important insights. The strategy is as follows: starting from the Doi-Peliti field theory derived in the previous Section, I will first convert to a description in terms of physical fields via a Cole-Hopf transformation, and then use a reverse Martin-Siggia-Rose/Janssen-De Dominicis procedure [MyPaper4]. In this procedure, a link is made between the field-theoretic action and Langevin equation for the fields. This programme can be followed exactly to the last stage, at which point the non-Gaussian noise that emerges at the exact level can be either made Gaussian, to give the Langevin equations, or suppressed to give deterministic hydrodynamics. The last stage is achieved by sending the linear size of the system $L \to \infty$ while keeping fixed the density of particles. In this limit, exact hydrodynamic PDEs emerge, describing the behaviour of hydrodynamic variables on scales comparable with L, while the leading order stochastic corrections give the Gaussian (Langevin) noises.

12.3.1   Mapping of a Doi-Peliti field-theory on a Langevin equation

Once the field theory has been derived, the action can be split into two contributions: one linear in the Doi-shifted creation field $\tilde{\phi}$ and one containing all the non-linearities of $\tilde{\phi}$:

$$\mathcal{S}[\phi, \tilde{\phi}] = \int \mathrm{d}\boldsymbol{x}\, \mathrm{d}t\, \tilde{\phi} \cdot \boldsymbol{\mathcal{F}}[\phi] - K_\theta[\phi, \tilde{\phi}]\,. \tag{12.40}$$

Note the absence of a term independent on $\tilde{\phi}$: this is a consequence of conservation of the total probability [125].

I would like to drive the reader's attention to the similarity between this action and that derived from a Martin-Siggia-Rose/Janssen-De Dominicis (MSRJD) formalism from a Langevin equation in Chapter 4. The connection between the two is not as straightforward as it might seem: in principle, the creation and annihilation fields ϕ^* and ϕ are complex, and in particular, one is the complex conjugate of the other. On the other hand, in the MSRJD formalism, the response field is integrated over the imaginary axis, while the physical field is always real. This riddle can be however solved by realising that through analytic continuation, the two field theories can be mapped one into the other [125].

Once the details of the integration domain of the fields are settled, one can find a set of Langevin equations describing the behaviour of ϕ by utilising the connection provided by the MSRJD formalism. In contrast to what is typically done, namely building a path-integral field-theory from a Langevin equation, here I am doing the opposite: in this sense, I will say to use a *reverse* MSRJD procedure. The behaviour of the field ϕ described by the action $\mathcal{S}$ is therefore equivalent to that described by the Langevin equation

$$\boldsymbol{\mathcal{F}}[\phi] - \boldsymbol{\theta} = 0\,. \tag{12.41}$$

Here $\boldsymbol{\theta}$ is a random noise, with zero mean and statistics defined by the cumulant generator function K_θ.

The interpretation of this Langevin equation is however not so clear: in some simple cases, as in the case of pair annihilation processes, the noise term can often turn out to have an imaginary amplitude [16, 125, 126]. Moreover, ϕ is a complex field, which is linked to physical observables through complex relations, as discussed in the previous section. All these complications can be partially solved, as I will show in the next section, by using what is known as a Cole-Hopf transformation.

The Cole-Hopf transformation

In the attempt to derive a set of Langevin equations describing the behaviour of the fields, by interpreting the Doi-Peliti field theory through a MSRJD formalism, it is convenient to first perform a Cole-Hopf transformation [16, 127]. This transformation connects the Doi-Peliti fields to physical observables, namely particle density fields. Moreover, the Cole-Hopf transformation avoids the well-known problem, discussed in the previous section, of imaginary-noise Langevin equations, which are obtained if the MSRJD interpretation is performed directly on the Doi-Peliti action [16, 125, 126].

For the one-species example of Sec 12.2.2, the transformed fields ρ and $\tilde{\rho}$ obey

$$\phi^* = e^{\tilde{\rho}}\,, \qquad \phi = e^{-\tilde{\rho}} \rho \tag{12.42}$$

Thus the density field $\rho = \phi^* \phi$ is analogue to the second-quantised number operator $\hat{n} = a^\dagger a$, while the correlation function of Eq. (12.28) now takes the more intuitive form

$$\mathbb{E}\left[n_{\boldsymbol{i}}(t)\, n_{\boldsymbol{j}}(t')\right] = \langle \rho_{\boldsymbol{i}}(t) \rho_{\boldsymbol{j}}(t')\rangle \tag{12.43}$$

More generally, for all density correlations evaluated at different times and/or different sites, one can now replace the expectation value by the average over the field-theoretical measure, and replace the particle number operators with the corresponding ρ fields.

However, to compute correlation functions on the same site at the same time, subtleties remain because the corresponding number operators must remain normal-ordered. Thus the correlator given in Eq. (12.29) obeys

$$\mathbb{E}\left[n_{\boldsymbol{i}}(t)^2\right] = \langle \rho_{\boldsymbol{i}}(t)^2 + \rho_{\boldsymbol{i}}(t)\rangle. \tag{12.44}$$

This non-intuitive result is the unavoidable price for building an exact theory in terms of (almost!) physical density fields. Below I will therefore pay careful attention when computing equal-time correlation functions.

Cole-Hopf transformation in field-theories for AIMs

The Cole-Hopf transformed action density reads

$$\mathcal{A} = \tilde{\rho}_{\boldsymbol{i}}^+ \partial_t \rho_{\boldsymbol{i}}^+ + \tilde{\rho}_{\boldsymbol{i}}^- \partial_t \rho_{\boldsymbol{i}}^- + \mathcal{A}_D^{CH} + \mathcal{A}_\epsilon^{CH} + \mathcal{A}_{\text{flip}}^{CH} \tag{12.45}$$

where $\tilde{\rho}^+$ and ρ^+ have replaced ϕ and ϕ^*, and $\tilde{\rho}^-$ and ρ^- have replaced ψ and ψ^*. The fields ρ^+ and ρ^- approach the physical densities for A and B particles respectively. The contributions to $\mathcal{A}^{CH}$ are found via the change of variables (12.42); their forms will be given as needed, below.

I first set, without loss of generality, the lattice spacing to $h = 1$, and then consider the system at diffusive hydrodynamic scales, achieved by a further rescaling of spatial coordinates, $\tilde{\boldsymbol{x}} = \boldsymbol{i}/L$, and of time, $\tilde{t} = t/L^2$. This choice of rescaling follows from requiring diffusion to be the process that fixes the hydrodynamic time scale. Under this change of coordinates, I have

$$\sum_{\boldsymbol{i}} = L^d \int \mathrm{d}\tilde{\boldsymbol{x}} \qquad \int \mathrm{d}t = L^2 \int \mathrm{d}\tilde{t} \qquad \mathcal{S} = \int \mathrm{d}\tilde{\boldsymbol{x}} \mathrm{d}\tilde{t}\, \tilde{\mathcal{A}} \tag{12.46}$$

where $\tilde{\mathcal{A}}$ is the hydrodynamic action density, which absorbs all the powers of L coming from space-time rescaling. This action density can be expanded in powers of L^{-1}, dropping sub-leading terms as $L \to \infty$. I continue to split $\tilde{\mathcal{A}}$ into contributions from spin-flip, diffusive and biased hopping processes, whose rates must however be rescaled such that all three contribute to the hydrodynamic limit. Finally, the conjugate fields must also be rescaled as $\tilde{\rho} \to L^{-d}\tilde{\rho}$.

12.3.2 Hydrodynamics for AIM1

For AIM1, with spin-flip rates given by (12.7), the deterministic hydrodynamic equations are known from Ref. [120], offering an important cross-check on my

methods. At leading order in L^{-1}, the action terms (dropping the CH superscript) are [MyPaper4]:

$$\tilde{\mathcal{A}}_D = -L^d D\tilde{\rho}^+ \tilde{\nabla}^2 \rho^+ - L^d D\tilde{\rho}^- \tilde{\nabla}^2 \rho^- - L^d D\rho^+ \left(\tilde{\boldsymbol{\nabla}}\tilde{\rho}^+\right)^2 - L^d D\rho^- \left(\tilde{\boldsymbol{\nabla}}\tilde{\rho}^-\right)^2 \quad (12.47)$$

$$\tilde{\mathcal{A}}_\epsilon = L^{d+1} v\tilde{\rho}^+ \partial_{\hat{x}}\rho^+ - L^{d+1} v\tilde{\rho}^- \partial_{\hat{x}}\rho^- \quad (12.48)$$

$$\tilde{\mathcal{A}}_{\text{flip}} = L^{d+2}\gamma\, e^{-\beta}\left(e^{\tilde{\rho}^+} - e^{\tilde{\rho}^-}\right) \times$$
$$\times \left(e^{-\tilde{\rho}^+}\rho^+ e^{\left(e^\beta - 1\right)\rho^- + \left(e^{-\beta}-1\right)\rho^+} - e^{-\tilde{\rho}^-}\rho^- e^{\left(e^{-\beta}-1\right)\rho^- + \left(e^\beta-1\right)\rho^+}\right) \quad (12.49)$$

For all three to contribute to the hydrodynamic limit, as previously discussed, then D has to be of order unity, while one must have that $\gamma \sim L^{-2}$ in (12.49) and $v \sim L^{-1}$ in (12.48). These choices ensure that the number of spin flips is order one in the time $\sim L^2/D$ needed for a particle to diffuse a distance L, and that propulsion likewise competes with both flipping and diffusion at this hydrodynamic scale [MyPaper4]. After redefining the parameters to absorb their scaling with L and rescaling $\tilde{\rho}$ as $\tilde{\rho} \to L^{-d}\tilde{\rho}$, I can look at all terms in $\tilde{\mathcal{A}}$ scaling as L^0, including the time derivative terms, as is required for the $L \to \infty$ limit to now be taken. I finally get to the hydrodynamic action density [MyPaper4]

$$\tilde{\mathcal{A}} = \tilde{\rho}^+\left(\partial_{\tilde{t}} - D\tilde{\nabla}^2 + v\partial_{\hat{x}}\right)\rho^+ + \tilde{\rho}^-\left(\partial_{\tilde{t}} - D\tilde{\nabla}^2 - v\partial_{\hat{x}}\right)\rho^- +$$
$$+ \gamma\, e^{-\beta}\left(\tilde{\rho}^+ - \tilde{\rho}^-\right)\left(\rho^+ e^{\left(e^\beta-1\right)\rho^- + \left(e^{-\beta}-1\right)\rho^+} - \rho^- e^{\left(e^{-\beta}-1\right)\rho^- + \left(e^\beta-1\right)\rho^+}\right) \quad (12.50)$$

The absence of higher powers of the $\tilde{\rho}$ fields finally allows me to map this field theory, via the inverse MSRJD procedure outlined in Sec. 4.2. This procedure involves mapping the action onto the noiseless limit of a set of stochastic PDEs – the noisy version is given in Sec. 12.3.2 below. The hydrodynamic equations governing ρ^+ and ρ^- are thereby found as

$$\partial_t \rho^+ = D\nabla^2 \rho^+ - v\partial_{\hat{x}}\rho^+ - \tilde{F}(\rho^+, \rho^-) \quad (12.51)$$

$$\partial_t \rho^- = D\nabla^2 \rho^- + v\partial_{\hat{x}}\rho^- + \tilde{F}(\rho^+, \rho^-) \quad (12.52)$$

where

$$\tilde{F}(\rho^+, \rho^-) = \gamma\, e^{-\beta}\left(\rho^+ e^{\left(e^\beta-1\right)\rho^- + \left(e^{-\beta}-1\right)\rho^+} - \rho^- e^{\left(e^{-\beta}-1\right)\rho^- + \left(e^\beta-1\right)\rho^+}\right) \quad (12.53)$$

If written in terms of magnetisation $m = \rho^+ - \rho^-$ and total number of particles $\rho = \rho^+ + \rho^-$, these equations become [MyPaper4]

$$\partial_t m = D\nabla^2 m - v\partial_{\hat{x}}\rho - 2F(m, \rho) \quad (12.54)$$

$$\partial_t \rho = D\nabla^2 \rho - v\partial_{\hat{x}}m \quad (12.55)$$

where $F(m, \rho) = \tilde{F}((\rho + m)/2, (\rho - m)/2)$, namely

$$F(m, \rho) = \gamma\, e^{-\beta - \rho + \rho\cosh\beta}(m\cosh[m\sinh\beta] - \rho\sinh[m\sinh\beta]) \quad (12.56)$$

Notably, the 'aligning force' F is exactly as found in Ref. [120]. There, the hydrodynamic equations were derived directly by averaging the microscopic process over a local Poisson measure. Although the derivation is quite different, the Doi-Peliti formalism ultimately gives an equivalent result because it is constructed from coherent states that also correspond to a Poisson distribution [16].

Fluctuating hydrodynamics

An advantage of this Doi-Peliti field theory is that it provides a systematic way to address *fluctuating* hydrodynamics. This can be done by keeping the next order in L^{-d} beyond the action (12.50). This captures for finite-size systems the leading order (small, Gaussian) fluctuations around Equations (12.54), (12.55), by adding to them Langevin noises scaling as $L^{-d/2}$. Adding these terms to the action (12.50), the equations for m and ρ become [MyPaper4]

$$\partial_t m = D\nabla^2 m - v\partial_{\hat{x}}\rho - 2F(m, \rho) + \frac{1}{\sqrt{L^d}}\theta \tag{12.57}$$

$$\partial_t \rho = D\nabla^2 \rho - v\partial_{\hat{x}}m + \frac{1}{\sqrt{L^d}}\boldsymbol{\nabla}\cdot\boldsymbol{\zeta} \tag{12.58}$$

where $F(m, \rho)$ is still given by (12.56), but now we have the noise contributions θ and $\boldsymbol{\zeta}$. The noise θ can be further split in two contributions $\theta = \eta + \boldsymbol{\nabla}\cdot\boldsymbol{\xi}$, where the latter arises from diffusion and thus conserves the total magnetisation. The statistics of these Gaussian noises is fully determined by a covariance matrix comprising

$$\langle\eta(\boldsymbol{x}, t)\eta(\boldsymbol{y}, s)\rangle = 4\gamma\, e^{-\beta-\rho+\rho\cosh(\beta)}\,\delta\left(\boldsymbol{x}-\boldsymbol{y}\right)\delta\left(t-s\right)\times$$
$$\times\left(\rho\cosh\left[m\sinh(\beta)\right] - m\sinh\left[m\sinh(\beta)\right]\right) \tag{12.59}$$

with other noise covariances being zero except for

$$\langle\xi_i(\boldsymbol{x}, t)\xi_j(\boldsymbol{y}, s)\rangle = 2\,D\,\rho\,\delta_{i,j}\delta\left(\boldsymbol{x}-\boldsymbol{y}\right)\delta\left(t-s\right)$$
$$\langle\zeta_i(\boldsymbol{x}, t)\zeta_j(\boldsymbol{y}, s)\rangle = 2\,D\,\rho\,\delta_{i,j}\delta\left(\boldsymbol{x}-\boldsymbol{y}\right)\delta\left(t-s\right)$$
$$\langle\xi_i(\boldsymbol{x}, t)\zeta_j(\boldsymbol{y}, s)\rangle = 2\,D\,m\,\delta_{i,j}\delta\left(\boldsymbol{x}-\boldsymbol{y}\right)\delta\left(t-s\right)$$

Note that $\boldsymbol{\xi}$ and $\boldsymbol{\zeta}$, namely the conservative noises, are Gaussian also beyond the large L limit. This can be seen from the fact that they arise from the action terms (12.47) and (12.48), where no term is more than quadratic in $\tilde{\rho}^{\pm}$. The non-conservative noise η, on the other hand, has non-Gaussian statistics, as higher powers of $\tilde{\rho}^{\pm}$ are present in (12.49), which becomes Gaussian only al large L in virtue of the central limit theorem.

12.3.3 Hydrodynamics for AIM2

The same procedure as used above for flip rates obeying (12.7) can be applied to the many-body rates (12.8)-(12.10). Spatial hopping is not affected, so all the contributions proportional to D and ϵ will remain unchanged. But the contribution $\tilde{\mathcal{S}}_{\text{flip}}$ to the hydrodynamic action now takes the form (before rescaling parameters)

$$\tilde{\mathcal{S}}_{\text{flip}} = L^{d+2}\gamma\left(e^{\tilde{\rho}^+} - e^{\tilde{\rho}^-}\right)\left(e^{-\tilde{\rho}^+}\rho^+ - e^{-\tilde{\rho}^-}\rho^-\right) -$$
$$-L^{d+2}\lambda\left(e^{\tilde{\rho}^+} - e^{\tilde{\rho}^-}\right)^2 e^{-\tilde{\rho}^+-\tilde{\rho}^-}\rho^+\rho^+ + \tag{12.60}$$
$$+L^{d+2}\frac{\tau}{2}\left(e^{-\tilde{\rho}^+} - e^{\tilde{\rho}^-}\right)\left(e^{\tilde{\rho}^+}\rho^+ - e^{\tilde{\rho}^-}\rho^+\right)\rho^+\rho^-$$

As done previously, I now rescale the rates γ, λ and τ by L^{-2} such that each type of flip competes with diffusion (and propulsion). Finally, by rescaling $\tilde{\rho}\to L^{-d}\tilde{\rho}$ and

taking $L \to \infty$, the resulting hydrodynamic action becomes equivalent to the same partial differential equations (12.52), (12.51), but with a different choice of $F(\rho^+, \rho^-)$. Again rewriting this in terms of magnetisation $m = \rho^+ - \rho^-$ and particle density $\rho = \rho^+ + \rho^-$, I recover (12.54) and (12.55), with (12.56) replaced by [MyPaper4]

$$F(m, \rho) = m \left(\gamma + \tau \frac{m^2 - \rho^2}{8} \right) . \tag{12.61}$$

Just as in Sec 12.3.2, I can compute leading-order fluctuation corrections, recovering (12.57) and (12.58), in which $F(m, \rho)$ obeys (12.61) and the noise correlator of η given by

$$\langle \eta(\boldsymbol{x}, t) \eta(\boldsymbol{y}, s) \rangle = \delta(\boldsymbol{x} - \boldsymbol{y}) \, \delta(t - s) \left[2\gamma\rho + \left(\lambda + \rho \frac{\tau}{4} \right) (\rho^2 - m^2) \right] \tag{12.62}$$

while all other correlators remain the same.

12.3.4 Homogeneous solutions

Spatially homogeneous but time-dependent solutions of the noiseless hydrodynamic equations are found by assuming $m(\boldsymbol{x}, t) = m(t)$ and $\rho(\boldsymbol{x}, t) = \rho(t)$ in Eq.s (12.54,12.55), which become

$$\partial_t m = -2F(m, \rho) \tag{12.63}$$

$$\partial_t \rho = 0 \tag{12.64}$$

The second of these expresses particle conservation: $\rho(t) = \rho_0$, the initial density. In contrast, m relaxes via the spin-flip dynamics, with an asymptotic solution $\lim_{t \to +\infty} m(t) = m_0$ obeying $F(m_0, \rho_0) = 0$. For both choices of F considered above in (12.56), (12.61), the disordered state $m_0 = 0$ is always a solution. However, it is unstable whenever $\partial_m F(m_0, \rho_0) < 0$, giving rise to a magnetised phase.

For definiteness I will here focus on AIM2 here (though AIM1 is similar [120]), for which the force $F(m, \rho)$ obeys (12.61) so that

$$\partial_m F = \left(\gamma - \frac{\tau}{8} \rho^2 \right) - \frac{3\tau}{8} m^2 \tag{12.65}$$

The state $m_0 = 0$ is thus stable for $\rho_0 \leq \rho_c$, and unstable for $\rho_0 > \rho_c$, where the *critical* density is given by [MyPaper4]

$$\rho_c = \sqrt{\frac{8\gamma}{\tau}} . \tag{12.66}$$

Above ρ_c, where $m_0 = 0$ is unstable, one has a symmetric pair of stable, magnetised states

$$m_0 = \pm \bar{m} \qquad\qquad \bar{m}^2 = \rho_0^2 - \rho_c^2 . \tag{12.67}$$

This resembles a standard, Ising-like spontaneous symmetry breaking where two vanishingly magnetic states merge at the critical point $\rho_0 = \rho_c$. However, in the passive Ising model, for all $\rho_0 > \rho_c$ the two solutions $m = \pm \bar{m}$ remain stable against *inhomogeneous perturbations*. For AIMs this is not the case: there is a region of parameter space where no homogeneous solution is stable, and AIM2 makes no exception. The AIM transition is thus better understood as a first-order transition, akin to a liquid-gas transition [71].

Linear stability of uniform states

To check the linear stability of homogeneous solutions $m = m_0$, $\rho = \rho_0$, I linearise the equations of motion and examine small perturbations δm and $\delta \rho$ which then obey [MyPaper4]:

$$\partial_t \delta m = D \, \nabla^2 \delta m - v \, \partial_x \delta\rho - 2 \, \alpha \left(\rho_0 \right) \delta m - 2 \, g \left(\rho_0 \right) \delta\rho \tag{12.68}$$

$$\partial_t \delta\rho = D \, \nabla^2 \delta\rho - v \, \partial_x \delta m \tag{12.69}$$

where

$$\alpha \left(\rho_0 \right) = \partial_m F \left(m_0, \rho_0 \right) \qquad\qquad g \left(\rho_0 \right) = \partial_\rho F \left(m_0, \rho_0 \right) . \tag{12.70}$$

For $\rho_0 \leq \rho_c$, where $m_0 = 0$, these two coefficients read

$$\alpha \left(\rho_0 \right) = \gamma \left(1 - \frac{\rho_0^2}{\rho_c^2} \right) \qquad\qquad g \left(\rho_0 \right) = 0 \, , \tag{12.71}$$

While for $\rho_0 > \rho_c$, where $m_0 = \pm\sqrt{\rho_0^2 - \rho_c^2}$, they read

$$\alpha \left(\rho_0 \right) = 2\gamma \left(\frac{\rho_0^2}{\rho_c^2} - 1 \right) \qquad\qquad g \left(\rho_0 \right) = \mp 2\gamma \frac{\rho_0}{\rho_c} \sqrt{\frac{\rho_0^2}{\rho_c^2} - 1} \tag{12.72}$$

Note that for all $\rho_0 \neq \rho_c$, the coefficient $\alpha \left(\rho_0 \right) > 0$, while it equals 0 only at $\rho_0 = \rho_c$.

In Fourier space the linearised dynamics becomes

$$\partial_t \begin{pmatrix} \delta m \\ \delta\rho \end{pmatrix} = M \left(\boldsymbol{k} \right) \begin{pmatrix} \delta m \\ \delta\rho \end{pmatrix} \tag{12.73}$$

Here I used Fourier-transformed fields, which are obtained from the real-space fields through the transformation

$$f \left(\boldsymbol{k}, t \right) = \int \mathrm{d}^d x \, f \left(\boldsymbol{x}, t \right) e^{-\mathrm{i}\boldsymbol{x} \cdot \boldsymbol{k}} \, . \tag{12.74}$$

The evolution matrix M is given by

$$M(\boldsymbol{k}) = \begin{pmatrix} -D \, k^2 - 2 \, \alpha(\rho_0) & -i \, v \, k_x - 2 \, g(\rho_0) \\ -i \, v \, k_x & -D \, k^2 \end{pmatrix} \tag{12.75}$$

and stability against perturbations at wave vector $\boldsymbol{k}$ requires both eigenvalues of $M(\boldsymbol{k})$ to have a nonpositive real part. These eigenvalues are given by

$$\lambda_{1/2} \left(\boldsymbol{k} \right) = \pm \sqrt{\alpha(\rho_0)^2 + 2i \, v \, g(\rho_0) k_x - v^2 k_x^2} - \alpha(\rho_0) - Dk^2 \tag{12.76}$$

Studying the eigenvalues at $k = 0$, one finds that

$$\lambda_1 = -2\alpha(\rho_0) \qquad\qquad \lambda_2 = 0 \, , \tag{12.77}$$

confirming the analysis made above concerning stability within the subspace of homogeneous mean-field solutions.

What happens if instead, I perturb the system, not with a homogeneous perturbation, but with a slowly varying one? As long as $\rho_0 \neq \rho_c$, and hence $\alpha(\rho_0)$ is positive, continuity in $\boldsymbol{k}$ requires $\Re(\lambda_1(\boldsymbol{k})) < 0$ at small $\boldsymbol{k}$. In contrast, λ_2 at small $\boldsymbol{k}$ takes the form

$$\lambda_2(\boldsymbol{k}) = \pm i \frac{v\, g(\rho_0)}{\alpha(\rho_0)} k_x - Dk^2 + v^2 \frac{g(\rho_0)^2 - \alpha(\rho_0)^2}{2\,\alpha(\rho_0)^3} k_x^2 + O(k^3) \tag{12.78}$$

Let me now distinguish the two cases $\rho_0 < \rho_c$ and $\rho_0 > \rho_c$.

1. At $\rho_0 < \rho_c$, where $g = 0$, the eigenvalue λ_2 becomes

$$\lambda_2(\boldsymbol{k}) = -Dk^2 - \frac{v^2}{2\alpha(\rho_0)} k_x^2 + O(k^3) \tag{12.79}$$

   indicating stability of the uniform, nonmagnetic solution for all $\rho_0 < \rho_c$, in agreement with the predictions of mean field theory.

2. At $\rho_0 > \rho_c$ the homogeneous solutions that appear stable from a mean-field argument has $m_0^2 = \rho_0^2 - \rho_c^2 \neq 0$. In this case, λ_2 becomes

$$\lambda_2(\boldsymbol{k}) = \mp i \frac{\rho_0\, v}{\sqrt{\rho_0^2 - \rho_c^2}} k_x - Dk^2 + v^2 \frac{\rho_c^4}{4\gamma\left(\rho_0^2 - \rho_c^2\right)^2} k_x^2 + O(k^3) \tag{12.80}$$

   The linear part (in $\boldsymbol{k}$) of $\lambda_2(\boldsymbol{k})$ is always imaginary, and hence does not affect the stability analysis. The quadratic part may, however, become positive for values of ρ_0 close to ρ_c. In particular, this happens when

$$\rho_0^2 - \rho_c^2 < \frac{v}{2\sqrt{\gamma D}} \rho_c^2. \tag{12.81}$$

As the r.h.s. is always strictly positive if $v > 0$, there is always an interval $[\rho_c, \rho_l]$, in which the homogeneous solution is unstable, with ρ_l given by

$$\rho_l = \rho_c \sqrt{1 + \frac{v}{2\sqrt{\gamma D}}} > \rho_c. \tag{12.82}$$

For low activity v, the instability window shrinks $\rho_l \to \rho_c$, and in particular

$$\rho_l = \rho_c + \frac{v}{4\sqrt{\gamma D}} \rho_c + \mathcal{O}(v^2) \tag{12.83}$$

In this second scenario, which arises for any nonzero propulsion v, the homogeneous magnetic phase becomes unstable to long wavelength perturbations. Only for $v = 0$ is the passive-Ising-like second order transition recovered; for all $v \neq 0$ there is a range of densities, $\rho_c(\gamma, \tau) < \rho_0 < \rho_l(\gamma, \tau, D)$, in which no homogeneous solution is stable. In this range, the system is therefore driven towards a spatiotemporal pattern.

Although I will not reproduce the full calculation, note that the same qualitative behaviour arises for AIM1, in which the force F in (12.63) is replaced by (12.56): here it is again possible to show that for any $v \neq 0$ there is a finite range of densities

$\rho_c < \rho_0 < \rho_l$ in which the ordered homogeneous solution is linearly unstable with respect to long-wavelength spatial perturbations. Hence, the transition is not second-order, but is better understood as a liquid-gas phase transition as in [71]. In both cases, for the zero propulsion limit $v \to 0$, one finds that $\rho_l \to \rho_c$, so that the homogeneous ordered and disordered phases are linearly stable on either side of ρ_c, and a second-order transition is therefore expected in that limit.

12.4 No flocking transition in a two-body interaction model

In the previous Section, I analysed the hydrodynamic behaviour of the AIM2, where the spin-flipping process is given by the set of reactions (12.9,12.10). Strikingly, the critical density $\rho_c = (8\gamma/\tau)^{1/2}$ depends on the AIM2.1 (random one-body flipping) spin-flip rate γ, and the AIM2.3 (three-body flipping) rate τ, but not on the AIM2.2 (two-body flipping) rate λ. As one switches off the AIM2.3 interaction $\tau \to 0$, the critical density diverges $\rho_c \to +\infty$. This means that contrary to naive expectation, two-body collisional alignment cannot by itself lead to ordering for any amount of random noise γ, no matter how large the rate λ at which two-body flipping occurs [MyPaper4].

A physical interpretation of the relevant process is that two close enough particles, *i.e.* sharing the same lattice site, bump into each other with some rate λ. When such a collision occurs, if the particles have opposite spin, they align (randomly choosing which of the two orientations to share). Since the spin sets the preferred direction of motion of the particle, the two colliding particles move in the same direction after the collision. This seems to capture a basic and intuitive mechanism through which flocking might occur, yet I find no ordered phase. Something closer to a 'majority rule' (which gets encoded in the three-body collision process of AIM2.3) is instead required [MyPaper4].

Intriguingly, several recent studies have proposed that two-body interactions are indeed not enough to sustain global alignment via a spontaneous breaking of an Ising-like symmetry [128, 129, 130, 131]. This work confirms this prediction, which I believe has not been given enough emphasis in the community. The advantage of the field-theoretical approach is that its exact analysis can cleanly and unambiguously rule out any ordered state induced by the two-body collision term in the hydrodynamic limit addressed here. Specifically, if one retains only the one-body (randomising) and two-body terms by setting $\tau = 0$ in AIM2, they would obtain (12.54,12.55) with a force term $F(m,\rho) = \gamma m$. The homogeneous solution at zero magnetisation, $m_0 = 0$, is then stable for all $\gamma > 0$, regardless of the global density ρ_0. Therefore, for any finite amount of random spin flipping, the two-body collision process described by the reaction (12.9) is not sufficient to induce collective motion [MyPaper4].

At $\gamma = 0$, things look slightly different. Without the two-body term ($\lambda = 0$), all solutions can be written as a superposition of waves which travel in the $\pm x$ direction with speed v and damping Dk^2. These solutions not only conserve the total density but also the total magnetisation; accordingly a state of uniform magnetisation cannot emerge from an unmagnetised initial state. Remarkably, this result is sustained, at the hydrodynamic level, even when the two-particle interaction (12.9) is switched

on [MyPaper4]. This result seems counter-intuitive. Indeed, in the absence of random spin-flipping but with two-body collisions ($\gamma = 0, \lambda > 0$) the system has two absorbing states: whenever particles are all either of the A or B kind, no further spin-flipping can occur. Either state would represent a permanently stable flock.

As I have shown, this physics does not emerge in the hydrodynamic limit. A key factor is that absorbing states are reached in a finite time only in a finite-size system. I must therefore switch attention to the fluctuating hydrodynamics of this system arising at finite L. The finite-size behaviour of the two-particle interaction model, at large but finite L, is given by

$$\partial_t m = D\nabla^2 m - v\partial_{\hat{x}}\rho + \frac{1}{\sqrt{L^d}}\left(\eta + \boldsymbol{\nabla}\cdot\boldsymbol{\xi}\right) \tag{12.84}$$

$$\partial_t \rho = D\nabla^2 \rho - v\partial_{\hat{x}}m + \frac{1}{\sqrt{L^d}}\boldsymbol{\nabla}\cdot\boldsymbol{\zeta} \tag{12.85}$$

I have already set $\gamma = 0$, so spin-flipping is given by the 'pure' AIM2.2 reactions, as defined by (12.9). As in the previous models, η, $\boldsymbol{\xi}$ and $\boldsymbol{\zeta}$ are Gaussian noises whose correlators are found by setting $\gamma = \tau = 0$ in the more general results given already for AIM2 in Sec. 12.3.3.

The noises $\boldsymbol{\xi}$ and $\boldsymbol{\zeta}$ arise from the diffusive motion of particles, and hence conserve the total magnetisation. Flocking, were it to emerge, would have to stem from the η noise term. But, as seen from the covariance results in Sec 12.3.3, specifically (12.62), the noise η is larger the smaller the magnetisation. When $m \sim 0$, this noise therefore pushes the system towards magnetised states with $m \neq 0$. The noise then weakens, so it is less likely for the system to return to $m \sim 0$. When eventually the system reaches the absorbing state $m = \pm\rho$, all particles flock in the same direction forever after. The η term therefore does push the system towards a flocking state; but it is the only term that does so. This means that for AIM2.2 any collective motion arises by a purely stochastic mechanism [MyPaper4], not a deterministic drift – a fact also clear from the shape of $F(m, \rho)$ when $\tau = 0$. As previously discussed, stochasticity, and hence the probability of achieving this flocked state, vanishes in the hydrodynamic limit $L \to \infty$. Therefore, exact conservation of the total magnetisation at deterministic level is not because spin-flipping processes are absent altogether, but because the probability of having a fluctuation that macroscopically changes m vanishes when $L \to \infty$. This peculiar scenario is of course radically changed by the three-body collisional coupling term τ, which restores a deterministic drift towards flocking that wins out above the critical density ρ_c.

12.5 The unbiased AIM critical point

The linear stability analysis performed in Sec 12.3.4 shows that AIMs generically undergo a first-order transition, with a continuous transition recovered for unbiased hopping rates $\epsilon = 0$ (equivalently $v = 0$): this accordingly defines the unbiased AIM critical point. Note that this critical point is unstable in the RG sense since any infinitesimal value of v brings back first-order behaviour. An important question concerns the universality class of this critical transition. The answer would be obvious if this limit recovered a reversible model, which would surely lie in the

kinetic Ising class known as Model C in Halperin and Hohenberg classification [40], as discussed further below. Indeed, numerical simulations in 2 dimensions of the AIM0 give results compatible with this prediction [71]. However, this outcome is not guaranteed because, as also shown in Sec. 12.1, the dynamics of AIM0 violates detailed balance even at $v = 0$, making the system out of equilibrium even in the absence of self-propulsion [71]. This is equally true of AIM1 and AIM2, and given their shared symmetries one can expect all these models to lie in a single universality class, that may or may not be that of equilibrium Model C.

A major advantage of the field-theoretic approach described in the present Chapter is that it creates a clear and unambiguous foundation for resolving this issue via a full renormalization group (RG) analysis. Here I will derive a suitable starting point for RG calculations on AIMs, compare it with the corresponding Model C equations, and review what is known about the two cases. I will focus on the case of AIM2, where spin-flipping is given by the reactions (12.8)-(12.10).

12.5.1 Relevant and irrelevant terms

The hydrodynamic methods used in Sec. 12.3 generally identify a limit in which noiseless, mean-field critical behaviour is recovered; this approach does not capture all relevant terms for RG purposes. To identify these, I start instead from a coarse-grained continuous version of the microscopic theory, describing the system on mesoscopic scales (much larger than h, the lattice spacing, and much smaller than L, the system size). I am hence not assuming anymore the scaling with L of the coefficients investigated in Sec. 12.3. I will instead take a continuum limit by sending the lattice spacing $h \to 0$. The continuum limit therefore represents a way to investigate the dynamics on scales much larger than h, but yet much smaller than L.

The continuum limit

I will develop the continuum limit of the theory. I will do so as I am interested in the behaviour of the system on scales $l \ll h$, and therefore assume the lattice spacing can be sent to $h \to 0$. Attention however must be paid to the most physical way to rescale the various parameters in this limit. Let me first change the spatial variable used to describe the system. Instead of using the lattice number i, I will use the continuous variable $x = hi$. Sums over lattice sites i are thus replaced by integrals over x, with the prescription

$$\int d\boldsymbol{x} f(\boldsymbol{x}) = h^d \sum_{\boldsymbol{i}} f_{\boldsymbol{i}} \,, \qquad f(h\boldsymbol{i}) = f_{\boldsymbol{i}} \,. \tag{12.86}$$

Second, one must carefully define the continuous-space fields. Say that I have already performed a Cole-Hopf transformation, and have a theory that describes the behaviour of the number of particle field ρ. In the case of more particle species, as it is for AIMs, the same procedure described here can be easily generalised.

While I leave the tilde fields $\tilde{\rho}^{\pm}$ unchanged, it is convenient to rescale the $\rho^{\pm}$ fields with the volume around each lattice site h^d. This comes from the fact that, when the $h \to 0$ limit is taken at a fixed total number of particles, the expected number of particles on each site vanishes. What remains constant is the density,

namely the average number of particles divided by the volume occupied by a single site h^d. Hence, it is convenient to rescale the annihilation fields by h^d, namely

$$\tilde{\rho}(h\boldsymbol{i}, t) = \tilde{\rho}_{\boldsymbol{i}}(t) \qquad\qquad \rho(h\boldsymbol{i}, t) = h^{-d}\rho_{\boldsymbol{i}}(t) \qquad (12.87)$$

Moreover, by observing that that

$$f(\boldsymbol{x}) - f(\boldsymbol{x} + h\hat{y}) = -h\,\partial_{\hat{y}}f(\boldsymbol{x}) + o(h)\,, \qquad (12.88)$$

it is straightforward to write the action contributions that describe processes involving different sites, namely the hopping process in the case of AIMs.

The final choice to be made concerns the scaling with h of the reaction and jump rates. For example, to keep finite the mean square displacement due to the diffusive process, the microscopic hopping rate D must diverge as h^{-2}. For the case of multiple-body interactions, all the rates must be rescaled to compensate for the vanishing probability of finding more than one particle on the same site. For example, the rate of an n-body interaction should diverge as $h^{-d(n-1)}$ to guarantee that a spin-flipping due to the n-body interaction occurs on average on the same time-scale as the other processes.

After these rescalings, the action becomes $\mathcal{S} = \int (\mathcal{A}_D + \mathcal{A}_{\text{flip}})\,d\boldsymbol{x}dt$, where [MyPaper4]

$$\mathcal{A}_D = -D\tilde{\rho}^+\tilde{\nabla}^2\rho^+ - D\tilde{\rho}^-\tilde{\nabla}^2\rho^- - D\rho^+\left(\tilde{\boldsymbol{\nabla}}\tilde{\rho}^+\right)^2 - D\rho^-\left(\tilde{\boldsymbol{\nabla}}\tilde{\rho}^-\right)^2 \qquad (12.89)$$

$$\mathcal{A}_{\text{flip}} = \gamma\left(e^{\tilde{\rho}^+} - e^{\tilde{\rho}^-}\right)\left(e^{-\tilde{\rho}^+}\rho^+ - e^{-\tilde{\rho}^-}\rho^-\right) + \frac{\tau}{2}\left(e^{-\tilde{\rho}^+} - e^{\tilde{\rho}^-}\right)\left(e^{\tilde{\rho}^+}\rho^+ - e^{\tilde{\rho}^-}\rho^+\right)\rho^+\rho^- \qquad (12.90)$$

I now want to change variables from $\rho^\pm$ to m and ρ. To do this in the field theory, one must also transform the $\tilde{\rho}^\pm$ fields according to

$$m = \rho^+ - \rho^- \qquad\qquad \rho = \rho^+ + \rho^- \qquad (12.91)$$

$$\tilde{m} = \frac{\tilde{\rho}^+ - \tilde{\rho}^-}{2} \qquad\qquad \tilde{\rho} = \frac{\tilde{\rho}^+ + \tilde{\rho}^-}{2} \qquad (12.92)$$

For RG purposes, it is sufficient to work as usual in a Landau-Ginzburg expansion in fluctuations around the homogeneous disordered state at $m = 0$, $\rho = \rho_0$, as my interest is the study of the transition as $\rho_0 \to \rho_c^-$. Hence I shall write $\rho = \rho_0 + \delta\rho$, and expand in powers of m and $\delta\rho$. The resulting action contains an infinite set of nonlinear terms of which only the first few are relevant, in the RG sense, near $d_c = 4$ dimensions, which is the upper critical dimension of the model. Retaining only these terms, the result is the sum of a Gaussian action density $\mathcal{A}_0$ and a non-Gaussian interaction part $\mathcal{A}_I$

$$\mathcal{A}_0 = \tilde{m}\left(\partial_t - D\,\nabla^2 + a\right)m - \tilde{\lambda}\,\tilde{m}^2 + \tilde{\rho}\left(\partial_t - D\,\nabla^2\right)\delta\rho - \tilde{D}\left(\boldsymbol{\nabla}\tilde{\rho}\right)^2 \qquad (12.93)$$

$$\mathcal{A}_I = b\,\tilde{m}\,m^3 + g\,\tilde{m}\,m\,\delta\rho + \text{irrelevant} \qquad (12.94)$$

with coefficients derived from microscopic parameters as follows:

$$a = \frac{1}{4}\left(8\gamma - \tau\rho_0^2\right)\,, \qquad\qquad b = \frac{\tau}{4}\,, \qquad\qquad g = -\frac{\tau\,\rho_0}{2}$$

$$\tilde{\lambda} = \frac{\rho_0}{4}\left(8\gamma + \rho_0^2\tau\right)\,, \qquad\qquad \tilde{D} = \rho_0\,D$$

This action can be cast in a more familiar form as a pair of Langevin equations, through the reverse MSRJD procedure illustrated in Sec. 12.3.1, which read [MyPaper4]

$$\partial_t m = D\nabla^2 m - a\, m - b\, m^3 - g\, \delta\rho\, m + \sqrt{2\tilde{\lambda}}\, \eta \qquad (12.95)$$

$$\partial_t \delta\rho = -\boldsymbol{\nabla} \cdot \boldsymbol{J}\,; \quad \boldsymbol{J} = -D\, \boldsymbol{\nabla}\delta\rho + \sqrt{2\tilde{D}}\, \boldsymbol{\zeta} \qquad (12.96)$$

with η and ζ_i independent uncorrelated Gaussian white noises of unit variance.

Note that any nonlinearity of the form $\boldsymbol{\nabla}(m^2)$ in the current $\boldsymbol{J}$ of (12.96), or equivalently a term $\tilde{\rho}\,\nabla^2(m^2)$ in the action (12.94), if present, would also be relevant in $d < 4$. However, since it is absent in the bare theory and there are no other non-Gaussian terms linear in $\tilde{\rho}$, it will not be generated during an RG transformation. More generally one expects any relevant term, even if absent in the original action, to be generated during the RG flow, unless its absence is protected by some kind of symmetry or conservation law. The physics that prevents the generation of this term in our case is as follows: *when $v = 0$, the dynamics of the mass density ρ is independent of the state of magnetisation m* [MyPaper4]. Such a condition survives coarse-graining, and can arguably be viewed as a symmetry between A and B particles (or up- and down-spins) at the microscopic level, stating that the diffusive jump rates of a particle are independent of its spin state.

It is however even more interesting to note that even in the presence of $v \neq 0$, the term $\nabla(m^2)$ in the current J, which would lead to Model C-like behaviour (see Eq.(12.98) below), is not generated. This is prevented by the absence of any deterministic non-linear coupling in the density equation so that other deterministic non-linear couplings cannot arise under the RG flow. This mechanism is however absent in a model with detailed balance, where the hopping rates *must* depend on the energy change caused by the hop, which does depend on the spin state. Since it is possible to construct an AIM that recovers detailed balance at $v = 0$ [122], one cannot view the symmetry found here as fundamental to all AIMs, but it remains a defining feature of all the AIMs studied in this Chapter (including AIM0).

12.5.2 Connection with Model C

The equations of motion of Model C are [40]

$$\partial_t m = \lambda\nabla^2 m - \lambda r\, m - \lambda u\, m^3 - \lambda\gamma\, \delta\rho\, m + \sqrt{2\lambda}\, \eta$$
$$\partial_t \delta\rho = -\boldsymbol{\nabla} \cdot \boldsymbol{J} \qquad (12.97)$$

$$\boldsymbol{J} = -D\, \boldsymbol{\nabla}\delta\rho - \frac{D\gamma}{2}\boldsymbol{\nabla}(m^2) + \sqrt{2D}\, \boldsymbol{\zeta} \qquad (12.98)$$

Here λ is a mobility parameter (unrelated to the previous use of the same symbol in this Chapter), while r, u, γ are coefficients in the free energy functional

$$\mathcal{H} = \int \mathrm{d}^d x\, \frac{1}{2}\left(\boldsymbol{\nabla}m\right)^2 + \frac{r}{2}m^2 + \frac{u}{4}m^4 + \frac{1}{2}\rho^2 + \frac{\gamma}{2}m^2\rho\,, \qquad (12.99)$$

that underlies the model. Model C obeys detailed balance with respect to this $\mathcal{H}$. The noise terms η and $\boldsymbol{\zeta}$ are independent Gaussian white noises of unit variance, just as in (12.95,12.96).

Strikingly, the *only difference* between (12.95,12.96) for the AIMs under study and Model C is the absence in the AIM case of the term $\boldsymbol{\nabla}(m^2)$ in the current $\boldsymbol{J}$. As already discussed, this term is relevant but structurally absent in our chosen AIMs, while in contrast, it is structurally present, with a coefficient fixed by detailed balance, in Model C. The difference between these two cases need not be accessible via any approach that attempts to perturbatively deform one model into the other, for instance by considering small departures from detailed balance. The change in parameters is not small and replaces one symmetry (time-reversal) with a different and unrelated one (spin-independent density dynamics).

Interestingly, a generalised model that includes both AIM and Model C as special cases has previously been introduced and studied using RG methods [132]. The model is defined by

$$\partial_t m = \lambda \, \nabla^2 m - a \, m - b \, m^3 - g_m \, m \, \delta\rho + \sqrt{2\tilde{\lambda}} \, \eta \qquad (12.100)$$

$$\partial_t \delta\rho = -\boldsymbol{\nabla} \cdot \boldsymbol{J}$$

$$\boldsymbol{J} = -D \, \boldsymbol{\nabla} \delta\rho - \frac{g_\rho}{2} \boldsymbol{\nabla}(m^2) + \sqrt{2\tilde{D}} \, \boldsymbol{\zeta} \qquad (12.101)$$

The AIM2 dynamics of (12.95,12.96) is recovered as

$$g_\rho = 0 \qquad\qquad g_m = g \qquad\qquad \lambda = D \qquad (12.102)$$

while equilibrium Model C corresponds to

$$a = \lambda r \qquad\qquad \lambda = \tilde{\lambda} \qquad\qquad g_m = \lambda\gamma \qquad (12.103)$$

$$b = \lambda u \qquad\qquad D = \tilde{D} \qquad\qquad g_\rho = D\gamma \qquad (12.104)$$

12.5.3 RG flow

In the present Chapter, I will quickly review the perturbative RG study by Akkineni and Taueber in [132], which in fact addresses a much larger class spanning Heisenberg as well as Ising symmetry, and Model D as well as Model C dynamics.

Briefly, for the model governed by (12.100,12.101), various fixed points of potential relevance to AIMs are considered in [132]. A Gaussian fixed point, stable for $d > 4$, becomes unstable for $\epsilon = 4 - d > 0$. In the absence of g_m, the m dynamics is decoupled from ρ, which is then ignorable. The unstable flow is therefore towards a Model A fixed point. For nonzero g_m, however, the Model A fixed point is unstable towards an equilibrium-like Model C fixed point where detailed balance is restored. The Model C fixed point is found to be perturbatively stable against detailed-balance violations; its basin of attraction should include all models in which such violation is *weak*.

Beyond this basin, in addition to the $g_m = 0$ manifold where Model A behaviour is recovered, lies a further unstable manifold at $g_\rho = 0$. The strongly non-equilibrium dynamics on this manifold describes situations, like the AIMs studied here, in which it is the dynamics of ρ that decouples from m. On this unstable manifold, a further fixed point was found, whose strongly non-equilibrium dynamics describes a situation in which m relaxes much faster than ρ at large scales. This fixed point is however unstable also within the $g_\rho = 0$ manifold. Interestingly, Akkineni and Tauber also

found another non-equilibrium fixed point at $g_\rho = 0$ for which the coupling g_m seemingly flows to infinity for $d < 4$. The latter caused them to conclude that no true non-equilibrium fixed point is accessible at order ϵ [132].

AIMs are not in Model C universality class

What is important to note for the present discussion is that the $g_\rho = 0$ sub-manifold does not contain the Model C critical point. This can be seen directly from the following argument. As previously explained, the Model C fixed point splits off from the Gaussian one below $d = 4$. Here the coupling term involving g_ρ is relevant. Only if it were irrelevant could the fixed-point value of this coupling constant become zero at the Model C fixed point. Therefore, this fixed point cannot lie on the $g_\rho = 0$ manifold to which our AIMs are confined. This strongly suggests that, whether or not the AIM critical point is perturbatively accessible to order ϵ [132], it should indeed lie in a different universality class from Model C [MyPaper4].

This suggestion is different from the one made concerning AIM0 in [71]. The situation is however delicate because, as previously stated, this result depends on a symmetry of all the AIMs considered here (including AIM0 of [71]) which might nonetheless be broken in more general models. Specifically, I know it *must* be broken in any AIM that restores detailed balance by construction at the critical point (e.g. [122]), in which case there can be little doubt that the Model C universality class prevails. I also note that numerical evidence favours equilibrium Ising exponents for AIMs in $d = 2$ [71], which I have also confirmed for myself numerically. It is unusual for universality classes to merge on reducing dimensionality, so this could indicate that while the Model C and AIM classes retain distinct exponents these are hard to distinguish numerically in two (and therefore possibly three) dimensions.

A possible new universality class for AIMs

I will now however argue that, despite the conclusions of [132], the non-equilibrium exponents describing the unbiased AIM critical point can be still computed within the one-loop perturbative RG approach proposed in [132]. This is caused by the fact that, although g_m flows to infinity, also the ratio $w = D/\lambda$ does [132].

When $w \to +\infty$, the effective relaxation coefficient of the magnetisation λ becomes much larger than the diffusivity $\lambda \ll D \to \lambda^{-1} \gg D^{-1}$, therefore meaning that the field m relaxes on time-scales much larger than ρ. One might therefore expect that ρ becomes a *fast* mode, and thus to recover Model A behaviour. However, by looking at the one-loop β-functions of [132] as $w \to 0$, one can see that g_m diverges, as previously mentioned. However, the ratio g_m/w remains finite along the RG flow, and quite surprisingly the one-loop critical exponents turn out to depend only on this ratio [MyPaper5]. A detailed discussion of the issues related to this RG flow is still in preparation [MyPaper5] and lies beyond the scope of this Chapter. However, if these results were confirmed, one would find a critical exponent ν at first order in ϵ given by

$$\nu = \frac{1}{2} + \frac{\epsilon}{8} \,. \tag{12.105}$$

This value of the exponent ν differs from the Ising equilibrium value of $\frac{1}{2} + \frac{\epsilon}{12}$,

hence suggesting that the phase transition of unbiased AIMs might fall in a different universality class than Ising models. Some caveats must be however solved before claiming this is the case: the presence of this non-equilibrium universality class strongly relies on the fact that g_m flows to infinity. If did was not the case, for $w \to 0$ Model A behaviour would be recovered. Understanding whether higher order terms might prevent g_m from flowing to infinity is therefore crucial in addressing the question of what is the universality class of the transition in unbiased AIMs.

12.6 Summary and future perspectives

In the present Chapter, I have considered a Doi-Peliti field theoretical formalism and exploited it to derive an exact field theory able to describe the behaviour of a class of different Active Ising Models (AIMs). I showed that this field-theoretical approach provides, as it so often does, a powerful framework to understand collective behaviour in active systems. Using this approach I derived several previously known results [MyPaper4], that include the deterministic hydrodynamic equations of AIM1 [120]; the peculiar behaviour of the two-body collisional interaction, which cannot sustain flocking via spontaneous symmetry breaking in the presence of noise [128]; and the linear instability of the homogeneous ordered phase close to the transition, leading to phase-separated profiles and a first order scenario [44, 36], [MyPaper3].

Thereafter I showed that the Doi-Peliti framework can take us far beyond these results. For example, it allows one to go beyond the deterministic hydrodynamic equations, complementing them with sub-leading fluctuation terms needed to describe the system on finite scales. Developing this field theory also allowed me to address the unbiased AIM critical point, defined as the second-order alignment transition arising when the self-propulsion term is turned off. I argue that this transition, contrary to expectation [71], is *not* governed by the Model C universality class [MyPaper4]. This result follows from the lack of detailed balance, and therefore need not hold for more general Active Ising Models, as those constructed so that detailed balance gets restored in the zero self-propulsion limit [122].

A complete RG analysis of AIMs is still missing, and a first attempt to understand their universality class is still in preparation [MyPaper5]. This represents an interesting future research direction, as it will allow us to understand whether coupling local alignment interactions with diffusive motion in space is enough to turn the phase transition from an equilibrium to a non-equilibrium one.

Conclusions and outlook

The work that has been done

Agreement between experiments on collective biological systems and renormalization group calculations have been scarce, challenging the extension of concepts as universality to the realm of biophysics. The central goal of my thesis has therefore been to probe field-theoretical approaches to the study of biological systems, by focusing on the case of natural swarms of midges in the field. Although lacking collective order, signatures of collective behaviour in swarms have been detected by the presence of scaling laws and scale-free correlations. These behaviours can be explained by the proximity of the system to a critical point, therefore allowing a theoretical treatment of collective swarming behaviour within the theory of dynamic critical phenomena. However, the value of the dynamic critical exponent of swarms, $z_{\mathrm{exp}} = 1.37 \pm 0.11$, was not predicted by any statistical theory. Explaining why swarms are characterised by exponent has therefore been the main goal of my work.

To approach the study of swarming behaviour within a field-theoretical framework, I first had to develop the appropriate field theory accounting for all relevant features observed in swarms. The collective properties of the system, as the dynamic critical exponent, can be then inferred through the renormalization group, in which short-wavelength details are integrated out to obtain an effective description of the large-scale degrees of freedom only. Universality, in this context, arises thanks to the fact that only a few effective theories describe the collective behaviour of a wider class of systems. Within each universality class, systems typically share the same general features as dimensionality, symmetries and conservation laws. Although universality has been widely confirmed in the context of physical systems, its applicability to living matter has long lacked confirmation, challenging its underlying principles within the context of biology.

Starting from the experimental evidence, I reviewed piece by piece all the *universal* features characterising swarms of midges and their collective behaviour. Here, by universal features, I mean symmetries (or lack of them) and conservation laws. Local effective alignment interactions between neighbouring midges are the first key ingredient that allows for a qualitative explanation of swarming behaviour. From the field-theoretical point of view, these interactions can be modelled within a Landau-Ginzburg approach, which accounts for the rotational symmetry in the system. The dynamic behaviour of a system described by the Landau-Ginzburg free energy that, as swarms, lacks the conservation of the order parameter is known as Model A. This statistical theory describes the behaviour of a time-dependent Landau-Ginzburg equation and thus represents the starting point for a field-theoretical description of

the dynamic collective behaviour of swarms. Near the critical point, however, Model A is known to have a dynamic exponent of $z \approx 2$, far from the value measured in experiments.

The agreement with experiments can be improved by realising that midges in swarms are inherently active, namely can use stored energy to perform self-propelled motion, and thus violate time-reversal symmetry and detailed balance. As a consequence of activity, the interaction network is not fixed in time, driving the system far from equilibrium. Since the time scale over which network rearrangements occur is compatible with those over which neighbouring midges align, activity is indeed strong and thus represents an important feature in the description of swarm. It is therefore possible to cast swarms into the framework of the Toner and Tu theory, which merges the behaviour of Model A with the Navier-Stokes equations, to account for the fact that the order parameter is the local direction of motion of midges.

The first problem arose when studying the near-ordering phase of the Toner and Tu theory, which is the relevant one for swarming behaviour. In particular, the coupling between fluctuations in the density and the direction of motion turns the phase transition, which was second-order in Model A, into a first-order one. As a consequence, no scaling laws should be observed in this regime. This contrasts with observations in swarms, where scaling laws have been detected. To attempt to explain the observed scaling behaviour, I assumed swarms to be nearly incompressible. In the incompressible limit, a renormalization group calculation of the Toner and Tu theory at the critical point was already performed by Chen, Toner and Lee. Their RG approach, while confirming the transition is continuous when density fluctuations are completely suppressed, predicted a dynamic exponent of $z = 1.73$ in the physical case of three dimensions. Although not filling the gap with experiments on swarms, this RG calculation showed that activity does reduce it, lowering z from the value $z \approx 2$ of Model A. The work of Chen, Toner and Lee therefore represents a fundamental stepping stone towards the understanding of swarming behaviour and serves as a springboard for my calculation on swarms.

Although incompressibility might be a sound approximation in swarms, it still lacked theoretical support. Understanding the role of density fluctuations therefore seemed to be the next step to take, before addressing other features of swarms. To understand the effects of weak density fluctuations in the behaviour of swarms, I studied the so-called Malthusian Toner and Tu theory, in which – thanks to birth-death processes – density fluctuations are partially suppressed. I showed, through a renormalization group approach, how in the Malthusian theory density fluctuations turn the phase transition into a first-order one. However, when the compressibility vanishes, I do recover a second-order transition falling in the same universality class as the incompressible theory. For finite-size systems, a crossover between these two behaviours emerges, with sufficiently small systems exhibiting a second-order phenomenology falling in the incompressible universality class. This suggests that even though most active systems are not strictly incompressible, whenever scaling laws are detected and the spatial profile is homogeneous, collective behaviour is described by the incompressible universality class. Swarms indeed fall into this description, as they are active and yet exhibit scaling laws, meaning that they live on the homogeneous, second-order side of this crossover. Incompressibility is therefore

fully justified as a tool to investigate the collective behaviour of swarms.

While my work on the effects of density fluctuations gives strong support to the assumption of incompressibility, the value of $z = 1.73$ predicted for active systems with alignment interactions is still far from the experimental result of swarms, meaning that new physics is required. Through an inspection of the shape of the temporal correlation functions of swarms, it turns out that they have a non-exponential. This feature can be explained by the presence of inertial behaviour in the orientational dynamics. Behavioural inertia can be viewed as a sort of resistance to adapt to social forces from neighbouring individuals, in the same way as inertia, namely the mass, is the resistance to the change of velocity when a force is applied. The presence of inertia in the collective behaviour of swarms can be accounted for by coupling the order parameter, namely the direction of motion, to the generator of its rotational symmetry, which I call spin in analogy with quantum mechanics. By Noether theorem, I expect the total spin to be conserved, as a consequence of the presence of a rotational symmetry. This coupling between the order parameter and its conserved spin has been already investigated in the context of equilibrium statistical models for collective behaviour in antiferromagnets, giving rise to the dynamic universality class of G respectively. In particular, in Model G, the presence of a mode-coupling interaction together with the conservation of the total spin lowers the dynamic critical exponent from the value of $z \approx 2$ of Model A to $z = 1.5$ in three dimensions.

After showing how inertia and activity are responsible, independently one from the other, for lowering the value of z from the value of $z = 2$ of Model A to $z = 1.73$ and $z = 1.5$ respectively, the natural attempt has been to combine these two features into a single field theory, which I referred to as Self-Propelled Model G. (Note that, in this terminology, the Toner and Tu theory can be identified as Self-Propelled Model A.) Because I aimed at working under the assumption of incompressibility, as motivated earlier, I had to understand how this constraint affected the behaviour of the spin. From a technical point of view, enforcing incompressibility is equivalent to requiring that the velocity field, and hence also the direction of motion, obey a solenoidal constraint. Understanding the effects of this constraint on the dynamics of the spin is an issue unrelated to the presence of activity, and hence I addressed it working in a fixed-network approximation. My analysis revealed that to be consistent with the desired static behaviour, the dynamics of a solenoidal-constrained version of Model G required the presence of an additional dynamic interaction, arising from the interplay of static ferromagnetic alignment and dynamic mode-coupling. Remarkably, although the static universality class changes in the presence of the solenoidal constraint, the dynamic universality class does not. This further strengthens the idea that, as long as the dynamic universality class is concerned, incompressibility should not affect critical behaviour.

Once all the required subtleties were settled, I was ready to perform the full renormalization group calculation for Self-Propelled Model G. The results of this calculation, which turned out to be quite hard and demanding, revealed a rich fixed-point phenomenology. In addition to the three aforementioned universality classes, namely that of equilibrium non-inertial systems with $z = 2$ (Model A), equilibrium inertial systems with $z = 1.5$ (Model G), and active non-inertial systems with $z = 1.73$ (Model A), a novel fixed-point at which both activity and inertia

are essential ingredients emerged. In three dimensions, the critical exponent at the new fixed point is $z = 1.35$, in very good agreement with the experimental result $z_{\mathrm{exp}} = 1.37 \pm 0.11$. Furthermore, this theoretical result is also in excellent agreement with numerical simulations of the Inertial Spin Model, a particle-based model for active inertial matter, in which the dynamic critical exponent was found to be $z_{\mathrm{num}} = 1.35 \pm 0.04$. This result provides one of the first successful tests of a renormalization group prediction against experiments on living active systems, establishing the renormalization group as a tool for the quantitative description of collective behaviour in biological systems.

In conclusion, my work contributed to establishing the predictive power of field theoretical techniques, above all the renormalization group, in the context of active biological systems. In particular, my theoretical analysis provided the first successful test of a renormalization group prediction in experiments on living systems, which was missing since the introduction of the first models for collective behaviour in living systems. With my research on the collective dynamics of insect swarms, I thus found a long-sought match between experiments and theory, suggesting that universality may play a decisive role also in strongly correlated biological systems.

Outlooks

The results attained here have an impact that perhaps goes far beyond the case of natural swarms of insects, as they pave the way for new research prospects. A theoretical renormalization group approach to the same theory of swarms, namely Self-Propelled Model G, in the symmetry-broken phase might give interesting insights into the collective behaviour of flocks of birds. Although midges and birds might not have much in common, it turns out that inertial behaviour is also relevant in the description of collective turns in starling flocks. The collective behaviour of flocks has, however, a different nature from that of swarms. While swarms behave collectively as a consequence of the proximity to a critical point, flocks do so because they live deeply in the ordered phase, where a continuous symmetry – rotational invariance – is spontaneously broken. This gives rise to what are known as spin-waves, massless excitations that exhibit scale-free correlations. The presence of inertia and activity suggests that the collective behaviour of flocks and swarms might be described by different phases of Self-Propelled Model G. Studying Self-Propelled Model G in its ordered phase is however not a piece of cake, and presents its peculiar technical difficulties compared to the sturdy performed here in the near-ordering phase. Thus, an RG approach to bird flocks is not a simple extension of the present work and requires the proper attention. If confirmed, this picture would push the concept of universality in biology even further, showing that different biological systems not only exhibit collective behaviours that uniquely depend on their symmetries and conservation laws but also share most of their universal features.

Once the behaviour of both flocks and swarms has been characterised through a renormalization group approach, an interesting question to address is how influential activity is at the level of the collective properties. While both midges and birds are inherently active at the individual scale, activity might not play the same role on the collective scale. In flocks, for example, the ordered motion of birds makes

rearrangements in the interaction network extremely slower than rearrangements in the orientation of neighbouring birds. Aligning dynamics therefore occurs in a state of quasi-local-equilibrium, and experiments on flocks showed that equilibrium inference, which assumes a fixed interaction network, gives results consistent with dynamical inference. In swarms, on the other hand, network rearrangements and reorientations of the direction of motion occur on the same time scale.

Within statistical mechanics, the strength of non-equilibrium features can be measured by looking at the entropy production rate of the system. To understand whether non-equilibrium effects are relevant at the collective scale of a system, the entropy production rate is the quantity to watch out for. While entropy is always produced at the individual's scale, as a consequence of self-propelled motion, often it is not on large scales. In this case, the system exhibits equilibrium-like collective behaviour. Using the tools of non-equilibrium statistical mechanics, in particular stochastic thermodynamics, it is possible to estimate the entropy production in an active field theory. Providing such an estimate in Self-Propelled Model G, both in the near-ordering and in the ordered phase, would allow one to compare the impact of activity on the collective behaviour of swarms and flocks. This comparison would help in understanding to what extent activity affects collective behaviour in flocks, and if the observed local equilibrium can be explained by the presence of a lower entropy-production rate.

Active matter beyond natural swarms

The last part of my PhD work has been dedicated to the broader topic of flocking transitions. To address some of its peculiar differences with phase transitions at equilibrium, a simplified class of models for flocking have been recently introduced. In this class of models, flocking arises as the consequence of the spontaneous breaking of a discrete, rather than continuous, symmetry. Because of the analogy with the equilibrium Ising model, this class of models is known as Active Ising Models (AIMs). My work has focused on the development of a field theoretical approach to AIMs, in an attempt to provide a comprehensive hydrodynamic theory that describes their emergent and collective behaviour. In particular, I used a Doi-Peliti formalism to map exactly the microscopic dynamics onto a field-theoretical action, from which hydrodynamic equations could be derived. To back up the validity of this approach, I first applied it to models whose hydrodynamic behaviour is known, recovering the correct results. Furthermore, I showed how my approach allows me to go beyond the exact hydrodynamic level, complementing the equations with a proper Langevin stochastic noise.

Finally, I used the resulting field theory for AIMs to address some properties of the phase transition. In the unbiased limit, where the coupling ruling activity is turned off, the system is still not at equilibrium. This is because the interplay of unbiased diffusive motion and alignment interactions violates detail balance. However, following numerical simulations showing Ising exponents in two dimensions, it has been conjectured that the universality class might have been that of Model C, an equilibrium model in which the order parameter (the magnetisation) is coupled to a conserved quantity (the density of particles). Through my field-theoretical

analysis, I could rule out this possibility and put forward the hypothesis that the transition belongs to a new non-equilibrium universality class.

Ordering transitions out of equilibrium, such as the flocking transition, still presents many features which have not yet been completely understood. Simple models, like the Active Ising Models, offer a useful simplified scenario in which some non-equilibrium features can be theoretically investigated. My analysis of the phase transition of unbiased AIMs, for example, suggests that when particle diffusion is added to Ising-like spin alignment, the phase transition might be ruled by a novel, yet to be determined, universality class with non-Ising exponents. A deeper RG analysis of this transition, currently in preparation, will shed light on whether particle diffusion is sufficient to turn an equilibrium ordering transition into a non-equilibrium one.

The development of a field theory that describes AIMs allows one to go even further, addressing the role of non-equilibrium fluctuations in the emergence of phase-separated profiles on the onset of flocking. A quantitative theoretical approach to this question involves the evaluation of non-equilibrium effects, which can be done by computing the entropy production rate. Furthermore, while the instability leading to phase separation is well understood, the mechanism through which this reflects into a first-order phase transition still lacks an unambiguous theoretical explanation. This field-theoretical approach might therefore help to improve our current understanding of flocking transitions.
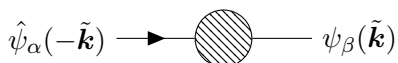
Appendix A

Feynman Diagrams of the incompressible Toner and Tu theory

At first order in $\epsilon = 4 - d$, the self-energies and vertex-functions of the incompressible Toner and Tu theory take contributions from the following diagrams.

A.1 Self Energies

A.1.1 Self Energy Σ

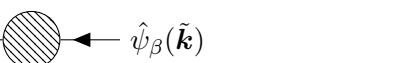The self energy $\Sigma_{\alpha\beta}$ corrects the inverse bare propagator of $\boldsymbol{\psi}$, and is given by

$$\Sigma_{\alpha\beta} \quad : \quad \hat{\psi}_\alpha(-\tilde{\boldsymbol{k}}) \longrightarrow \bigotimes \longleftarrow \psi_\beta(\tilde{\boldsymbol{k}}) \qquad (A.1)$$

with the following non-vanishing diagrams contributing to it

A.1.2 Self Energy $\tilde{\Sigma}$

The self energy $\tilde{\Sigma}_{\alpha\beta}$ corrects the noise variance of $\boldsymbol{\psi}$, and is given by

$$\tilde{\Sigma}_{\alpha\beta} \quad : \quad \hat{\psi}_\alpha(-\tilde{\boldsymbol{k}}) \longrightarrow \bigotimes \longleftarrow \hat{\psi}_\beta(\tilde{\boldsymbol{k}}) \qquad (A.2)$$

with no non-vanishing diagram contributing to it.

A.2 Vertex functions

A.2.1 Vertex function of the advection vertex of ψ

The vertex function $V^{\hat{\psi}\psi\psi}$ represents the corrections to the advection vertex in the equation of $\boldsymbol{\psi}$, and is given by

$$
V^{\hat{\psi}\psi\psi}_{\alpha\beta\gamma}(\tilde{\boldsymbol{k}},\tilde{\boldsymbol{q}}) \quad : \quad \hat{\psi}_\alpha(-\tilde{\boldsymbol{k}}) \longrightarrow \qquad \qquad \tag{A.3}
$$

$\psi_\beta(\tilde{\boldsymbol{q}})$

$\psi_\gamma(\tilde{\boldsymbol{k}}-\tilde{\boldsymbol{q}})$

with the following non-vanishing diagrams contributing to it
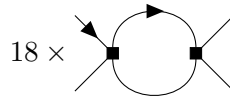
$12 \times$ $\qquad$ $6 \times$

A.2.2 Vertex function of the ferromagnetic vertex of ψ

The vertex function $V^{\hat{\psi}\psi\psi\psi}$ represents the corrections to the ferromagnetic vertex in the equation of $\boldsymbol{\psi}$, and is given by

$$
V^{\hat{\psi}\psi\psi\psi}_{\alpha\beta\gamma\nu}(\tilde{\boldsymbol{k}},\tilde{\boldsymbol{q}},\tilde{\boldsymbol{h}}) \quad : \quad \hat{\psi}_\alpha(-\tilde{\boldsymbol{k}}) \longrightarrow \qquad \psi_\gamma(\tilde{\boldsymbol{h}}) \tag{A.4}
$$

$\psi_\beta(\tilde{\boldsymbol{q}})$

$\psi_\gamma(\tilde{\boldsymbol{k}}-\tilde{\boldsymbol{q}}-\tilde{\boldsymbol{h}})$

with the following non-vanishing diagram contributing to it
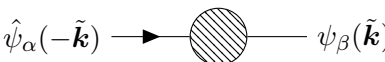
$18 \times$

Appendix B

Feynman Diagrams of the Malthusian Toner and Tu theory

At first order in $\epsilon = 4 - d$, the self-energies and vertex-functions of the Malthusian Toner and Tu theory take contributions from the following diagrams.

B.1 Self Energies

B.1.1 Self Energy Σ

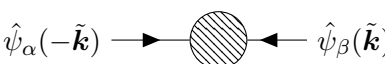The self energy $\Sigma_{\alpha\beta}$ corrects the inverse bare propagator of $\boldsymbol{\psi}$, and is given by

$$\Sigma_{\alpha\beta} \quad : \quad \hat{\psi}_\alpha(-\tilde{\boldsymbol{k}}) \longrightarrow \!\!\!\text{⬤}\!\!\!\longrightarrow \psi_\beta(\tilde{\boldsymbol{k}}) \tag{B.1}$$

with the following non-vanishing diagrams contributing to it
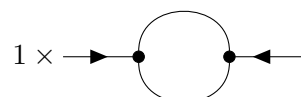

B.1.2 Self Energy $\tilde{\Sigma}$

The self energy $\tilde{\Sigma}_{\alpha\beta}$ corrects the noise variance of $\boldsymbol{\psi}$, and is given by

$$\tilde{\Sigma}_{\alpha\beta} \quad : \quad \hat{\psi}_\alpha(-\tilde{\boldsymbol{k}}) \longrightarrow \!\!\!\text{⬤}\!\!\!\longleftarrow \hat{\psi}_\beta(\tilde{\boldsymbol{k}}) \tag{B.2}$$

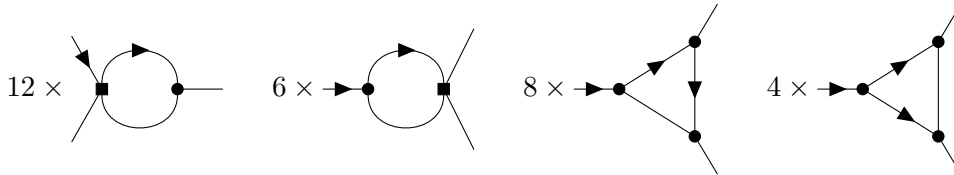with only the following non-vanishing diagram contributing to it

B.2 Vertex functions

B.2.1 Vertex function of the advection vertex of ψ

The vertex function $V^{\hat{\psi}\psi\psi}$ represents the corrections to the advection vertex in the equation of $\boldsymbol{\psi}$, and is given by

$$V^{\hat{\psi}\psi\psi}_{\alpha\beta\gamma}(\tilde{\boldsymbol{k}}, \tilde{\boldsymbol{q}}) \quad : \quad \hat{\psi}_\alpha(-\tilde{\boldsymbol{k}}) \longrightarrow \qquad\qquad \tag{B.3}$$

with the following non-vanishing diagrams contributing to it
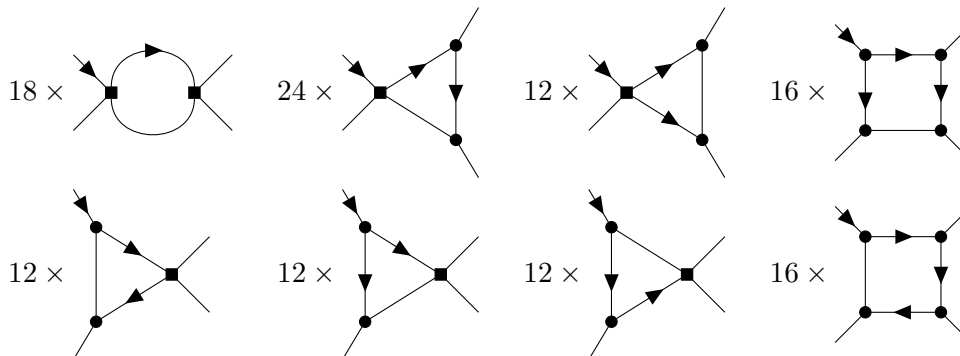

B.2.2 Vertex function of the ferromagnetic vertex of ψ

The vertex function $V^{\hat{\psi}\psi\psi\psi}$ represents the corrections to the ferromagnetic vertex in the equation of $\boldsymbol{\psi}$, and is given by

$$V^{\hat{\psi}\psi\psi\psi}_{\alpha\beta\gamma\nu}(\tilde{\boldsymbol{k}}, \tilde{\boldsymbol{q}}, \tilde{\boldsymbol{h}}) \quad : \quad \hat{\psi}_\alpha(-\tilde{\boldsymbol{k}}) \longrightarrow \qquad \psi_\gamma(\tilde{\boldsymbol{h}}) \tag{B.4}$$

with the following non-vanishing diagrams contributing to it

Appendix C

Feynman Diagrams of Self-Propelled Model G

C.1 Self Energies
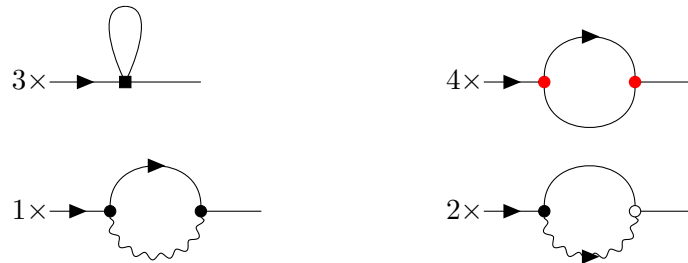
C.1.1 Self Energy Σ

The self energy $\Sigma_{\alpha\beta}$ corrects the inverse bare propagator of $\boldsymbol{\psi}$, and is given by

$$\Sigma_{\alpha\beta} \quad : \quad \hat{\psi}_\alpha(-\tilde{\boldsymbol{k}}) \longrightarrow \hspace{-0.3em}\bigcirc\hspace{-0.3em} \longrightarrow \psi_\beta(\tilde{\boldsymbol{k}}) \tag{C.1}$$

with the following non-vanishing diagrams contributing to it

C.1.2 Self Energy Π

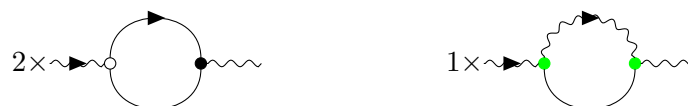The self energy $\Pi_{\alpha\beta\gamma\nu}$ corrects the inverse bare propagator of $\boldsymbol{s}$, and is given by

$$\Pi_{\alpha\beta\gamma\nu} \quad : \quad \hat{s}_{\alpha\beta}(-\tilde{\boldsymbol{k}}) \sim\hspace{-0.5em}\blacktriangleright\hspace{-0.3em}\bigcirc\hspace{-0.3em}\sim s_{\gamma\nu}(\tilde{\boldsymbol{k}}) \tag{C.2}$$

with the following non-vanishing diagrams contributing to it

C.1.3   Self Energy $\tilde{\Sigma}$

The self energy $\tilde{\Sigma}_{\alpha\beta}$ corrects the noise variance of $\boldsymbol{\psi}$, and is given by

$$\tilde{\Sigma}_{\alpha\beta} \quad : \quad \hat{\psi}_\alpha(-\tilde{\boldsymbol{k}}) \longrightarrow \! \longleftarrow \hat{\psi}_\beta(\tilde{\boldsymbol{k}}) \tag{C.3}$$

with the following non-vanishing diagram contributing to it

$$\frac{1}{2} \times$$

C.1.4   Self Energy $\tilde{\Pi}$

The self energy $\tilde{\Pi}_{\alpha\beta\gamma\nu}$ corrects the noise variance of $\boldsymbol{s}$, and is given by

$$\tilde{\Pi}_{\alpha\beta\gamma\nu} \quad : \quad \hat{s}_{\alpha\beta}(-\tilde{\boldsymbol{k}}) \leadsto\!\!\blacktriangleright\!\!\leadsto \! \blacktriangleleft\!\!\leadsto \hat{s}_{\gamma\nu}(\tilde{\boldsymbol{k}}) \tag{C.4}$$

with the following non-vanishing diagrams contributing to it

$$1 \times \qquad\qquad\qquad\qquad \frac{1}{2} \times$$

C.2   Vertex functions

C.2.1   Vertex function of the Mode-Coupling vertex of ψ

The vertex function $V^{\hat{\psi}\psi s}$ represents the corrections to the mode-coupling vertex in the equation of $\boldsymbol{\psi}$ and is given by

$$V^{\hat{\psi}\psi s}_{\alpha\beta\gamma\nu}(\tilde{\boldsymbol{k}}, \tilde{\boldsymbol{q}}) = \quad \hat{\psi}_\alpha(-\tilde{\boldsymbol{k}}) \longrightarrow \qquad (C.5)$$

with the following non-vanishing diagrams contributing to it

C.2.2 Vertex function of the Mode-Coupling vertex of s

The vertex function $V^{\hat{s}\psi\psi}$ represents the corrections to the mode-coupling vertex in the equation of $\boldsymbol{s}$, and is given by

$$V^{\hat{s}\psi\psi}_{\alpha\beta\gamma\nu}(\tilde{\boldsymbol{k}}, \tilde{\boldsymbol{q}}) = \hat{s}_{\alpha\beta}(-\tilde{\boldsymbol{k}}) \quad \tag{C.6}$$

with the following non-vanishing diagrams contributing to it
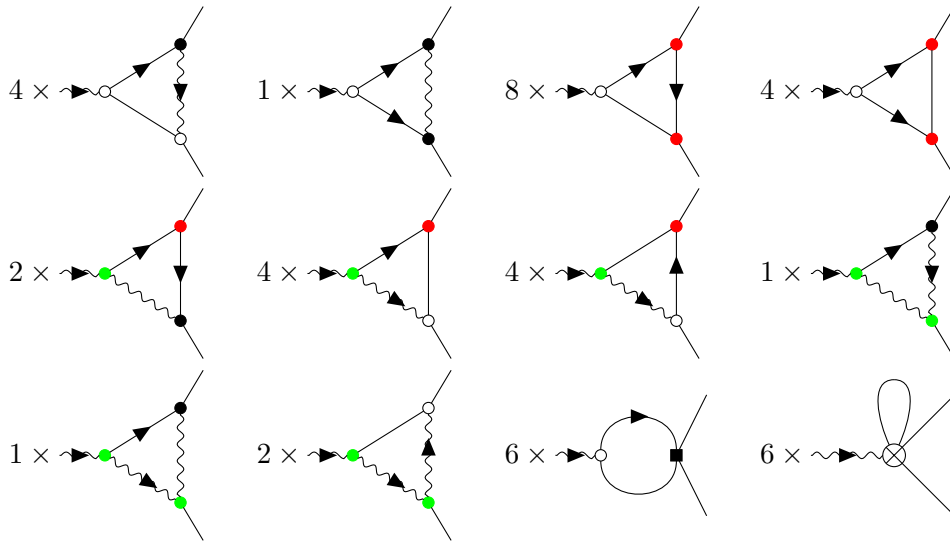
C.2.3 Vertex function of the advection vertex of ψ

The vertex function $V^{\hat{\psi}\psi\psi}$ represents the corrections to the advection vertex in the equation of $\boldsymbol{\psi}$, and is given by

$$V^{\hat{\psi}\psi\psi}_{\alpha\beta\gamma}(\tilde{\boldsymbol{k}}, \tilde{\boldsymbol{q}}) = \hat{\psi}_\alpha(-\tilde{\boldsymbol{k}}) \longrightarrow \quad \psi_\beta(\tilde{\boldsymbol{q}}) \atop \psi_\gamma(\tilde{\boldsymbol{k}} - \tilde{\boldsymbol{q}}) \tag{C.7}$$

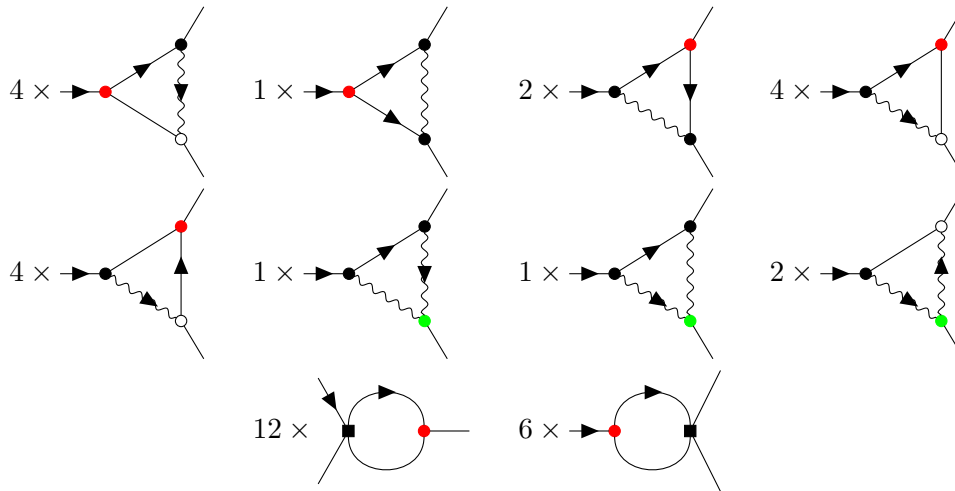with the following non-vanishing diagrams contributing to it

C.2.4   Vertex function of the advection vertex of s

The vertex function $V^{\hat{s}s\psi}$ represents the corrections to the advection vertex in the equation of s, and is given by

$$V^{\hat{s}s\psi}_{\alpha\beta\gamma\nu\eta}(\tilde{\boldsymbol{k}}, \tilde{\boldsymbol{q}}) = \ \hat{s}_{\alpha\beta}(-\tilde{\boldsymbol{k}}) \quad \overset{s_{\gamma\nu}(\tilde{\boldsymbol{q}})}{\underset{\psi_\eta(\tilde{\boldsymbol{k}} - \tilde{\boldsymbol{q}})}{}} \tag{C.8}$$

with the following non-vanishing diagrams contributing to it
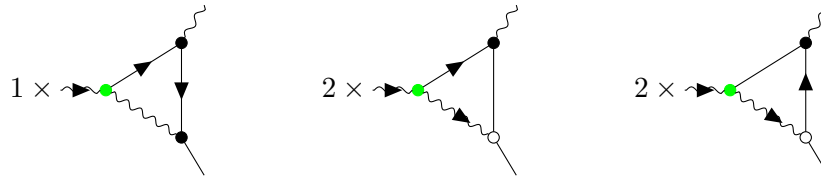
C.2.5   Vertex function of the ferromagnetic vertex of ψ

The vertex function $V^{\hat{\psi}\psi\psi\psi}$ represents the corrections to the ferromagnetic vertex in the equation of $\boldsymbol{\psi}$, and is given by

$$V^{\hat{\psi}\psi\psi\psi}_{\alpha\beta\gamma\nu}(\tilde{\boldsymbol{k}},\tilde{\boldsymbol{q}},\tilde{\boldsymbol{h}}) = \quad \hat{\psi}_\alpha(-\tilde{\boldsymbol{k}}) \quad \psi_\gamma(\tilde{\boldsymbol{h}}) \tag{C.9}$$

with the following non-vanishing diagrams contributing to it
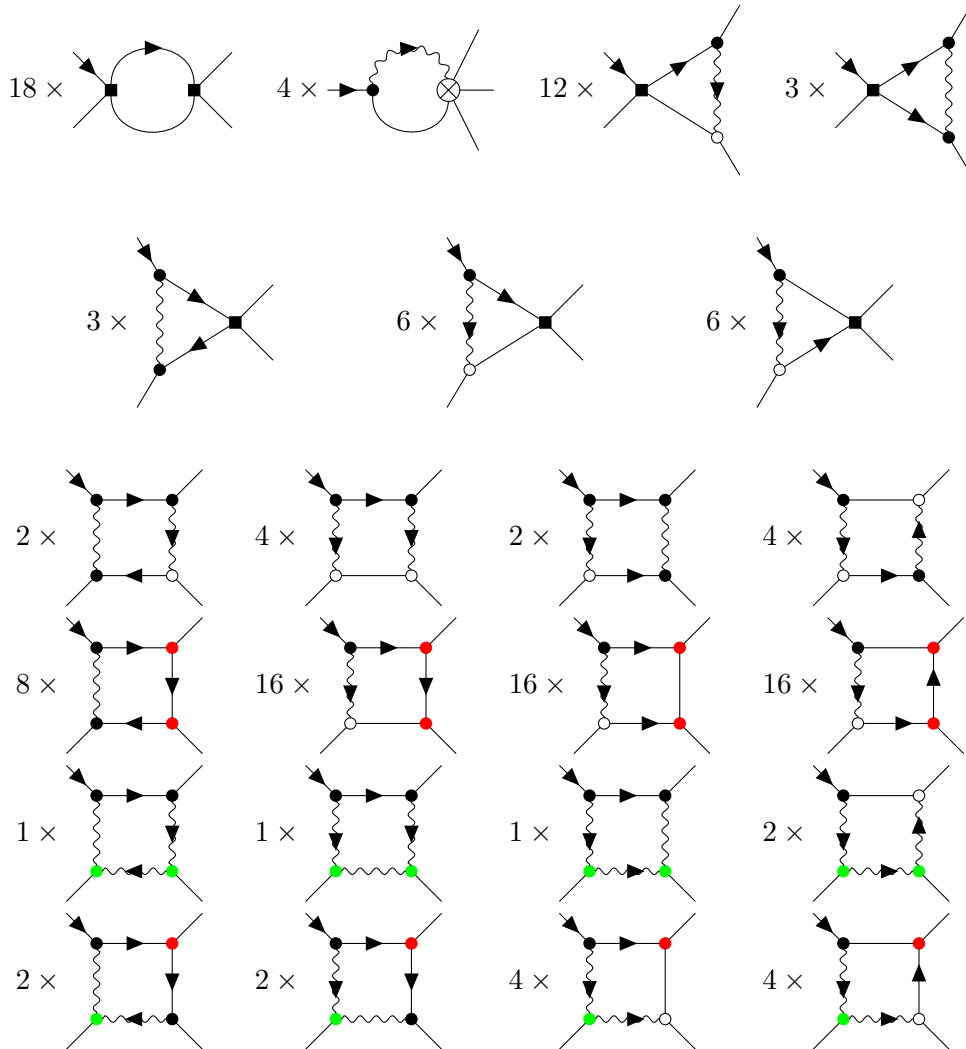
C.2.6 Vertex function of the DYS vertex of s

The vertex function $V^{\hat{s}\psi\psi\psi}$ represents the corrections to the DYS vertex in the equation of s, and is given by
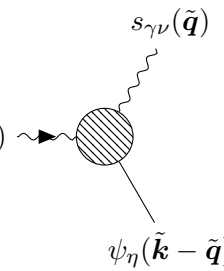
$$V^{\hat{s}\psi\psi\psi}_{\alpha\beta\gamma\sigma\tau}(\tilde{\boldsymbol{k}}, \tilde{\boldsymbol{q}}, \tilde{\boldsymbol{h}}, \tilde{\boldsymbol{p}}) = \hat{s}_{\alpha\beta}(-\tilde{\boldsymbol{k}}) \quad \tag{C.10}$$

with the following non-vanishing diagrams contributing to it
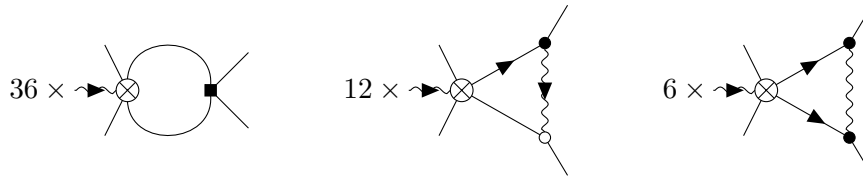
Appendix D

Field-theoretical approach to Active Ising Models

D.1 Master Equation

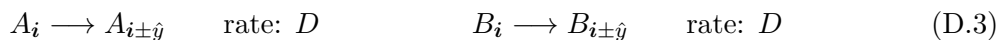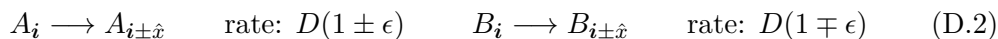Here I will give the explicit form of the Master Equation for the different AIMs introduced in Chapter 12.

Since the Master Equation is linear in P, each different process gives an independent contribution. For the AIMs considered here the Master Equation can be always written in the form

$$\partial_t P = \mathcal{L}_{\text{hop}}[P] + \mathcal{L}_{\text{flip}}[P] \,, \tag{D.1}$$

where $\mathcal{L}_{\text{hop}}$ is the contribution coming from hopping, while $\mathcal{L}_{\text{hop}}$ is the contribution coming from spin-flipping processes.

D.1.1 Hopping

For all the AIMs introduced here, the dynamics in space is represented by the biased hopping, described by the reactions

$$A_{\boldsymbol{i}} \longrightarrow A_{\boldsymbol{i}\pm\hat{x}} \quad \text{rate: } D(1\pm\epsilon) \qquad B_{\boldsymbol{i}} \longrightarrow B_{\boldsymbol{i}\pm\hat{x}} \quad \text{rate: } D(1\mp\epsilon) \tag{D.2}$$
$$A_{\boldsymbol{i}} \longrightarrow A_{\boldsymbol{i}\pm\hat{y}} \quad \text{rate: } D \qquad\qquad B_{\boldsymbol{i}} \longrightarrow B_{\boldsymbol{i}\pm\hat{y}} \quad \text{rate: } D \tag{D.3}$$

These rates for a random jump, expressed in terms of the number of $A_{\boldsymbol{i}}$ and $B_{\boldsymbol{i}}$ particles, $n_{\boldsymbol{i}}^+$ and $n_{\boldsymbol{i}}^-$ respectively, then take the following form

$$A_{\boldsymbol{i}} \to A_{\boldsymbol{i}\pm\hat{y}} \quad W\left(n_{\boldsymbol{i}}^+ - 1, n_{\boldsymbol{i}\pm\hat{y}}^+ + 1 | n_{\boldsymbol{i}}^+, n_{\boldsymbol{i}\pm\hat{y}}^+\right) = n_{\boldsymbol{i}}^+ D \qquad \forall \hat{y} \neq \hat{x} \tag{D.4}$$

$$B_{\boldsymbol{i}} \to B_{\boldsymbol{i}\pm\hat{y}} \quad W\left(n_{\boldsymbol{i}}^- - 1, n_{\boldsymbol{i}\pm\hat{y}}^- + 1 | n_{\boldsymbol{i}}^-, n_{\boldsymbol{i}\pm\hat{y}}^-\right) = n_{\boldsymbol{i}}^- D \qquad \forall \hat{y} \neq \hat{x} \tag{D.5}$$

$$A_{\boldsymbol{i}} \to A_{\boldsymbol{i}\pm\hat{x}} \quad W\left(n_{\boldsymbol{i}}^+ - 1, n_{\boldsymbol{i}\pm\hat{x}}^+ + 1 | n_{\boldsymbol{i}}^+, n_{\boldsymbol{i}\pm\hat{x}}^+\right) = n_{\boldsymbol{i}}^+ D(1\pm\epsilon) \tag{D.6}$$

$$B_{\boldsymbol{i}} \to B_{\boldsymbol{i}\pm\hat{x}} \quad W\left(n_{\boldsymbol{i}}^- - 1, n_{\boldsymbol{i}\pm\hat{x}}^- + 1 | n_{\boldsymbol{i}}^-, n_{\boldsymbol{i}\pm\hat{x}}^-\right) = n_{\boldsymbol{i}}^- D(1\mp\epsilon) \tag{D.7}$$

The contribution of these processes to the master equation can be split as

$$\mathcal{L}_{\text{hop}} = \mathcal{L}_D + \mathcal{L}_\epsilon \,, \tag{D.8}$$

where $\mathcal{L}_D$ is obtained by setting $\epsilon = 0$ and therefore gives rise to simple, unbiased, diffusion, while $\mathcal{L}_\epsilon$ is instead the contribution arising from active self-propulsion and will vanish if ϵ does. Hence, $\mathcal{L}_D$ and $\mathcal{L}_\epsilon$ always take the form

$$\mathcal{L}_D[P] = D \sum_{\boldsymbol{i}} \sum_{\boldsymbol{j}:|\boldsymbol{i}-\boldsymbol{j}|=h} (n_{\boldsymbol{i}}^+ + 1) P(\boldsymbol{n}^+ + \boldsymbol{1}_{\boldsymbol{i}} - \boldsymbol{1}_{\boldsymbol{j}}, \boldsymbol{n}^-; t) - n_{\boldsymbol{i}}^+ P(\boldsymbol{n}^+, \boldsymbol{n}^-; t) + \tag{D.9}$$

$$+ (n_{\boldsymbol{i}}^- + 1) P(\boldsymbol{n}^+, \boldsymbol{n}^- + \boldsymbol{1}_{\boldsymbol{i}} - \boldsymbol{1}_{\boldsymbol{j}}; t) - n_{\boldsymbol{i}}^- P(\boldsymbol{n}^+, \boldsymbol{n}^-; t)$$

$$\mathcal{L}_\epsilon[P] = \epsilon D \sum_{\boldsymbol{i}} (n_{\boldsymbol{i}}^+ + 1) P(\boldsymbol{n}^+ + \boldsymbol{1}_{\boldsymbol{i}} - \boldsymbol{1}_{\boldsymbol{i}+h\hat{x}}, \boldsymbol{n}^-; t) - (n_{\boldsymbol{i}}^+ + 1) P(\boldsymbol{n}^+ + \boldsymbol{1}_{\boldsymbol{i}} - \boldsymbol{1}_{\boldsymbol{i}-h\hat{x}}, \boldsymbol{n}^-; t) -$$

$$- (n_{\boldsymbol{i}}^- + 1) P(\boldsymbol{n}^+, \boldsymbol{n}^- + \boldsymbol{1}_{\boldsymbol{i}} - \boldsymbol{1}_{\boldsymbol{i}+h\hat{x}}; t) + (n_{\boldsymbol{i}}^- + 1) P(\boldsymbol{n}^+, \boldsymbol{n}^- + \boldsymbol{1}_{\boldsymbol{i}} - \boldsymbol{1}_{\boldsymbol{i}-h\hat{x}}; t) \tag{D.10}$$

Here I used a compact notation, denoting by $\boldsymbol{n}^\pm$ the vector collecting the number of $\pm$ particles on all sites $\boldsymbol{i}$ of the lattice $\{n_{\boldsymbol{i}}^\pm\}$, representing the state of the system. The vector $\boldsymbol{1}_{\boldsymbol{i}}$ has the same dimension as $\boldsymbol{n}^\pm$, and contains a 1 in the entry $\boldsymbol{i}$ while all the other entries are 0. In this way, adding $\boldsymbol{1}_{\boldsymbol{i}}$ to $\boldsymbol{n}^+$ corresponds to the addition of one + particle to the $\boldsymbol{i}$ site.

D.1.2 Spin-flipping

AIM0 rates

In the AIM0, the spin-flipping process occurs on each site with the rates of a fully-connected Ising model, namely

$$A_{\boldsymbol{i}} \longrightarrow B_{\boldsymbol{i}} \qquad \text{rate: } \gamma \exp\left(-\beta \frac{m_i}{\rho_i}\right) = \gamma \exp\left(\beta \frac{n_i^- - n_i^+}{n_i^+ + n_i^-}\right) \tag{D.11}$$

$$B_{\boldsymbol{i}} \longrightarrow A_{\boldsymbol{i}} \qquad \text{rate: } \gamma \exp\left(\beta \frac{m_i}{\rho_i}\right) = \gamma \exp\left(\beta \frac{n_i^+ - n_i^-}{n_i^+ + n_i^-}\right) \tag{D.12}$$

The global rates associated to this process are

$$A_{\boldsymbol{i}} \to B_{\boldsymbol{i}} \qquad W\left(n_i^+ - 1, n_i^- + 1 | n_i^+, n_i^-\right) = \gamma\, n_i^+ \exp\left(\beta \frac{n_i^- - n_i^+}{n_i^+ + n_i^-}\right) \tag{D.13}$$

$$B_{\boldsymbol{i}} \to A_{\boldsymbol{i}} \qquad W\left(n_i^+ + 1, n_i^- - 1 | n_i^+, n_i^-\right) = \gamma\, n_i^- \exp\left(\beta \frac{n_i^+ - n_i^-}{n_i^+ + n_i^-}\right) \tag{D.14}$$

which contribute to the Master Equation as

$$\mathcal{L}_{\text{flip}}[P] = \gamma \sum_{\boldsymbol{i}} (n_i^+ + 1) \exp\left(\beta \frac{n_i^- - n_i^+ - 2}{n_i^+ + n_i^-}\right) P(\boldsymbol{n}^+ + \boldsymbol{1}_{\boldsymbol{i}}, \boldsymbol{n}^- - \boldsymbol{1}_{\boldsymbol{i}}; t) -$$

$$- n_i^+ \exp\left(\beta \frac{n_i^- - n_i^+}{n_i^+ + n_i^-}\right) P(\boldsymbol{n}^+, \boldsymbol{n}^-; t) +$$

$$+ (n_i^- + 1) \exp\left(\beta \frac{n_i^+ - n_i^- - 2}{n_i^+ + n_i^-}\right) P(\boldsymbol{n}^+ - \boldsymbol{1}_{\boldsymbol{i}}, \boldsymbol{n}^- + \boldsymbol{1}_{\boldsymbol{i}}; t) - \tag{D.15}$$

$$- n_i^- \exp\left(\beta \frac{n_i^+ - n_i^-}{n_i^+ + n_i^-}\right) P(\boldsymbol{n}^+, \boldsymbol{n}^-; t)$$

AIM1 rates

In the AIM1, the spin-flipping process occurs with rates which are reminiscent of some Ising-like behaviour, namely given by

$$A_i \longrightarrow B_i \qquad \text{rate: } \gamma \exp\left(-\beta\, m_i\right) = \gamma \exp\left[\beta\left(n_i^- - n_i^+\right)\right] \tag{D.16}$$

$$B_i \longrightarrow A_i \qquad \text{rate: } \gamma \exp\left(\beta\, m_i\right) = \gamma \exp\left[\beta\left(n_i^+ - n_i^-\right)\right] \tag{D.17}$$

The global rates associated to this process are

$$A_i \to B_i \qquad W\left(n_i^+ - 1, n_i^- + 1 | n_i^+, n_i^-\right) = \gamma\, n_i^+ \exp\left(\beta\left(n_i^- - n_i^+\right)\right) \tag{D.18}$$

$$B_i \to A_i \qquad W\left(n_i^+ + 1, n_i^- - 1 | n_i^+, n_i^-\right) = \gamma\, n_i^- \exp\left(\beta\left(n_i^+ - n_i^-\right)\right) \tag{D.19}$$

which contribute to the Master Equation as

$$
\begin{aligned}
\mathcal{L}_{\text{flip}}[P] = \gamma \sum_i\, & (n_i^+ + 1) \exp\left[\beta\left(n_i^- - n_i^+ - 2\right)\right] P(\boldsymbol{n}^+ + \mathbf{1}_i\,, \boldsymbol{n}^- - \mathbf{1}_i\,; t) - \\
& -n_i^+ \exp\left[\beta\left(n_i^- - n_i^+\right)\right] P(\boldsymbol{n}^+, \boldsymbol{n}^-; t) + \\
& +(n_i^- + 1) \exp\left[\beta\left(n_i^+ - n_i^- - 2\right)\right] P(\boldsymbol{n}^+ - \mathbf{1}_i\,, \boldsymbol{n}^- + \mathbf{1}_i\,; t) - \\
& -n_i^- \exp\left[\beta\left(n_i^+ - n_i^-\right)\right] P(\boldsymbol{n}^+, \boldsymbol{n}^-; t)
\end{aligned}
\tag{D.20}
$$

AIM2

In the case of the AIM2, particles undergo multiple-particle collisions. Here, I consider one-, two- and three-particle collision processes, with rates denoted γ, λ and τ respectively. These three processes are what I call in the main text AIM2.1, AIM2.2 and AIM2.3. In this case, the contribution $\mathcal{L}_{\text{flip}}$ can be further written as

$$\mathcal{L}_{\text{flip}} = \mathcal{L}_\gamma + \mathcal{L}_\lambda + \mathcal{L}_\tau \tag{D.21}$$

AIM2.1: one-particle collision

The one-particle collision (random) spin-flipping process is defined by the reactions

$$A_i \longrightarrow B_i \qquad \text{rate: } \gamma \qquad\qquad B_i \longrightarrow A_i \qquad \text{rate: } \gamma \tag{D.22}$$

The rates for a random spin flipping, expressed in terms of the number of A_i and B_i particles, n_i^+ and n_i^- respectively, take the following form

$$A_i \longrightarrow B_i \qquad\qquad W(n_i^+ - 1, n_i^- + 1 | n_i^+, n_i^-) = \gamma\, n_I^+ \tag{D.23}$$
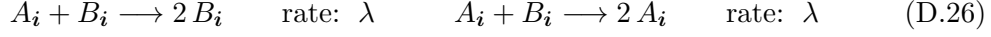
$$B_i \longrightarrow A_i \qquad\qquad W(n_i^+ + 1, n_i^- - 1 | n_i^+, n_i^-) = \gamma\, n_i^- \tag{D.24}$$

From these rates, I can write down the contribution $\mathcal{L}_\gamma\,[P]$ of the random spin-flipping to the Master Equation, as

$$
\begin{aligned}
\mathcal{L}_\gamma\,[P] = \gamma \sum_i\, & (n_i^+ + 1)\, P(\boldsymbol{n}^+ + \mathbf{1}_i\,, \boldsymbol{n}^- - \mathbf{1}_i\,; t) - n_i^+\, P(\boldsymbol{n}^+, \boldsymbol{n}^-; t) + \\
& +(n_i^- + 1)\, P(\boldsymbol{n}^+ - \mathbf{1}_i\,, \boldsymbol{n}^- + \mathbf{1}_i\,; t) - n_i^-\, P(\boldsymbol{n}^+, \boldsymbol{n}^-; t)
\end{aligned}
\tag{D.25}
$$

AIM2.2: two-particle collision

In terms of reactions, the two-particle collision process can be expressed as

$$A_i + B_i \longrightarrow 2\,B_i \qquad \text{rate: } \lambda \qquad A_i + B_i \longrightarrow 2\,A_i \qquad \text{rate: } \lambda \qquad \text{(D.26)}$$

Note that the two rates must be equal if one wants to preserve the symmetry by spin inversion, which is a symmetry under exchange of A and B particles. The rates associated to this process are

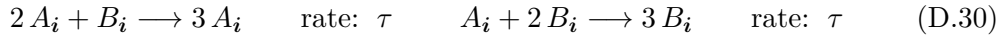$$A_i \longrightarrow B_i \qquad\qquad W(n_i^+ - 1, n_i^- + 1 | n_i^+, n_i^-) = \lambda\, n_i^+ n_i^- \qquad \text{(D.27)}$$
$$B_i \longrightarrow A_i \qquad\qquad W(n_i^+ + 1, n_i^- - 1 | n_i^+, n_i^-) = \lambda\, n_i^+ n_i^- \qquad \text{(D.28)}$$

which contribute to the Master Equation as

$$\mathcal{L}_\lambda[P] = \lambda \sum_i (n_i^+ + 1)(n_i^- - 1)\, P(\boldsymbol{n}^+ + \mathbf{1}_i, \boldsymbol{n}^- - \mathbf{1}_i; t) - n_i^+ n_i^-\, P(\boldsymbol{n}^+, \boldsymbol{n}^-; t) +$$
$$+ (n_i^- + 1)(n_i^+ - 1)\, P(\boldsymbol{n}^+ - \mathbf{1}_i, \boldsymbol{n}^- + \mathbf{1}_i; t) - n_i^+ n_i^-\, P(\boldsymbol{n}^+, \boldsymbol{n}^-; t)$$
$$\text{(D.29)}$$

AIM2.2: two-particle collision

In terms of reactions, the three-particle collision process can be expressed as

$$2\,A_i + B_i \longrightarrow 3\,A_i \qquad \text{rate: } \tau \qquad A_i + 2\,B_i \longrightarrow 3\,B_i \qquad \text{rate: } \tau \qquad \text{(D.30)}$$

Again, if one wants the system to obey a symmetry under the exchange of A and B species, which is a symmetry under global spin flipping, the rates with which the two reactions take place must be the same. The global rates associated to this process are

$$A_i \longrightarrow B_i \qquad W(n_i^+ - 1, n_i^- + 1 | n_i^+, n_i^-) = \frac{\tau}{2}\, n_i^+ n_i^- \left(n_i^- - 1\right) \qquad \text{(D.31)}$$

$$B_i \longrightarrow A_i \qquad W(n_i^+ + 1, n_i^- - 1 | n_i^+, n_i^-) = \frac{\tau}{2}\, n_i^+ \left(n_i^+ - 1\right) n_i^- \qquad \text{(D.32)}$$

which contributes to the Master Equation as

$$\mathcal{L}_\tau[P] = \frac{\tau}{2} \sum_i (n_i^+ + 1)n_i^+(n_i^- - 1)\, P(\boldsymbol{n}^+ + \mathbf{1}_i, \boldsymbol{n}^- - \mathbf{1}_i; t) - n_i^+(n_i^+ - 1)n_i^-\, P(\boldsymbol{n}^+, \boldsymbol{n}^-; t) +$$
$$+ (n_i^- + 1)n_i^-(n_i^+ - 1)\, P(\boldsymbol{n}^+ - \mathbf{1}_i, \boldsymbol{n}^- + \mathbf{1}_i; t) - n_i^+ n_i^-(n_i^- - 1)\, P(\boldsymbol{n}^+, \boldsymbol{n}^-; t)$$
$$\text{(D.33)}$$

D.2   Doi-Peliti Action

The action of the Doi-Peliti field theory of an AIM will have a form similar to that presented in Sec. 12.2.1. Since two particle species are present in an AIM, namely A and B particles with $+1$ and -1 spin respectively, I will need to take this into account by introducing two sets of creation and annihilation fields. The action therefore reads

$$\mathcal{S} = \sum_i \int \mathrm{d}t\, \phi_i^*(t)\partial_t \phi_i(t) + \psi_i^*(t)\partial_t \psi_i(t) + \int \mathrm{d}t\, \frac{\langle \boldsymbol{\phi}^*(t), \boldsymbol{\psi}^*(t) | \hat{H} | \boldsymbol{\phi}(t), \boldsymbol{\psi}(t) \rangle}{\langle \boldsymbol{\phi}^*(t), \boldsymbol{\psi}^*(t) | \boldsymbol{\phi}(t), \boldsymbol{\psi}(t) \rangle} \quad \text{(D.34)}$$

Where $\hat{H}$ is derived from $\mathcal{L}$ through the procedure described in Sec. 12.2.1. Since $\mathcal{L} = \mathcal{L}_D + \mathcal{L}_\epsilon + \mathcal{L}_{\text{flip}}$, therefore also

$$\hat{H} = \hat{H}_D + \hat{H}_\epsilon + \hat{H}_{\text{flip}} \tag{D.35}$$

and in turn the action can be written as $\mathcal{S} = \sum_i \int \mathrm{d}t\, \mathcal{A}$ where

$$\mathcal{A} = \phi_i^*(t)\partial_t \phi_i(t) + \psi_i^*(t)\partial_t \psi_i(t) + \mathcal{A}_D + \mathcal{A}_\epsilon + \mathcal{A}_{\text{flip}} \tag{D.36}$$

D.2.1 Hopping

As done for the Master Equation in Appendix D.1, I split in two the contribution of hopping also in the field-theoretical action.

Passive diffusion

Starting from the diffusive contribution to the Master Equation $\mathcal{L}_D$, one can derive the second-quantised evolution operator associated with it, given by

$$\begin{aligned}
\hat{H}_D &= -D \sum_i \sum_{j:|i-j|=h} a_j^\dagger a_i - a_i^\dagger a_i + b_j^\dagger b_i - b_i^\dagger b_i = \\
&= D \sum_i \sum_{j:|i-j|=h} \left(a_i^\dagger - a_j^\dagger\right) a_i + \left(b_i^\dagger - b_j^\dagger\right) b_i = \\
&= \frac{D}{2} \sum_i \sum_{j:|i-j|=h} \left(a_i^\dagger - a_j^\dagger\right)(a_i - a_j) + \left(b_i^\dagger - b_j^\dagger\right)(b_i - b_j) ,
\end{aligned} \tag{D.37}$$

Since $\hat{H}_D$ is already normal-ordered, the contribution $\mathcal{A}_D$ to the Doi-Peliti action density is straightforward to compute and takes the form

$$\mathcal{A}_D = \frac{D}{2} \sum_{j:|i-j|=h} \left[\left(\phi_i^*(t) - \phi_j^*(t)\right)(\phi_i(t) - \phi_j(t)) + \left(\psi_i^*(t) - \psi_j^*(t)\right)(\psi_i(t) - \psi_j(t))\right] \tag{D.38}$$

The final contribution to the total action is obtained by summing over sites i and integrating over time.

Active self-propulsion

Starting from the active self-propulsion contribution to the Master Equation $\mathcal{L}_\epsilon$, one can derive the second-quantised evolution operator associated to it, given by

$$\begin{aligned}
\hat{H}_\epsilon &= -\epsilon D \sum_i a_{i+h\hat{x}}^\dagger a_i - a_{i-h\hat{x}}^\dagger a_i - b_{i+h\hat{x}}^\dagger b_i + b_{i-h\hat{x}}^\dagger b_i = \\
&= -\epsilon D \sum_i \left(a_{i+h\hat{x}}^\dagger - a_{i-h\hat{x}}^\dagger\right) a_i - \left(b_{i+h\hat{x}}^\dagger - b_{i-h\hat{x}}^\dagger\right) b_i = \\
&= -\epsilon D \sum_i \left(a_{i+h\hat{x}}^\dagger - a_{i-h\hat{x}}^\dagger\right) a_i - \left(b_{i+h\hat{x}}^\dagger - b_{i-h\hat{x}}^\dagger\right) b_i
\end{aligned} \tag{D.39}$$

Since $\hat{H}_\epsilon$ is already normal-ordered, the contribution $\mathcal{A}_\epsilon$ to the Doi-Peliti action density is straightforward to compute, and takes the form

$$\mathcal{A}_\epsilon = -\epsilon D \left[\left(\phi_{i+h\hat{x}}^*(t) - \phi_{i-h\hat{x}}^*(t)\right)\phi_i(t) - \left(\psi_{i+h\hat{x}}^*(t) - \psi_{i-h\hat{x}}^*(t)\right)\psi_i(t)\right] \tag{D.40}$$

D.2.2 Spin-flipping

AIM0 action

For the AIM0, one can derive the second-quantised evolution operator associated to $\mathcal{L}_{\text{flip}}$, which is given by

$$\hat{H}_{\text{flip}} = \gamma \sum_{\boldsymbol{i}} \left(a_{\boldsymbol{i}}^\dagger - b_{\boldsymbol{i}}^\dagger \right) \left[a_{\boldsymbol{i}} \exp\left(\beta \frac{b_{\boldsymbol{i}}^\dagger b_{\boldsymbol{i}} - a_{\boldsymbol{i}}^\dagger a_{\boldsymbol{i}}}{a_{\boldsymbol{i}}^\dagger a_{\boldsymbol{i}} + b_{\boldsymbol{i}}^\dagger b_{\boldsymbol{i}}} \right) - b_{\boldsymbol{i}} \exp\left(\beta \frac{a_{\boldsymbol{i}}^\dagger a_{\boldsymbol{i}} - b_{\boldsymbol{i}}^\dagger b_{\boldsymbol{i}}}{a_{\boldsymbol{i}}^\dagger a_{\boldsymbol{i}} + b_{\boldsymbol{i}}^\dagger b_{\boldsymbol{i}}} \right) \right] \quad \text{(D.41)}$$

In terms of $\hat{H}^{(\gamma)}$ the contribution to the action will be given by

$$S_\gamma = \sum_{\boldsymbol{i}} \int \mathrm{d}t \, S_\gamma(\phi_{\boldsymbol{i}}^*(t), \psi_{\boldsymbol{i}}^*(t), \phi_{\boldsymbol{i}}(t), \psi_{\boldsymbol{i}}(t)) \quad \text{(D.42)}$$

The main issue with this form of $\hat{H}_{\text{flip}}$ is that it is not normal-ordered. To write down an explicit action for the field theory, normal ordering $\hat{H}_{\text{flip}}$ is a crucial step. However, this task seems very hard, due to the presence of operators at the denominator in the exponential. However, it is still possible to find a formal expression for the action density $\mathcal{A}_{\text{flip}}$.

In terms of $\hat{H}_{\text{flip}}$, the contribution to the action density will be given by

$$\mathcal{A}_{\text{flip}} = \frac{\langle \phi^*, \psi^* | \hat{H}_{\text{flip}} | \phi, \psi \rangle}{\langle \phi^*, \psi^* | \phi, \psi \rangle} \quad \text{(D.43)}$$

Here I dropped the subscript $\boldsymbol{i}$ to make the reading easier, as the process involves particles on the same site. The coherent states on a single site are given by

$$|\phi, \psi\rangle = e^{\phi a^\dagger + \psi b^\dagger}|0\rangle = \sum_{l_1, l_2} \frac{\phi^{l_1} \psi^{l_2}}{l_1! l_2!} (a^\dagger)^{l_1} (b^\dagger)^{l_2}|0\rangle = \sum_{l_1, l_2} \frac{\phi^{l_1} \psi^{l_2}}{l_1! l_2!} |l_1, l_2\rangle \quad \text{(D.44)}$$

$$\langle \phi^*, \psi^* | = \langle 0 | e^{\phi^* a + \psi^* b} = \langle 0 | \sum_{m_1, m_2} \frac{(\phi^*)^{m_1} (\psi^*)^{m_2}}{m_1! m_2!} a^{m_1} b^{m_2} = \sum_{m_1, m_2} \langle m_1, m_2 | (\phi^*)^{m_1} (\psi^*)^{m_2}$$
$$\text{(D.45)}$$

The summation here runs from 0 to ∞, while the states $|l_1, l_2\rangle$ and $\langle m_1, m_2|$ are defined as

$$|l_1, l_2\rangle = (a^\dagger)^{l_1} (b^\dagger)^{l_2}|0\rangle \qquad \langle m_1, m_2| = \langle 0| \frac{a^{m_1} b^{m_2}}{m_1! m_2!}. \quad \text{(D.46)}$$

The slightly different definition is chosen to ensure the correct normalisation

$$\langle m_1, m_2 | l_1, l_2 \rangle = \delta_{m_1, l_1} \delta_{m_2, l_2}. \quad \text{(D.47)}$$

Thus, the action density $\mathcal{A}_{\text{flip}}$ reads

$$
\begin{aligned}
\mathcal{A}_{\text{flip}} =& \gamma\, e^{-\phi^*\phi - \psi^*\psi} \sum_{l_1, l_2, m_1, m_2} \left[\langle m_1, m_2 | \left(a^\dagger - b^\dagger \right) a \, \exp\left(\beta \frac{b^\dagger b - a^\dagger a}{a^\dagger a + b^\dagger b} \right) | l_1, l_2 \rangle - \right. \\
& \left. - \langle m_1, m_2 | \left(a^\dagger - b^\dagger \right) b \, \exp\left(\beta \frac{a^\dagger a - b^\dagger b}{a^\dagger a + b^\dagger b} \right) | l_1, l_2 \rangle \right] \frac{(\phi^*)^{m_1} (\psi^*)^{m_2} \phi^{l_1} \psi^{l_2}}{l_1! \, l_2!} = \\
=& \gamma\, e^{-\phi^*\phi - \psi^*\psi} \sum_{l_1, l_2, m_1, m_2} \left[\exp\left(\beta \frac{l_2 - l_1}{l_1 + l_2} \right) \langle m_1, m_2 | \left(a^\dagger a - b^\dagger a \right) | l_1, l_2 \rangle - \right. \\
& \left. - \exp\left(\beta \frac{l_1 - l_2}{l_1 + l_2} \right) \langle m_1, m_2 | \left(a^\dagger b - b^\dagger b \right) | l_1, l_2 \rangle \right] \frac{(\phi^*)^{m_1} (\psi^*)^{m_2} \phi^{l_1} \psi^{l_2}}{l_1! \, l_2!} = \\
=& \gamma\, e^{-\phi^*\phi - \psi^*\psi} \sum_{l_1, l_2, m_1, m_2} \left[l_1 \exp\left(\beta \frac{l_2 - l_1}{l_1 + l_2} \right) \left(\langle m_1, m_2 | l_1, l_2 \rangle - \langle m_1, m_2 | l_1 - 1, l_2 + 1 \rangle \right) - \right. \\
& \left. - l_2 \exp\left(\beta \frac{l_1 - l_2}{l_1 + l_2} \right) \left(\langle m_1, m_2 | l_1 + 1, l_2 - 1 \rangle - \langle m_1, m_2 | l_1, l_2 \rangle \right) \right] \frac{(\phi^*)^{m_1} (\psi^*)^{m_2} \phi^{l_1} \psi^{l_2}}{l_1! \, l_2!}
\end{aligned}
\tag{D.48}
$$

Hence, by reminding that $\langle m_1, m_2 | l_1, l_2 \rangle = \delta_{m_1, l_1} \delta_{m_2, l_2}$, I can write the action as:

$$
\begin{aligned}
\mathcal{A}_{\text{flip}} = \gamma\, e^{-\phi^*\phi - \psi^*\psi} \sum_{l_1, l_2} \phi^{l_1} \psi^{l_2} \left[l_1 \frac{(\phi^*)^{l_1} (\psi^*)^{l_2} - (\phi^*)^{l_1 - 1} (\psi^*)^{l_2 + 1}}{l_1! \, l_2!} \exp\left(\beta \frac{l_2 - l_1}{l_1 + l_2} \right) + \right. \\
\left. + l_2 \frac{(\phi^*)^{l_1} (\psi^*)^{l_2} - (\phi^*)^{l_1 + 1} (\psi^*)^{l_2 - 1}}{l_1! \, l_2!} \exp\left(\beta \frac{l_1 - l_2}{l_1 + l_2} \right) \right]
\end{aligned}
\tag{D.49}
$$

By shifting the start of the sum

$$
\mathcal{A}_{\text{flip}} = \gamma\, e^{-\phi^*\phi - \psi^*\psi} \sum_{l_1 = 0}^{\infty} \sum_{l_2 = 0}^{\infty} \frac{(\phi^*\phi)^{l_1} (\psi^*\psi)^{l_2}}{l_1! \, l_2!} \left(\phi^* - \psi^* \right) \left[\phi \exp\left(\beta \frac{l_2 - l_1 - 1}{l_1 + l_2 + 1} \right) - \psi \exp\left(\beta \frac{l_1 - l_2 - 1}{l_1 + l_2 + 1} \right) \right]
\tag{D.50}
$$

This is, of course, only a formal expression. I was not able to compute the result of this series explicitly, and thus the problem of what the Doi-Peliti field theoretical action for the AIM0 is remains an open question. I must, however, notice that both series in l_1 and l_2 are expected to be absolute convergent since the two factors $\exp\left(\beta \frac{l_2 - l_1 - 1}{l_1 + l_2 + 1} \right)$ and $\exp\left(\beta \frac{l_1 - l_2 - 1}{l_1 + l_2 + 1} \right)$ remain bounded for any l_1 and l_2 and the presence of $l_1! \, l_2!$ in the denominator guarantees convergence. This allows me to rewrite the sum over l_1 and l_2 as follows

$$
\sum_{l_1, l_2} f(l_1, l_2) = \sum_{k=0}^{+\infty} \sum_{l=0}^{k} f(k - l, l)
\tag{D.51}
$$

Using this new form, I can perform the sum over l, which leads to the form of the action density provided in the main text.

AIM1 action

For the AIM1, one can derive the contribution to the action of spin-flipping starting from $\mathcal{L}_{\text{flip}}$. The second-quantised evolution operator associated with this process is given by

$$\hat{H}_{\text{flip}} = \gamma \sum_i \left(a_i^\dagger - b_i^\dagger \right) \left\{ a_i \exp\left[\beta \left(b_i^\dagger b_i - a_i^\dagger a_i \right) \right] - b_i \exp\left[\beta \left(a_i^\dagger a_i - b_i^\dagger b_i \right) \right] \right\} \quad \text{(D.52)}$$

From $\hat{H}_{\text{flip}}$, it is possible to derive the contribution $\mathcal{A}_{\text{flip}}$ to the Doi-Peliti action density by averaging over coherent states, as done for the AIM0. The derivation is quite similar to the AIM0, with the difference that the summation can be performed exactly, and the action density takes the form

$$\mathcal{A}_{\text{flip}} = \gamma \left(\phi_i^* - \psi_i^* \right) e^{-\beta - \psi_i^* \psi_i - \phi_i^* \phi_i} \left(\phi_i\, e^{e^\beta \psi_i^* \psi_i + e^{-\beta} \phi_i^* \phi_i} - \psi_i\, e^{e^{-\beta} \psi_i^* \psi_i + e^\beta \phi_i^* \phi_i} \right) \quad \text{(D.53)}$$

AIM2 action

In the case of the AIM2, the action $\mathcal{A}_{\text{flip}}$ can be written as

$$\mathcal{A}_{\text{flip}} = \mathcal{A}_\gamma + \mathcal{A}_\lambda + \mathcal{A}_\tau \quad \text{(D.54)}$$

I derive in what follows each contribution.

AIM2.1: one-particle collision

Starting from $\mathcal{L}_\gamma$, one can derive the associated second-quantised evolution operator

$$\hat{H}_\gamma = \gamma \sum_i \left(a_i^\dagger - b_i^\dagger \right) \left(a_i - b_i \right) \quad \text{(D.55)}$$

which is already normal-ordered. Hence the contribution $\mathcal{S}_\gamma$ to the Doi-Peliti action density is straightforward to compute and takes the form provided in the main text in Eq. (12.37), namely

$$\mathcal{A}_\gamma = \gamma \left(\phi^* - \psi^* \right) \left(\phi - \psi \right) \quad \text{(D.56)}$$

AIM2.2: two-particle collision

Starting from $\mathcal{L}_\lambda$, one can derive the associated second-quantised evolution operator

$$\hat{H}_\lambda = -\lambda \sum_i \left(a_i^\dagger - b_i^\dagger \right)^2 a_i\, b_i \quad \text{(D.57)}$$

Since $\hat{H}_\lambda$ is already normal-ordered, the contribution $\mathcal{A}_\lambda$ to the Doi-Peliti action density is straightforward to compute and takes the form provided in the main text in Eq. (12.38), namely

$$\mathcal{A}_\lambda = -\lambda \left(\phi^* - \psi^* \right)^2 \phi\, \psi \quad \text{(D.58)}$$

AIM2.3: three-particle collision

Starting from $\mathcal{L}_\tau$, one can derive the associated second-quantised evolution operator

$$\hat{H}_\tau = -\frac{\tau}{2} \sum_i \left(a_i^\dagger - b_i^\dagger \right) \left[\left(a_i^\dagger \right)^2 a_i - \left(b_i^\dagger \right)^2 b_i \right] a_i\, b_i \quad \text{(D.59)}$$

Since $\hat{H}_\tau$ is already normal-ordered, the contribution $\mathcal{A}_\tau$ to the Doi-Peliti action is straightforward to compute and takes the form provided in the main text in Eq. (12.39), namely

$$\mathcal{A}_\tau = -\frac{\tau}{2} \left(\phi^* - \psi^* \right) \left[(\phi^*)^2 \phi - (\psi^*)^2 \psi \right] \phi\, \psi \quad \text{(D.60)}$$

My papers

[MyPaper1] Cavagna, A., Di Carlo, L., Giardina, I., Grigera, T. S., Melillo, S., Parisi, L., Pisegna, G. & Scandolo, M. Natural swarms in 3.99 dimensions. *Nature Physics* **19**, 1043–1049 (2023). DOI: 10.1038/s41567-023-02028-0.

[MyPaper2] Cavagna, A., Di Carlo, L., Giardina, I., Grigera, T., Pisegna, G. & Scandolo, M. Dynamical renormalization group for mode-coupling field theories with solenoidal constraint. *Journal of Statistical Physics* **184**, 26 (2021). DOI: 10.1007/s10955-021-02800-7.

[MyPaper3] Di Carlo, L. & Scandolo, M. Evidence of fluctuation-induced first-order phase transition in active matter. *New Journal of Physics* **24**, 123032 (2022). DOI: 10.1088/1367-2630/aca9ed.

[MyPaper4] Scandolo, M., Pausch, J. & Cates, M. E. Active ising models of flocking: a field-theoretic approach. *The European Physical Journal E* **46**, 103 (2023). DOI: 10.1140/epje/s10189-023-00364-w.

[MyPaper5] Scandolo, M., Pausch, J. & Cates, M. E. In preparation (2023).

Bibliography

[1] Cardy, J. *Scaling and renormalization in statistical physics* (Cambridge University Press, 1996).

[2] Parisi, G. *Statistical field theory.* Frontiers in Physics (Addison-Wesley, 1988).

[3] Kardar, M. *Statistical physics of fields* (Cambridge University Press, 2007).

[4] Leggett, A. J. A theoretical description of the new phases of liquid ^{3}He. *Reviews of Modern Physics* **47**, 331–414 (1975).

[5] Cavagna, A. *et al.* Scale-free correlations in starling flocks. *Proceedings of the National Academy of Sciences* **107**, 11865–11870 (2010).

[6] Cavagna, A. & Giardina, I. Bird flocks as condensed matter. *Annual Review of Condensed Matter Physics* **5**, 183–207 (2014).

[7] Ginelli, F. *et al.* Intermittent collective dynamics emerge from conflicting imperatives in sheep herds. *Proceedings of the National Academy of Sciences* **112**, 12729–12734 (2015).

[8] Zhang, H. P., Be'er, A., Florin, E.-L. & Swinney, H. L. Collective motion and density fluctuations in bacterial colonies. *Proceedings of the National Academy of Sciences* **107**, 13626–13630 (2010).

[9] Cavagna, A., Giardina, I. & Grigera, T. S. The physics of flocking: Correlation as a compass from experiments to theory. *Physics Reports* **728**, 1–62 (2018).

[10] Goldstone, J., Salam, A. & Weinberg, S. Broken symmetries. *Physical Review* **127**, 965–970 (1962).

[11] Nambu, Y. Quasi-particles and gauge invariance in the theory of superconductivity. *Physical Review* **117**, 648–663 (1960).

[12] Attanasi, A. *et al.* Collective behaviour without collective order in wild swarms of midges. *PLOS Computational Biology* **10**, 1–10 (2014).

[13] Cavagna, A. *et al.* Dynamic scaling in natural swarms. *Nature Physics* **13**, 914–918 (2017).

[14] Binney, J. J., Dowrick, N. J., Fisher, A. J. & Newman, M. E. J. *The theory of critical phenomena: an introduction to the renormalization group* (Oxford University Press, 1992).

[15] Goldenfeld, N. *Lectures on Phase Transitions and the Renormalization Group* (Perseus Books, 1992).

[16] Täuber, U. C. *Critical dynamics: a field theory approach to equilibrium and non-equilibrium scaling behavior* (Cambridge University Press, 2014).

[17] Wilson, K. G. Renormalization group and critical phenomena. i. renormalization group and the kadanoff scaling picture. *Physical Review B* **4**, 3174–3183 (1971).

[18] Marchetti, M. C. *et al.* Hydrodynamics of soft active matter. *Reviews of Modern Physics* **85**, 1143–1189 (2013).

[19] Toner, J. & Tu, Y. Long-range order in a two-dimensional dynamical xy model: how birds fly together. *Physical Review Letters* **75**, 4326–4329 (1995).

[20] Toner, J. & Tu, Y. Flocks, herds, and schools: A quantitative theory of flocking. *Physical Review E* **58**, 4828–4858 (1998).

[21] Chen, L., Lee, C. F. & Toner, J. Incompressible polar active fluids in the moving phase in dimensions $d > 2$. *New Journal of Physics* **20**, 113035 (2018).

[22] Toner, J. Giant number fluctuations in dry active polar fluids: A shocking analogy with lightning rods. *The Journal of Chemical Physics* **150**, 154120 (2019).

[23] Chen, L., Toner, J. & Lee, C. F. Critical phenomenon of the order-disorder transition in incompressible active fluids. *New Journal of Physics* **17**, 042002 (2015).

[24] Škultéty, V., Birnšteinová, i. c. v., Lučivjanský, T. & Honkonen, J. Universality in incompressible active fluid: Effect of nonlocal shear stress. *Physical Review E* **102**, 032616 (2020).

[25] Mishra, S., Simha, R. A. & Ramaswamy, S. A dynamic renormalization group study of active nematics. *Journal of Statistical Mechanics: Theory and Experiment* **2010**, P02003 (2010).

[26] Ramaswamy, S. The mechanics and statistics of active matter. *Annual Review of Condensed Matter Physics* **1**, 323–345 (2010).

[27] Toner, J., Tu, Y. & Ramaswamy, S. Hydrodynamics and phases of flocks. *Annals of Physics* **318**, 170–244 (2005).

[28] Caballero, F., Nardini, C. & Cates, M. E. From bulk to microphase separation in scalar active matter: a perturbative renormalization group analysis. *Journal of Statistical Mechanics: Theory and Experiment* **2018**, 123208 (2018).

[29] Maggi, C., Gnan, N., Paoluzzi, M., Zaccarelli, E. & Crisanti, A. Critical active dynamics is captured by a colored-noise driven field theory. *Communications Physics* **5**, 55 (2022).

[30] Cagnetta, F., Škultéty, V., Evans, M. R. & Marenduzzo, D. Universal properties of active membranes. *Physical Review E* **105**, L012604 (2022).

[31] Mahdisoltani, S., Zinati, R. B. A., Duclut, C., Gambassi, A. & Golestanian, R. Nonequilibrium polarity-induced chemotaxis: Emergent galilean symmetry and exact scaling exponents. *Physical Review Research* **3**, 013100 (2021).

[32] Gelimson, A. & Golestanian, R. Collective dynamics of dividing chemotactic cells. *Physical Review Letters* **114**, 028101 (2015).

[33] Deseigne, J., Dauchot, O. & Chaté, H. Collective motion of vibrated polar disks. *Physical Review Letters* **105**, 098001 (2010).

[34] Mahault, B., Ginelli, F. & Chaté, H. Quantitative assessment of the toner and tu theory of polar flocks. *Physical Review Letters* **123**, 218001 (2019).

[35] Tu, Y., Toner, J. & Ulm, M. Sound waves and the absence of galilean invariance in flocks. *Physical Review Letters* **80**, 4819–4822 (1998).

[36] Chaté, H., Ginelli, F., Grégoire, G. & Raynaud, F. Collective motion of self-propelled particles interacting without cohesion. *Physical Review E* **77**, 046113 (2008).

[37] Ginelli, F., Peruani, F., Bär, M. & Chaté, H. Large-scale collective properties of self-propelled rods. *Physical Review Letters* **104**, 184502 (2010).

[38] Doostmohammadi, A., Shendruk, T. N., Thijssen, K. & Yeomans, J. M. Onset of meso-scale turbulence in active nematics. *Nature Communications* **8**, 15326 (2017).

[39] Nishiguchi, D., Nagai, K. H., Chaté, H. & Sano, M. Long-range nematic order and anomalous fluctuations in suspensions of swimming filamentous bacteria. *Physical Review E* **95**, 020601 (2017).

[40] Hohenberg, P. C. & Halperin, B. I. Theory of dynamic critical phenomena. *Reviews of Modern Physics* **49**, 435–479 (1977).

[41] Cavagna, A. *et al.* Dynamical renormalization group approach to the collective behavior of swarms. *Physical Review Letters* **123**, 268001 (2019).

[42] Vicsek, T., Czirók, A., Ben-Jacob, E., Cohen, I. & Shochet, O. Novel type of phase transition in a system of self-driven particles. *Physical Review Letters* **75**, 1226–1229 (1995).

[43] Landau, L. D. & Lifshitz, E. M. *Fluid mechanics. Landau and Lifshitz: course of theoretical physics*, vol. 6 (Pergamon Press, 1987).

[44] Grégoire, G. & Chaté, H. Onset of collective and cohesive motion. *Physical Review Letters* **92**, 025702 (2004).

[45] Toner, J. Birth, death, and flight: A theory of malthusian flocks. *Physical Review Letters* **108**, 088102 (2012).

[46] Forster, D., Nelson, D. R. & Stephen, M. J. Large-distance and long-time properties of a randomly stirred fluid. *Physical Review A* **16**, 732–749 (1977).

[47] Martin, P. C., Siggia, E. D. & Rose, H. A. Statistical dynamics of classical systems. *Physical Review A* **8**, 423 (1973).

[48] Mermin, N. D. & Wagner, H. Absence of ferromagnetism or antiferromagnetism in one- or two-dimensional isotropic heisenberg models. *Physical Review Letters* **17**, 1133–1136 (1966).

[49] Hohenberg, P. C. Existence of long-range order in one and two dimensions. *Physical Review* **158**, 383–386 (1967).

[50] Widom, B. Equation of state in the neighborhood of the critical point. *The Journal of Chemical Physics* **43**, 3898–3905 (1965).

[51] Kadanoff, L. P. Scaling laws for ising models near t_c. *Physics Physique Fizika* **2**, 263–272 (1966).

[52] Wilson, K. G. & Kogut, J. The renormalization group and the ε expansion. *Physics Reports* **12**, 75–199 (1974).

[53] Wilson, K. G. & Fisher, M. E. Critical exponents in 3.99 dimensions. *Physical Review Letters* **28**, 240–243 (1972).

[54] Downes, J. A. The swarming and mating flight of diptera. *Annual Review of Entomology* **14**, 271–298 (1969).

[55] Sullivan, R. T. Insect swarming and mating. *The Florida Entomologist* **64**, 44–65 (1981).

[56] Attanasi, A. *et al.* Finite-size scaling as a way to probe near-criticality in natural swarms. *Physical Review Letters* **113**, 238102 (2014).

[57] Fyodorova, M. V. & Azovsky, A. I. Interactions between swarming chironomus annularius (diptera: Chironomidae) males: Role of acoustic behavior. *Journal of Insect Behavior* **16**, 295–306 (2003).

[58] Pennetier, C., Warren, B., Dabiré, K. R., Russell, I. J. & Gibson, G. "Singing on the wing" as a mechanism for species recognition in the malarial mosquito anopheles gambiae. *Current Biology* **20**, 131–136 (2010).

[59] Ballerini, M. *et al.* Interaction ruling animal collective behavior depends on topological rather than metric distance: Evidence from a field study. *Proceedings of the National Academy of Sciences* **105**, 1232–1237 (2008).

[60] Ferrell, R. A., Menyhárd, N., Schmidt, H., Schwabl, F. & Szépfalusy, P. Dispersion in second sound and anomalous heat conduction at the lambda point of liquid helium. *Physical Review Letters* **18**, 891–894 (1967).

[61] Halperin, B. I. & Hohenberg, P. C. Generalization of scaling laws to dynamical properties of a system near its critical point. *Physical Review Letters* **19**, 700–703 (1967).

[62] Taylor, J. R. *An Introduction to Error Analysis: The Study of Uncertainties in Physical Measurements.* ASMSU/Spartans.4.Spartans Textbook (University Science Books, 1997).

[63] Woolley, E. B. The method of minimized areas as a basis for correlation analysis. *Econometrica* **9**, 38–62 (1941).

[64] Samuelson, P. A. A note on alternative regressions. *Econometrica: Journal of the Econometric Society* **10**, 80–83 (1942).

[65] Mora, T. *et al.* Local equilibrium in bird flocks. *Nature Physics* **12**, 1153–1157 (2016).

[66] Cavagna, A., Culla, A., Di Carlo, L., Giardina, I. & Grigera, T. S. Low-temperature marginal ferromagnetism explains anomalous scale-free correlations in natural flocks. *Comptes Rendus Physique* **20**, 319–328 (2019).

[67] Cavagna, A. *et al.* Marginal speed confinement resolves the conflict between correlation and control in collective behaviour. *Nature Communications* **13**, 2315 (2022).

[68] Ginelli, F. The physics of the vicsek model. *The European Physical Journal Special Topics* **225**, 2099–2117 (2016).

[69] Cavagna, A., Di Carlo, L., Giardina, I., Grigera, T. S. & Pisegna, G. Equilibrium to off-equilibrium crossover in homogeneous active matter. *Physical Review Research* **3**, 013210 (2021).

[70] Solon, A. P. & Tailleur, J. Revisiting the flocking transition using active spins. *Physical Review Letters* **111**, 078101 (2013).

[71] Solon, A. P. & Tailleur, J. Flocking with discrete symmetry: The two-dimensional active ising model. *Physical Review E* **92**, 042119 (2015).

[72] Partridge, B. & Lee, C. F. Critical motility-induced phase separation belongs to the ising universality class. *Physical Review Letters* **123**, 068002 (2019).

[73] Doostmohammadi, A., Ignés-Mullol, J., Yeomans, J. M. & Sagués, F. Active nematics. *Nature Communications* **9**, 3246 (2018).

[74] Dadhichi, L. P., Maitra, A. & Ramaswamy, S. Origins and diagnostics of the nonequilibrium character of active systems. *Journal of Statistical Mechanics: Theory and Experiment* **2018** (2018).

[75] Dadhichi, L. P., Kethapelli, J., Chajwa, R., Ramaswamy, S. & Maitra, A. Nonmutual torques and the unimportance of motility for long-range order in two-dimensional flocks. *Physical Review E* **101**, 052601 (2020).

[76] Toner, J. Reanalysis of the hydrodynamic theory of fluid, polar-ordered flocks. *Physical Review E* **86**, 031918 (2012).

[77] Bertin, E., Droz, M. & Grégoire, G. Hydrodynamic equations for self-propelled particles: microscopic derivation and stability analysis. *Journal of Physics A: Mathematical and Theoretical* **42**, 445001 (2009).

[78] Janssen, H.-K. On a lagrangean for classical field dynamics and renormalization group calculations of dynamical critical properties. *Zeitschrift für Physik B Condensed Matter* **23**, 377–380 (1976).

[79] De Dominicis, C. Techniques de renormalisation de la théorie des champs et dynamique des phénomènes critiques. *Journal de Physique Colloques* **37**, C1–247–C1–253 (1976).

[80] Doi, M. Stochastic theory of diffusion-controlled reaction. *Journal of Physics A: Mathematical and General* **9**, 1479 (1976).

[81] Doi, M. Second quantization representation for classical many-particle system. *Journal of Physics A: Mathematical and General* **9**, 1465 (1976).

[82] Peliti, L. Path integral approach to birth-death processes on a lattice. *J. Phys. France* **46**, 1469–1483 (1985).

[83] Baglietto, G. & Albano, E. V. Finite-size scaling analysis and dynamic study of the critical behavior of a model for the collective displacement of self-driven individuals. *Physical Review E* **78**, 021125 (2008).

[84] Gönci, B., Nagy, M. & Vicsek, T. Phase transition in the scalar noise model of collective motion in three dimensions. *The European Physical Journal Special Topics* **157**, 53–59 (2008).

[85] Aldana, M., Larralde, H. & Vázquez, B. On the emergence of collective order in swarming systems: A recent debate. *International Journal of Modern Physics B* **23**, 3661–3685 (2009).

[86] Fisher, M. E. & Aharony, A. Dipolar interactions at ferromagnetic critical points. *Physical Review Letters* **30**, 559–562 (1973).

[87] Aharony, A. & Fisher, M. E. Critical behavior of magnets with dipolar interactions. I. Renormalization group near four dimensions. *Physical Review B* **8**, 3323–3341 (1973).

[88] Vicsek, T. & Zafeiris, A. Collective motion. *Physics Reports* **517**, 71–140 (2012).

[89] Solon, A. P., Chaté, H. & Tailleur, J. From phase to microphase separation in flocking models: The essential role of nonequilibrium fluctuations. *Physical Review Letters* **114**, 068101 (2015).

[90] Besse, M., Chaté, H. & Solon, A. Metastability of constant-density flocks. *Physical Review Letters* **129**, 268003 (2022).

[91] Chen, L., Lee, C. F. & Toner, J. Universality class for a nonequilibrium state of matter: A $d = 4 - \epsilon$ expansion study of malthusian flocks. *Physical Review E* **102**, 022610 (2020).

[92] Chen, L., Lee, C. F. & Toner, J. Moving, reproducing, and dying beyond flatland: Malthusian flocks in dimensions $d > 2$. *Physical Review Letters* **125**, 098003 (2020).

[93] Martin, D. *et al.* Fluctuation-induced phase separation in metric and topological models of collective motion. *Physical Review Letters* **126**, 148001 (2021).

[94] De Dominicis, C. & Giardina, I. *Random fields and spin glasses: a field theory approach* (Cambridge University Press, 2006).

[95] Aharony, A. Critical behavior of magnets with dipolar interactions. III. Antiferromagnets. *Physical Review B* **8**, 3349–3357 (1973).

[96] Toner, J. Renormalization-group treatment of the dislocation loop model of the smectic-A—nematic transition. *Physical Review B* **26**, 462–465 (1982).

[97] Dasgupta, C. & Halperin, B. I. Phase transition in a lattice model of superconductivity. *Physical Review Letters* **47**, 1556–1560 (1981).

[98] Amit, D. J. & Martin-Mayor, V. *Field Theory, the Renormalization Group, and Critical Phenomena: Graphs to Computers Third Edition* (World Scientific Publishing Company, 2005).

[99] Oerding, K., Van Wijland, F., Leroy, J. P. & Hilhorst, H. J. Fluctuation-induced first-order transition in a nonequilibrium steady state. *Journal of Statistical Physics* **99**, 1365–1395 (2000).

[100] Attanasi, A. *et al.* Information transfer and behavioural inertia in starling flocks. *Nature Physics* **10**, 691–696 (2014).

[101] Zwanzig, R. *Nonequilibrium statistical mechanics* (Oxford University Press, 2001).

[102] Cavagna, A. *et al.* Flocking and turning: a new model for self-organized collective motion. *Journal of Statistical Physics* **158**, 601–627 (2015).

[103] Sasvári, L., Schwabl, F. & Szépfalusy, P. Hydrodynamics of an n-component phonon system. *Physica A: Statistical Mechanics and its Applications* **81**, 108–128 (1975).

[104] Sasvári, L. & Szépfalusy, P. Dynamic critical properties of a stochastic n-vector model. *Physica A: Statistical Mechanics and its Applications* **87**, 1–34 (1977).

[105] Mori, H., Fujisaka, H. & Shigematsu, H. A New Expansion of the Master Equation. *Progress of Theoretical Physics* **51**, 109–122 (1974).

[106] Zwanzig, R. Memory effects in irreversible thermodynamics. *Physical Review* **124**, 983–992 (1961).

[107] De Dominicis, C. & Peliti, L. Field-theory renormalization and critical dynamics above t_c: Helium, antiferromagnets, and liquid-gas systems. *Physical Review B* **18**, 353–376 (1978).

[108] Cavagna, A. *et al.* Renormalization group crossover in the critical dynamics of field theories with mode coupling terms. *Physical Review E* **100**, 062130 (2019).

[109] Cavagna, A. *et al.* Silent flocks: constraints on signal propagation across biological groups. *Physical Review Letters* **114**, 218101 (2015).

[110] Pelissetto, A. & Vicari, E. Critical phenomena and renormalization-group theory. *Physics Reports* **368**, 549–727 (2002).

[111] Bruce, A. D. & Aharony, A. Critical exponents of ferromagnets with dipolar interactions: Second-order ϵ expansion. *Physical Review B* **10**, 2078–2087 (1974).

[112] Ma, S.-k. & Mazenko, G. F. Critical dynamics of ferromagnets in $6 - \epsilon$ dimensions: General discussion and detailed calculation. *Physical Review B* **11**, 4077–4100 (1975).

[113] Frey, E. & Schwabl, F. Critical dynamics of magnets. *Advances in Physics* **43**, 577–683 (1994).

[114] Halperin, B. I., Hohenberg, P. C. & Siggia, E. D. Renormalization-group treatment of the critical dynamics of superfluid helium, the isotropic antiferromagnet, and the easy-plane ferromagnet. *Physical Review B* **13**, 1299 (1976).

[115] Fruchart, M., Hanai, R., Littlewood, P. B. & Vitelli, V. Non-reciprocal phase transitions. *Nature* **592**, 363–369 (2021).

[116] Yang, X. & Marchetti, M. C. Hydrodynamics of turning flocks. *Physical Review Letters* **115**, 258101 (2015).

[117] Sokal, R. R. & Rolf, F. J. *Biometry: the principals and practice of statistics in biology research* (W. H. Freeman and Company, 2012).

[118] Nardini, C. *et al.* Entropy production in field theories without time-reversal symmetry: Quantifying the non-equilibrium character of active matter. *Physical Review X* **7**, 021007 (2017).

[119] Caballero, F. & Cates, M. E. Stealth entropy production in active field theories near ising critical points. *Physical Review Letters* **124**, 240604 (2020).

[120] Kourbane-Houssene, M., Erignoux, C., Bodineau, T. & Tailleur, J. Exact hydrodynamic description of active lattice gases. *Physical Review Letters* **120**, 268003 (2018).

[121] Kolmogoroff, A. Zur theorie der markoffschen ketten. *Mathematische Annalen* **112**, 155–160 (1936).

[122] Fodor, E., Agranov, T., Jack, R. & Cates, M. E. In preparation (2023).

[123] Garcia-Millan, R. & Pruessner, G. Run-and-tumble motion in a harmonic potential: field theory and entropy production. *Journal of Statistical Mechanics: Theory and Experiment* **2021**, 063203 (2021).

[124] Pruessner, G. & Garcia-Millan, R. Field theories of active particle systems and their entropy production (2022). `arXiv:2211.11906`.

[125] Wiese, K. J. Coherent-state path integral versus coarse-grained effective stochastic equation of motion: From reaction diffusion to stochastic sandpiles. *Physical Review E* **93**, 042117 (2016).

[126] Cardy, J. Field theory and non-equilibrium statistical mechanics (1999).

[127] Lefèvre, A. & Biroli, G. Dynamics of interacting particle systems: stochastic process and field theory. *Journal of Statistical Mechanics: Theory and Experiment* **2007**, P07024 (2007).

[128] Chatterjee, P. & Goldenfeld, N. Three-body interactions drive the transition to polar order in a simple flocking model. *Physical Review E* **100**, 040602 (2019).

[129] Suzuki, R., Weber, C. A., Frey, E. & Bausch, A. R. Polar pattern formation in driven filament systems requires non-binary particle collisions. *Nature Physics* **11**, 839–843 (2015).

[130] Jhawar, J. *et al.* Noise-induced schooling of fish. *Nature Physics* **16**, 488–493 (2020).

[131] Garcia-Millan, R. The concealed voter model is in the voter model universality class. *Journal of Statistical Mechanics: Theory and Experiment* **2020**, 053201 (2020).

[132] Akkineni, V. K. & Täuber, U. C. Nonequilibrium critical dynamics of the relaxational models c and d. *Physical Review E* **69**, 036113 (2004).